SOVIET PHYSICS

JETP

A translation of the Zhurnal Éksperimental'noĭ i Teoreticheskoĭ Fiziki.

Vol. 14, No. 4, pp 705-950 (Russ. orig. Vol. 41. No. 4, pp 993-1336, October, 1961) April, 1962

STUDY OF THREE-PRONG STARS PRODUCED IN NUCLEAR EMULSION BY INELASTIC pn INTERACTIONS AT 9 Bev

V. A. BOTVIN, Zh. S. TAKIBAEV, I. Ya. CHASNIKOV, N. P. PAVLOVA, and É. G. BOOS

Institute of Nuclear Physics, Academy of Sciences, Kazakh S.S.R.

Submitted to JETP editor January 20, 1961

J. Exptl. Theoret. Phys. (U.S.S.R.) 41, 993-1002 (October, 1961)

Three-prong stars produced in nuclear emulsion in pn interactions involving 9-Bev primary protons are analyzed. The c.m.s. proton and pion angular distributions, energy spectra, and transverse momentum distributions are studied. The magnitude of the asymmetry in the angular distributions is considered in detail. Each type of reaction is analyzed separately, and the fraction of energy carried off by a proton and pion is found to be independent of the type of reaction. The distribution of the true inelasticity coefficients K is given for the reaction $p + n \rightarrow p + p + \pi^- +$ neutral particles. A tendency for the formation of two peaks is observed in the K distribution and this may indicate the existence of two different mechanisms of multiple production.

INTRODUCTION

INTERACTIONS of 9-Bev protons with free and quasi-free emulsion nucleons have been studied in a number of experiments.[1-7] The results obtained, however, differ in a number of respects. In [2,4,5] the total angular distribution of the secondary particles in pp and pn interactions was considered as a function of the multiplicity under the assumption that the velocity of the secondary particles in the center-of-mass system (c.m.s.) is equal to the velocity of the c.m.s. relative to the laboratory system (l.s.) ($\beta_i' = \beta_c$). It was noted that a marked asymmetry resulting from the preferential emission of secondary particles in the forward direction is observed in the angular distribution of pn interactions of low multiplicity, and it was concluded that this asymmetry was due to protons.

Subsequently, individual cases of three-prong stars in which it was possible to determine the nature and energy of all secondary particles were analyzed in [6]. It was shown that the secondary particles from the interactions selected for analysis in [6] were emitted preferentially in the forward direction and that this asymmetry was not due to protons, but to pions.

Meanwhile, it was noted[7] that the c.m.s. angular distribution of protons emitted in pn interactions is almost symmetric. Although there was a certain tendency to the forward emission of protons, the large errors make it impossible to establish the existence of an asymmetry for the protons.

Taking these facts into account, we have studied in detail the characteristics of the secondary particles in three-prong stars from pn interactions.

1. EXPERIMENTAL ARRANGEMENT

A stack consisting of 250 NIKFI-R 10×10 cm emulsion pellicles was exposed to the internal beam of the proton synchrotron of the Joint Institute of Nuclear Research. The pellicles were scanned along the proton tracks by the fast scanning method.[8] From all the recorded cases of primary proton interactions in the emulsion we selected for analysis proton-nucleon interactions which satisfied the appropriate selection criteria.[1,3,5]

In the present experiment we were interested only in inelastic pn interactions in which the stars have three prongs. The number of such cases was 110.

For these interactions we measured the angles in the plane of the emulsion λ_i and the dip angles φ_i of the secondary charged particles. From these measurements we determined the angle of emission of the secondary particles θ_i: $\cos\theta_i = \cos\lambda_i \cos\varphi_i \cos\varphi_0 + \sin\varphi_i \sin\varphi_0$, where φ_0 is the angle of the primary particle with respect to the plane of the emulsion. When the angles λ_i were very small, we measured them by the coordinate method; for large angles, the measurements were made with an eyepiece goniometer with scale divisions of 6′.

In order to identify the secondary charged particles we made multiple scattering and ionization measurements. We selected for measurement all tracks making an angle φ_i with the plane of the emulsion less than a cutoff angle $\varphi^0 = 8°$.

To ensure good statistical reliability for the scattering and ionization measurements, we followed the secondary tracks into the neighboring pellicles, so that the length of the measured track was at least 5000 μ for measurements with 250-μ cells and at least 10000 for measurements with 500-μ cells. When it was necessary to use a bigger cell, we increased the track length correspondingly by following the tracks further, so that the error in determining the energy did not exceed 20 — 25%.

The scattering measurements were made with 250 — 4000 μ cells. The optimum cell length for a given track was chosen with the aid of the parameter $\rho\bar{D}'''/\bar{D}$ where $\bar{D}$ and $\bar{D}'''$ are the mean second and third differences.[9] For pure Coulomb scattering $\rho_C = \sqrt{3/2} = 1.225$; for spurious scattering $\rho_S = 1.75 + 0.07$. The cells were recalculated for larger cell lengths until ρ was less than 1.4 — 1.5. The value of $\bar{D}_C$ for pure Coulomb scattering was found from the formula

$$\bar{D}_c = [(\rho_s \bar{D}^2 - \bar{D}'''^2)/(\rho_s^2 - \rho_c^2)]^{1/2}.$$

At the same time, the value of $\bar{D}_C$ was estimated from the formula

$$\bar{D}_c = \sqrt{\bar{D}^2 - \bar{n}^2},$$

where $\bar{n}$ is the mean value of the spurious scattering. The numerical value of $\bar{n}$ was determined from scattering measurements along 9-Bev proton tracks and was based on a large volume of statistical material.[10] The values of $\bar{D}_C$ found from these two formulas, and also, in some cases, with smaller cells[9] were in agreement with one another.

The ionization was measured by blob counting along the secondary particle tracks and along several beam tracks in the vicinity of the secondary track. The correction for the dip angle was based on the method of Viryasov and Pisareva.[11] As a measure of the ionization we used the ratio $b^* = B/B_0$, where B and B_0 are the blob densities of the secondary and primary particle tracks, respectively. For the identification of the tracks we used the b* versus $p\beta c$ curves. In the region $p\beta c \gtrsim 1$ Bev, the measurement error of b* was no greater than 3%.

To check choice of the correct curves we identified the particles by means of the following curves which have been used by various investigators: a) the curves based on Barkas and Young's tables;[12] b) the curve given by Edwards et al.;[13] c) the curve given recently by Jongejans.[14] It should be noted that the curves of Barkas and Young practically coincide with those of Jongejans. Figure 1 shows the above-mentioned curves of b* vs ($p\beta c$) and the experimental points. From the position of the experimental points it seems to us that the best agreement is obtained with curves lying between those of Barkas and Young and those of Edwards et al.

Following Wang et al[7] we assumed that most of the particles in the region $1.5 \leq p\beta c \leq 2.5$ Bev were pions.

All the b* vs $p\beta c$ curves are of similar shape. The difference involves only the rate of rise of the ionization from the minimum to the plateau. To facilitate the use of these curves, the value of b* on primary particle tracks is usually taken as unity. This leads to the renormalization of the curves and results in a certain relative displacement of the curves. As can be seen from Fig. 1, however, the choice of the b* vs. $p\beta c$ curves will not actually affect the conclusions, since the number of points representing particles whose identification will be changed is small.

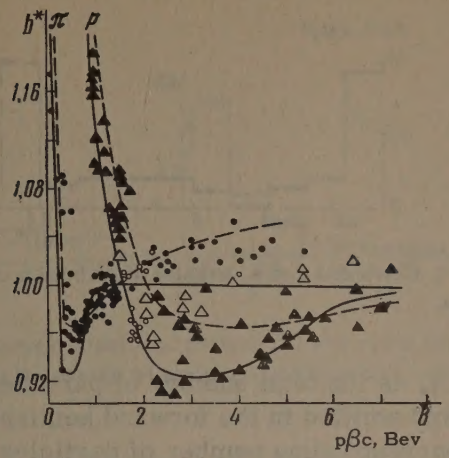

FIG. 1. Plot of b* vs. pβc for protons and pions; dotted curves – according to Barkas and Young, solid curves – according to Edwards et al.

2. PROTON AND PION C.M.S. ANGULAR DISTRIBUTION

To construct the c.m.s. angular distribution we used particles which could be identified under the conditions of the experiment. Since we could not determine the nature of all secondary particles in all interactions, but took, as a rule, a given sample of tracks ($\varphi_i \leq \varphi^0 = 8°$), it was necessary to introduce geometrical corrections which took into account particles with large dip angles. We arrived at these corrections in different ways.

A. If it is assumed that there is azimuthal symmetry in the l.s. (which is an entirely reasonable assumption), then each measured particle emitted at an angle θ in the l.s. should be assigned a statistical weight determined from the expression [15]

$$P = \frac{\pi}{2 \arcsin(\sin\varphi^0 / \sin\theta)}. \quad (1)$$

But we noted that the introduction of a statistical weight in this way increases somewhat the number of particles emitted at large angles (the sum of the statistical weights found from the measured particles is greater than the actual number of observed particles emitted at large angles).

B. Along with this approach, we determined the statistical weights in another way. The experimentally observed angular distribution of secondary particles in the l.s. was used to find the "experimental statistical weight" of each measured particle. We knew the number of measured particles and the total number of particles for any angular interval of the experimentally obtained histogram of the l.s. angular distribution. We could therefore determine the statistical weight for the given interval of angles θ as the ratio of the total number of secondary particles to the number of measured particles falling in the given angular interval. The experimental statistical weight determined in this way can be used in two cases: a) when particle tracks with $\varphi \leq \varphi^0$ are selected for identification, b) when all the particles are measured, even those with gray tracks in the emulsion. The experimental statistical weight determined for the second case will give the upper limit for the number of particles emitted in the backward hemisphere in the c.m.s.

We note that the introduction of the experimental statistical weights under assumption a) or using formula (1) and the taking into account of all gray tracks with a statistical weight of unity does not change the results.

In a previous experiment [16] we gave the experimental characteristics for different methods of introducing geometrical corrections. It was shown that the majority of the experimental data depend weakly on the choice of the statistical weights. However, more reliable results (in particular, for the $p_\perp$ distribution of protons) are obtained with the use of the experimental statistical weights under assumption b). We therefore present here the experimental results corresponding to the method of introducing the experimental statistical weights under assumption b).

The c.m.s. pion and proton angular distributions are shown in Figs. 2a and 2b. In these figures, as in those which follow, the dotted histograms correspond to the identification of particles with the curves of Barkas and Young and the solid histograms correspond to the curves of Edwards et al (unless indicated otherwise). It is seen from the pion c.m.s. angular distribution that the number of pions emitted forward is larger than the number of pions emitted backward. On the other hand, the opposite is observed for protons.

For a more careful check of this result, we assumed that all particles with pβc ≥ 2.5 Bev in

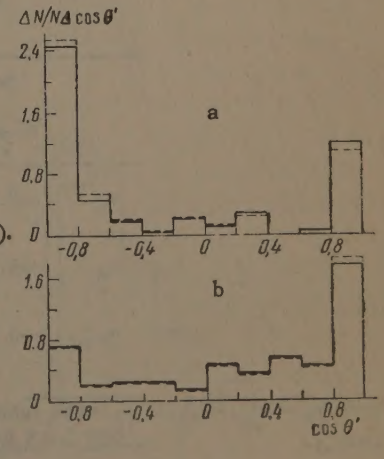

FIG. 2. C.m.s. angular distribution for protons (a) and pions (b).

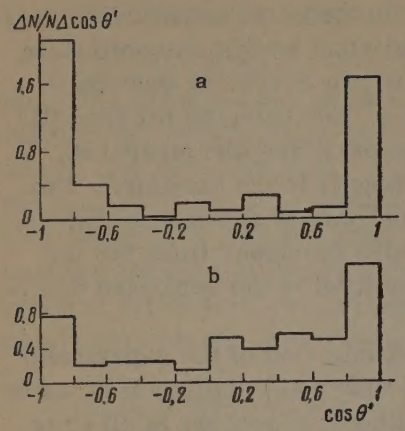

FIG. 3. Angular distributions of protons (a) and pions (b) under the assumption that all particles with $p\beta c \geq 2.5$ Bev (l.s.) are protons.

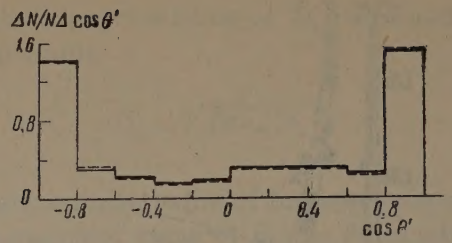

FIG. 4. Combined c.m.s. angular distribution of protons and pions.

the l.s. are protons, which is clearly not in accordance with the experimental data. The proton and pion angular distributions constructed under this assumption are given in Figs. 3a and 3b. It is quite evident that even under such an extreme assumption we did not observe a redistribution of the protons in the forward hemisphere, and we can say only that the protons are emitted symmetrically forward and backward in the c.m.s.

The combined angular distribution of the protons and pions is shown in Fig. 4. It is readily seen that the distribution is symmetric.

Since the question of the asymmetry of the angular distribution is very important, we analyzed all the assumptions involved in the introduction of the geometrical corrections. We shall consider qualitatively the question of the asymmetry of the particles. We define the asymmetry in terms of the quantity

$$\eta = (N_+ - N_-)/(N_+ + N_-), \qquad (2)$$
$$N_+ + N_- = N,$$

where N_+ is the total number of particles of a given kind emitted in the forward hemisphere, N_- is the corresponding number of particles for the backward hemisphere. The values of η for protons and pions and also for the combined distribution are shown in Table I for geometrical corrections introduced in various ways. The errors shown in the table were calculated with the aid of the binomial distribution of the values of N_+/N, where to determine the errors in the quantities N_+ and N we used different numbers of measured particles without taking into account their statistical weight. It is seen from the table that there is a significant tendency for the preferential emission of protons in the backward hemisphere and of pions in the forward hemisphere (in the c.m.s.); the value of the asymmetry determined by (2) lies outside the limits of error.

Hence we can conclude that the symmetry of the particles in the angular distribution for three-prong stars in the pn interactions found in [4,5] is the result of the unjustified assumption that the c.m.s. velocity of the secondary particles is equal to the velocity of the c.m.s. relative to the l.s. ($\beta_1' = \beta_c$). In fact, the combined proton and pion

Table I. Value of asymmetry in pion and proton distributions and combined angular distribution for different methods of introducing geometrical corrections and different assumptions on the relation between the ionization and the momentum of the particles

	Statistical weight from Eq. (1)		Experimental statistical weight			
			for case a		for case b	
	Barkas and Young	Edwards et al.	Barkas and Young	Edwards et al.	Barkas and Young	Edwards et al.
η_p	−0.36±0.15	−0.43±0.12	−0.32±0.11	−0.41±0.12	−0.35±0.10	−0.42±0.10
	−0.17±0.10*		−0.16±0.10		−0.16±0.09	
η_π	+0.14±0.07	+0.16±0.06	+0.31±0.07	+0.32±0.06	+0.40±0.07	+0.41±0.07
	+0.07±0.08		+0.22±0.08		+0.31±0.08	
$\eta_{p+\pi}$	+0.04±0.07	+0.04±0.07	+0.06±0.07	+0.05±0.07	+0.09±0.06	+0.08±0.06
	−0.03±0.07		+0.05±0.07		+0.08±0.06	

*The values in these curves correspond to the assumption that all particles with $p\beta c \geq 2.5$ Bev are protons.

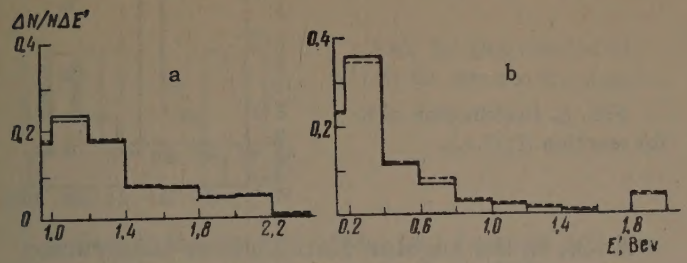

FIG. 5. Energy spectra of protons (a) and pions (b) in the c.m.s.; E' – total energy of protons and pions ($\Delta E'$ – in units of $\mu_\pi c^2$).

angular distribution (Fig. 4) is symmetric. Despite the fact that no asymmetry is observed, in the combined angular distribution of all particles, even under the stronger assumption as regards the nature of the high-energy particles ($p\beta c \geq 2.5$ Bev), we are inclined to believe that the observed strong tendency for the emission of pions in the forward hemisphere and of protons in the backward hemisphere in the c.m.s. reflects the existence of a real physical phenomenon which has not been explained as yet.

3. ENERGY CHARACTERISTICS OF SECONDARY PARTICLES, DISTRIBUTION OF TRANSVERSE MOMENTA AND INELASTICITY COEFFICIENTS

The experimental proton and pion c.m.s. energy distributions are shown in Fig. 5. We cannot, at present, make a direct comparison with the various theories of meson multiple production, since we do not have the calculated energy spectrum for reactions involving only three charged particles among the secondary particles.

We give below the mean values of the proton and pion energies in the c.m.s. $\bar{E}'_{tot}$ and the corresponding values for particles emitted in the forward $\bar{E}_f$ and backward $\bar{E}_b$ hemispheres (in Bev):

	E'_{tot}	$\bar{E}'_f$	$\bar{E}'_b$
Protons:	1.426 ± 0.044	1.365 ± 0.046	1.453 ± 0.045
Pions:	0.460 ± 0.024	0.449 ± 0.050	0.487 ± 0.052

It is seen that these values do not differ from one another, within the limits of experimental error, which, of course, indicates that the particle energies were measured correctly.

The transverse momentum distributions of the protons and pions are shown in Fig. 6. The mean values of $\bar{p}_\perp$ for protons and pions were (in Bev):

	$\bar{p}_\perp$	$\bar{p}_\perp$, forward	$\bar{p}_\perp$, back
Protons:	0.317 ±0.025	0.359 ± 0.052	0.297 ± 0.028
Pions	0.212 ±0.012	0.205 ± 0.012	0.229 ± 0.036

Also shown in the table are the corresponding mean values for the forward and back hemispheres in the c.m.s.

From the mean values of the energy carried away by pions and nucleons, we estimated the inelasticity coefficient and the fraction of c.m.s. energy expended on the production of neutral mesons. If the mean number of pions per three-prong star is 1.76 and their mean energy is 0.460 ± 0.024 Bev, then the fraction of energy expended on the production of charged mesons is (31 ± 5) %. The fraction of energy carried away by nucleons is (37 ± 3) % and, correspondingly, the inelasticity coefficient is (63 ± 4) %. Hence (32 ± 6) % of the primary energy remains for the production of neutral mesons.

If it is considered that the number of neutral mesons is one-half the number of charged mesons (this is confirmed at high energies in the cosmic ray region), then it should be assumed that the π^0-meson energy spectrum in three-prong stars is of lower energy than the charged-meson spectrum but this seems unlikely.

If it is assumed that the neutral and charged mesons have the same energy spectra, then we arrive at the conclusion that the mean number of neutral mesons per three-prong star should be approximately equal to the number of charged mesons.

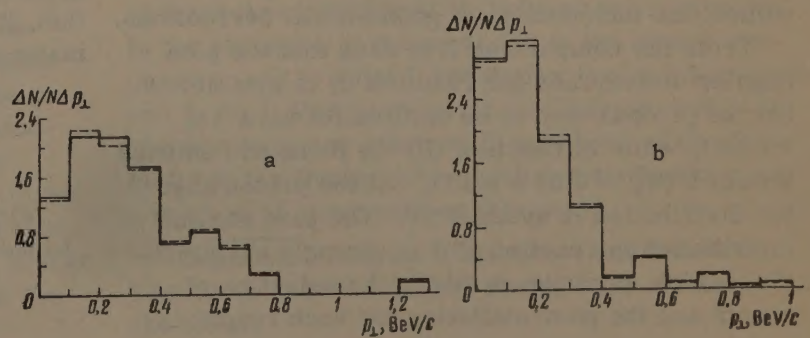

FIG. 6. Transverse momentum distributions of protons (a) and pions (b) ($p_\perp$ in units of Bev/c).

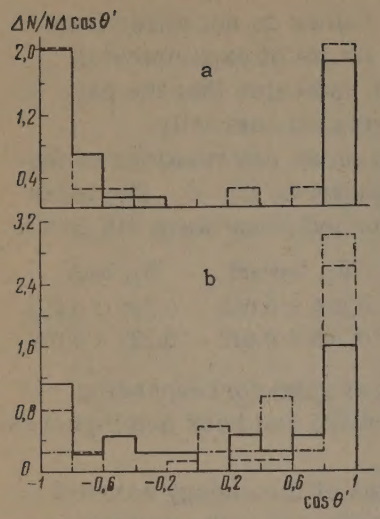

FIG. 7. Angular distribution of protons (a) and pions (b) for different types of reactions: solid line – reaction (I); dotted line – reaction (II); dash-dots – reaction (III).

4. ANALYSIS OF INTERACTIONS IN WHICH THE NATURE OF ALL SECONDARY CHARGED PARTICLES WERE IDENTIFIED

In the determination of the nature of the secondary charged particles, we were able to identify all three charged secondary particles in 41 cases. If we do not consider reactions in which strange particles and nucleon-antinucleon pairs are produced (the cross section of such interactions is quite small), then it is necessary to analyze only the following reactions:

$$p + n \to p + p + \pi^- + k\pi^0, \quad \text{(I)}$$
$$p + n \to p + n + \pi^+ + \pi^- + k\pi^0, \quad \text{(II)}$$
$$p + n \to n + n + \pi^+ + \pi^+ + \pi^- + k\pi^0, \quad \text{(III)}$$

where $k = 1, 2, 3, \ldots$ is the number of π^0 mesons produced. For the cases in which all particles could be measured, the cross sections of reaction (I), (II), and (III) are in the ratio $\sigma_I : \sigma_{II} : \sigma_{III} = 1.71 : 3.14 : 1$. The angular distributions of pions and protons for these reactions are shown in Fig. 7.

In order to improve the statistics, we included in the proton angular distribution of reaction (I) protons in which as a result of the measurements two particles were identified as protons and the third particle (unidentified) was evidently a pion. The number of such cases was 10. All curves correspond to the number of measured particles without the introduction of geometrical corrections.

From the comparison it is seen that the pion angular distribution for reaction (I) is symmetric, but the protons tend to be emitted forward ($\eta_p^I = 0.18$), while in reaction (II) the pions are emitted forward ($\eta_\pi^{II} = 0.55 \pm 0.13$), but the proton angular distribution is symmetric. The pion angular distribution in reaction (III) is strongly asymmetric (which, perhaps, is due to the selection of events and the poor statistics for such reactions).

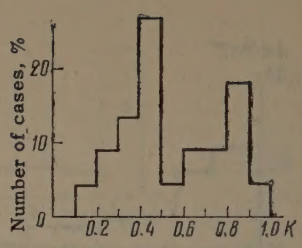

FIG. 8. Distribution of K for reaction (I) (l.s.).

Hence, in the angular distributions constructed for all reactions (Fig. 2), the asymmetry of backward protons is apparently due to reaction (I), while the forward asymmetry of the pions is due to reactions (II) and (III). The possibility of such an interpretation will be considered separately in another article.

Cases of interaction in which two protons are among the identified particles are of interest, since they permit an estimate of the true value of the inelasticity coefficient K, i.e., the fraction of the primary particle energy expended on the production of charged and neutral particles. In the l.s., the value of K for each interaction was determined from the relation

$$K = \left(E_0 + M - \sum E_p\right) / T_0,$$

where E_0 is the total energy of the primary proton, ΣE_p is the sum of the total energy for the two secondary protons, $T_0 = 9$ Bev is the kinetic energy of the primary proton. The value of the inelasticity coefficient K′ in the c.m.s. is

$$K' = \left(2M\gamma_c - \sum E_p'\right) / 2M(\gamma_c - 1),$$

where M is the proton mass.

Figure 8 shows the distribution of K (in the l.s.) for 22 cases. The corresponding K′ distribution (for the c.m.s.) is shown in Fig. 9.

It should be noted that the inelasticity coefficient distribution for reaction (I) does not have a clearly visible maximum, on the contrary the distribution is very broad and a tendency is observed for the formation of two maxima in the intervals $0.4 - 0.5$ and $0.8 - 0.9$ in both the l.s. and c.m.s. This suggests the existence of two mechanisms of inelastic interaction. But in order to establish this, it is necessary to increase the statistical material.

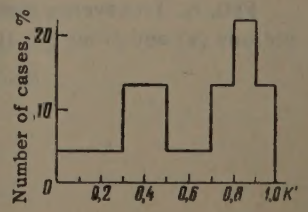

FIG. 9. Distribution of K′ for reaction (I) (c.m.s.).

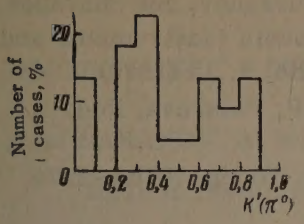

FIG. 10. Distribution of $K'(\pi^0)$ for reaction (I) (c.m.s.).

Knowing the energy of the two protons and the pion, we can also find the value of $K'(\pi^0)$, which is the fraction of energy expended in the production of neutral particles only. The corresponding distribution for reaction (I) is shown in Fig. 10. This distribution is also very broad.

Table II*

Type of reaction	Mean fraction of energy per proton, %	Mean fraction of energy per proton, %	Mean fraction of energy for all π^0 mesons, %
(I)	18.6 ± 0.8	16.4 ± 0.9	46.4 ± 2.5
(II)	15 ± 0.8	18 ± 0.8	34 ± 2.4
(III)	0	19.7 ± 1.1	4 ± 3.3
Mean values with allowance for the experimental statistical weights (case b)	18.7 ± 0.8	17.6 ± 0.9	–

*All data refer to the c.m.s.

One can still estimate the mean fraction of energy carried away by a single proton and a single charged pion for the various reactions. These values are shown in Table II. It is readily seen that the mean value of the energy carried away by a single proton and a single charged pion is practically independent of the form of the reaction. If it is assumed that the mean fraction of the energy carried away by the neutron in reaction (II) is equal to the mean fraction of energy carried away by protons in the same reaction and the mean fraction of energy for reaction (III) is the same as the corresponding value for reaction (I), then we can estimate the fraction of energy expended on the production of π^0 mesons. This value is also given in Table II (column 3). If it is assumed that the mean fraction of energy expended in the production of one π^0 is the same as the mean fraction of energy expended on the production of one charged pion, then it should be expected that, on the average, there are two to three π^0 mesons in reaction (I) and one to two π^0 mesons in reaction (II). In reaction (III) ~4% of the energy goes into neutral mesons, which is within the limits of experimental error.

The fraction of energy expended on the production of both charged and neutral mesons in reaction I is ~63%, while 59% of all the energy in reaction III is expended on the production of charged mesons only. These values are close to one another, which, indicates the absence of π^0 mesons in reaction (III), or, at most, the presence of only one π^0 meson.

On the basis of the foregoing discussion, it can be assumed that, with an increase in the multiplicity of the charged pions, the number of π^0 mesons decreases. Qualitatively, this also follows from other data. If it is considered that the mean energy of the pions does not depend on the multiplicity,[7] then, for $n_s = 7 - 8$, a negligible fraction of the energy should go into neutral particles. An analysis carried out in another experiment[17] indicates this, too.

CONCLUSIONS

1. The combined pion and proton c.m.s. angular distribution is symmetric.

2. The proton and pion angular distributions each show an asymmetry in the c.m.s., where the sign of the asymmetry is different; the protons are emitted preferentially in the backward hemisphere, while the pions are emitted preferentially in the forward hemisphere.

3. The estimate of the inelasticity coefficient based on the protons and pions indicates that half the energy going into the production of pions is carried away by π^0 mesons. If it is assumed that the energy spectra of the neutral and charged mesons are the same, then the number of π^0 mesons is equal to the number of $\pi^\pm$ mesons.

4. It has been shown that the mean energy carried away by one charged pion and one proton does not depend on the type of reaction.

5. The distribution of the true coefficient of inelasticity has no clearly discernible maximum; instead, we observe a tendency for the formation of two maxima. This conclusion, however, has to be confirmed with larger statistical material.

In conclusion, we consider it our pleasant duty to thank Academician V. I. Veksler for assistance in the exposure of the emulsion in the proton synchrotron of the Joint Institute for Nuclear Research and to M. I. Podgoretskii, K. D. Tolstov, and I. M. Gramenitskii and other staff members of the Joint Institute for Nuclear Research for discussions and a number of comments on this work.

[1] Bogachev, Bunyatov, Merekov, and Sidorov, DAN SSSR 121, 617 (1958), Soviet Phys.-Doklady 3, 785 (1959).

[2] V. I. Veksler, Proceedings of the Second Intern. Conf. on the Peaceful Uses of Atomic Energy, Geneva, 1958.

[3] Barashenkov, Belyakov, Bubelev, Wang, Maltsev, Gyn, and Tolstov, Nucl. Phys. **9**, 74 (1958).

[4] V. I. Veksler, Proceedings of the Ninth Annual Intern. Conf. on High Energy Physics, Kiev, 1959.

[5] Bogachev, Bunyatov, Gramenitskii, Lyubimov, Merekov, Podgoretskii, Sidorov, and Tuvdendorzh, JETP **37**, 1225 (1959), Soviet Phys. JETP **10**, 872 (1960).

[6] Takibaev, Botvin, and Chasnikov, DAN SSSR **135**, 571 (1960), Soviet Phys.-Doklady **5**, 1249 (1961).

[7] Wang, Visky, Gramenitskii, Grishin, Dalkhazhav, Lebedev, Nomofilov, Podgoretskii, and Strel'tsov, JETP **39**, 957 (1960), Soviet Phys. JETP **12**, 663 (1961).

[8] Yu. P. Bannik and M. I. Podgoretskii, Pribory i tekhnika eksperimenta (Instruments and Experimental Techniques) No. 3, 36 (1960).

[9] I. Ya. Chasnikov, Trudy Instituta yadernoĭ fiziki AN Kaz SSSR (Trans. Nuclear Phys. Institute, Kazakh S.S.R.) **3**, 64 (1960).

[10] Chasnikov, Takibaev, Tursunov, and Sharapov, Pribory i tekhnika eksperimenta (Instruments and Experimental Techniques) No. 5, 15 (1960).

[11] N. M. Viryasov and L. P. Pisareva, ibid. No. 2, 17 (1960).

[12] W. H. Barkas and D. M. Young, UCRL-2579, 1954.

[13] Edwards, Losty, Perkins, Pinkau, and Reynolds, Phil. Mag. **3**, 237 (1960).

[14] B. Jongejans, Nuovo cimento **16**, 625 (1960).

[15] Bogachev, Bunyatov, Visky, Merekov, Sidorov, and Yarba, JETP **38**, 432 (1960), Soviet Phys. JETP **11**, 317 (1960).

[16] Botvin, Takibaev, Chasnikov, Boos, and Pavlova, Trudy Instituta yadernoĭ fiziki AN KazSSR (Trans. Nuclear Phys. Institute, Kazakh S.S.R.) **5** (in press).

[17] Boos, Botwin, Takibaev, Chasnikov, and Pavlova, JETP **42**, No. 1 (1962).

Translated by E. Marquit
173

ANISOTROPIC FISSION OF U^{238} INDUCED BY 3-Mev NEUTRONS

I. A. BARANOV, A. N. PROTOPOPOV, and V. P. ÉĬSMONT

Radium Institute, Academy of Sciences, U.S.S.R.

Submitted to JETP editor April 11, 1961

J. Exptl. Theoret. Phys. (U.S.S.R.) 41, 1003-1006 (October, 1961)

A double ionization chamber with grids was used to investigate the dependence of the angular anisotropy of U^{238} fission induced by 3-Mev neutrons on the mass ratio of the fission fragment pairs. The anisotropy was found to be constant for mass ratios between 1.25 and 1.65. It was also established that the angular distribution of light and heavy fragments is symmetrical with respect to 90° to within a 3% uncertainty.

In one of the first investigations into the angular distribution of fission fragments[1] a dependence was observed between angular anisotropy and mass asymmetry, in which it was found that the angular anisotropy was greater for asymmetric fission than for symmetric fission. Subsequent research[2-4] showed that such a dependence of angular anisotropy on mass asymmetry persists for cases where the fission of various nuclei is induced by various particles.*

However, these investigations were all conducted under such conditions that fission of nuclei with different excitation energies could occur. Therefore, it was impossible to say whether this dependence was purely accidental and external in nature or an intrinsic characteristic of the fission process itself. The possibility of this being an intrinsic characteristic has been discussed by A. Bohr[5] (the influence of spin and parity of various fission channels) and by Strutinskii[6] (the dependence of the density of the fragment energy levels on the magnitude of their spin).

However, Halpern and Strutinskii[7] showed that this dependence may also be of a purely accidental nature. Actually, since the excitation energies of the fissioning nuclei in all the experiments thus far have been such that nuclear fission could occur either with no preliminary "shedding" of neutrons or with a preliminary "shedding" of one, two, or more neutrons, the temperatures of the nuclei immediately before the division into fragments could be different. Nuclei that have "shed" neutrons will fission in a "cooler" state and therefore more anisotropically than nuclei that have experienced no preliminary neutron "shedding."

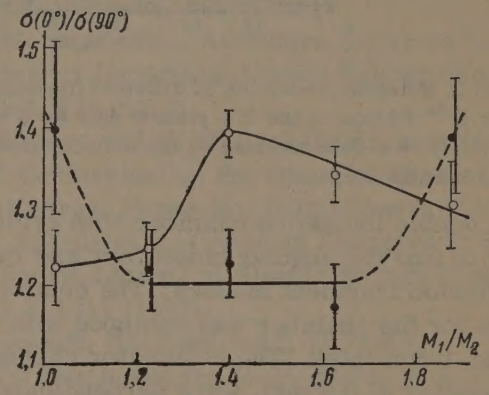

FIG. 1. Dependence of angular anisotropy on fragment mass ratios. o – data obtained for 14.9 Mev neutrons; • – data obtained for 3 Mev neutrons.

Fission asymmetry is also related to the excitation energy of the nucleus. The lower the excitation energy of the nuclei before fission, the greater will be their contribution toward asymmetric fission. Thus it is that nuclei that have "shed" neutrons before fission undergo more asymmetric and anisotropic fission than nuclei that have not first "shed" neutrons.

Experiments in which the excitation of the nucleus is strictly limited should provide an insight into the nature of the dependence between the angular and mass asymmetries. In such a case the excitation must be small enough so that the fission cannot follow the "shedding" of a neutron. These conditions are fulfilled when the experiments involve monoenergetic neutrons with energies up to 5 Mev.

The neutrons used in the present investigation were obtained from the D(d, n)He^3 reaction. These neutrons, which bombarded a uranium target, had an energy of 3 Mev. Because of the slowing down of the deuterons in the thick target and the finite solid angle a neutron energy as low as 0.2 Mev was possible.

*What is meant here is the fission of heavy nuclei at excitation energies that do not exceed 50 Mev.

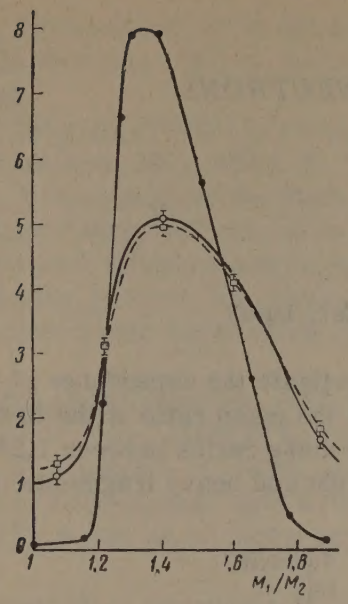

FIG. 2. Relative probability of different fragment mass ratios for U^{238} fission. □ and ○ – present data for 0° and 90° respectively; ● – data obtained by the radiochemical method[9] (fission spectra neutrons).

A double ionization chamber with grids was used to find the angular anisotropy and ratio of the fission fragment masses. The common electrode for the chamber was equipped with a collimator 1 mm thick. The collimator channels, with a diameter of 0.3 mm, were perpendicular to the collimator surface. Because of the low intensity of the neutron flux the target used was rather thick, consisting of natural uranium in the form $(NH_4)_2U_2O_7$ with an overall density of 450 $\mu g/cm^2$. The electrostatic spraying method was used to apply the target to a collodion film.[8]

Measurements were made alternately when the chamber was in two positions relative to the direction of the neutron beam. In the first position (0°) the direction of the neutron beam coincided with the axis of the collimator channels, i.e. with the direction in which the fragments were separated. In the second position (90°) the neutron beam entered almost perpendicularly to the axis of the collimator channels. The angular resolution was such that the direction of emission of the fragments did not deviate by more than 28° from the fixed direction of 0° or 90°. In other respects the experimental conditions and technique were the same as described earlier.[4] A total of about 4,000 fissions were recorded in each of the two directions.

To check the reliability of the method under thick target conditions we repeated previous measurements of the dependence of anisotropy on mass asymmetry for 14.9-Mev neutrons in which better energy resolution was had.[4] The results coincided satisfactorily.

Figure 1 shows the measured dependence of angular anisotropy, i.e., the ratios of cross sections $\sigma(0°)/\sigma(90°)$, on the mass ratio of the fragments M_1/M_2 for fission induced by 14.9- and 3-Mev neutrons. One can see that the dependence of anisotropy on the mass ratio for 3-Mev neutrons is of a different nature from the corresponding dependence for 14.9-Mev neutrons. It is essential to note that the measured anisotropy for symmetric and very asymmetric fissions does not reflect the true anisotropy in the corresponding region of the fragment mass ratios. This is evidenced by the fact that the distribution of the mass ratio for fragment pairs (see Fig. 3) for fission at 0° and 90° angles proved to be 1.5 times as wide as the distribution obtained by the radio-chemical method.[9]

The use of a thick target was the main reason for such a wide distribution. A conclusion that can be drawn from a comparison of our mass distribution with the radiochemical one is that in our case the major portion of the symmetric and very asymmetric fissions was composed of fissions that did not in fact belong to the given range of mass ratios. Thus, the major contribution to anisotropy for the mass ratio 1.07 was made by fissions with a mass ratio > 1.07, while the anisotropy for the mass ratio 1.87 was mainly due to fissions with a mass ratio < 1.87. Therefore, when the dependence of angular anisotropy on mass asymmetry was under investigation, only mass ratios between 1.25 and 1.65 could properly be used.

It is nevertheless important that the anisotropy values for mass ratios of 1.07 and 1.87 lie no lower than the anisotropy values for mass ratios between 1.25 and 1.65, as in the case of 14.9-Mev neutrons. What may to some extent account for the somewhat higher position of these points over the others is the fact that the distribution of pulses from fission fragments where the fission is at 0° must be somewhat wider than a distribution recorded at 90°, because of the effect of the motion of the center of mass. The anisotropy is constant for mass ratios between 1.25 and 1.65, which tends to indicate an accidental dependence of anisotropy on asymmetry such as was noted earlier in the case of fission induced by particles of medium energy. In order to determine the degree of anisotropy in the symmetric and very asymmetric regions, measurements with a better resolution are necessary.

Our investigation also resolved the question of a difference in distributions of directions in which light and heavy fragments are emitted. Previous

work[2,4,10] on fission by particles with energies not in excess of several tens of Mev has shown that there is no difference between the angular distributions for light and heavy fragments. In the work of Brolley et al.[11] on the fission of Np^{237} by 14.3 Mev neutrons it was found that the light and heavy fragments do not have identical distributions. However, the technique used in their experiment was incapable of ensuring a reliable solution of the problem.[4] We attempted to compare the directions in which light and heavy fragments were emitted from the fission of U^{238} induced by 3-Mev neutrons, since our experimental conditions permit us to distinguish a light fragment from a heavy fragment and to determine its direction of emission. The result was such that the number of emissions of a light fragment (relative to the total number of fissions) in the 0°, 90°, and 180° directions were 48 ± 3, 48.0 ± 2, and (49.8 ± 3)% respectively. It can be seen here that to within 3% the angular distribution of the light fragments is symmetrical with respect to 90° and does not differ from the distribution for heavy fragments.

Also included in our study was a comparison between the mean kinetic energy of both fragments that separated at an angle of 0° to the neutron beam and the kinetic energy of fragments that separated at 90° to the beam, for mass ratios between 1.3 and 1.6. The total kinetic energy of both kinds of fragments that separated at 0° proved to be on the average 0.9 ± 0.5 Mev greater than the energy of the fragments that separated at 90°.

In conclusion the authors wish to express their gratitude to Yu. A. Selitskii for preparing the uranium target.

[1] Fairhall, Halpern, and Winhold, Phys. Rev. 94, 733 (1954).

[2] Cohen, Ferrell-Bryan, Coombe, and Hullings, Phys. Rev. 98, 685 (1955).

[3] Cohen, Jones, McCormick, and Ferrell, Phys. Rev. 94, 625 (1954).

[4] A. N. Protopopov and V. P. Éismont, Atomnaya Énergiya 6, 644 (1959); Soviet Journal of Atomic Energy (Eng. Transl.) 6, 475 (1960).

[5] A. Bohr, First International Conference on the Peaceful Uses of Atomic Energy, Vol. 2, p. 175 (Russ. Ed.) (Geneva, 1955).

[6] V. M. Strutinskii, Atomnaya Énergiya 2, 508 (1957); Soviet Journal of Atomic Energy (Eng. Transl.) 2, 621 (1957).

[7] I. Halpern and V. M. Strutinskii, Second International Conference on the Peaceful Uses of Atomic Energy, Paper No. 1513 (Geneva, 1958).

[8] Yu. A. Selitskii, Atomnaya Énergiya 7, 554 (1959); Soviet Journal of Atomic Energy (Eng. Transl.) 7, 1019 (1961).

[9] S. Katcoff, Nucleonics 16, 78 (1958).

[10] R. B. Leachman and G. P. Ford, Nucl. Phys. 19, 366 (1960).

[11] Brolley, Dickinson, and Henkel, Phys. Rev. 99, 159 (1955).

Translated by A. Skumanich
174

INVESTIGATION OF HYPERNUCLEI PRODUCED BY 8.8-Bev PROTONS

V. A. TUMANYAN, M. G. SARINYAN, D. A. GALSTYAN, A. R. KANETSYAN, M. E. ARUSTAMOVA, and G. S. SARKISYAN

Physics Institute, Academy of Sciences, Armenian S.S.R.

Submitted to JETP editor April 17, 1961

J. Exptl. Theoret. Phys. (U.S.S.R.) **41**, 1007-1012 (October, 1961)

Hyperfragment production in nuclear emulsion by ~ 9-Bev protons was investigated. Fifty-four hyperfragment decays were detected. The hypernuclei B^{10}_{Λ}, C^{11}_{Λ}, C^{14}_{Λ}, C^{15}_{Λ}, and N^{14}_{Λ} were observed for the first time. ~ 30% of the observed events can be explained by the single-nucleon mechanism of Λ^0-hyperon interaction. Two decays with anomalously large energy release were observed.

1. EXPERIMENTAL PROCEDURE

THE production of hyperfragments was investigated in a 10×20 cm nuclear emulsion stack 400 μ thick bombarded in the 8.8-Bev internal proton beam of the proton synchrotron at the Joint Institute for Nuclear Research. The beam density was 2.7×10^5 protons/cm^2.

In scanning under 150x total magnification all "connected" stars within a single pellicle were registered. All definite instances of nuclear interaction, σ stars, and elastic scattering were subsequently eliminated. The remaining events satisfied the following criteria: 1) length of connecting track $\geq 20\,\mu$; 2) the existence of scattering at the end of the connecting track; 3) for $Z \geq 4$, thindown at the end of the connecting track.

In 72 cm^3 of emulsion 81 presumable decays of hyperfragments were found satisfying the given criteria. Six mesonic decays and 46 nonmesonic decays were distinguished by means of appropriate treatment and kinematic analysis.

Particle identification depended on previous calibration of the emulsion. The charge of particles having ranges under 1000 μ was determined with calibration curves relating track width d and dip (the d method). Measurements were performed on the tracks of 63 protons, 48 α particles from Be^8 decay and 29 α particles from Li^8 decay. For $Z \geq 4$ the charge was determined mainly on the basis of charge conservation, but also from the thin-down length l.

The mass of singly-charged particles was determined by Perkins' method,[1] for which integral calibration curves were plotted relating the gap count N to the residual range R [the N(R) method] for the tracks of π^+ mesons selected from $\pi^+ \rightarrow \mu^+$ decays. In some cases the mass was also determined from measurements of multiple scattering and range.

The Λ^0-hyperon binding energy in the hypernucleus was calculated from

$$B_\Lambda = M + M_{\Lambda^0} - \sum M_i - Q,$$

where M is the rest mass of the nucleus to which the Λ^0 was bound, M_{Λ^0} is the Λ^0 rest mass, 1115.06 ± 0.21 Mev,[2] M_i is the rest mass of emitted particles, and Q is the kinetic energy of all emitted particles. Nuclear masses were taken from [3].

The maximum error in B_Λ was determined from

$$\delta B_\Lambda = \delta_{exp+str} + \delta_{sp} + \delta Q_0 + \delta R_l,$$
$$\delta_{exp+str} = \sum (\delta^2_{i\,exp} + \delta^2_{i\,str})^{1/2}, \quad \delta Q_0 = \delta M + \delta M_{\Lambda^0} + \sum \delta M_l,$$

where $\delta_{i\,str}$ includes errors in range determination resulting from the Born approximation, and from microscopic distortion and inhomogeneity of the emulsion; $\delta_{i\,exp}$ represents errors of the MBI-9 microscope; $\delta_{sp} = 3 \times 10^{-4} Q$ is an error associated with the introduction of a correction for the stopping power of the NIKFI-R emulsion; $\delta R_i = 42 \times 10^{-4} Q'$ represents errors arising from the use of range-energy tables,[4] and Q′ is the total energy of emitted charged particles.

In all cases except when mesons decayed without emitting a neutral particle, the maximum error in determining B_Λ was of the same order as B_Λ. It can be assumed that normal errors will be smaller than the maximum errors; this is indicated by an estimate based on the distribution of binding energies for hyperfragments with close mass numbers.

Table I

No. of event	Length of connecting track, μ	Decay scheme	B_Λ, Mev
1	84	$He^4_\Lambda \to \pi^- + p + p + p + n$	0.02±1.59
2*	785	$He^4_\Lambda \to \pi^- + p + He^3$	1.79±0.94
			0.32±0.91
3**	114	$He^5_\Lambda \to \pi^- + p + He^4$	2.19±0.62
		$He^7_\Lambda \to \pi^- + p + He^6$	2.42±0.61
4	102	$Li^7_\Lambda \to p + d + t + n$	9.09
5	145	$Li^7_\Lambda \to p + d + t + n$	5.83±7.65
6	115	$Be^7_\Lambda \to p + Li^5 + n$	3.40±4.56
7	50	$Li^8_\Lambda \to p + He^6 + n$	10.08±9.72
8	84	$Li^8_\Lambda \to t + He^4 + n$	4.42±2.95
9	145	$Be^8_\Lambda \to d + d + He^3 + n$	6.36±4.83
10	176	$Li^8_\Lambda \to p + He^6 + n$	7.93±4.67
		$Be^8_\Lambda \to He^3 + He^4 + n$	9.50±4.57
		$Be^8_\Lambda \to He^4 + He^3 + n$	10.79±6.49
11	59	$Li^9_\Lambda \to d + He^6 + n$	11.29±6.13
12	61	$Be^9_\Lambda \to He^4 + He^4 + n$	5.49±5.06
13	166	$Be^{10}_\Lambda \to p + Li^8 + n$	3.06
14	23	$B^{10}_\Lambda \to p + d + t + He^3 + n$	$10.78^{+19.25}_{-4.67}$
		$B^{11}_\Lambda \to p + p + d + He^6 + n$	8.38±13.44
15	105	$C^{11}_\Lambda \to He^3 + He^4 + He^3 + n$	5.13±15.51
		$C^{11}_\Lambda \to He^4 + He^3 + He^3 + n$	12.49±14.94
		$C^{12}_\Lambda \to He^4 + He^4 + He^3 + n$	12.68±16.67
16	131	$C^{14}_\Lambda \to Li^6 + Li^7 + n$	12.24±10.80
17	215	$N^{14}_\Lambda \to p + C^{12} + n$	13.28±18.57
		$C^{15}_\Lambda \to d + B^{12} + n$	14.50±17.64

*The geometry did not permit an unambiguous determination of the pion range.

**The ground state of He^6 is always assumed.

We selected only values of B_Λ agreeing with the average of values given in the literature or with the expected values within the error limits for individual cases.

We note that nonmesonic decays were not regarded as possible π^0 decays of hyperfragments; the estimated number of the latter was ~ 3.

2. RESULTS

Our analysis classified all observed events as either clear or doubtful. Forty-two hyperfragment decays were clear; of these 6 were mesonic (including one instance of decay in flight), while the remainder were nonmesonic.

The binding energy B_Λ was determined in three mesonic decays, although the result was unambiguous in only one instance. B_Λ was determined in 14 nonmesonic decays, including 10 unambiguous values. Table I gives the values of B_Λ and the error limits.

We were apparently the first to observe the decay of certain heavy hyperfragments. Thindown and scattering at the end of each connecting track indicate definitely that these are hyperfragment decays. Confirmation is furnished by the reasonable values of B_Λ obtained from the kinematic analysis. Table II gives details for the decays of the newly discovered hypernuclei, which include B^{10}_Λ, C^{10}_Λ, C^{14}_Λ, C^{15}_Λ, and N^{14}_Λ. It must be noted that the existence of these hypernuclei, with the exception of C^{14}_Λ, is not absolutely certain. Events Nos. 14 and 15 could also be assigned to the previously discovered nuclei B^{11}_Λ and C^{12}_Λ, respectively.[5-7] Event No. 17 could involve either of the previously undiscovered hypernuclei N^{14}_Λ or C^{15}_Λ.

Table II

No. of event	Hyperfragment and its charged decay-products* a	b	c	Ranges, μ	Indentification method	Azimuth	Dip angle	B_Λ
14	B^{10}_Λ	B^{11}_Λ		23	*d*	0	+25°50′	$10.78^{+19.25}_{-4.67}$
	He^3	He^6		39	*d*	31°3′	—32°20′	8.38±13.44
	t	*p*		6.7	From charge conservation	30°	—32°20′	
	d	*d*		7523	*N* (*R*)	220°30′	+ 5°20′	
	p	*p*		10711	*N* (*R*)	56°30′	20°25′	
15	C^{11}_Λ	C^{11}_Λ	C^{12}_Λ	105	*l*, *d*	0	—47°5′	5.13±15.51
	He^3	He^4	He^4	51	*d*	267°24′	+46°	12.49±14.94
	He^4	He^3	He^4	149	*d*	32°54′	—25°30′	12.68±16.67
	He^3	He^3	He^3	521	*d*	27°24′	76°50′	
16	C^{14}_Λ			131	*l*, *d*	0	+29°30′	
	Li^7			42	*d*	97°	— 7°52′	12.24±10.80
	Li^6			6.4	From charge conservation	202°30′	—21°12′	
17	N^{14}_Λ	C^{15}_Λ		215	*l*, *d*	0	+24°10′	13.28±18.57
	p	*d*		558	*d*	30°12′	—16°20′	14.5±17.64
	C^{12}	B^{12}		5.5	From charge conservation	196°30′	—13°	
18**	C_Λ	N_Λ		234	*l*, *d*	0	+18°20′	—113±24
	p	*p*		1235	*N* (*R*)			
				2044	*n* (Δ*R*)	131°4′	— 4°10′	
	d	*d*		40968	*N* (*R*)	310°15′	+17°20′	
	Be	B		2.4	From charge conservation	335°39′	—63°47′	
19**	Li_Λ	Be		70	*l*, *d*	0	—15°20′	—63±9
	p	*d*		31664	*N* (*R*)	226°36′	—50°50′	
	He	Li		3049	*d*	32°39′	+66°50′	

*a, b, c — different interpretations of the same event.
**In events Nos. 18 and 19 the mass numbers of the hyperfragments could not be determined unambiguously.

We also observed decays of other rarely observed hyperfragments. For example, a second instance of Be^{10}_Λ decay was observed, which was reported for the first time by Silverstein.[8] The decay of Be^7_Λ was observed, although the presence of a previously undetected Li^5 nucleus among the decay products makes this case doubtful. The decay of He^7_Λ also deserves mention.

The absence of hyperfragments with Z = 1 is accounted for by the scanning procedure, whereby connected tracks within a single pellicle were registered.

Two nonmesonic decays with unusually high energy release were observed; in both instances the connecting track exhibited clear thindown and scattering. The best values of B_Λ obtained for these two events were -113 ± 24 and -63 ± 9 Mev, respectively. Table II gives the principal parameters of these events. The tracks were traced and measured by four observers for the purpose of eliminating errors.

In event No. 18 the range of the first particle was not determined unambiguously. At a distance of 1235 μ from the decay point, this particle probably experienced a nuclear interaction with small energy release, producing a star with a small number of prongs. Two possible residual ranges were therefore considered for this particle. In the first case it was assumed that the end of the track coincided accidentally with the center of the star and that the range was $R = 1235\,\mu$; in the second case it was assumed that the particle interacted in flight.

In order to determine the mass of this particle the measured gap density on the track was compared with the corresponding densities on the differential calibration curves for protons and pions [the $n(\Delta R)$ method]. The results were 1520 ± 243 and $1778 \pm 290\,m_e$, so that this particle may be considered a proton. On the basis of this assumption the residual range for the second case was found to be 2044 μ. The nuclear interaction energy computed from these data was ~ 12 Mev.

It is important to emphasize that the anomalous character of this decay is maintained in both cases.

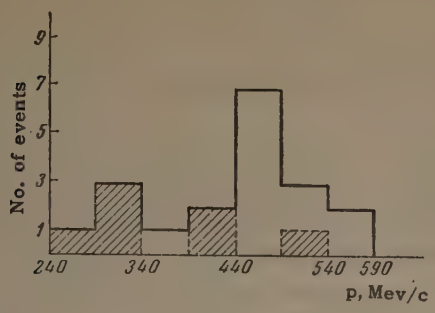

FIG. 1. Momentum spectrum of fast nucleons from nonmesonic decays of hyperfragments. Shaded rectangles – fast protons; unshaded rectangles – fast neutrons.

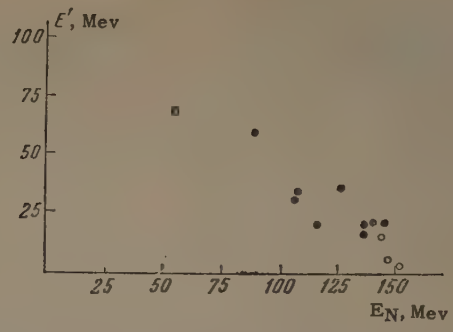

FIG. 2. Relationship between the total energy E_N of fast nucleons and the energy E' of all other particles in decays for which B_Λ was determined definitely. ● – neutron energy in the absence of a fast proton; ○ – combined proton and neutron energy.

3. DISCUSSION

All of the observed events involving new hyperfragments had been predicted on Iwao's shell model.[9] Since all hypernuclei known at present agree with Iwao's scheme, the shell-model theory of hypernuclei can be considered to agree satisfactorily with experiment. In the present work members of isotopic multiplets were observed, some for the first time. However, the appreciable errors incurred in determining B_Λ and the small number of events prevent any quantitative check of the consequences of charge independence.

In nonmesonic decays of hyperfragments the ratio of the numbers of decays induced by Λ^0 interactions with neutrons and protons respectively, $R = W_1(\Lambda^0 n \rightarrow nn)/W_2(\Lambda^0 p \rightarrow np)$, can furnish information[10] regarding the character of Λ^0-nucleon interactions. For direct hyperon-nucleon interactions $R \leq 1$, while for interactions through a virtual Σ state $R \geq 0.06$.

In Λ^0 decay induced by a Λ^0-proton interaction the proton acquires energy. Estimates taking into account the energy release in decay and the momentum distribution of nucleons and Λ^0 hyperons in the nucleus indicate that the lower limit of this acquired energy is ~ 30 Mev. The ratio R was computed for definite hyperfragment decays. Accordingly, we take the probability W_2 to equal the number of decays in which protons were emitted with energy above 30 Mev, while W_1 is the number of decays without a fast proton. Our result was $R = 2.43$. According to the results obtained by Ferrari and Fonda[10] this value of R corresponds to a Λ^0-nucleon interaction through a virtual Σ state with nonconservation of parity in the decay.

Figure 1 shows the momentum spectrum of fast nucleons emitted in nonmesonic decays. The momenta are given for all fast protons from definite decay events and for neutrons from events for which definite values of B_Λ were obtained. The higher range of neutron momenta compared with proton momenta agrees with Silverstein's results.[8] This difference in the energy ranges cannot be accounted for by the interaction of a Λ^0 with a single nucleon.

Approximately equal mean proton and neutron momenta are observed in decays where a fast proton is produced. Therefore the mechanism of interaction between a Λ^0 and a single nucleon can account for only about 30% of the observed events. When a Λ^0 interacts with a single nucleon the decay products should always include two fast nucleons, whereas in a considerable number of events in which B_Λ was determined definitely only a fast neutron was observed (Fig. 2). We must therefore assume either that in most cases chance values of B_Λ were obtained or that the single-nucleon process is an unsatisfactory hypothesis. An explanation can be sought in the possibility that a Λ^0 interacts with two or more nucleons or individual nuclei. It is evident from Fig. 2 that some events can be explained in this manner, although the energy distribution among the different decay products then remains unaccounted for.

The ratio of nonmesonic to mesonic decays of hyperfragments confirms spin $\frac{1}{2}$ for the Λ^0 hyperon.

Events involving anomalously high energy release cannot be accounted for easily in the conventional manner. An estimated ratio of ~ 0.2 is obtained for accidental passage of a connecting track through a secondary-star center. Some possibility therefore exists that the end fragment track will coincide accidentally with a star center.

If the possibility of chance coincidences is ignored the effect cannot be accounted for satisfactorily by assuming the existence of a Λ^0 hyperon in the nucleus. The existence of hypernuclei with other known hyperons is excluded because of the

possibility of strong interactions. The anomaly can then be accounted for by the existence of other strange particles allowed by the scheme of Gell-Mann and Nishijima. The existence of a hyperon with mass $\sim 3000\,m_e$ and strangeness +1 would then account for the large energy release in the aforementioned events.

The authors wish to thank Professor A. I. Alikhanyan for his interest, and Academician V. I. Veksler for supplying the emulsion stack irradiated at the Joint Institute for Nuclear Research. The authors are also indebted to L. G. Aĭrumyan, S. P. Rafaélyan, S. P. Papazyan, and A. O. Ovsepyan for measurements.

[1] D. H. Perkins, Nature **159**, 126 (1947).
[2] W. E. Slater, Nuovo cimento Suppl. **10**, 1 (1958).
[3] E. Segrè, editor, Experimental Nuclear Physics (John Wiley and Sons, Inc., New York, 1953), vol. I, p. 745.
[4] Fay, Gottstein, and Hain, Nuovo cimento Suppl. **11**, 236 (1954).
[5] Ammar, Levi Setti, Slater, Limentani, Schlein, and Steinberg, Nuovo cimento **15**, 181 (1960).
[6] Gorgé, Koch, Lindt, Nikolić, Subotić-Nikolić, and Winzeler, Nuclear Phys. **21**, 599 (1960).
[7] J. Sacton, Nuovo cimento **18**, 266 (1960).
[8] E. M. Silverstein, Nuovo cimento Suppl. **10**, 41 (1958).
[9] S. Iwao, Nuovo cimento **17**, 491 (1960).
[10] F. Ferrari and L. Fonda, Nuovo cimento **7**, 320 (1958).

Translated by I. Emin
175

(γ, n) *REACTION THRESHOLDS FOR SILICON ISOTOPES*

A. K. BERZIN and R. P. MESHCHERYAKOV

Institute for Nuclear Physics, Electronics, and Automation; Tomsk Institute of Technology

Submitted to JETP editor April 19, 1961

J. Exptl. Theoret. Phys. (U.S.S.R.) 41, 1013-1014 (October, 1961)

The thresholds of the (γ, n) reaction are determined for the three silicon isotopes Si^{28}, Si^{29}, and Si^{30}.

OWING to the large neutron binding energy of the most abundant of the silicone isotopes, Si^{28}, direct measurement of the yield of the (γ, n) reaction close to threshold is made difficult by the large neutron background. On the other hand the short half-life of Si^{27} (4.07 sec) and the low intensity of the present day circular accelerators lead to large statistical fluctuations in the obtained saturation activity. It is thus impossible to use the method of induced activity in the region of interest to us with the usual experimental setup in which the counting of the reaction products is performed after the irradiation of the sample (during a time interval of 10 to 12 $T_{1/2}$).

In order to obtain trustworthy data we performed the counting of the induced activity in between the pulses of the betatron. The advantages of this system were pointed out earlier.[1] The apparatus used for the measurements has been described by one of the authors.[2]

Since it is advantageous to prolong the counting time for the measurement of a 4.07-sec activity, the control system of the betatron was connected to the counting system. The channel duration of the 16-channel time analyzer was chosen to be 4096 μsec, which gives a repetition rate of 14 cps. In order to account for the background from short-lived activities [principally due to the (γ, n) reaction in the bismuth contained in the material used to shield the detector from the direct bremsstrahlung beam] the count in the first channels was made separately. The contribution of long-lived activities was determined by measuring the background after turning on the apparatus.

The decay products of Si^{27} were detected by a stilbene crystal and a photomultiplier. The smallness of the scintillator light flash produced upon incidence of the bremsstrahlung on the sample ensured very good reproducibility of the results, for in this case gain changes of the photomultiplier are negligible.[3]

The precision of the measurement at a sufficient distance from the threshold is limited by the accuracy of the reproducibility of the dose received by the sample. A calculation has shown that the possible fluctuations in the yield of the accelerator and the finite time constant of the dosimeter can lead to a relative error not exceeding $\pm 0.3\%$. The reliability of the data close to threshold is considerably smaller.

All measurements were performed with samples of natural isotopic composition. The thresholds for the (γ, n) reaction of the two other isotopes was determined by direct measurement. The betatron energy control system is basically the same as described earlier.[4] It contains a multivibrator with a response level of the order of millivolts. This leads to higher stability than obtainable with a dc amplifier. In order to compensate for slow drifts the control system was regularly checked. The following (γ, n) thresholds were used as energy calibration points: H^2 (2.226 ± 0.02 Mev), Bi^{209} (7.43 ± 0.05 Mev), Cu^{63} (10.826 ± 0.02 Mev), and also the kink in the photoneutron yield curve from oxygen at 17.27 ± 0.04 Mev.

The measurements were performed after the setup reached thermal equilibrium. The extrapolation to threshold was performed in the usual manner. The following values were obtained for the threshold energies:

$$Si^{28} = 17.14 \pm 0.12 \text{ Mev}, \quad Si^{29} = 8.47 \pm 0.07 \text{ Mev}, \quad Si^{30} = 10.618 \pm 0.07 \text{ Mev}.$$

These values agree well with values recently reported in the literature.[5]

[1] Ferrero, Malvano, and Tribuno, Nuovo cimento 2, 1135 (1955).

[2] Vlasov, Meshcheryakov, and Kislov, Proceedings of the Third All-University Accelerator Conference (in press).

[3] R. P. Meshcheryakov and G. P. Mikhaĭlov, Proceedings of the Ninth All-Union Conference on Nuclear Spectroscopy (in press).

[4] Berzin, Meshcheryakov, and Nemkov, Proc. Tomsk Inst. Technology 87, 219 (1957).

[5] V. A. Kravtsov, Usp. Fiz. Nauk 65, 451 (1958).

Translated by M. Danos
176

ELECTROSTATIC INSTABILITY OF AN INTENSE ELECTRON BEAM IN A PLASMA

M. V. NEZLIN

Submitted to JETP editor April 24, 1961

J. Exptl. Theoret. Phys. (U.S.S.R.) 41, 1015-1022 (October, 1961)

It is demonstrated that the current density in a quasi-neutral fast electrom beam propagating in a plasma has an upper limit above which the beam becomes unstable against formation of a virtual cathode. The mechanism of this instability is discussed.

THE experimental data reported earlier by Pierce [1] and recently by Volosov [2] show that if the current density j in a quasi-neutral electron beam propagating in vacuum exceeds a certain limit j_b, then small negative potential perturbations build up progressively with time in the beam. This results in the production of a virtual cathode, i.e., to the "blocking" of the beam by its own space charge. The limiting current j_b exceeds the maximum beam current without ions j_m by a factor of only 5 or 6, [1,2] i.e., cancellation of the space charge hardly contributes to an appreciable increase in the maximum beam current.

The purpose of the present investigation was to determine the stability of a quasi-neutral electron beam in a concentrated plasma, or, what is the same, the maximum stable current of an electron beam in a plasma.

1. EXPERIMENTAL PROCEDURE

The stability of the electron beam in the plasma was investigated with the apparatus shown schematically in Figs. 1 and 2. An intense beam of fast electrons and a concentrated highly-ionized "cold" plasma were produced in lithium vapor in a strong longitudinal magnetic field by a gas discharge with an incandescent tungsten cathode with direct current. After leaving the discharge chamber (15 cm long with diaphragms 1.2 cm in diameter) the fast electrons of the beam and the plasma particles propagated in a vacuum volume 12.5 cm in diameter and struck an anode which was usually at a distance L = 100 cm from the cathode. In this volume the pressure p of the residual gas was $(3-6) \times 10^{-6}$ mm Hg, the lithium-vapor pressure in the discharge chamber was on the order of 10^{-4} mm Hg, the discharge voltage V_d which determined the beam electron energy could be adjusted from several to 400 volts, the beam current I_d was 0.5—5 amp, and the magnetic field H could be varied from 400 to 2000 oe. The beam diameter was approximately 1 cm.

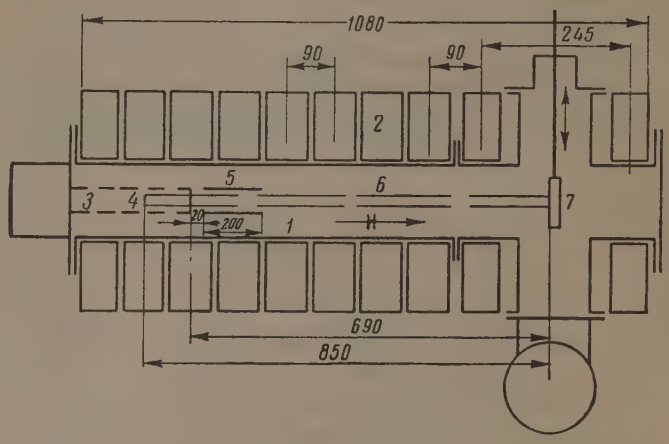

FIG. 1. Experimental apparatus: 1 – vacuum, 2 – solenoid, 3 – plasma source, 4 – cathode of source, 5 – filter, 6 – beam, 7 – anode. The dimensions are in millimeters.

The plasma concentration in the investigated volume was regulated either by changing the lithium vapor pressure and the discharge chamber (but not below the discharge ignition threshold) or by using a special filter. The filter consisted of two water-cooled copper plates cut to fit the beam; these plates surrounded the beam over a length of 20 cm and could be brought together or moved apart during the experiment without interfering with the beam. Since the plates "froze out" the vapor and some of the lithium ions emerging from the discharge chamber, the plasma concentration decreased along the filter.

The beam and plasma electron concentrations, n_{e_1} and n_{e_2}, were measured by a probe method, using the volt-ampere characteristic of a bulky collector situated behind a small hole (2 mm in diameter) drilled in the center of the anode. The ion branch of the probe characteristic (Figs. 3 and 4) was determined by the Bohm formula, [3] according to which

$$j_+ = 0{,}4n_+\sqrt{2T_e/m_+}, \qquad (1)$$

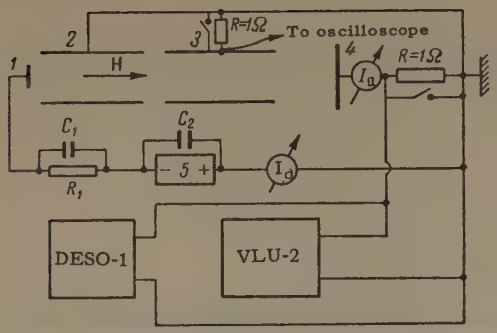

FIG. 2. Electric circuit of apparatus: 1 – cathode, 2 – discharge chamber, 3 – filter, 4 – anode, $C_1 = C_2 = 100\ \mu f$, $R_1 = 40$ ohm, 5 – discharge rectifier.

where j_+ is the ion current density in the probe (collector), n_+ the concentration of the ions in the plasma, m_+ their mass, and T_e the temperature of the plasma electrons. In our case

$$n_+ = n_{e1} + n_{e2}, \tag{2}$$

$$n_{e1} = j_{e1}/v_{e1}, \qquad n_{e2} = 4j_{e2}/v_{e2}, \tag{3}$$

and j_{e_1} and j_{e_2} are the current densities of the beam and of random plasma electrons. The value of j_{e_1} was assumed equal to the collector current density at zero collector potential (j_0).

We neglect here the plasma-electron current in the probe, i.e., we assume that in the expression

$$j_0 \approx j_{e1} + \frac{n_{e2} v_{e2}}{4} \exp\left(-\frac{e\varphi_a}{T_e}\right), \tag{4}$$

where φ_a is the potential of the plasma relative to the probe (anode)*; the second term in the right half can be neglected compared with the first. The validity of this assumption will be justified later on. Equations (1)–(4) were used to determine the relative plasma concentration ($\alpha = n_{e_2}/n_{e_1}$):

$$\alpha + 1 \approx 2.5 \sqrt{\frac{m_+}{m_e}\frac{eU}{T_e}}\ \frac{j_+}{j_{e1}} \approx \frac{1.6 \cdot 10^3 \sqrt{U}}{j_{e1}/j_+}, \tag{5}$$

where eU is the energy of the beam electrons (hundreds of ev) and $T_e = 3$ ev (the latter was obtained from probe measurements). We assumed U to equal the discharge voltage V_d.

2. EXPERIMENTAL DATA

In the first series of measurements we plotted the dependence of the time-averaged electron current in the anode, I_{av}, on the plasma concentration. In these measurements I_d (the time-averaged total beam electron current) served as the parameter for the family of functions $I_{av}(n_+)$.

*In the discharge considered here the plasma has a positive potential on the order of several times T_e/e relative to the anode.

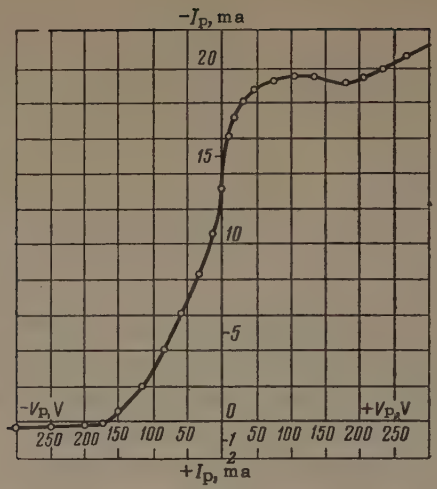

FIG. 3. Probe characteristic: $I_d = 1.2$ amp; $V_d = 120$ v, $I_{av} = 0.96$ amp; H = 1800 oe; L = 85 cm; $p = 5 \times 10^{-6}$ mm Hg.

We measured simultaneously the amplitude A of the oscillations in the beam passing through the plasma. A typical result (Fig. 5) shows that there are two qualitatively different modes of electron beam propagation in the plasma.

1. If the relative concentration of the plasma exceeds a certain "critical" value ($\alpha > \alpha_c$), the beam is stable in the plasma. All the electrons that leave the cathode pass freely through the plasma and reach the anode. The anode electron current I_a is practically independent of the time (i.e., it is equal to I_{av}) and exceeds somewhat the cathode electron current I_d, owing to the plasma-electron current.

2. When $\alpha < \alpha_c$, the beam is unstable in the plasma, as shown by the fact that the electron current in the anode oscillates intensely from practically zero to a maximum value somewhat greater than I_d.

The current oscillations in the unstable beam (Fig. 6) are made up of a relaxation component, with period $T \approx 10^{-4} - 10^{-3}$ sec, and a high-

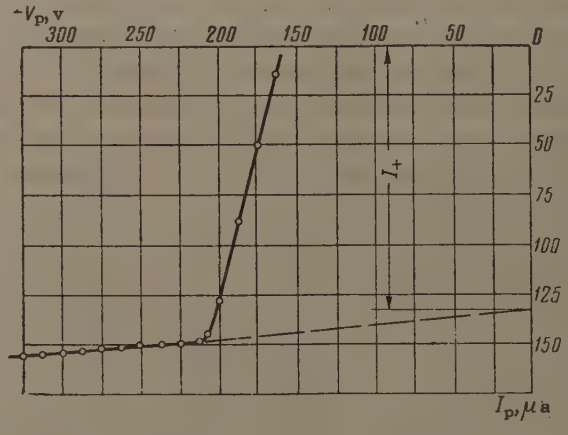

FIG. 4. Ion branch of probe characteristic under the conditions of Fig. 3.

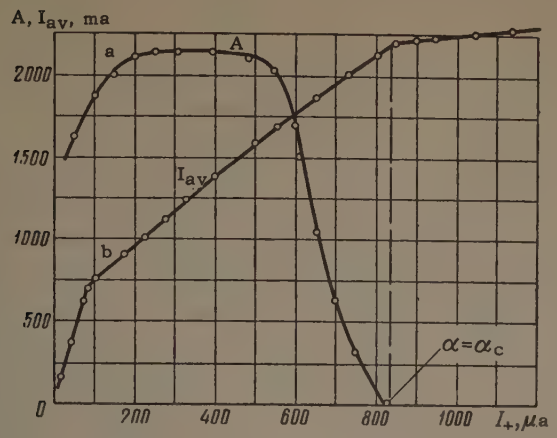

FIG. 5. Dependence of I_{av} and A on the concentration of the plasma. I_+ – ion current in probe collector; I_d = 2 amp; V_d, H, L, and p are the same as in Fig. 3.

frequency component with period $\tau \approx (1-3) \times 10^{-7}$ sec. The high-frequency oscillations (Fig. 7) occupy a portion T_1 of the period of the relaxation oscillations, and their amplitude is somewhat greater than I_d. This means that when $\alpha < \alpha_c$ (we refer here to time-averaged quantities) the beam passes freely through the plasma only during a time interval $T_2 = T - T_1$, while during the time interval T_1 it alternately passes through the plasma (with period τ) or is cut off. Consequently the average anode current I_{av} comprises only part of the total electron current, the remainder of this current (as shown by measurements and by Fig. 8) going to the discharge chamber (or to the filter, if used). With increasing α, the value of T_2/T increases, causing a corresponding increase in I_{av} (Fig. 5); when $\alpha = \alpha_c$ we have $T_2/T = 1$ and I_{av} practically reaches saturation (at a value somewhat greater than I_d).

3. MECHANISM OF INSTABILITY OF THE ELECTRON BEAM IN THE PLASMA

It must be emphasized that these current oscillations in the electron beam are not connected with

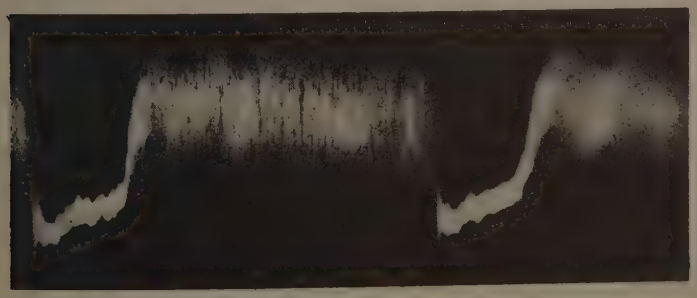

FIG. 6. Dependence of the anode current on the time. Upward deflection corresponds to an increase in the electron current. T = 500 μsec; τ = 0.15 μsec; peak-to-peak oscillation A = 2 amp; I_d = 1.8 amp; V_d = 180 v; I_{av} = 1 amp; H = 1800 oe; p = 4×10^{-6} mm Hg; L = 100 cm.

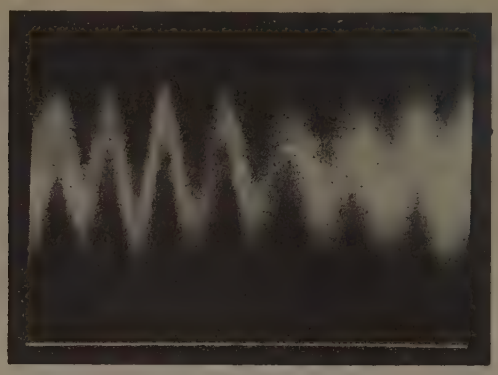

FIG. 7. Sweep of high-frequency oscillations of Fig. 6.

instability in the discharge arc. Such an instability arises, as is well known,[3] when the ratio of the cathode ion current to the cathode electron current does not satisfy the Langmuir relation

$$j_+ / j_{e1} \geqslant \sqrt{m_e / m_+}. \qquad (6)$$

In our experiments such an instability was produced artificially by decreasing V_d to 10 or 15 volts, and manifested itself in the fact that the discharge was alternately ignited and extinguished, with a period on the order of 200—500 μsec (Fig. 9); it is particularly important here that the oscillations of the anode and discharge-chamber current were in step with the oscillations of the total discharge current (no filter was used in this experiment). Unlike the oscillations due to such an instability of the discharge arc itself, the investigated oscillations in the anode and discharge-chamber currents (Fig. 8) are out of phase and are consequently of a different nature (there was likewise no filter in this experiment).

We note that all these phenomena looked qualitatively alike, regardless of whether a filter was used or not, and regardless of the length of the

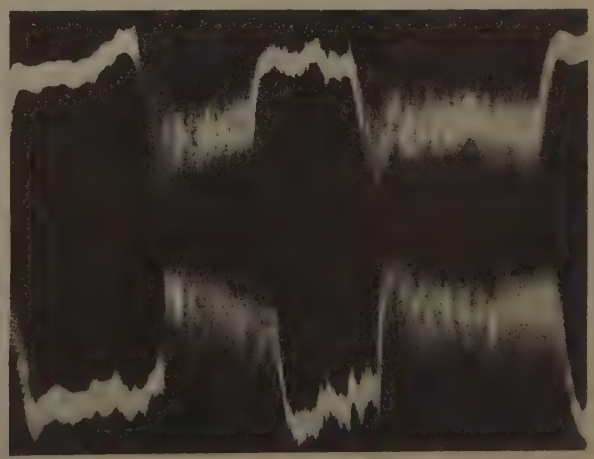

FIG. 8. Oscillograms of anode current (below) and discharge-chamber current (above) in a low-voltage discharge. I_d = 1 amp; V_d = 15 v; T = 300 μsec.

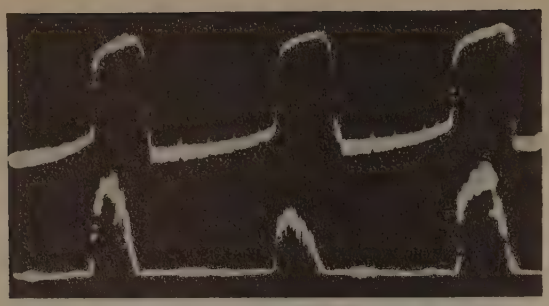

FIG. 9. Oscillations of anode current (top) and discharge-chamber current (bottom). Deflection upward corresponds to an increase in the electron current; T = 300 μsec; τ = 0.1 μsec; A = 2.1 amp; I_d = 2 amp; V_d = 200 v; I_{av} = 1 amp; H = 1800 oe; L = 100 cm; p = 3×10^{-6} mm Hg.

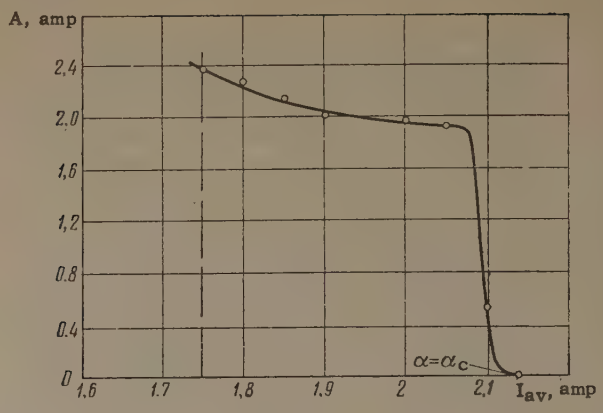

FIG. 10. Dependence of A on the concentration of the plasma at l = 2 cm, I_d = 2 amp, V_d = 120 v, H = 1800 oe.

plasma beam, particularly when the anode was at a distance l = 2 cm from the discharge chamber. The latter is illustrated in Fig. 10, where the measure of α is the quantity $\beta = I_{av}/I_d$ (I_{av} = 1.75 amp corresponds to the threshold of discharge ignition).

We thus arrive, on the basis of the data presented above, at the conclusion that the beam instability observed in the plasma when $\alpha < \alpha_c$ is connected with the alternate appearance and disappearance (with a period $\tau \approx 10^{-7}$ sec) of a virtual cathode in the beam. In these oscillations the vanishing of anode current does not signify extinction of the discharge, but that the electrons reflected from the virtual cathode "drop out" into the discharge chamber and the filter (Fig. 8). As to the coordinates of the virtual cathode, a special experiment, with a probe moving along the beam (on the edge of the beam) has shown that in a long beam the virtual cathode is produced between the discharge chamber and the anode (for example in the filter, if the filter plates are brought sufficiently close together).

Let us explain qualitatively why the oscillations have the appearance shown in Figs. 6 and 8. If the inequality $\alpha < \alpha_c$ obtains at some instant of time, the beam can pass through the plasma only during the time interval τ_0 when the negative potential perturbations do not have time to produce a virtual cathode in the beam. This time interval ($\sim 10^{-7}$ sec), as follows from Figs. 6 and 8, is of the same order as the transit time (τ_{e_1}) of a beam electron in the system. After formation of the virtual cathode, the "beam plus plasma" system, deprived of the potential barrier which confines the plasma electrons, is likewise not stationary. The duration τ_{co} of the cut-off state of the beam will be equal to the time in which the plasma electrons remove from the system a corresponding excess of negative charge, after which the beam is again resumed, etc. This can explain why the virtual cathode pulsates in time (Figs. 6—8).

During these oscillations the plasma electrons apparently "heat up" and begin to ionize the lithium vapor more effectively. If at the same time the plasma concentration increases to the critical value α_c, the oscillations will stop and the plasma electrons will begin to "cool down." Then the plasma concentration, after reaching a certain limit, will again decrease and when $\alpha < \alpha_c$ the oscillations resume and eventually increase the concentration of the plasma to a level $\alpha > \alpha_c$, etc. In our opinion this is precisely why the high-frequency oscillations are modulated by the relaxation oscillations, and why the latter have "platforms" corresponding to the stable state of the beam (the part T_2 of the oscillation period T in Figs. 6 and 8). It is easy to see that the less the time average of α differs from α_c, the greater should be the ratio T_2/T and the average current through the plasma (I_{av}). As already noted, this is indeed observed in the experiments (Fig. 5). If $\alpha \ll \alpha_c$, then the "platforms" of Figs. 6 and 8 should disappear, in spite of the additional ionization of the lithium by the plasma electrons. This phenomenon also takes place when $\beta < 0.2$—0.3.

4. LIMITING STABLE CURRENT OF ELECTRON BEAM IN A PLASMA

Thus, as the electron beam passes through the plasma, there is an upper limit to the current density, beyond which the beam becomes unstable with respect to formation of a virtual cathode. The limiting stable (or critical) beam current density j_c has been shown by the measurements to be proportional to the plasma concentration and to be determined by the relation

$$j_c \approx 0.7\, j_{e2} \approx n_{e2}\, v_{e2} / 6. \qquad (7)$$

Thus, for example, the values of I_c are 1.05, 2, and 4 amp for $n_{e_2} = 2.4$, 5, and 1.5×10^{12} cm^{-3}, etc. (These data pertain to $V_d = 120$ v). Here

$$\alpha_c \approx 6 v_{e1} / v_{e2} \approx 30 - 40. \quad (8)$$

From relations (8), (6), and (1) it follows that α_c is approximately double the relative plasma concentration corresponding to the discharge ignition threshold. Consequently a discharge with a stable arc can be unstable with respect to formation of a virtual cathode (as follows from Fig. 10).

It is easy to see that the presence of a concentrated plasma ($\alpha \approx 30$—40) increases by many times the limiting current and the stable electron beam. In fact, in the absence of plasma ($\alpha = 0$) the limiting current in our case ($V_d = 120$ v, beam diameter 1 cm, diameter of vacuum volume 12 cm) would be [1,2]

$$j_b \approx 30 \text{ ma cm}^{-2} \approx 10^{-2} j_c. \quad (9)$$

In other words, the plasma exerts an appreciable stabilizing action on an electron beam propagating through it. This action is obviously connected with the fact that when a perturbation of potential occurs in the beam, a sufficient number of plasma electrons leave the system under the influence of the resultant electric field, and the development of the perturbation is slowed down, ceasing completely when $\alpha > \alpha_c$.

We can make the following suggestions concerning the mechanism of this additional departure of the plasma electrons. This beam instability, as already noted, develops in a time on the order of the transit time τ_{e_1} of the beam electrons. Within this time the plasma electrons do not have a chance to "drop out" of the beam along the magnetic field, since their velocities are much lower than the velocities of the beam electrons. Thus, there is apparently no time for the longitudinal drift of plasma electrons to come into play, and the principal factor stabilizing the system is the transverse (perpendicular to H) drift of the plasma electrons.

The following data favor this conclusion. First, when $\alpha < \alpha_c$ the flow of beam electrons transverse to the discharge chamber is approximately equal to the total electron current from the cathode (Fig. 8) i.e., it amounts to two or three amperes, which is easily verified to be several orders of magnitude greater than the transverse flow of these electrons due to collision with ions and atoms. Second, measurement with a probe located 40 mm away from the beam axis have shown that when $\alpha < \alpha_c$ the plasma electron and ion currents in the probe increase by several times, in spite of the considerable decrease (by several times) of the current in the beam passing through the plasma (the half-width of the beam also increases appreciably). In other words, when $\alpha < \alpha_c$ a very effective ("anomalous") transverse diffusion of electrons is produced in the plasma beam.

Third, experiments have shown that the beam stability depends strongly on the intensity of the magnetic field. It turns out that when α is neither too small nor too large the beam is stable only within a definite range of H, for example from 800 to 1400 oe (this range is greatly extended on both sides as α increases, and its upper limit goes beyond 2000 oe). Fourth, as already noted, in a long beam the virtual cathode is formed between the discharge chamber and the anode. This means that different parts of the beam (having different longitudinal coordinates) are not equally stable against the formation of the virtual cathode. The greatest stability is possessed by the discharge-chamber region. This can be attributed to the greater effectiveness of the transverse motion of the plasma electrons in this region, owing to the increased concentration of the plasma and to the proximity of the walls.

To find a general quantitative criterion of the above instability of a beam in a plasma, and to explain its origin, additional research must be carried out. The same holds for the explanation of the role of the boundary conditions. In the present investigation the "beam plus plasma" system was open and was bounded by electrodes, one of which was the source of the electron beam and the other the receiver. The question whether a similar instability can arise in a closed system, say in a torus, still remains unanswered.

The author is deeply grateful to G. I. Budker, at whose initiative the present work was carried out, for useful advice; to A. M. Solntsev for very effective help with the work, and to A. V. Zharinov, M. S. Ioffe, B. B. Kadomtsev, and A. A. Vedenov for valuable discussions and advice.

[1] J. R. Pierce, Theory and Design of Electron Beams, (Russian translation), Soviet Radio Press, 1956, p. 165. [Van Nostrand, 1949].

[2] V. I. Volosov, J. Tech. Phys. (U.S.S.R.), in press.

[3] D. Bohm, The Characteristics of Electrical Discharges in Magnetic Fields, N.Y. 1949.

Translated by J. G. Adashko
177

THE $Ne^{21}(n, \alpha)O^{18}$ *REACTION ON SLOW NEUTRONS*

A. I. ABRAMOV and M. G. YUTKIN

Submitted to JETP editor April 25, 1961

J. Exptl. Theoret. Phys. (U.S.S.R.) **41**, 1023-1024 (October, 1961)

The nuclear reaction $Ne^{21}(n, \alpha)O^{18}$ has been detected in a neon-filled ionization chamber irradiated by thermal neutrons. The energy and effective cross section of the reaction have been measured.

CALCULATION based on the nuclear masses shows that neutrons can produce in neon isotopes only one exothermal reaction with emission of charged particles, namely $Ne^{21}(n, \alpha)O^{18}$ (the atomic masses used in the calculations were taken from the tables of [1,2]).

To observe this reaction we placed a spherical ionization chamber,[3] filled with pure neon to a pressure of 10 atm, in a beam of slow neutrons from the thermal column of the BR-5 reactor. A continuous discriminator was used to plot a blanking curve, differentiation of which yielded a pulse spectrum in the form of a peak with a "tail" stretching to the left. The reaction energy $Q = 0.696 \pm 0.019$ Mev, obtained from the peak position, coincides within the limits of experimental accuracy with the calculated value $Q = 0.704$ Mev.[4] No pulses of comparable amplitude were observed in control measurements with an argon filled chamber. This circumstance confirmed indirectly that the pulses registered in the main experiment were to due to the neon itself. The high cadmium ratio (> 100) measured with the neon-filled chamber indicates that the reaction noted is induced by thermal neutrons.

The effective cross section of the $Ne^{21}(n, \alpha)O^{18}$ reaction on thermal neutrons was measured by comparing it with the cross section of the $He^3(n, p)H^3$ reaction. For this purpose, two identical chambers, one with neon and the other with He^3, were placed successively at the same point in space and the ratio of the counting rates from the chambers was then determined. Since the helium chamber counted too many pulses per second in the direct neutron beam, all the measurements were made with scattered neutrons several meters away from the open damper of the thermal column. The ratio of the counting rates was found to be 13090 ± 208. Knowing the content of He^3 in the working mixture and of Ne^{21} in natural neon (0.257%), we could readily determine the cross section ratio: $\sigma_{Ne^{21}}/\sigma_{He^3} = 0.0177 \pm 0.0059$. The uncertainty in the result indicated here is the total experimental error, which reflects, in particular, the difference in the shape of the pulse spectra obtained from different chambers. Assuming now the cross section of the (n, p) reaction on He^3 for thermal neutrons to be 5400 ± 200 b,[5] we obtain finally $\sigma[Ne^{21}(n, \alpha)O^{18}] = 96 \pm 33$ b. The use of the value $\sigma_{He^3} = 5400$ b, obtained for a neutron velocity 2200 m/sec, is fully justified in this case, for it was established in physical tests on the BR-5 reactor that the spectrum of the neutrons leaving its thermal column is quite close to Maxwellian.

We note that the $Ne^{21}(n, \alpha)O^{18}$ reaction can be used for the spectrometry of fast neutrons along with the $He^3(n, p)H^3$ reaction. If the first of these reactions is used, pulses from the recoil nuclei will not interfere with the measurements up to a neutron energy ~ 4 Mev.

[1] B. S. Dzhelepov and L. K. Peker, Skhemy raspada radioaktyvnykh yader (Decay Schemes of Radioactive Nuclei), AN SSSR, 1958.

[2] Everling, Konig, and Mattauch, Nucl. Phys. **18**, 529 (1960).

[3] A. I. Abramov, PTÉ (Instrum. and Meas. Techn.) **4**, 56 (1958).

[4] Bell, Bonner, and Gabbard, Nucl. Phys. **14**, 270 (1959).

[5] D. Hughes and R. B. Schwartz, Neutron Cross Sections, New York, 1958.

Translated by J. G. Adashko
178

ELASTIC SCATTERING OF 2.8 Bev/c PIONS ON NEUTRONS

Yu. D. BAYUKOV, G. A. LEKSIN, and Ya. Ya. SHALAMOV

Institute of Theoretical and Experimental Physics, Academy of Sciences, U.S.S.R.

Submitted to JETP editor April 28, 1961

J. Exptl. Theoret. Phys. (U.S.S.R.) **41**, 1025-1030 (October, 1961)

The differential cross sections for 2.8-Bev π^-n scattering are determined for c.m.s. angles from 10 to 180°. The probability for nondiffractional scattering of π^- mesons is found to be small and to drop sharply with increasing incident meson energy.

INTRODUCTION

THERE is now much experimental material[1-8] on the elastic scattering of pions in πN collisions at energies above 1 Bev. These data deal mostly with scattering in the region of the first diffraction maximum. Appreciable interest is attached, however, to scattering of pions by nucleons at larger angles, called arbitrarily non-diffraction scattering. We have obtained earlier[9] certain information on the cross section for the elastic scattering of negative 2.8-Bev/c pions by neutrons at 140—180° in the c.m.s. In the present work the measurements have been continued to determine the differential cross section of elastic π^-n scattering at all angles outside the diffraction-scattering region.

There is only one published paper[1] devoted to a study of π^+p scattering (which is isotopically symmetrical to π^-n scattering) at 1.8 Bev in the entire angle interval. However, if it is assumed that in this energy range the character of scattering of positive and negative pions by nucleons is the same, the results of the present investigation can be compared with the results of [2-5] which deal with non-diffraction elastic π^-p scattering. In particular, a study was made[2,3] of the angular distribution for elastic scattering of 1.2- and 1.3-Bev negative pions in the c.m.s. angle interval up to 180°. Approximately 100—200 cases each of elastic scattering outside the diffraction region were registered. For 5-Bev negative-pion energies, seven[4] and two[5] cases of non-diffraction elastic scattering were found. In [2] a comparison was made of the angular distributions for elastic π^-p scattering at energies 0.97 Bev,[10] 1.2 Bev,[2] and 1.3 Bev.[3] The differential backward scattering cross section curves for 1.2 and 1.3 Bev do not differ from each other, within the limits of experimental error, but lie somewhat lower than the corresponding curve for π^-p scattering at 970 Mev. The authors call attention to this tendency. The presence of non-diffraction scattering at 1.3 Bev is emphasized in [5], where it is indicated that it apparently interferes with the diffraction scattering. Not much attention has been paid to non-diffraction scattering at high energies, nor have any deductions been drawn concerning its character and its variation with energy.

EXPERIMENTAL SETUP

To study elastic π^-n scattering we scanned approximately 5000 stereo pairs, obtained with a 17-liter freon bubble chamber[11] 50 cm long. The negative-pion beam had a momentum 2.8 ± 0.3 Bev/c. The bubble chamber was operated without a magnetic field. The freon working mixture (CF_3Cl and CF_2Cl_2) contains light nuclei and has at the same time a sufficiently high specific gravity (1.12 g/cm^3) and low conversion length (30 cm); the latter is particularly important, since the main source of the background was a process involving the creation of neutral pions, which were effectively registered in the chamber via the decay γ quanta.

In scanning the stereo pairs we selected the single-prong stars. These were assumed to occur upon interaction between the negative pions and the quasi-free neutrons of the nuclei contained in the freon. Additional selection criteria, taking the kinematics of elastic π^-n scattering into account, were the conditions that a) the scattered particle must not stop in the chamber substance, b) the ionization of the scattered particle must not differ by more than a factor of three from the ionization of the primary particle, and c) the track of the scattered particle must not have a deflection greater than three bubbles (~ 2 mm), and consequently the angle of multiple scattering of

the particle should be less than that for 200-Mev/c pions.

The film was scanned by two observers independently. The efficiency of detecting a single-prong star with secondary-particle emission angle > 15° in the laboratory system of coordinates (l.s.) is close to unity. Information on the scattering in the ~ 5—15° range in the l.s. were obtained after an additional thorough examination of approximately one tenth of the entire material. This is necessary because, on the one hand, scattering at small angles is frequently encountered, and on the other, it is more difficult to search for such scattering on the film than for scattering at larger angles. Scattering at angles < 5° in the l.s. was not investigated, for in this range of angles scattering on the nucleus as a whole begins to compete with scattering on the quasi-free nucleons.

The distribution of selected single-prong stars by the secondary-particle l.s. emission angles is shown by the smooth curve of Fig. 1. The dashed curve on the same figure shows the angular distribution of those single-prong stars, from among the total number selected, which were accompanied by 1, 2, or 3 electron-positron pairs directed toward the interaction point. These events were due to the reaction

$$\pi^- + n \to \pi^- + n + m\pi^0, \qquad (1)$$

where m = 1, 2, ... is the number of mesons produced in the given process. This distribution includes five single-prong stars connected with creation of strange particles: one Λ^0 (or Σ^0) and four K^0 mesons. In two cases the creation of the K^0 meson was accompanied by emission of pions, since electron-positron pairs due to conversion of the γ quanta from the neutral pion decay were registered. It is natural to assume that the Λ^0 and K^0 particles were created in interactions of the type

$$\pi^- + n \to \pi^- + \Lambda^0 (\Sigma^0) + K^0 + m\pi^0, \qquad (2)$$

$$\pi^- + n \to K^- + K^0 + n + m\pi^0, \qquad (3)$$

$$\pi^- + n \to \pi^- + n + K^0 + \overline{K}^0 + m\pi^0, \qquad (4)$$

where m = 0, 1, 2 ....

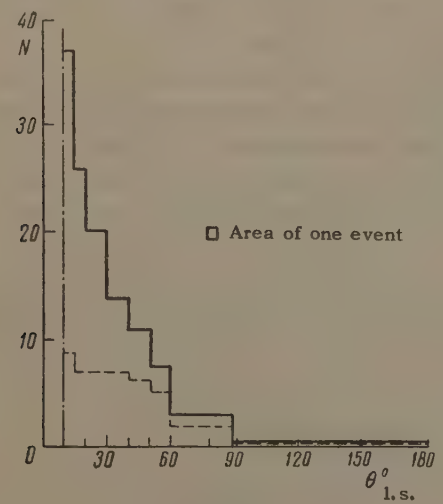

FIG. 1

We note that seven single-prong stars were registered in the interval of negative-pion emission angles from 90 to 180° in the l.s. Five of these were accompanied by electron-positron pairs or a K^0 meson. This fact is in good agreement with the result of the preceding investigation.[9]

SUBTRACTION OF BACKGROUND

The reactions (1)—(4) are background reactions relative to the investigated process, and the single-prong stars due to these reactions must be eliminated from the total number of selected cases. There exists a finite probability of not registering a π^0, K^0, or Λ^0 particle. The registration efficiencies of the neutral particles must therefore be taken into account in the subtraction of the background.

Let us consider reaction (1). It is first necessary to estimate the efficiency of registration of the γ quanta from the neutral-pion decay. For each γ quantum producing a pair directed toward the selected single-prong star we measured the distance L along the direction of motion of the γ quantum, from the point of interaction to the boundaries of that region of the chamber in which the conversion pair could still be registered in the scanning. This distance, for a known conversion length L_K = 30 cm, enables us to determine by means of the formula $\epsilon = 1 - \exp(-L/L_K)$ the efficiency ϵ of registering a γ quantum emitted from a given point in a given direction. The average efficiency of registration of the γ quantum from reaction (1) was calculated from the formula $\bar{\epsilon} = n/\Sigma \epsilon_i^{-1}$, where n is the number of registered electron-positron pairs.

Within the limits of statistical errors, the average efficiency of registering the γ quanta remains the same for neutral-pion emission in different angular ranges. This enabled us to calculate the average γ-quantum registration efficiency for the entire chamber, independently of the angle of emission of the neutral pion. The average registration efficiency of the γ quantum produced by reaction (1) is 0.33 ± 0.03.

To determine the number of single-prong stars due to reaction (1), but not accompanied by conversion pairs, we must know the multiplicity of forma-

Angle interval	N_1	N_2	N_3	N	N^*	N_0
0—30°	30	13	0	56	43	29±4
30—60°	24	8	3	49	35	20±3
60—180°	8	6	2	26	16	5±3

tion of neutral pions. The table lists the following data for three negative-pion emission angle intervals: N^* —number of single-prong stars with electron-positron pairs directed towards the interaction point, N_1, N_2, and N_3 —numbers of single-prong stars with 1, 2, and 3 electron-positron pairs, respectively, N —total number of registered γ quanta from reaction (1).

A change in the multiplicity of creation of the neutral pions in reaction (1) influences the sought number of single-prong stars unaccompanied by electron-positron pairs in the chamber (N_0), as well as the ratios N_1/N^*, N_2/N^*, N_3/N^*, and N/N^*. Starting from these experimentally-determined ratios, and assuming that the registration efficiency of the γ quanta is 0.33, we calculated N_0. The resultant values of N_0 are listed in the last column of the table.

The efficiency of registration of reactions (2)—(4) was estimated starting from the following considerations: a) the K^0 and $\bar{K}^0$ mesons behave in half the cases like long-lived K_2^0 mesons and leave the chamber; b) in one-third of the cases the K_1^0 meson decays into two neutral pions, and such cases were not registered in the chamber; c) there is a finite probability that the K_1^0 meson will leave the chamber; d) the Λ^0 particle can decay into a neutral pion and neutron and may thus not be registered; e) the Λ^0 particle can leave the chamber; f) in reactions (2) and (4), the neutral strange particles should be taken into account twice; g) some part of the reactions (2)—(4) are accompanied by the creation of neutral pions, which can be registered in the chamber and accounted for together with reactions (1). The calculated value of the registration efficiency of a single-prong star connected with the observed creation of strange particles in reactions (2)—(4) is approximately 0.4. The error in this quantity is of little significance, since the number of registered events due to reactions (2)—(4) is small.

DISCUSSION OF THE RESULTS

It is assumed that all the single-prong stars remaining after subtracting the background, i.e., not due to reactions (1)—(4), are cases of quasi-elastic π^-n scattering on quasi-free neutrons of the nuclei. In quasi-elastic π^-n scattering, half of the neutrons in each nucleus of the freon mixture effectively participates on the average in the quasi-elastic π^-n scattering. The other half of the neutrons is screened by the remaining nucleons of the nucleus, since the secondary particles produced in the elastic π^-n scattering, initiate a nuclear cascade, which results in stars having > 1 prong. The value of the screening coefficient n = 0.5 was discussed earlier.[9]

The angular distribution of elastic π^-n scattering referred to a single free neutron is shown in Fig. 2. The abscissas show the cosines of the angles and the negative-pion emission angles themselves in the c.m.s. of the negative pion and the nucleon. The ordinates represent the differential cross sections of the elastic π^-n scattering. The left-hand scale pertains to angles < 38° in the c.m.s. and the right-hand scale, which has been changed by a factor of one hundred, pertains to scattering angles > 38°. The errors indicated on the figure are statistical. Error bars parallel to the abscissa axis indicate the width of the angle interval over which the average was taken.

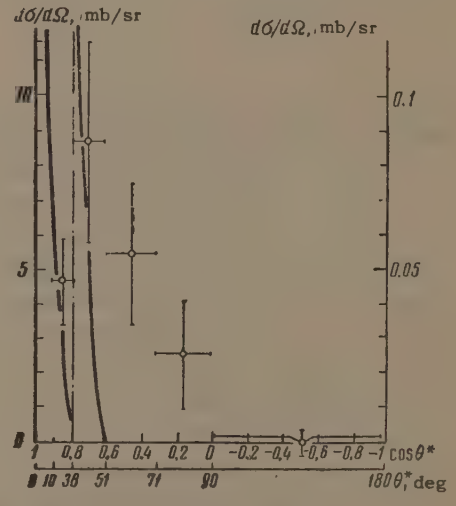

FIG. 2

The continuous curve in Fig. 2 shows the calculated angular distribution of the diffraction scattering of 2.8-Bev/c pions. The calculations were based on the formulas of the optical model, which are customarily used in this case,[12] under the assumption that the nucleon is a sphere with sharp boundary and constant refractive index. The parameters of the optical model were taken from [6], namely: the change in the real part of the wave number K_1 is zero, the coefficient of absorption of the nucleon is $K = 0.71 \times 10^{-13}$ cm^{-1}, and the radius of the sphere is $R = 1.05 \times 10^{-13}$ cm. These parameters agree with all the known experimental data on elastic πN scattering.[1-8] It is seen from

Fig. 2 that the points corresponding to 50° scattering in the c.m.s. lie on the calculated curve, i.e., it can be assumed that the results obtained in the present investigation in the region of diffraction πN scattering do not contradict the aggregate of presently known results.

From the data obtained in this investigation we can conclude that, accurate to 0.006 mb/sr, there is no elastic π^-n scattering in the range 90—180° (c.m.s.). This confirms the previous [9] deduction concerning compensation of diagrams with one virtual nucleon (Fig. 3) at high energies in π^-n scattering, while the data on the wider angle range confirm the conclusion that the contributions of different phase shifts with small orbital momenta cancel each other in c.m.s. backward scattering, or else that these phase shifts themselves are small.

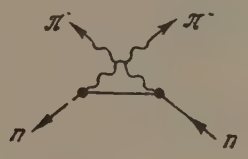

Рис. 3

It is seen from Fig. 2 that elastic π^-n scattering is observed at 50—90° in the c.m.s. Strictly speaking, we cannot exclude the possibility of fitting this part of the scattering in the framework of the optical model by suitable choice of the parameters and by increasing their number (for example, by taking account of the diffuse boundary of the nucleon). At the present statistical accuracy of the experimental material, however, such a description is meaningless.

It is interesting to compare the results obtained with the corresponding results from [1-5]. One can hope that the conclusion concerning the compensation of the diagram of Fig. 3 makes a comparison of π^-n scattering with π^-p scattering valid. Otherwise the scattering of negative pions by neutrons and protons at c.m.s. angles $> 90°$ would be different, since the diagram of Fig. 3, which yields backward scattering at high energies, does not hold for π^-p scattering, owing to the charge-conservation law.

The known data on potential, non-diffraction scattering of pions by nucleons are compared in Fig. 4, where the abscissas represent the c.m.s. momentum p* transferred in the scattering and the ordinates are the differential cross sections in terms of the square of the pion wavelengths in the c.m.s. The data of [1,3] have been averaged over the intervals designated by the horizontal

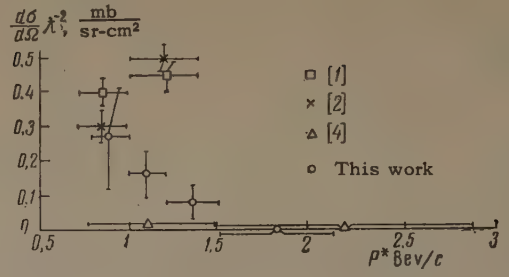

FIG. 4

error bars in the figure. The data of Thomas [4] are given for the seven cases he has noted outside the region of diffraction scattering, with notice of the fact that not a single case of elastic scattering was registered at 90—180° c.m.s. The error shown in the figure for this region corresponds to a single case. As can be seen from the foregoing results, subject to the accuracy indicated in the figure, the nucleon does not acquire a c.m.s. momentum greater than 1.5 Bev in elastic πN scattering, and the probability of acquiring a momentum 1—1.5 Bev decreases with increasing energy of the incoming meson.

The character of scattering at high energies is such that in elastic pp scattering the maximum c.m.s. momentum transfer is 1.6 Bev/c, accurate to 0.01 mb/sr. Such a transfer was registered in the scattering of 4.4-Bev protons in [13]. With increasing energy of incoming protons the probability of transferring a momentum ≥ 1 Bev/c decreases. [13-16] It is interesting to note (see [17]) that the Λ^0 particles produced in the interaction between 2.8-Bev/c negative pions and nucleons also have in the laboratory system a maximum momentum of 1.6 Bev/c.

The authors are deeply grateful to I. Ya. Pomeranchuk, who called our attention to this problem, for numerous discussions during the work. We are grateful to Academician A. A. Alikhanov and M. S. Kozodaev for interest in the work and for useful discussions of the results obtained, to Yu. S. Krestnikov and V. A. Shebanov who graciously supplied the film obtained with the chamber, and also to N. S. Khropov and M. U. Chudakova for help in the measurements.

[1] L. O. Roeling and D. A. Glaser, Phys. Rev. **116**, 1001 (1959).

[2] Bertanza, Carrara, Drago, Franzini, Mannelli, Silvestrini, and Stoker, Nuovo cimento **19**, 467 (1961).

[3] Chretien, Leitner, Samios, Schwartz, and Steinberger, Phys. Rev. **108**, 383 (1957).

[4] R. G. Thomas, Phys. Rev. **120**, 1015 (1960).

[5] Maenchen, Fowler, Powell, and Wright, Phys. Rev. **108**, 850 (1957).

[6] Wang, Wang, Ting, Ivanov, Katyshev, Kladnitskaya, Kulyukina, Nguyen Din Ty, Nikitin, Otvinovskii, Solov'ev, Sosnovskii, and Shafranov, JETP **38**, 426 (1960), Soviet Phys. JETP **11**, 313 (1960).

[7] Eisberg, Fowler, Lea, Shephard, Shutt, Thorndike, and Whittemore, Phys. Rev. **97**, 797 (1955).

[8] W. D. Walker, Phys. Rev. **108**, 872 (1957).

[9] Bayukov, Leksin, Suchkov, Shalamov, and Shebanov, JETP **41**, 52 (1961), Soviet Phys. JETP **14**, 40 (1962).

[10] A. R. Ezwin and J. K. Kopp, Phys. Rev. **109**, 1364 (1958).

[11] Blinov, Lomanov, Meshkovskii, Shalamov, and Shebanov, PTÉ (Instrum. and Meas. Techn.) **1**, 35 (1958).

[12] Ferback, Serber, and Taylor, Phys. Rev. **75**, 1352 (1948).

[13] Cork, Wentzel, and Causey, Phys. Rev. **107**, 859 (1957).

[14] Lyubimov, Markov, Tsyganov, Cheng, and Shafranova, JETP **37**, 910 (1959), Soviet Phys. JETP **10**, 651 (1960).

[15] Bogachev, Bunyatov, Merekhov, and Sidorov, DAN SSSR **121**, 617 (1958), Soviet Phys.-Doklady **3**, 785 (1959).

[16] Kalbach, Lord, and Tsao, Phys. Rev. **113**, 330 (1959).

[17] Shalamov, Shebanov, and Grashin, JETP **40**, 1302 (1961), Soviet Phys. JETP **13**, 917 (1961).

Translated by J. G. Adashko
179

SPECTRUM OF ELECTRONS EMITTED IN THE DECAY OF NEGATIVE MUONS IN NUCLEAR EMULSION

A. O. VAĬSENBERG, E. A. PESOTSKAYA, and V. A. SMIRNIT-SKII

Submitted to JETP editor April 28, 1961

J. Exptl. Theoret. Phys. (U.S.S.R.) 41, 1031-1036 (October, 1961)

The spectra of electrons produced in the decay of μ^- mesons in light (C, N, O) and heavy (Ag, Br) mesic atoms in a nuclear emulsion have been measured. In the first case, the spectrum is identical with the positron spectrum in the μ^+-e decay. In the second case, the spectrum shape seems to be softer. The spectrum of Auger electrons accompanying the μ^--e decay has been obtained. The probability of Auger electron production in light mesic atoms is shown to agree with the theoretical prediction.

1. INTRODUCTION

THE purpose of the present experiment is to compare the spectrum of the electrons produced in μ^--e^- decays of mesic atoms of light (C, N, O) and heavy (Ag, Br) emulsion nuclei with the positron spectra in the μ^+-e^+ decay of "free" μ^+ mesons. The decay probabilities and the spectra in the μ^+ and μ^- decay may differ considerably, and this difference should increase for heavy nuclei. This is due to the decrease in the number of final states of the decay electrons, to relativistic effects caused by the motion of the μ^- mesons in the K orbit of the mesic atom, and to the action of the Coulomb field of the nucleus on the decay electrons.

All these effects, both for a point and an extended nucleus, were investigated theoretically by a number of authors.[1-3] For an illustration of the magnitude of the expected effect, the decay electron spectra for free μ^+ mesons (curve 1) and for the decay of mesic atoms with Z = 7 and Z = 40 (curves 2 and 3, taken from [2]) are shown in Fig. 1. Here and in the following figures, the x axis represents the energy $\epsilon = E[\text{Mev}]/52.8$. These curves have been obtained for the four-fermion V-A interaction. Thus, curve 1 corresponds to the Michel parameter $\rho = 3/4$.

In the present experiments, we have measured the following electron spectra: 1) spectrum from 2969 π^+-μ^+-e^+ decays; 2) spectrum from 604 μ^--e^- decays; and 3) spectrum from 207 μ^--e^- decays accompanied by the production of Auger electrons.

The spectra 1) and 2) have been used earlier[4] to determine the Michel parameter ρ and the asymmetry parameter δ. The same reference describes in detail the irradiation of the emulsion chambers in the π^+ and μ^- meson beams using the proton synchrotron of the Joint Institute for Nuclear Research, the method of spectrum measurement, and the selection criteria.

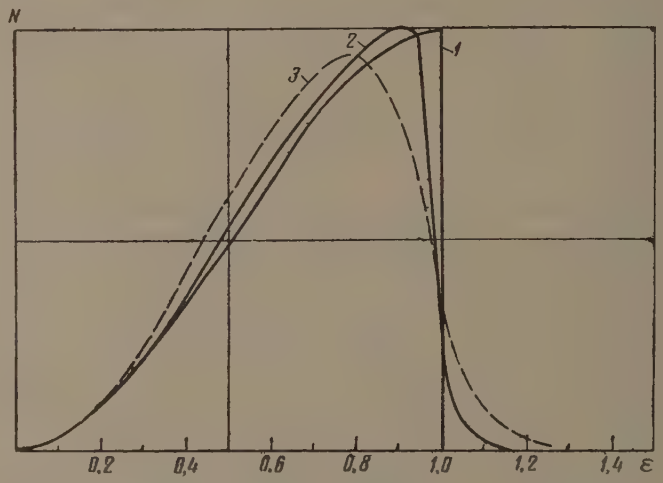

FIG. 1. Spectra of decay electrons for V – A interaction: 1 – Z = 0; $\rho = 3/4$; 2 – Z = 7; 3 – Z = 40. The calculations refer to an extended nucleus.[2]

2. COMPARISON OF THE ELECTRON SPECTRA IN μ^--e^- DECAY IN LIGHT EMULSION ATOMS WITH THE POSITRON SPECTRUM IN μ^+-e^+ DECAY

The positron spectrum obtained from 2969 μ^+-e^+ decays and the spectrum of electrons from 604 μ^--e^- decays in light emulsion atoms is shown in Fig. 2. The solid curve indicates the theoretical spectrum, blurred by the experimental conditions, with a Michel parameter $\rho = 0.68$.[4] An analysis of these spectra leads to the conclusion that the electron spectrum for the decay in light emulsion atoms (C, N, O) is almost in full agreement

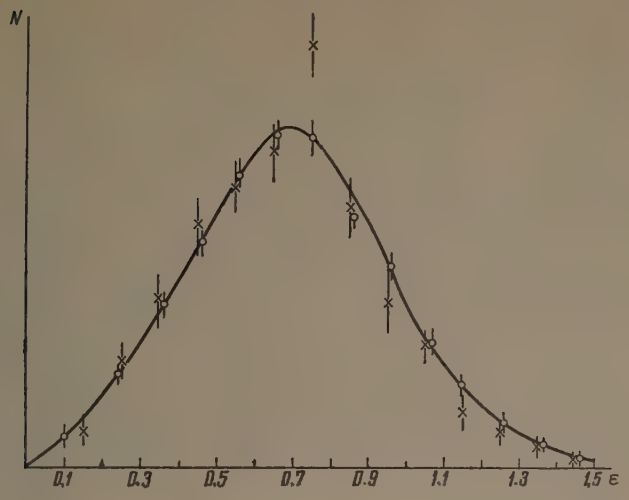

FIG. 2. Electron spectra for the $\mu^+ - e^+$ decay (○) and for the $\mu^- - e^-$ decay (×) in light emulsion atoms.

with the spectrum of positrons from the μ^+-e^+ decay. This result is not unexpected, since the influence of the above-mentioned effects connected with the bound μ^- meson should be small for low Z (see curve 2 in Fig. 1), and the blurring of both spectra due to the dispersion of the measurement makes them even more indistinguishable.

Analogous results have also been obtained by Bloch et al,[5] who compared the electron spectrum in μ^--e^- decays in He with the positron spectrum in the μ^+-e^+ decay.

3. SELECTION OF DECAYS IN HEAVY EMULSION ATOMS

Most μ^- meson decays in emulsion occur in mesic atoms of light nuclei. If we assume that ~ 40% of the μ^- mesons stop in the gelatine and ~ 60% in the silver-halide crystals[6] and use the known values for the μ^- meson lifetime in mesic atoms of C, N, O, Ag, and Br,[7] we find that approximately only one out of 15 μ^--e^- decays in the emulsion occurs in the mesic atoms of silver halides. In order to select such decays, we have used as a selection criterion the presence of a track of an Auger electron in addition to the decay-electron track. Tracks were classified as due to Auger electron if they contained not less than four grains or blobs, with the first not more than 4 μ from the point were the μ^- meson stopped, and in which, moreover, the large scattering characteristic of slow electron tracks is observed.

The spectrum of Auger electrons selected by such a criterion was estimated in the following way: for each Auger electron track, we count the number of grains or blobs. Then, on plane tracks whose range is easy to measure, we establish the approximate blob density vs. range relation which, in the range of 4 — 50 blobs, is of the form $R(\mu) = 1.85\,N$ (blobs). From this relation we can determine the range of the remaining tracks that are more inclined, for which the number of blobs can be measured while the range can be measured only with great difficulty. After the range has been estimated, the energy is found by using the range-energy relations for slow electrons.[8]

The energy spectrum of Auger electrons accompanying the μ^--e^- decay as obtained by us is shown in Fig. 3. The comparison of this spectrum with the probabilities, calculated in [9], of transitions in C, N, O, Ag, and Br atoms leads to the conclusion that, for our selection criterion, about 85 — 90% of the μ^--e^- decays accompanied by Auger electrons occurred in mesic atoms of Ag or Br.

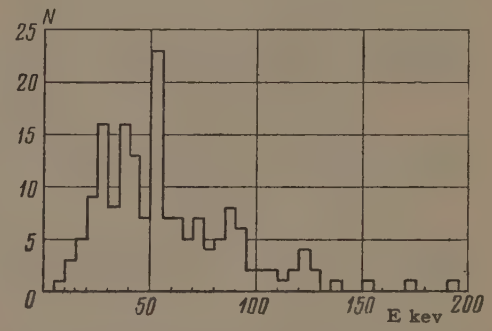

FIG. 3. Spectrum of Auger electrons accompanying the $\mu^- - e^-$ decay.

As a direct check of the accuracy of such a selection criterion, we have used the presence of Auger electrons in σ_μ capture stars on light nuclei of the emulsion. The capture by a light nucleus was identified by the presence of a two-prong star, with one prong representing the track of the recoil nucleus with a range less than 10 μ, while the second prong represents the track of an α particle. In scanning 500 such stars, we found an Auger electron track which satisfied our selection criterion, with energy $\gtrsim$ 25 kev, in only two cases. In selecting the μ^--e^- decays in the emulsion, we found that, using our selection criterion, about 60 normal μ^- meson decays occurred for each decay event accompanied by an Auger electron. Hence, it follows that, in our spectrum of 202 particles, not more than $(2/500) \times 60 \approx 25\%$ of μ^- meson decays in light atoms may be present as an admixture. This analysis confirms the correctness of our selection criteria for decays in heavy atoms.

4. COMPARISON OF ELECTRON SPECTRA IN μ^--e^- DECAY IN HEAVY EMULSION ATOMS WITH THE POSITRON SPECTRUM

This comparison is shown in Fig. 4, where curve 1 represents the positron spectrum (taken from Fig. 2), while curve 2 represents the theoretical electron spectrum from the μ meson decay in heavy emulsion atoms ($Z = 40$) calculated by Überall and blurred by our experimental conditions. The circles represent the experimental electron spectrum. A comparison shows that, because of instrumental errors, spectrum 2 is shifted towards lower energies. The parameter of the spectrum sensitive to the low-energy region is the inverse energy averaged over the whole spectrum $\langle 1/\epsilon \rangle$. The values of $\langle 1/\epsilon \rangle$ for the experimental spectrum and for the theoretical spectra are shown in the table.

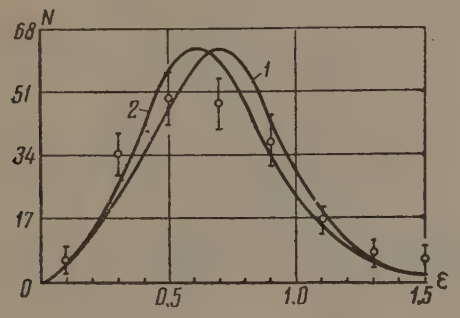

FIG. 4. Comparison of the electron spectra for the $\mu^+ - e^+$ and $\mu^- - e^-$ decays in Ag and Br emulsion nuclei. 1 – experimental spectrum of electrons in the $\mu^+ - e^+$ decay taken from Fig. 2; 2 – electron spectrum calculated by Überall[3] in the $\mu^- - e^-$ decay for $Z = 40$ and blurred because of our instrumental errors.

Spectrum	$\langle 1/\varepsilon \rangle$
Theoretical spectrum of positrons ($\rho = 0.68$)	1.79
Experimental spectrum of 2969 positrons	1.77 ± 0.07
Theoretical electron spectrum	
according to Überall[3]	1.91
according to Terent'ev[2]	2.06
Experimental spectrum of 202 electrons	1.92 ± 0.30

It can be seen from the table that the mean values of $\langle 1/\epsilon \rangle$ for the theoretical and experimental positron spectra and for the electron spectra respectively are in good agreement. For an experimental check of the statistical significance of this agreement, we have divided the spectrum of μ^+-e^+ decays consisting of 2969 positrons and the similar spectrum of 604 electrons from μ^- meson decays in mesic atoms of light emulsion nuclei into spectra consisting of 200 particles each, and have compared the number of particles in the low energy range ($\Delta\epsilon = 0 - 0.4$) of these 17 spectra with the number of particles in the same range in the spectrum of μ^- decays in heavy atoms (the latter being equal to 39). In addition, we have also compared the mean values of the inverse energy for each of the spectra. It was found that in none of the 17 spectra is the number of particles in the interval $\Delta\epsilon = 0 - 0.4$ greater than the number of particles in the electron spectrum (39), and all values of $\langle 1/\epsilon \rangle$ are less than 1.92. Thus, the experimental estimate of the probability that the measured spectrum of electrons is a fluctuation of the positron spectrum gives the value of $\sim 1/17 \lesssim 10\%$.

5. NEUTRINOLESS DECAY OF μ^- MESONS INTO ELECTRONS

Our experimental data on the electron spectra in the μ^--e^- decay makes it possible to obtain the upper limit for the probability of the neutrinoless decay of μ^- mesons into electrons on the X nucleus: $\mu^- + X \rightarrow X^* + e^-$. This process is forbidden in the first approximation of the four-fermion interaction theory, and is absolutely forbidden if the electron and meson neutrinos are different. It could occur with a μ^- meson captured on the K orbit of the mesic atom: the whole recoil would be absorbed by the X nucleus, and the energy carried away by the electron would be close to the rest energy of the μ^- meson ~ 100 Mev, or somewhat less if the nucleus were excited.

Let us consider the spectra of positrons and electrons in the energy range $\epsilon > 1.0$. For the positron spectrum, we limit ourselves to this range because of the dispersion of the scattering measurements which, under our conditions, amounts to 15 – 25% at the limit of the spectrum.

The analysis carried out by us showed that most of the particles with energy $\epsilon > 1$ correspond to short tracks of length $l \leq 1.5$ mm, for which the dispersion of the measurements is considerable. Thus, the background in the range of large energies ($\epsilon \sim 2$), when we are looking for monochromatic electrons of ~ 100 Mev from the μ^--e^- decay, is determined by the dispersion of the scattering measurements.

The second source of the background in this energy range is due to the fact that the electron spectrum exceeds the limit $\epsilon = 1$ because of the effects of the μ^- meson binding in the mesic atom. The blurring of the spectra in our experiment[4] showed, however, that this background is negligibly small as compared with the first source.

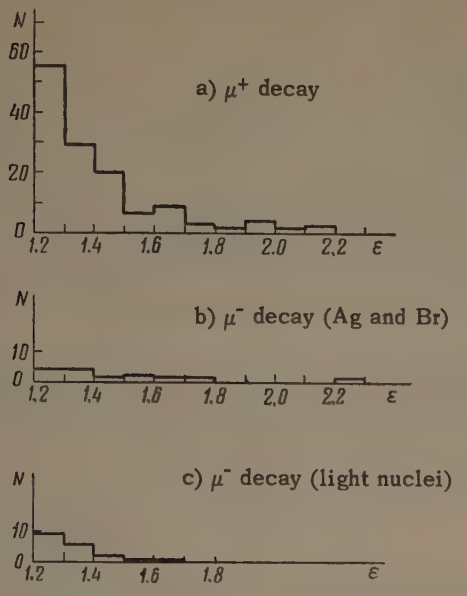

FIG. 5. Comparison of the "tails" of the spectra for $\mu^+ - e^+$ and $\mu^- - e^-$ decays.

Figure 5 shows the spectra for an energy $\epsilon > 1.2$ for a) 2980 positrons, b) 604 electrons originating in the decays in light emulsion atoms, and c) 207 electrons in the decays in heavy emulsion atoms. We shall assume that the particles of the spectrum a) determine the background of the measurement for the spectra b) and c). This background in the energy range $\Delta\epsilon = 1.7 - 2.3$ amounts to $\sim 0.06\%$ of the total spectrum in the energy range $\Delta\epsilon = 0.1$. In the spectrum c) of decays in heavy emulsion nuclei in the range $\Delta\epsilon = 1.6 - 2.3$, two particles are present. It should be added that the tracks of electrons starting with $\epsilon = 1.5$ are very short in this spectrum, namely 1.0, 1.25, 1.1, and 1.0 mm, and their energy is therefore measured with an increased spread. We can therefore maintain that the spectrum of electrons from μ^--e^- decays in heavy mesic atoms in the emulsion as obtained by us does not indicate the presence of electrons in the range of 80 — 120 Mev in numbers greater than that determined by the background.

We shall now estimate the upper limit of the probability of the process $\mu^- + X \rightarrow X^* + e^-$ to which these results correspond. In order to determine this probability, it is necessary to find the number of captures corresponding to the measured number of decays. Under the condition that the decay probability is the same for μ^- and μ^+ mesons, the number of captures $N_c = N_d(\tau_0/\tau - 1)$, where N_d is the number of decays, τ_0 is the lifetime of the μ^+ mesons, and τ is the lifetime of the meson in the given mesic atom. We shall furthermore assume that the captures in the Ag and Br crystals are distributed between the Ag and Br according to the Fermi-Teller law, i.e., proportional to Z.

The number of captures corresponding to 207 decays of heavy nuclei is equal to

$$N_c = 207\left\{\frac{47}{82}\left(\frac{2200}{84} - 1\right) + \frac{35}{82}\left(\frac{2200}{100} - 1\right)\right\} = 4150.$$

Thus, for the ratio of the probability of the $\mu^- + X \rightarrow X + e^-$ process to the probability of the capture of a μ^- meson by heavy emulsion nuclei (AgBr, $Z \sim 40$), we find

$$\varkappa = w(\mu^- + X \rightarrow X^* + e^-)/w(\mu^- + X_z \leftrightarrow X_{z-1} + \nu) \lesssim 2.5 \cdot 10^{-4}.$$

6. PRINCIPAL RESULTS

The principal results obtained in the comparison of the electron and positron spectra in the μ-e decay are as follows:

1) The electron spectrum for the decays in mesic atoms of light emulsion nuclei is identical with the positron spectrum under our experimental conditions.

2) The electron spectrum for the decays in mesic atoms of Ag and Br indicates a considerable increase in the mean value of the inverse energy $\langle 1/\epsilon \rangle$.

Both these conclusions are in agreement with the predictions of the theory of the μ-e decay of a bound μ^- meson.

3) The relative probability of a neutrinoless electron decay of a μ^- meson estimated from our data is less than $\kappa \approx 2.5 \times 10^{-4}$. This value refers to the capture by Ag and Br emulsion nuclei. The probability of such a transition on the Cu nuclei was investigated in experiments [10-12] by other methods. In this experiment, the neutrinoless electron decay of a μ^- meson was also not observed, and the following upper limits were obtained for the value of κ: $\sim 10^{-3}$,[10] $(4^{+3}_{-2}) \times 10^{-6}$,[11] and 7×10^{-6}.[12]

4) The spectrum of Auger electrons produced in the capture of μ^- mesons by the heavy emulsion nuclei was measured.

5) It was shown that the number of Auger electrons with energy greater than ~ 25 kev in the capture of μ^- mesons by light nuclei amounts to more than a few tenth of a percent of the number of captures. These results confirm the theory of nonradiative transitions in mesic atoms.[9,13,14]

---

[1] C. E. Porter and H. Primakoff, Phys. Rev. **83**, 849 (1951).

[2] M. V. Terent'ev, JETP **39**, 6, 1734 (1960), Soviet Phys. JETP **12**, 1211 (1960).

[3] H. Überall, Phys. Rev. **119**, 365 (1960).

[4] Vaĭsenberg, Smirnit-skii, and Kolganova, JETP **40**, 1042 (1961), Soviet Phys. JETP **13**, 734 (1961).

[5] Bloch, Fiorini, Kikuchi, Giacomelli, and Ratti, Proc. of the 1960 Ann. Int. Conf. on High Energy Phys., Univ. of Rochester, 1960, p. 553.

[6] W. E. Fry, Nuovo cimento **10**, 490 (1953).

[7] Progress in Elementary Particle and Cosmic Ray Physics, ed. by J. G. Wilson and S. A. Wouthuysen (North-Holland Publishing Co., Amsterdam, 1960), Vol. V, p. 386.

[8] M. Ross and B. Zajac, Nature **164**, 311 (1949).

[9] G. R. Burbridge and A. H. Borde, Phys. Rev. **89**, 189 (1953).

[10] J. Steinberger and H. B. Wolf, Phys. Rev. **100**, 1490 (1955).

[11] Sard, Growe, and Kruger, Proc. of the 1960 Ann. Int. Conf. on High Energy Phys., Univ. of Rochester, 1960, p. 557.

[12] Conversi, di Lella, Egidi, Rubbia, and Toller, Nuovo cimento **18**, 1283 (1960).

[13] R. A. Ferell, Phys. Rev. Letters **4**, 425 (1960).

[14] M. A. Ruderman, Phys. Rev. **118**, 1632 (1960).

Translated by H. Kasha
180

NONSTATIONARY ELASTIC SLOWING DOWN OF NEUTRONS IN GRAPHITE AND IRON

A. I. ISAKOV

P. N. Lebedev Physics Institute, Academy of Sciences, U.S.S.R.

Submitted to JETP editor April 28, 1961

J. Exptl. Theoret. Phys. (U.S.S.R.) **41**, 1037-1039 (October, 1961)

The slowing down time distribution for neutrons slowed down from 14 Mev to 4.9 Mev in graphite and iron has been measured with a pulsed neutron source. The results agree satisfactorily with the nonstationary theory of elastic slowing down of neutrons. The cross section for neutron capture in iron has also been measured and found to be 2.57 ± 0.04 bn for E = 0.0253 ev.

THE nonstationary slowing down of neutrons in lead was investigated in recent experiments.[1-3] A pulsed neutron source, together with a specimen having an isolated resonance at an energy E_0, was introduced into a lead prism. The intensity of the γ rays emitted upon capture of the neutrons in the specimen were measured as a function of the slowing-down time. In the limiting case of a very narrow resonance, the ratio of the intensity of the radiation emitted in the capture to the neutron density yields directly the distribution of the neutron slowing-down time to a final energy E_0. The average slowing-down time in the lead used in that investigation was in good agreement with theory, but the dispersion in the slowing-down times was 50 percent greater. In order to determine the causes of this discrepancy and to test the theory on other moderators, we undertook to measure the nonstationary elastic slowing down of neutrons in graphite and in iron.

The measurement procedure was the same as before.[1-3] The measurements were made on cylindrical gold specimens (E_0 = 4.906 ev) of effective thickness $\bar{l}$ = 0.4 mm. The γ rays from the capture of the slowed-down neutrons by the gold were registered with a proportional counter, over which the specimen was placed. The γ-ray count $I_\gamma(t)$ was normalized to a lithium-counter counting rate $I_{Li}(t)$ proportional to the neutron density.

The dots on Figs. 1 and 2 show the experimental results, obtained in graphite* and in iron respectively. The solid curve is a plot of the formula

$$I_\gamma(t)/I_{Li}(t)=\text{const}\cdot\int_0^\infty F(E,t)\,v\,(1-e^{-N\bar{l}\sigma(E)})\,dE, \qquad (1)$$

*The measurements were made with the prism described by Dlougy.[4]

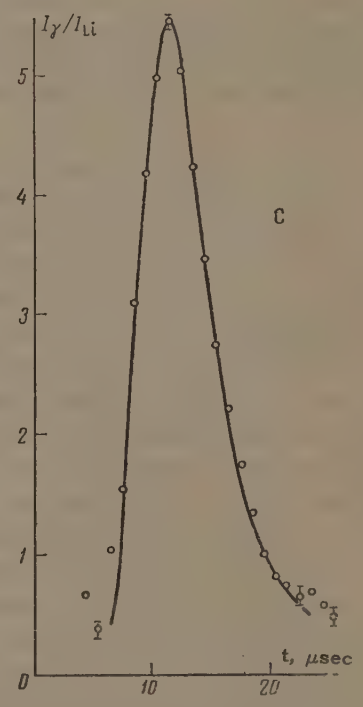

FIG. 1. Dependence of I_γ/I_{Li} on the slowing-down time for gold in a prism of graphite: o – experimental points; continuous curve – calculated line shape.

where F(E,t) is a function of the energy distribution of the slowed-down neutrons, calculated after Kazarnovskii,[5] with account of the small corrections for the apparatus spectral broadening, for broadening due to thermal motion of the atoms of the moderator, and for the 0.2% admixture of carbon in the case of iron; E and v are the energy and velocity of the moderated neutron; N is the number of nuclei per cm^3; $\sigma(E)$ is the total cross section for the interaction between the neutrons and the nuclei of the specimen. We neglect in (1) the potential scattering.

In the calculation of F(E,t) we used the tabulated[6] scattering cross sections of iron and copper.

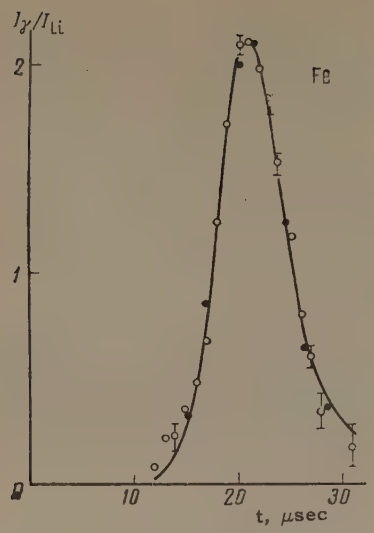

FIG. 2. Dependence of I_γ/I_{Li} on the slowing-down time for gold in an iron prism; ○ – experimental points, continuous curve – calculated line shape, ● – points calculated under the assumption that the spectrum of the moderated neutrons is Gaussian.

As can be seen from Figs. 1 and 2, the theoretical curves describe satisfactorily the shape of the line, its width, and its position, for either graphite or iron. The full circles of Fig. 2 have been calculated from (1) under the assumption that F(E,t) is a Gaussian function. As can be seen from the figure, the difference between the exact and approximate functions is insignificant.

We cannot use the Gaussian approximation for light moderators, since the spectrum of the moderated neutrons is not symmetrical, as can be seen from Fig. 1. The agreement with the theory of nonstationary elastic slowing down of neutrons, observed for graphite and iron moderators, enables us to conclude that the discrepancy between theory and experiment can be attributed in the case of lead to impurities of light nuclei.

We also undertook a direct measurement of the mean lifetime of neutrons in an iron prism. The intensity of registration of the neutrons with a lithium counter I_{Li} and the slowing-down time t are connected by the relation [1]

$$\ln I = -\alpha \ln t - t/T + \text{const},$$

where t is the neutron slowing down time and T the mean lifetime of the neutrons prior to capture. In a time interval 10 – 150 μsec, the neutron density decreased practically exponentially. The term $\alpha \ln t$, which characterizes the "leakage" of neutrons from the prism, was insignificant in this case. The measurement results are shown in Fig. 3.

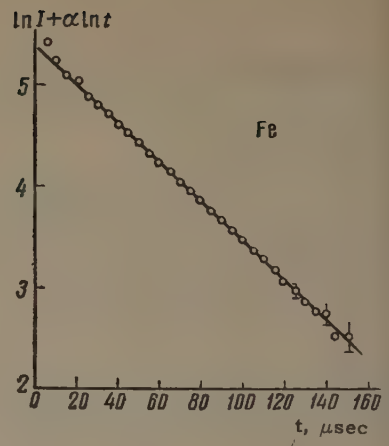

FIG. 3. Dependence of the neutron intensity I on the slowing-down time in an iron prism.

The mean lifetime in iron is T = 22.2 ± 0.15 μsec. After introducing corrections for the impurities in the iron and for the effect of the measuring channel, we obtain for the lifetime T = 21.30 ± 0.30 μsec. From the measured values of the mean lifetime and the density of the iron prism we obtain for the capture cross section of 0.0253-ev neutrons $\sigma_c = 2.57 \pm 0.04$ b. This result agrees with the latest published data $\sigma_c = 2.53 \pm 0.06$ b [6a] and $\sigma_c = 2.62 \pm 0.06$ b. [6b]

In conclusion I take this opportunity to thank F. L. Shapiro, at whose initiative the experiments were undertaken, for constant help and collaboration in this work.

[1] Bergman, Isakov, Murin, Shapiro, Shtranikh, and Kazarnovskii, Trans. First Geneva Conference, vol. 4, p. 166 (Russ. ed.), 1955.

[2] Bergman, Isakov, Popov, and Shapiro, JETP 33, 9 (1957), Soviet Phys. JETP 6, 6 (1958).

[3] Bergman, Isakov, Popov, and Shapiro, Nuclear Reactions at Low and Medium Energies (Trans. of All-Union Conference of November 1957), AN SSSR, 1958.

[4] Z. Dlougy, Atomnaya energiya (Atomic Energy) 9, 182 (1960).

[5] M. V. Kazarnovskii, Dissertation, Phys. Inst. Acad. Sci., 1955; Trudy, Phys. Inst. Acad. Sci. 11, p. 176.

[6] a) Neutron Cross Sections, BNL 325, Second ed., 1958;

b) Neutron Cross Sections, BNL-325, Supplement to Second ed., 1960.

Translated by J. G. Adashko
181

INELASTIC SCATTERING OF PROTONS ON F^{19} NUCLEI

S. S. VASIL'EV, E. A. ROMANOVSKII, and G. F. TIMUSHEV

Institute of Nuclear Physics, Moscow State University

Submitted to JETP editor May 3, 1961

J. Exptl. Theoret. Phys. (U.S.S.R.) 41, 1040-1042 (October, 1961)

A magnetic analysis is performed on 6.6-Mev protons inelastically scattered on F^{19} with the excitation of five levels. The cross sections and angular distributions are measured. Conclusions are drawn regarding the spin, parity, and nature of the levels.

THE F^{19} nucleus has only three nucleons beyond the closed shell of the O^{16} nucleus. We can therefore calculate numerically the properties of F^{19} low-lying levels in the intermediate coupling model of shell theory [1] and also classify the levels within the framework of the nucleon cluster model. [2] On the other hand, three extra nucleons can lead to a pronounced deformation of the nucleus, so that the presence of rotational levels in F^{19} can be expected. [3]

For this reason, a more precise determination of the excited state properties of the F^{19} nucleus is of interest. In the present article we investigate the inelastic scattering of 6.6-Mev protons by F^{19} nuclei. The measurement techniques have been described earlier. [4] The measured angular distributions, which correspond to excitation of the levels at 0.198 ± 0.012, 1.553 ± 0.012, 1.344 ± 0.012, 1.458 ± 0.012, and 2.789 ± 0.006 Mev, are presented in the figure.

All the angular distributions are asymmetric about 90°. The absolute values of the cross sections vary sharply with small changes in the energy of the excited level. The total cross section for excitation of the five F^{19} levels ($\sigma_t \sim 400$ mb) is comparable with the geometric one. The enumerated facts allow us to conclude that the inelastic scattering is, on the whole, due to direct interaction.

In excitation of the 0.198 and 1.553-Mev levels, the transferred orbital angular momentum is $l = 2$, and the possible spin and parity values are in accord with the tables of [5], being respectively $5/2^+$ and $3/2^+$. In the case of excitation of the 1.334 and 1.458-Mev levels, $l = 1$ and our measurements confirm the correct assignment of odd parity to these levels (determined on the basis of data on the decay of O^{19} [6]).

The measured total cross sections for excitation of the 1.344, 1.458, and 2.789-Mev levels are, respectively, 25, 25, and 15 mb. The total cross section for the (p,n) reaction on F^{19} is about 55 mb. [7] On the other hand, the total cross sections for excitation of the 0.198 and 1.553-Mev

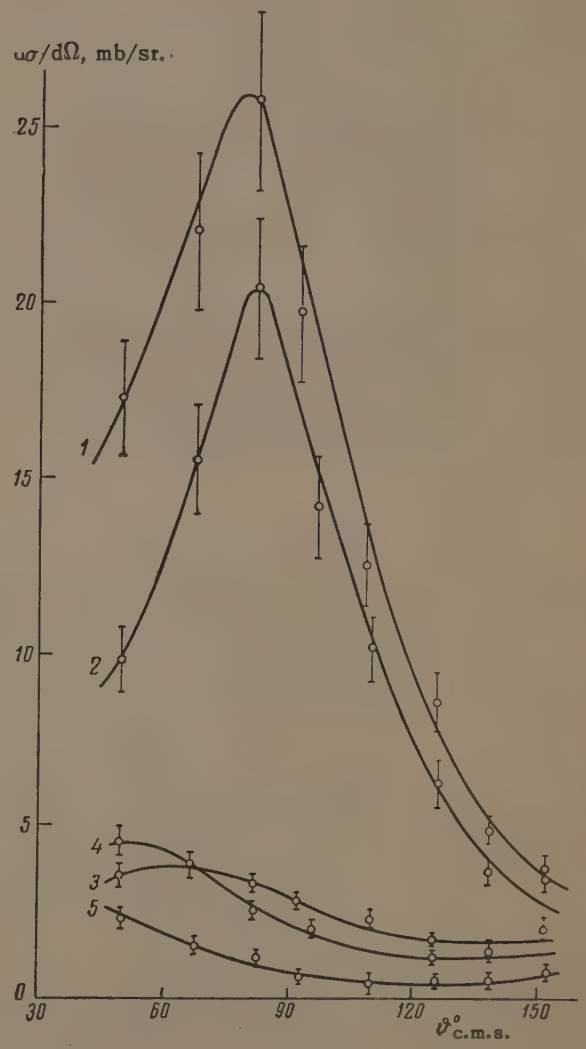

Angular distributions of protons (E_p = 6.6 Mev) inelastically scattered on F^{19} with excitation of the following levels: 1 – 0.198 Mev, 2 – 1.553 Mev, 3 – 1.344 Mev, 4 – 1.458 Mev, and 5 – 2.789 Mev.

levels are 180 and 130 mb. The total cross sections for excitation of the 0.198 and 1.553-Mev levels, which are large in comparison with the cross sections for the excitation of other levels as well as with the cross section for the (p,n) reaction on F^{19}, indicate the collective nature of these excited states (in accord with Cohen's hypothesis[8]). This conclusion confirms the assumption[3] that the ground state and the 0.198 and 1.553-Mev states belong to one rotational series.

The small cross section for excitation of the 1.344- and 1.458-Mev levels indicates a single-particle mechanism in the excitation of these states. They can be interpreted as "hole" states[9] or as states possessing a nucleon cluster structure which differs from that of the ground state.[2]

In the excitation of the 2.789-Mev level $l = 0$, and consequently the spin and parity are $\frac{1}{2}^+$ or $\frac{3}{2}^+$ and not $\frac{7}{2}^\pm$ or $\frac{9}{2}^\pm$ as assumed earlier.[10] Paul and Rakavy[3] propose that the spin and parity of this level are $\frac{9}{2}^+$, and on this basis conclude that the 2.789-Mev level belongs to the rotational series indicated above. On the basis of our measurements, it seems more probable that the 2.789-Mev excited state has a single-particle nature. The rotational level with spin and parity $\frac{9}{2}^+$ must, it seems, lie higher than 2.789 Mev.

In conclusion the authors express their gratitude to Yu. A. Vorob'ev, A. A. Danilov, E. F. Kir'yanov, and V. P. Khlapov for assuring the good functioning of the cyclotron and to Z. F. Kalacheva, M. Kh. Listov, and P. I. Osipova for help in the work.

[1] J. P. Elliott and B. H. Flowers, Proc. Roy. Soc. **A229**, 536 (1955).

[2] B. Roth and K. Wildermuth, Nucl. Phys. **20**, 10 (1960).

[3] E. B. Paul, Phil. Mag. **2**, 311 (1957); G. Rakavy, Nucl. Phys. **4**, 375 (1957).

[4] Vasil'ev, Romanovskii, and Timushev, JETP **40**, 972 (1961), Soviet Phys. JETP **13**, 678 (1961).

[5] F. A. Ajzenberg-Selove and T. Lauritsen, Nucl. Phys. **11**, 1 (1959).

[6] Johnson, Jones, Phillips, and Wilkinson, Proc. Roy. Soc. **A252**, 1 (1959).

[7] Blaser, Boehm, Marmier, and Scherrer, Helv. Phys. Acta **24**, 465 (1951).

[8] B. L. Cohen, Phys. Rev. **116**, 426 (1959).

[9] C. S. Warke and G. Abraham, Nucl. Phys. **10**, 306 (1959).

[10] J. M. Freeman, Phil. Mag. **2**, 628 (1957).

Translated by Mrs. J. D. Ullman
182

ABSORPTION OF NUCLEAR-ACTIVE COSMIC RAY PARTICLES IN AIR

G. BOZOKI, E. FENYVES, T. SANDOR,* O. BALEA, M. BATAGUI, E. FRIEDLANDER,† B. BETEV, S. KAVLAKOV, and L. MITRANI‡

Submitted to JETP editor May 4, 1961

J. Exptl. Theoret. Phys. (U.S.S.R.) **41**, 1043-1045 (October, 1961)

Absorption of nuclear-active cosmic-ray particles in air was studied by the coincidence method at 80, 410, 950, and 2925 m above sea level. The μ-meson background was determined by measuring the underground flux. The absorption mean free path for nuclear-active particles in air is found to be $\lambda_a = (119 \pm 1)$ g/cm^2. The mean energy of the investigated nuclear-active particles estimated from the magnitude of their flux is ~ 30 Bev.

THE absorption of the nuclear-active component of cosmic radiation was investigated by measuring its flux at different altitudes above sea level (Bucharest—80 m, Budapest—410 m, Busteni—950 m, Stalin's Peak—2925 m). The experimental setup was an array of counters connected for coincidence and placed in a lead block (Fig. 1). This registered the electron-nuclear showers produced by the nuclear-active particles in the lead. A layer of lead 10 cm thick was placed between the upper (1 — 4) and the lower (5 — 8) counters while 5 cm of lead was placed between the lower counters. The counters were covered on the top and on the sides by 15 cm of lead. The counter diameter was 4 cm and the effective length 80 cm. The lower counters 5 — 7 and 6 — 8 were connected in parallel pairs and the frequency of the sixfold coincidences (1, 2, 3, 4, 5 — 7, 6 — 8) was measured.

Since the muon background at low altitudes is considerable compared with the overall frequency of coincidences due to nuclear-active particles, we have determined the frequency of the background events by underground measurements. The investigations were carried out in Budapest 8 m below ground (17 m water equivalent). At this depth, the nuclear-active component is practically completely absorbed and thus the sixfold coincidences obtained can be caused only by the muons.

By measuring the intensity of the muon component underground and on the earth's surface at different heights above sea level, we can determine the background produced by the muons in different places, so that corrections can be made for the frequency of the measured coincidences.

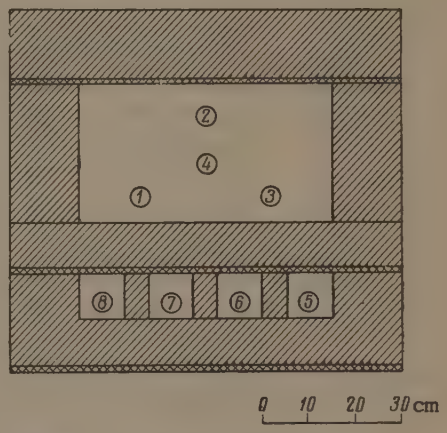

FIG. 1. Diagram of experimental apparatus.

The measurement results are shown in the table and in Fig. 2. It is clearly seen from Fig. 2 that the absorption curve deviates insignificantly from exponential.

The free path for absorption in air was determined directly from the measurements, with allowance for the background, by the maximum-likelihood method[1]

$$\lambda_a = 119 \pm 1 \text{ g/cm}^2.$$

This value agrees well with the results of Tinlot[2] (118 ± 2 g/cm^2), Hodson[3] (118 ± 1.1 g/cm^2), Azimov, Vishnevskii, and Khil'ko[4] (123 ± 6 g/cm^2), Schultz[5] (125 ± 5 g/cm^2), George and Jason[6] (114 ± 10 g/cm^2), Ryzhkova and Sarycheva,[7] and also with other results obtained with similar experimental arrays. All obtained approximately 120 g/cm^2 for the absorption free path in air.

The mean energy of the registered nuclear-active particles can be estimated from the frequency of the coincidences by assuming that the energy spectrum follows a power law and that the

*Central Physics Research Institute of the Hungarian Academy of Sciences, Budapest.

†Institute of Nuclear Physics, Bucharest Rumania.

‡Physics Institute with Atomic Scientific-Experimental Base, Sofia, Bulgaria.

Location	Depth, g/cm²	Frequency of coincidences	
		without correction	with correction
Bucharest (80 m)	1009	1,17±0,02	1,00±0,04
Budapest (410 m)	969	1,73±0,03	1,55±0,04
Busteni (950 m)	907	2,57±0,03	2,37±0,04
Stalin's Peak (2925 m)	703	13,96±0,10	13,67±0,11

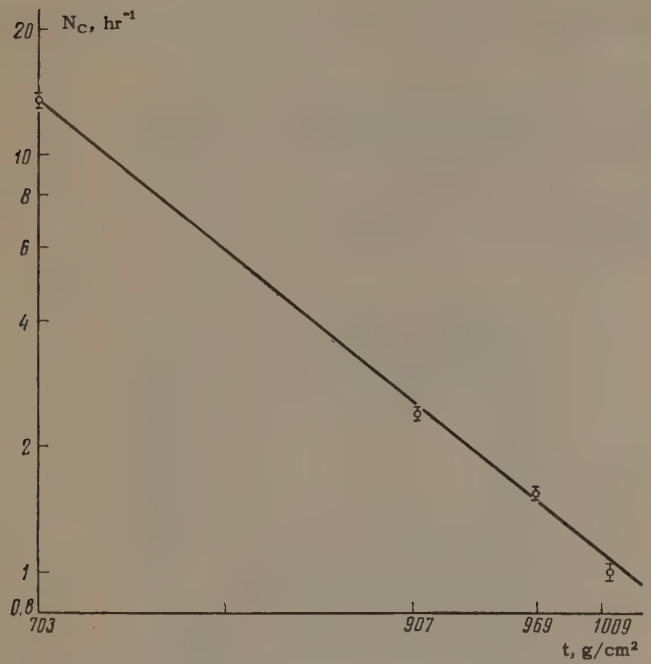

FIG. 2. Frequency of coincidences N_c (with correction for background) as a function of the depth t in the atmosphere.

probability of operation of the apparatus approaches a step function with zero value below a certain limiting energy E_0 and constant value K (determined by the geometry of the apparatus) at energies greater than E_0. Using the spectrum obtained by Bridge and Rediker [8] we find that the mean energy of the nuclear-active particles is roughly 30 Bev.

The authors are grateful to Professors L. Janossy, G. Nadzhakov, and I. Auslaender for deep interest and valuable advice during the experiments, to N. Akhababyan, I. H. Ionn, J. Koch, G. Thaler, K. Ziegelman, and J. Schnirer for wiring and operating the apparatus, and to E. Rupp for help with the calculations.

[1] L. Janossy and E. Rupp, M.T.A. K.F.K. I. Közl. (News, Central Phys. Res. Inst. Hung. Acad. Sci.) **8**, 71 (1960).

[2] I. Tinlot, Phys. Rev. **74**, 1197 (1948).

[3] L. Hodson, Proc. Phys. Soc. **A65**, 702 (1952).

[4] Azimov, Vishnevskii, and Khil'ko, DAN SSSR **78**, 231 (1951).

[5] H. Schultz, Z. Naturforsch. **9a**, 419 (1954).

[6] E. P. George and A. Jason, Proc. Phys. Soc. **A63**, 1081 (1950).

[7] K. P. Ryshkova and L. I. Sarycheva, JETP **28**, 618 (1955), Soviet Phys. JETP **1**, 572 (1955).

[8] H. S. Bridge and R. H. Rediker, Phys. Rev. **88**, 206 (1952).

Translated by J. G. Adashko
183

A METHOD FOR STUDYING ELASTIC SCATTERING AT HIGH ENERGIES

V. N. KUZ'MIN

Radium Institute, Academy of Sciences, U.S.S.R.

Submitted to JETP editor May 10, 1961

J. Exptl. Theoret. Phys. (U.S.S.R.) 41, 1046-1047 (October, 1961)

A nuclear recoil technique is described in which nuclear photographic plates are employed as a nuclear detector. The scattering of 660-Mev protons on He^4 is used to illustrate the application of the method. The possibilities of the method are discussed.

A basic difficulty in the study of elastic scattering of high-energy nucleons (hundreds of Mev and higher) is the separation of pure elastic scattering from competing inelastic processes. Moreover, unfavorable background effects lead to certain difficulties in the study of small-angle scattering at high energies.

All these difficulties can be removed relatively simply if the recoil-nucleon technique is employed. The method is based on the following. When a particle of mass of M_1 is scattered on a nucleus (particle) of mass M_2, the latter, as a result of the collision, acquires an energy E_2. The energy E_2 can be readily calculated from the kinematics of an elastic collision. By recording the recoil nucleus, we can establish the very act of scattering, while the energy distribution of the recoil nuclei can provide a check on the elasticity of the scattering process.

The angle by which the particle of mass M_1 is scattered can be estimated from the approximate formula

$$\operatorname{tg}\vartheta_1 \approx \sqrt{2M_2E_2}/p_0 \ll 1, \qquad (1)^*$$

where p_0 is the momentum of the incident particle.

If we choose a detector which can record low-energy recoil nuclei, then it is possible to study small-angle elastic scattering. The best such detector is nuclear emulsion for the following reasons:

1) If the recoil-nucleus tracks are chosen in a given direction, the background can be readily eliminated.

2) From a study of the recoil-nucleus range distribution the elasticity of the scattering process can be checked.

3) Scattering at different angles can be studied with the aid of nuclear emulsion in a single experiment. In this way, the error in determining the intensity of the bombarding beam is eliminated.

4) In polarization measurements, nuclear emulsion makes possible an estimate of the scattering intensity to the right and to the left of the beam in the same experiment.

We used the recoil-nucleus technique for the study of elastic scattering of 660-Mev protons on He_2^4. After passing through a window covered by a copper foil 70 μ thick, the proton beam entered a volume filled with helium at atmospheric pressure. The recoil nuclei (α particles) emitted at a given angle relative to the direction of the proton beam were recorded with the aid of nuclear emulsion plates.

The α-particle tracks were selected in accordance with the following criteria: 1) a given angle of inclination relative to the plane of the plate; 2) the angle between the track and a given direction in the plate was $\leq \varphi_0$; 3) the track should be located in a given area of the emulsion.

These criteria can be obtained by calculation and also by means of a radioactive source. A radioactive source of α particles also serves to determine the geometrical conditions of the experiment (solid angle of the detector).

The figure shows the energy distribution of the α particles recorded at angles $\theta = 81°$ and $\theta = 84°$. As seen from the figure, the half-width of the peak

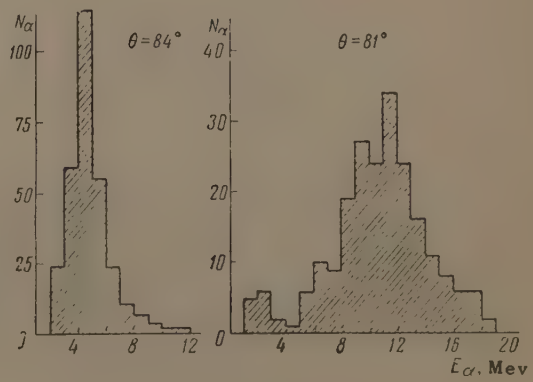

*tg = tan.

is 3 — 6 Mev. This corresponds to a resolution of ~ 1% of the energy of the recorded scattered nucleons. The method permits the accumulation of relatively good statistics (statistical error ~ 8%) in 3 — 4 hr of accelerator operation and a small expenditure of time on the measurements.

The position of the peak in the energy distribution of the recoil nuclei uniquely determines the scattering angle, which gives an additional independent check of the angle.

Elastic scattering down to angles θ_{min} can be studied by this method. The lower limit θ_{min} is determined by the minimum range of the recoil nucleons which can be reliably measured in the emulsion. To illustrate the characteristics of these minimum angles we consider energies available in the existing proton accelerators. We give below the values of θ_{min} (in the l.s.):

Proton energy, Mev	660	1000	10000	25000
θ_{min} (pp scattering), deg	2.5	1.5	0.25	0.1
θ_{min} (pHe_2^4 scattering), deg	7.5	4.5	0.8	0.3

For the scattering of protons by deuterons, tritons, and He_2^3, the angles lie between those of pp and pHe_2^4 scattering. The proposed nuclear-recoil technique can be applied to the scattering of elementary particles (nucleons, electrons, photons) by light nuclei ($A \leq 4$) as well as to the scattering of complex nuclei composed of 2 — 4 nucleons by the corresponding light nuclei. Information on polarization can be obtained from the study of the scattering of recoil nuclei with nonzero spin by emulsion nuclei. For this, of course, it is necessary to know the properties of the emulsion as a polarization analyzer.

In conclusion, the author takes this opportunity to express his gratitude to Professor A. P. Zhdanov for his constant interest in this work.

Translated by E. Marquit
184

IONIZATION OF ARGON BY ATOMS, AND SINGLY OR DOUBLY CHARGED IONS OF NEON AND ARGON

V. V. AFROSIMOV, R. N. IL'IN, V. A. OPARIN, E. S. SOLOV'EV, and N. V. FEDORENKO

Leningrad Physico-Technical Institute, Academy of Sciences, U.S.S.R.

Submitted to JETP editor May 13, 1961

J. Exptl. Theoret. Phys. (U.S.S.R.) **41**, 1048-1055 (October, 1961)

The total ionization cross section σ_- and the total cross sections σ_{0n} for the production of slow ions with charges n = 1, 2, 3, 4 are measured in the ionization of argon by 20 — 180 kev Ne and Ar atoms and Ne^+ and Ar^+ ions, and by 20 — 360 kev Ne^{2+} and Ar^{2+} ions. σ_- decreases with increasing fast-particle charge. This is accounted for by the decreasing probability of fast-particle stripping with increasing charge. The yield of slow multiply-charged ions increases with the charge of fast incident particles. Charge exchange and ionization with pickup apparently make the principal contributions to the cross section for slow multiply-charged ion production.

INTRODUCTION

INELASTIC atomic collisions accompanied by charge exchange can be described in general by

$$A^{k+} + B \rightarrow A^{m+} + B^{n+} + (m + n - k)e, \qquad (1)$$

where A is the incident particle with charge k before and charge m after the collision, and B is a gas atom transformed by the collision into an ion with charge n. We shall designate the incident particles as fast or primary, while the ions and atoms formed from these primary particles will be called fast secondary particles. Ions formed out of gas target atoms will be called slow ions.* The cross section for process (1) will be denoted by σ_{0n}^{km}, where the upper and lower indices pertain to the charges of the fast and slow particles, respectively.

The widely used potential (or capacitor) method for determining ionization and charge exchange cross sections permits measurement of the total cross section for the production of free electrons, interpreted as the total ionization cross section [2]

$$\sigma_- = \sum_{m,\,n} (m + n - k)\,\sigma_{0n}^{km} \qquad (2)$$

and the total cross section for slow-ion production (with weighting by charge units)

$$\sigma_+ = \sum_n n\sigma_{0n}, \qquad (3)$$

where σ_{0n} is the total cross section for the production of slow ions with charge n (see [3]). Electrons can be freed both from the target gas atoms and from fast particles. Therefore the total ionization cross section is the sum of the cross sections σ_i for gas ionization and σ_l for fast-particle stripping:

$$\sigma_- = \sigma_l + \sigma_i. \qquad (4)$$

Mass-spectrometer methods measure the total cross sections for the production of n-fold charged slow ions out of gas atoms (σ_{0n}), or the total cross sections for the production of fast secondary ions with charge m out of fast primary particles (σ^{km}). These are expressed in terms of partial cross sections by

$$\sigma_{0n} = \sum_m \sigma_{0n}^{km}, \qquad \sigma^{km} = \sum_n \sigma_{0n}^{km}. \qquad (5)$$

The dependence of the total ionization cross section on the primary-particle charge has not been investigated thoroughly. On the one hand, at high (Mev) energies the theory of collision ionization predicts a quadratic dependence. On the other hand, no definite charge dependence has been found at tens of kev. [3,4,5]

In the present work we have investigated the intermediate region of a few hundred kev, concurrently with measurements of the cross sections σ_{0n} for the production of slow ions with different charges. Argon gas was bombarded with fast Ar, Ar^+, Ar^{2+}, Ne, Ne^+, and Ne^{2+}. The cross sections for electron capture by these fast particles

*It was established in [1] that ions, especially multiply-charged ions, resulting from gas ionization can possess energies up to a few percent of the fast primary energy. Although the fraction of these relatively energetic ions is small their presence can reduce somewhat the measured cross sections for the production of multiply-charged ions.

had previously been measured in our laboratory.[6,7] A comparison of the cross sections for the formation of slow ions and of fast secondary ions can be used to determine the correlation between processes occurring in the shells of both colliding particles. More complete information concerning the relationship of these processes requires a new technique combining mass analysis and a coincidence scheme for registering the colliding particles.

EXPERIMENTAL PROCEDURE

In investigating the total ionization cross section σ_-, the total cross section σ_+ for slow-ion production, and the total cross section σ_{0n} for the production of n-fold charged slow ions, we used the experimental apparatus described in [8] and [9] in conjunction with devices for producing and registering a fast-atom beam. The apparatus is shown schematically in Fig. 1.

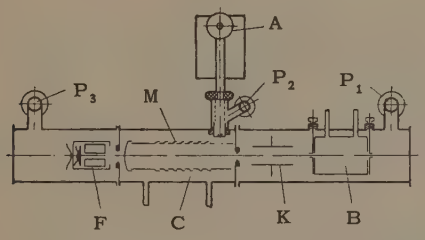

FIG. 1. Experimental apparatus. B – auxiliary charge-exchange chamber, K – capacitor, C – collision chamber, M – measuring capacitor, A – mass analyzer of slow ions, F – fast-particle collector. P_1, P_2, and P_3 – pumps.

Fast neutral atoms were produced by resonant charge exchange of a monochromatic ion beam in the auxiliary charge-exchange chamber B, where the gas pressure was $10^{-3}-10^{-2}$ mm Hg. A pressure differential of the order 1:200 existed between the entrance and exit channels of chamber B. The neutral-atom beam leaving the charge-exchange chamber was cleared of unneutralized fast ions by the electric field of the capacitor K and entered the collision chamber C, which contained a sectional capacitor M for measuring the cross sections σ_- and σ_+. The cross sections σ_{0n} were determined by the slow-ion analyzer A, which was joined to the collision chamber.

The fast-ion beam intensity was measured by means of the secondary electron emission and was monitored by the thermal effect of the beam in the collector F, which is represented in Fig. 2. The beam impinged on the 15 μ thick 20×20 mm grounded nickel foil N. The current of secondary electrons ejected from the foil to the positively biased electrodes E_1 and E_2 was measured. The

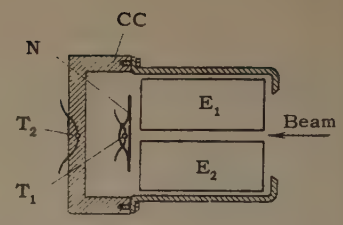

FIG. 2. Fast-atom collector. N – nickel foil, T_1 and T_2 – thermistors, E_1 and E_2 – electrodes, CC – heavy copper casing.

thermistor T_1 was cemented to the back of the foil. The bead thermistor used in the collector was of 0.2 mm diameter, with a temperature coefficient of −4.5% per degree at 20° C. A second identical thermistor T_2 was cemented to the heavy copper casing CC of the collector in order to compensate for the ambient temperature. The two thermistors were incorporated in a bridge for measuring the beam intensity P from the thermistor ratio R_{T_1}/R_{T_2}. The calibration curve $R_{T_1}/R_{T_2} = f(P)$ from which the fast-atom beam intensity was determined had been plotted using a beam of fast singly-charged ions. Control runs showed that f(P) is independent of particle mass and velocity. The thermal-type collector permitted the registration of beam variations as small as 0.1 mw. Beam intensity usually varied in the range 5 — 10 mw.

By means of the thermal collector it was found that the coefficients of secondary-electron emission from the surface of the foil were very close for fast atoms and singly-charged ions of the same element (neon or argon) with identical velocities. It was found more convenient to measure atom-beam intensity by means of secondary-electron emission than with the thermal collector, which is subject to considerable inertia.

A constant check was maintained during all measurements to ensure that the entire beam traversing the collision chamber was also entering the collector located directly behind the chamber.

In the work with ion beams the charge-exchange chamber B was maintained at the extreme vacuum, and the fast-atom collector was used as a Faraday cage consisting of the foil N and the electrodes E_1 and E_2. In this case a transverse electric field between the electrodes prevented secondary electrons ejected from the foil from leaving the collector. Argon gas pressure in the collision chamber was maintained low at $(2-4)\times10^{-4}$ mm, providing the condition for single scattering. Differential pumping was performed by the pumps P_1, P_2, and P_3. The residual pressure in the collision chamber was $(1-2)\times10^{-6}$ mm.

Random errors incurred in measuring cross sections are estimated at ±12% for fast ions and ±15% for fast atoms.

RESULTS AND DISCUSSION

We measured the total ionization cross section σ_-, the total cross section for slow-ion production σ_+, and the total cross sections for the production of singly, doubly, triply and quadruply charged slow ions (σ_{01}, σ_{02}, σ_{03}, and σ_{04}) when argon was ionized by fast Ne and Ar atoms and by the ions Ne^+, Ne^{2+}, Ar^+, and Ar^{2+}. The energy range for fast atoms and singly charged ions was 20 — 180 kev; the range for doubly charged ions was 20 — 360 kev.

A. Total Ionization Cross Section σ_-

The total cross sections $\sigma_-(v)$ for the ionization of argon by fast Ar atoms and by Ar^+ and Ar^{2+} ions are shown in Fig. 3. Corresponding data for fast Ne atoms and for Ne^+ and Ne^{2+} ions are shown in Fig. 4. σ_- increases monotonically over the entire range to a maximum of the order $(1-1.5)\times 10^{-15}$ cm^2. This velocity dependence of the ionization cross sections was to be expected, since their maxima must correspond to higher velocities.[10]

A comparison of the $\sigma_-(v)$ curves for fast ions and atoms of the same element shows a dependence on the fast-particle charge. For the ionization of argon by fast Ne atoms this dependence is exhibited very clearly, beginning at $v \sim 8\times 10^7$ cm/sec. σ_- diminishes with increasing charge.

The observed behavior of σ_- can be accounted for as follows. At low velocities the ion stripping cross section σ_l plays only a small part compared with the gas ionization cross section σ_i. With increasing velocity the stripping contribution to σ_- increases [Eq. (4)], its magnitude being inversely correlated with the fast particle charge. For the

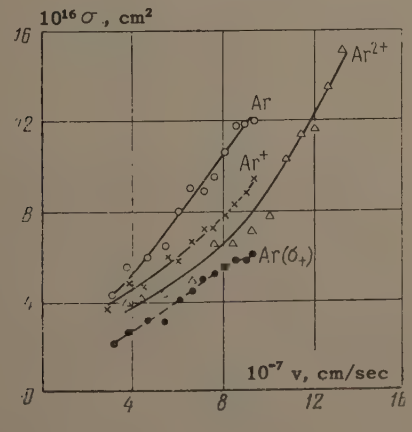

FIG. 3. Velocity dependence of argon ionization cross sections. Solid curves — total ionization cross sections σ_- for fast Ar, Ar^+, and Ar^{2+}. Dashed curves — total cross section σ_+ for slow-ion production by fast Ar atoms.

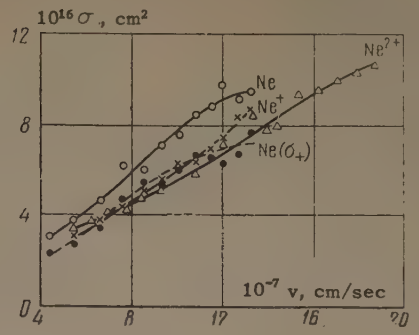

FIG. 4. Velocity dependence of neon ionization cross sections. Solid curves — total ionization cross section σ_- for fast Ne, Ne^+, and Ne^{2+}. Dashed curves — total cross section σ_+ for slow-ion production by fast Ne atoms.

symmetric Ar-Ar pair, stripping assumes a large role, since electrons must be removed from the shells of both colliding particles with equal probability. Since the equality $\sigma_+ = \sigma_i$ must be fulfilled in gas ionization by fast atoms, we have for the Ar-Ar pair

$$\sigma_l = \sigma_i = \sigma_+ = \sigma_-/2. \qquad (6)$$

The data on σ_+ and σ_- (Fig. 3) for argon ionization by fast argon atoms confirm (6); this is an additional check on the operation of the measuring capacitor. For singly charged fast Ar^+ ions stripping makes a small contribution to σ_- (σ_l is 10 — 15% of σ_- for Ar^+-Ar according to [11]); for Ar^{2+} the contribution should be even smaller. For fast neon ions and atoms the charge dependence of σ_- in the same energy range, i.e., at somewhat higher velocities (Fig. 4), is not so strong as for fast argon particles. This is associated with the fact that neon has higher ionization potentials than argon and smaller stripping cross sections.

A comparison of σ_- for fast argon and neon particles with the same charge and the same velocity (Figs. 3 and 4) shows that the total ionization cross section σ_- is larger for fast particles having a large number of shell electrons. This qualitative conclusion had been reached previously for fast singly charged ions.[8,10,12]

Firsov[13] has used statistical concepts to estimate the total ionization cross section in collisions of heavy atomic particles. In Fig. 5 our data are compared with Firsov's universal curve, which is based on his approximate theory that yields cross sections within a factor of 2. The experimental and theoretical cross sections are in agreement within these limits.

In Fig. 6 our results for σ_- in the ionization of argon by Ne^+ are compared with the results given in [14], [8], and [3], and are seen to be in

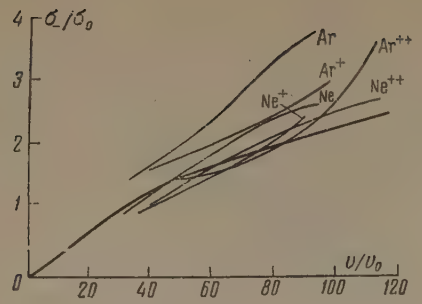

FIG. 5. Total ionization cross sections σ_- compared with Firsov's theoretical curve (heavy line). The fast primary particles are designated at the end of each experimental curve (thinner lines). v_0 and σ_0 are characteristic values of the velocity and cross section calculated from [13].

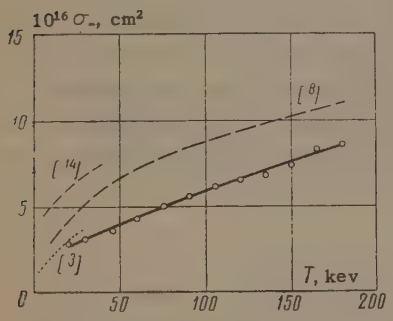

FIG. 6. Total cross sections for argon ionization by Ne^+ given by different authors. The solid curve represents our present work.

best agreement with [3]. The cross section given in [8] exceeds somewhat the experimental error limit in our work and in [3]. The curve in [14] lies considerably above all other curves.

The measurements of σ_- in the ionization of argon by fast Ne and Ar atoms are compared in Fig. 7. Our curve for Ar-Ar agrees well with [5], while for Ne-Ar our results agree with [3] within the limits of error.

The discrepancies between the total ionization cross sections given by different investigators result mainly from the difficulty of excluding extraneous effects while measuring electron currents, and also possibly while measuring gas pressures. The differences between the most recent values given for the cross sections [3,5,8] do not exceed $\pm 25-30\%$, which is smaller than the discrepancies in earlier work.

B. Total Cross Sections σ_{0n} for the Production of Slow Ions with Different Charges

Figure 8 shows curves of the total cross sections σ_{0n} for the production of slow argon ions with different charges as functions of the velocities of Ar atoms and of Ar^+ and Ar^{2+} ions. Figure 9 shows analogous curves for fast Ne atoms and for Ne^+ and Ne^{2+} ions. The total cross section for the production of slow ions with a given charge is always smaller for fast atoms than for fast ions of the same element. The largest

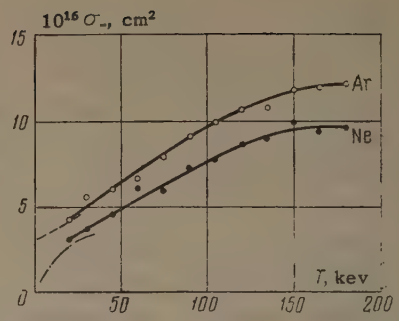

FIG. 7. Total cross sections for argon ionization by fast Ne and Ar atoms given by different authors. Solid curves – present work; dashed curve – from [3] for Ne-Ar; dash-dot curve – from [5] for Ar-Ar.

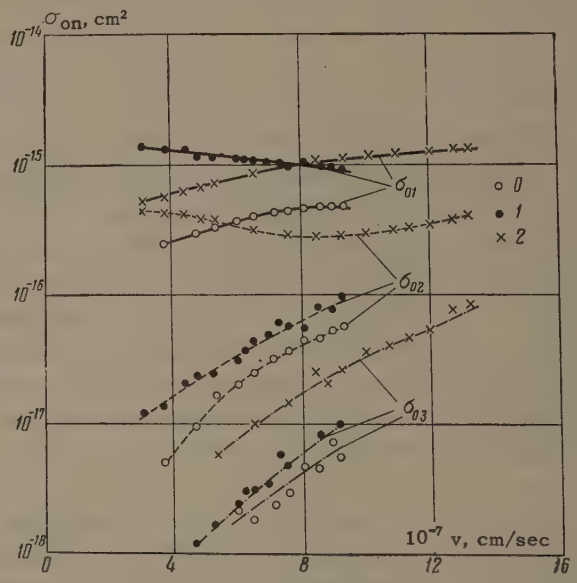

FIG. 8. Total cross sections σ_{01}, σ_{02}, σ_{03} for the production of slow ions with different charges in the ionization of argon by fast Ar, Ar^+, and Ar^{2+}. The fast-particle charges are identified by the numbers 0, 1, and 2.

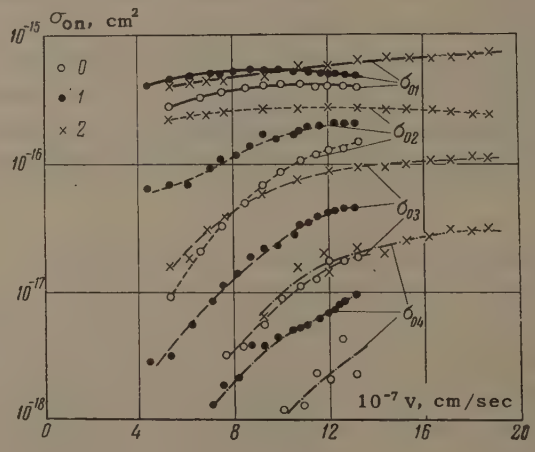

FIG. 9. Total cross sections σ_{01}, σ_{02}, σ_{03} and σ_{04} for the production of slow ions with different charges in the ionization of argon by fast Ne, Ne^+, and Ne^{2+}. The fast-particle charges are identified by the numbers 0, 1, and 2.

total cross sections for the production of slow ions with charges 2, 3, and 4 are achieved with doubly charged ions.

This basic experimental result can be accounted for as follows. The magnitudes and energy depend-

ences of the cross sections for slow-ion production must reflect the characteristics of the basic processes, which can vary for the different cases. In atom-atom collisions slow ions are produced mainly through pure ionization. In ion-atom collisions analogous cross sections can include a considerable contribution from charge-exchange and from ionization with pickup. It follows from [6] and [7] that charge-exchange processes can possess large cross sections, especially if the fast ions are multiply charged and the charge-exchange process is exothermic. Pure ionization cross sections should increase with velocity up to $v \approx e^2/\hbar$ (electron velocity in the Bohr hydrogen atom).[10] Therefore σ_{0n} in atom-atom collisions increases continuously in the given velocity range. The cross sections for different processes of electron capture by fast ions can either increase or decrease with increasing velocity; therefore the curve of the total cross section $\sigma_{0n}(v)$ in ion-atom collisions can exhibit a minimum.

This situation can be illustrated by comparing some of our curves with those given by Flaks and Solov'ev[6] who measured with mass spectrometers the cross sections for electron capture by fast Ar^{2+} ions in argon. For Ar^{2+}-Ar, Fig. 10 gives our cross sections σ_{01} and σ_{02}, and also σ^{20} and σ^{21} for the production of fast Ar and Ar^+, respectively, taken from [6]. These four

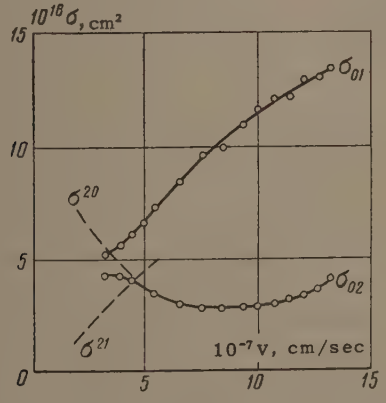

FIG. 10. Total cross sections for the production of slow ions with charges 1 and 2 (σ_{01} and σ_{02}), and cross sections for the production of fast secondary particles (σ^{21} and σ^{20}) in the Ar^{2+}–Ar case. The curves for σ^{21} and σ^{20} were taken from [6].

cross sections can be expressed in terms of partial cross sections for the most probable processes requiring the lowest relative energy expenditure, as follows:

$$\sigma_{01} \approx \sigma_{01}^{22} + \sigma_{01}^{21}, \quad (7)$$

$$\sigma_{02} \approx \sigma_{02}^{22} + \sigma_{02}^{21} + \sigma_{02}^{20}, \quad (8)$$

$$\sigma^{21} \approx \sigma_{01}^{21} + \sigma_{02}^{21}, \quad (9)$$

$$\sigma^{20} \approx \sigma_{02}^{20}, \quad (10)$$

where σ_{01}^{22} and σ_{02}^{22} are the cross sections for pure ionization with the removal of one or two electrons from gas atoms, σ_{01}^{21} is the cross section for single-electron charge exchange, σ_{02}^{21} is the cross section for ionization with single-electron pickup, and σ_{02}^{20} is the cross section for resonant two-electron charge exchange.

In Fig. 10 the lower end of the σ^{20} curve is seen to coincide with the σ_{02} curve. This can occur only if in (8) we have

$$\sigma_{02}^{20} \gg \sigma_{02}^{22} + \sigma_{02}^{21}, \quad (11)$$

i.e., slow doubly-charged argon ions are produced at velocities $v \leq 6 \times 10^7$ cm/sec mainly through resonant two-electron charge exchange. The two other possible processes—ionization with single-electron pickup and pure ionization with the removal of two electrons—are endothermic with an energy expenditure of the order of tens of electron volts. Therefore their contributions to σ_{02} should increase with velocity, leading us to expect the minimum of the $\sigma_{02}(v)$ curve that is actually observed.

The curves for σ_{01} and σ^{21} also exhibit appreciable similarity. These cross sections are of the same order of magnitude and both curves rise, with $\sigma_{01} > \sigma^{21}$ at their intersection. From (7) and (9) we obtain

$$\sigma_{01}^{22} > \sigma_{02}^{21}. \quad (12)$$

The energy expenditure for both processes is of the order of the first ionization potential of argon. However, it seems to us that the inequality of these cross sections reveals a general phenomenological characteristic of inelastic processes that is worth noting. This characteristic is the fact that with the same energy expenditure the less probable process is that in which more electrons participate. The cross section for pure single-electron ionization is on the left in inequality (12), while on the right we have the cross section for ionization with pickup. In the latter process two electrons are removed from the atom, and one of these is captured by the ion, i.e., at least two electrons participate in the process.

In conclusion the authors wish to thank Professor V. M. Dukel'skii for his interest, and I. T. Sheftel' for providing the thermistors and making valuable suggestions regarding their utilization.

[1] V. V. Afrosimov and N. V. Fedorenko, ZhTF

27, 2557 (1957), Soviet Phys.-Tech. Phys. 2, 2378 (1957).

[2] Il'in, Afrosimov, and Fedorenko, JETP 36, 41 (1959), Soviet Phys. JETP 9, 29 (1959).

[3] I. P. Flaks, ZhTF 31, 367 (1961), Soviet Phys.-Tech. Phys. 6, 263 (1961).

[4] Fedorenko, Flaks, and Filippenko, JETP 38, 719 (1960), Soviet Phys. JETP 11, 519 (1960).

[5] Sluyters, de Haas, and Kistemaker, Physica 25, 1376 (1959).

[6] I. P. Flaks and E. S. Solov'ev, ZhTF 28, 599 (1958), Soviet Phys.-Tech. Phys. 3, 564 (1958).

[7] I. P. Flaks and E. S. Solov'ev, ZhTF 28, 612 (1958), Soviet Phys.-Tech. Phys. 3, 577 (1958).

[8] Fedorenko, Afrosimov, and Kaminker, ZhTF 26, 1929 (1956), Soviet Phys.-Tech. Phys. 1, 1861 (1956).

[9] N. V. Fedorenko and V. V. Afrosimov, ZhTF 26, 1941 (1956), Soviet Phys.-Tech. Phys. 1, 1872 (1956).

[10] N. V. Fedorenko, UFN 68, 481 (1959), Soviet Phys.-Uspekhi 2, 526 (1960).

[11] D. M. Kaminker and N. V. Fedorenko, ZhTF 25, 1843 (1955).

[12] Afrosimov, Il'in, and Fedorenko, ZhTF 28, 2266 (1958), Soviet Phys.-Tech. Phys. 3, 2080 (1958).

[13] O. B. Firsov, JETP 36, 1517 (1959), Soviet Phys. JETP 9, 1076 (1959).

[14] H. B. Gilbody and J. B. Hasted, Proc. Roy. Soc. (London) A240, 382 (1957).

Translated by I. Emin
185

SOME OBSERVATIONS ON THE SOLIDIFICATION OF HELIUM

A. I. SHAL'NIKOV

Institute for Physics Problems, Academy of Sciences, U.S.S.R.

Submitted to JETP editor May 18, 1961

J. Exptl. Theoret. Phys. (U.S.S.R.) 41, 1056-1058 (October, 1961)

Visual observations of the solidification of helium have been made. The difficulty of obtaining large blocks, even under conditions when the crystallization process can be controlled, in noted.

In all experiments on the properties of solid helium, it has usually been obtained under conditions where the apparatus itself (the pressure chamber) is connected to the external apparatus that produces the gas pressure by means of a narrow capillary. This method came under criticism in Cwilong's work[1] on the determination of the solidification point of helium in a glass piezometer, the pressure in which was produced by a change in volume of a metal bellows connected to it. The melting curves obtained by Cwilong below 1.8° K are considerably different from the curves obtained by Keesom and Keesom[2] and by Swenson[3] by the blocked capillary method. Unfortunately, Cwilong did not carry out observations on the characteristics of the solidified helium and confined himself only to the determination of the melting point, which was registered by the cessation of motion of magnetic needles placed inside the piezometer.

Keesom,[4] who first used a glass piezometer, could not for some reason observe the boundaries between the liquid and solid helium.

Since we wished to investigate the motion of electric charges in solid helium,[5] we naturally had to be sure of the quality of the crystals studied. For observation of the solidification process we initially used a glass test tube (Fig. 1a) made of No. 29 glass of diameter $^7/_9$ mm, the upper part of which was sealed to an iron-chromium stopper (N47KhB). This seal (in contrast with a 3S5 seal to kovar) stood up to any number of coolings and heatings without cracking. A 0.5 mm diameter platinum wire was sealed into the bottom of the tube.* The tube was connected through a 0.9/1.6 mm diameter capillary, shielded by a vacuum jacket, to a helium gasifier† by means of which a relative pressure up to 100 atm could be produced and maintained.

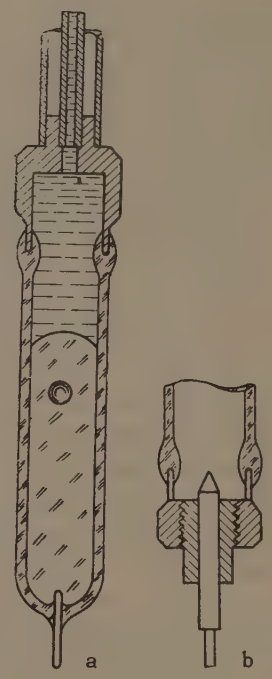

FIG. 1

Since the thermal conductivity of iron-chromium is very low, the test tube in apparatus already used in studying the motion of charges was provided with an iron-chromium stopper, through which a 2 mm diameter copper conductor of cold was passed (Fig. 1b).

With a favorable choice of illumination, the boundaries between the solid and liquid helium are very well visible, so that the solidification process could be recorded on motion picture film (Fig. 2).

The means by which the liquid solidifies depends on many factors, difficult to control because the heat generated on solidification must be led away through the two-phase system produced, the overall thermal conductivity of which varies within wide limits.

*The platinum wire (Fig. 1a) had no noticeable effect on the duration of the crystallization process.

†I would like to thank A. I. Filimonov and V. K. Tkachenko for the possibility of using the gasifier set up by them.

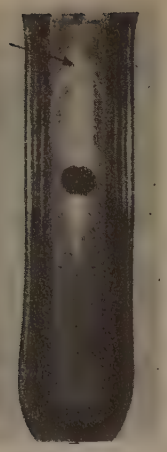

FIG. 2

It is difficult to obtain macroscopic blocks of solid helium even when the process is carried out very slowly, for it is very difficult in practice to achieve conditions under which the heat removal is through the lowest part of the apparatus. Even under conditions when the capillary transmitting the pressure is insulated from the ambient by vacuum shielding, it is not always possible to prevent the formation of centers in it.

In order to avoid this we even had to resort to heating the part of the capillary inside the vacuum shield (40 mm in length) which was in the immediate neighborhood of the tube. This procedure, however, produces at the same time a temperature gradient in the tube itself.

The following types of crystallization are generally observed.

1. If the pressure is increased relatively rapidly (~ 0.1 atm/sec) blocking of the capillary is observed and then an instantaneous solidification of the whole volume of the tube, which in this case appears to be filled with a mass reminiscent of "wet" snow. This mass only becomes transparent gradually when the pressure is increased considerably.

2. Sometimes on reaching the solidification point a "hail" of solid spherulites starts to precipitate in the liquid, and these gradually fill the whole volume of the tube.

3. For a sufficiently slow increase of the pressure ($\sim 0.01 - 0.05$ atm/min) the formation of an ideally transparent crystal starts at the surface of the copper rod let into the tube, and the layer of solid helium formed duplicates the contours of the cold conductor, as though marking out a surface of constant temperature. As the crystal grows its boundary deforms and the phase boundary, which crosses the tube by its continuous upward movement, becomes uneven. Formation of a crystal at the surface of the cold conductor is eased if a temperature gradient is produced in the liquid filling the tube, by heating the capillary or, correspondingly, by lowering the level of the liquid helium in the external bath. However, even when these measures are taken, the growth of several regular spherulites starting from the side walls of the tube is observed, which in the end usually leads to the blocking off of some volume of the liquid, which because of the small compressibility of solid helium cannot be transformed into the solid state, even upon considerable increase in pressure.

4. Apparently the purity of the helium also affects the crystallization process. Generally, in the first experiments with newly assembled apparatus, blocking of the capillary takes place more easily and also the formation of centers of crystallization, leading to the falling out of "hail."

We carried out some experiments with He^3 along with the observations of the crystallization of He^4.

We did not observe any special features in the solidification of He^3, but we have the impression that the formation of large blocks in He^3 is appreciably easier and that the whole solidification process proceeds more regularly. We used apparatus with electrodes [5] in the experiments with He^3. After the formation of a crystal at the cold conductor and the subsequent gradual filling of the apparatus with "ice," the appearance of a transparent solid phase in the interelectrode region was invariably observed. We intend to study the solidification of He^3 in more detail later.

A report has recently appeared [6] on the observation of a new modification of solid He^4. There was no evidence of this new modification in our observations on the crystallization process. This can be explained, however, by the very limited region of existence of the new crystalline modification and the low accuracy in the measurement of pressure in our experiments.

In conclusion I would like to thank B. N. Esel'son for discussion and D. I. Vasil'ev for help in the experiments.

[1] B. M. Cwilong, Phys. Rev. **88**, 135 (1952).

[2] W. H. Keesom and Miss A. P. Keesom, Leiden Comm. **20**, 224d, 224e (1933).

[3] C. A. Swenson, Phys. Rev. **79**, 626 (1950).

[4] W. H. Keesom, Leiden Comm. **17**, 184b (1926).

[5] A. I. Shal'nikov, JETP **41**, 1059 (1961), this issue, p. 755.

[6] J. H. Vignos and H. A. Fairbank, Phys. Rev. Lett. **6**, 265 (1961).

Translated by R. Berman
186

MOTION OF CHARGES IN LIQUID AND SOLID HELIUM

A. I. SHAL'NIKOV

Institute for Physics Problems, Academy of Sciences, U.S.S.R.

Submitted to JETP editor May 18, 1961

J. Exptl. Theoret. Phys. (U.S.S.R.) 41, 1059-1063 (October, 1961)

The motion of charges in liquid and solid helium has been investigated over the temperature range between 4.2 and 1.5° K. A dependence of the currents in solid helium upon the quality of the crystals produced has been established.

THE nature of electric charges in liquid helium and the mechanism of their motion cannot as yet be regarded as completely explained, despite the fact that a considerable number of papers have already been devoted to this question.[1-8] In particular, the fundamental problem of the nature of the anomalously large effective masses, whose possible existence was pointed out in our first note,[6] still remains unsolved.

The polarization and conductivity hysteresis phenomena which we observed led us at that time to suggest that the current carriers consist principally of submicroscopic impurity particles carrying charges of both signs. If one accepts Atkins' hypothesis,[5] however, the polarization phenomena evidently find a satisfactory explanation within its framework without assuming the presence of impurities, which can, nevertheless, exert a strong influence upon the conditions of a real experiment.

We present here, briefly, the results of experiments on the motion of charges in liquid helium, under pressures ranging from equilibrium to the solidification point, which, it seems to us, can provide further data on the nature of the charge carriers.

We employed both all-glass and glass-metal systems (Fig. 1), whose construction permitted measurement of weak electrical currents in liquid and solid helium over a wide range in pressure, as well as visual observation of the helium solidification process.

The experimental volume containing the electrodes was connected through a glass or metal capillary, protected by a Dewar jacket, to a helium gasifier capable of producing and maintaining pressures up to 100 atm.* To one of the electrodes, made of stainless steel, there was attached a molybdenum disc (4 mm in diameter), covered with a layer of titanium tritide which served as a source, emitting electrons of 5.7 kev average energy. Another molybdenum disc—the electrometer electrode—was rigidly fastened to the first through a system consisting of two pairs of glass beads into which were sealed ferrochromium wires serving as guard electrodes.

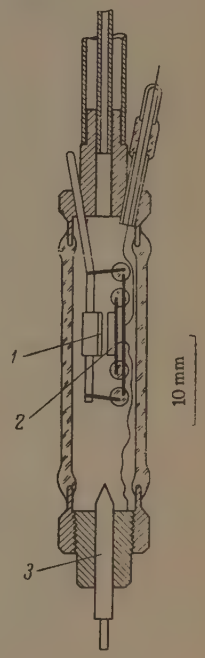

FIG. 1. Diagram of the apparatus: 1 – source, 2 – electrometer electrode, 3 – copper rod.

Prior to an experiment the experimental volume and the gasifier reservoir connected to it were filled with liquid helium, condensed from a glass gasholder and passed, before condensation, through a trap containing highly-purified activated charcoal at 90° K.

The current through the interelectrode gap was measured with an ÉMU electrometer. For the current measurements in solid helium an electrostatic screen, manipulated through the cover of the surrounding helium Dewar, was moved into place over the normally uncovered experimental chamber.

*Throughout this article, pressure is to be understood to mean relative (above atmospheric).

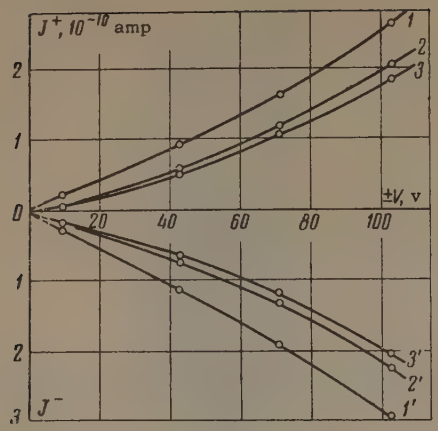

FIG. 2. Variation of current with field intensity in liquid helium: curves 1, 1′ – for 0 atm, 4.2 °K; curves 2, 2′ – for 5 atm, 1.65 °K; curves 3, 3′ – for 10 atm, 1.65 °K.

Voltage-current characteristics for one of our systems (with a source emitting 7.95×10^7 electrons/sec and an interelectrode spacing of 500 μ), at temperatures of 1.65 and 4.2° K and pressures of 0.5 and 10 atm, are shown in Fig. 2. As can be seen from the figure, the current in the liquid helium reaches 2.5×10^{-10} amp for an electric field intensity of ~2000 v/cm; this is only an order of magnitude less than the total saturation ion current of the source.

Curves showing the variation in current (for a field intensity of 3000 v/cm) with increasing pressure at temperatures between 2.0 and 4.2° K (obtained in an apparatus containing a source emitting 7.15 electrons/sec, with an electrode spacing of 340 μ), as well as the pressure dependence of the liquid density,[9] are presented in Figs. 3 and 4.

In our first systems, in which the electrodes were arranged horizontally, we were quite unable, by further increase in pressure, to cause crystallization to take place in such a way as to insure

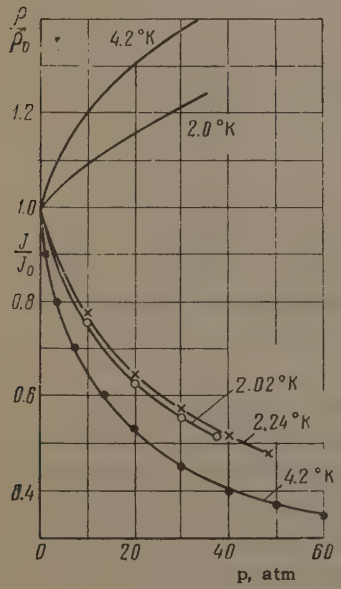

FIG. 3. Relative variation of current with pressure in liquid helium, and relative variation of liquid helium density with pressure.

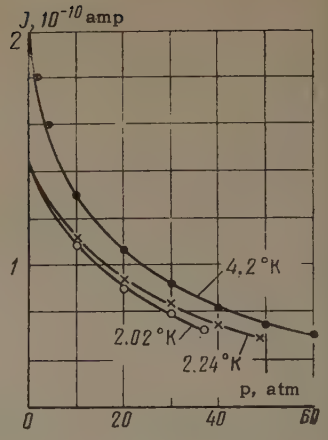

FIG. 4. Variation of current in liquid helium pressure.

that none of the liquid phase was blocked off in the space between the electrodes. We made use thereafter of systems in which the interelectrode region extended vertically, which considerably simplified the process.

As is evident from Figs. 5 and 6, the current changes discontinuously at the solidification point; the ratio of the currents before and after the discontinuity depends critically, however, upon the conditions under which crystallization occurs. Thus, besides the true decrease in the current resulting from the change in the character of the motion of the charges due to the transition of the helium into the crystalline solid state, discontinuities are very frequently observed whose magnitude is governed by partial freezing of the helium filling the space between the electrodes.

However, even the "true" discontinuity is found to depend upon the way in which the liquid helium crystallizes. When the helium solidifies into a finely-crystalline mass ("wet snow")[9] with subsequent compaction under pressure, the discontinuity is found to be most pronounced: the current falls by 30 — 50 times, while beyond the

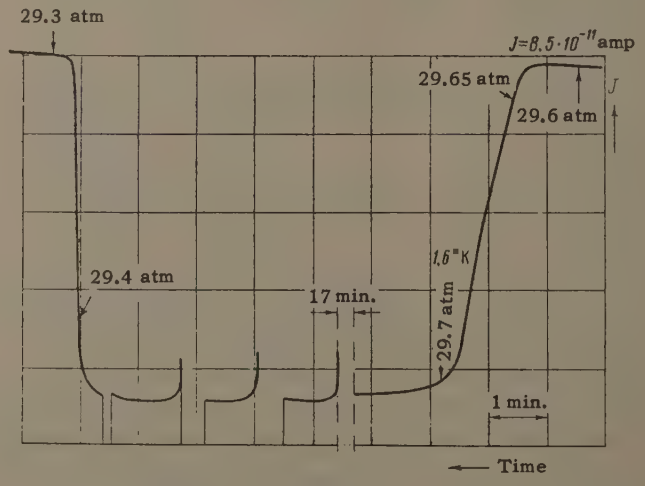

FIG. 5. Currents during solidification and melting, and currents in solid helium (pressure given at points indicated by arrows).

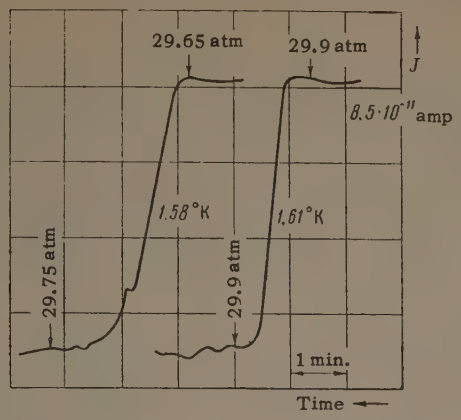

FIG. 6. Currents for two successive helium solidification runs.

discontinuity, even in the solid helium, there is observed a current variation of the type associated with polarization, as well as a general instability of the conductivity evidently connected with changes in the mechanical stresses and deformations.*

In certain cases, however, (Fig. 6), we succeeded in observing currents in solid helium (evidently monocrystalline or composed of coarse crystals) which differed in all by only a few times (≥ 3) from the currents in the liquid prior to its solidification. Figure 5 shows a current record during the solidification process, obtained with an ÉMU electrometer and a chart recorder. In this experiment the current in the solid helium fell by a factor of seven as compared with the current in the liquid at 29.6 atm, i.e., to 1.2×10^{-11} amp.†

It is evident from the curves showing the variation of current with time (Fig. 5), the measurement beginning within a fraction of a second after registering the capacitive surge, that as the pressure is removed and then reapplied, polarization and hysteresis effects are observed which are characteristic of a solid body in which charges of both signs are in motion.

An equilibrium value for the current is reached more rapidly when the charges moving in the region between the electrodes are predominantly negative in sign; when the polarity is reversed, equilibrium is established somewhat more slowly.

It must also be noted that reversible variations of current with pressure are observed only for good crystals, and only over that small pressure interval for which the boundary of the growing crystal is in direct contact with a sufficiently extensive liquid surface. Once the crystal has completely filled the experimental space, and the phase boundary has risen into the capillary, the pressure ceases for all practical purposes to be exerted throughout the whole volume of the crystal.

Although we performed many measurements over a broad temperature range from 4.2 to 1.3° K, disturbances associated with polarization made it hard nevertheless to secure reproducible results. It is difficult therefore to draw definite conclusions regarding the temperature dependence of the current-pressure relation below 2° K (where the effect of temperature is relatively slight), or the influence of the direction of the field within the interelectrode region upon the observed effects. It must be borne in mind that under our experimental conditions the measurements were performed over a period on the order of ten minutes, and if, for example, the current at the beginning of the measurement were higher by 15 — 20% for one polarity than for the other, then at the end of the experiment, the opposite pattern would usually be observed.

Nevertheless, on the basis of all of our observations we can draw the following definite conclusions:

1. The currents in solid helium are governed principally by the quality of the crystals obtained, and are near, in order of magnitude, to the currents in the liquid. The conclusion reached by Careri, Fasoli, and Gaeta [7] regarding the impossibility of observing the movement of charges in solid helium is, as follows from our experiments, in error.*

2. Inasmuch as charges of both signs may move in solid helium, we have no basis whatever for regarding their structure as different from that which they possess in the liquid.

3. Besides the charge carrier structure common to both liquid and solid helium, there are also present in the liquid charges whose structure is associated with the presence of impurities in the helium.

4. An increase in the density of liquid helium leads to a decrease in the mobility of carriers of both signs.

*This, clearly, is the situation encountered by Careri, Fasoli, and Gaeta, [7] who conclude that currents in solid helium cannot be measured at all.

†The slopes of the curves in Figs. 5 and 6 are determined by the ratio of the areas of the interelectrode regions occupied by the liquid and solid phases as the liquefaction or solidification proceeds.

*We have also performed a few exploratory experiments with He^3 which we propose to describe in more detail at some later date. We shall only mention here that the current in solid He^3 falls by only a small amount ($\sim 40\%$) as compared with that in the liquid. A substantial decrease in the current with a further, relatively slight, increase in pressure is also characteristic of solid He^3.

5. In liquid helium it is evident that charges are transported chiefly by carriers (of large effective mass) associated with the presence of impurities. At the same time, currents in liquid helium may also be carried by other kinds of charges (for example, electrons and holes), which, evidently, are responsible for currents in crystalline helium.

In conclusion, I wish to thank D. I. Vasil'ev for his aid in conducting the measurements.

[1] R. L. Williams, Can. J. Phys. **35**, 134 (1957).

[2] Careri, Reuss, Scaramuzzi, and Thomson, 5th Int. Conf. on Low Temp. Phys., 1957, Wisconsin, p. 79; Proc. 5th Int. Conf. on Low Temp. Phys. and Chem., 1957, Univ. of Wisconsin Press, 1958, p. 155.

[3] L. Meyer and F. Reif, Phys. Rev. **110**, 279 (1958).

[4] Careri, Scaramuzzi, and Thomson, Nuovo cimento **13**, 186 (1959).

[5] K. R. Atkins, Phys. Rev. **116**, 1339 (1959).

[6] R. G. Arkhipov and A. I. Shal'nikov, JETP **37**, 1247 (1959), Soviet Phys. JETP **37**, 888 (1960).

[7] Careri, Fasoli, and Gaeta, Nuovo cimento **15**, 774 (1960).

[8] F. Reif and L. Meyer, Phys. Rev. Lett. **5**, 1 (1960); Phys. Rev. **119**, 1164 (1960).

[9] A. I. Shal'nikov, JETP **41**, 1056 (1961), this issue, p. 753.

Translated by S. D. Elliott
187

ASYMMETRY OF DOUBLE MOTT SCATTERING OF 45--245 kev ELECTRONS

P. E. SPIVAK, L. A. MIKAÉLYAN, I. E. KUTIKOV, V. F. APALIN, I. I. LUKASHEVICH, and G. V. SMIRNOV

Submitted to JETP editor May 18, 1961

J. Exptl. Theoret. Phys. (U.S.S.R.) 41, 1064-1068 (October, 1961)

By using double Mott scattering from gold, we have measured the asymmetry in the scattering of electrons, for energies 45 — 245 kev, using angles $\theta_1 = \theta_2 = 120°$.

1. INTRODUCTION

MOTT scattering of electrons is the most sensitive method for measuring their polarization, and has attracted the attention of experimenters in connection with nonconservation of parity in β decay. The sensitivity of the method is characterized by the quantity S which determines the azimuthal asymmetry of the scattering: $I \sim 1 + PS \cos \varphi$ where I is the intensity of the scattered electrons, P their degree of polarization, and φ the azimuthal angle. The quantity S depends on the polar angle, the electron energy and the atomic number of the scatterer. Since the asymmetry is expressed in terms of the product PS, to determine the polarization one must have reliable data concerning the value of S.

The function S was first calculated theoretically by Mott.[1,2] The most precise values for the case of scattering by mercury[3] and gold[4] were computed by Sherman and Nelson, neglecting the screening by the atomic electrons. The screening was included in the work of Mohr and Tassie,[5] Bartlett and Welton,[6] which showed that for electron energies around 120 kev the effect of screening is still very noticeable and that its effect on the value of S can amount to 10 — 15%. However, it is now not clear just how reliable these estimates are.

The quantity S can be found from an experiment on double Mott scattering of unpolarized electrons,[1] since in this case the asymmetry is equal to the product $S(\theta_1) S(\theta_2)$, where θ_1 and θ_2 are the angles for the first and second scatterings. The authors of [7] were the first to succeed in observing the asymmetry in double scattering. Later there was a whole series of experiments for the purpose of obtaining a quantitative measure of the effect. A Japanese group[8] obtained values for S in the energy range 60 — 120 kev. The data were almost half the theoretical values. These authors did not include the depolarizing effect of multiple scattering, which is probably the main reason for the large discrepancy.

The angular dependence of S was studied in papers by Pettus[9] and Nelson and Pidd.[10] The results quantitatively confirm the predictions of the theory. But the precision of these measurements is left in doubt, since the authors did not take into account multiple scattering in the scatterers and also apparently did not succeed in eliminating the effect of electrons scattered from the walls of the apparatus. In the present work, we have set ourselves the task of obtaining much more precise values of the function S for the energy range 45 — 245 kev, for an angle $\theta = 120°$. From the point of view of measurements of the degree of polarization, the value of S in the region of 120° is of most interest, since it reaches a maximum there.

2. MAIN FEATURES OF THE EQUIPMENT AND CONTROL EXPERIMENTS

Description of the arrangement. We used a rectifier which supplied voltages up to 300 kev, with a value known to ±2%. After a preliminary magnetic analysis, the well-collimated beam of electrons 1 (cf. Fig. 1) 12 mm in diameter entered a chamber containing the first scatterer 2. Electrons scattered through an angle of 120° passed into another chamber containing the second scatterer 3, and after a second scattering at an angle of 120° ± 3° were recorded by a pair of Geiger ring counters 4 and 5, placed at a distance of about 20 cm from the second scatterer.

Scattering from the walls of the apparatus. Electron spectra. The main difficulties which must be overcome in an experiment on double scattering are due to unwanted scattering of the electrons from the walls of the apparatus. To reduce this effect, we provided "traps" at the points of maxi-

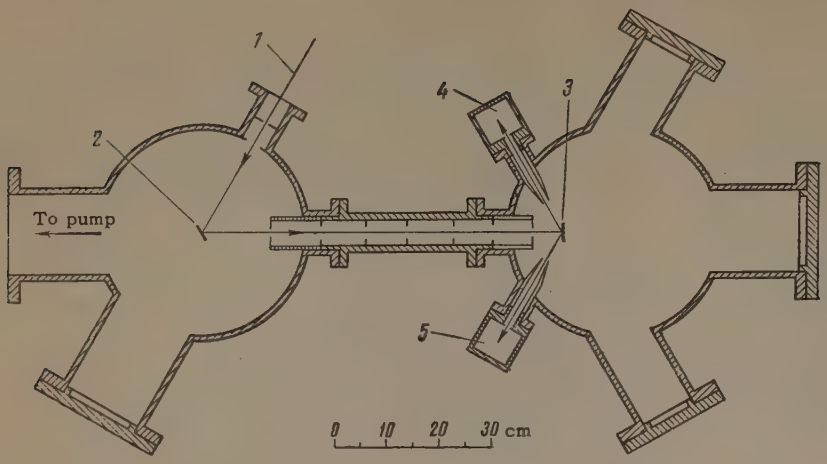

FIG. 1. Experimental arrangement: 1 – beam of accelerated electrons, 2 –first scatterer, 3 – second scatterer, 4, 5 – Geiger counters.

mum irradiation of the walls, the linear dimensions of the chambers were made relatively large (40 cm) and their internal surfaces were covered with Plexiglas. The separation of the first and second scatterers was chosen equal to ~ 75 cm, which enabled us to eliminate the direct bombardment of the second scatterer by electrons scattered from the walls of the first chamber and from the holder of the first scatterer.

Nevertheless this does not completely eliminate the background of scattered electrons. Electrons scattered from the walls of the first chamber can always strike the first scatterer, be scattered from it and enter the beam going toward the second scatterer. Similarly, electrons scattered from the walls of the second chamber can enter the counters. The second chamber had been used previously in an experiment for measuring the longitudinal polarization of β electrons.[11] Detailed studies made earlier and repeated for various electron energies in the present work showed that the effect of scattering from the walls is negligibly small.

To study the number of extraneous electrons which can reach the second scatterer from the first chamber, a series of control experiments was made. At the position of the second scatterer we placed a Geiger ring counter with a window which passed electrons with energy above 15 kev. Then the first scatterer was removed, and instead a thin foil was placed somewhat further from the center of the chamber along the axis of the primary beam, arranged so that electrons scattered from it could not enter directly into the second chamber, but gave a strong "illumination" of the walls of the first chamber. As was to be expected, no increase in counting rate was observed. Then another scatterer was placed at the entrance of the collimator leading to the second chamber. This scatterer was shielded from electrons directly scattered from the foil, but could be struck by electrons scattered from the walls. We thus succeeded in imitating the actual conditions of arrival of extraneous electrons at the second scatterer.

These experiments showed that there are extraneous electrons arriving at the second scatterer. There were very few at low energies, but their number increased markedly with increasing energy, and in the range 150 — 200 kev the fraction of such electrons reached 1.5 — 2%. Further study showed that these electrons have an energy which is several times smaller than that of the main group. Therefore their relative intensity is strongly increased at the second scattering, which can lead to considerable errors.

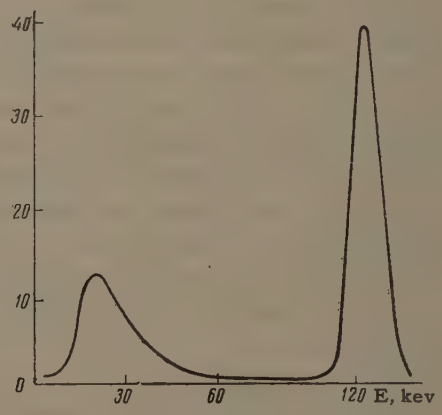

FIG. 2. Spectrum of doubly scattered electrons.

As an example we show in Fig. 2 the spectrum of the doubly scattered electrons, obtained under operating conditions using a spectrometer placed at the location of one of the counters. To get a sizeable counting rate, the resolving power was set equal to 10%, which explaines the rather large width of the main peak. Its true halfwidth did not exceed 2%. Similar spectra were measured over the whole energy range from 45 to 250 kev.

E, kev	$S_{theor}(120°)$	$S_{exp}(120°)$	$\Delta S/S_{exp}$, %	S_{exp}/S_{theor}
45	0.364	0.286	4	0.79
63	0.382	0.337	4	0.88
83	0.397	0.365	2.5	0.92
133	0.418	0.385	2.5	0.92
170	0.424	0.390	2.5	0.92
204	0.427	0.413	2	0.97
245	0.426	0.411	2	0.96

These measurements disclosed the following picture. The "soft" electrons begin to appear for accelerating voltages around 60 kv, their relative intensity increases rapidly with increasing accelerating voltage, and at 250 kv already exceeds somewhat the intensity of the main group. In addition, the "soft" electrons have an energy which is 4 — 6 times smaller than that of the main group, and between these groups there is a large energy interval from which electrons are practically absent. This made it possible to get rid of the extraneous electrons by using aluminum filters. The filter thicknesses were chosen by using the spectrometer. They increased with increasing primary energy, going from 0.3 mg/cm^2 at 45 kev to 12 mg/cm^2 for 245 kev. Later on, under operating conditions at several energies it was shown that a reduction of the filter thickness by $1\frac{1}{2}$ — 2 times did not change the measured value of S by more than 2%.

Scatterers. We used gold scatterers with thicknesses ranging from 16 to 200 μg/cm^2. The second scatterers were obtained by evaporating gold onto a film of collodion, whose thickness was 20 μg/cm^2 for the thinnest scatterers. The fraction of electrons scattered from the film was found experimentally by "difference" irradiation in the electron beam before and after depositing the gold. For the thinnest scatterers this fraction amounted to 6%. An aluminum sheet 0.1 μ thick was used as the backing for the first scatterers. The fraction of electrons scattered from the aluminum was 1 — 12%.

3. MEASUREMENTS AND RESULTS

Treatment of multiple scattering. As the measurements of the value of S^2 for different scatterer thicknesses showed, the depolarizing effect of multiple scattering is very large even for relatively thin layers. For example, the thickness of second scatterer, for which the value of S^2_{exp} is reduced by a factor of 1.3 relative to the value for zero thickness, is 350 μg/cm^2 for 245 kev, and 140 and 50 μg/cm^2 for energies of 133 and 60 kev. Because of this, at each energy we made measurements for several (usually six or seven) scatterers and extrapolated the results to zero thickness. For a correct extrapolation it is necessary to know precisely only the relative thicknesses of the layers. These were found to ~ 1% by comparing the intensities of electrons scattered from the various foils. To reduce the errors from the extrapolation, we used very thin scatterers; the extrapolated value of the asymmetry differed from the value obtained with the thinnest scatterer by no more than 5 — 8%. The only exceptions were the scatterers used for the measurements at 45 kev, for which this difference reached 15%. Here it was unreasonable to use thinner scatterers, because of the large increase in the corrections for scattering of electrons from the backing.

Elimination of apparatus asymmetry. To eliminate apparatus asymmetries, the measurements with the gold scatterer were followed by measurements in which the first scatterer was replaced by a foil of aluminum. One must be very careful in such measurements. When one uses thick layers of aluminum, there is a noticeable "softening" of the electrons. For example, as was shown by the measurements with scatterer thickness 5 μ and accelerating voltage 45 kv, the energy spread of the scattered electrons is 30 — 40%. This can lead to errors, since it is very difficult to achieve the condition where the relative efficiency of the counters shielded by filters is energy independent to a high degree. In this connection we recall that an error of 1% in determining the apparatus asymmetry coefficient leads to an error of 5 — 10% in the value of S^2. For this reason we used quite thin layers of aluminum in the measurements: 1 μ for the lowest energies, 2 μ for energies 80 and 133 kev, and chose a foil thickness of 5 μ starting from an energy of 170 kev.

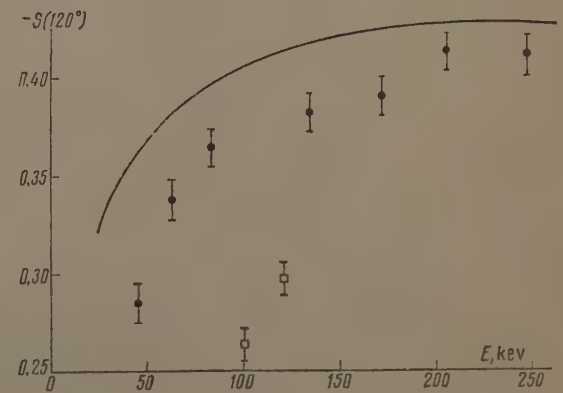

FIG. 3. Experimental results: • — this paper; □ — data of[8]. The solid curve is the computation of[3,4], which does not include screening.

Corrections. The following corrections were made to the measurements of S. Corrections for:

1. Scattering of electrons from the backing of the gold layers, amounting to a total of 1 — 10% for both scatterers.

2. Polarization of electrons scattered by the aluminum in the measurements of apparatus asymmetry, 3 — 4%.

3. Finite angular spread, 0.5%.

The results of the measurements are given in the table. The last column gives the ratio of the experimental value of S to the value obtained from the computations.[3,4] The errors arising in the interpolation of the data of [3,4] do not spoil the precision of the computations, which are estimated by the author to be 1%. As we see from the table, the discrepancy between the theoretical values, which were obtained omitting screening, and the experimental values decreases with increasing energy. But even at energies of 200 — 250 kev, there remain small deviations amounting to 3 — 4% ± 2%.

Figure 3 shows the data of the present work, the results of Sherman's calculations,[3,4] and the data of Ryu[8] for energies of 100 and 120 kev. We are not aware of any other measurements of the value of S(120°) by experiments on double scattering.

In conclusion, we mention the work of Bienlein et al[12] who studied the asymmetry of Mott scattering, using the polarized electrons from Co^{60} as a source. They studied the angular dependence of S and its dependence on the atomic number of the scatterer. In their work the absolute values of S(120°) for energies of 120, 155 and 209 kev were obtained under the assumption that the polarization of the β electrons is exactly equal to the ratio of the velocity of the electron to the velocity of light. Such a determination of S is not an internally complete experiment, and the result may turn out to be wrong, since even in the case of allowed transitions one observes considerable differences in the polarization of the electrons emitted from different nuclei.[11]

[1] N. F. Mott, Proc. Roy. Soc. (London) **A124**, 425 (1929).

[2] N. F. Mott, Proc. Roy. Soc. (London) **A135**, 429 (1932).

[3] N. Sherman, Phys. Rev. **103**, 1601 (1956).

[4] N. Sherman and D. Nelson, Phys. Rev. **114**, 1541 (1959).

[5] C. B. O. Mohr and L. J. Tassie, Proc. Phys. Soc. (London) **A67**, 711 (1954).

[6] J. H. Bartlett and T. A. Welton, Phys. Rev. **59**, 281 (1941).

[7] Shull, Chase, and Myers, Phys. Rev. **63**, 29 (1943).

[8] N. Ryu, J. Phys. Soc. Japan **7**, 125, 130 (1952); **8**, 804 (1953).

[9] W. G. Pettus, Phys. Rev. **109**, 1458 (1958).

[10] D. Nelson and R. Pidd, Phys. Rev. **114**, 728 (1959).

[11] L. A. Mikaélyan and P. E. Spivak, JETP **37**, 1168 (1959), Soviet Phys. JETP **10**, 831 (1960); Nuclear Phys. **20**, 475 (1960).

[12] H. Bienlein et al., Z. Physik **154**, 376 (1959); **155**, 101 (1959).

Translated by M. Hamermesh
188

*INELASTIC INTERACTION OF PROTONS AND NUCLEONS AT AN ENERGY OF 9 Bev**

T. VISKY, I. M. GRAMENITSKII, Z. KORBEL, A. A. NOMOFILOV, M. I. PODGORETSKII, L. ROB, V. N. STREL'TSOV, D. TUVDENDORZH, and M. S. KHVASTUNOV

Joint Institute for Nuclear Research

Submitted to JETP editor May 18, 1961

J. Exptl. Theoret. Phys. (U.S.S.R.) 41, 1069-1075 (October, 1961)

The multiplicity dependence of the angular and energy characteristics of secondary particles in proton-nucleon collisions at 9 Bev is studied. A comparison is made with results of calculations [15,16] based on the single-meson scheme.

THE general properties of proton-nucleon (pN-interactions) at 9 Bev were described in earlier papers [2,3] (see also [4]). Certain important details of the phenomena, however, remained unclear, particularly those concerning the dependence of the angle and energy characteristics on the multiplicity and on the asymmetry of the c.m.s. angular distribution of the secondary protons in pn interactions. The present study was aimed at an investigation of these problems and at better results, which we had hoped to attain by increasing the statistical material and improving the procedure (more stringent selection of events, more accurate ionization measurement, and measurement of the signs of the secondary-particle charges).

We scanned the primary-proton tracks, by the accelerated method (see [5]), in a pellicle stack made up of NIKFI-R emulsions irradiated by 9-Bev protons inside the proton synchrotron of the Joint Institute for Nuclear Research. We scanned a total of 3 km of track and found about 8000 interactions. The mean free path for the interaction was found to be 35.9 ± 0.4 cm.

From among the interactions found we sorted out the cases that satisfied the criteria for collisions between protons and free or quasi-free nucleons. [2,3] A total of about 900 events of this type were found. In order to obtain the cleanest material on the proton-nucleon interaction, particular attention was paid to absence of a cluster in the center of the event, which could be due either to a very slow recoil nucleus or to a slow electron. We therefore chose for the measurement 425 such "clean" cases, of which 251 had an even number of secondary charged particles (pp interactions) and 174 had an odd number of prongs (pn interactions).

The fast secondary particles were identified by measuring the multiple scattering and the ionization density. We used the g/g_0 (relative ionization density) vs. $p\beta$ (for pions and protons) curves calculated by Barkas and Young. [6] These curves are shown in Fig. 1 together with the experimental points.

In addition, we determined the signs of the charges of the secondary particles from the deflection in the magnetic field of the proton synchrotron.* Using the procedure described by Gramenitskii et al, [7] we determined the quantity $\gamma_m = \theta_{meas}/\bar{\theta}_{mult}\sqrt{t}$, where θ_{meas} — actual change in the direction of the particle over the length t, and $\bar{\theta}_{mult}$ — mean square of the multiple-scattering angle at the same length. The length of the track was not less than 6 cm here. To verify the method we measured γ_m on the tracks of positive particles (particles from 2-prong events in pp interactions and particles identified as protons from the measurements of the ionization and scattering). For 14 out of 90 positive particles γ_m was negative, i.e., the sign of the charge, is incorrectly determined in (16 ± 4)% of the cases, owing to the influence of multiple scattering.

We also analyzed three-prong events among the pn interactions. In this case the number of positive particles was twice the number of negative ones. Actually 57 and 28 particles were observed with positive and negative γ_m, respectively, i.e., the ratio of the number of positive to negative particles was 2.0 ± 0.47. It can be concluded from this check that the sign of the charge of a particle with track longer than 6 cm is correctly determined in 80—85 percent of the cases.

The fast particles were measured and identified with tracks having dip angles φ less than or

*Some results of this investigation were also reported by V. I. Veksler. [1]

*During the time of irradiation the stack was in the 12 000 oe magnetic field of the proton synchrotron.

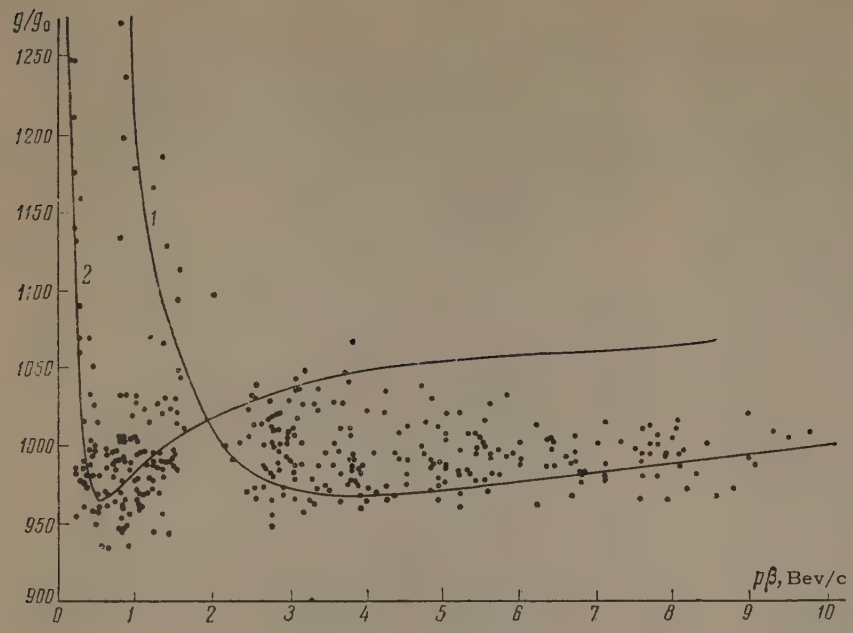

FIG. 1. The dependence of the relative cluster density g/g_0 on $p\beta$: 1 – proton; 2 – pions.

equal to 5°. Therefore to obtain the angle and momentum distributions and the mean values of the various quantities we introduced geometrical corrections [7] for the number of particles which have an angle φ greater than 5° for a given direction angle θ. In the calculation of the statistical errors under these conditions we used the previously obtained results.[8]

As noted earlier,[3] particles with $p\beta$ ranging from 1.5 to 2.5 Bev/c (region where the pion and proton curves intersect in Fig. 1) cannot be identified in practice by their ionization and scattering. The same reference cites some indirect arguments in favor of assuming the greater part of the particles entering into this region being pions. In addition to the foregoing, we can also advance the following arguments. It is natural to assume the ratio of the total number of pions to the number of charged particles in the pp interactions to be close to 1.5. This ratio, calculated from the inelasticity coefficient under the assumption that all the particles in the intersection region are protons, was found to be 2.41 ± 0.35. Thus, the assumption that all the particles in the "intersection region" are protons must be excluded.

Table I*

Multiplicity	Protons		Pions	
	p_c	$p_\perp$	p_c	$p_\perp$
2	1280±60	368±36	662±78	414±72
4	1010±50	439±37	393±30	260±28
6–8	920±70	549±71	442±43	355±45

*Momenta given in Mev/c units.

To estimate the percentage of protons in those particles we can use the result of indirect identification of the secondary positively-charged particles in the momentum interval 2.3—2.9 Bev/c, obtained with the aid of electronic circuitry in a study of the interaction between 9-Bev protons and beryllium nuclei. It was shown that in the secondary particles emitted with this momentum at 0—2° the number of protons is almost equal to the number of positive pions.*

If we assume that this is true in the entire "intersection region," then we obtain for pp interactions the ratio $n(\pi^{\pm 0})/n(\pi^{\pm}) = 1.40 \pm 0.23$.† It must be noted that many other characteristics of pp interaction, particularly the natural requirement of symmetry of the angular distribution of the pions and protons in the c.m.s., likewise do not contradict the foregoing assumption, which we have subsequently used in the reduction of all the experimental results.

In the analysis of the pp interactions, great interest is attached to the comparison of various characteristics of the secondary particles at different multiplicities. Table I lists the mean values of the c.m.s. momentum (p_c) and the transverse momentum of the secondary protons and pions from the pp interactions.

*The authors are grateful to M. F. Likhachev, V. S. Stavinskii, Ts'ui Yun-ch'an and Chang Nai-hsien, who communicated the results cited.

†In the calculation we assumed all the negative particles from the "intersection region" to be negative pions, and each positive particle was assumed equally likely to be a proton or a positive pion.

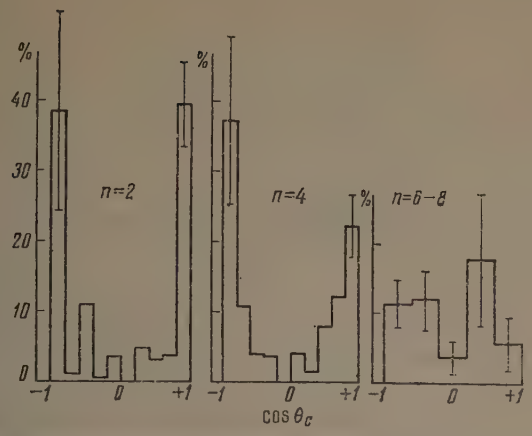

FIG. 2. Angular distribution of protons in the c.m.s. for different multiplicities in pp interactions. The ordinates represent the percentage of events.

From the data of Table I we can conclude that the average characteristics depend relatively little on the number of charged particles.*

The angular distribution of the protons in the c.m.s. for pp-interactions (Fig. 2) is highly isotropic at low multiplicity, and becomes close to isotropic on going to n = 6—8.

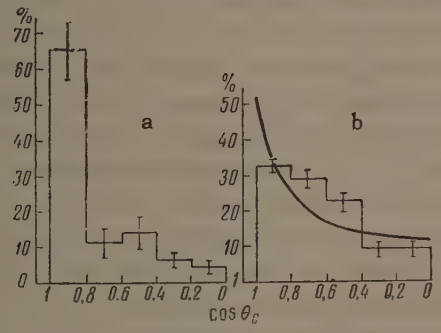

FIG. 3. Angular distribution of secondary protons (a) and pions (b) in the c.m.s., obtained in pp interactions; the smooth curve is calculated by the single-meson scheme.

Figure 3 shows the summary c.m.s. angular distributions of the protons and ions for all pp interactions. It is seen from the plot that the angular distribution of the pions is much closer to isotropic.

From the data of Table I we can readily calculate the total number of mesons as a function of the multiplicity. Table II lists the results of such a calculation together with data on the number of protons per interaction. It can be seen that the total number of mesons increases somewhat with increasing number of charged particles. In the case of large multiplicity (n = 6—8) there are practically no neutral mesons.

*The coefficient of inelasticity and the fraction of the energy lost by the proton (in the laboratory system) to the formation of pions were 0.56 ± 0.08 and 0.40 ± 0.05, respectively, for all pp interactions. These data agree, within the limits of errors, with the earlier results (see[3]).

Table II

Multiplicity	Total number of mesons	Number of charged mesons	Number of neutral mesons	Number of protons
2	2.0±0.26	0.96±0.16	1.04±0.30	1.04±0.16
4	4.16±0.34	2.72±0.18	1.44±0.38	1.28±0.18
6–8	4.12±0.44	5.04±0.26	—	1.32±0.26

For all the pp interactions taken together, the average number of protons, charged pions, and neutral pions is respectively 1.18 ± 0.10, 2.24 ± 0.14, and 0.90 ± 0.30. An analogous analysis was made for pn interactions.

Table III*

Multiplicity	Protons		Pions	
	p_c	$p_\perp$	p_c	$p_\perp$
3	1010±40	355±43	428±39	252±33
5	918±70	441±45	437±41	291±39
7–9	813±80	543±75	420±90	228±25

*Momenta given in Mev/c units.

Table III lists the mean values of the c.m.s. momentum and of the transverse momentum for different multiplicities.

As in the case of pp interactions, the dependence of the average secondary-particle characteristics on the multiplicity is relatively weak. The mean number of protons, charged pions, and neutral pions per pn interaction is respectively 1.11 ± 0.10, 2.82 ± 0.21 and 1.61 ± 0.49.*

The c.m.s. angular distribution of the protons shown in Fig. 4 is asymmetric, in accord with the results of the earlier investigations[2-4] (see also [10,11]).

As was shown in [12], the c.m.s. angular distribution of the charged pions should be symmetrical for pn interactions. The observed angular distribution of the pions (see Fig. 4) does not contradict this statement, for the difference in the number of pions emitted in the forward and backward hemispheres is 73 ± 50.

The analysis shows that the pN interactions have the following characteristic features:

1) A relatively small fraction of the primary energy of the proton (~ 40%) goes in the mean into pion production.

*It must be noted that the values given pertain only to pn interactions with n > 1 secondary prongs. The average number of protons per event for all pn interactions should be unity (see[9]). With our sampling, the average number of protons should be somewhat greater than unity.

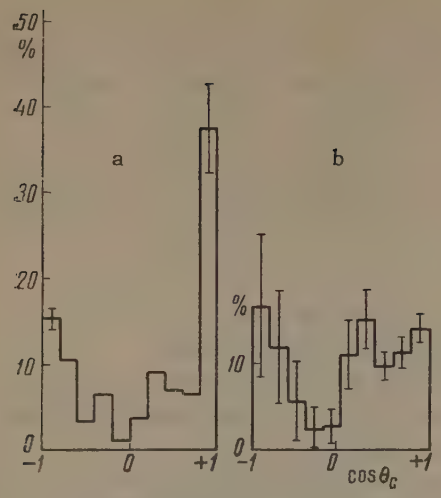

FIG. 4. Angular distribution of protons (a) and pions (b) in the c.m.s. for pn interactions.

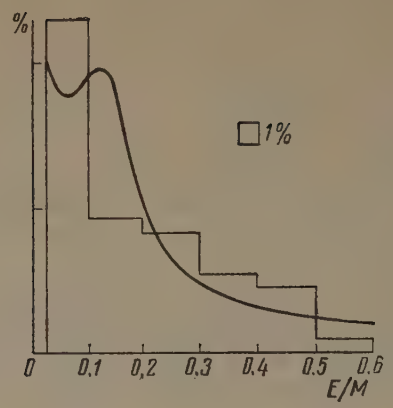

FIG. 6. Energy distribution of the recoil nucleons in pp interactions. Smooth curve – result of calculation by the single-meson scheme. Area under each column of the histogram corresponds to the number of cases in percent. The square on the figure indicates the scale.

2) The angular distribution of the protons in pp interactions is sharply anisotropic in the c.m s., and the degree of anisotropy decreases with increasing multiplicity.

3) The c.m.s. angular distribution of the pions is much closer to isotropic than that of the protons.

4) The average characteristics of the secondary particles ($\bar{p}_c$, $\bar{p}_\perp$, $\bar{n}_p$, $\bar{n}_\pi$) change relatively little with changing multiplicity.

5) A noticeable asymmetry is observed in the angular proton distribution for pn interactions.

At present there exists no consistent theory capable of describing the entire pN interaction picture. The statistical theory of multiple particle production describes well only certain characteristics of the interaction, for example the distribution by multiplicities (see [13,14]). On the other hand, the angular distributions of the secondary particles cannot be explained within the framework of the statistical theory. It is important that the statistical theory does not consider in principle the structure of the interacting particles, whereas even the crudest model representations are capable of yielding rather interesting results. If, for example, we assume that the nucleon consists of a "meson cloud" surrounding a central "core," [15] then we can expect two types of collisions to be present, "central" and "peripheral." This division is, of course, arbitrary.

On going from small to large multiplicities it is natural to expect the relative role of the "central" collisions to increase. This agrees with the experimental data, which indicate certain changes in the momentum and angular characteristics of the secondary nucleons (see Tables I and III and Fig. 2). On the other hand it is known that the number of charged secondary particles is not a sufficiently sensitive parameter capable of separating the "central" collisions from the "peripheral" ones (see [16]). One might think that the energy loss would be a more suitable criterion. If we assume arbitrarily that the "purely central" collisions are characterized by greater energy losses, we must conclude that the number of such collisions is small, for only in about 6% of all the pN interactions with two secondary protons were both protons emitted in the same c.m.s. direction.

It is apparently natural to classify as "peripheral" collisions in which the recoil nucleon acquires little energy. We can attempt to describe such collisions by using the single-meson scheme in the pole approximation. [16,17] Calculation shows that the cross section of the inelastic pN interaction should amount to about 18 mb, i.e., an appre-

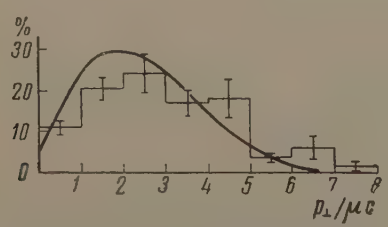

FIG. 5. Distribution of transverse momenta of protons in pp interactions. Smooth curve – result of calculation by the single-meson scheme.

Table IV

pp interactions			pn interactions		
n	number of events, %		n	number of events, %	
	exp	theor		exp	theor
2	44.8±4.2	35	1	29.9±4.2	18.4
4	42.2±4.1	58	3	46.0±5.1	65.2
6	10.6±2.1	6.0	5	16.1±3.1	15.7
8	2.4±0.6	0.1	7	7.5±2.1	0.7
$\bar{n}_{pp}$	3.42±0.10	3.46	9	0.6±0.6	—
			$\bar{n}_{pn}$	3.06±0.14	2.96

ciable portion of the corresponding experimental value, which is approximately 30 mb.[1,18]

It is therefore interesting to compare the experimental and calculated data pertaining to the entire statistical material. Figure 5 shows the experimental and theoretical distributions of the transverse momenta of the proton for pp interactions, while Figs. 3 and 6 show the angular distribution of the pions in the c.m.s. and the energy distribution of the recoil nucleons in the l.s. Table IV lists the theoretical and experimental distributions by number of charged particles for pp and pn interactions.

For pn interactions we have calculated the quantity

$$\Delta = (n_{\text{forw.}} - n_{\text{backw.}})/N$$

(N — total number of interactions) which characterizes the degree of asymmetry of the angular distribution in the c.m.s. We give below values of Δ for different multiplicites

n	1	3	5	7 — 9
$\Delta_{\text{exp.}}$	—	$+0.55\pm0.09$	0.0 ± 0.21	-0.64 ± 0.64
$\Delta_{\text{theor.}}$	$+0.43$	$+0.61$	-0.03	-0.68

We do not give the experimental value of Δ for cases with n = 1, for which only cases with $\theta_1 \geq 5°$ were considered.

A comparison of the experimental data with the calculations based on the one-meson scheme indicates that they are in qualitative agreement. It is hardly expected to obtain quantitative agreement because, in addition to single-meson interactions, an appreciable role can be played also by processes that follow more complicated schemes.

The authors are grateful to V. I. Veksler, I. M. Dremin, and D. S. Chernavskii for valuable discussions, to the proton-synchrotron crew for help with irradiating the emulsion, and to the chemical processing crew for developing the stack. The authors are particulary grateful to the laboratory staff who performed the difficult task of scanning and measuring.

[1] V. I. Veksler, Proc. 1960 Ann. Intern. Conf. on High Energy Physics, Rochester, 1960, p. 810.

[2] Bogachev, Bunyatov, Gramenitskii, Lyubimov, Merekov, Podgoretskii, Sidorov, and Tuvdendorzh, JETP **37**, 1225 (1959), Soviet Phys. JETP **10**, 872 (1960).

[3] Wang, Visky, Gramenitskii, Grishin, Dalkhazhav, Lebedev, Nomofilov, Podgoretskii, and Strel'tsov, JETP **39**, 957 (1960), Soviet Phys. JETP **12**, 663 (1961).

[4] Bogachev, Bunyatov, Merekov, Sidorov, and Yarba, JETP **38**, 1346 (1960), Soviet Phys. JETP **11**, 968 (1960).

[5] B. P. Bannik and M. I. Podgoretskii, PTÉ (Instrum. and Exptl. Techn.) **3**, 36 (1960).

[6] W. H. Barkas and D. M. Young, UCRL-2579, 1954.

[7] Gramenitskii, Korbel', and Rob, loc. cit. [5], No. 1, 42 (1961).

[8] Visky, Gramenitskii, and Podgoretskii, Preprint R-636, Joint Inst. Nuc. Res., 1960.

[9] M. S. Khvastunov, Preprint R-748, Joint Inst. Nuc. Res., 1961.

[10] Fowler, Shutt, Thorndike, Whittemore, Garrison, and Morris, Phys. Rev. **95**, 1026 (1954).

[11] F. N. Holmquist, UCRL-8559, 1958.

[12] Grishin, Nikitin, and Podgoretskii, Preprint R-480, Joint Inst. Nuc. Res., 1960.

[13] Belenkii, Maksimenko, Nikishov, and Rozental', Usp. Fiz. Nauk **62**, 1 (1957).

[14] Barashenkov, Belyakov, Bubelev, Wang, Mal'tsev, Ding, and Tolstov, Nucl. Phys. **9**, 74 (1960).

[15] D. I. Blokhintsev, CERN Symposium **2**, 155 (1956).

[16] Gramenitskii, Dremin, Maksimenko, and Chernavskii, JETP **40**, 1093 (1961), Soviet Phys. JETP **13**, 771 (1961).

[17] I. M. Dremin and D. S. Chernavskii, JETP **38**, 229 (1960), Soviet Phys. JETP **11**, 167 (1960).

[18] Achmore, Cocconi, Diddens, and Wetherell, Phys. Rev. Lett. **5**, 576 (1960).

Translated by J. G. Adashko
189

ELECTRON PARAMAGNETIC RESONANCE IN CONCENTRATED AQUEOUS SOLUTIONS OF VO^{2+}

N. S. GARIF'YANOV, B. M. KOZYREV, R. Kh. TIMEROV, and N. F. USACHEV

Physico-Technical Institute, Kazan' Branch, Academy of Science, U.S.S.R.

Submitted to JETP editor May 19, 1961

J. Exptl. Theoret. Phys. (U.S.S.R.) 41, 1076-1078 (October, 1961)

Highly concentrated aqueous solutions of $VOCl_2$ are investigated by the EPR method. The dependence of EPR line shape on concentration and temperature is in agreement with the predictions of the exchange-narrowing theory. An exchange frequency $\omega_e \approx 5 \times 10^{10}$ sec^{-1} is estimated for a concentration of 6 M.

1. Liquid solutions of vanadyl (VO^{2+}) salts are convenient systems in which to test the existing theories of paramagnetic relaxation in solutions.[1-3]

Using the method proposed in [4] we have investigated the behavior of EPR (electron paramagnetic resonance) line width in aqueous solutions of $VOCl_2$ over the temperature range 278 to 390° K at concentrations from M = 6 M to M = 1 M at the frequency ν = 9430 Mc.

As was shown earlier in a qualitative way,[5] pronounced exchange interactions between the VO^{2+} ions are observed in this range of concentrations. Kubo and Tomita[3] have developed the most complete theory of exchange effects in EPR. Hence the following discussion will be based, for the most part, on the results of [3] and [6], in which the effect of exchange on the magnetic dipole-dipole interaction[3] and on the hyperfine interaction[6] is considered. It can be shown[6] that with very strong exchange, when the exchange narrowing predominates over motional narrowing, the absorption line has the Lorentz shape with half-width (at half-height) $\Delta\omega_{1/2}$

$$\Delta\omega_{1/2} = \Delta\omega_{ss} + \Delta\omega_{hf} + \Delta\omega_z^a, \qquad (1)$$

where $\Delta\omega_{ss}$ is the dipole contribution to the half-width,[3]

$$\Delta\omega_{ss} = \hbar^{-2} g^4 \beta^4 S(S+1) \sum_j \langle r_{ij}^{-6} \rangle \omega_e^{-1} \left[\tfrac{3}{5} E_0 + E_1 + \tfrac{2}{5} E_2\right], \qquad (2)$$

$\Delta\omega_{hf}$ is the contribution to the half-width from the hyperfine interaction[6]

$$\Delta\omega_{hf} = \tfrac{1}{3} I(I+1)(a^2 + \tfrac{1}{2} b^2)\, \omega_e^{-1} [E_0 + E_1], \qquad (3)$$

and $\Delta\omega_Z^a$ is the contribution of the anisotropic part of the Zeeman energy[6]

$$\Delta\omega_z^a = \tfrac{1}{15} (\Delta g \beta H/\hbar)^2 \tau_c \left[\tfrac{4}{3} + (1 + \omega_0^2 \tau_c^2)^{-1}\right]. \qquad (4)$$

Here

$$a = (A + 2B)/3, \quad b = 2(A - B)/3, \quad \Delta g = g_\parallel - g_\perp,$$

$$E_k = (\pi/2)^{1/2} \exp(-k^2 \omega_0^2 / 2\omega_e^2),$$

$$\omega_e = [\tfrac{2}{3} J^2 S(S+1)]^{1/2}, \quad J^2 = N^{-1} \sum_{j \neq k} J_{jk}^2;$$

ω_e is the exchange frequency, J^2 is the mean value of the square of the exchange integral effective at one ion, and τ_c is the correlation time of Brownian motion. Equations (2) and (3) are obtained under the conditions of strong exchange $\omega_e^2 \tau_c^2 \gg 1$ and coincidence of exchange frequencies for $\Delta\omega_{ss}$ and $\Delta\omega_{hf}$.[6]

We note that the contribution $\Delta\omega_Z^a$ does not depend on exchange, since the anisotropic part of the Zeeman energy is neutralized only by thermal motion and not by exchange.

2. Experimentally, the concentration dependence of the half-width of the EPR line in $VOCl_2$ solutions in concentration region I (6 to 2 M) differs in an essential way from that in region II (1 to 0.001 M).

In the present paper we limit ourselves to a consideration of the results pertaining to region I. These concentrations are characterized by a complete absence of any kind of hyperfine structure (hfs). In this region the shape and width of the single EPR are strongly concentration dependent (see the table). For the highest concentration M = 6 M the ratio $r = \langle \Delta H^4 \rangle^{1/4} / \langle \Delta H^2 \rangle^{1/2} = 1.49$ indicates a Lorentz shape for the absorption line. The smallest value of the width at these concentrations occurs at M = 6 M and is 175 oe, signifying strong exchange interaction in the sample (so-called "exchange narrowing"). The line gradually widens with dilution and at M ~ 2 M acquires a wide plateau-like shape with r = 1.20, which is close to the value 1.16 computed for this ratio for an idealized rectangular-shaped absorption line.

From this it can be seen that Eqs. (1) — (4) for the half-width $\Delta\omega_{1/2}$ of a Lorentz absorption line

Concentration, M	r	ΔH, oe	g-factor
6	1.49	174	1.963±0.005
5	1,36	251	1,963±0.005
4	1.30	347	1,963±0.005
3	1.26	502	—
2	1.20	653	—

in the case of strong exchange are suitable for the description of EPR in 5 — 6 M solution. An additional substantial argument in support of their applicability is the very weak dependence of the line width on temperature in the highly concentrated solutions. Thus, at a concentration of 6 M the width decreases from 175 to 160 oe as the temperature increases from 293 to 323° K, and with further heating it remains unchanged. Such a dependence can be explained on the basis of Eqs. (1) — (4) when it is realized that only the contribution from the anisotropic part of the Zeeman energy [Eq. (4)] depends on the temperature (through the correlation time τ_c). When τ_c becomes short enough with increasing temperature so that $\Delta\omega_z^a$ is negligible relative to $\Delta\omega_{ss} + \Delta\omega_{hf}$, the line width does not depend strongly on the temperature in accordance with Eqs. (2) and (3). In this temperature range the behavior of concentrated $VOCl_2$ solutions is completely analogous to that of paramagnetic solids having strong exchange interaction (free radicals, many magnetically concentrated ionic salts of elements of the first transition group, etc.).[7]

Using Eqs. (2) and (3) we can estimate from the temperature independent part of the half-width the exchange frequency ω_e, a parameter difficult to measure by other means. Taking $\Delta H = 160$ oe at $M = 6$ M, $A = 200$ oe, $B = 76$ oe, $I = 7/2$, and $S = 1/2$ we obtain $\omega_e \approx 5 \times 10^{10}$ rad/sec. Here we have used the values for the hyperfine coupling constants A and B obtained earlier in [8] from EPR spectra of super-cooled ethanol solutions of hydrated complexes of $VOCl_2$. Dilute liquid solutions in ethanol and water have isotropic hyperfine coupling constants $a = 110$ oe and $a = 117$ oe, respectively. The small difference between these values leads to the expectation that the use of the measurements of A and B in supercooled ethanol solutions is adequately justified. The strong exchange condition $\omega_e^2\tau_c^2 \gg 1$ for our solutions is apparently satisfied, since the viscosity of concentrated aqueous solutions of $VOCl_2$ is rather large (at room temperature the viscosity of a 6 M solution amounts to 141 centipoise).

When the concentration becomes somewhat lower than 2 M, traces of resolved hfs can be seen on the wide plateau-shaped absorption line. However, the dipole width of each peak in the concentration range 2 to 1 M is comparable to the hfs constant $a = (1/3)(A + 2B)$. Hence the hfs is either not resolved at all (2 M) or there are only traces of a resolved structure (1 M). In this case the relations $\Delta H \sim 2Ia = 7 \times 117 = 819$ oe should be satisfied. Experiment gives the somewhat larger value $\Delta H = 930$ oe for a 1 M solution, as was to be expected.

In discussing the results obtained at intermediate concentrations (2 — 1 M), we are limited to purely qualitative considerations, since existing theories [1-3,6] do not treat this case.

[1] H. McConnell, J. Chem. Phys. **25**, 709 (1956).

[2] S. A. Al'tshuler and K. A. Valiev, JETP **35**, 947 (1958), Soviet Phys. JETP **8**, 661 (1959).

[3] R. Kubo and K. Tomita, J. Phys. Soc. Japan **9**, 888 (1954).

[4] Avvakumov, Garif'yanov, Kozyrev, and Tishkov, JETP **37**, 1564 (1959), Soviet Phys. JETP **10**, 1110 (1960).

[5] N. S. Garif'yanov and B. M. Kozyrev, DAN SSSR **98**, 929 (1954).

[6] D. Kivelson, J. Chem. Phys. **27**, 1087 (1957); **33**, 1094 (1960).

[7] S. A. Al'tshuler and B. M. Kozyrev, Elektronnyi paramgnitnyi rezonans (Electron Paramagnetic Resonance), Fizmatgiz, 1961, pp. 211, 274.

[8] N. S. Garif'yanov, DAN SSSR **103**, 41 (1955).

Translated by L. M. Matarrese
190

CONCERNING THE FERMI SURFACE OF TIN

N. E. ALEKSEEVSKII and Yu. P. GAĬDUKOV

Institute for Physics Problems, Academy of Sciences, U.S.S.R.

Submitted to JETP editor May 26, 1961

J. Exptl. Theoret. Phys. (U.S.S.R.) 41, 1079-1081 (October, 1961)

It is shown that besides the model of the Fermi surface for tin proposed earlier,[1] another topologically equivalent surface satisfies the experimental data from galvanomagnetic measurements. The surface suggested is compared with the Fermi surface derived by Gold and Priestley[2] from a study of the de Haas–van Alphen effect.

WE reported earlier[1] that some general deductions could be made about the form of the Fermi surface of tin on the basis of a study of the galvanomagnetic properties.

Recently Gold and Priestley[2] reported the results of an investigation of the Fermi surface of tin obtained by measuring the de Haas–van Alphen effect. It was therefore of interest to compare the results of these two methods of studying the Fermi surface of metals.

The main experimental result of galvanomagnetic measurements is a stereographic projection of the singular magnetic field directions.[3] A unique interpretation of this projection is not always possible. The stereographic projection we obtained previously[1] made possible the following proposed model of an open Fermi surface: a plane net of "corrugated cylinders" with axes parallel to the [010] direction. The dimensions of the "cylinders" are such that [110] is an additional open direction.

However, along with such a surface, the stereographic projection of the singular magnetic field directions for tin can agree with an open Fermi surface formed by "corrugated cylinders" with axes directed along [110]. The [010] direction is then the additional open direction.

This surface, as well as the surface discussed above, is equivalent, in a topological way, to a surface formed by two corrugated planes, parallel to the (001) plane and connected in the [001] direction by tubular "bridges." The mean diameter of the "bridges" can be calculated by using the experimental data and Eqs. (3) and (4) of the previous paper[1]: $d = 0.55b$ and the mean distance between the planes: $h = 0.5b$, where $b = 2(2\pi/a)$, $a = 5.84$ A. An open surface of this type is shown schematically in Fig. 1.

Both variants of an open Fermi surface for tin are topologically equivalent and can be obtained, one from the other, by rotating the axes through an angle $\pi/4$ in the (001) plane and changing the scale by a factor $\sqrt{2}$.*

From the experimental data it also follows that tin has a closed surface (or several surfaces), with a volume equal to the volume of the open surface, but of opposite sign. According to measurements of the Hall effect the closed surface corresponds to "electrons" and the open to "holes." Using the value of the Hall constant in the [001] direction, $R_{[001]} = 5 \times 10^{-3}$ cgs emu, the volume of the "bridges" can be calculated, which agrees with the principal dimensions of the open surface. This is the model of the Fermi surface of tin which results from the galvanomagnetic data.

Gold and Priestley proposed a model, according to which the Fermi surface of tin consists of seven closed and two open surfaces, the closed surfaces (except for one) being "electronic" and the open, "hole." The total volumes of the "electron" and "hole" surfaces are roughly equal. Gold and Priestley found that the results of their experiments on the de Haas–van Alphen effect could be explained within the framework of this

*The Bravais lattice of tin can be chosen in two ways: it is either a face-centered tetragonal lattice with axial ratio $a/c \approx 2.6$, or a body-centred tetragonal lattice with axial ratio $a/c \approx 1.8$. Both lattices are equivalent in principle and differ from one another in that their periods in the (001) plane differ by $\sqrt{2}$. In the previous paper the analytic expression for the isoenergetic surfaces is given in the axial system of a face-centred tetragonal crystal lattice, while the axial ratio a/c for tin was given in error for a body-centred lattice ($a/c \approx 1.8$). However, for the qualitative analysis of the topology of the isoenergetic surfaces only the property that $a/c > 1$ was used, and not the quantitative expression for a/c.

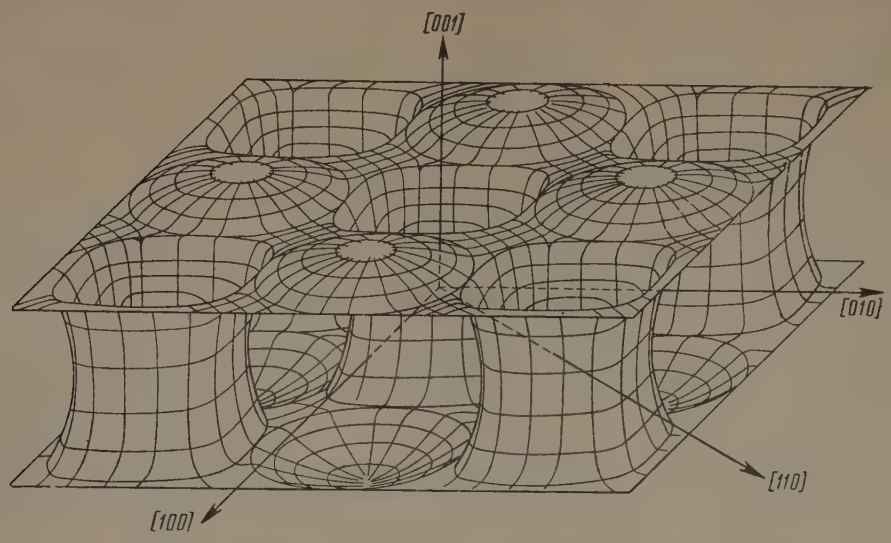

model. There is thus a qualitative agreement between the two models of the Fermi surface of tin considered.

We can only make a quantitative comparison for the open surfaces. Of the two open surfaces in Gold and Priestley's model we must choose that which lies in the fourth Brillouin zone, since a surface in the third zone cannot give anything new for the galvanomagnetic properties.

The open surface is the fourth zone consists of two "corrugated planes," joined by "bridges" in the [001] direction. This surface agrees topologically with both variants of the Fermi surface proposed by us. It agrees approximately in shape with the surface shown in Fig. 1. The difference between these surfaces consists only in the first having the [110] direction open, while the second has both the [110] and the [010] directions open. However, this difference is insignificant since, keeping the cross-section area of the "bridges" constant, it is possible by small "deformation" of this cross-section to make the [010] direction open as well. The area of certain sections of the surface in the fourth zone can be calculated from the values of the periods of the oscillation of susceptibility determined by Gold and Priestley, and its characteristic dimensions can then be found. The diameter of the "bridges" and the distance between the "planes" are roughly equal to 0.5 b.

The Fermi surface of tin obtained on the basis of the data of galvanomagnetic measurements is thus in good agreement with the surface derived by Gold and Priestley.

We should also remark that the topological type of open surface suggested earlier[1] and in the present work is shown up in experiments on magnetoacoustic resonance,[4] in which, in particular, open trajectories along the [110] direction are found.

The authors express their thanks to Prof. I. M. Lifshitz and V. G. Peschanskii for their valued comments.

[1] Alekseevskii, Gaĭdukov, Lifshitz, and Peschanskii, JETP **39**, 1201 (1960), Soviet Phys. JETP **12**, 837 (1961).

[2] A. V. Gold and M. G. Priestley, Phil. Mag. **5**, 1089 (1960).

[3] I. M. Lifshitz and V. G. Peschanskii, JETP **35**, 1251 (1958), Soviet Phys. JETP **8**, 875 (1959).

[4] Galkin, Kaner, and Korolyuk, JETP **39**, 1517 (1960), Soviet Phys. JETP **12**, 1055 (1961).

Translated by R. Berman
191

NUCLEAR MAGNETIC RESONANCE IN METALLIC THALLIUM

Yu. S. KARIMOV and I. F. SHCHEGOLEV

Institute for Physics Problems, Academy of Sciences, U.S.S.R.

Submitted to JETP editor May 26, 1961

J. Exptl. Theoret. Phys. (U.S.S.R.) 41, 1082-1090 (October, 1961)

Nuclear magnetic resonance has been investigated in metallic thallium in a sample of natural isotopic abundance and in samples enriched in Tl^{205} and Tl^{203}. Measurements were carried out over a range of fields from 550 to 5500 oe at helium temperatures. In a sample with natural isotopic abundance, it was observed that in weak fields the indirect exchange interaction between the nuclei, due to the presence of conduction electrons, caused the lines due to the two isotopes to merge. The experimental results agree well with calculations based on the Kubo and Tomita theory of magnetic resonance absorption. A value A/h = 37.5 kc/sec has been obtained for the indirect exchange interaction constant.

INTRODUCTION

SEVERAL years ago Ruderman and Kittel [1] noted that in metals, in addition to the usual dipole-dipole interaction between nuclear spins, there can also exist an indirect exchange interaction due to conduction electrons. The operator for the indirect exchange interaction between the nuclear spins I_α and I_β has the form $\tilde{A}_{\alpha\beta} I_\alpha \cdot I_\beta$. The constant $\tilde{A}_{\alpha\beta}$ depends on quantities characterizing the behavior of electrons in the metal and an expression for it was obtained in the one electron approximation by Ruderman and Kittel. [1]

In the case of a metal containing several different isotopes possessing magnetic moments, this interaction must lead to additional broadening of the nuclear magnetic resonance (n.m.r.) line, and this was shown in a convincing manner by Bloembergen and Rowland [2] who measured widths of n.m.r. lines in samples of metallic thallium of different isotopic composition. However, in addition to line broadening such an interaction, if it is sufficiently large, must give rise to another curious effect: it must make the resonance lines of the individual isotopes approach one another, and it must make them merge completely in weak fields when the energy difference between the Zeeman levels of the individual isotopes becomes smaller than the energy of the exchange interaction. This is due to the fact that in weak fields the nuclei of the different isotopes coupled by the exchange interaction behave as a single system. In strong fields the coupling between them is broken and each isotope gives rise to its own absorption line. This effect, which is to a certain extent analogous to the Paschen-Back effect, has been observed in electron paramagnetic resonance, [3,4] and we have attempted to observe it in the case of nuclear spins in metallic thallium.

Thallium has two stable isotopes, Tl^{203} and Tl^{205}, whose natural abundance is respectively 30 and 70%. Both isotopes have spin $\frac{1}{2}$, and their magnetic moments differ by only 1%. Such a small difference between the magnetic moments on the one hand, and the appreciable value of the indirect exchange interaction on the other hand, have caused us to observe a complete merging of the lines of the two isotopes into one relatively narrow symmetric line even in fields $\lesssim 1$ koe. To convince ourselves that the observed effects are associated specifically with the presence in the sample of two different thallium isotopes, and are not due to some other causes, we have carried out measurements on isotopically enriched samples, one with 97.6% Tl^{205} and the other with 90% Tl^{203}. These measurements also enabled us to determine accurately the displacement of the lines from their initial position in a sample of natural isotopic abundance. Moreover, they have enabled us to obtain quantitative data characterizing the narrowing of the line as the magnetic field is decreased.

In order to describe the results obtained we have carried out calculations on the basis of the theory of Kubo and Tomita, [5] which have turned out to be in good agreement with experiment. The indirect exchange interaction constant enters into several quantities which can be measured experimentally and the values obtained from these different measurements agree with one another.

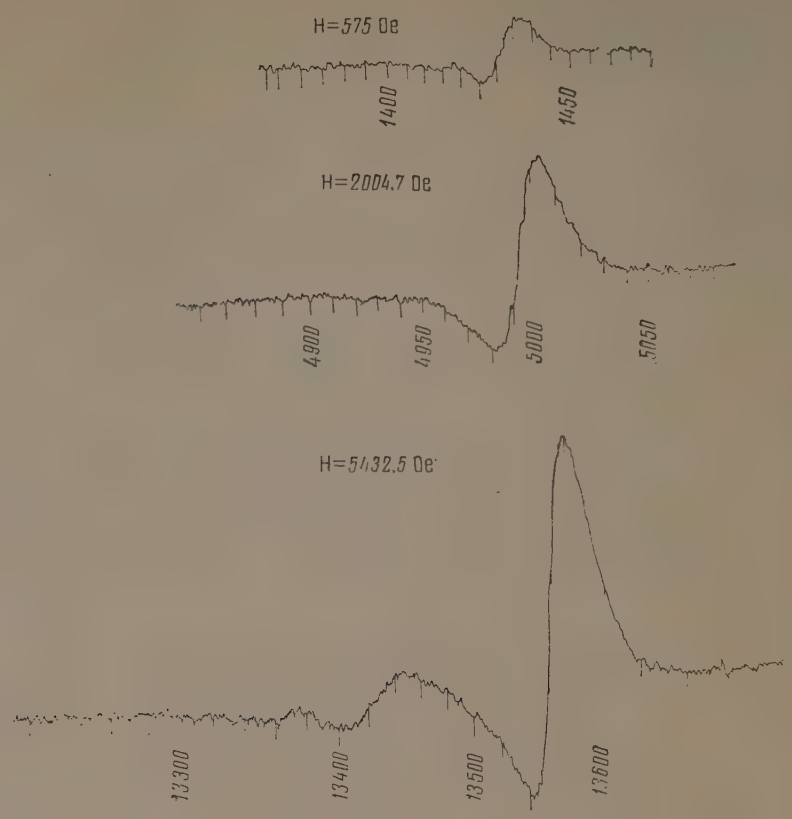

FIG. 1. Recorded derivatives of absorption lines in a sample of natural isotopic abundance.

EXPERIMENT

All the measurements were carried out at helium temperatures, since it is difficult to obtain a good signal-to-noise ratio in weak fields by any other method.

The sample of natural isotopic abundance was prepared from metal of 99.9% purity. The sample enriched in Tl^{205} contained 97.6% Tl^{205}, 2.4% Tl^{203} and less than 0.1% impurities, the principal one of which was Si. The sample enriched in Tl^{203} contained 90% Tl^{203}, 10% Tl^{205} and less than 0.2% impurities, the principal one of which was again Si. These samples consisted of finely dispersed metallic powder mixed with vacuum grease. The metallic powder was obtained by reducing the oxide Tl_2O_3 in an atmosphere of hydrogen at 265° C. The size of the particles in the samples did not exceed 1μ, which is much smaller than the skin depth in thallium at helium temperatures in the frequency range used. Measurements in the case of natural isotopic composition were also carried out on a sample obtained by filing thallium with a barette file. The size of the particles in this case was $10-30\mu$ and was, apparently, somewhat greater than the skin depth. The position and the shape of the lines obtained for all these different samples agreed within experimental error.

The n.m.r. spectrometer was briefly described previously.[6] The magnetic field was measured by means of proton resonance, and the accuracy of the measurement was limited by the instability of the magnetic field which did not exceed 10^{-2}%. The modulation amplitude was different depending on the line width, and was so chosen that the cor-

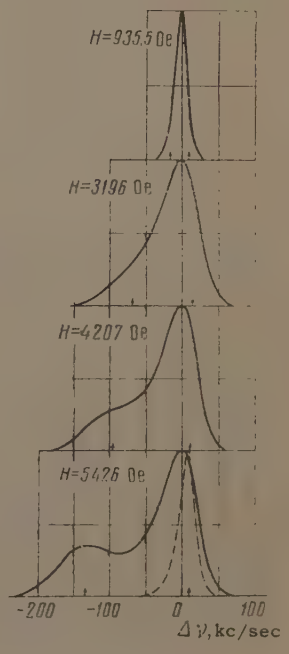

FIG. 2. Absorption lines in a sample of natural isotopic abundance for different intensities of the magnetic field. The dotted curve shows the form which the Tl^{205} absorption line has in an enriched sample.

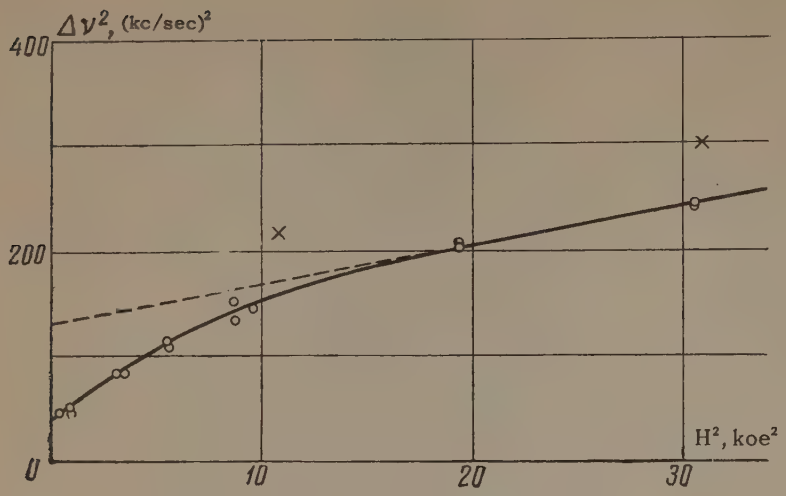

FIG. 3. Dependence on the square of the field of the second moment of the Tl^{205} absorption line in an enriched sample.

rection to the second moment due to the finite modulation[7] did not exceed 1%.

RESULTS

Figure 1 shows recorded derivatives of absorption lines in metallic thallium of natural isotopic abundance in three different magnetic fields. Figure 2 shows the integrated line shape in the different fields. It can be seen that in weak fields there exists only one relatively symmetric resonance line. As the field is increased the line broadens, becomes asymmetric, and in the highest fields two lines appear due to the two different isotopes of thallium, and these were the lines observed by Bloembergen and Rowland.[2]

The absorption lines of Tl^{205} in the enriched sample behave differently. An increase in the magnetic field broadens the line only slightly. The absorption lines of Tl^{203} in the enriched sample behave similarly, but the broadening is much more pronounced in this case since this sample contains a greater amount of the "foreign" isotope. From these measurements we have obtained for metallic Tl^{205} the ratio $\nu_{res}/H_{res} = 2.4975 \pm 0.0003$ kc/sec · oe, and for metallic Tl^{203} the value $\nu_{res}/H_{res} = 2.4723 \pm 0.0003$ kc/sec · oe. These values were used to indicate in Fig. 2 by arrows those frequencies at which the Tl^{205} and Tl^{203} lines occur in the corresponding fields. For comparison we have shown by a dotted curve in this figure the appearance of the Tl^{205} absorption line in the enriched sample in a high field.

Figure 3 illustrates the manifestation in the line widths of the process of the smearing obliteration of the differences between the spins of the different isotopes as a result of the indirect exchange interaction.* Here we have shown the dependence of the second moment of the Tl^{205} absorption line in the enriched sample on the square of the external field. The linear dependence of the second moment on the square of the field observed in the highest fields is due to the anisotropy of the Knight shift. The dotted line extrapolates this linear dependence into the weak field region. The dotted line shows the manner in which the second moment would vary if the spins of the two isotopes of thallium would remain different at all times. However, we see that in weak fields the second moment becomes smaller than it ought to be by approximately a factor of four. The origin of this effect can be easily understood: in high fields there exist nuclei of two different thallium isotopes and the exchange interaction between them gives a contribution to the second moment. In low fields all the spins become the same and, as is well known, the exchange interaction between identical spins gives no contribution to the second moment.

*We say that the spins are different if their gyromagnetic ratios are different.

THEORY

For a quantitative description of the observed process of the merging of the lines and of the process of their narrowing we shall utilize the theory of magnetic resonance absorption developed by Kubo and Tomita.[5] It enables us to calculate the first and the second moments of the absorption lines in a sample containing two kinds of spins. The first moments describe the effect of the shift

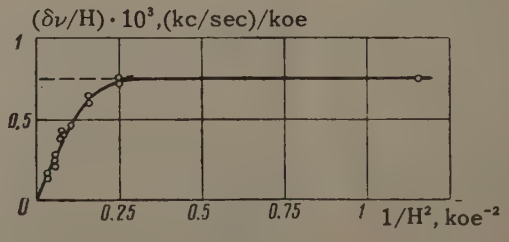

FIG. 4

of the lines from their initial position, while the second moments describe the line narrowing effect.

1. Following Van Vleck[8] we write the Hamiltonian for a system containing two different kinds of spins in the form

$$\mathcal{H} = -\hbar\gamma H\sum_i I_{iz} - h\gamma' H\sum_{i'} I_{i'z} + \sum_{i>k} B_{ik}I_{iz}I_{kz} + \sum_{i'>k'} B_{i'k'}I_{i'z}I_{k'z} + \sum_{i,k'} B_{ik'}I_{iz}I_{k'z} + \sum_{i>k} A_{ik}\mathbf{I}_i\mathbf{I}_k + \sum_{i'>k'} A_{i'k'}\mathbf{I}_{i'}\mathbf{I}_{k'} + \sum_{i,k'} A_{ik'}\mathbf{I}_i\mathbf{I}_{k'} = \mathcal{H}_z + \mathcal{H}_B + \mathcal{H}_A.$$

The unprimed quantities in this expression refer to spins of one kind, and the primed quantities to spins of the other kind. The first two terms describe the interaction with the external field H; the terms with the coefficients

$$B_{\alpha\beta} = -\tfrac{3}{2}(\gamma^2\hbar^2 r_{\alpha\beta}^{-3} + \widetilde{B}_{\alpha\beta})(3\gamma_{\alpha\beta}^2 - 1)$$

take into account the dipole and the pseudodipole[2] interactions; the terms with the coefficients

$$A_{\alpha\beta} = \tfrac{1}{2}(\gamma^2\hbar^2 r_{\alpha\beta}^{-3} + \widetilde{B}_{\alpha\beta})(3\gamma_{\alpha\beta}^2 - 1) + \widetilde{A}_{\alpha\beta},$$

take into account in addition to the dipole and the pseudodipole interactions also the isotropic exchange interaction. The subscripts α and β can refer both to spins of one kind and to spins of the other kind. In all the expressions for the coefficients we assume that the gyromagnetic ratios of both kinds of spins are the same: $\gamma' = \gamma$; $r_{\alpha\beta}$ is the distance between the nucleus α and the nucleus β; $\gamma_{\alpha\beta}$ is the cosine of the angle between the vector $\mathbf{r}_{\alpha\beta}$ and the external field. We have omitted from the Hamiltonian all terms which lead to satellite absorption lines at frequencies that are multiples of the Larmor frequency, and we have not taken into account the Knight shift.

2. In the case of high fields when two lines appear we choose (for notation see [5]):

$$\mathcal{H}_0 = \mathcal{H}_z, \qquad \mathcal{H}' = \mathcal{H}_A + \mathcal{H}_B.$$

In accordance with formulas (4.22) and (5.3) of the paper by Kubo and Tomita[5] we find by second order perturbation theory, for the case of spins $I = I' = \frac{1}{2}$, that in a polycrystalline sample the center of gravity of the line which was initially situated at the frequency $\nu = \gamma H/2\pi$ will be shifted by an amount

$$\delta\nu = -\frac{1}{4\pi(\nu-\nu')h^2}\sum_{k'}(\widetilde{A}_{ik'}^2 - b_{ik'}^2),$$

$$b_{ik'} = -(\gamma^2\hbar^2 r_{ik'}^{-3} + \widetilde{B}_{ik}). \qquad (1)$$

For the second moment with respect to the undisplaced position of the line we obtain in this approximation Van Vleck's expression:

$$\overline{\Delta\nu^2} = \frac{9}{20h^2}\sum_k b_{ik}^2 + \frac{9}{45h^2}\sum_{k'} b_{ik'}^2 + \frac{1}{4h^2}\sum_{k'}\widetilde{A}_{ik'}^2. \qquad (2)$$

We shall see later that in our case $b_{\alpha\beta} \ll \widetilde{A}_{\alpha\beta}$, and, therefore, in making comparisons with experiment we can neglect the quantities $b_{\alpha\beta}^2$ in comparison with $\widetilde{A}_{\alpha\beta}^2$. Further, the expression obtained by Ruderman and Kittel[1] shows that $\widetilde{A}_{\alpha\beta}$ is inversely proportional to the cube of the distance between the nucleus α and the nucleus β, at any rate at large distances. Therefore, the summation in formulas (1) and (2) can be restricted to only the twelve nearest neighbors in the hexagonal close packed lattice of metallic thallium by taking $\widetilde{A}_{\alpha\beta} = A$, $b_{\alpha\beta} = b$ for the nearest neighbors, and $\widetilde{A}_{\alpha\beta} = b_{\alpha\beta} = 0$ in all the other cases. As a result of this we obtain (cf. [9]):

$$\delta\nu/H = -6\pi(A^2/h^2)\, f/(\gamma-\gamma')\, H^2, \qquad (1a)$$

$$\overline{\Delta\nu^2} = \tfrac{27}{5}(b^2/h^2)(1-f) + 3(A^2/h^2) f. \qquad (2a)$$

Here f is the concentration of the "foreign," primed isotope.

The line displacement given by (1a) causes the second moment with respect to the center of gravity to be smaller than (2a) by an amount $(\delta\nu)^2$. However, this decrease is of the same order of smallness as the correction to the second moment which arises in fourth-order approximation of perturbation theory. We therefore obtain the total decrease in the second moment if we add to the above expression the correction evaluated in the fourth-order approximation (we note that all the third-order corrections vanish). As a result of this we have

$$\delta(\overline{\Delta\nu^2}) = \frac{1}{16(\nu-\nu')^2h^4N}\Big\{5\sum_{ik'}\widetilde{A}_{ik'}^4 + \sum_{ilk'\neq}[\widetilde{A}_{ik'}^2\widetilde{A}_{lk'}^2 - \widetilde{A}_{il}^2(\widetilde{A}_{ik'}-\widetilde{A}_{lk'})^2] + \sum_{ik'l'\neq}[4\widetilde{A}_{ik'}^2\widetilde{A}_{il'}^2 - \widetilde{A}_{k'l'}^2(\widetilde{A}_{ik'}-\widetilde{A}_{il'})^2]\Big\} + (\delta\nu)^2, \qquad (3)$$

where N is the number of unprimed spins. Summing this expression in the same manner as in the derivation of formulas (1a) and (2a) we obtain

$$\delta(\overline{\Delta\nu^2}) = 3\pi^2(A^4/h^4)(2f + 45f^2)/(\gamma-\gamma')^2 H^2. \qquad (3a)$$

3. In the weak field case we have only one resonance line, and we choose

$$\mathcal{H}_0 = -\hbar\gamma H\Big\{\sum_i I_{iz} + \sum_{i'} I_{i'z}\Big\},$$

$$\mathcal{H}' = \hbar(\gamma-\gamma')\, H\sum_{i'} I_{i'z} + \mathcal{H}_B + \mathcal{H}_A.$$

In accordance with formulas (4.22) and (5.3) of the paper by Kubo and Tomita[5] we find that the cen-

ter of gravity of the line will be displaced with respect to the frequency $\nu = (\gamma/2\pi)\,H$ by an amount

$$\delta\nu = -(\nu - \nu')\,f, \qquad (4)$$

and the second moment with respect to the center of gravity will be given in a polycrystalline sample by

$$\overline{\Delta\nu^2} = \frac{9}{20h^2}\left\{\sum_k b_{ik}^2 + \sum_{k'} b_{ik'}^2\right\} + (\nu - \nu')^2 f\,(1 - f). \qquad (5)$$

On carrying out the summation in this case in the same manner as before we obtain

$$\overline{\Delta\nu^2} = 27b^2/5h^2 + (2\pi)^{-2}(\gamma - \gamma')^2 H^2 f\,(1 - f). \qquad (5a)$$

Similar formulas were obtained by a different method by Pryce.[10]

The magnetic field which separates the region of strong fields from the region of weak fields is given by the following expression[5]

$$H^* = \left\{\sum_{k'} \widetilde{A}_{ik'}^2\right\}^{1/2} \Big/ 2\hbar\,(\gamma - \gamma') \approx \pi\sqrt{12f}A/h\,(\gamma - \gamma'). \qquad (6)$$

COMPARISON OF EXPERIMENT WITH THEORY

Our problem is to determine how well the expressions (1a) — (5a) describe the experimental data, and to obtain the values of the constants A and b, which describe the interaction of the nuclear spins in metallic thallium. A rough estimate for the indirect exchange interaction constant can be obtained directly from the data shown in Fig. 2. The lines due to the different isotopes begin to be resolved in fields of approximately 1.5 — 2 koe. If we assume that the difference in the energies of the Zeeman levels of the two isotopes in such fields is just of the order of the exchange energy, then we obtain for the constant A the estimate $A/h \approx 35 - 50$ kc/sec.

In order to justify the simplification introduced in obtaining formulas (1a) — (5a), whereby we neglected the quantity b^2 compared to A^2, we now obtain the value of the constant b, which characterizes the dipole and the pseudodipole interactions. This can be directly accomplished on the basis of the data shown in Fig. 3. As we have noted already, in the weakest fields when any difference between the gyromagnetic ratios of the spins of the different isotopes completely disappears, the value of the second moment is determined basically only by the dipole and the pseudodipole interactions, and is given by expression (5a). From this we obtain b/h = 2.7 kc/sec. The values of the second moment in weak fields in a sample of natural isotopic abundance and in the sample enriched in Tl^{203} give for b/h respectively the values of 2.6 and 2.9 kc/sec.

From the data of Fig. 3 it is possible to obtain also a more accurate value for the constant A by making use of the following considerations. In the strongest fields the second moment is given by formula (2a) and must be constant. As we have noted already, the observed linear increase is due to the anisotropy of the Knight shift which was not taken into account in the derivation of this formula. It can be taken into account if we add to the right hand side of formula (2a) a term proportional to the square of the field. A sharp decrease in the second moment in weak fields compared to the value which would be given by the linear dependence is due to the disappearance from formula (2a) of the term $3(A^2/h^2)f$, i.e., of the contribution made to the second moment by the exchange interaction between the different isotopes. Without this term formula (2a) goes over into formula (5a) (if f is sufficiently small), which specifically describes the second moment in weak fields. Thus, by equating the quantity $3(A^2/h^2)f$ to the difference between that value of the second moment which is obtained by extrapolating the linear dependence into the weak field region and the actual value of the second moment we obtain A/h = 36.0 kc/sec. A similar procedure applied to the data obtained with the sample enriched in Tl^{203} gives A/h = 34.0 kc/sec.

We shall now see how well the process of the merging of the lines is described by the theory. Formula (1a) referring to this is valid for fields $H > H^* \approx 1.4$ koe [this value is obtained from formula (6) by putting A/h = 36 kc/sec and f = 0.3]. Figure 4 shows the experimentally measured dependence on $1/H^2$ of the relative displacement $\delta\nu/H$ for the Tl^{205} line in metal of natural isotopic abundance. The dotted line here shows the limiting value obtained in accordance with formula (4a) to which the value of $\delta\nu/H$ tends as $H \to 0$ [$\delta\nu/H = -(\gamma - \gamma')f/2\pi$]. The initial portion of this curve indeed turns out to be linear for fields $H \gtrsim 3$ koe. From its slope we find that A/h = 36.5 kc/sec.

The process of line narrowing shown in Fig. 3 is described by formula (3a) which is valid for fields $H > H^* \approx 500$ oe. [This value is obtained by means of formula (6) for A/h = 36 kc/sec and $f = 2.4 \times 10^{-2}$.] Figure 5 shows the dependence of $\delta\overline{(\Delta\nu^2)}$ on $1/H^2$. It can be seen that the initial rectilinear portion of this curve extends from high fields down to $H \approx 1.5$ koe. From its slope we obtain A/h = 38.5 kc/sec. Similar measurements in the case of Tl^{203} yield A/h = 35 kc/sec.

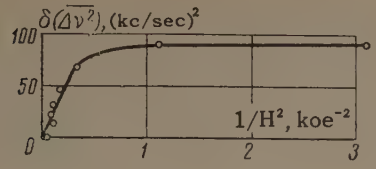

FIG. 5

The good agreement between the values of the indirect exchange interaction constant obtained from the different measurements testifies that the theory of Kubo and Tomita describes the situation sufficiently well. The linear dependence on $1/H^2$ predicted by the theory with respect to the shift $\delta\nu/H$ and the decrease in the second moment $\delta(\overline{\Delta\nu^2})$ is confirmed by experiment, as can be seen from Figs. 4 and 5.

DISCUSSION

Thus, as a result of the reduction of the experimental data we have obtained the following values for the constants describing the interaction between the nuclear spins in the metal: A/h = 36.0 kc/sec, b/h = 2.7 kc/sec. The ordinary dipole-dipole interaction constant in thallium is $\gamma^2\hbar^2a^{-3}$ = 1 kc/sec (a is the distance between nearest neighbors). Thus, it can be seen that the pseudodipole interaction is of approximately the same magnitude as the dipole interaction, and does not exceed 10% of the isotropic exchange interaction described by the constant A.

As we have noted already, Ruderman and Kittel [1] have obtained an expression relating the constant A to the properties of the conduction electrons, which in the case $I = I' = \frac{1}{2}$ has the form

$$\tilde{A}_{ik} = \Omega^2 m^* \langle a_k^2 \rangle (8\pi r_{ik}^4)^{-1} [2k_m r_{ik} \cos(2k_m r_{ik}) - \sin(2k_m r_{ik})],$$

where Ω is the atomic volume, m* is the effective mass, $\langle a_k \rangle$ is the value of the hyperfine interaction constant between the nucleus and the electron averaged over the Fermi surface, $\hbar k_m$ is the momentum of the electron on the Fermi surface. Unfortunately, this expression was obtained under highly simplifying assumptions; in particular, it was assumed that the energy is a quadratic function of the momentum: $E = \hbar^2k^2/2m^*$. Apparently the last circumstance is completely excluded in the case of thallium. [11] Therefore, the estimates given below must be regarded more as an illustration, and we cannot assume that they have any serious significance at all.

As can be seen, the expression for A contains three unknown quantities: m*, $\langle a_k \rangle$ and k_m. However, we have at our disposal also the data on the Knight shift, in the expression for which obtained under the same restrictive assumptions these quantities appear in a different combination (cf., for example, [12]):

$$\Delta H/H = 3\pi\beta_0 \langle a_k \rangle m^*/\hbar^2\gamma k_m^2,$$

where β_0 is the Bohr magneton. The method of averaging the quantity a_k in this expression generally speaking differs from the method of averaging it in the expression for A, but for order of magnitude estimates this is not significant. According to our measurements, which agree well with the data of Bloembergen and Rowland, [2] $\Delta H/H = 1.52\%$. If for the value of the maximum Fermi momentum we take $k_m = \pi/a$, then we obtain $\langle a_k \rangle = 10^{11}$ cps, which exceeds the hyperfine interaction constant in the free atom by a factor 10, and m* = 0.2 m. But if we take m* = 1.2 m, which follows from data on specific heat, [14] we obtain $k_m \approx 5.5 \times 10^8$ cm^{-1}, and $\langle a_k \rangle = 10^{12}$ cps.

In conclusion we would like to note that there is an appreciable disagreement between our values of the constants and the values obtained by Bloembergen and Rowland [2]: A/h = 17.5 kc/sec, b/h = 5.5 kc/sec. In Fig. 4 we have shown by crosses those values of the second moment which are given in [2] for the sample enriched in Tl^{205} which contained 1.3% Tl^{203}. The values of the second moment themselves agree very satisfactorily with the values obtained in the present work if we take into account the fact that in the evaluation of second moments fairly large errors can arise, particularly if the signal-to-noise ratio is not very great. An attempt might be made to explain the small systematic discrepancy which, apparently, nevertheless exists by means of additional line broadening due to the influence of the spin-lattice relaxation time T_1: Bloembergen and Rowland have carried out their measurements at 77° K and T_1 might not have yet reached very high values. However, these authors have made an error in the reduction of the results of their experiments. They assumed that the second moment obtained by extrapolating to zero field the linear dependence at high fields is determined only by the dipole and the pseudodipole interactions. But in fact, as has been discussed above, the indirect exchange interaction also makes an appreciable contribution to it. Their neglect of this circumstance caused them to grossly overestimate the magnitude of this pseudodipole interaction and to correspondingly underestimate the magnitude of the indirect exchange interaction.

We express our deep gratitude to Academician P. L. Kapitza for continued interest in and support of this work, and to N. N. Mikhaĭlov for the preparation of the samples of metallic thallium. A. S. Borovik-Romanov has kindly read the manuscript and has made a number of valuable suggestions which were gratefully adopted.

[1] M. A. Ruderman and C. Kittel, Phys. Rev. **96**, 99 (1954).

[2] N. Bloembergen and T. J. Rowland, Phys. Rev. **97**, 1679 (1955).

[3] D. M. S. Bagguley and J. H. E. Griffiths, Proc. Roy. Soc. (London) **A206**, 366 (1950).

[4] Abe, Ono, Hayashi, Shimada, and Iwanaga, J. Phys. Soc. Japan **9**, 814 (1954).

[5] R. Kubo and K. Tomita, J. Phys. Soc. Japan **9**, 888 (1954).

[6] Yu. S. Karimov and I. F. Shchegolev, JETP **40**, 3 (1961), Soviet Phys. JETP **13**, 1 (1961).

[7] E. R. Andrew, Phys. Rev. **91**, 425 (1953).

[8] J. H. Van Vleck, Phys. Rev. **74**, 1168 (1948).

[9] M. Yokota and S. Koide, J. Phys. Soc. Japan **9**, 953 (1954).

[10] M. H. L. Pryce, Nature **162**, 538 (1948).

[11] N. E. Alekseevskii and Yu. P. Gaĭdukov, JETP **37**, 672 (1959), Soviet Phys. JETP **10**, 481 (1960).

[12] E. R. Andrew, Nuclear Magnetic Resonance, Cambridge Univ. Press, 1955.

[13] Landolt-Börnstein, Zahlenwerte and Funktionen, **1**, Teil 5, 1952.

[14] J. G. Daunt, Progr. Low Temp. Phys., ed. by C. J. Gorter **1**, 1955, p. 202.

Translated by G. Volkoff
192

PHOTODEUTERONS FROM Al^{27}

E. D. MAKHNOVSKII

Leningrad Institute for Physics and Technology, Academy of Sciences, U.S.S.R.

Submitted to JETP editor May 30, 1961

J. Exptl. Theoret. Phys. (U.S.S.R.) 41, 1091-1093 (October, 1961)

The ratio of the photodeuteron to photoproton yield was measured for Al^{27} irradiated with γ rays with $E_{\gamma max} = 35$ Mev. Within an energy range from 2.9 to 10 Mev the ratio was found to be 0.009 ± 0.007 (which is much smaller than the ratio for Cu at $E_{\gamma max} = 70$ Mev [3]).

THE experimental data on photodeuterons of energies > 15 Mev can be interpreted on the basis of the so-called pickup process.[1,2] The study of photodeuterons of energy < 15 Mev has met with difficulties due to the small yield of the (γ, d) reaction and due to the lack of a sufficiently trustworthy method of distinguishing between singly charged particles of low energy. The investigations of the relative yields of photodeuterons have led to rather conflicting results which also are sometimes difficult to compare.

In the present work the ratio of the yield of photodeuterons and photoprotons was measured for Al^{27} irradiated with bremsstrahlung of $E_{\gamma max} = 35$ Mev. The charged particles were identified by the radius of curvature of their trajectory in a magnetic field and by their range in a nuclear emulsion.[3] Compared to the more frequently used method of grain counting in the residual range this method is less cumbersome to apply and more sensitive in distinguishing between singly charged particles.

The target was an aluminum foil of 7 mg/cm^2 thickness. Together with the nuclear emulsion it was placed inside a vacuum chamber in a transverse constant magnetic field with H = 13 500 oe. The nuclear emulsions, type NIKFI-Ya2 400 μ thick, were distributed in the interval 50° to 120° with respect to the photon beam. In addition to the range of the particles, the orientations of their tracks were measured in order to determine the radius of curvature of their trajectories in the magnetic field. The irradiation dose was measured with a quantometer.[4] The background due to (n, p) reactions in the vacuum chamber and due to (γ, p) reaction in the aluminum foil windows was determined in a run with the target foil removed from the chamber. A correction for the background was applied to the results.

The distribution of the radii of curvature as a function of the range is given in the figure. The solid curves give the calculated dependence $\rho(R)$ for protons, deuterons, α particles and tritons. The "range of errors" also is indicated: for the protons by solid lines, for the deuterons by lines with crosses. The corresponding curves for tritons and α particles are not given. The measured events are indicated by open circles.

From the analysis of the data we obtain for the ratio of the yield of photodeuterons of energy 2.9 to 10 Mev to the yield of photoprotons of the same energies, $Y(\gamma, d)/Y(\gamma, p) = 0.009 \pm 0.007$. Thus the deuteron yield is less than two percent of the proton yield. Recently Forkman[5] has used a method analogous to ours to measure the yield of photodeuterons from S, Co and Cu. His results agree in the order of magnitude with the results of the present paper.

According to the evaporation model the yield of photodeuterons from light and medium nuclei (at $E_{\gamma max} = 30$ Mev) is also a fraction of a percent of the photoproton yield. However, despite the agreement of the experimental data with the results obtained from the evaporation model the question of the mechanism of the production of photodeuterons remains open so long as the angular and energy distributions are unknown. Another probable process along with evaporation of deuterons is one in which a deuteron is emitted when an evaporated proton picks up a neutron while leaving the nucleus. Byerly and Stephens[6] point out that this process is more probable than simple evaporation. However, at present one can only confirm that if such a process of production of low energy photodeuterons exists its probability is of the same order of magnitude as the probability of the evaporation process.

In the earlier paper[3] somewhat too large val-

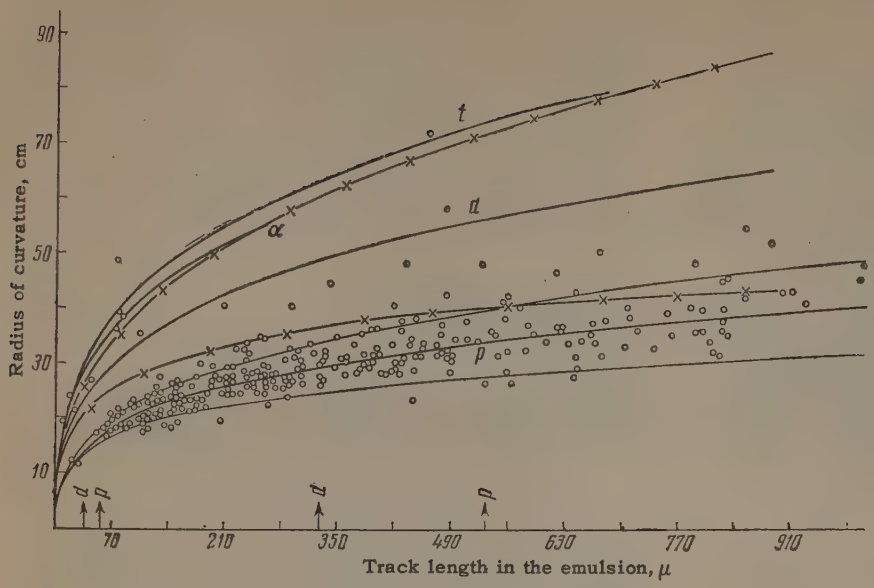

Dependence of the radius of curvature on the track length of the particles in the emulsion. The arrows on the abscissa indicate the limits of the range of the particles corresponding to the energy interval 2.9 to 10 Mev.

ues were given for the ratio $Y(\gamma, d)/Y(\gamma, p)$ for copper at $E_{\gamma\,max} = 70$ Mev. When the data are more correctly analyzed with account of the background, we obtain for particles with energies in the range 4 to 10 Mev $Y(\gamma, d)/Y(\gamma, p) = 0.04 \pm 0.01$ and for the range 3 to 10 Mev $Y(\gamma, d)/Y(\gamma, p) = 0.05 \pm 0.01$.

Chizhov and Kul'chitskii [1] have shown that the yield ratio for particles of a given energy interval increases with increasing bremsstrahlung energy. Such a tendency has been confirmed by our experiments. The observed rather sharp increase of the yield ratio is obviously due not to evaporation but to a different process of deuteron production.

In the present work we also have estimated the ratio of the yield of photoalphas to the yield of photoprotons from Al^{27}. Neglecting a possible contribution from phototritons we obtain for particle energies 8.8 to 14 Mev $Y(\gamma, \alpha)/Y(\gamma, p) = 0.023 \pm 0.019$. This relative yield of α particles is not in contradiction with the available experimental information for light and medium nuclei.

The author thanks I. Dregich for help in the measurements and to the synchrotron crew of the A. P. Ioffe Physics Institute of the U.S.S.R. Academy of Sciences for running the synchrotron.

[1] V. P. Chizhov and L. A. Kul'chitskii, JETP **36**, 345 (1959), Soviet Phys. JETP **9**, 393 (1959).

[2] V. P. Chizhov, JETP **38**, 809 (1960), Soviet Phys. JETP **11**, 587 (1960).

[3] Komar, Makhnovskii, and Poddubnov, DAN SSSR **133**, 797 (1960), Soviet Phys.-Doklady **5**, 824 (1960).

[4] A. P. Komar and S. P. Kruglov, ZhTF **30**, 1369 (1960), Soviet Phys.-Tech. Phys. **5**, 1299 (1961).

[5] B. Forkman, preprint.

[6] P. R. Byerly and W. E. Stephens, Phys. Rev. **83**, 54 (1951).

Translated by M. Danos
193

SLOW-IONS PRODUCED IN GASES UPON PASSAGE OF FAST ATOM AND ION BEAMS

I. P. FLAKS, G. N. OGURTSOV, and N. V. FEDORENKO

Leningrad Physico-Technical Institute, Academy of Sciences, U.S.S.R.

Submitted to JETP editor May 29, 1961

J. Exptl. Theoret. Phys. (U.S.S.R.) 41, 1094-1103 (October, 1961)

The cross section σ_{0k} for production of slow ions with various charges in single collisions of fast Ne^0 atoms and Ne^+, Ne^{2+}, Ne^{3+} ions with Ne, Ar, Kr, Xe atoms and of fast Kr^0, Kr^+, Kr^{2+}, Kr^{3+} atoms and ions with Kr and Xe atoms was measured at accelerating potentials from 3 to 30 kv. The experimental data show that with increasing charge of the fast particle the cross section σ_{0k} increases as a rule. In atom-atom collisions slow ions are produced only by ionization and the cross section σ_{0k} continuously grows with increasing velocity of the fast ionizing particle. The main processes that determine the cross sections σ_{0k} and their energy dependence in ion-atom collisions are charge exchange and ionization with capture.

INTRODUCTION

WHEN fast atomic particles I^{n+} collide with atoms A of a gas, slow ions can be produced by three processes: pure ionization

$$I^{n+} + A \to I^{n+} + A^{k+} + ke, \qquad (1)$$

charge exchange

$$I^{n+} + A \to I^{m+} + A^{k+} \qquad (m + k = n) \qquad (2)$$

and ionization with capture*

$$I^{n+} + A \to I^{m+} + A^{k+} + (m + k - n)e. \qquad (3)$$

The cross sections of processes (1)—(3) can be written in general form as σ_{0k}^{nm}, where the superscripts pertain to the initial and final charge states of the fast particle while the subscripts pertain to the charge state of the slow atomic particle. Since the ionization of atoms can also be accompanied by "stripping" of fast particles, the indices n, m, and k can range in principle from zero to the total number of electrons Z_I and Z_A in the shells of the colliding atomic particles, and to describe the processes one must have complete data on the charge states of both particles before and after collision. Data of this kind can be obtained only by the coincidence method.

Considering the limited capabilities of mass-spectrometric methods, which enable us to investigate separately the charge states of only fast or only slow secondary ions, we use a two-index system. The cross sections for the production of fast secondary ions will be designated by superscripts (σ^{nm}), while the cross sections for the formation of slow ions will be denoted by subscripts (σ_{0k}). In both cases, the first index denotes the initial charge state and the second the final state.

In our earlier papers [3,4] we reported measurements of the total cross sections for the formation of slow ions, denoted by σ_+, and the total cross section for the formation of free electrons (or the total ionization cross sections) σ_-, while in [5,7] we measured the charge-exchange cross sections σ^{nm} of differently charged ions. These measurements never determined the charge composition of the slow ions and the dependence of this composition on the charge of the fast atomic particles. The first qualitative data of this kind were obtained for Ar^+ and Ar^{2+} and for the atoms Ar and Kr. [8] The purpose of the present investigation was to determine the cross sections for the formation of slow ions of different charges (σ_{0k}), and to determine their connection with the charge of the fast atomic particle by comparison with our earlier data. [5-7]

The procedure used to measure the cross sections σ_{0k} was similar to that employed earlier, [2] but was modified somewhat. The choice of objects for the investigation was determined by the best conditions under which this procedure can be applied, when the mass of the fast ionizing particle does not exceed the mass of the gas atom. We investigated the following pairs: Ne^{n+}–Ne, Ne^{n+}–Ar, Ne^{n+}–Kr, Ne^{n+}–Xe and Kr^{n+}–Kr, Kr^{n+}–Xe. The charge n varied from 0 to 3, and the accelerated voltage V varied from 3 to 30 kv.

*The possible existence of processes of group (3) was first pointed out in [1,2].

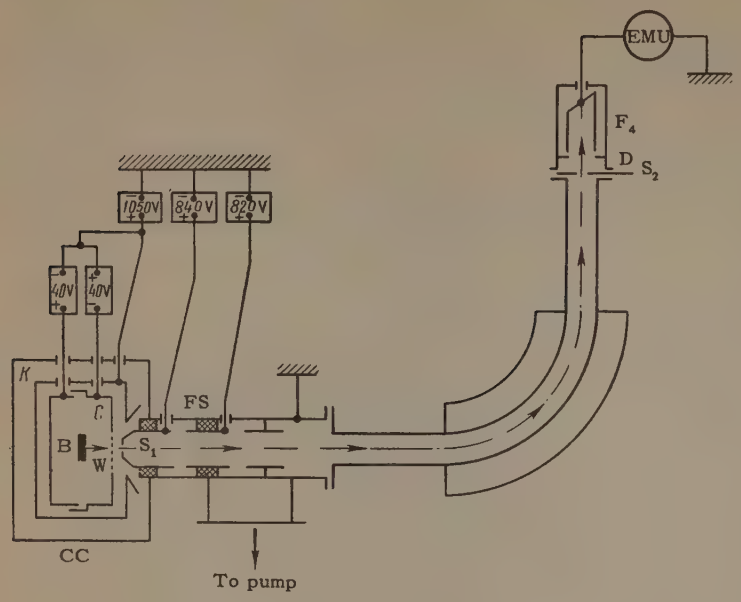

FIG. 1. Analyzer for slow ions.

1. MEASUREMENT PROCEDURE

The cross sections for the formation of slow ions of different charges were measured in the experimental setup described in [3,4], supplemented with a secondary-ion analyzer. A diagram of this analyzer is shown in Fig. 1. The slow ions were produced in a gas broached by a fast atom or ion beam B. They were extracted from this volume by a potential $V_C = \pm 40$ v applied to the plates of a capacitor C in a metallic container K insulated from the ground. To accelerate slow ions, an accelerating voltage $V_p = +1050$ v was applied to the container K and to the electrodes in it.* The ions then proceeded to the analyzer through a window W in the capacitor plates; the window was covered with a loose metal grid.

The potentials V_C and V_p and the potentials on the focusing system FS were determined by control experiments similar to those described in [2].

The analyzer was a sector type magnetic mass spectrometer with a deflection angle 90°, an average trajectory radius 150 mm, and a 10 mm gap between magnetic poles. The analyzer was connected to the grounded outer container of the collision chamber CC. The measuring part of the analyzer was also at ground potential. This was the principal difference between our method of measuring cross sections and the method described in [2], where the analyzer and the ion receiver connected to the input of a vacuum-tube electrometer were at approximately 1000 v relative to ground, so that the sensitivity of the electrometer could not be fully utilized.

The beam of slow ions entered the analyzer through a slit S_1 (1.5×10 mm). At the output of the analyzer was a slit S_2 (2×14 mm), which served to determine exactly the position of the lines in the mass spectrum and to verify the beam focusing conditions. When the cross sections σ_{0k} were measured, the slit S_2 was moved out and the input aperture of receiver F_4 was limited by the aperture of the diaphragm D (25 mm dia). Receiver F_4 was connected to a type ÉMU-2 electrometer with maximum sensitivity 2×10^{-15} amp/div.

The analyzer chamber was evacuated with a TsVL-100 supplementary pump. In the presence of gas in the collision chamber the pressure in the analyzer chamber was less than 1×10^{-5} mm Hg. That the collisions were single was confirmed by the presence of practically linear portion on the slow-ion beam intensity vs collision-chamber gas pressure curve. The pressure of the investigated gas did not exceed 2×10^{-4} mm Hg.

The slow ions were identified by comparing the spectrograms with and without the investigated gas in the collision chamber.

The cross sections for the formation of differently charged slow ions was determined from the formula

$$\sigma_{0k} = \frac{1}{k} \alpha_k \sigma_+, \qquad (4)$$

where α_k — relative intensity of the lines of slow ions with charge k and σ_+ — total cross section for the production of slow ions (per unit charge).

*In measurements with fast ions the accelerating voltage V was increased by the same amount.

The cross sections σ_+ for the atom-atom and single-charge ion-atom pairs investigated in the present work were measured by us earlier.[3] For doubly-charged and triply-charged ions, the cross sections σ_+ were measured simultaneously with σ_{0k}. It is obvious that σ_+ is the sum

$$\sigma_+ = \sigma_{01} + 2\sigma_{02} + 3\sigma_{03} + \ldots . \quad (5)$$

In most cases the overall error in the measurement of the cross section σ_{0k}, estimated from the reproducibility of the results, did not exceed 15%. In measurements made with krypton, the lines of the slow Kr^{3+} ions were masked by a large background due to the N_2^+ which has the same ke/M, so that an additional systematic error has crept into the measurement of the cross sections σ_{03} in krypton.

2. MEASUREMENT RESULTS AND DISCUSSION

We investigated the dependence of the cross sections for the production of slow ions of various charges (σ_{0k}) on the kinetic energy T of the fast ionizing particles. The results of the measurements for fast Ne^0, Ne^+, Ne^{2+}, and Ne^{3+} particles are shown in Figs. 2—5 for the Ne, Ar, Kr, and Xe atoms, respectively, while the result for the fast Kr^0, Kr^+, Kr^{2+}, and Kr^{3+} particles are shown in Figs. 6 and 7 for the Kr and Xe atoms respectively.

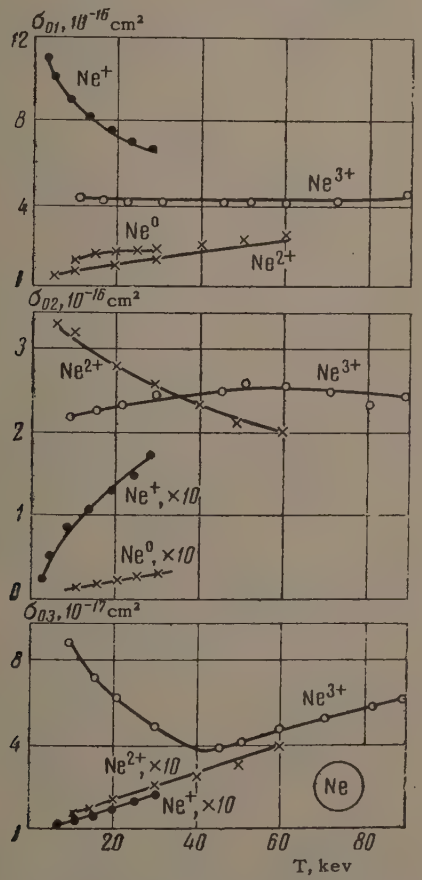

FIG. 2. Dependence of the cross sections for the production of slow singly-charged (σ_{01}), doubly-charged (σ_{02}), and triply-charged (σ_{03}) ions in neon on the energy T of the ionizing particles. The ionizing particles were Ne^0, Ne^+, Ne^{2+}, and Ne^{3+}.

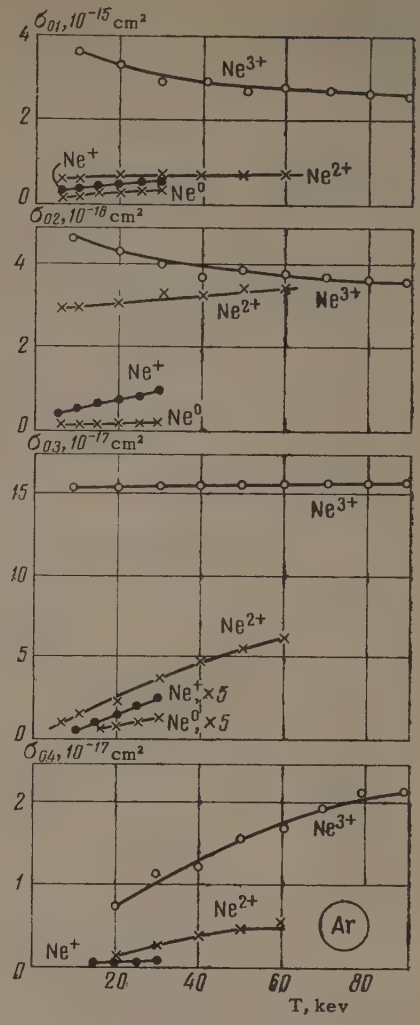

FIG. 3. Cross sections for the production of slow ions in argon.

It can be established, first, that in any given gas the cross sections σ_{0k} for the production of slow ions, increase as a rule with increasing fast-particle charge n, and that for neutral atoms the $\sigma_{0k}(T)$ curves lie lower than all other curves. The course of the $\sigma_{0k}(T)$ curves for different pairs of colliding atomic particles is not the same; in the case of fast neutral atoms the σ_{0k} increase continuously with increasing cross-section energy, while for the ion-atom pairs the σ_{0k} both increase and decrease. In some cases the variation of σ_{0k} was not monotonic.

A. Formation of Singly-Charged Slow Ions

It can be seen from the general schemes (1)—(3) that when a neutral inert-gas atom I^0 collides

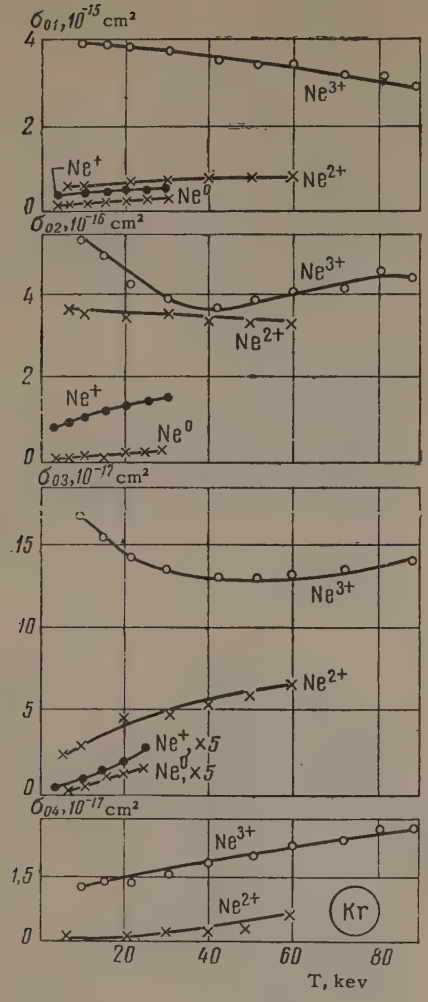

FIG. 4. Cross sections for the production of slow ions in Kr.

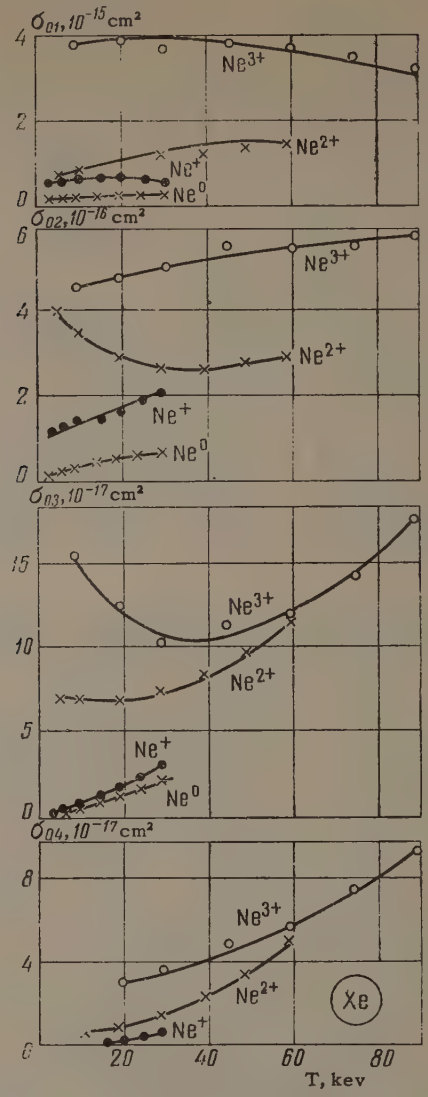

FIG. 5. Cross sections for the production of slow ions in Xe.

with gas atoms A slow singly-charged ions A^+ are produced only via pure ionization

$$I^0 + A \rightarrow I^0 + A^+ + e. \qquad (6)$$

In the energy interval 3—30 kev, simultaneous "stripping" and ionization ($I^0 + A \rightarrow I^+ + A^+ + 2e$) can be neglected since σ_{01}^{01} is small compared with σ_{01}^{00}.

It follows from general considerations that the maximum of the energy dependence of the pure ionization should lie above the Bohr velocity $e^2/\hbar$, i.e., beyond the investigated energy interval in the case of heavy fast particles.[9] In this connection, all the $\sigma_{01}(T)$ curves for fast neutral atoms increase with energy (Figs. 2—7).

In the case of ion-atom collisions, single-charged slow ions can be created both via pure ionization

$$I^{n+} + A \rightarrow I^{n+} + A^+ + e, \qquad (7)$$

and via single-electron charged exchange

$$I^{n+} + A \rightarrow I^{(n-1)+} + A^+. \qquad (8)$$

The form of the curves $\sigma_{01}(T)$ for the like pairs Ne^+–Ne and Kr^+–Kr (Figs. 2 and 6) shows clearly that the predominant role in the formation of singly-charged ions is played by resonant charge exchange, the cross section of which decreases continuously with increasing energy. For other I^+–A pairs, σ_{01} increases with energy because of the increase in the cross section for the non-resonant charge exchange and pure ionization.

As a rule, σ_{01} increases with increasing n, owing to the increase in the relative role of the charge-exchange processes. Only for the like pairs Ne^+–Ne and Kr^+–Kr is σ_{01} greater than for the pairs Ne^{2+}–Ne, Kr^{2+}–Kr and Ne^{3+}–Ne, Kr^{3+}–Kr, since the cross section of the resonant single-electron charge exchange, σ^{10}, is greater than the cross sections for the single-electron charge exchange σ^{21} and σ^{32}.[5-7]

From a comparison of the data of the present paper and the earlier data[5-7] we can also es-

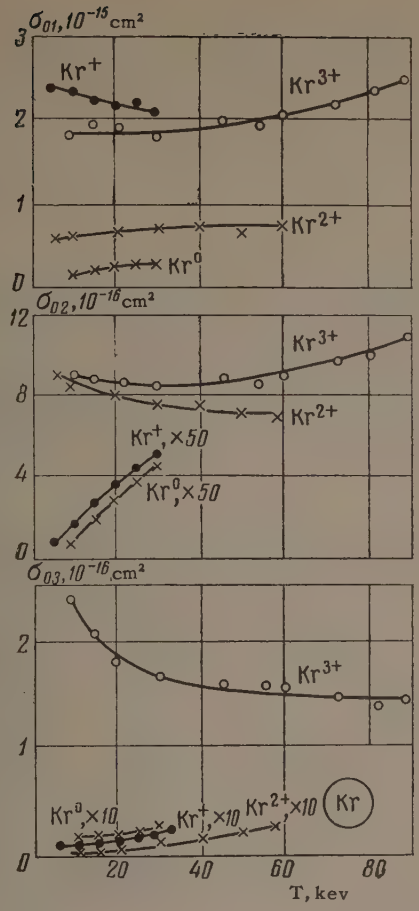

FIG. 6. The same as Fig. 4; the ionizing particles are Kr^0, Kr^+, Kr^{2+}, and Kr^{3+}.

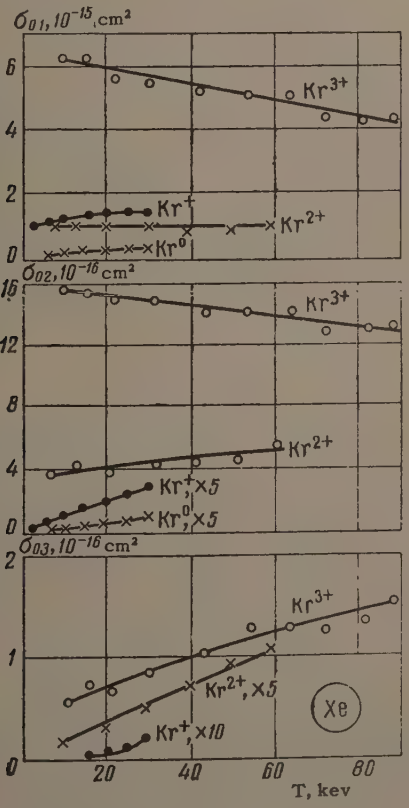

FIG. 7. The same as Fig. 5; the ionizing particles are Kr^0, Kr^+, Kr^{2+}, and Kr^{3+}.

tablish that the $\sigma_{01}(T)$ curves for fast doubly-charged ions are similar to the $\sigma^{21}(T)$ curves for single-electron charge-exchange, while for the Ne^{3+}–Kr pair and the same velocity σ_{01} is very close to the charge-exchange cross section σ^{32}. For the like pairs Ne^{3+}–Ne and Kr^{3+}–Kr, the cross sections σ_{01} and σ^{32} are also close in magnitude and increase simultaneously with increasing energy. We have no data to compare the pairs Ne^{3+}–Ar, Ne^{3+}–Xe, and Kr^{3+}–Xe, but the large values of σ_{01} undoubtedly indicate that the charge-exchange cross sections of the fast triply-charged ions, which have not yet been measured, are large.

B. Doubly-Charged Slow Ions

For the I^0–A pairs, the production of A^{2+} ions, as of all slow ions with larger charge, must be ascribed to pure ionization. For the I^{n+}–A pairs, a considerable contribution to the cross sections σ_{02} is made by ionization with capture, and when $n \geq 2$ the two-electron charge exchange processes also contribute.

An examination of Figs. 2—7 shows that for all the investigated I^0–A pairs σ_{02} continuously increases with increasing energy T and with decreasing energy of double ionization of the gas atom. In the initial region of the energies, the cross sections for the formation of slow ions, $\sigma_{02}(I^0)$ and $\sigma_{01}(I^0)$ differ by one order of magnitude and more; with increasing energy, this difference decreases because of the steeper variation of the $\sigma_{02}(T)$ curves.

For I^+–A pairs $\sigma_{02}(I^+)$ also increases continuously with the energy, but much more slowly than $\sigma_{02}(I^0)$. The great difference between $\sigma_{02}(I^+)$ and $\sigma_{02}(I^0)$ shows that ionization with capture plays the predominant role in the production of A^{2+} ions, since this process involves less energy loss than pure ionization, by an amount equal to the energy required to neutralize the fast single-charge ion.

With increasing charge of the fast ions, the cross sections σ_{02} increase and the character of their energy dependence changes. In the case of the like pairs Ne^{2+}–Ne and Kr^{2+}–Kr, doubly-charged slow ions are formed predominantly by resonant two-electron charge exchange, and the cross sections σ_{02} decrease monotonically with increasing energy. It is easily seen that $\sigma_{02}(I^{2+})$ exceeds $\sigma_{01}(I^{2+})$ in the initial energy range (6—40 kev), since the resonant charge-exchange cross section σ^{20} exceeds the charge-exchange cross section σ^{21}.[5]

For the Ne^{2+}–Kr and Ne^{2+}–Xe pairs, a greater contribution may be made to σ_{02} by ionization with capture

$$I^{2+} + A \rightarrow I^{+} + A^{2+} + e, \qquad (9)$$

rather than by charge exchange ($I^{2+} + A \rightarrow I + A^{2+}$). This is confirmed by the fact that the cross sections σ_{02} for these pairs are greater than the charge-exchange cross sections σ^{20} measured in [6], and the $\sigma_{02}(T)$ and $\sigma^{20}(T)$ curves are different. This relation obtains between the cross sections because processes (9) are exothermic for these pairs.

For the remaining two pairs, Ne^{2+}–Ar and Kr^{2+}–Xe, processes (9) are endothermic and their contributions to σ_{02} is apparently smaller. For these pairs both the σ_{02} and the σ^{20} increase continuously with the energy T.

In the case of triply-charged fast ions the cross sections σ_{02} for the like pairs Ne^{3+}–Ne and Kr^{3+}–Kr are only 2 or 2.5 times smaller than the corresponding cross sections σ_{01}, while for the unlike pairs they differ by a factor 6 or 7. We obtained the same relation for the cross sections of two-electron (σ^{31}) and single-electron (σ^{32}) charge-exchange.[7] However, for the pairs Ne^{3+}–Ne, Ne^{3+}–Kr, and Kr^{3+}–Kr, which are comparable with the data of [7], the σ_{02} greatly exceed the capture cross sections σ^{31}, since the σ_{02} include ionization with capture

$$I^{3+} + A \rightarrow I^{2+} + A^{2+} + e, \qquad (10)$$

a process that is exothermic for all the investigated pairs except Kr^{3+}–Kr.

C. Triply-Charged Slow Ions

The cross section σ_{03} for pure triple ionization was measured only for the pairs Ne^{0}–Ar, Ne^{0}–Kr, Ne^{0}–Xe, and Kr^{0}–Kr. For the remaining two pairs, Ne^{0}–Ne and Kr^{0}–Xe, the currents corresponding to triply-charged slow ions where below the sensitivity limit of the electrometer.

For I^{n+}–A pairs with $n \geq 1$, A^{3+} ions are also produced by ionization with capture, while when $n \geq 3$ three-electron charge exchange is added to these processes. An examination of Figs. 2–7 readily shows that the $\sigma_{03}(I^{+})$ differ from the $\sigma_{03}(I^{0})$ in the mean by only 1.5–2 times, since pure ionization and ionization with capture

$$I^{+} + A \rightarrow I^{0} + A^{3+} + 2e \qquad (11)$$

are strongly endothermic processes and the relative decrease in the energy of reaction (11) is small compared with the energy of triple ionization of the gas atom. With increasing energy T, $\sigma_{03}(I^{0})$ and $\sigma_{0}(I^{+})$ increase continuously.

For I^{2+}–A pairs, the ionization with capture processes

$$I^{2+} + A \rightarrow I^{+} + A^{3+} + 2e, \qquad (12)$$

$$I^{2+} + A \rightarrow I^{0} + A^{3+} + e, \qquad (13)$$

are also endothermic and the cross sections σ_{03} increase with energy. However, the reaction energy of the process (12), and particularly of (13), is considerably less than the energy of the pure ionization process, and therefore the $\sigma_{03}(I^{2+})$ greatly exceed $\sigma_{03}(I^{0})$ for almost all the I^{2+}–A pairs.

In the collision of triply-charged ions with gas atoms, I^{3+}–A, the predominant role in the formation of A^{3+} ions is played in the case of the like pairs Ne^{3+}–Ne and Kr^{3+}–Kr by the resonant charge-exchange processes. The cross sections σ_{03}, like the three-electron charge exchange cross section σ_{30}, decrease with increasing energy.[7] For the Ne^{3+}–Ne pair at energies ~45–90 kev, the charge-exchange cross section σ^{30} is practically constant and the increase in the cross sections σ_{03} with increasing energy is due to the endothermal processes of ionization with capture

$$I^{3+} + A \rightarrow I^{2+} + A^{3+} + 2e, \qquad (14)$$

$$I^{3+} + A \rightarrow I^{+} + A^{3+} + e, \qquad (15)$$

and also to pure ionization.

A comparison of σ_{03} with σ^{30} for the Ne^{3+}–Kr pair shows that for the same energy σ_{03} is 4–5 times greater than σ_{30},[7] since the processes (14) are exothermic for this pair, as well as for the Ne^{3+}–Ar and Ne^{3+}–Xe pairs, and it is probable that these processes make a greater contribution to σ_{03} than the three-electron charge-exchange processes.

D. Quadruply-Charged Slow Ions

The cross sections σ_{04} were measured only for the collisions of Ne ions with Ar, Kr and Xe atoms. As can be seen from the data of Figs. 4–6, the cross sections σ_{04} increase sharply with increasing energy and with increasing charge of the fast ions. The cross section σ_{04} is on the order of 10^{-19} cm^2 for the Ne^{+}–Ar pair and on the order of 10^{-18} cm^2 for the Ne^{+}–Xe pairs. With increasing fast-ion charge, the number of ionization processes with capture increases and the energies of these reactions are greatly reduced, thereby increasing σ_{04}. For the Ne^{3+}–Xe pair ionization with capture ($Ne^{3+} + Xe \rightarrow Ne^{0} + Xe^{4+} + e$) is an

Charge-exchange cross section σ^{10} (in units of 10^{-16} cm^2) calculated from (18) and (19) (in parentheses) and determined by measuring the difference $(\sigma_+ - \sigma_-)$ [3]

Energy	$Ne^+ - Ne$		$Ne^+ - Ar$		$Ne^+ - Kr$		$Ne^+ - Xe$		$Kr^+ - Kr$		$Kr^+ - Xe$	
T, kev	σ^{10}	$\sigma_+ - \sigma_-$	σ^{10}	$\sigma_+ - \sigma_-$	σ^{10}	$\sigma_+ - \sigma_-$	σ^{10}	$\sigma_+ - \sigma_-$	σ^{10}	$\sigma_+ - \sigma_-$	σ^{10}	$\sigma_+ - \sigma_-$
6	—	—	2.4	2.5	3.6	3.6	5.8	5.6	—	—	10.8	8,4
15	6.7 (5.4)	5.6	2,75	3.0	4.0	4.2	5,4	5.3	20,1 (17.8)	18	12.5	9.3
25	5.7 (4,1)	4.2	3.3	3.45	4,25	4,3	5,0	4,8	19,1 (16,4)	16,5	12,8	9,3

exothermal process and this is apparently why σ_{04} reaches a value close to 1×10^{-16} cm^2 for this pair.

E. Estimate of the Cross Section for Ionization with Capture

By examining the experimental data for the simplest cases, when the fast particles are singly-charged ions and σ_{0k} is the sum of only two cross sections, we can attempt to estimate quantitatively the contribution of the individual cross sections to the overall cross sections σ_{0k}, starting from the assumption that the pure-ionization cross sections are the same for fast neutral atoms and for singly-charged ions

$$\sigma_{0k}^{11}(I^+) = \sigma_{0k}^{00}(I^0). \qquad (16)$$

In this case the charge-exchange cross section σ_{01}^{10}, which enters in $\sigma_{01}(I^+)$, and the cross sections for ionization with capture, σ_{02}^{10} and σ_{03}^{10}, which enter in σ_{02} and σ_{03}, are differences of the cross sections

$$\sigma_{0k}^{10} = \sigma_{0k}(I^+) - \sigma_{0k}(I^0). \qquad (17)$$

The assumption (16) can be verified by comparing the summary charge-exchange cross sections, obtained by adding the cross sections calculated from (17)

$$\sigma^{10} = \sigma_{01}^{10} + \sigma_{02}^{10} + \sigma_{03}^{10} \qquad (18)$$

and measured in [3] by determining the difference of the cross sections $(\sigma_+ - \sigma_-)$.

The values of σ^{10} and $(\sigma_+ - \sigma_-)$ are compared in the table for 6, 15, and 25 kev (the cross sections are given in units of 10^{-16} cm^2).

As can be seen from the table, assumption (16) is valid only for the pairs Ne^+–Ar, Ne^+–Kr and Ne^+–Xe. For the remaining cases, the cross sections for pure ionization of gas atoms by singly-charged ions and by fast ions may differ appreciably. In particular, in the ionization of gas atoms by fast atoms of the same gas, the same amount of energy is consumed in ionization and in "stripping," and the cross sections of these processes should be equal. [3]

In ionization by ions with relatively low energy (3–30 kev), we can neglect the "stripping" of the ions and instead of (16) we can assume for the like ion-atom and atom-atom pairs

$$\sigma_{0k}^{11}(I^+) \approx 2\sigma_{0k}^{00}(I^0), \qquad (19)$$

thereby obtaining a good agreement between σ^{10} and $(\sigma_+ - \sigma_-)$ [the values of σ^{10} determined from (19) are shown in the table in parentheses].

By way of an example, Fig. 8 shows the estimated charge-exchange cross sections σ_{01}^{10} and

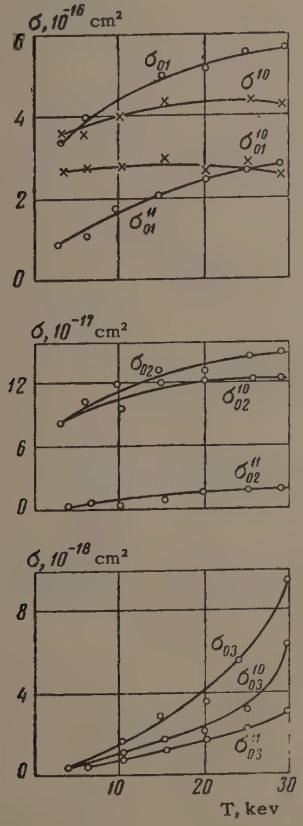

FIG. 8. Dependence of the cross sections of different processes in Kr on the energy of the fast Ne^+ particle. σ_{01}, σ_{02}, σ_{03} – cross sections for the production of singly-, doubly-, and triply-charged ions; σ_{01}^{11}, σ_{02}^{12}, σ_{03}^{11} – cross sections for pure ionization: σ_{01}^{10}, σ_{02}^{10}, σ_{03}^{10} – cross sections for ionization with capture; σ^{10} – charge-exchange cross section.

the cross sections for ionization with capture σ_{02}^{10} and σ_{03}^{10} for the pair Ne^+–Kr. The same figure shows also the summary cross sections σ_{01}, σ_{02}, and σ_{03} as well as the pure-ionization cross sections σ_{01}^{11}, σ_{02}^{11} and σ_{03}^{11}, determined under the assumption (16), and also the summary charge-exchange cross sections σ^{10}. It is seen from these data that in the initial energy range the relative contribution of charge exchange to σ_{01} predominates over the contribution from pure ionization. But since the pure-ionization cross section increases more rapidly with energy than does the charge-exchange cross section, the contributions from both processes are approximately the same at the limiting energy value. Pure ionization plays a small role in the formation of doubly-charged slow ions, while pure ionization and ionization with capture are approximately of equal weight in the production of triply-charged slow ions. All these conclusions are in good agreement with remarks in the preceding sections, based on energy considerations, concerning the relative probability of various processes.

In conclusion, the author is deeply grateful to Professor V. M. Dukel'skii for a discussion of the results of the work.

[1] Fedorenko, Afrosimov, and Kaminker, ZhTF **26**, 1929 (1956), Soviet Phys.-Tech. Phys. **1**, 1861 (1957).

[2] N. V. Fedorenko and V. V. Afrosimov, ibid. **26**, 1941 (1956) [translation **1**, 1872 (1957)].

[3] I. P. Flaks, ibid. **31**, 367 (1961),[translation **6**, 263 (1961)].

[4] Fedorenko, Flaks, and Filippenko, JETP **38**, 719 (1960), Soviet Phys. JETP **11**, 519 (1960).

[5] I. P. Flaks and E. S. Solov'ev, ZhTF **28**, 599 (1958), Soviet Phys.-Tech. Phys. **3**, 564 (1958).

[6] I. P. Flaks and E. S. Solov'ev, ibid. **28**, 612 (1958) [translation **3**, 577 (1958)].

[7] I. P. Flaks and L. G. Filippenko, ibid. **29**, 1100 (1959) [translation **4**, 1005 (1960)].

[8] N. V. Fedorenko, ibid. **24**, 1950 (1954).

[9] N. V. Fedorenko, UFN **68**, 481 (1959), Soviet Phys.-Uspekhi **2**, 526 (1960).

Translated by J. G. Adashko
194

TWO-ELECTRON CHARGE EXCHANGE OF PROTONS IN HELIUM DURING FAST COLLISIONS

V. I. GERASIMENKO

Physico-Technical Institute, Academy of Sciences, Ukranian S.S.R.

Submitted to JETP editor September 23, 1960; resubmitted July 6, 1961

J. Exptl. Theoret. Phys. (U.S.S.R.) 41, 1104-1106 (October, 1961)

The integral cross section for capture of two electrons by protons in helium is calculated in the first Born approximation.

SEVERAL recent theoretical and experimental papers are devoted to the capture of electrons in atomic collisions. The purpose of these papers, in addition to a determination of the effective capture cross sections, was to ascertain, by comparison of the theoretical and the experimental results, whether a particular approximate calculation method is applicable.[1] It has become clear, in particular, that the cross section for the capture of one electron by the protons in hydrogen, calculated in the first Born approximation, agrees with the experimental cross section up to the limits of applicability of the Born approximation.

It must be noted that most published papers have been devoted to single-electron processes. In the present communication we determine the cross section for one of the many-electron processes, namely the cross section for the capture of two electrons in a collision between fast protons and helium atoms (when the Born approximation is valid). In this case the Born threshold is about 100 kev (in the laboratory frame). This process has already been investigated theoretically[2] at low colliding-particle velocities, and experimentally[3] at medium velocities.

The differential c.m.s. cross section of the transition of two electrons from the ground state of the helium atom to the ground state of the H^- ion is

$$d\sigma = \frac{k_2}{k_1}|f(\theta)|^2 do;$$

$$f(\theta) = \frac{\mu}{2\pi}\int\int\int e^{-i\mathbf{k}_2\mathbf{r}}\psi(r_1, r_2)\, V(\mathbf{p}_1, \mathbf{p}_2, \mathbf{r}_1)\, e^{i\mathbf{k}_1\mathbf{s}}\varphi(p_1, p_2) \times d\mathbf{r}_1 d\mathbf{r}_2 d\mathbf{r},$$

$$V(\mathbf{p}_1, \mathbf{p}_2, \mathbf{r}_1) = 2/p_1 + 2/p_2 - 2/|\mathbf{r}_1 - \mathbf{p}_1|.$$

Here $\mathbf{s}(\mathbf{r})$ is the radius vector of the proton (α particle) relative to the center of gravity of the helium atom (the H^- ion); $\mathbf{r}_1, \mathbf{r}_2(\mathbf{p}_1, \mathbf{p}_2)$ are the radius vectors of the electrons relative to the proton (α particle); $\mathbf{k}_1(\mathbf{k}_2)$ is the wave vector before (after) scattering, with $k_1^2 = \mu E$, $K_2^2 = \mu(E - E_1 + E_2)$, where E —energy of relative motion, E_1 and E_2 are respectively the energies of the H^- and He ground states, $\mu = {}^4/_5\epsilon$ —reduced mass, ϵ —the ratio of the mass of the electron to the mass of the proton;

$$\psi = (z^3/\pi)^2 e^{-z(r_1+r_2)}, \qquad \varphi = (z'^3/\pi)^2 e^{-z'(p_1+p_2)}$$

—respectively the wave functions of the ground state of the H^- ion and the helium atom; $z = 0.69$, $z' = 1.69$. These formulas are written in atomic units ($\hbar = e = m = 1$); the cross section is in a_0^2 units ($a_0 = 0.529 \times 10^{-8}$ cm^2).

The scattering amplitude can be reduced to a form convenient for numerical integration. Transformations analogous to those used in [4] yield

$$f(\theta) = 48\mu z^4\alpha^4\pi^{-2}(J_1 - J_2);$$

$$J_1 = 16\int_0^1\int_0^1 dx\, dy\, xy\,(1-y)\, a^{-3}b^{-5}A^{-5}F_1(x, y),$$

$$J_2 = \int_0^1\int_0^1 dx\, dy\, xy\,(1-x)(1-y)\, a^{-5}b^{-5}A^{-5}F_2(x, y).$$

$$F_1 = a^3A^2 + 2Ab(a+b)^2(3a^2 - 2ab + b^2) + 16ab^2(a+b)^4,$$

$$F_2 = 3A^4 + 2A^3(2a^2 + 3ab + 2b^2) + 8A^2[(a+b)^4 - ab(2a^2 + 3ab + 2b^2)] + 48Aab(a^2 + b^2)(a+b)^2 + 128a^2b^2(a+b)^4,$$

$$a^2 = 1 + (\alpha^2 - 1)x + \varkappa^2(1-x)x,$$

$$b^2 = 1 + (\alpha^2 - 1)y + \varkappa^2(1-y)y,$$

$$A = (a+b)^2 + (\mathbf{g} + \varkappa x + \varkappa y)^2, \qquad \alpha = z/z',$$

$$\mathbf{g} = \frac{1}{z'}\left(\frac{2}{2+\varepsilon}\mathbf{k}_1 - \mathbf{k}_2\right), \quad \varkappa = \frac{\varepsilon}{z'}\left(\frac{\mathbf{k}_1}{4+2\varepsilon} + \frac{\mathbf{k}_2}{1+2\varepsilon}\right),$$

$$\cos\theta = \frac{\mathbf{k}_1\mathbf{k}_2}{k_1k_2}.$$

The integrals J_1 and J_2 in the cross section are brought about by the interaction between the

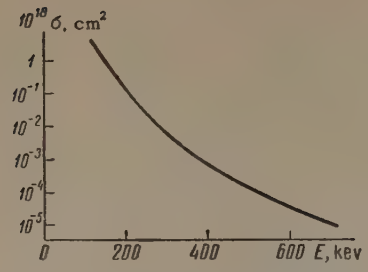

electrons and the incoming proton and by the interaction between the nuclei, respectively. At very high energies, they decrease with energy in like fashion. Indeed, as $E \to \infty$ we have

$$J_1 \sim \int_0^1 x\,dx \int_0^1 \frac{y(1-y)}{b^5 A^3}\,dy, \quad J_2 \sim \int_0^1 \frac{x(1-x)}{a^5}\,dx \int_0^1 \frac{y(1-y)}{b^5 A}\,dy.$$

A is proportional to E in the entire range of values of x and y, and hardly depends on x or y; therefore

$$J_1 \sim \frac{1}{E^3}\int_0^1 \frac{y(1-y)}{b^5}\,dy, \quad J_2 \sim \frac{1}{E}\left\{\int_0^1 \frac{y(1-y)}{b^5}\,dy\right\}^2,$$

hence, after integration,

$$J_1 \sim E^{-5}, \quad J_2 \sim E^{-5}.$$

From the physical point of view, it becomes obvious that the contribution to the cross section from the interaction between the nuclei should decrease with increasing E more rapidly than the contribution due to the interaction between the electrons and the incoming particle.

Such a difficulty exists also in the analysis of the capture of a single electron.[5,6] Several authors[7,8] were able to reconcile the calculated cross section with the physical notions regarding the nature of the charge-exchange process. At low energies, however, the single charge exchange cross sections calculated in[5-8] are practically the same. In the present note we calculate the double charge exchange cross section for energies where the corrections proposed in [7,8] are apparently still insignificant.

The calculated integral cross section is shown in the figure as a function of the energy of the incoming protons in the laboratory frame. At the present time there are no experimental data for energies greater than 100 kev. It would be desirable to obtain such data and to compare them with the results of this paper. We note that the negative hydrogen ion apparently has no excited levels. The calculated cross section can therefore be directly compared with experiment.

[1] D. R. Bates and A. Dalgarno, The Airglow and the Aurorae, p. 328, London (1955).

[2] L. N. Rozentsveĭg and V. I. Gerasimenko, Trudy, Khar'kov State University **6**, 86 (1956).

[3] Fogel', Mitin, Kozlov, and Romashko, JETP **35**, 565 (1958), Soviet Phys. JETP **8**, 390 (1959).

[4] V. I. Gerasimenko and L. N. Rozentsveĭg, JETP **31**, 684 (1956), Soviet Phys. JETP **4**, 509 (1957).

[5] D. R. Bates and A. Dalgarno, Proc. Phys. Soc. **A65**, 919 (1952).

[6] J. D. Jackson and H. Schiff, Phys. Rev. **89**, 359 (1953).

[7] D. R. Bates, Proc. Roy. Soc. **A247**, 294 (1958).

[8] R. H. Baisel and E. Gerjuoy, Phys. Rev. **117**, 749 (1960).

Translated by J. G. Adashko
195

PARTICLE ACCELERATION BY PASSAGE OF A HYDROMAGNETIC SHOCK WAVE FRONT

V. P. SHABANSKII

Institute of Nuclear Physics, Moscow State University

Submitted to JETP editor February 15, 1961

J. Exptl. Theoret. Phys. (U.S.S.R.) **41**, 1107-1111 (October, 1961)

An expression for the momentum increment of a high-energy particle (compared with the particles comprising the bulk of a plasma) due to passage of a hydromagnetic shock wave is derived and discussed.

We consider a plane hydromagnetic shock wave propagating in a direction perpendicular to a magnetic field (perpendicular shock wave). The velocity of the front relative to the medium 1 ahead of the front is v_1, and that relative to medium 2 behind the front is v_2. Let a charged particle of velocity $v \gg v_1$ be incident from medium 1 on the front of the shock wave. The particle-velocity component parallel to the magnetic field will not change on passing through the front. We therefore choose a system of coordinates in which the particle moves in a plane perpendicular to the magnetic field. We assume that the Larmor radius of the particle is much greater than the width of the front and that this width can be neglected. Moving alternately between regions 1 and 2, the particle will describe circular arcs in coordinate systems that are stationary with respect to media 1 and 2, respectively, the Larmor radius being determined by the magnetic field in region 1 or 2. Thus, a particle remains "tied" to the front for some time.

If the angle between the particle velocity and the normal to the front, directed from 1 into 2, is denoted by φ, then the central angle ϑ swept by the particle in medium 2 is connected with φ by the relation $\vartheta = \pi + 2\varphi$. Here $-\pi/2 \leq \varphi \leq \pi/2$ and $0 \leq \vartheta \leq 2\pi$, and φ is positive when $\vartheta > \pi$. If $v \gg v_1$ the displacement of the front Δx relative to the medium 2 during the stay $\Delta t = \vartheta/\omega$ of the particle in medium 2 (ω is the Larmor frequency) is equal to $\Delta x = v_2 \Delta t = v_2 \vartheta/\omega$. On the other hand, $\Delta x = r\Delta\vartheta \cos\varphi$, where r is the Larmor radius. Inasmuch as $\Delta\vartheta = 2\Delta\varphi$, and $\omega r = v = pc^2/\epsilon$ (where p is the momentum of the relativistic particle, ϵ is the total energy, and c is the velocity of light), we have for the change of the angle due to the finite stay of the particle in medium 2

$$\Delta\varphi_2 = (v_2/2v)(\pi + 2\varphi)/\cos\varphi. \quad (1)$$

We obtain similarly the change in the angle during the stay of the particle in medium 1. It is necessary to take account of the fact here that the front moves in medium 1 with velocity v_1, and that the same angle φ, which by definition is positive on going from medium 1 into 2, is negative on going from medium 2 into 1. Then

$$\Delta\varphi_1 = (v_1/2v)(\pi - 2\varphi)/\cos\varphi. \quad (2)$$

Along with the angle changes (1) and (2) due to the finite time of stay of the particle in each region (1 or 2), the angle will be increased by the change in momentum of the particle upon reflection from medium 2. The particle momentum component normal to the boundary, $p_\perp = p\cos\varphi$, is increased by $\Delta p_\perp = 2(v_1 - v_2)\epsilon/c^2$, while the increment of the parallel component $p_\parallel = p\sin\varphi$ is $\Delta p_\parallel = 0$. From the equations

$$\Delta p \sin\varphi + p\Delta\varphi' \cos\varphi = 0,$$

$$\Delta p \cos\varphi - p\Delta\varphi' \sin\varphi = 2(v_1 - v_2)\,\varepsilon/c^2$$

we obtain for the increment $\Delta\varphi'$ of the angle and for the change Δp of the momentum the following expressions

$$\Delta\varphi' = -2(v_1 - v_2)\,\varepsilon/pc^2 = -2(v_1 - v_2)\,v^{-1}\sin\varphi, \quad (3)$$

$$\Delta p = 2(v_1 - v_2)\,\varepsilon c^{-2}\cos\varphi. \quad (4)$$

The increment in the angle over the cycle (within a complete revolution of the particle through regions 2 and 1) is made up of the incre-

ments* (1), (2), and (3), viz., $\Delta\varphi = \Delta\varphi_1 + \Delta\varphi_2 + \Delta\varphi'$. Dividing by the increment of momentum over the cycle as given by (4), and taking (1) and (2) into account, we obtain a differential equation relating p and φ:

$$dp/d\varphi = pf(\varphi), \tag{5}$$

where $f(\varphi)$ will be written out below.

The angle at which the particle can no longer leave region 2 is $\varphi = \pi/2$. We therefore, have for the complete increment of the particle-momentum component perpendicular to the magnetic field upon passage of the shock wave front

$$p = p_0 \exp I(\varphi_0), \tag{6}$$

$$I(\varphi_0) = \int_{\varphi_0}^{\pi/2} f(\varphi)\, d\varphi = \int_{\varphi_0}^{\pi/2} \frac{4(1 - v_2/v_1)\cos^2\varphi\, d\varphi}{(\pi + 2\varphi)\, v_2/v_1 + (\pi - 2\varphi) - 4(1 - v_2/v_1)\sin\varphi\cos\varphi}, \tag{7}$$

where φ_0 is the initial angle of entrance into region (2).

The particle will experience maximum acceleration when $\varphi_0 = -\pi/2$, i.e., when it travels parallel to the front in the same direction as the Lorentz force acting from medium 2 towards this front.†

It is characteristic that the magnetic field does not enter explicitly into this equation. The increment in momentum is determined only by the ratio of velocities of the front relative to the gas ahead and behind the shock-wave front, and increases with increasing density discontinuity, since

$$1 - v_2/v_1 = 1 - \rho_1/\rho_2 = (\rho_2 - \rho_1)/\rho_2,$$

where ρ_1 and ρ_2 are the densities of the medium in the regions 1 and 2. Since in a weak shock wave the density discontinuity decreases with increasing ratio of the magnetic pressure $H_1^2/8\pi$ to the gas pressure P_1 for equal wave intensity, the weak-field case is the most favorable from the point of view of particle acceleration on the front.

In the general case of hydromagnetic waves the expressions for v_2/v_1 are quite cumbersome. We shall consider two limiting cases, weak and strong waves.

In the case of weak waves we are interested only in the increment of the momentum of the particle under consideration, compared with the momentum increment of the average-energy particles making up the plasma in which the shock wave propagates. For simplicity we assume that the gas consists of particles with two degrees of freedom. Then the equation of state, which relates the pressure $P^* = P + H^2/8\pi$ and the energy $E^* = E + H^2/4\pi$, coincides with the equation for a perfect gas, and

$$v_2/v_1 = [(\gamma - 1)M_1^{*2} + 2]/[(\gamma + 1)M_1^{*2}], \tag{8}$$

where the generalized Mach number $M_1^* = v_1/c_1^*$ is connected with the ordinary Mach number $M_1 = v_1/c_1$ by the relation

$$M_1^{*2} = M_1^2/(1 + H_1^2/8\pi P_1);$$

γ is the adiabatic exponent, and in our case $\gamma = 2$; $c_1^{*2} = \gamma P_1/\rho_1$ is the magnetohydrodynamic speed of sound.

Let us assume that $M_1^* = 1 + \delta$, $\delta \ll 1$. This means that $M_1 \ll \sqrt{3}\,(1 + H_1^2/8\pi P_1)^{1/2}$ and, generally speaking, we can also have $M_1 \gg 1$. In first order in δ we find from (8) that $v_2/v_1 = 1 - 2\delta/(\gamma + 1)$. Expression (7) yields in this case

$$I(\varphi_0) = \int_{\varphi_0}^{\pi/2} \frac{4\delta\cos^2\varphi\, d\varphi}{\pi(\gamma + 1)} = \frac{2\delta}{\pi(\gamma + 1)}\left(\frac{\pi}{2} - \varphi_0 - \sin 2\varphi_0\right), \tag{9}$$

$$I(-\pi/2) = 2\delta/(\gamma + 1). \tag{10}$$

Substituting the maximum value of I as given by (10) in (6), we obtain for $\delta \ll 1$

$$\Delta p/p_0 = (p - p_0)/p_0 = 2\delta/(\gamma + 1). \tag{11}$$

Let us consider now the momentum increment of the particles of a medium in which a weak shock wave propagates. It can be shown that in the linear approximation in δ the temperature discontinuity in a gas with two degrees of freedom is equal to the

*Direct calculation of the increment of the angle in the coordinate system 1 over the cycle reduces to the following. We determine the increment $\Delta\varphi_1$ in medium 1 during the stay of the particle in this medium [formula (2)]. Then the angle $\varphi + \Delta\varphi_1$ is transformed to the coordinate system 2, using the relativistic transformation formulas.

We calculate the increment $\Delta(\varphi + \Delta\varphi_1)'$ during the stay of the particle in medium 2, and then the angle $(\varphi + \Delta\varphi_1)' + \Delta(\varphi + \Delta\varphi_1)'$ is again transformed to system 1 and the angle increment over the cycle is calculated, viz., $\Delta\varphi = \varphi - (\varphi + \Delta\varphi_1)'' - \Delta(\varphi + \Delta\varphi_1)''$. The momentum change in system 1, corresponding to this angle increment, is determined upon reflection from the medium with account of the fact that the particle energy does not change during its stay in medium 2. The results of this much more cumbersome calculation agrees with the data given in the text, apart from terms of higher order in the smallness parameter v_1/v. But even without this calculation it is seen from the physics of the problem that the angle increment is the result of the effects listed in the text. It does not matter in what system of coordinates we determine subsequently the momentum increment from the differential equation (5), since the relative difference between p in system 1 and p' in system 2 is of order $v_1/c_1 \ll 1$.

†It is easy to see that if the source of fast particles is far from the front (at a distance greater than the Larmor radius of the particle in the medium 1), then the initial angle of entry will always be $\varphi_0 = -\pi/2$, and the acceleration will be a maximum. This is indeed the real case.

discontinuity of total energy E*, i.e., in our approximation almost all the energy on the front is dissipated into heat. Therefore, using the expressions for the discontinuity of E*, we obtain

$$\frac{T_2}{T_1}=\frac{E_2^*}{E_1^*}=\frac{[2\gamma M_1^{*2}-(\gamma-1)]\,[(\gamma-1)\,M_1^{*2}+2]}{(\gamma+1)^2\,M_1^{*2}}\approx 1+2\delta\frac{\gamma-1}{\gamma+1}. \quad (12)$$

The increment of the mean momentum (velocity) of the particles of the medium, $\bar{p}_2/\bar{p}_1=\sqrt{T_2/T_1}$, is

$$\Delta\bar{p}/\bar{p}_1=(\bar{p}_2-\bar{p}_1)/\bar{p}_1=\delta\,(\gamma-1)/(\gamma+1). \quad (13)$$

We see therefore that in our case ($\gamma=2$), which corresponds to a greater heating of the medium particles then in the real case of particles of a gas with three degrees of freedom, the increment (13) of the momentum of the particles of the medium is half as large as the maximum increment of the momentum of the particle under consideration (11), and is equal to the momentum increment of the accelerated particle if the latter is perpendicularly incident on the front ($\varphi_0=0$).

The formulas given above are valid for a real particle gas with three degrees of freedom in the case when $H_1^2/8\pi P_1\ll 1$. Then $M^*\approx M=1+\delta$. The increment of the average momentum of the particles of the medium (13) is $\delta/4$, and that of the accelerated particle (11) is $3\delta/4$, i.e., three times greater.

Let us consider a strong shock wave ($M_1^*\gg 1$). In this case $\rho_1/\rho_2=v_2/v_1=(\gamma-1)/(\gamma+1)$ and expression (7) reduces to

$$I(\varphi_0)=\int_{\varphi_0}^{\pi/2}f(\varphi)\,d\varphi=\int_{\varphi_0}^{\pi/2}\frac{4\cos^2\varphi d\varphi}{\gamma\pi-2\varphi-4\sin\varphi\cos\varphi}. \quad (14)$$

The results of the numerical integration of this expression with $\gamma=5/3$ and substitution in (6) are shown in the figure. The maximum increment of the accelerated-particle momentum amounts to $p/p_0=5.23$ when $\varphi_0=-\pi/2$. This means that the energy, say, of a nonrelativistic particle increases 27 times on passing through the front, while the energy of an ultrarelativistic particle increases 5.3 times.

When $M_1^*\gg 1$ we obtain instead of (12)

$$\frac{T_2}{T_1}<\frac{E_2^*}{E_1^*}=\frac{2\gamma(\gamma-1)}{(\gamma+1)^2}M_1^{*2}. \quad (15)$$

For a particle gas with two degrees of freedom ($\gamma=2$) (for which the heating is greatest), and when $M_1^{*2}<60$, this quantity is less than the maximum increment in the energy of the accelerated particles. Therefore not only weak waves but also intense waves up to $M_1^*\lesssim 8$ will be most favorable for the acceleration of particles of the energy component of the plasma with minimum heating of the bulk of the gas, and can contribute to the decomposition of the plasma into two energy components, hot and cold.

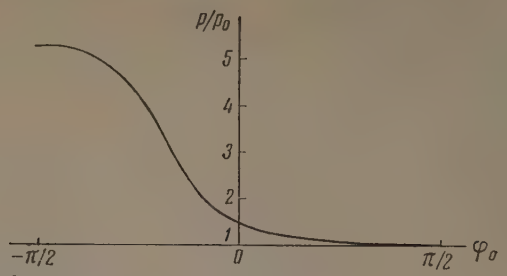

Ratio of momentum p of accelerated particle after passage of the front to the initial momentum p_0, as a function of the angle of incidence φ_0

An attempt to determine the particle acceleration on the front of a hydrodynamic shock wave was made earlier by Dorman and Freĭdman.[1] However, the approximation used in [1] was too crude and not rigorously founded. The formula for the energy increment obtained in that paper did not reflect the dependence of the increment on the angle of incidence of the particle on the front* and had the form

$$\Delta\varepsilon=\varepsilon-\varepsilon_0=\frac{4}{\pi}\frac{(cp_0)^2}{\varepsilon_0}\frac{v_1/v_2-1}{v_1/v_2+1}.$$

For a strong wave [$v_1/v_2\sim(\gamma+1)/(\gamma-1)\sim 4$] we have

$$\Delta\varepsilon=\frac{4}{\pi}\frac{3}{5}\frac{(cp_0)^2}{\varepsilon_0}.$$

In the nonrelativistic case the total energy $\epsilon_0\sim mc^2$ and we obtain for the increment in the kinetic energy

$$\frac{\Delta\varepsilon}{\varepsilon_k^0}=\frac{\varepsilon_k-\varepsilon_k^0}{\varepsilon_k^0}\sim\frac{4}{\pi}\frac{3\cdot 2}{5}\sim 1.6$$

($\epsilon_k/\epsilon_k^0\sim 2.6$), where $\epsilon_k=mv_0^2/2$. In the ultrarelativistic case $\epsilon_0\sim cp_0$ and $\Delta\epsilon/\epsilon_0\sim 4\times\frac{3}{5}\pi\sim 0.8$. The authors themselves state that their estimate of $\Delta\epsilon$ is approximate, accurate to a coefficient ~ 2—3 (as can be seen from the text of the present paper, the error is considerably greater). It is therefore difficult to judge on the basis of the paper by Dorman and Freĭdman whether particles can be accelerated on the front of a hydromagnetic shock wave.

[1] L. I. Dorman and G. I. Freĭdman, Voprosy magnitnoi gidrodinamiki i dinamiki plazmy (Problems of Magnetohydrodynamics and Plasma Dynamics), Riga, (1959).

Translated by J. G. Adashko
196

*By averaging expression (6) over the angles, assuming isotropic incidence of these fast particles on the front, we would obtain a formula which would coincide with the results of[1] in order of magnitude. But this must not be done since, as already noted, in the real case the fast particles are incident on the front at an angle $\varphi_0=-\pi/2$.

SHIFT OF ATOMIC ENERGY LEVELS IN A PLASMA

L. É. PARGAMANIK

Khar'kov State University

Submitted to JETP editor February 16, 1961; resubmitted June 19, 1961

J. Exptl. Theoret. Phys. (U.S.S.R.) **41**, 1112-1118 (October, 1961)

A diagram technique is used for analyzing level shifts in single-electron atoms in an equilibrium plasma at a finite temperature. The level shifts are computed to first and second order in the coupling constant $e^2/2aT$ (a is the Bohr radius). Debye shielding is taken into account by summing over diagrams. At high temperatures ($T \gtrsim 10^{6\circ}$ K) the shift is determined by the electron-electron exchange interaction and increases as $T^{1/2}$. The problem of calculating level widths is discussed.

1. INTRODUCTION

In recent years considerable progress has been made[1] in analyses of the effect of a plasma on the spectra of atoms in the plasma; these analyses consider effects due to electrons and ions by a combination of collision and statistical methods, using both quantum mechanical and classical descriptions; the correlation between charged particles has also been included. Nonetheless, the problem of describing these effects by means of a unified point of view remains unsolved. The application of quantum field theory techniques in quantum statistics (the Matsubara technique[2] and the further development of the Green's function technique[3-5]) open the possibility of a new approach to the problem. In this case one can formulate a quantum description of the entire plasma and then take account of correlation with the atoms.

Using the point of view of field theory we shall consider the state of an electron in the plasma in terms of single-electron excitations. These excitations will correspond to bound electron states in the atom if these states become single-electron states in an isolated atom as the charged-particle density of the plasma approaches zero. To use this approach we isolate one of the ions and consider the entire plasma in the Coulomb field of this ion. The energy changes of the single-electron excitations then represent shifts of the atomic energy levels in the plasma while their imaginary parts represent the widths of the corresponding levels.

2. SINGLE-ELECTRON EXCITATIONS

We compute the energy level shifts for single-electron atoms in an equilibrium plasma at temperature $T = \beta^{-1}$. The entire plasma is considered in the "external" field due to an isolated ion, which is assumed to be fixed. The kinetic energy of the electrons and ions is included in the unperturbed plasma Hamiltonian H_0 while the interaction Hamiltonian is written in the form

$$H_1 = H_{ee} + H_{ei} + H_{ii} + V_e + V_i; \tag{1}$$

$$H_{ee} = \int dx\, dy\, \psi^+(x)\, \psi^+(y)\, u(x-y)\, \psi(y)\, \psi(x),$$

$$V_e = \int dx\, \psi^+(x)\, \psi(x)\, V(\mathbf{x}),$$

$$H_{ii} = Z^2 \int dx\, dy\, \varphi^+(x) \varphi^+(y)\, u(x-y) \varphi(y) \varphi(x),$$

$$V_i = -Z \int dx \varphi^+(x)\, \varphi(x) V(\mathbf{x}),$$

$$H_{ei} = -Z \int dx\, dy\, \psi^+(x)\, \psi(x)\, u(x-y)\, \varphi^+(y)\, \varphi(y). \tag{2}$$

Here, ψ^+ and ψ are electron creation and annihilation operators while φ^+ and φ are the same for ions in the temperature representation of the interaction, $u(x-y) = u(\mathbf{x}-\mathbf{y})\, \delta(x^0 - y^0)$ is the potential energy of the interaction for an electron pair, $V(\mathbf{x})$ is the potential energy of an electron in the external field, Z is the charge of nucleus* and the subscripts e and i refer to electrons and ions respectively. The integration over the 4-vector x is carried out over the entire three-dimensional space of the vector $\mathbf{x}$ and over the interval $(0, \beta)$ of the temperature variable x^0.

It follows from the spectral representation of the single-particle Green's function[3,5] that its poles give the energy spectrum of the single-particle excitations. We consider the single-electron temperature Green's function[2,4]

$$G(x, y) = \langle S(\beta) \rangle^{-1} \langle T\{\psi^+(x)\, \psi(y)\, S(\beta)\} \rangle, \tag{3}$$

*When $Z > 1$ we assume that all perturbing ions are completely ionized.

where $S(\beta)$ is the Matsubara S-matrix, the T ordering is carried out over the temperature variable, while the averaging is taken by means of the density matrix of the noninteracting particles $\exp\{\Omega + \mu N - H_0)\beta\}$. As is well known, the Green's function G satisfies the Dyson equation

$$G(x, y) = S(x-y) + \int dx'dy' S(x-x')\,\Sigma^*(x', y')\,G(y', y), \tag{4}$$

where $S(x-y)$ is the Green's function for the free electron

$$\left(\frac{\partial}{\partial x^0} + \mu + \frac{1}{2m}\Delta_x\right) S(x-y) = \delta(x-y), \tag{5}$$

while Σ^* is the compact self-energy part. The quantity Σ^* represents the sum of all compact diagrams with two external electron lines. In Fig. 1 we show these diagrams for first $(1-4)$ and second (in H_1) order perturbation theory. The single solid line corresponds to the electron,

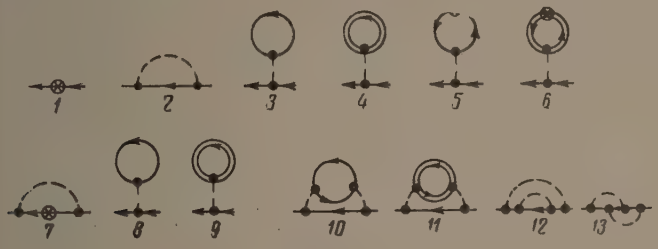

FIG. 1

the double solid line corresponds to the ion, the dashed line corresponds to the Coulomb interaction and the starred line corresponds to the external field. Using Eq. (5) we can obviously rewrite Eq. (4) in the form

$$\left(\frac{\partial}{\partial x^0} + \mu + \frac{1}{2m}\Delta_x\right) G(x-y)$$

$$-\int dz\,\Sigma^*(x, z)\,G(z, y) = \delta(x-y). \tag{6}$$

The Green's function is an antiperiodic function of the difference $x^0 - y^0$ [4,5]; hence the integral in Eq. (6) must be the same function of this difference. This requirement is satisfied by two functional forms of the dependence of $\Sigma^*(x, z)$ on $x^0 - z^0$: a delta function and an antiperiodic function. All diagrams in Fig. 1 except for 10, 11, and 13 refer to the first function; 10, 11, and 13 refer to the second.

We remove from Σ^* the term corresponding to diagram 1 of Fig. 1, which is independent of plasma density, and introduce the mass operator M defined by $\Sigma^*(x, z) = V(x)\delta(x-z) + M(x, z)$. Then, from Eq. (6) we obtain the equation

$$\left[\frac{\partial}{\partial x^0} + \mu + \frac{1}{2m}\Delta_x - V(x)\right] G(x, y)$$

$$-\int dz M(x, z)\,G(z, y) = \delta(x-y). \tag{7}$$

We let the density of charged particles in the plasma approach zero so that the mass operator approaches zero and (7) becomes an equation for the Green's function of the single-electron atom. Thus, the mass operator in (7) takes account of the effect of the plasma on the atom.

It is well known [4,5] that we can carry out a Fourier transformation over "time" x^0 within the temperature diagram technique:

$$G(\omega_n) = \frac{1}{2}\int_{-\beta}^{\beta} e^{i\omega_n x_0}\,G(x_0)\,dx_0, \tag{8}$$

where $\omega_n = \pi(2n+1)/\beta$ for electrons. In the frequency representation Eq. (7) is

$$\left[-i\omega_n + \mu + \frac{1}{2m}\Delta_x - V(x)\right] G(x, y, \omega_n)$$

$$-\int dz M(x, z, \omega_n)\,G(z, y, \omega_n) = \delta(x-y)$$

or, in operator form*

$$G^{-1}(\omega_n) = -i\omega_n + \mu + \Delta_x/2m - V(x) - M(\omega_n).$$

The poles of G (zeros of G^{-1}) in the complex plane $E = -i\omega_n + \mu$ determine the spectrum of the energy of single electron excitations of the system; thus, the determination of this spectrum reduces to solution of the equation

$$\left[-\frac{1}{2m}\Delta_x + V(x) + M(\omega_n = iE_\nu - i\mu)\right]\chi_\nu = E_\nu\chi_\nu. \tag{9}$$

Using the perturbation method, we find the zeroth approximations (in M) of the energy levels E_ν^0 and the eigenfunctions χ_ν^0 of the single-electron atom; in the first approximation

$$E_\nu = E_\nu^0 + M_{\nu\nu}(\omega_n = iE_\nu^0 - i\mu), \tag{10}$$

where $M_{\nu\nu}$ is the matrix element of M in the basis χ_ν^0. This matrix element gives the shift of the energy level for the state χ_ν^0.

3. MASS OPERATOR

In the first approximation we obtain for $M^{(1)}$ three terms, corresponding to diagrams 2, 3 and 4 in Fig. 1. Diagram 2, which describes the exchange interaction between electrons, corresponds to the matrix

*For the delta-function terms in $x^0 - y^0$ we take $M(x, y, \omega_n)$ to mean the multiplier for $\delta(x^0 - y^0)$ in $M(x, y)$.

$$M_2^{(1)}(x, y) = S(x-y)\,u(x-y)$$
$$= \delta(x^0 - y^0)\,Ne^2\,|\mathbf{x}-\mathbf{y}|^{-1}\exp[-(\mathbf{x}-\mathbf{y})^2/4\lambda\!\!\!^{-2}], \quad (11)$$

where $\lambda\!\!\!^{-} = (\beta/2m)^{1/2}$.

Diagrams 3 and 4 correspond to the matrices

$$M_3^{(1)}(x, y) = \delta(x-y)\int dz u(\mathbf{x}-\mathbf{z})\,N,$$
$$M_4^{(1)}(x, y) = -\delta(x-y)\int dz u(\mathbf{x}-\mathbf{z})\,ZN_i,$$

which describe the interaction of the atomic electron with the self-consistent field of the electrons and ions (mean densities M and N_i). Each of these integrals diverges separately; however they balance each other in a quasi-neutral plasma ($N = ZN_i$). In the second approximation there are three pairs of compensating diagrams; these are not shown in Fig. 1.

In the second approximation, we first must consider diagrams 5, 6, 8, 9, 10, and 11, which lead to divergent integrals and make the largest contribution to the level shift. Diagram 5, which describes the interaction of the atomic electron with the plasma electrons (which are polarized by the field of the nucleus), corresponds to the matrix

$$M_5^{(2)}(x, y) = \delta(x-y)(2\pi)^{-3}\int dk e^{-i\mathbf{kx}} P_e^{(2)}(\mathbf{k}, 0)\,V(\mathbf{k})\,u(\mathbf{k}), \quad (12)$$

where $u(\mathbf{k}) = 4\pi e^2\mathbf{k}^{-2}$.

Diagram 10, which describes the exchange interaction (taking account of the polarization of the plasma electrons), corresponds to a matrix of the following form in the momentum-frequency representation:

$$M_{10}^{(2)}(\mathbf{p}, \omega_n) = 2(2\pi)^{-3}\beta^{-1}$$
$$\times \sum_m \int dk S(\mathbf{p}-\mathbf{k}, \omega_{n-m})\,P_e^{(2)}(\mathbf{k}, \omega_m)\,u^2(\mathbf{k}), \quad (13)$$

where $S(\mathbf{p}, \omega_n) = (-i\omega_n + \mu - \epsilon_{\mathbf{p}})^{-1}$ for odd frequencies while the second-order electron polarization operator is

$$P_e^{(2)}(\mathbf{k}, \omega_{2n}) = (2\pi)^{-3}\int d\mathbf{p}\,\frac{(f_{\mathbf{p}} - f_{\mathbf{p}-\mathbf{k}})(\varepsilon_{\mathbf{p}} - \varepsilon_{\mathbf{p}-\mathbf{k}})}{(\varepsilon_{\mathbf{p}} - \varepsilon_{\mathbf{p}-\mathbf{k}})^2 + \omega_{2n}^2}$$

and zero for odd frequencies; here, $f_{\mathbf{p}}$ and $\epsilon_{\mathbf{p}}$ are the Fermi function and the kinetic energy of an electron with momentum $\mathbf{p}$. For a nondegenerate plasma and zero frequency we have

$$P_e^{(2)}(\mathbf{k}, 0) = -N\beta I(\lambda\!\!\!^{-}\mathbf{k}) \cong -N\beta\left(1 + \frac{1}{2}\lambda\!\!\!^{-2}\mathbf{k}^2\right),$$
$$I(\xi) = \int_0^1 e^{-\xi^2(1-s^2)/4} ds; \quad (14)$$

for nonvanishing frequencies and small k we have

$$P_e^{(2)}(\mathbf{k}, \omega_{2n}) \cong -N\beta 2\left(\frac{\lambda\!\!\!^{-}\mathbf{k}}{2\pi n}\right)^2.$$

Diagrams 6 and 11 correspond to the expressions obtained from (12) and (13) when the electron polarization operator is replaced by the ion operator $P_i^{(2)}$. The last is obtained from (14) if N is replaced by N_i and $\lambda\!\!\!^{-}$ by $\kappa\lambda\!\!\!^{-}$, where κ^2 is the ratio of electron mass to ion mass.

The integrals in the matrix elements (12) and (13) diverge at small k. In order to avoid this divergence we must take account of the Debye shielding[2,5,6], that is to say we must consider plasma polarization in all the orders. This can be done by introducing the effective electron interaction potential, obtained by summing the most important polarization diagrams of Fig. 2, containing successively m electron and n ion branches. We replace these branches by the most general compact polarization diagrams; then,

FIG. 2

taking account of the equal and independent contributions of diagrams differing in order of alternation of the electron and ion polarization operators P_e^* and P_i^* we find the effective electron interaction potential:

$$\tilde{u}(\mathbf{k}, \omega_s) = u(\mathbf{k}, \omega_s)\sum_{m,n=0}^{\infty}\frac{(m+n)!}{m!\,n!}$$
$$\times [u(\mathbf{k}, \omega_s)P_e^*(\mathbf{k}, \omega_s)]^m [Z^2 u(\mathbf{k}, \omega_s)P_i^*(\mathbf{k}, \omega_s)]^n$$
$$= u(\mathbf{k}, \omega_s)/\{1 - [P_e^*(\mathbf{k}, \omega_s) + Z^2 P_i^*(\mathbf{k}, \omega_s)]\,u(\mathbf{k}, \omega_s)\}, \quad (15)$$

where $u(\mathbf{k}, \omega_s) = u(\mathbf{k})/2$. Thus, $\tilde{u} = u$ for odd frequencies. The effective potential is obtained from Eq. (15) by multiplying by $-Z$ for the electron-ion interaction and by Z^2 for the ion-ion interaction.

The divergences in (12) and (13) can be avoided by taking account in Eq. (15) of the polarization operators P_e^* and P_i^* in the first nonvanishing approximation; they are replaced by $P_e^{(2)}$ from (14) and by $P_i^{(2)}$.

Summation of diagrams of type 5, in which the line of interaction is replaced by the chain of Fig. 2, obviously means that the function $u(\mathbf{k}, 0)$ is replaced by $\tilde{u}(\mathbf{k}, 0)$ in Eq. (12). Adding a similar summation of diagrams of type 6, we have

$$M_{\text{pol}}(x, y) = \delta(x-y)\, 2(2\pi)^{-3}\int d\mathbf{k} e^{-i\mathbf{kx}} [P_e^{(2)}(\mathbf{k}, 0) + Z^2 P_i^{(2)}(\mathbf{k}, 0)] V(\mathbf{k})\tilde{u}(\mathbf{k}, 0)$$
$$\cong \delta(x-y)(Ze^2/d)(1 - |\mathbf{x}|/2d), \quad (16)$$

where $d = [4\pi e^2 (1+Z) N\beta]^{-1/2}$ is the Debye radius.*

In summing the exchange diagrams of type 10 and 11, in which the interaction line is replaced by the chain of Fig. 2, we must take account of the fact that the exchange diagram 2 is a first-order delta function in $x^0 - y^0$, while in all the remaining orders it is antiperiodic. Hence the summation can be carried out conveniently starting with second-order diagrams 10 and 11. This means that in Eq. (13) the quantity $u^2 P_e$ is replaced by $\tilde{u} - u$:

$$M_{\text{exc}}(\mathbf{p}, \omega_{2n+1}) = \frac{1}{2}(2\pi)^{-3}\beta^{-1}\sum_m \int d\mathbf{k} S(\mathbf{p}-\mathbf{k}, \omega_{2n+1-2m}) \times \frac{[P_e^{(2)}(\mathbf{k}, \omega_{2m}) + Z^2 P_i^{(2)}(\mathbf{k}, \omega_{2m})] u^2(\mathbf{k})}{1 - \frac{1}{2}[P_e^{(2)}(\mathbf{k}, \omega_{2m}) + Z^2 P_i^{(2)}(\mathbf{k}, \omega_{2m})] u(\mathbf{k})}. \quad (17)$$

In this sum the term with $m = 0$ is appreciably greater than the sum of all the remaining terms so that as an approximation we can write

$$M_{\text{exc}}(\mathbf{p}, \omega_{2n+1} = iE_\nu - i\mu) = \frac{1}{2\pi} e^4 N(1+Z)\int \frac{d\mathbf{k}}{k^2(k^2 + 1/2\, d^2)(|E_\nu| + \varepsilon_{p-k})}. \quad (18)$$

Diagrams 8 and 9 also give divergent matrix elements and the divergence is again avoided by replacing u by $\tilde{u}$. Using diagram 8, which describes the interaction of the atomic electron with the plasma electrons (taking account of the interaction between the latter), we obtain the matrix element

$$M_8^{(2)}(x, y) = \delta(x-y)\frac{4\pi}{\sqrt{5}}\frac{e^2}{a}\left(\frac{\lambda}{a}\right)^2 Na^3 \quad (19)$$

(a is the Bohr radius). The matrix element for diagram 9 is obtained from (19) by multiplying by $-\kappa^2$; consequently these do not compensate.

4. LEVEL SHIFT

Equation (10) shows that to find the energy level shift for state χ_{nlm} caused by the plasma we must compute the diagonal element $M(\mathbf{x}, \mathbf{y}, \omega_n = iE_n^0 - i\mu)$ in the basis χ_{nlm}. The shift due to plasma polarization is obtained from (10) and (16):

$$\delta E_{nl\,\text{pol}} = \frac{Ze^2}{a}\left\{\frac{a}{d} - \frac{1}{4}\left(\frac{a}{d}\right)^2 [3n^2 - l(l+1)]\right\}, \quad (20)$$

and falls off with temperature as $T^{-1/2}$. Diagram 8 corresponds to the level shift obtained from (19):

$$\delta E_{nl} = \frac{4\pi}{\sqrt{5}}\frac{e^2}{a}\left(\frac{\lambda}{a}\right)^2 Na^3, \quad (21)$$

and falls of as T^{-1} with increasing temperature.

To compute the level shift which corresponds to the exchange diagram with the effective potential we note that the matrix element (18) depends on the difference $\mathbf{x} - \mathbf{y}$ in the coordinate representation. Hence it is diagonal in the momentum representation; using the appropriate hydrogen functions, we have from (18)

$$\delta E_{nl\,\text{exc}} = \int d\mathbf{p} |\chi_{nlm}(\mathbf{p})|^2 M_{\text{exc}}(\mathbf{p}, \omega_{2n+1} = iE_n^0 - i\mu) = C_{nl} T\frac{a}{d} = C_{nl}\sqrt{\frac{2aT}{e^2}}\omega_0, \quad (22)$$

where ω_0 is the plasmon energy, $\omega_0 = (4\pi e^2 N m^{-1})^{1/2}$. The numerical factor C_{nl} depends on the quantum numbers n and l of the state being considered, being 0.442 for the 1s state, 3.3 for the 2p state, and 3.58 for the 3d state. This shift increases with temperature as $T^{1/2}$.

We now clarify the region of applicability of the results that have been obtained. For this purpose we note that perturbation theory has been used twice in the above—in solving Eq. (9) and in calculating the mass operator. The mass operator in (9) is small because it is proportional to the plasma charge density. The effect of the plasma on the atom is characterized by the number of electrons inside the Bohr orbit, that is, the parameter Na^3, which is small compared with unity for the gas state. All the mass operator diagrams are proportional to N but the summation carried out above leads to a dependence of the form $M \sim N^{1/2}$ for the largest terms.

We have computed the mass operator above by means of the thermodynamic perturbation theory, i.e., expansion of $S(\beta)$ in H_1. The largest term in H_1 is the interaction energy of the atomic electron with the nucleus $\sim e^2/a$; thus in the present case the role of the coupling constant is played by the quantity $e^2/2aT = (\lambda/a)^2$, i.e., the ratio of the atomic ionization energy to the thermal energy. We can limit ourselves to the lowest approximations in $S(\beta)$ in the expansion of $e^2/2aT \ll 1$.* Thus, the obtained results apply for high temperatures, (temperatures appreciably greater than 1.5×10^5° K).

*This part of the mass operator describes the additional energy of the electron in the Debye field and can be obtained by expansion of the Debye potential $-(Ze^2/r)\exp(-r/d)$ in r/d.

*For example, at high temperatures the ratio of level shifts corresponding to diagrams 7 and 2 is of order e^2/aT.

A comparison of the shifts (20) and (22) shows that at high temperatures the important factor is the exchange shift (22), which is a rather large quantity. Thus, when $N = 10^{16}$ cm^{-3} and $T = 10^{6}$° K the $H_\alpha(3d \rightarrow 2p)$ line is shifted by 9.4 A.

The level shifts corresponding to the alpha second-order diagrams not considered in detail above are found to be of order (21) or even smaller at high temperatures and for this reason need not be considered.

The accuracy in the measurement of the shift of a spectral line depends on line width. For this reason we must consider the possibility of computing the broadening of the levels due to the effect of charges in the plasma (Stark broadening). The notion of level width applies only in a continuous energy spectrum which, in the scheme considered above, occurs only when $E_\nu > 0$, (unbound electron states). Analytic continuation of the mass operator for computing the level shift of this state makes it necessary to deform the integration contour and gives an imaginary part in δE_ν. The latter can arise only in those terms of the mass operator which depend only on frequency ω_n, i.e., terms that are not diagonal in $x^0 - y^0$ in the temperature representation. For example, in computing the exchange shift of the energy of the unbound state we find an imaginary part in the zero-frequency term in the sum (17):

$$\begin{aligned} \operatorname{Im} M_{\text{exc}}(\mathbf{p},\ \omega_{2n+1} = iE_\nu^{\upsilon} - i\mu) &= \frac{1+Z}{2} e^4 N \int \frac{d\mathbf{k}}{k^2(k^2+d^{-2})}\, \delta(E_\nu - \varepsilon_{\mathbf{p}-\mathbf{k}}) \\ &= \frac{T}{2ap} \ln \frac{1 + d^{-2}(p-p_\nu)^{-2}/2}{1 + d^{-2}(p+p_\nu)^{-2}/2}, \end{aligned} \tag{23}$$

where $p_\nu = (2mE_\nu^{1/2})$. To compute the level width we must average this expression over unbound electron states.

In the scheme being considered we have a discrete energy spectrum for the bound electron states ($E_\nu < 0$). Analytic continuation of the mass operator for these energies leads to an integral which has no singularities along the contour of integration and is thus real. Hence, the width of the negative levels is zero in this scheme. This result is due to our assumption that the nuclei are fixed. Actually, the atomic energy spectrum for bound states is continuous because of the kinetic energy of the atom. Consequently we must take account of the motion of the nuclei in computing the width of the energy levels for the bound states. This approach can be carried out by describing the atom in the plasma by means of the two-particle electron-ion Green's function.

The author wishes to thank A. I. Akhiezer, I. M. Lifshitz, I. A. Akhiezer, and S. V. Peletminskii for discussions of the present work.

[1] Greim, Kolb, and Shen, Phys. Rev. **116**, 4 (1959).

[2] T. Matsubara, Progr. Theor. Phys. **11**, 351 (1955).

[3] L. D. Landau, JETP **34**, 262 (1958), Soviet Phys. JETP **7**, 183 (1958).

[4] Abrikosov, Gor'kov, and Dzyaloshinskii, JETP **36**, 900 (1959), Soviet Phys. JETP **9**, 636 (1959).

[5] E. S. Fradkin, JETP **36**, 1286 (1959), Soviet Phys. JETP **9**, 912 (1959).

[6] V. P. Galaĭko and L. É. Pargamanik, DAN SSSR **123**, 999 (1958), Soviet Phys.-Doklady **3**, 1225 (1958).

Translated by H. Lashinsky
197

QUANTUM-MECHANICAL DIELECTRIC TENSOR FOR AN ELECTRON PLASMA IN A MAGNETIC FIELD

P. S. ZYRYANOV and V. P. KALASHNIKOV

Ural Polytechnic Institute

Submitted to JETP editor March 4, 1961; resubmitted July 5, 1961

J. Exptl. Theoret. Phys. (U.S.S.R.) 41, 1119-1124 (October, 1961)

A quantum mechanical analysis is given for the complex dielectric tensor of an electron plasma in a magnetic field; the orbital motion of the electrons in the magnetic field is quantized in this treatment. The transition to the classical and quasi-classical cases is studied and the relation to well-known results is established.[1,3,4] The limiting quantum case is investigated. An expression is derived for the anti-Hermitian part of the tensor, which is responsible for dissipation. The magnetic-field dependence of the interaction screening range is discussed.

1. The dielectric tensor of an electron plasma with a Maxwellian distribution function in a uniform magnetic field has been given by Sitenko and Stepanov[1] on the basis of classical kinetic theory. In strong magnetic fields, however, the energy of a Larmor quantum is of the same order as or larger than that of the random motion of the particles and the classical theory no longer applies because the orbital electron motion must be quantized.

In the present paper we derive the quantum-mechanical dielectric tensor $\epsilon_{ij}(\omega, \mathbf{q})$, which plays a central role in investigations of the electromagnetic properties of plasma; the correlation energy of the particles is expressed in terms of this tensor. As has recently been shown by Silin,[2] this tensor also plays an important role in shielding of the Coulomb field of particles in the collision integral, so that the formulation of the quantum collision integral for Coulomb particles in a magnetic field also depends on the quantum-mechanical tensor $\epsilon_{ij}(\omega, \mathbf{q})$.

In computing $\epsilon_{ij}(\omega, \mathbf{q})$ we shall use the linear, self-consistent field approximation. The orbital electron motion in the magnetic field is quantized by describing the particle motion with a single-particle statistical operator $\hat{\rho}$, whose equation of motion assumes the following form in the present approximation:

$$i\hbar\partial\hat{\rho}'/\partial t = [\hat{\mathcal{H}}_0, \hat{\rho}']_- + [\hat{\mathcal{H}}', \hat{\rho}_0]_+, \qquad (1)$$

where $[A, B]_-$ and $[A, B]_+$ are the commutators and anticommutators for the operators A and B; ρ_0 is the ground state operator, $\hat{\rho}'$ is the perturbed value of $\hat{\rho}$ ($\hat{\rho} = \hat{\rho}_0 + \hat{\rho}'$), which is a linear functional of the self-consistent field

$$\hat{\mathcal{H}}_0 = (\hat{\mathbf{p}} - e\mathbf{A}_0/c)^2/2\mu, \qquad (2)$$

$\mathbf{A}_0 \equiv \{-Hy, 0, 0\}$ is the vector potential of the uniform magnetic field

$$\hat{\mathcal{H}}' = -\frac{e}{2\mu c}\left[\mathbf{A}', \left(\hat{\mathbf{p}} - \frac{e}{c}\mathbf{A}_0\right)\right]_+, \qquad (3)^*$$

and $\mathbf{A}'$ is the vector potential of the self-consistent field. We shall use the gauge:

$$\varphi \equiv 0, \qquad \operatorname{div}(-\dot{\mathbf{A}}') = 4\pi c \operatorname{Sp}\{\hat{\rho}'(\mathbf{r}')\,\delta(\mathbf{r} - \mathbf{r}')\}. \qquad (4)$$

The vector $\mathbf{E} = -(1/c)\dot{\mathbf{A}}'$ obeys the equation

$$\operatorname{rot}\operatorname{rot}\mathbf{E} = -\frac{4\pi}{c^2}\frac{\partial}{\partial t}\left(\mathbf{j} + \frac{1}{4\pi}\frac{\partial}{\partial t}\mathbf{E}\right), \qquad (5)\dagger$$

where

$$\mathbf{j} = \frac{e}{2\mu}\operatorname{Sp}\left\{\hat{\rho}(\mathbf{r}')\left[\left(\hat{\mathbf{p}} - \frac{e}{c}\mathbf{A}_0 - \frac{e}{c}\mathbf{A}'\right), \delta(\mathbf{r} - \mathbf{r}')\right]_+\right\}. \qquad (6)$$

2. To form $\epsilon_{ij}(\omega, \mathbf{q})$ we use Eq. (1) to express $\hat{\rho}'$ in terms of $\mathbf{A}$ and then find the current-density vector (6); Eq. (5) can then be used to find $\epsilon_{ij}(\omega, \mathbf{q})$ directly. This calculation is carried out conveniently in the representation based on the eigenfunctions of the operator $\hat{\mathcal{H}}_0$ (Landau representation):

$$\hat{\mathcal{H}}_0|k_x, k_z, n\rangle = E_{k_z, n}|k_x, k_z, n\rangle,$$
$$E_{k_z, n} \equiv E_\nu = \hbar\Omega(n + 1/2) + \hbar^2 k_z^2/2\mu, \qquad (7)$$

$$\nu\rangle \equiv |k_x, k_z, n\rangle$$
$$= (4\pi^2\alpha)^{-1/2}\exp(ik_x x + ik_z z)\,\Phi_n[(y + \alpha^2 k_x)/\alpha)],$$
$$\alpha^2 = \hbar/\mu\Omega, \qquad \Omega = |e|H/\mu c. \qquad (8)$$

---

*$[\mathbf{A}', (\hat{\mathbf{p}} - \frac{e}{c}\mathbf{A}_0)] = \mathbf{A}' \times (\hat{\mathbf{p}} - \frac{e}{c}\mathbf{A}_0)$.

†rot = curl.

Assuming that $\hat{\rho}' \sim E \sim \exp(i\omega t - i\mathbf{q}\cdot\mathbf{r})$, using (1) we find the following expression for the matrix elements of the operator $\hat{\rho}$

$$\langle \nu' | \hat{\rho} | \nu \rangle = f_0(\nu)\,\delta_{\nu\nu'} + \frac{f_0(\nu') - f_0(\nu)}{E_{\nu'} - E_\nu - \hbar\omega - i\Delta} \langle \nu' | \hat{\mathcal{H}}' | \nu \rangle. \tag{9}$$

From (3) and (8) we have

$$\langle k_x, k_z, n | \hat{\mathcal{H}}' | k_x + q_x, k_z + q_z, n' \rangle = (e/\mu c)\, \mathbf{K}_{nn'}(q_x, q_z)\, \mathbf{A}'(q_x, q_z);$$

$$\mathbf{K}_{nn'}(q_x, q_z) \equiv {}^1/_2 \{ \langle n | \mu\Omega\, [\hat{y}, \hat{J}]_+ | n' \rangle, \langle n | [\hat{p}_y, \hat{J}]_+ | n' \rangle, \langle n | (2\hbar k_z + \hbar q_z)\hat{J} | n' \rangle \}. \tag{10}$$

Here, $\hat{J} = \exp\{\alpha^2 q_x^2 \partial/\partial y\}$ and $\mathbf{A}'(q_x, q_z)$ is the Fourier transform of the self-consistent vector potential.

The operator $\hat{J}$ is unitary:

$$\hat{J}\hat{J}^+ = \hat{I}, \tag{11}$$

where $\hat{I}$ is the unit operator.

To compute the current density we must write the matrix elements for the kinetic momentum operator

$$\langle k_x', k_z', n' | \hat{\mathbf{p}} - e\mathbf{A}_0/c | k_x, k_z, n \rangle = \delta(k_z - k_z' + q_z)\, \delta(k_x - k_x' + q_x) \{ \langle n' | \mu\Omega y | n \rangle, \langle n' | \hat{p}_y | n \rangle, \langle n' | \hbar k_z | n \rangle \}. \tag{12}$$

Using (6) and (9) – (12) we obtain from (5)

$$\sum_{i=1}^{3} \{ n^2(\varkappa_i \varkappa_j - \delta_{ij}) + \varepsilon_{ij}(\omega, \mathbf{q}) \} E_i = 0, \tag{13}$$

$$n = cq/\omega, \qquad \varkappa_i = q_i/q;$$

$$\varepsilon_{ij}(\omega, \mathbf{q}) = \delta_{ij} + 4\pi\sigma_{ij}(\omega, \mathbf{q})/i\omega, \tag{14}$$

$$\sigma_{ij}(\omega, \mathbf{q}) = \frac{e^2 N_0}{\mu i\omega}\,\delta_{ij} + \frac{e^2}{\mu^2 i\omega}\,\frac{1}{2\pi^2\alpha^2} \times \lim_{\Delta\to 0} \sum_{n, n'} \int dk_z\, \frac{f_0(k_z + q_z, n') - f_0(k_z, n)}{E_{k_z+q_z, n'} - E_{k_z, n} - \hbar\omega - i\Delta} (\mathbf{K}^*_{nn'})_i (\mathbf{K}_{n'n})_j, \tag{15}$$

where N_0 is the mean particle-number density:

$$N_0 = (2\pi^2\alpha^2) \sum_n \int dk_z f_0(E_{k_z, n}).$$

The tensor $\epsilon_{ij}(\omega, \mathbf{q})$ [and consequently $\sigma_{ij}(\omega, \mathbf{q})$] satisfies the well-known Onsager symmetry relation

$$\varepsilon_{ij} = (-1)^a \varepsilon_{ji}, \qquad \varepsilon_{ij}(\mathbf{q}, \mathbf{H}, \omega) = \varepsilon_{ji}(-\mathbf{q}, -\mathbf{H}, \omega) \tag{16}$$

(the number a indicates how many times y appears in the indices i and j).

3. We now consider limiting cases of Eq. (14). First we show that (14) yields the classical result of Sitenko and Stepanov.[1] We assume that f_0 is a Maxwellian distribution function and expand the difference

$$f_0(E_{k_z+q_z, n'}) - f_0(E_{k_z, n}) = -f_0(E_{k_z, n})\,(E_{k_z+q_z, n'} - E_{k_z, n}) \tag{17}$$

in terms of q_Z and $n' - n$.

Since the operator $\hat{J}$ is unitary (11), we have

$$(N_0 (2\pi)^2 \mu\theta\alpha^2)^{-1} \sum_{n'n} \int dk_z f_0(k_z, n) (\mathbf{K}^*_{nn'})_i (\mathbf{K}_{n'n})_j = \delta_{ij}. \tag{18}$$

The components of the vectors $\mathbf{K}_{nn'}$ are replaced by their asymptotic expressions for large n, corresponding to the transition to the classical limit ($n \to \infty$, $\hbar \to 0$, $n\hbar$ is finite):

$$\lim \langle n | \hat{J} | n' \rangle = \lim \exp(-\alpha^2 q_x^2/4)\, (n'!\, n!)^{-1/2} \times (\alpha q_x/\sqrt{2})^{n'-n} L_n^{n'-n}(\alpha^2 q_x^2/2) = (-1)^{n'-n} J_{n'-n}(\alpha q_x \sqrt{n' + n + 1}), \tag{19}$$

for $n' \geq n$. Here $L_n^{n'-n}(x)$ is the Laguerre polynomial and $J_{n'-n}(x)$ is the Bessel function of order $(n'-n)$.

Using the recurrence formulas for the Bessel functions we have

$$\langle n | [\hat{y}, \hat{J}]_+ | n' \rangle = \sqrt{2n}\, \frac{n J_{n'-n}(\alpha q_x \sqrt{n' + n + 1})}{q_x \sqrt{n + n' + 1}},$$

$$\langle n | [\hat{p}_y, \hat{J}]_+ | n' \rangle = \frac{\hbar}{i\alpha} \sqrt{2n} J'_{n'-n}(\alpha q_x \sqrt{n' + n + 1}),$$

$$(\hbar k_z + \hbar q_z/2) \langle n | \hat{J} | n' \rangle = \hbar k_z J_{n'-n}(\alpha q_x \sqrt{n' + n + 1}); \tag{20}$$

in which we have taken account of the fact that $[\hat{y}, \hat{J}]_- = 0$ in the classical limit. Converting to the variables

$$(\hbar k_z)^2/2\mu\theta = y^2, \quad n\hbar\Omega/\theta = t^2, \quad s = \sqrt{3\theta/\mu},$$

$$\sqrt{{}^3/_2}\,(\omega - n\Omega)/(sq_z) = Z_n, \quad \lambda = \sqrt{{}^2/_3}\, sq_x/\Omega, \quad \omega_0^2 = 4\pi e^2 N_0/\mu,$$

we have from (14) in the classical limit

$$\varepsilon_{ij}(\omega, q) = \delta_{ij} - \frac{4\omega_0^2}{\sqrt{\pi}\omega^2} \sum_{n=-\infty}^{\infty} \int_0^\infty t e^{-t^2} dt \int_{\mathcal{C}} \frac{e^{-y^2} dy}{Z_n - y} \times (\mathbf{D}(n/\lambda;\ i\partial/\partial\lambda, y)\, J_n(\lambda t))_i \times (\mathbf{D}(n/\lambda, -i\partial/\partial\lambda, y)\, J_n(\lambda t))_j;$$

$$\mathbf{D}(n/\lambda, i\partial/\partial\lambda, y) \equiv \{ n/\lambda, i\partial/\partial\lambda, y \}, \tag{21}$$

which coincides with Eq. (11) of Sitenko and Stepanov.[1]

We now find the quasi-classical limit for ϵ_{ij} for a plasma with a Fermi distribution function. This case is of importance in the plasma model

of a metal. For complete degeneracy we have

$$f_0(k_z + q_z, n') - f_0(k_z, n) = -\delta[\hbar^2 k_z^2/2\mu - \hbar\Omega(n_0 - n)]\,[E_{k_z+q, n'} - E_{k_z, n}], \tag{22}$$

and, from Eq. (11),

$$(2\pi^2\mu N_0\alpha^2)^{-1}\sum_{n'n}\int dk_z\delta\left[\frac{\hbar^2k_z^2}{2\mu} - \hbar\Omega(n_0 - n')\right] \times (\mathbf{K}^*_{nn'})_i(\mathbf{K}_{n'n})_j = \delta_{ij}, \tag{23}$$

where $\hbar\Omega n_0 = E_0 - \hbar\Omega/2$, E_0 is the Fermi energy (more precisely, the chemical potential).

Using the asymptotic forms of (19) and (20) and assuming that $n = n_0 \sin^2\vartheta$ we have from Eq. (14)

$$\varepsilon_{ij}(\omega, q_x, q_z) = \delta_{ij} - \frac{3\omega_0^2}{2\omega}\sum_{n=-\infty}^{\infty}\int_0^{\pi}\frac{\sin\vartheta\, d\vartheta}{v_0 q_z\cos\vartheta + n\Omega - \omega} \times\left(\mathbf{D}\left(\frac{n}{x}, \frac{i\partial}{\partial x}, \cos\vartheta\right)J_n(x\sin\vartheta)\right)_i \times\left(\mathbf{D}\left(\frac{n}{x}, -\frac{i\partial}{\partial x}, \cos\vartheta\right)J_n(x\sin\vartheta)\right)_j. \tag{24}$$

We note that two components of Eq. (15) for $\sigma_{ij}(\omega, \mathbf{q})$ have been obtained by Mattis and Dresselhaus [3] for a purely transverse field (σ_{xx} and σ_{zz}). This equation has also been obtained in the quasi-classical limit being considered here by Cohen, Harrison, and Harrison. [4] In both of these papers Im $\omega = 1/\tau$ was assumed to be known and independent of magnetic field, and the frequency ω was identified with the frequency of the collisions between the electrons and the impurities or the lattice. There is reason to believe that these assumptions do not apply in the quantum region (strong magnetic fields) or in the short-wave region, where spatial dispersion is important.

We now consider the limiting quantum case corresponding to small quantum numbers n or strong magnetic fields. In this case $n = n' = 0$ if $n_0 < 1$; this means that all the particles are in the $n = 0$ level and that all $n > 0$ levels are empty. For these magnetic field strengths

$$\varepsilon_{ij}(\omega, q_x, q_z) = (1 - \omega_0^2/\omega^2)\,\delta_{ij} - \exp(-\alpha^2 q_x^2/2)\,\omega_0^2\omega^{-2}(2\pi^2\alpha^2\mu N_0)^{-1} \times\lim_{\Delta\to 0}\int dk_z\frac{f_0(k_z + q_z) - f_0(k_z)}{\hbar^2(q_z^2 + 2k_z q_z)/2\mu - \hbar\omega - i\Delta} \times(\mathbf{D}(0, i\hbar q_z, 2\hbar k_z + \hbar q_z))_i(\mathbf{D}(0, -i\hbar q_z, 2\hbar k_z + \hbar q_z))_j. \tag{25}$$

It follows from this formula that the tensor ϵ_{ij} reduces to a scalar and there is no spatial dispersion for waves characterized by $q_z = 0$ and $q_x \neq 0$, i.e., waves that propagate at right angles to the magnetic field:

$$\varepsilon_{ij}(\omega) = (1 - \omega_0^2/\omega^2)\,\delta_{ij}. \tag{26}$$

This result follows from the fact that a strong magnetic field inhibits particle motion perpendicular to the field. This feature does not apply for waves characterized by $q_z \neq 0$.

The quantity n_0 increases as the magnetic field is reduced, and as soon as $n_0 \geq 1$ motion across the magnetic field develops discontinuously. When $1 \leq n_0 < 2$ [for waves that propagate across the field ($q_x \neq 0$, $q_z = 0$)] the expression for ϵ_{ij} becomes

$$\varepsilon_{xx} = 1 - \frac{\omega_0^2}{\omega^2}\left\{1 - \frac{\Omega^2}{\omega^2 - \Omega^2}\exp\left(-\frac{\alpha^2 q_x^2}{2}\right)\right\},$$

$$\varepsilon_{yy} = 1 - \frac{\omega_0^2}{\omega^2}\left\{1 - \frac{\Omega^2(1 - \alpha^2 q_x^2/2)}{\omega^2 - \Omega^2}\exp\left(-\frac{\alpha^2 q_x^2}{2}\right)\right\},$$

$$\varepsilon_{zz} = 1 - \frac{\omega_0^2}{\omega^2}\left\{1 + \tfrac{4}{3}n_0\frac{\Omega^2}{\omega^2 - \Omega^2}\exp\left(-\frac{\alpha^2 q_x^2}{2}\right)\right\},$$

$$\varepsilon_{xy} = -\varepsilon_{yx} = \frac{i\omega_0^2}{\omega^2 - \Omega^2}\frac{\Omega}{\omega}\left(1 - \frac{\alpha^2 q_x^2}{2}\right)\exp\left(-\frac{\alpha^2 q_x^2}{2}\right). \tag{27}$$

Furthermore, $\epsilon_{zj} = 0$ when $j \neq z$.

As the magnetic field is reduced, n_0 increases still further and when $n_0 = m$ (m is a whole number) the tensor $\epsilon_{ij}(\omega, \mathbf{q})$ changes discontinuously and a new level becomes populated.

4. The investigation of the dissipative properties of the plasma is based on the anti-Hermitian part of the tensor $\epsilon_{ij}(\omega, \mathbf{q})$ which we denote by $\epsilon''_{ij}(\omega, \mathbf{q})$ below. Using the general formulas (14) and (15) we find

$$\varepsilon''_{ij}(\omega, \mathbf{q}) = \frac{\omega_0^2}{2\pi N_0\mu\alpha^2\omega^2}\sum_{nn'}\int dk_z\{f_0(k_z + q_z, n') - f_0(k_z, n)\}(\mathbf{K}^*_{nn'})_i(\mathbf{K}_{n'n})_j\,\delta[E_{k_z+q_z, n'} - E_{k_z, n} - \hbar\omega]. \tag{28}$$

For waves propagating across the magnetic field ($q_z = 0$)

$$\varepsilon''_{ij}(\omega, q_x) = \frac{\omega_0^2}{\omega^2}(2\pi\alpha^2 N_0\mu)^{-1}\sum_{nn'}\int dk_z[f_0(k_z, n') - f_0(k_z, n)] \times(\mathbf{K}^*_{nn'})_i(\mathbf{K}_{n'n})_j\,\delta(\hbar\Omega(n' - n) - \hbar\omega). \tag{29}$$

Using the asymptotic expressions for the vectors $\mathbf{K}_{nn'}$ as $n \to \infty$ and assuming a Maxwellian distribution function we have from Eq. (29)

$$\varepsilon''_{ij}(\omega, q_x) = 4\sqrt{\pi}\frac{\omega_0^2}{\omega^2}\int_0^\infty dt \cdot te^{-t^2}\left(\mathbf{D}\left(\frac{\omega}{\lambda\Omega}, i\frac{\partial}{\partial\lambda}, 0\right)J_{\omega/\Omega}(\lambda t)\right)_i$$

$$\times\left(\mathbf{D}\left(\frac{\omega}{\lambda\Omega}, -\frac{i\partial}{\partial\lambda}, 0\right)J_{\omega/\Omega}(\lambda t)\right)_j$$

$$+\delta_{zz}\frac{2\pi\omega_0^2}{\omega\Omega}\int_0^\infty dt \cdot te^{-t^2}J^2_{\omega/\Omega}(\lambda t),$$

$$\varepsilon''_{zj} = 0 \quad \text{for } j \neq z, \tag{30}$$

while for a degenerate Fermi distribution we have

$$\varepsilon''_{ij}(\omega, q_x) = \frac{3\pi\omega_0^2}{2\omega\Omega}\int_0^{\pi/2}\left(\mathbf{D}\left(\frac{\omega}{x\Omega}, \frac{i\partial}{\partial x}, \cos\vartheta\right)J_n(x\sin\vartheta)\right)_i$$

$$\times\left(\mathbf{D}\left(\frac{\omega}{x\Omega}, -\frac{i\partial}{\partial x}, \cos\vartheta\right)J_n(x\sin\vartheta)\right)_j \sin\vartheta d\vartheta, \tag{31}$$

where $x = q_x v_0/\Omega$. We may note that ϵ''_{ij} in Eq. (31) approaches zero when the magnetic field is switched off; this follows from the asymptotic behavior of the Bessel functions.

The results of the present work can be easily extended to the case of several particle species subjected to Coulomb interactions in a fixed magnetic field.

5. We discuss briefly the potential φ of a charge e moving with velocity $\mathbf{v}_0$ in a medium for which $\epsilon_{ij}(\omega, \mathbf{q})$ is given. The expression for φ is

$$\varphi(\mathbf{r}, t) = (2\pi)^{-3}$$

$$\times\int 4\pi e\, d\mathbf{q}\, d\omega e^{i\mathbf{qr}-i\omega t}(q_i q_j \varepsilon_{ij}(\omega, \mathbf{q}))^{-1}\,\delta(\omega - \mathbf{qv}_0). \tag{32}$$

The denominator in (32) is the longitudinal dielectric constant $\epsilon(\omega, \mathbf{q})$:

$$q^2\varepsilon(\omega, \mathbf{q}) = q_i q_j \varepsilon_{ij}(\omega, \mathbf{q}), \tag{33}$$

which, by (14), is

$$\varepsilon(\omega, \mathbf{q}) = 1 - \frac{4\pi e^2}{2\pi^2\alpha^2}\lim_{\Delta\to 0}\sum_{nn'}|\langle n|\hat{f}|n'\rangle|^2$$

$$\times\int dk_z \frac{f_0(k_z + q_z, n') - f_0(k_z, n)}{E_{k_z+q_z, n'} - E_{k_z, n} - \hbar\omega - i\Delta}. \tag{34}$$

In the classical limit and with $\mathbf{v}_0 = 0$ we use (32) and (34) to find the isotropic exponential decay of potential with distance (Debye shielding with radius r_D). This case corresponds to the inequality $r_D \gg \lambda\!\!\!^{-}_F$ ($\lambda\!\!\!^{-}_F$ is the de Broglie wavelength of an electron at the Fermi surface). When $r_D \sim \lambda\!\!\!^{-}_F$ the potential oscillates and the shielding differs considerably from Debye shielding, depending on the magnetic field if such a field is present. The oscillations of the potential of a point charge in a plasma are associated with the diffraction of the electron de Broglie waves in the inhomogenous potential produced by the point charge; this effect does not appear in the classical limit.

In strong magnetic fields the Larmor radius r_L plays the role of the Debye radius. The inequality $r_L < \lambda\!\!\!^{-}_F$ holds for Fermi statistics with $n_0 \lesssim 1$ and we obtain the following expression for the potential φ (cylindrical coordinates):

$$\varphi(\rho, z) = \frac{e}{\pi}\int_0^\infty dq_\perp q_\perp J_0(\rho q_\perp)\int_{-\infty}^{+\infty} dq_z e^{iq_z z}$$

$$\times\left\{q^2 - \frac{1}{2\pi}(2\mu e^2/\hbar)^2\frac{\Omega}{\hbar q_z}\exp(-\alpha^2 q_\perp^2/2)\right.$$

$$\left.\times\left[\ln\frac{-\sqrt{2n_0} + q_z\alpha/2}{\sqrt{2n_0} + \alpha q_z/2} + \ln\frac{\sqrt{2n_0} - \alpha q_z/2}{-\sqrt{2n_0} - \alpha q_z/2}\right]\right\}^{-1},$$

where $q_\perp^2 = q_x^2 + q_y^2$ while $\epsilon(\omega, \mathbf{q})$ is computed in [5]. Analysis of this formula shows that when $n_0 \lesssim 1$ the anisotropic shielding is important only in a region of space characterized by dimension a. Electromagnetic wave propagation can be studied in the quantum case by means of the dispersion equation which follows from (13); the determinant of the system is set equal to zero.

[1] A. G. Sitenko and K. N. Stepanov, JETP **31**, 642 (1956), Soviet Phys. JETP **4**, 512 (1957).

[2] V. P. Silin, JETP **40**, 1768 (1961), Soviet Phys. JETP **13**, 1244 (1961).

[3] D. C. Mattis and G. Dresselhaus, Phys. Rev. **111**, 403 (1958).

[4] Cohen, Harrison and Harrison, Phys. Rev. **117**, 937 (1960).

[5] P. S. Zyryanov, JETP **40**, 1065 (1961), Soviet Phys. JETP **13**, 751 (1961).

Translated by H. Lashinsky
198

CALCULATION OF THE FRACTION OF HIGH-ENERGY ELECTRONS AND PHOTONS NEAR THE AXIS OF EXTENSIVE AIR SHOWERS

I. V. RAKOBOL'SKAYA

Nuclear Physics Institute, Moscow State University

Submitted to JETP editor March 6, 1961

J. Exptl. Theoret. Phys. (U.S.S.R.) 41, 1125-1129 (October, 1961)

The fraction of high-energy electrons and photons in extensive air showers located at distances of up to 3 m from the shower axis is calculated assuming that π^0 mesons are produced continuously throughout the atmosphere. The angles of emission of the π^0 mesons are taken into account. It is shown that the theoretical calculations can be made consistent with the experimental results if, besides taking the π^0 meson emission angles into account, we assume that the energy spectrum of the photons produced is much softer than the spectrum of the nuclear-active component in EAS of energy $\geq 10^{11} - 10^{12}$ ev.

It has been shown [1-3] that, in the core of extensive air showers (EAS) at distances of 0 — 3 m from the shower axis, the energy spectra of the electron-photon component are considerably softer than should be expected from calculations based on the electromagnetic cascade theory. The fraction of high-energy ($E \geq 10^9$ ev) electrons and photons at 0 — 3 m from the shower axis has been determined experimentally and theoretically:

$$\Delta = N(\geqslant 10^9)/N(>0).$$

The experimental value Δ for showers with a total number of particles $N = 10^4 - 5 \times 10^4$ equals $(16 \pm 3)\%$. For a cascade parameter $s = 1.2$, the theoretical calculation of Δ (see [4]) at different energies E_0 of the primary photon gives

E_0, eV:	10^{10}	10^{11}	10^{12}	10^{13}	10^{14}
Δ, %:	15	33	35	39	44

The variation of Δ with the initial photon energy E_0 and the depth of production of the cascade shower t is illustrated in Table I (where t is expressed in radiation lengths, E_0 in ev, and Δ in percent).

It can be seen from the table that in order to make the theoretical calculations based on the purely electromagnetic theory of EAS development consistent with the experimental value of Δ it is necessary to satisfy one of two conditions: either the electron-photon component of EAS is produced mainly by protons with energy $\leq 10^{10}$ ev, or the energy spectrum of secondary photons with an energy 10^8 ev or higher should be characterized by a large value of the cascade parameter s (> 1.4). It is very difficult to reconcile either of these assumptions with a number of experimental facts.

A comparison of the data on the energy flux carried by electrons and photons near the axis of EAS [5,6] and on the mean energy per electron at various distances from the shower axis [7] with the calculations based on the electromagnetic cascade theory has also shown that the core region in EAS is poor in high-energy electrons.

In the present paper, we attempt to explain this deficiency of electrons by taking into account the

Table I

E_0 \ t		3	5	7	9	11	13	15	17	19	21	23
10^{10}	Δ	32	24	15	9							
	s	0,75	1,0	1,27	1.4							
10^{11}	Δ		46	40	34	29	21					
	s		0,75	1,10	1,12	1,3	1,4					
10^{12}	Δ			56	50	44	36	30	25			
	s			0,8	0,95	1.1	1.2	1.3	1,4			
10^{13}	Δ				63	58	50	44	36	30	27	
	s				0,8	0,9	1,05	1,15	1,24	1,3	1,4	
10^{14}	Δ					70	62	54	46	40	34	29
	s					0,85	0,95	1,03	1,11	1,22	1,26	1,34

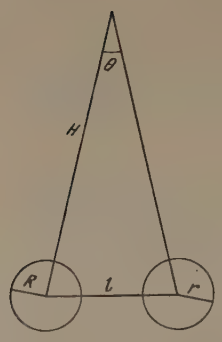

angles of emission of π^0 mesons. We have carried out the calculation of the fraction of high-energy electrons and photons in the range of 0 — 3 m from the shower axis assuming a continuous production of π^0 mesons in the atmosphere, and taking their angles of emission into account. The lateral distribution of the nuclear-active particles in the showers was neglected; it was assumed that the π^0 mesons are produced within the shower core.* The transverse momentum obtained by the π^0 mesons was assumed to be constant, independent of the energy, and equal to $p_\perp = 4 \times 10^8$ ev/c. The angle θ at which π^0 mesons are inclined to the EAS axis is equal to $\theta = p_\perp c/E_0$.

It has been assumed that the γ rays produced in the decay of π^0 mesons conserve their direction of emission. If the γ ray is produced at an atmospheric depth t, then, at the observation level t_0, the axis of the cascade shower produced by the photon deviates from the center of the EAS by a distance $l \approx H\theta = Hp_\perp c/E_0$ (where H is in meters).

The number of electrons and photons $N(t_0, R, E)$ at depth t_0 in a circle with radius R around the EAS axis in a shower with total energy E′ is equal to

$$N(t_0, R, E) = \int_0^{t_0} \int_0^{E'} \Phi(E_0, t) F(E_0, E, R, t_0 - t)\, dE_0\, dt.$$

where $F(E_0, E, R, t_0 - t)$ is a function giving the number of electrons and photons with energy $\geq E$ arriving at the depth t_0 within a circle with radius R originating from one proton with energy E_0 produced at the depth t and deviating from the shower axis by the angle θ, and $\Phi(E_0, t)$ is the number of photons with energy E_0 produced at the depth t as a result of π^0 meson decay.

For the function $F(E_0, E, R, t_0 - t)$ we have

$$F = 2 \int_{l-R}^{l+R} r\rho \arccos \frac{r^2 + l^2 - R^2}{2lr}\, dr, \quad l \geqslant R,$$

$$F = \int_0^{R-l} \pi r\rho\, dr + 2 \int_{R-l}^{R+l} r\rho \arccos \frac{r^2 + l^2 - R^2}{2lr}\, dr, \quad l < R,$$

where $\rho(r, E_0, E, t_0 - t)$ is the flux density of particles with energy $\geq E$ at a distance r from the cascade shower axis. From the cascade theory, we have

$$\rho = r_1^{-2} f(r, E_0, E, t_0 - t)\, N / 2\pi,$$

$$r_1 = E_s / E, \quad E_s = 21 \text{ Mev},$$

where $f(r, E_0, E, t_0 - t)$ is the lateral distribution function of electrons and photons with energy $\geq E$ at a depth t_0 produced by a photon with energy E_0 at a depth t,[4] and $N(E_0, E, t_0 - t)$ is the total number of such electrons and photons.[8]

Similarly, the number of electrons with energy greater than 0 in the circle of radius R was determined. For this, it was necessary to use the results of the cascade theory taking the ionization losses into account.

1. We have assumed that the primary photons in the atmosphere are produced according to the function $e^{-\mu t}$, and have determined how the fraction Δ of high-energy electrons and photons varies as compared with all electrons within a 3 m radius as a function of the initial photon energy E_0 and of the factor μ (Table II). The calculation was carried out numerically.

Furthermore, we have determined what the photon spectrum $\Phi(E_0, t)$ should be so that the theoretical value of Δ will agree with the experimental one for $1/\mu = 160$ g/cm^2. The spectrum was assumed to be represented by a power law $\Phi(E_0, t) = AE^{-\gamma}$, and the following possibilities were considered:

1) If $\gamma = 2.0$* in the $10^9 - 2 \times 10^{12}$ ev energy range, then $\Delta = 19\%$.

2) If $\gamma = 1.5$ in the $10^9 - 10^{11}$ ev energy range and $\gamma = 2.5$ in the $2 \times 10^{11} - 2 \times 10^{12}$ ev energy range, then $\Delta = 20\%$.

3) If we choose $\gamma = 1.3$ and consider the photon spectrum up to 2×10^{12} ev, then $\Delta = 43\%$.

It is impossible to determine the exact analytical shape of the spectrum from these calculations. It is, however, clear that the flatter the spectrum for low energies, the steeper it should become at higher energies.

*The correction for the lateral distribution of nuclear-active particles in the shower was introduced only for small altitudes (< 1 t), where it plays a larger role than the deflection of photons.

*Earlier,[2,3] the value $\gamma = 1.7$ was obtained for the electron and photon spectra within a 3 m radius about the EAS axis in the $2 \times 10^9 - 10^{10}$ ev energy range. We can assume that the spectrum of photons produced by the electron-photon shower component is not less steep.

Table II. Calculated values of Δ, %

$1/\mu$, g/cm²	E_0, ev				
	$7\cdot10^{10}$	$2\cdot10^{11}$	$5.5\cdot10^{11}$	$1.5\cdot10^{12}$	$4\cdot10^{12}$
180	5	47	59	64	70
160	4	40	53	60	66
120	3.5	31	38	45	
70	1,7	9	17	25	

Table III

	Experiment	Calculations based on the model of [9]					
		Neglecting the π^0 meson angles of emission	Taking into account the π^0 meson angles of emission		Taking into account the angle of emission of π^0 mesons and cutting the spectrum off at 1.5×10^{12} ev	
E', ev*	$(1-5)\cdot10^{14}$	10^{14}	10^{14}	10^{16}	10^{14}	10^{16}
Δ, %	16 ± 3	45	27	39	18	24

*For $E' = 10^{16}$ ev, Δ is somewhat larger, since at this energy the π^0 meson spectrum is flatter than for $E' = 10^{14}$ ev.

2. We have used the theoretical spectra of photons produced as a result of the π^0 meson decay at various depths in the atmosphere for an initial nuclear energy $E_1' = 10^{14}$ ev and $E_2' = 10^{16}$ ev calculated by Guzhavin and Zatsepin [9] using the Landau model [10] of the nuclear collision. If the spectrum $\Phi(E_0, t)$ is assumed to be of the power law form $\Phi = AE^{-\gamma}$, then, as shown in [9], the value γ varies with the depth of the atmosphere. The mean value of γ (for $E_1' = 10^{14}$ ev) is then $\bar{\gamma} \approx 1.8$ in the $5.5\times10^{11} - 1.1\times10^{13}$ ev energy range, while $\bar{\gamma} \approx 0.9$ in the $1.35\times10^{9} - 10^{10}$ ev energy range.

If we assume that the nuclear-active component produces photons with a probability decreasing as $e^{-\mu t}$, then, according to [9], the value for $1/\mu$ varies with photon energy from 70 g/cm² for $E_0 = 4\times10^{12}$ ev to 190 g/cm² for $E_0 = 4\times10^{9}$ ev.

Using this spectrum $\Phi(E_0, t)$, we have determined the values of Δ for E_1' and E_2' within a 3 m radius about the EAS axis, both taking into account and neglecting the angles of emission of π^0 mesons (Table III). As can be seen from the table, when the angles of emission of π^0 mesons are taken into account, the fraction of high-energy electrons and photons within a 3 m radius about the shower axis decreases by a factor of 1.5. However, the theoretical and experimental values of Δ are still markedly different. In order to obtain an agreement with the experiment, we have assumed that the photon spectrum is softer than that calculated by Guzhavin and Zatsepin. [9] In fact, we have simply cut off the spectrum $\Phi(E_0, t)$ at the energy $E_0 = 1.5\times10^{12}$ ev at all depths of the atmosphere, obtaining for Δ a value of 18%.*

From the above discussion it can be seen that the calculated value of Δ may agree with the experimental one without making any assumptions concerning the steepness of the π^0 production spectrum in the low-energy range ($10^8 - 10^{10}$ ev). Taking the emission angles of π^0 mesons into account decreases the difference between the theoretical and experimental values of Δ, and enables us to assume a less steep spectrum in this energy range. However, for energies $> 10^{11}$ ev, we still have to assume that the spectrum of the produced photon may be considerably steeper than the spectrum of the nuclear-active component in the showers.* The difference between the spectra of π^0 mesons and the spectra of the nuclear-active particles produced with mesons has been observed independently by the Bristol group. [11]

I am pleased to express my deep gratitude to Prof. G. T. Zatsepin for constant attention and helpful advice, to S. I. Nikol'skii and L. I. Sarycheva for discussion of the results, and to V. V. Guzhavin for making the detailed calculations of [9] available.

*In the calculation, we have not taken the distribution of $p_\perp$ into account, but have assumed its value to be constant. In order to estimate the influence of $p_\perp$, we have calculated Δ for $E' = 10^{14}$ ev for $p_\perp = 2\times10^8$ and 8×10^8 ev/c, and have obtained Δ = 28% and 26% respectively. After cutting off the spectrum at the energy 1.5×10^{12} ev, we have obtained Δ = 20% and 16% instead of 18% as given in Table III. Hence, it can be seen that taking the exact distribution of $p_\perp$ into account cannot introduce any significant changes.

*A value $\gamma = 1.0$ for energies $\leq 10^{13}$ ev has been obtained experimentally ([5,12] and others) for the spectrum of nuclear-active components in EAS.

[1] Hazen, Williams, and Randall, Phys. Rev. **93**, 578 (1954).

[2] Danilova, Dovzhenko, Nikol'skii, and Rakobol'skaya, JETP **34**, 841 (1958), Soviet Phys. JETP **7**, 582 (1958).

[3] Dovzhenko, Nikol'skii, and Rakobol'skaya, JETP **38**, 1361 (1960), Soviet Phys. JETP **11**, 981 (1960).

[4] V. V. Guzhavin and I. P. Ivanenko, Proc. Cosmic Ray Conf. IUPAP, Moscow, 1959, vol. 2, p. 253.

[5] Goryunov, Erlykin, Zatsepin, and Kamnev, Proc. Cosmic Ray Conf. IUPAP, Moscow, 1959, vol. 2, p. 71.

[6] N. N. Goryunov, Dissertation, Moscow State University, 1960.

[7] Vernov, Goryunov, Dmitriev, Kulikov, Nechin, Solov'eva, Strugal'skii, and Khristiansen, Proc. Cosmic Ray Conf. IUPAP, Moscow, 1959, vol. 2, p. 7.

[8] S. Z. Belen'kii, Lavinnye protsessy v kosmicheskikh luchakh (Cascade Processes in Cosmic Rays) Gostekhizdat, 1948.

[9] V. V. Guzhavin and G. T. Zatsepin, JETP **32**, 365 (1957), Soviet Phys. JETP **5**, 312 (1957).

[10] L. D. Landau, Izv. AN SSSR, Ser. Fiz. **17**, 51 (1953).

[11] Duthie, Fisher, Fowler, Kaddoura, Perkins, and Pinkau, Proc. Cosmic Ray Conf. IUPAP, Moscow, 1959, vol. 1, p. 28.

[12] Dovzhenko, Zatsepin, Murzina, Nikol'skii, and Yakovlev, Proc. Cosmic Ray Conf. IUPAP, Moscow, 1959, vol. 2, p. 144.

Translated by H. Kasha
199

DEGREE OF GROWTH OF MATRIX ELEMENTS IN THE AXIOMATIC APPROACH

B. V. MEDVEDEV and M. K. POLIVANOV

Mathematics Institute, Academy of Sciences, U.S.S.R. and Joint Institute for Nuclear Research

Submitted to JETP editor March 22, 1961

J. Exptl. Theoret. Phys. (U.S.S.R.) 41, 1130-1141 (October, 1961)

It is shown that within the "axiomatic" approach for the construction of the scattering matrix, supplemented by the requirement that the theory be "renormalizable," some very strong restrictions arise on the possible degree of growth of the matrix elements.

1. INTRODUCTION

In the last five years a lot of attention has been devoted to the study of the general structure of local quantum field theory.[1-4] A central question in these investigations is the problem to what extent is the theory determined by only general requirements—relativistic invariance, unitarity and completeness of the system of positive energy states, locality—and without specific dynamic assumptions, that are made when the theory is constructed on the basis of the Hamiltonian approach.

The basic system of physical assumptions may be formulated in various ways. It seems convenient to us to start from the scattering matrix S, as was first proposed by Heisenberg,[5] and to formulate these physical assumptions as requirements that must be satisfied by the matrix elements of S. In addition to the S matrix it is necessary to introduce into the theory some local operators, since without them different points in space-time cannot be distinguished and the causality requirement cannot be formulated. This can be done (cf.[4]) by writing the S matrix as an expansion in normal products of asymptotic fields:

$$S = \sum_{n=0}^{\infty} \frac{(-i)^n}{n!} \int dx_1 \ldots \; dx_n \, \Phi^n(x_1, \ldots, x_n) : \varphi(x_1) \ldots \varphi(x_n) : \tag{1}$$

and then extending it off the energy shell by removing the condition

$$(\Box - m^2)\varphi(x) = 0. \tag{2}$$

Then Heisenberg local operators can be constructed by variational differentiation with respect to the fields $\varphi(x)$.

A system of basic assumptions of this type has been formulated by Bogolyubov[6] for a theory with adiabatic switching on and off of the interaction; this system, as was shown by Bogolyubov and Shirkov,[7] gave within the framework of perturbation theory the same results as the conventional Lagrangian formulation and renormalization theory. Later this set of assumptions was reformulated and made more precise by Bogolyubov and the authors[4]* especially for derivation of dispersion relations and spectral representations of the Källen-Lehmann type. We shall refer to this approach for the construction of quantum field theory, based on the set of fundamental assumptions of BMP, Sec. 2, and resting on the methods of dispersion theory, as the dispersion approach. The significance of the dispersion approach to quantum field theory is not restricted to the limited number of exact results, that have been obtained with its help, but determines a new method for the construction of the entire theory.

In particular, if one attempts to satisfy the fundamental conditions of the dispersion approach by a formal series expansion in powers of some small parameter, then one will, as always in perturbation theory, be able to obtain consistently one term in the expansion after another. The advantage over the conventional theory will lie in the fact that it will now no longer be necessary to resort to the physically unsatisfactory adiabatic switching on and off procedure, and one will be able to work with only renormalized quantities, thus avoiding the meaningless in the modern theory question of the relation between "renormalized" and "unrenormalized" quantities. As was recently shown,[8] the consecutive terms in the expansion are determined in this way accurately to within a finite number of constants, whose sig-

*To be referred to in the following as BMP.

nificance is that of the counter terms in the conventional Hamiltonian approach.*

The number of such constants is determined by the degree of growth of the matrix elements. Given the interaction Lagrangian, these degrees of growth are determined in a well known manner. It has been repeatedly suggested [1,4] that specifying the degree of growth replaces in the dispersion approach the specification of the Lagrangian. It was obvious at the same time, [1,8] that the degree of growth could not be specified completely arbitrarily.

This work is devoted to the clarification of the extent of the arbitrariness with which the degree of growth of various matrix elements can be specified. We find, somewhat unexpectedly, that this arbitrariness is quite limited, and that for the important class of "properly renormalizable" theories the degree of growth need not be specified as a separate postulate, since it is almost uniquely determined by the set of basic assumptions of BMP and the transformation properties of the fields.

It turns out that the investigation for the simplest case of a self-interacting spin-zero field can be carried out without explicit use of perturbation theory.

2. EQUATIONS FOR THE MATRIX ELEMENTS

From the set of basic physical assumptions formulated in BMP one can deduce in a variety of ways [9] a system of equations that couple with each other generalized vertices with various numbers of legs, i.e., matrix elements corresponding to various numbers of particles in the initial and final states. Since in the derivation of this system of equations use is made of the causality condition it is necessary, as has been already remarked, to consider in addition to the S matrix some kind of local Heisenberg operators. A minimum of two such operators must be introduced, their significance being that of first and second variational derivatives of the scattering matrix or, more precisely, of "radiation operators" (see BMP) of first and second order. We then can formulate the theory in such a way that all other "legs," except for one and two respectively, can be real and lie on the energy shell.*

We thus investigate the matrix elements of two Hermitian operators J and J(x) taken between states on the energy shell:

$$J(p_1, \ldots, p_l; q_1, \ldots, q_s) = \langle \mathbf{p}_1, \ldots, \mathbf{p}_l | J | \mathbf{q}_1, \ldots, \mathbf{q}_s \rangle, \tag{3}$$

$$J(x | p_1, \ldots, p_l; q_1, \ldots, q_s) = \langle \mathbf{p}_1, \ldots, \mathbf{p}_l | J(x) | \mathbf{q}_1, \ldots, \mathbf{q}_s \rangle \tag{4}$$

The operator J is simply the Heisenberg current operator evaluated at the origin of the coordinate system in order to exclude its trivial x-dependence

$$J = j(0), \qquad j(x) = i \frac{\delta S}{\delta \varphi(x)} S^+. \tag{5}$$

As a consequence of translational invariance its matrix elements are related to the matrix elements $\mathrm{j}(\mathrm{x} | \ldots \mathrm{p} \ldots ; \ldots \mathrm{q} \ldots)$ of the operator j(x) by the formula

$$J(p_1, \ldots, p_l; q_1, \ldots, q_s) = j(x | p_1, \ldots, p_l; q_1, \ldots, q_s) \exp\{-i(\Sigma p_i - \Sigma q_j) x\}. \tag{6}$$

The second operator, J(x), is the retarded radiation operator from which again the trivial coordinate dependence has been removed:

$$J(x) = -\delta j\left(-\frac{x}{2}\right) \Big/ \delta \varphi\left(\frac{x}{2}\right), \qquad J^+(x) = J(x). \tag{7}$$

Its matrix elements (4) coincide with the functions $F^{\mathrm{ret}}_{\omega\omega'}$ introduced in BMP. Let us note that in fact the matrix elements (3) contain one momentum that does not lie on the energy shell

$$P - Q \neq 0, \qquad P = \sum_1^l p_i, \qquad Q = \sum_1^s q_j, \tag{8}$$

and the matrix elements (4) contain two such momenta: (8) and the momentum corresponding to the explicitly appearing coordinate x.

It is easy to see that the matrix elements (3) and (4) are connected, independently of the causality condition, by the relations†

$$J(p, p_1, \ldots, p_l; q_1, \ldots, q_s) = P\left(\frac{q_1}{q_2, \ldots, q_s}\right) \times \delta(\mathbf{p} - \mathbf{q}_1)\, J(p_1, \ldots, p_l; q_2, \ldots, q_s) - \frac{1}{(2\pi)^{3/2}\sqrt{2p^0}} \times \int dx\, J(x | p_1, \ldots, p_l; q_1, \ldots, q_s) \times \exp\left\{i\left(p + \frac{P-Q}{2}\right)x\right\}, \tag{9'}$$

*Let us note, by the way, that in the dispersion approach—and this represents another of its advantages—the origin of the counter terms, as well as the reason for the appearance of divergences in the conventional theory when ϑ-functions are unjustifiably multiplied by insufficiently regular functions, become particularly clear. Such an operation reduces in momentum representation to an application of the integral Cauchy formula to a function that does not vanish at infinity without taking into account the integral along the large circle (cf. discussion in BMP, Secs. 1 & 4).

*The authors are grateful to N. N. Bogolyubov who called their attention to the usefulness of such an approach.

†The operator P in Eq. (9) is the symmetrization operator in the appropriate arguments, as defined by Bogolyubov (see [7], §18).

$$J(p_1, \ldots, p_l; q, q_1, \ldots, q_s) = P\left(\frac{p_1}{p_2, \ldots, p_l}\right)\delta(\mathbf{p}_1 - \mathbf{q})\, J(p_2, \ldots, p_l; q_1, \ldots, q_s) - \frac{1}{(2\pi)^{3/2}\sqrt{2q^0}}\int dx\, J(x|p_1, \ldots, p_l; q_1, \ldots, q_s) \times \exp\left\{i\left(-q + \frac{P-Q}{2}\right)x\right\}, \quad (9'')$$

$$J(x) - J(-x) = i\{j(x/2)\, j(-x/2) - j(-x/2)\, j(x/2)\}, \quad (10)$$

and the causality condition imposes on the operator $J(x)$ the additional restriction

$$J(x) = 0 \text{ for } x \lesssim 0. \quad (11)$$

And so we have obtained a system of equations (9) — (11) for determining the matrix elements of the operators J and $J(x)$. It may be that this system is sufficient to determine the operators in question; in any case it can be shown, by methods analogous to those used previously,[8] that this is indeed so within the framework of perturbation theory.

In order to exclude from the above system the operator $J(x)$ we first rewrite Eq. (10) in terms of matrix elements:

$$J(x|p_1, \ldots, p_l; q_1, \ldots, q_s) - J(-x|p_1, \ldots, p_l; q_1, \ldots, q_s) = i\sum_{\nu=0}^{\infty}\frac{1}{\nu!}\int d\mathbf{k}_1 \ldots d\mathbf{k}_\nu\, J(p_1, \ldots, p_l; k_1, \ldots, k_\nu) \times J(k_1, \ldots, k_\nu; q_1, \ldots, q_s) \times \left[\exp\left\{i\left(\frac{P+Q}{2} - K\right)x\right\} - \exp\left\{-i\left(\frac{P+Q}{2} - K\right)x\right\}\right], \quad K = \sum_{\kappa=1}^{\nu} k_\kappa. \quad (12)$$

Now one must further take into account the restriction imposed on $J(x)$ by the causality condition (11), as a consequence of which $J(-x|\ldots p\ldots; \ldots q\ldots)$ vanishes when $x^0 < 0$. Formally this can be accomplished by introducing into Eq. (12) a factor $\theta(x^0)$:

$$J(x|p_1, \ldots, p_l; q_1, \ldots, q_s) = i\sum_{\nu=0}^{\infty}\frac{1}{\nu!}\int d\mathbf{k}_1 \ldots d\mathbf{k}_\nu\, J \times (p_1, \ldots, p_l; k_1, \ldots, k_\nu)\, J(k_1, \ldots, k_\nu; q_1, \ldots, q_s^*)\, \theta(x^0) \times \left[\exp\left\{i\left(\frac{P+Q}{2} - K\right)x\right\} - \exp\left\{-i\left(\frac{P+Q}{2} - K\right)x\right\}\right]. \quad (13)$$

Naturally this operation, as is well known, may turn out to be devoid of precise meaning if the integrands do not fall off sufficiently rapidly and would then result, when applied literally, in the appearance of divergences. In such cases, as is known from dispersion relations, it is necessary to perform a subtraction under the integral sign, as a consequence of which a certain polynomial will appear in momentum representation on the right hand side of Eq. (13). It is in this sense precisely that we will understand Eq. (13) and will not, in what follows, write out the polynomial explicitly.

Keeping these reservations in mind we can substitute Eq. (13) into, for example, Eq. (9′). We then arrive at an infinite system of coupled equations:

$$J(p, p_1, \ldots, p_l; q_1, \ldots, q_s) = P\left(\frac{q_1}{q_2, \ldots, q_s}\right)\delta(\mathbf{p} - \mathbf{q}_1)\, J(p_1, \ldots, p_l; q_2, \ldots, q_s) - \frac{(2\pi)^{3/2}}{\sqrt{2p^0}}\sum_{\nu}^{\infty}\frac{1}{\nu!}\int d\mathbf{k}_1 \ldots d\mathbf{k}_\nu\, J(p_1, \ldots, p_l; k_1, \ldots, k_\nu) \times J(k_1, \ldots, k_\nu; q_1, \ldots, q_s) \times \left\{\frac{\delta(\mathbf{p} + \mathbf{P} - \mathbf{K})}{K^0 - P^0 - p^0 - i\varepsilon} - \frac{\delta(\mathbf{p} - \mathbf{Q} + \mathbf{K})}{-K^0 + Q^0 - p^0 - i\varepsilon}\right\} \quad (14)$$

and an analogous system, arising from Eq. (9″), from which to determine the matrix elements of the operator J.

It will be more convenient to deal not directly with the matrix elements of the operator J but rather with the relativistically invariant matrix elements

$$I(p_1, \ldots, p_l; q_1, \ldots, q_s) = \sqrt{2p_1^0 \ldots 2p_l^0 2q_1^0 \ldots 2q_s^0}\, J(p_1, \ldots, p_l; q_1, \ldots, q_s), \quad (15)$$

which are normalized in the conventional manner. (In order to establish the connection with the usual results let us recall that since we have already taken translational invariance into account, the number of arguments explicitly appearing in the matrix element is by one less than the number of legs of the corresponding generalized diagram.) For the matrix elements $I(\ldots p\ldots; \ldots q\ldots)$ the basic set can be rewritten in the form

$$I(p, p_1, \ldots, p_l; q_1 \ldots, q_s) = P\left(\frac{q_1}{q_2, \ldots, q_s}\right)\sqrt{2p^0 2q_1^0}\,\delta(\mathbf{p} - \mathbf{q}_1) \times I(p_1, \ldots, p_l; q_2, \ldots, q_s) - (2\pi)^{3/2}\sum_{\nu}^{\infty}\frac{1}{\nu!}\int\frac{d\mathbf{k}_1 \ldots d\mathbf{k}_\nu}{2k_1^0 \ldots 2k_\nu^0} \times I(p_1, \ldots, p_l; k_1, \ldots, k_\nu)\, I(k_1, \ldots, k_\nu; q_1, \ldots, q_s) \times \left\{\frac{\delta(\mathbf{p} + \mathbf{P} - \mathbf{K})}{K^0 - P^0 - p^0 - i\varepsilon} - \frac{\delta(\mathbf{p} - \mathbf{Q} + \mathbf{K})}{-K^0 + Q^0 - p^0 - i\varepsilon}\right\}. \quad (16')$$

The lower limit in the summation over ν is deduced from the following considerations. First of all, as is easy to show, only connected diagrams contribute to the current J; therefore the summation over ν cannot include the value $\nu = 0$. Next, we recall the conditions for the stability of the

vacuum and the one-particle states, BMP I, Eq. (6), as a result of which it is necessary to set

$$I(-;-) = I(p;-) = I(-;q) = 0. \qquad (17)$$

Therefore, if even one of the numbers l or s is equal to zero, then the summation over ν starts at two.

The second half of the system of coupled equations is obtained in a fully analogous manner from Eq. (9″)

$$I(p_1, \ldots, p_l; q, q_1, \ldots, q_s) = P\left(\frac{p_1}{p_2, \ldots, p_l}\right)\delta(\mathbf{p}_1 - \mathbf{q})\sqrt{2p_1^0 2q^0} \times I(p_2, \ldots, p_l; q_1, \ldots, q_s) - (2\pi)^{3/2}\sum_{\nu}^{\infty}\frac{1}{\nu!}\int\frac{dk_1 \ldots dk_\nu}{2k_1^0 \ldots 2k_\nu^0} \times I(p_1, \ldots, p_l; k_1, \ldots, k_\nu)\, I(k_1, \ldots, k_\nu; q_1, \ldots, q_s) \times \left\{\frac{\delta(-\mathbf{q}+\mathbf{P}-\mathbf{K})}{K^0 - P^0 + q^0 - i\varepsilon} - \frac{\delta(-\mathbf{q}-\mathbf{Q}+\mathbf{K})}{-K_0 + Q^0 + q^0 - i\varepsilon}\right\}. \qquad (16'')$$

We recall once more the polynomials discussed in connection with Eq. (13)—although not explicitly written out they should not be forgotten on the right sides of Eqs. (16).

In accordance with Eq. (17), matrix elements with two legs on the energy shell are absent from the system (16). Therefore it is necessary to go off the energy shell in order to be able to include proper energy parts in the considerations. It is convenient to do so by defining the four-dimensional Fourier transform of the matrix elements (4) by the formula

$$\tilde{I}(k\,|\,p_1, \ldots, p_l; q_1, \ldots, q_s) = [2p_q^0 \ldots\ 2p_l^0 2q_1^0 \ldots\ 2q_s^0]^{-1/2} \times \int e^{ikx} J(x\,|\,p_1, \ldots, p_l; q_1, \ldots, q_s)\, dx. \qquad (18)$$

According to Eq. (12) we obtain for these Fourier transforms the following expressions

$$\tilde{I}(k\,|\,p_1, \ldots, p_l; q_1, \ldots, q_s) = (2\pi)^3\sum_{\nu}^{\infty}\frac{1}{\nu!}\int\frac{dk_1 \ldots dk_\nu}{2k_1^0 \ldots 2k_\nu^0} I(p_1, \ldots, p_l; k_1, \ldots, k_\nu) \times I(k_1, \ldots, k_\nu; q_1, \ldots, q_s) \times \left\{\frac{\delta[\mathbf{k} + (\mathbf{P}+\mathbf{Q})/2 - \mathbf{K}]}{-k^0 - (P^0+Q^0)/2 + K^0 - i\varepsilon} - \frac{\delta[\mathbf{k} - (\mathbf{P}+\mathbf{Q})/2 + \mathbf{K}]}{-k^0 + (P^0+Q^0)/2 - K^0 - i\varepsilon}\right\}, \qquad (19)$$

which, in particular, make it possible to find the proper energy parts when the remaining matrix elements on the energy shell are known. It can be said that Eqs. (19) represent the formulas for "leaving the energy shell," since the vector $\mathbf{k}$ in them is not restricted by the condition $\mathbf{k}^2 = m^2$.

One can also write the inverse relations:

$$I(p, p_1, \ldots, p_l; q_2, \ldots, q_s) = P\left(\frac{q_1}{q_2, \ldots, q_s}\right)\sqrt{2p^0 2q_1^0}\, I(p_1, \ldots, p_l; q_2, \ldots, q_s) - (2\pi)^{-3/2}\tilde{I}\left(p + \frac{P-Q}{2}\,\middle|\, p_1, \ldots, p_l; q_1, \ldots, q_s\right) \qquad (20)$$

under the condition $\mathbf{p}^2 = m^2$.

Without going into the ways of solving the system (16),* which represents in essence the relativistic analogue of the Low equation, we shall make use of it to make estimates of possible degrees of growth of the matrix elements of the operator J.

3. DEGREE OF GROWTH OF MATRIX ELEMENTS

The dependence of the matrix elements on the many momenta may be quite complex and we do not pretend here to discover what it is in detail. We address ourselves to a much simpler problem. Namely, in analogy to the procedure followed in perturbation theory (cf., for example, [7], Sec. 26) when it is desired to establish the degree of growth of some diagram, we will be interested only in the total degree of growth when all momenta are uniformly stretched.

We require for every matrix element l and s the existence for every kind of momentum of a finite growth exponent—that is a minimal integer $\omega(l, s)$ such that upon stretching of all momenta

$$p_1 = \xi_1 P, \ldots, \quad p_l = \xi_l P, \quad q_1 = \eta_1 P, \ldots, \quad q_s = \eta_s P, \quad P \to \infty \qquad (21)$$

the matrix element $I(p_1, \ldots, p_l; q_1, \ldots, q_s)$ grows slower than $P^{\omega(l,s)+\alpha}$ for an arbitrary $\alpha > 0$. We will refer to theories for which this condition is satisfied as renormalizable.† In what follows we consider only renormalizable theories.

*Difficulties of two kinds stand in the way of getting a solution for a system of this type. Such systems express lower matrix elements (i.e. matrix elements with fewer arguments) in terms of higher ones; it is therefore altogether not clear how to go about getting an exact solution for such a system. If, on the other hand, an approximation of some sort is being considered then one is faced with the problems arising from the overdeterminacy of the system—from the causality condition follows not only the system (16), but also a large variety[9] of other infinite systems of similar character. If we were to find an exact solution of the system (16), then that solution would automatically satisfy all the other possible systems; an approximation, on the other hand, good for one system may turn out to be very poor for another system.

†Such a definition of renormalizable theories is somewhat broader than the conventional definition, wherein it is also required that the number of matrix elements with nonnegative growth exponents be finite. The discussion that follows tends to support the view that the difference of the classes of theories defined in these two ways is empty.

We now wish to see whether the equations in (16) impose some kind of restrictions on the possible choice of the numbers $\omega(l, s)$. The right side of (16) consists, except for the uninteresting contribution from nonconnected diagrams, of an (infinite) sum of nonlinear terms of identical structure:

$$\int \frac{dk_1 \dots dk_\nu}{2k_1^0 \dots 2k_\nu^0} I(p_1, \dots, p_l; k_1, \dots, k_\nu)$$

$$\times I(k_1, \dots, k_\nu; q_1, \dots, q_s)$$

$$\times \left\{ \frac{\delta(\mathbf{p}+\mathbf{P}-\mathbf{K})}{K^0 - P^0 - p^0 - i\varepsilon} - \frac{\delta(\mathbf{p}-\mathbf{Q}+\mathbf{K})}{-K^0 + Q^0 - p^0 - i\varepsilon} \right\}.$$

Each of them contains 3ν integrations over the components of the momenta $\mathbf{k}$, ν factors k^0 in the denominator, and the three-dimensional δ-function divided by a one-dimensional energy denominator. In addition there appears under the integral sign the product of the matrix elements I corresponding to the numbers l, ν and ν, s, whose precise dependence on the momenta is unknown. Clearly, therefore, we cannot determine the momentum dependence of the entire integral. If, however, we make the plausible assumption that in the integration over $\mathbf{k}_1, \dots, \mathbf{k}_\nu$ the important contributions come from large values of the momenta, then it will be sufficient to know the asymptotic behavior of the matrix elements in the integrand when all momenta are increased, which is governed by the growth exponent $\omega(l, \nu)$ or $\omega(\nu, s)$. But then the determination of the behavior of the integral when all momenta are increased reduces, just as in perturbation theory, to the counting of the powers of momenta. In view of what has been said such a count gives

$$3\nu - \nu - 3 - 1 + \omega(l, \nu) + \omega(\nu, s)$$

$$= \omega(l, \nu) + \omega(\nu, s) + 2\nu - 4. \qquad (22)$$

In order to make now an estimate of the entire right side degree of growth we remark that it would be most unnatural if the higher momentum powers in various terms in the summation over ν on the right side of Eq. (16) were to cancel each other without some physical reason. Such a cancellation could only be due to the existence of some sort of a group, as is for example the case for the well known compensation of high powers in electrodynamics as a consequence of the group of gauge transformations.

Therefore, if the theory does not admit any groups (which is assumed to be the case in what follows for the sake of simplicity*) it follows from Eq. (16) that the exponent of growth of the matrix element on the left side can in no case be less than the degree of growth (22) of each term of the right side. In this way we arrive at the two sets of inequalities:

$$\omega(l+1, s) \geqslant \omega(l, \nu) + \omega(\nu, s) + 2\nu - 4, \qquad (23')$$

$$\omega(l, s+1) \geqslant \omega(l, \nu) + \omega(\nu, s) + 2\nu - 4, \qquad (23'')$$

which must be satisfied for all l, s, and ν which fulfill the conditions

$$\nu \geqslant 1, \quad l + s \geqslant 1, \quad \nu + l \geqslant 2, \quad \nu + s \geqslant 2. \qquad (24)$$

In a fully analogous manner we obtain from Eq. (19) an estimate for the degree of growth of the off the energy shell matrix element $\tilde{I}$:

$$\tilde{\omega}(l, s) \geqslant \omega(l, \nu) + \omega(\nu, s) + 2\nu - 4. \qquad (25)$$

It is easy to imagine that the degree of growth should not depend on the numbers l and s separately, but only on their sum (that is the total number of legs in the diagram), i.e., that

$$\omega(l, s) = \Omega(l+s). \qquad (26)$$

In that case the two sets (23) become one:

$$\Omega(l + s + 1) \geqslant \Omega(l + \nu) + \Omega(\nu + s) + 2\nu - 4, \qquad (27)$$

with the same conditions (24) on the numbers l, s, and ν. It is easy to see that if all the inequalities are replaced by equalities then the system (27) has as a particular solution

$$\Omega_0(n) = 3 - n. \qquad (28)$$

Therefore the general solution can be conveniently looked for in the form of a sum of the particular solution and a certain addition N(n):

$$\Omega(n) = 3 - n + N(n). \qquad (29)$$

After this substitution the basic system takes on the form

$$N(l + s + 1) \geqslant N(l + \nu) + N(s + \nu). \qquad (30)$$

The considerations that have led us to Eq. (30) cannot, of course, be taken as yet as a rigorous mathematical proof. A mathematician would call them heuristic and would try to produce counter examples. Without attempting to give here a rigorous proof let us present one more argument. The matrix elements in the integrands on the right side of Eq. (16) consist, in part, of the counterterms. Since the momentum dependence of the counterterms is in the form of polynomials the integrand is explicitly known and so the part of the integral involved in the counter term can be exhaustively studied by elementary methods. Actually such a study is unnecessary since exactly the same prob-

*The case when such a group exists must be investigated separately.

lem has been studied in detail in the theory of R-operation (see [7], Sec. 26).

Let us go on to an investigation of the system of inequalities (30). We establish first of all that all N(n) are nonpositive. To prove this it is sufficient for odd n to set in Eq. (30) $\nu = s + 1 \geq 2$, l —arbitrary. Then the left side cancels the first term on the right and we get

$$0 \geqslant N(2s+1) \text{ for } s \geqslant 1. \tag{31}$$

For even n we set $s = l \geq 1$ and $\nu \geq 1$, which again is allowed by the conditions (24). We then get

$$2N(l+\nu) \leqslant N(2l+1) \leqslant 0, \tag{32}$$

where we have used Eq. (31) for the last inequality. Thus

$$\Omega(n) \leqslant \Omega_0(n) = 3 - n \text{ for all } n \geqslant 2. \tag{33}$$

In this way we verify that the particular solution (28) gives the maximum possible growth exponent for the matrix elements $I(p_1, \ldots p_l; q_1, \ldots q_s)$. From this result it follows in particular that the number of matrix elements with positive growth exponents is finite and that consequently our definition of renormalizable theories coincides with the conventional one.

We show next that the possible growth exponents are bounded not only from above but also from below. To this end we set $\nu = 1$ —its minimum possible value, and denote the argument on the left side of Eq. (30) by the single letter n, so that

$$N(n) \geqslant N(n-s) + N(s+1), \tag{34}$$

where n and s are restricted according to Eq. (24) by the conditions

$$n \geqslant s+2, \quad s \geqslant 1. \tag{35}$$

The same formula (with a new value for n) can be applied again to the first term on the right side of Eq. (34). Repeating this procedure k times we obtain for N(n) the lower bound

$$N(n) \geqslant N(n-ks) + kN(s+1)N. \tag{36}$$

At that, in view of Eq. (35), in choosing k one must satisfy the condition

$$k \geqslant (n-2)/s. \tag{37}$$

Setting in Eq. (36) s = 1 and k equal to its maximum possible value k = n − 2, we find that for all $n \geq 2$ we must have

$$N(n) \geqslant N(2) + (n-2)N(2) = (n-1)N(2). \tag{38}$$

The result (38) is not an underestimate, by which we mean that the lower bound for the values of N(n) indicated by it can actually be attained. Indeed, if we let the N(n) in the basic system (30) take on the minimum values allowed by Eq. (38), then that system reduces to the condition $\nu \geq 1$, which is satisfied according to Eq. (24).

The limitations on the possible values of N(n) are not exhausted by the above conditions (32) and (38). Namely, should N(n) for some $n = n_0 > 2$ exceed the minimum value (38) then new restrictions are imposed on N(n) for $n > n_0$, which can be derived from Eq. (36) by setting in it s equal to some number larger than one. We will not derive these conditions here.

Finally, relations (25) provide us with a lower bound for the growth exponent for diagrams with two legs off the energy shell:

$$\tilde{N}(1) = \tilde{\Omega}(1) - 2 = \tilde{\omega}(1 \mid -; -) - 2 \geqslant 2N(\nu), \quad \nu \geqslant 2. \tag{38'}$$

In this case there is no upper bound.

4. PROPERLY RENORMALIZABLE THEORIES

In the preceding section we have derived from the basic equations (16) of the theory the system of inequalities (23) by assuming the theory to be renormalizable. To that end we made use of the requirement that the growth exponent on the left side of Eq. (16) could not be exceeded by the growth exponent of any of the terms on the right side, i.e., it had to be either larger than or equal to the largest growth exponent of the terms on the right side. It would be desirable to make this condition stronger and replace the inequality by an equality. Since, as we have repeatedly emphasized, in addition to the explicitly written out integrals it is understood that there appear on the right side of Eq. (16) certain counter terms, such a strengthening of the conditions requires an additional assumption.

We shall call a theory properly renormalizable if the power of the polynomials added to the T products does not exceed the growth exponent of the corresponding T products. Let us now suppose that we are dealing with a properly renormalizable theory. Then the conditions (23) can indeed be rewritten in the stronger form:

$$\omega(l+1, s) = \max_{\nu} \{\omega(l, \nu) + \omega(\nu, s) + 2\nu - 4\},$$
$$\omega(l, s+1) = \max_{\nu} \{\omega(l, \nu) + \omega(\nu, s) + 2\nu - 4\}. \tag{39}$$

For the quantities N(n) the stronger conditions become

$$N(l+s+1) = \max \{N(l+\nu) + N(s+\nu)\}, \tag{40}$$

where the maximum is to be taken over all values of the arguments allowed by the conditions (24).

Table I

2							
5=3+2	*4*						
7=4+3	5+2	*6*					
9=5+4	6+3	7+2	*8*				
11=6+5	7+4	8+3	9+2	*10*			
13=7+6	8+5	9+4	10+3	11+2	*12*		
15=8+7 17=9+8	9+6 10+7 ...	10+5 11+6 ...	11+4 12+5 ...	12+3 13+4 ...	13+2 14+3 ...	*14* 15+2 ...	...

Table II

4=2+2	*3*				
6=3+3	4+2	*5*			
8=4+4	5+3	6+2	*7*		
10=5+5	6+4	7+3	8+2	*9*	
12=6+6 14=7+7	7+5 8+6 ...	8+4 9+5 ...	9+3 10+4 ...	10+2 11+3 ...	*11* 12+2 ... ...

We attempt to solve this system. Let us write it in the form:

$$N(n_1) = \max\{N(n_2) + N(n_3)\}, \tag{41}$$

where now the maximum is sought over values of n_2 and n_3 satisfying the set of conditions

$$n_2 + n_3 = n_1 - 1 + 2\nu, \quad n_2 > \nu \geqslant 1, \; n_3 > \nu \geqslant 1. \tag{42}$$

To obtain a solution of the system (41) we write the totality of pairs N(n), over which the maximum on the right side of Eq. (41) is taken, in the form of two tables (I and II, for even and odd values separately) with two entries, in which the rows are labeled by the sums of n_2 and n_3 and the columns by the differences. The sums in the cells in the tables represent all possible decompositions of $n_1 - 1 + 2\nu$ into the sum of n_2 and n_3, satisfying Eq. (42); it is obvious that they represent simultaneously the sums standing under the maximum sign in Eq. (41). If any of these combinations of n_2 and n_3 satisfy the inequalities (42) then so will obviously, for fixed n_1, all the combinations appearing below in the same column since displacement downwards in a column corresponds simply to an increase in ν. By giving ν the smallest possible value $\nu = 1$ we convince ourselves that, according to the first equality (42), only the rows with $n_2 + n_3 \geq n_1 + 1$ enter into the region over which the maximum in Eq. (41) is sought for a given n_1. As regards the number of columns that enter this region, this is determined from the condition $(n_2 - n_3) \leq (n_2 + n_3) - 4$ which follows from Eq. (42). The resultant regions are shown in Tables I and II and marked by the corresponding values of n_1, which are denoted in italics. It follows right away from a study of Tables I and II that

$$N(2) \leqslant N(4), \tag{43}$$

since it is seen from Table I that the region over which the maximum for N(2) is sought, is fully contained within the region over which the maximum for N(4) is sought.

Next the situation becomes more complicated since in passing from N(3) to N(5) not only a new (the third in Table II) column is added, but also the element 2 + 2 gets eliminated from the first row. However as a consequence of Eq. (43) N(2) + N(2) ≤ N(4) + N(2), and the combination 4 + 2 also enters both allowable regions. Consequently we may write a new inequality:

$$N(3) \leqslant N(5). \tag{44}$$

It is easy to see that this state of affairs will be preserved at each successive step. That is, each time as we go from n to n+2 the shrinkage of the region over which the maximum is sought will turn out to be immaterial as soon as chains of inequalities of the type Eqs. (43), (44) are established for all $k \leq n+1$. In this manner a complete induction turns out to be possible and we arrive at the infinite chains

$$N(2) \leqslant N(4) \leqslant N(6) \leqslant \ldots \leqslant N(2k) \leqslant \ldots, \tag{45'}$$

and

$$N(3) \leqslant N(5) \leqslant N(7) \leqslant \ldots \leqslant N(2k+1) \leqslant \ldots. \tag{45''}$$

On the other hand, however, all N(n) are bounded from above by the condition (33). Thus the two nondecreasing sequences of integers (34) should reach their upper bounds, i.e., there should exist

$$\max N(2k) = -a \leqslant 0 \quad \text{and}$$

$$\max N(2k+1) = -b \leqslant 0 \quad (k \geqslant 1). \tag{46}$$

Observing now that the region (42), over which the maximum in Eq. (41) is sought, includes for any n_1 arbitrarily large n_2 and n_3 we conclude that instead of Eq. (41) we could write

$$N(2k) = \max\{-a-b\} = -a-b,$$
$$N(2k+1) = \max\{(-a-a),(-b-b)\}. \tag{47}$$

Consequently N(2k) and N(2k+1) are independent of k. But then

$$N(2k) = -a = -a-b, \text{ i. e. } b = 0,$$

and, further,

$$N(2k+1) = -b = \max\{-2a, -2b\},$$

i.e., $-a \leq 0$.

And so the solution of the system (40) is of the form

$$N(2k) = -a, \quad N(2k+1) = 0, \tag{48}$$

where a is an arbitrary nonnegative integer. According to Eq. (29) this means that the general expression for the possible growth exponents of matrix elements I in a properly renormalizable theory is given by

$$\Omega(2k) = 3 - 2k - a,$$
$$\Omega(2k+1) = 2 - 2k, \quad a \geqslant 0, \; a \in N. \tag{49}$$

There remains to write the condition for the growth exponent for the diagram with two legs:

$$\tilde{N}(1) = 2\max_{\nu \geqslant 2} N(\nu) = 0, \quad \tilde{\Omega}(1) = \tilde{N}(1) + 2 = 2. \tag{50}$$

5. DISCUSSION

The most important of the results obtained in the two preceding sections is the upper bound (33) for the possible growth exponents. Only matrix elements with three or four legs (n = 2 or 3) (beside the proper energy parts, that do not enter the system (16)) can have nonnegative exponents. But this means that only these matrix elements may possess counterterms (being polynomials in the momenta they could not have negative growth exponents!). We thus see that within the dispersion approach framework the "dynamical principle" is almost superfluous—the specification of the transformation properties of the fields alone specializes the character of admissible interactions accurate to within a small number of constants. For the case of the spinless field here considered only two such constants appear—the constant quadrilinear counterterm (n = 3) as well as the trilinear one (the formally admissible linear counterterm is forbidden by relativistic invariance considerations).

Particularly strong limitations arise in properly renormalizable theories. We note that a condition, that appears to be identical to the proper renormalizability condition, is always imposed in the conventional construction of perturbation theory; namely the choice for counterterms in momentum representation of polynomials of the minimum possible degree (cf., for example, [7], Sec. 26) (without such a condition it would be impossible to construct the R-operation). A significant difference arises, however, in the following point. Conventionally one deals in fact with counterterms (in a broad sense) of two kinds. Along with proper counter terms (renormalization constants), arising in the determination of products of singular functions, one also considers "charges," which come from the original Lagrangian. The degrees of the corresponding polynomials are not determined from a minimality condition but are prescribed ad hoc when the theory is formulated. In our approach all counterterms are treated uniformly, the "charges" appearing on the same footing as the "renormalization constants." Both kinds play the role of inhomogeneities or a kind of boundary conditions for the basic system (16); there are reasons to believe that in their absence only the trivial zero solution would be admissible. This is certainly so if we accept an expansion in some small parameter in the spirit of [8].

In that connection the requirement of minimum growth adds to the logical scheme of the theory a particular beauty: in the absence of counterterms the system (16) would possess only the trivial solution; nontrivial solutions are obtained only if counter terms are introduced; introducing them, however, does not add extraneous elements to the system (16) but rather use is made of the nonuniqueness present in the system, owing to its singular nature. Were the system (16) regular there would be no internal reason for adding counterterms and we would arrive at a unique—zero—solution (cf. [10]).

We thus impose the condition of "minimal growth" also on the counterterms, normally included in the "bare Lagrangian." This, naturally, may lead to stronger restrictions on the acceptable class of theories—the class of properly renormalizable theories already is the class of theories renormalizable in the conventional sense. In particular this eliminates the theory with one trilinear interaction of scalar particles—the Hurst-Thirring field. In this theory the growth exponent of the simplest diagram with three legs is equal to minus two, and is even smaller for more complicated three-legged diagrams. Therefore from the point of view of minimal growth such diagrams should not be accompanied by counterterms and the charge should be equal to zero.*

It is interesting that a properly renormalizable theory with two types of scalar interactions—trilinear and quadrilinear simultaneously—is pos-

*It is interesting to compare these considerations with the indications that have appeared in the literature[11] that this theory is internally inconsistent.

sible. Indeed, the growth exponent of the trilinear vertex $\Omega(2)$ may be chosen in Eq. (49) either equal to zero or negative on account of a, but the one corresponding to the quadrilinear vertex $\Omega(3)$ is necessarily equal to zero, i.e., in the theory of interacting spin zero particles there necessarily appears the quadrilinear interaction.

The authors are grateful to N. N. Bogolyubov, V. S. Vladimirov, and I. F. Ginzburg for fruitful discussion and a series of valuable remarks.

[1] Lehmann, Symanzik, and Zimmermann, Nuovo cimento **1**, 205 (1955).

[2] R. Haag, Mat.-Fis. Medd. Dan. Vid. Selsk. **29**, 12 (1955).

[3] A. S. Wightman, Colloque international en Lille, June, 1957.

[4] Bogolyubov, Medvedev, and Polivanov, Voprosy teorii dispersnykh sootnoshenii (Problems in the Theory of Dispersion Relations), Fizmatgiz (1958).

[5] W. Heisenberg, Z. Physik **120**, 513, 673 (1943).

[6] N. N. Bogolyubov, Izv. AN SSSR, Ser. Fiz. **19**, 237 (1955), Columbia Tech. Transl., p. 215.

[7] N. N. Bogolyubov and D. V. Shirkov, Introduction to Quantum Field Theory, Interscience, 1959.

[8] B. V. Medvedev, DAN SSSR **135**, 1087 (1960), Soviet Phys.–Doklady **5**, 1206 (1961).

[9] B. V. Medvedev, JETP **40**, 826 (1961), Soviet Phys. JETP **13**, 580 (1961).

[10] V. L. Bonch-Bruevich and B. V. Medvedev, JETP **22**, 425 (1952).

[11] Gordon Baym, Phys. Rev. **117**, 886 (1960).

Translated by A. M. Bincer
200

THERMAL CONDUCTIVITY OF PURE SUPERCONDUCTORS AND ABSORPTION OF SOUND IN SUPERCONDUCTORS

B. T. GEĬLIKMAN and V. Z. KRESIN

Moscow State Pedagogical Institute

Submitted to JETP editor March 30, 1961

J. Exptl. Theoret. Phys. (U.S.S.R.) 41, 1142-1150 (October, 1961)

The electron thermal conductivity produced in very pure superconductors by scattering of electron excitations on phonons is calculated on the basis of the microscopic theory of superconductivity. The absorption of sound in superconductors is also discussed.

We consider in this paper the electron thermal conductivity of superconductors, due to the scattering of electrons on phonons. This interaction plays a major role in the investigation of the thermal conductivity of very pure semiconductors. In addition, it makes a certain contribution also when the impurity concentration is not too high.[1] The final formula for the corresponding coefficient of thermal conductivity was given earlier.[2] We present here more detailed calculations and a comparison with experiment. We consider also the absorption of ultrasound in superconductors.

1. THERMAL CONDUCTIVITY OF PURE SUPERCONDUCTORS

The electron distribution function satisfies the kinetic equation

$$\frac{\partial f}{\partial x}\frac{\partial \varepsilon}{\partial p_x} - \frac{\partial f}{\partial p_x}\frac{\partial \varepsilon}{\partial x} = \left(\frac{\partial f}{\partial t}\right)_{st}, \qquad (1.1)$$

where f is the electron distribution function, which we seek, as usual, in the form

$$f = f_0 + \frac{\partial f_0}{\partial \varepsilon}\varphi(\varepsilon, \Omega)\frac{\partial T}{\partial x}.$$

In the electron-phonon interaction Hamiltonian

$$H = \sum_{\mathbf{k}, \mathbf{k}', s} V_{\mathbf{k}\mathbf{k}'} a^+_{\mathbf{k}'s} a_{\mathbf{k}s} b_{\mathbf{q}} + \text{ c.c.}$$

we change over to new Fermi amplitudes that describe the electron excitations of the superconductor by making a canonical transformation, following Bogolyubov[3]:

$$a_{k0} = u_k a_{k,1/2} - v_k a^+_{k,-1/2},$$
$$a_{k1} = u_k a_{-k,-1/2} + v_k a^+_{k,1/2},$$
$$u_k^2 = \tfrac{1}{2}(1 + \xi/\varepsilon), \quad v_k^2 = \tfrac{1}{2}(1 - \xi/\varepsilon)$$

(ξ — energy of ordinary electron reckoned from the Fermi surface, ϵ — energy of electron excitation, $\epsilon = \sqrt{\xi^2 + \Delta^2(T)}$, $\Delta(T)$ — size of gap in the energy spectrum).

We now rewrite the kinetic equation in terms of the new amplitudes (the left half is transformed in accordance with [4]):

$$f_0^2 e^{\varepsilon/T}\frac{\xi}{\varepsilon}\frac{\varepsilon}{T}\frac{\partial T}{\partial x} = \int |V|^2 N_0\left(1 + \frac{\xi\xi' - \Delta^2}{\varepsilon\varepsilon'}\right)$$
$$\times [\varphi(\varepsilon', \Omega') - \varphi(\varepsilon, \Omega)]\, e^{\varepsilon'/T} f_0(\varepsilon) f_0(\varepsilon')$$
$$\times \delta(\varepsilon' - \varepsilon - \hbar\omega)\, d\mathbf{q} + \int |V|^2 N_0\left(1 + \frac{\xi\xi' - \Delta^2}{\varepsilon\varepsilon'}\right)[\varphi(\varepsilon', \Omega')$$
$$- \varphi(\varepsilon, \Omega)]\, e^{\varepsilon/T} f_0(\varepsilon) f_0(\varepsilon')\, \delta(\varepsilon - \varepsilon' - \hbar\omega)\, d\mathbf{q}$$
$$+ \int |V|^2 N_0\left(1 - \frac{\xi\xi' - \Delta^2}{\varepsilon\varepsilon'}\right)[\varphi(\varepsilon', \Omega') - \varphi(\varepsilon, \Omega)]$$
$$\times e^{\hbar\omega/T} f_0(\varepsilon) f_0(\varepsilon')\, \delta(\varepsilon' + \varepsilon - \hbar\omega)\, d\mathbf{q},$$
$$N_0 = (e^{\hbar\omega/T} - 1)^{-1}. \qquad (1.2)$$

We recognize further that the phonon wave vector $\mathbf{q}$ is small compared with $|\mathbf{p}|$. We therefore expand $\varphi(\Omega')$ in powers of $\mathbf{q}' = \mathbf{p} - \mathbf{p}^*$ ($\mathbf{p}^*$ is a vector directed in the $\mathbf{p}$ direction of length $|\mathbf{p}'|$). This method of investigating the kinetic equation was first developed by Landau and Pomeranchuk.[5] Integrating then over the angle ϑ (the polar axis is chosen in the direction of the vector $\mathbf{p}$), we obtain*

$$f_0^2 e^{\varepsilon/T}\frac{\varepsilon}{T}\frac{p_x}{m} = \int N_0 |V|^2 \frac{\varepsilon\varepsilon'}{|\xi||\xi'|}\left(1 + \frac{\xi\xi' - \Delta^2}{\varepsilon\varepsilon'}\right)$$
$$\times [\varphi(\varepsilon + \hbar\omega, \Omega) - \varphi(\varepsilon, \Omega)]\frac{e^{(\varepsilon+\hbar\omega)/T}}{(e^{\varepsilon/T} + 1)(e^{(\varepsilon+\hbar\omega)/T} + 1)}$$
$$\times \frac{m}{pq} q^2\, dq\, d\varphi + \int N_0 |V|^2 \frac{\varepsilon\varepsilon'}{|\xi||\xi'|}\left(1 + \frac{\xi\xi' - \Delta^2}{\varepsilon\varepsilon'}\right)$$
$$\times [\varphi(\varepsilon - \hbar\omega, \Omega) - \varphi(\varepsilon, \Omega)]\frac{e^{\varepsilon/T}}{(e^{\varepsilon/T} + 1)(e^{(\varepsilon-\hbar\omega)/T} + 1)}$$
$$\times \frac{m}{pq} q^2\, dq\, d\varphi + \int N_0 |V|^2 \frac{\varepsilon\varepsilon'}{|\xi||\xi'|}$$
$$\times \left(1 - \frac{\xi\xi' - \Delta^2}{\varepsilon\varepsilon'}\right)[\varphi(\hbar\omega - \varepsilon, \Omega) - \varphi(\varepsilon, \Omega)]$$

*The temperature is in energy units throughout.

$$\times \frac{e^{\hbar\omega/T}}{(e^{\varepsilon/T}+1)(e^{(\hbar\omega-\varepsilon)/T}+1)} \frac{m}{pq} q^2\, dq\, d\varphi$$

$$+\int N_0 |V|^2 \frac{\varepsilon\varepsilon'}{|\xi||\xi'|}\left(1+\frac{\xi\xi'-\Delta^2}{\varepsilon\varepsilon'}\right)$$

$$\times \frac{e^{(\varepsilon+\hbar\omega)/T}}{(e^{\varepsilon/T}+1)(e^{(\varepsilon+\hbar\omega)/T}+1)} \frac{m}{pq} \frac{\partial^2\varphi}{\partial\Omega^2} q_i q_j q^2\, dq\, d\varphi$$

$$+\int N_0 |V|^2 \frac{\varepsilon\varepsilon'}{|\xi||\xi'|}\left(1+\frac{\xi\xi'-\Delta^2}{\varepsilon\varepsilon'}\right) \frac{e^{\varepsilon/T}}{(e^{\varepsilon/T}+1)(e^{(\varepsilon-\hbar\omega/T}+1)}$$

$$\times \frac{m}{pq} \frac{\partial^2\varphi}{\partial\Omega^2} q_i q_j q^2\, dq\, d\varphi + \int N_0 |V|^2 \frac{\varepsilon\varepsilon'}{|\xi||\xi'|}\left(1-\frac{\xi\xi'-\Delta^2}{\varepsilon\varepsilon'}\right)$$

$$\times \frac{e^{\hbar\omega/T}}{(e^{\varepsilon/T}+1)(e^{(\varepsilon-\hbar\omega)/T}+1)} \frac{m}{pq} \frac{\partial^2\varphi}{\partial\Omega^2} q_i q_j q^2\, dq\, d\varphi. \qquad (1.2')$$

We make the approximate substitution

$$\frac{\varepsilon\varepsilon'}{|\xi||\xi'|}\left(1\pm\frac{\xi\xi'-\Delta^2}{\varepsilon\varepsilon'}\right)\approx 2,$$

as was done in the calculation of the phonon thermal conductivity,[6] and integrate both parts of (1.2′) with respect to ξ. In the right half we make at the same time the expansion[5] $p_x/p = (p_x/p)_p = p_0 + a_x\xi$. We then seek a solution in the form $\varphi(\epsilon, \Omega) = \varphi_1(\Omega) + \varphi_2(\epsilon, \Omega)$, with $\varphi_1 \gg \varphi_2$. Using $d\xi = \epsilon\, d\epsilon/\xi$ to change over to integration with respect to ϵ we obtain

$$\int_b^\infty f_0^2 e^z a_x z\sqrt{z^2-b^2}\, dz = |V'|^2 T^2 \int_0^\infty \frac{x^2\, dx}{e^x-1}\int [\varphi_2(z+x,\Omega)$$

$$-\varphi_2(z,\Omega)]\frac{e^{z+x}\, dz\, d\varphi}{(e^z+1)(e^{z+x}+1)}$$

$$+|V'|^2T^2\int_0^\infty \frac{x^2\, dx}{e^x-1}\int_{b+x}^\infty [\varphi_2(z-x,\Omega)-\varphi_2(z,\Omega)]$$

$$\times\frac{e^z\, dz\, d\varphi}{(e^z+1)(e^{z-x}+1)}+|V'|^2T^2\int_{2b}^\infty \frac{x^2\, dx}{e^x-1}\int_b^{x-b}[\varphi_2(x-z,\Omega)$$

$$-\varphi_2(z,\Omega)]\frac{e^x\, dz\, d\varphi}{(e^z+1)(e^{x-z}+1)}$$

$$+|V'|^2T^4\int_0^\infty \frac{x^4\, dx}{e^x-1}\int_b^\infty \frac{e^{z+x}\, dz\, d\varphi}{(e^z+1)(e^{z-x}+1)}\frac{\partial^2\varphi_1}{\partial\Omega^2}$$

$$+|V'|^2T^4\int_0^\infty \frac{x^4\, dx}{e^x-1}\int_{b+x}^\infty \frac{e^z\, dz\, d\varphi}{(e^z+1)(e^{z-x}+1)}\frac{\partial^2\varphi_1}{\partial\Omega^2}$$

$$+\frac{1}{2}|V'|^2T^4\int_{2b}^\infty \frac{x^4\, dx}{e^x-1}\int_b^{x-b}\frac{e^x\, dz\, d\varphi}{(e^z+1)(e^{x-z}+1)}\frac{\partial^2\varphi_1}{\partial\Omega^2}.$$

We use the notation $\epsilon/T = z$; $\hbar\omega/T = x$; $\Delta/T = b$; $|V'|^2 = |V^2|/q$.

The first integrals, which contain $\varphi_2(\epsilon, \Omega)$, make a zero contribution (to verify this we make the substitutions $z \to z + x$ in the second integrand and $z \to x - z$ in the third). We then find

$$\varphi = \frac{a(\Omega)}{T^4\Phi(T)}\int_b^\infty f_0^2 e^z z\sqrt{z^2-b^2}\, dz\frac{\partial T}{\partial x};$$

$$\Phi(T) = \int_0^\infty \frac{4x^4}{e^x-1}\int_b^\infty \frac{dz}{(e^z+1)(e^{-z-x}+1)}$$

$$+\int_{2b}^\infty \frac{x^4\, dx}{e^x-1}\int_b^{x-b}\frac{dz}{(e^z+1)(e^{-z}+e^{-x})} \qquad (1.3)$$

where $a(\Omega)$ depends on the angles that determine the direction of motion of the electron.

We calculate next the heat flux from the formula $Q = \int \epsilon v_x f\, dp$. Taking (1.3) into account, we obtain

$$Q = \frac{\text{const}}{\Phi(T)T^2}\overline{a(\Omega)}\left[\int_b^\infty f_0^2 e^z z\sqrt{z^2-b^2}\, dz\right]^2\frac{\partial T}{\partial x}. \qquad (1.4)$$

Calculation of the integrals in (1.4) leads ultimately to

$$\varkappa = -Q\Big/\frac{\partial T}{\partial x} = \frac{\text{const}}{\Phi(T)T^2}\left[b^2\sum_{s=1}^\infty K_2(bs)\right]^2, \qquad (1.5)$$

where $K_2(bs)$ is a Bessel function of imaginary argument, and

$$\Phi(T) = 96\zeta(4)\ln(1+e^{-b}) + \sum_{s=1}^\infty s^{-5}e^{-2bs}(80b^4s^4$$

$$+160b^3s^3+240b^2s^2+240bs+120)$$

$$-\ln(e^b+1)\sum_{s=1}^\infty s^{-4}e^{-2bs}(64b^3s^3+96b^2s^2+96bs+48). \qquad (1.6)$$

In the temperature region close to T_C, where the contribution of the electron-phonon interaction to the heat flux is most significant, we obtain

$$\varkappa = \varkappa_n\frac{36}{\pi^4}\frac{\Phi(T_c)}{\Phi(T)}\left[2\sum_{s=1}^\infty\frac{(-1)^{s+1}}{s^2}e^{-bs}\right.$$

$$\left.+2b\ln(1+e^{-b})-\frac{b^2}{2(e^b+1)}\right]^2, \qquad (1.7)$$

where κ_n —thermal conductivity of the normal metal. The results obtained agree quite well with the experimental data.[7,8]

Expression (1.5) for κ differs from that obtained by Bardeen, Rickayzen, and Tewordt.[9] These authors used a direct variational method and trial functions for f that differed appreciably from the true function (1.3).

2. ABSORPTION OF ULTRASOUND IN SUPERCONDUCTORS

Let us examine the absorption of sound in superconductors when the frequency satisfies the condition $\omega \gg 1/\tau$ (ω —frequency of sound, τ —relaxation time for electron excitations; see below).

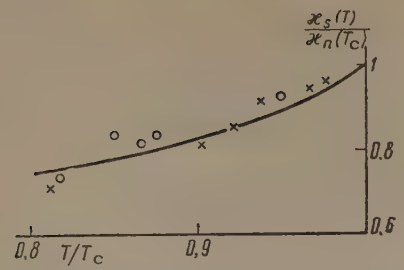

FIG. 1. Experimental points correspond to × – tin,[7] ○ – indium,[8] solid curve – theoretical.

Since the period of the sound wave is in this case less than the relaxation time, we can disregard the relaxation processes completely and consider only the absorption of sound quanta (the number of which is $N \gg 1$) by the electron excitations.

Writing for the probability of absorption of a sound quantum

$$W_I = \sum_k |V|^2 [(u_k u_{k'} - v_k v_{k'})^2 N f (1-f') \delta(\varepsilon' - \varepsilon - \hbar\omega) + (u_k v_{k'} + u_{k'} v_k)^2 N (1-f)(1-f') \delta(\varepsilon' + \varepsilon - \hbar\omega)]$$

(f – number of electron excitations with energy ϵ, N – number of phonons of frequency ω) and for the probability of the reverse process

$$W_{II} \sim \sum_k |V|^2 [(u_k u_{k'} - v_k v_{k'})^2 (N+1) \times (1-f) f' \delta(\varepsilon' - \varepsilon - \hbar\omega) + (u_k v_{k'} + u_{k'} v_k)^2 (N+1) f f' \delta(\varepsilon' + \varepsilon - \hbar\omega)]$$

and substituting the expressions for u_k and v_k, we obtain for the absorption coefficient, which is proportional to the difference $W_I - W_{II}$, the expression

$$\gamma \sim \int |V|^2 \left\{ \left(1 + \frac{\xi\xi' - \Delta^2}{\varepsilon\varepsilon'}\right)(f - f') \delta(\varepsilon' - \varepsilon - \hbar\omega) + \left(1 - \frac{\xi\xi' - \Delta^2}{\varepsilon\varepsilon'}\right)(1 - f - f') \delta(\varepsilon' + \varepsilon - \hbar\omega) \right\} \times \frac{p^2 dp \sin\vartheta\, d\vartheta\, d\varphi}{4\pi^2\hbar^4}. \quad (2.1)$$

From the momentum conservation law we obtain for the angle ϑ between $\mathbf{p}$ and $\mathbf{q}$, in the case of the scattering of electrons by phonons ($\mathbf{p}' = \mathbf{p} + \mathbf{q}$)

$$\cos\vartheta = (2m\xi' - 2m\xi + q^2)/2pq.$$

In the creation of excitation pairs ($\mathbf{p} + \mathbf{p}' = \mathbf{q}$) we have

$$\cos\vartheta = (-2m\xi' + 2m\xi + q^2)/2pq.$$

Taking these relations into account, we obtain upon integration over the angles (the polar axis is chosen in the direction of the vector $\mathbf{q}$) and after changing to integration with respect to ϵ

$$\gamma = \text{const} \cdot \left[\int_\Delta^\infty \left(1 - \frac{\xi\xi' - \Delta^2}{\varepsilon\varepsilon'}\right)(f - f') \frac{\varepsilon\varepsilon'}{|\xi||\xi'|} d\varepsilon + D\left(\frac{\hbar\omega}{T}\right) \int_\Delta^{\hbar\omega - \Delta} \frac{1}{2}\left(1 - \frac{\xi\xi' - \Delta^2}{\varepsilon\varepsilon'}\right)(1 - f - f') \frac{\varepsilon\varepsilon'}{|\xi||\xi'|} d\varepsilon \right];$$

$$D\left(\frac{\hbar\omega}{T}\right) = \begin{cases} 1, & \hbar\omega \geqslant 2\Delta \\ 0, & \hbar\omega < 2\Delta. \end{cases} \quad (2.2)$$

The function $D(\hbar\omega/T)$ has been introduced because creation of excitation pairs is possible only when $\hbar\omega \geq 2\Delta$.

We put approximately

$$1 \pm (\xi\xi' - \Delta^2)/\varepsilon\varepsilon' \approx 2; \quad (2.3)$$

and consider here frequencies that satisfy the condition $\hbar\omega < T$. We then obtain

$$\gamma = \text{const} \cdot T \left[\int_b^\infty (f - f')\, dz + D(x) \int_b^{x-b} (1 - f - f')\, dz \right];$$

$$f = (e^z + 1)^{-1}, \quad b = \Delta/T, \quad z = \varepsilon/T, \quad x = \hbar\omega/T.$$

Simple integration results in a general formula for the ratio of the ultrasound absorption coefficients in the normal and superconducting states [1]

$$\gamma_s/\gamma_n = \{x - \ln[(e^{b+x} + 1)(e^b + 1)^{-1}] + D(x)[2b - x + 2\ln[(e^{x-b} + 1)(e^b - 1)^{-1}]]\} / \ln[(e^x + 1)/2]. \quad (2.4)$$

When $x \ll 1$ we have $\gamma_s/\gamma_n = 2/(e^b + 1)$, which agrees with the result obtained by Bardeen, Cooper, and Schrieffer [10] and experimentally confirmed by Morse and Bohm. [11]

3. ABSORPTION OF LONG-WAVE SOUND

We now investigate the absorption of sound in superconductors for the case when $\omega \ll 1/\tau$; for electron excitations we have according to [11] $\tau \sim 10^{-7} - 10^{-6}$ sec. We consider first the absorption of sound by electron excitations, which makes the main contribution to this absorption. We consider the sound field as a factor that deforms the lattice. The irreversibility of the deformation process indeed leads to the absorption of sound energy. The problem thus reduces to a solution of the corresponding kinetic equation and subsequent calculation of the dissipation function, which determines the absorption of the sound wave.

We write the kinetic equation

$$-\left(\frac{\partial f}{\partial t}\right)_s = \sum_q |V|^2 (u_k u_{k'} - v_k v_{k'})^2 \{[f'(1-f)(N+1) - f(1-f')N] \delta(\varepsilon' - \varepsilon - \hbar\omega) + [f'(1-f)N - f(1-f')(N+1)] \delta(\varepsilon - \varepsilon' - \hbar\omega)\} + |V|^2 (u_k v_{k'} + u_{k'} v_k)^2 [N(1-f)(1-f') - (N+1) f f'] \delta(\varepsilon' + \varepsilon - \hbar\omega); \quad (3.1)$$

where N is the number of phonons of frequency ω.

When the sound field is turned on, the electron is in a lattice with a somewhat modified constant, so that its momentum becomes dependent on the deformation tensor.[12] Therefore

$$\left(\frac{\partial f}{\partial t}\right)_s = \frac{\partial f}{\partial \varepsilon}\frac{\xi}{\varepsilon}\varepsilon_{ik}(\mathbf{k})\,u_{ik}$$

(u_{ik} —deformation tensor; $\epsilon_{ik}(\mathbf{k})$ —tensor dependent on the direction of k). We assume that $l \gg \lambda$ (l —mean free path, λ —wavelength of sound). We can then neglect the electric deformation fields.[13]

We seek the distribution function, as usual, in the form $f = f_0 + g(\epsilon, \Omega)$, where $f_0 = (e^{\epsilon/T}+1)^{-1}$ and $g(\epsilon, \Omega)$ depends on the energy of the electron excitation and on the angles that determine its direction of motion. We expand $g(\epsilon, \Omega)$ in Legendre polynomials and confine ourselves as usual to the first term of the expansion, i.e., we assume $g(\epsilon, \Omega) = g(\epsilon)p_x/p$ (p —electron momentum, p_x —its projection on the direction of the sound), $g(\epsilon)$ being sought in the form

$$g(\varepsilon) = \frac{\partial f_0}{\partial \varepsilon}\varphi(\varepsilon)\frac{\xi}{|\xi|}.$$

Then (3.1) is rewritten as

$$\begin{aligned} f_0^2 e^{\varepsilon/T}\frac{|\xi|}{\varepsilon}\varepsilon_{ik}u_{ik} &= \int N_0|V|^2\left(1+\frac{\xi\xi'-\Delta^2}{\varepsilon\varepsilon'}\right)\\ &\times\left[\varphi(\varepsilon')\frac{p_x'}{p'}-\varphi(\varepsilon)\frac{p_x}{p}\right]f_0 f_0' e^{\varepsilon'/T}\delta(\varepsilon'-\varepsilon-\hbar\omega)\,d\mathbf{q}\\ &+\int N_0|V|^2\left(1+\frac{\xi\xi'-\Delta^2}{\varepsilon\varepsilon'}\right)\left[\varphi(\varepsilon')\frac{p_x'}{p'}\right.\\ &\left.-\varphi(\varepsilon)\frac{p_x}{p}\right]f_0 f_0' e^{\varepsilon/T}\delta(\varepsilon-\varepsilon'-\hbar\omega)\,d\mathbf{q}\\ &+\int N_0|V|^2\left(1-\frac{\xi\xi'-\Delta^2}{\varepsilon\varepsilon'}\right)\left[\varphi(\varepsilon')\frac{p_x'}{p'}\right.\\ &\left.-\varphi(\varepsilon)\frac{p_x}{p}\right]f_0 f_0' e^{\hbar\omega/T}\delta(\varepsilon+\varepsilon'-\hbar\omega)\,d\mathbf{q}. \end{aligned} \tag{3.2}$$

For the momentum projection averaged over the azimuth φ we have $q_x = 2\pi(p_x/p)q\cos\vartheta$ (ϑ —angle between $\mathbf{p}$ and $\mathbf{q}$; the polar axis is chosen in the direction of the vector $\mathbf{p}$), with $\cos\vartheta \approx -q/2p$. We integrate further over the angle ϑ and put approximately

$$\left(1\pm\frac{\xi\xi'-\Delta^2}{\varepsilon\varepsilon'}\right)\frac{\varepsilon\varepsilon'}{|\xi||\xi'|}\approx 2.$$

We seek $\varphi(\epsilon)$ in the form $\varphi(\epsilon) = \varphi_0 + \varphi_1(\epsilon)$, with $\varphi_0 \gg \varphi_1$ ($\varphi_0 = \text{const}$). Introducing further the variables $z = \epsilon/T$, $b = \Delta/T$, $x = \hbar\omega/T$ and integrating with respect to z and with respect to the angles in the momentum space of the electrons, we obtain

$$\begin{aligned} \int_b^\infty \frac{e^z}{(e^z+1)^2}\varepsilon_{ik}\dot{u}_{ik}\,dz\,d\Omega &= |V'^2|\,T^5\int_0^\infty\frac{2x^4\,dx}{e^x-1}\int_b^\infty\frac{dz\,d\Omega\varphi_0}{(e^z+1)(e^{-z-x}+1)}\\ &+|V'|^2\frac{T^5}{2}\int_{2b}^\infty\frac{x^4\,dx}{e^x-1}\int_b^\infty\frac{e^z\,dz\,d\Omega}{(e^z+1)(e^{x-z}+1)}\varphi_0, \end{aligned}$$

$|V'|^2 = |V|^2/q$.

We see therefore that the sought function φ has the form

$$\varphi = \frac{\text{const}}{T^5}\frac{1}{(e^b+1)\Phi(T)}. \tag{3.3}$$

For $\Phi(T)$ see (1.6).

The impurities do not play any role in this process. They cause elastic scattering of the electrons, and their effect can be accounted for by adding a term $(f-f_0)/\tau$ to (3.1). This term, however, drops out in the integration over the angles in the momentum space of the electrons, a natural fact, for in this case elastic scattering cannot lead to establishment of equilibrium.

We now find the dissipation function, which determines the absorption of the sound energy. The entropy of a gas of electron excitations is

$$S = \sum_k\{(f_k-1)\ln(1-f_k) - f_k\ln f_k\},$$

which leads to the following expression for the dissipation function:

$$W = T\dot{S} = -T\sum_k \dot{f}_k\frac{g}{(1-f_0)f_0}. \tag{3.4}$$

Substituting f_k from (3.1) and then integrating with respect to ϵ and the angles in the phonon momentum space, we obtain, with account of approximation (2.3),

$$\begin{aligned} W &= \int_0^\infty x^2\,dx\int_b^\infty dz\varphi(z)\,[\varphi(z+x,\,\Omega')-\varphi(z,\,\Omega)]\\ &\times\frac{e^{z+x}}{(e^x-1)(e^z+1)(e^{z+x}+1)}+\int_0^\infty x^2\,dx\int_{b+x}^\infty dz\,\varphi(z)\\ &\times[\varphi(z-x,\,\Omega')-\varphi(z,\,\Omega)]\frac{e^z}{(e^x-1)(e^z+1)(e^{z-x}+1)}\\ &-\frac{1}{2}\int_{2b}^\infty x^2\,dx\int_b^{x-b}\varphi(z)\,[\varphi(x-z,\,\Omega')\\ &-\varphi(z,\,\Omega)]\frac{e^x\,dz}{(e^z+1)(e^{x-z}+1)(e^x-1)}. \end{aligned}$$

We therefore find

$$W = \frac{\text{const}}{T^5}\frac{1}{(e^b+1)^2\Phi(T)}. \tag{3.5}$$

This formula was first derived in [2]; it is seen from (3.5) that W is a universal temperature function. Consequently, the coefficient of absorption of long-wave sound by electron excitations, which

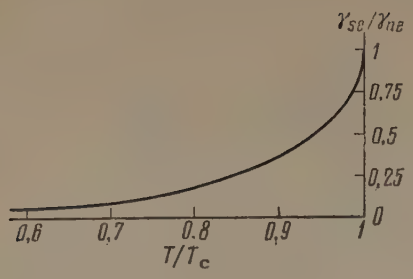

FIG. 2

is proportional to W, is given by

$$\gamma_{se} = \gamma_{ne} \frac{4\Phi(T_c)}{(e^b+1)^2\,\Phi(T)}, \qquad (3.6)$$

where $\gamma_{ne} = \text{const}/T^5$ is the coefficient of absorption of sound in the normal metal [13]; $\Phi(T)$ is given by (1.6) (see Fig. 2).

We determine similarly the absorption of sound energy by phonons. The sound field changes the phonon frequency to $\omega' = \omega(1 + \alpha_{i\nu} u_{i\nu})$; here $\alpha_{i\nu}$ is a tensor dependent on the direction of the phonon wave vector and $u_{i\nu}$ the deformation tensor. The kinetic equation for the distribution function of phonons interacting with electrons in a superconductor in a sound field has the form

$$-N_0^2 e^{\hbar\omega/T}\frac{\hbar\omega}{T}\alpha_{i\nu}\dot{u}_{i\nu} = \int |V|^2 \{2(u_k u_{k'} - v_k v_{k'})^2 \times [f'(1-f)(N+1) - Nf(1-f')]\,\delta(\varepsilon' - \varepsilon - \hbar\omega) + (u_k v_{k'} + u_{k'} v_k)^2 [(N+1)ff' - N(1-f)(1-f')]\,\delta(\varepsilon' + \varepsilon - \hbar\omega)\}\, p^2 dp\, d\cos\vartheta\, d\varphi. \qquad (3.7)$$

The perturbation of the phonon distribution function $R = N - N_0$ can be determined from this equation by a method similar to that used in [6], and has the form

$$R = -N_0^2 e^x r(x)/T;$$

$$\frac{1}{r} = \frac{\text{const}}{x}\left\{\int_b^\infty \frac{e^z\,dz}{(e^z+1)(e^{z+x}+1)} + D(x)\int_b^{x-b}\frac{dz}{(e^z+1)(e^{x-z}+1)}\right\}$$

$$\left(D(x) = \begin{cases} 0, & x < 2b \\ 1, & x \geqslant 2b \end{cases}\right).$$

For the dissipation function of the phonon gas we have

$$W_{ph} = -T\sum_q R\dot{N}/N_0(N_0+1).$$

Evaluation of this function yields (see Fig. 3)

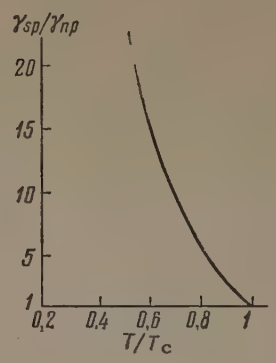

FIG. 3

$\gamma_{sp}/\gamma_{np} = F(T)/F(T_c)$;

$$F(T) = -8(b^4+b^3)(e^b-1)^{-1} - 6\zeta(3)(e^b+1) - 3(e^b+1)\sum_{s=1}^{\infty} s^{-3}e^{-2bs}(4b^2s^2+4bs+2) + 6\zeta(4)(e^b-1) - (e^b-1)\sum_{s=1}^{\infty} s^{-4}e^{-2bs}(8b^3s^3+12b^2s^2 + 12bs+6) + 32b^3(e^{2b}-1)^{-1} - a^4\sum_{s=1}^{\infty}\{se^{-2bs}\,\text{Ei}[-s(2b-a)]\} + 6\sum_{s=1}^{\infty} s^{-3}e^{-2bs};$$

$a \approx 2b - 0.16;$

$$\zeta(s) = \sum_{n=1}^{\infty} n^{-s}; \quad \zeta(3) = 1.202; \quad \zeta(4) = 1.082. \qquad (3.8)$$

Here γ_{sp} and γ_{np} are the coefficients of absorption of sound by phonons in the superconducting and normal states. γ_{sp} is also a universal function of the temperature. The total absorption coefficient is $\gamma_s = \gamma_{se} + \gamma_{sp}$.

The absorption of sound by phonons increases with decreasing temperature because the phonon mean free path is increased by the deduction in the number of electron excitations. This absorption mechanism is significant at temperatures not too close to T_C.

[1] B. T. Geĭlikman and V. Z. Kresin, JETP **36**, 959 (1959), Soviet Phys. JETP **9**, 677 (1959).

[2] V. Z. Kresin, JETP **36**, 1947 (1959), Soviet Phys. JETP **9**, 1385 (1959).

[3] N. N. Bogolyubov, JETP **34**, 58 (1958), Soviet Phys. JETP **7**, 41 (1958).

[4] B. T. Geĭlikman, JETP **34**, 1042 (1958), Soviet Phys. JETP **7**, 721 (1958).

[5] L. D. Landau and P. A. Pomeranchuk, JETP **7**, 180 (1937).

[6] B. T. Geĭlikman and V. Z. Kresin, DAN SSSR **123**, 259 (1958).

[7] A. M. Guenelt, Intern. Conf. on Superconductivity, Cambridge, (1959).

[8] E. E. Jones and A. M. Toxen, Trans. Intern. Conf. on Low-temperature Physics, Toronto, 1960. Phys. Rev. **120**, 1167 (1960).

[9] Bardeen, Rickayzen, and Tewordt, Phys. Rev. **113**, 982 (1959).

[10] Bardeen, Cooper, and Schrieffer, Phys. Rev. **108**, 1175 (1957).

[11] R. W. Morse and H. V. Bohm, Phys. Rev. **108**, 1175 (1957).

[12] A. I. Akhiezer, JETP **8**, 1330 (1938).

[13] V. L. Gurevich, JETP **38**, 532 (1960) [sic!].

Translated by J. G. Adashko
201

THEORY OF PLASMA DIFFUSION IN A MAGNETIC FIELD

V. L. GUREVICH and Yu. A. FIRSOV

Institute of Semiconductors, Academy of Sciences, U.S.S.R.

Submitted to JETP editor April 1, 1961

J. Exptl. Theoret. Phys. (U.S.S.R.) 41, 1151-1167 (October, 1961)

The transverse diffusion coefficient for particles in a fully ionized plasma in a magnetic field is calculated by a graphical method. The Born parameter $e^2/\hbar v_T$ is assumed small. The magnetic field is considered to be strong, the electron Larmor frequency being considerably larger than the collision frequency. Account is taken of the role of electrons and ions in screening the electron-ion interaction, of the deformation of the interacting-particle Debye clouds, and of the inelastic nature of electron-ion scattering. The numerical factor in the Coulomb logarithm is estimated in the case when the electron Larmor radius is much greater than the Debye radius. Corrections to the diffusion coefficient due to the effect of the magnetic field on electron-ion collisions are estimated. The case when the Debye radius is smaller than the Larmor radius of the electron but larger than that of the ion and when the magnetic field exerts a significant influence on the collision act is also considered.

1. A characteristic feature of the kinetic properties of a system of particles interacting in accordance with Coulomb's law is the divergence of the Coulomb scattering cross section at small momentum transfers. In a neutral system, the interaction between charged particles, which leads to screening, cuts off the interaction potential at distances on the order of the Debye radius $1/\kappa = (4\pi ne^2/kT)^{-1/2}$ (n — plasma electron concentration, e — electron charge, T — temperature). The cross section for the scattering on a screened potential is always finite, and the principal role is played by collisions with small momentum transfers, on the order of $\hbar\kappa$. Starting from these considerations, Landau [1] derived a kinetic equation for a system of charged particles.

These qualitative considerations, however, still leave a few points not completely clear. Thus, the Debye clouds of the particles colliding in the plasma can become noticeably deformed, and it would be interesting to ascertain the influence of this effect on the kinetic phenomena. Further, the screening of the interaction in an electron-ion plasma should be not only by the electrons but also by the ions, and it would be necessary to ascertain the extent of the ion contribution. Finally, we wish to know whether low inelasticity of the collisions between the electrons and ions of the plasma is essential; such inelasticity would cause, for example, the interaction between the electrons and ions to proceed via exchange of collective excitations of the plasmon type.

These questions are answered to some extent by Konstantinov and Perel', [2] whose proposed diagram technique [3] yielded a kinetic equation for the plasma electrons in a weak electric field. The Born parameter $e^2/\hbar v_T$ was assumed small ($v_T = \sqrt{2kT/m}$, where m is the electron mass).

In the present paper we investigate, also in the Born approximation, the transverse diffusion of particles of a completely ionized plasma in a magnetic field H. We consider the case $\Omega\tau \gg 1$ ($\Omega = eH/mc$ is the Larmor frequency and τ is the electron relaxation time). In this case both the screening by the ions (see [2]) and the deformation of their Debye clouds proved to be significant. However, exchange processes between the electron and the ion via plasmon-like oscillations, although theoretically possible, always make a negligibly small contribution.

When $\kappa R \gg 1$ ($R = v_T/\Omega$), the coefficient of transverse diffusion is proportional to $\ln(q_T/\kappa)$, [4,5] where $q_T = mv_T/\hbar$. An account of the foregoing factors enables us to find the coefficient under the sign of this logarithm. The corrections for the diffusion due to the effect of the magnetic field on the electric scattering are small when $\kappa R \gg 1$. We also investigated the case $\kappa R \ll 1$, when the effect of the magnetic field on the electron scattering cannot be neglected, and the solution cannot be obtained by iterating the equation of [2], the left half of which contains the Lorentz force. In this case the Coulomb logarithm is a function of H.

2. Let the magnetic field **H** be directed along the z axis and let the electron and ion concentration gradients and the electric field **E** be directed along the x axis. Then we have for the electron and ion current densities (the ions are assumed to be singly charged) in the linear approximation ($\mathbf{E} = -\nabla\varphi$):

$$i_x^e = -D_{xx}^{ee}\nabla_x n_e - D_{xx}^{ei}\nabla_x n_i + \sigma_{xx}^e \nabla_x \varphi/e, \quad (1)$$

$$i_x^i = -D_{xx}^{ie}\nabla_x n_e - D_{xx}^{ii}\nabla_x n_i - \sigma_{xx}^i \nabla_x \varphi/e. \quad (2)$$

The first term in (1) is the diffusion electron current, while the second is the electron current proportional to the gradient of the ion concentration, brought about by the action of the non-equilibrium ion distribution on the equilibrium electron distribution, i.e., the "dragging" of the electrons by the ions. The expression for σ_{xx}^e has the following form [2,6]

$$\sigma_{xx}^e = \sigma_{xx}^{ee} - \sigma_{xx}^{ei}, \quad (3)$$

$$\sigma_{xx}^{ee} = \frac{e^2\beta}{V_0}\,\mathrm{Re}\int_{-\infty}^{0} e^{st}\,dt \sum_{\lambda\lambda'}\sum_{\mu\mu'} \left\langle e^{-\beta\mathcal{H}_0'} T_C \exp\left[\int U(z)\,\frac{dz}{i\hbar}\right] \right.$$

$$\left. \times\, (a_\mu^+ a_{\mu'})_0\,(a_\lambda^+ a_{\lambda'})_t \right\rangle v_{\lambda\lambda'}^x v_{\mu\mu'}^x; \quad (4)$$

$$\sigma_{xx}^{ei} = \frac{e^2\beta}{V_0}\,\mathrm{Re}\int_{-\infty}^{0} e^{st}\,dt \sum_{\lambda\lambda'}\sum_{\mu\mu'} \left\langle e^{-\beta\mathcal{H}_0'} T_C \exp\left[\int U(z)\,\frac{dz}{i\hbar}\right] \right.$$

$$\left. \times\, (a_\mu^+ a_{\mu'})_0\,(A_\lambda^+ A_{\lambda'})_t \right\rangle V_{\lambda\lambda'}^x v_{\mu\mu'}^x. \quad (5)$$

Here $\beta = 1/kT$, V_0 is the normalization volume, s is the adiabatic parameter ($s > 0$, $s \to 0$),

$$\langle \ldots \rangle = \mathrm{Sp}\,(\ldots)/\mathrm{Sp}\,\exp(-\beta\mathcal{H}_0'),$$

$$\mathcal{H}' = \mathcal{H}_0 - \zeta_e N_e - \zeta_i N_i + U = \mathcal{H}_0' + U, \quad (6)$$

$\mathcal{H}_0$ is the Hamiltonian of the free electrons and ions, N_e (N_i) is the operator of the number of electrons (ions), ζ_e (ζ_i) is the chemical potential of the electrons (ions), and T_C is the symbol of ordering along the contour C, shown in the figures as a dash-dot line. Furthermore,

$$U(z) = \exp(\mathcal{H}_0 z/i\hbar)\; U \exp(-\mathcal{H}_0 z/i\hbar);$$

$U = U_{ee} + U_{ei} + U_{ii}$ is the interaction operator, with

$$U_{ee} = \tfrac{1}{2}\sum_{\gamma\gamma'}\sum_{\delta\delta'}\sum_{\mathbf{q}} u_{\mathbf{q}} \langle\gamma|e^{i\mathbf{qr}}|\gamma'\rangle\langle\delta|e^{-i\mathbf{qr}}|\delta'\rangle a_\gamma^+ a_{\gamma'} a_\delta^+ a_{\delta'}, \quad (7)$$

$$U_{ei} = -\sum_{\gamma\gamma'}\sum_{\delta\delta'}\sum_{\mathbf{q}} u_{\mathbf{q}} \langle\gamma|e^{i\mathbf{qr}}|\gamma'\rangle\langle\delta|e^{-i\mathbf{qr}}|\delta'\rangle a_\gamma^+ a_{\gamma'} A_\delta^+ A_{\delta'}, \quad (8)$$

$$U_{ii} = \tfrac{1}{2}\sum_{\gamma\gamma'}\sum_{\delta\delta'}\sum_{\mathbf{q}} u_{\mathbf{q}} \langle\gamma|e^{i\mathbf{qr}}|\gamma'\rangle\langle\delta|e^{-i\mathbf{qr}}|\delta'\rangle A_\gamma^+ A_{\gamma'} A_\delta^+ A_{\delta'}. \quad (9)$$

Here a_γ^+ and a_γ (A_γ^+ and A_γ) are the operators of creation and annihilation of the electron (ion) in the state γ; when the vector-potential has a gauge $\mathbf{A} = (0, Hx, 0)$ this state is determined by the quantum numbers n, p_z (momentum projection on the z axis), and X (coordinate of the center of the Landau oscillator); $\epsilon_\gamma(E_\gamma)$ is the energy of the electron (ion) in this state

$$u_{\mathbf{q}} = \int d^3r\, u(\mathbf{r})\, e^{i\mathbf{qr}}/V_0 = 4\pi e^2/V_0 q^2;$$

$v_{\lambda\lambda'}^x$ ($V_{\lambda\lambda'}^x$) are the matrix elements of the operator of the x component of the electron (ion) velocity.

From the meaning of the formula (3) [2] it is clear that σ_{xx}^{ee} determines the electric current due to the action of the external electric field on the electrons only, while σ_{xx}^{ei} is the electron current due to action of the electric field on the ions only, which then drag the "equilibrium" electrons. The possibility of representing σ_{xx}^e in the form of a difference of these two quantities stems from the fact that the current is calculated in an approximation which is linear in the field. But such a representation enables us to relate σ and D with the aid of the Einstein equations

$$D_{xx}^{ee} = \sigma_{xx}^{ee}/ne^2\beta, \qquad D_{xx}^{ei} = \sigma_{xx}^{ei}/ne^2\beta \quad (10)$$

(analogously for D_{xx}^{ie} and D_{xx}^{ii}).

On the other hand, it is clear from general consideration that $\sigma_{xx}^e = \sigma_{xx}^i = 0$. This can be verified by writing out the equations of motion for the system of interacting electrons and ions and going over to a new system of coordinates with the aid of the transformation $\mathbf{r} = \mathbf{r}' + ct[\mathbf{E}\times\mathbf{H}]/H^2$ (see [4,5]). But then

$$\sigma_{xx}^{ee} = \sigma_{xx}^{ei}, \qquad \sigma_{xx}^{ii} = \sigma_{xx}^{ie}. \quad (11)$$

Finally, it is easy to show that $\sigma_{xx}^{ei} = \sigma_{xx}^{ie}$. Of the equal quantities given in (11), we deemed it most expedient to calculate σ_{xx}^{ee}.

The general formula (4) can be expanded in powers of the small parameter $1/\Omega\tau$. We note that the first term to be calculated in this expansion contains the electron-electron interaction only to the extent that it determines the screening of the electron-ion potential, while the direct electron-electron scattering produces a zero contribution.

3. To calculate σ_{xx}^{ee} we apply to Eq. (4) the Konstantinov and Perel' diagram technique. [3,2] We calculate the term of lowest (namely second) order in the particle concentration n in σ_{xx}^{ee}. For this purpose it is necessary to take into account graphs with not more than two irregular lines, and the factor $1 - n_\gamma$ corresponding to the regular lines must be replaced by unity.

If the electron-ion potential were to fall off

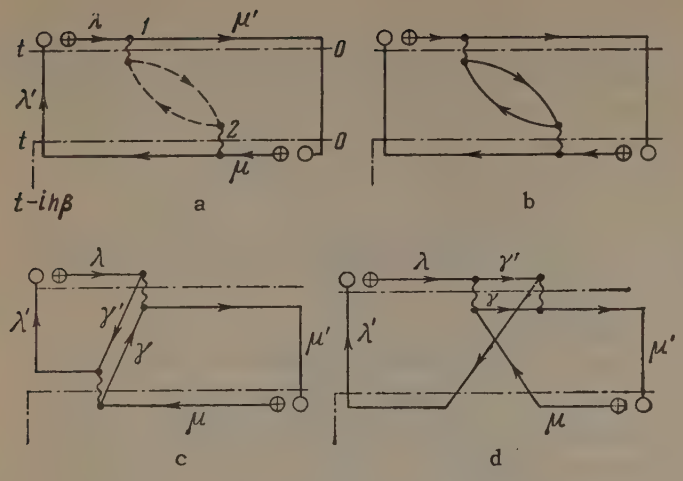

FIG. 1

with distance more rapidly than the Coulomb potential, then the conductivity would be determined in the Born approximation by the sum of the graph 1a and the other graphs of the like type with vertices 1 and 2 occupying all possible positions on the contour C. In order to eliminate the Coulomb divergence at small q, it is necessary to add here the sum of other graphs of higher order in the concentration, but containing on the other hand higher powers of 1/q. These renormalizing graphs are chains which can end only in ion loops and have in the middle either ion or electron loops, since both particles participate in the screening of the electron-ion interaction. It can be shown that if we sum over all the electron (or ion) indices on which such a loop depends, then the incoming and outgoing momenta are equal, and therefore such chains actually produce an accumulation of divergences in 1/q.

As noted earlier, direct electron-electron interaction does not contribute to σ_{xx}^{ee}. But we cannot draw such a conclusion beforehand when this interaction is renormalized via the ions. Consequently we must consider along with the chain-like graphs of type 1a also graphs of types 1b, c, and d.

To calculate the sums of these graphs we employ the procedure proposed in [2]. We consider the expression

$$l_q(z_1, z_2) = \langle e^{-\beta\mathcal{H}'} T_C [(B_q)_{z_1} (B_{-q})_{z_2}] \rangle, \quad (12)$$

which we call the plasmon line. Here

$$B_q = \sum_{\gamma\gamma'} \langle \gamma | e^{iqr} | \gamma' \rangle (a_\gamma^+ a_{\gamma'} - A_\gamma^+ A_{\gamma'}). \quad (13)$$

The plasmon line is the sum of all the graphs attached by means of the two interaction lines to the point z_1 and z_2, and consequently is the renormalized interaction line.

If the plasmon line is regular (z_2 ahead of z_1 on the contour), then

$$l_q(z_1, z_2) = l_q(z_1 - z_2) = \int_{-\infty}^{\infty} d\omega \Phi_q(\omega) e^{i\omega(z_1 - z_2)}. \quad (14a)$$

On the other hand if the plasmon line is irregular, then

$$l_q(z_1, z_2) = \bar{l}_q(z_1 - z_2) = \int_{-\infty}^{\infty} d\omega \Phi_q(\omega) e^{\hbar\omega\beta} e^{i\omega(z_1 - z_2)}. \quad (14b)$$

Here

$$\Phi_q(\omega) = Z^{-1} \sum_{kk'} e^{-\beta\mathcal{H}'_k} |\langle k | B_q | k' \rangle|^2 \delta(\omega_{kk'} - \omega)$$

$$= e^{-\hbar\omega\beta} \Phi_q(-\omega), \quad (15)$$

k and k' label the states of the entire interacting electron-ion system; $Z = \mathrm{Sp}\, e^{-\beta\mathcal{H}'}$; $\mathcal{H}'_k = \langle k | \mathcal{H}' | k \rangle$.

We put furthermore

$$l_q(t) = \frac{1}{2\pi i} \int_{\sigma - i\infty}^{\sigma + i\infty} L_q(\eta) e^{\eta t} d\eta, \quad \bar{l}_q(x) = \frac{1}{2\pi i} \int_{\sigma - i\infty}^{\sigma + i\infty} \bar{L}_q(\eta) e^{\eta t} d\eta, \quad (16)$$

$$L_q(\eta) = \int_0^{\infty} e^{-\eta t} l_q(t)\, dt = \int_{-\infty}^{\infty} d\omega \Phi_q(\omega) \frac{1}{\eta - i\omega}, \quad (17a)$$

$$\bar{L}_q(\eta) = \int_0^{\infty} e^{-\eta t} \bar{l}_q(t)\, dt = \int_{-\infty}^{\infty} d\omega \Phi_q(\omega) e^{\hbar\omega\beta} \frac{1}{\eta - i\omega}; \quad (17b)$$

$L_q(\eta)$ and $\bar{L}_q(\eta)$ are functions analytic in the right half of the complex η plane.

In the calculations it was found convenient to leave the integrals with respect to λ, but carry out the integration with respect to t. If we consider each graph as a result of such an integration, then the rules for setting up the analytic expressions in correspondence with the diagrams are as follows: 1) to each regular fermion line corresponds a factor $1 - n_\gamma$, and to each irregular line—a factor n_γ; 2) to each vertex on the upper (lower) time axis corresponds a factor $u_q/i\hbar$ ($-u_q/i\hbar$); 3) to each point on the "temperature" axis corresponds a factor $(-u_q)$ and one integration with respect to dλ; 4) to each regular plasmon line corresponds a factor $L_q(\eta)$; 5) to each interval between points on the horizontal portion of the contour corresponds a factor $[s + i(\omega_i - \omega_e)]^{-1}$ where $\hbar\omega_i$ is the total energy of the lines entering from the left into this interval and $\hbar\omega_e$ the total energy of the lines leaving to the right; the plasmon line is assigned a direction from left to right and an "energy" $i\hbar\eta$; 6) the graph is multiplied by $(-1)^{P_i + P_e}$, where $P_{i,e}$ is the number of intersections of the fermion lines of one type with each other; 7) in the final expression the summation is over all the electrons and ion indices and over all q, and the integration is over λ and η. The integration over η can be carried out by closing the contour in the right half-plane.

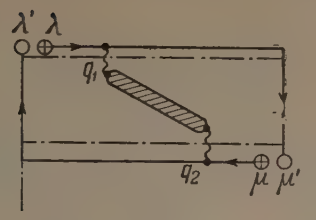

FIG. 2

4. Our problem is to express the sought sum of graphs in terms of known functions $\Phi_{\mathbf{q}}(\omega)$ and $K_{\mathbf{q}}(\omega)$ (see below).

The sum of the graphs 1a and b assumes after renormalization the form of a graph with a single plasmon line (Fig. 2). There are six graphs of this type with different placements of the vertices on the contour C (see Fig. 3). Graphs with points on the "temperature" axis only are pure imaginary and therefore not considered here. For the case when one end of the plasmon line is on the "temperature" axis, the integral with respect to λ is calculated in Appendix 1.

The sum of graphs of the type of Fig. 2, with the points placed as in Figs. 3a, b, and c, is

$$-\frac{2}{\hbar^2}\sum_{\mathbf{q}} u_{\mathbf{q}}^2 \operatorname{Re}\sum_{\lambda\mu} n_\lambda L_{\mathbf{q}}(s+i\omega_{\mu\lambda})\langle\lambda|(x-X_\lambda)e^{i\mathbf{qr}}|\mu\rangle \times\langle\mu|(x-X_\mu)e^{-i\mathbf{qr}}|\lambda\rangle.$$

We made use here of the identity

$$v_{\lambda\lambda'}/(s+i\omega_{\lambda\lambda'}) = \langle\lambda|x-X_\lambda|\lambda'\rangle \qquad (s\to 0). \quad (18)$$

The sum of the graphs of the type of Fig. 2, with points situated as in Figs. 3d, e, and f, is

$$\frac{2}{\hbar^2}\sum_{\mathbf{q}} u_{\mathbf{q}}^2 \operatorname{Re}\sum_{\lambda\mu} n_\lambda L_{\mathbf{q}}(s+i\omega_{\mu\lambda})\langle\lambda|(x-X_\mu)e^{i\mathbf{qr}}|\mu\rangle \times'\langle\mu|(x-X_\mu)e^{-i\mathbf{qr}}|\lambda\rangle.$$

Consequently the sum of all the graphs of the type shown in Fig. 2 is

$$\frac{2}{\hbar^2}\sum_{\mathbf{q}} u_{\mathbf{q}}^2 \operatorname{Re}\sum_{\lambda\mu}(X_\lambda - X_\mu) n_\lambda L_{\mathbf{q}}(s+i\omega_{\mu\lambda})\langle\lambda|e^{i\mathbf{qr}}|\mu\rangle \times\langle\mu|(x-X_\mu)e^{-i\mathbf{qr}}|\lambda\rangle. \quad (19)$$

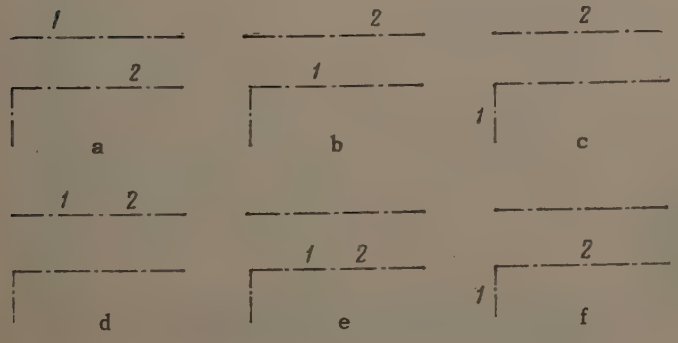

FIG. 3

We interchange the dummy indices λ and μ in (19) and take half the sum of the resultant expressions. We also take account of the fact that

$$(X_\lambda - X_\mu)^2 = (c/eH)^2 (p_{y\lambda} - p_{y\mu})^2 = (c\hbar/eH)^2 q_y^2, \quad (20)$$

and that the difference

$$L_{\mathbf{q}}(s-i\omega) - e^{\hbar\omega\beta} L_{\mathbf{q}}(s+i\omega)$$

is, on the basis of (17) pure imaginary when $s \to 0$. Then we obtain ultimately

$$\frac{\pi}{\hbar^2}\left(\frac{c\hbar}{eH}\right)^2 \sum_{\mathbf{q}} q_y^2 u_{\mathbf{q}}^2 \sum_{\lambda\mu} n_\lambda |\langle\lambda|e^{i\mathbf{qr}}|\mu\rangle|^2 \Phi_{\mathbf{q}}(\omega_{\mu\lambda}). \quad (21)$$

We consider now non-renormalized electron-electron interaction graphs such as Figs. 1c and d. Their sum is

$$-\pi\left(\frac{c}{eH}\right)^2 \sum_{\mathbf{q}} q_y^2 u_{\mathbf{q}}^2 \sum_{\lambda\mu}\sum_{\gamma\gamma'} n_\lambda n_\gamma \delta(\omega_{\mu\lambda} + \omega_{\gamma'\gamma}) |\langle\lambda|e^{i\mathbf{qr}}|\gamma'\rangle|^2 |\langle\mu|e^{i\mathbf{qr}}|\gamma\rangle|^2. \quad (22)$$

There can be four types of electron-electron scattering graphs with a single plasmon line, each type including 14 graphs. Figure 4 shows the principal graphs of the first type. The remainder are obtained by transferring the non-renormalized vertex from the upper segment of the time axis to the lower one (or vice versa). Figure 5 shows the characteristic graphs of the three remaining types. For the cases when both ends of the plasmon line (or one end and one simple vertex) are on the temperature axis, the integrals with respect to λ are calculated by a method similar to that developed in Appendix 1.

The sum of graphs with one plasmon line is

$$\left(\frac{2\pi}{\hbar}\right)\left(\frac{c}{eH}\right)^2 \sum_{\mathbf{q}} q_y^2 u_{\mathbf{q}}^3 \sum_{\lambda\mu}\sum_{\gamma\gamma'} |\langle\gamma|e^{i\mathbf{qr}}|\lambda\rangle|^2 \times |\langle\gamma'|e^{i\mathbf{qr}}|\mu\rangle|^2 n_\lambda n_{\gamma'}\delta(\omega_{\lambda\mu} + \omega_{\gamma'\gamma}) \operatorname{Re} K_{\mathbf{q}}(\omega_{\gamma'\beta} - is). \quad (23)$$

We have introduced here the notation

$$\bar{L}_{\mathbf{q}}(s+i\omega) - L_{\mathbf{q}}(s+i\omega) = iK_{\mathbf{q}}(\omega - is), \quad (24)$$

the meaning of which will become clear below (see Sec. 5).

There are four types of graphs with two plasmon lines (see Fig. 6). Each corresponds to 30 graphs. Their sum is

$$-\frac{\pi}{\hbar^2}\left(\frac{c}{eH}\right)^2 \sum_{\mathbf{q}} q_y^2 u_{\mathbf{q}}^4 \sum_{\lambda\mu}\sum_{\gamma\gamma'} |\langle\gamma|e^{i\mathbf{qr}}|\lambda\rangle|^2 |\langle\gamma'|e^{i\mathbf{qr}}|\mu\rangle|^2 \times n_\lambda n_{\gamma'}\delta(\omega_{\mu\lambda} + \omega_{\gamma\gamma'}) |K_{\mathbf{q}}(\omega_{\gamma'\mu} - is)|^2. \quad (25)$$

The total contribution to the conductivity from the renormalized electron-electron interaction is the sum of the expressions (22), (23), and (25):

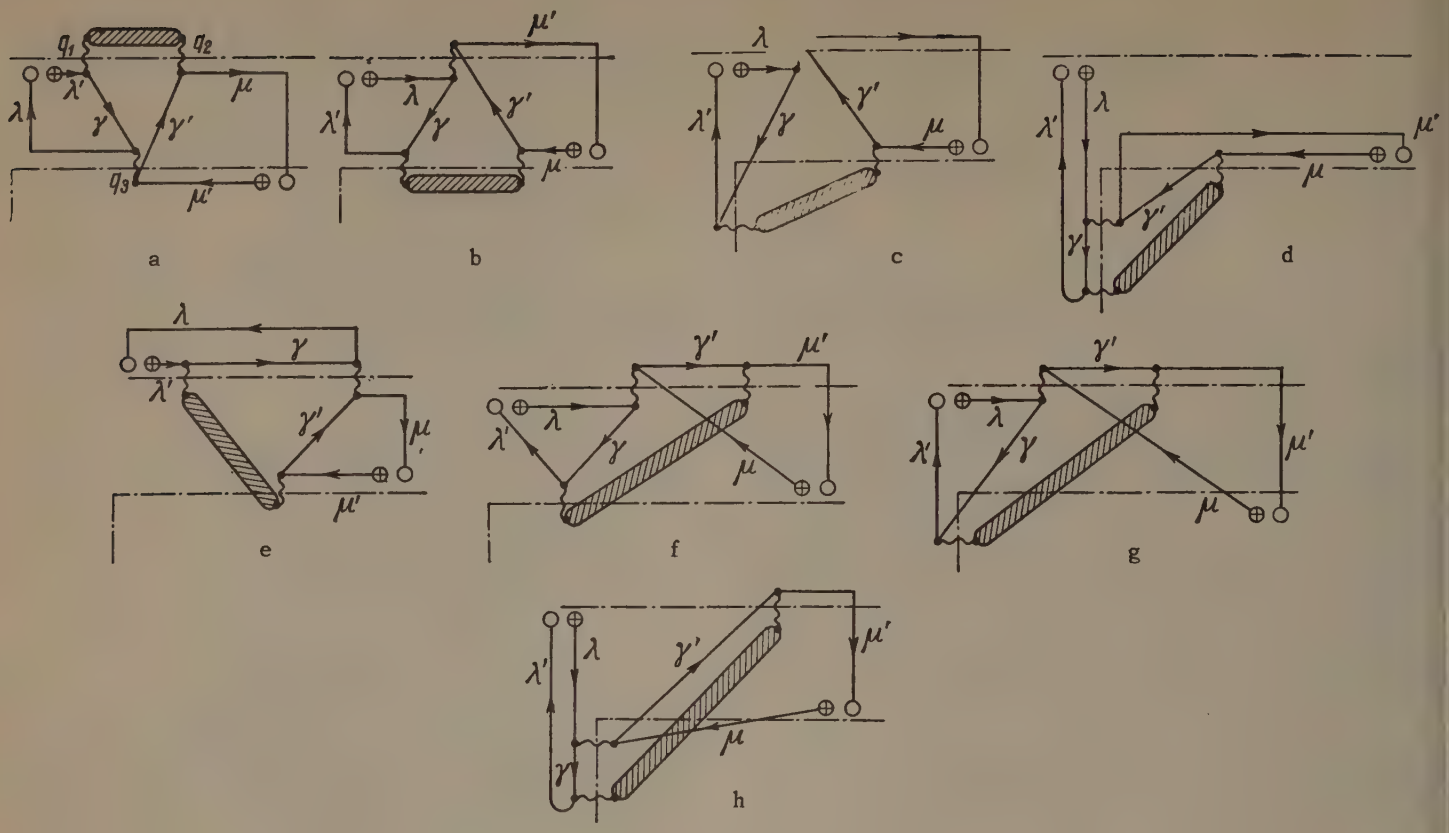

FIG. 4

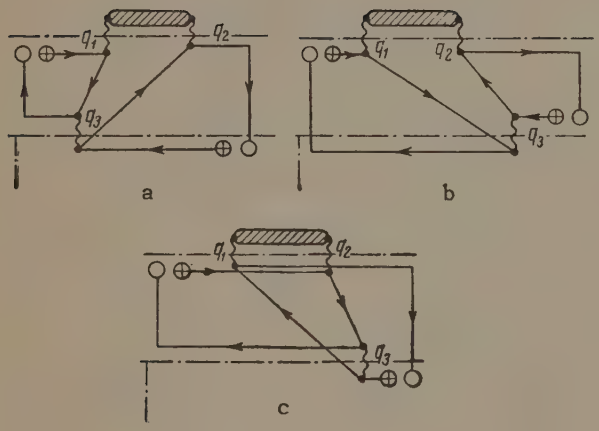

FIG. 5

$$-\pi\left(\frac{c}{eH}\right)^2 \sum_{\mathbf{q}} q_y^2 u_{\mathbf{q}}^2 \sum_{\lambda\mu} \sum_{\gamma\gamma'} n_{\gamma'} n_\lambda \delta(\omega_{\lambda\mu} + \omega_{\gamma'\gamma}) \times |\langle\lambda|e^{i\mathbf{qr}}|\gamma\rangle|^2 |\langle\mu|e^{i\mathbf{qr}}|\gamma'\rangle|^2 |1 - (u_{\mathbf{q}}/\hbar) K_{\mathbf{q}}(\omega_{\gamma'\mu} - is)|^2. \quad (26)$$

5. Generalizing the methods of [2,7] to the case $H \neq 0$, we obtain for $e^2 n^{1/3}/kT \ll 1$ the following expression

$$K_{\mathbf{q}}(\omega) = \beta\hbar n V_0 [P_{\mathbf{q}}^e(\omega) + P_{\mathbf{q}}^i(\omega)] \{1 + (\varkappa^2/q^2)[P_{\mathbf{q}}^e(\omega) + P_{\mathbf{q}}^i(\omega)]\}^{-1}. \quad (27)$$

The function $P_{\mathbf{q}}^e(\omega)$ has been calculated in [8,9] and is equal to

$$P_{\mathbf{q}}^e(\omega) = \frac{2}{\hbar\beta} \int_0^\infty dt\, e^{-i\omega t} \sin\left(\frac{\hbar q_z^2}{2m} t + \frac{\hbar q_\perp^2}{2m\Omega} \sin\Omega t\right) \times \exp\left(-\frac{q_z^2}{2m\beta} t^2 - \frac{\hbar q_\perp^2}{m\Omega} \operatorname{cth}\frac{\hbar\Omega\beta}{2} \sin^2\frac{\Omega t}{2}\right), \quad (28)^*$$

where $q_\perp^2 = q_x^2 + q_y^2$ and $P_{\mathbf{q}}^i(\omega)$ is obtained by replacing the electron mass m in (28) by the ion mass M.

In analogy with [2] we obtain relations (24) and

$$L_{\mathbf{q}}(s + i\omega) + \bar{L}_{\mathbf{q}}(s + i\omega) = 2\pi\Phi_{\mathbf{q}}(\omega) = \operatorname{Im} K_{\mathbf{q}}(\omega - is)/(1 - e^{\hbar\omega\beta}). \quad (29)$$

The first of these was already used.

We note that in the absence of interaction

$$\Phi_{\mathbf{q}}^0(\omega) = nV_0 e^{-\hbar\omega\beta/2} [F_{\mathbf{q}}^e(\omega) + F_{\mathbf{q}}^i(\omega)], \quad (30)$$

where

$$F_{\mathbf{q}}^e(\omega) = \hbar\beta \frac{\operatorname{Im} P_{\mathbf{q}}^e(\omega)}{2\pi \operatorname{sh}(\hbar\omega\beta/2)} = \frac{1}{nV_0} e^{\hbar\omega\beta/2} \sum_{\lambda\lambda'} |\langle\lambda|e^{i\mathbf{qr}}|\lambda'\rangle|^2 n_\lambda \delta(\omega - \omega_{\lambda\lambda'}) \quad (31)$$

and similarly for the ion function.

We represent the δ function in (26) in the form

$$\int_{-\infty}^{\infty} d\omega \delta(\omega + \omega_{\lambda\gamma}) \delta(-\omega + \omega_{\gamma'\mu}) \quad (32)$$

and transform this expression using (31). We introduce into (21) an additional integration with re-

*cth = coth.

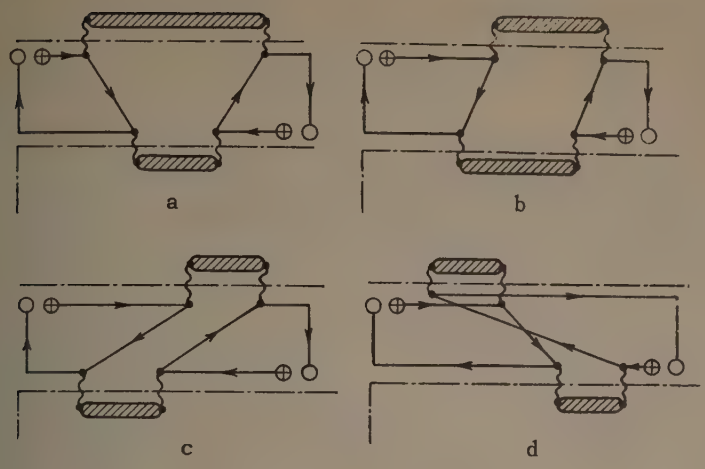

FIG. 6

spect to $d\omega$, with a factor $\delta(\omega - \omega_{\mu\lambda})$, and again use (31). Adding the two resultant expressions we obtain ultimately

$$D_{xx}^{ee} = \frac{n}{8\pi^2}\left(\frac{c}{eH}\right)^2 \int d^3q\, q^2 q_y^2 \left(\frac{4\pi e^2}{q^2}\right)^2 \int_{-\infty}^{\infty} d\omega \frac{F_q^i(\omega)\, F_q^e(\omega)}{A^2(\omega, q) + B^2(\omega, q)}$$

$$\equiv [ne^4/\pi\sqrt{2}m^{3/2}(kT)^{1/2}\Omega^2]\,\mathcal{Y}, \qquad (33)$$

$$A(\omega, \mathbf{q}) = 1 + \varkappa^2 q^{-2}\,[\mathrm{Re}\,P_q^e(\omega) + \mathrm{Re}\,P_q^i(\omega)], \qquad (34)$$

$$B(\omega, \mathbf{q}) = \varkappa^2 q^{-2}\,[\mathrm{Im}\,P_q^e(\omega) + \mathrm{Im}\,P_q^i(\omega)]. \qquad (35)$$

The products of the electron functions in the numerator of the sum of (21) and (26) cancel each other, i.e., the electron-electron scattering, even when renormalized with the ions, makes no contribution to σ_{xx}^{ee} or D_{xx}^{ee}.

The final expression is an integral over all the momentum transfers $\hbar\mathbf{q}$ and the energy transfer $\hbar\omega$ due to the product of the electron and ion functions, divided by the renormalizing denominator. If the interaction potential were to decrease with distance more rapidly than the Coulomb potential, simple considerations following Titeica[10] would yield for D_{xx}^{ee} the formula (33), but without the renormalizing denominator. In the case of Coulomb interaction, this denominator takes into account both the screening of the electron-ion potential and non-static effects connected with the inelasticity of the electron-ion collisions. In particular, the quantity A can vanish for certain connections between ω and $\mathbf{q}$. If B is also small, then this connection between ω and $\mathbf{q}$ yields the dispersion of the collective excitations in the plasma. An integrand with a sharp maximum in (33) corresponds in this case to a process in which the electron and ion exchange one of these excitations with each other.

Let us make one fundamental remark. The functions $F_q^e(\omega)$ and $F_q^i(\omega)$ tend to infinity as

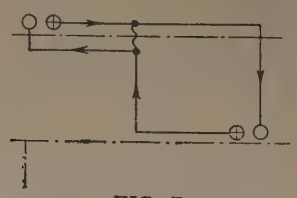

FIG. 7

$q_z \to 0$ and $\omega \to 0$. By virtue of this fact, Eq. (33) diverges logarithmically at small q_z when integrated with respect to ω. This divergence is connected with the specific properties of scattering in a magnetic field, discussed, for example, by Adams and Holstein[11] and by Skobov.[12] It is eliminated in fact by taking some cutoff mechanism into account. This gives rise in the expression for D_{xx}^{ee} to a term containing $\ln q_c R$, where q_c is the characteristic cutoff momentum (which can be estimated[11,12]). In many interesting cases, however, the coefficient of this logarithm is so small that the entire term can be discarded compared with the others. Then the final expression does not contain q_c at all. This is precisely the case, for example, when $\kappa R \gg (m/M)^{1/2}$.

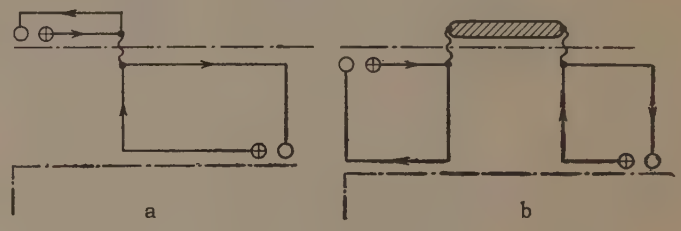

FIG. 8

6. Let us ascertain on what basis we can discard other graphs with four (or less) points.

The contribution from graphs such as shown in Fig. 7, being pure imaginary, is zero. The graphs consisting of two parts connected by a single interaction line or by a single plasmon line (Figs. 8a and b) are proportional to $u_q|_{q=0}$ and are consequently equal to zero. The graphs on Fig. 9 represent corrections to the electron-ion scattering in an approximation higher than that of Born, and are therefore disregarded. The graphs on Fig. 10 are corrections to σ_{xx}^{ee} of next higher order in

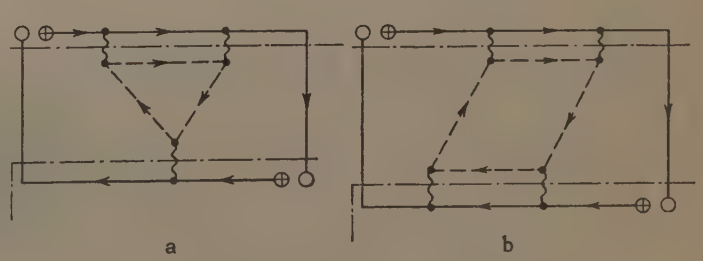

FIG. 9

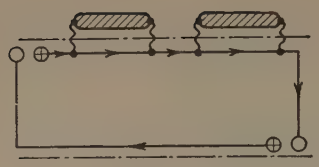

FIG. 10

$1/\Omega\tau$, and should therefore yield zero when summed. Graphs with overlapping or superimposed plasmon lines were estimated in [2] for the case H = 0. They are in any case small if $e^2/\hbar v_T \ll 1$.

7. Let us start with an investigation of the case $\kappa R \gg 1$. Expression (28) is no longer dependent on H and is noticeably simplified when $q_z \gg 1/R$. In fact, the terms significant in the integral of (28) are those with $t^2 \lesssim m\beta/q_z^2$. But for these values of t we have $\Omega t \lesssim (m\beta)^{1/2}\Omega/q_z = 1/q_z R \ll 1$, and we must therefore expand the sinusoidal terms in (28) in powers of the small parameter Ωt, retaining the first term. Then for $\hbar\Omega/kT \ll 1$ (this is the case of interest to us) we obtain

$$P_q^e(\omega) = \frac{2}{\hbar\beta}\int_0^\infty dt e^{-i\omega t}\sin\left(\frac{\hbar q^2 t}{2m}\right)\exp\left(-\frac{q^2t^2}{2m\beta}\right). \quad (36)$$

Hence [7]

$$\mathrm{Re}\,P_q^e(\omega) = \frac{q_T}{q}\left[W\left(\frac{\omega}{qv_T}+\frac{q}{2q_T}\right) - W\left(\frac{\omega}{qv_T}-\frac{q}{2q_T}\right)\right], \quad (37)$$

$$\mathrm{Im}\,P_q^e(\omega) = -\sqrt{\pi}\,\frac{q_T}{q}\,\mathrm{sh}\,\frac{\hbar\omega\beta}{2}\exp\left[-\left(\frac{\omega}{qv_T}\right)^2 - \left(\frac{q}{2q_T}\right)^2\right], \quad (38)^*$$

and $P_q^i(\omega)$ is obtained from $P_q^e(\omega)$ by replacing q with q/γ, where $\gamma^2 = M/m$. Here

$$W(x) = e^{-x^2}\int_0^x e^{y^2}dy = \begin{cases} 1/2x & \text{for } x \gg 1, \\ x & \text{for } x \ll 1. \end{cases} \quad (39)$$

Obviously, the values $q \gtrsim \kappa$ play a role in (33). But if $\kappa R \gg 1$ and q is significant, we can use (37) and (38) for $P_q^e(\omega)$, and consequently also for $P_q^i(\omega)$. The entire dependence of D_{xx} on the magnetic field is determined by the factor $1/\Omega^2$ in (33). Therefore, to calculate D_{xx} in this case it is natural to replace $P_q^e(\omega)$ and $P_q^i(\omega)$ by their limiting values (37) and (38) with H = 0 over the entire region of q, and then verify that the contribution from $q_z \lesssim 1/R$ is small where such a substitution cannot be made.

Let us substitute (37) and (38) in (33) and take (32) into account. It is easiest to integrate over the angles, and the matter reduces to calculating the expression

$$\mathcal{J}(\xi) = \frac{8\pi}{3}\int_0^\infty \frac{dz}{z}\exp\left[-\frac{z^2(1+\gamma^{-2})}{4}\right]\int_{-\infty}^{\infty}\exp\left[-x^2(1+\gamma^{-2})\right]\frac{dx}{A^2+B^2}, \quad (40)$$

where the dimensionless variables are $z = q/q_T$, $x = \hbar\omega\beta\gamma/2z$;

$$4\xi^2 = \varkappa^2/q_T^2 \ll 1. \quad (41)$$

If $A \neq 0$, then the exponential term in the numerator of the integrand of (40) makes $x \lesssim 1$, $z \lesssim 1$ the significant region of the variables. In this region A and B are given by the following expressions (we neglect quantities of order $1/\gamma$):

$$A = 1 + 8(\xi/z)^2 a(x), \qquad B = 8(\xi/z)^2 b(x),$$
$$a(x) = 1 - x\,W(x), \qquad b(x) = (x\sqrt{\pi}/2)\,e^{-x^2}. \quad (42)$$

We show later that only this region plays any role, since the contribution from the region where A = 0, i.e., from the collective effects, is negligibly small. Then the expression for D_{xx} can be represented for $\xi \ll 1$ in the form

$$D_{xx} = \frac{2}{3}\left(\frac{2\pi m}{kT}\right)^{1/2}\left(\frac{c}{eH}\right)^2 ne^4\left\{\ln\frac{1}{2eC_1\xi^2} - \frac{1}{\sqrt{\pi}}\int_0^\infty e^{-x^2}\ln[a^2(x) + b^2(x)]\,dx - \frac{2}{\sqrt{\pi}}\int_0^\infty\left[\frac{a(x)}{b(x)}\,\mathrm{arctg}\,\frac{b(x)}{a(x)} - 1\right]e^{-x^2}dx\right\}, \quad (43)^*$$

where $C = \ln C_1 = 0.577$ is Euler's constant.

The quantity $x = \hbar\omega\beta\gamma q_T/2q$ serves as a measure of the screening role of the ions. When $x \ll 1$ the screening can be regarded as static. If we replace a(x) and b(x) in (43) by a(0) and b(0), then the second and third terms vanish, corresponding to inclusion of the static effects only. To the contrary, when $x \gg 1$, the ions practically do not participate in the screening. If we replace a(x) and b(x) in (43) by $a(\infty)$ and $b(\infty)$, then the expression in the curly brackets becomes equal to $\ln(1/eC_1\xi^2)$, i.e., the factor under the logarithm sign is twice as large as in the first case, corresponding to complete neglect of the ion screening.

Actually, however, the sum of the second and third terms in the curly brackets of (43) is ln 1.34 = 0.296 and is different from the two limiting values because of the non-static ion screening. Finally

$$D_{xx} = \frac{2}{3}\left(\frac{2\pi m}{kT}\right)^{1/2}\left(\frac{c}{eH}\right)^2 ne^4\ln(0{,}55q_T^2/\varkappa^2). \quad (44)$$

This result differs from the expressions obtained earlier with logarithmic accuracy (see [5], where references can be found to earlier papers) in that the factor under the logarithm sign is exact.

We note that the same methods can be used to calculate the transverse conductivity σ_{xx} of a semiconductor with quadratic carrier dispersion law, if $e^2/\epsilon\hbar v_T \ll 1$ (ϵ is the dielectric constant of the semiconductor). The ions must be regarded here as stationary, and the scattering of the electrons by the ions must be assumed elastic. When

*sh = sinh.

*arctg = $\tan^{-1}$.

$\kappa R \gg 1$ we obtain for σ_{xx} the following formula, with an exact coefficient under the logarithm sign (compare with the result of Brooks [13]):

$$\sigma_{xx} = \frac{ne^2}{m^*\Omega^2\bar{\tau}}, \qquad \frac{1}{\bar{\tau}} = \frac{2}{3}\left(\frac{2\pi}{m^*}\right)^{1/2}\frac{n_i}{(kT)^{3/2}}\left(\frac{e^2}{\varepsilon}\right)^2 \ln\frac{1}{eC_1\xi^2}$$

(n_i is the concentration of the ions and m* the effective mass).

8. We show now that the contribution to (33) from regions where the collective effects are significant, i.e., where $A(\omega, q) = 0$, is negligibly small. First we determine when the second or third term of (34) can actually be negative, which is the necessary condition for $A(\omega, q)$ to vanish. The second term can be negative when $\omega/qv_T \gg 1$. The third term is small in this case, and $A(\omega, q)$ is in the first approximation independent of q and has a value $A = 1 - 4\pi ne^2/m\omega^2 = 1 - \omega_p^2/\omega^2$. When $\omega = \omega_p$ we have $A = 0$ (plasma "pole").

But if $\omega/qv_T \gg 1$, then Im $P_q^e(\omega)$ is exponentially small [essentially like $\exp(-\omega^2/q^2v_T^2)$] and Im $P_q^i(\omega)$ is small [like $\exp(-\gamma^2\omega^2/q^2v_T^2)$]. Inasmuch as when $A = 0$ the denominator of (33) is proportional to the square of the sum of these functions, i.e., in fact to the square of the greater of the two [Im $P_q^e(\omega)$], and the numerator is proportional to their product, the contribution to (33) from the plasma poles is exponentially small, essentially like $e^{-\gamma^2}$.

If $\gamma\omega/qv_T \gg 1 \gg \omega/qv_T$, the second term in (34) is positive and the third is negative, so that with account of the inequality $q/\gamma q_T \ll 1$ the function A assumes the form $A = 1 + 2(\kappa^2/q^2)\times[1 - xW(x)]$. Since $xW(x) < 1$, A does not vanish in this region. This is demonstrated by the known fact [14] that sound cannot propagate in a fully ionized Boltzmann gas.

9. We proceed to investigate the region $q_z \lesssim 1/R$. We separate in this region two intervals of the variation of q_z. In the first region, where

$$1/R \gtrsim q_z \gtrsim 1/R_i \qquad (45)$$

($R_i = \gamma R$ is the ionic Larmor radius) we must use for $P_q^e(\omega)$ the exact expression (28) and for $P_q^i(\omega)$ the approximate formulas (37) and (38). In the second interval, where

$$1/R_i \gtrsim q_z \gtrsim q_c, \qquad (46)^*$$

we must use the exact expressions for both quantities. In (46) q_c is the characteristic value of the wave vector introduced above, which cuts off the divergence at small q_z.

*cth = coth.

For what follows we must use the series expansion obtained in [9] for the integral in (28):

$$F_q^e(\omega) = \frac{1}{\sqrt{\pi}\,|q_z|\,v_T}\exp\left\{-\frac{u^2}{2}\,\alpha\,\mathrm{cth}\,\alpha\right\}\sum_{n=-\infty}^{\infty} I_n\left(\frac{\alpha u^2}{2\,\mathrm{sh}\,\alpha}\right)$$
$$\times\exp\left[-\left(\frac{n\Omega-\omega}{q_z v_T}\right)^2 - \left(\frac{q_z}{2q_T}\right)^2\right]. \qquad (47)$$

By the methods of [9] we obtain a similar expansion for Re $P_q^e(\omega)$:

$$\mathrm{Re}\,P_q^e(\omega) = \frac{q_T}{|q_z|}\exp\left\{-\frac{u^2}{2}\,\alpha\mathrm{cth}\alpha\right\}\sum_{n=-\infty}^{\infty} e^{\alpha n} I_n\left(\frac{\alpha u^2}{2\,\mathrm{sh}\,\alpha}\right)$$
$$\times[W(z_n^+) + W(z_n^-)]. \qquad (48)$$

Here

$$u = q_\perp R, \qquad \alpha = \frac{\hbar\Omega}{2kT}, \qquad z_n^{\pm} = \frac{\hbar q_z^2/2m \pm \omega + n\Omega}{|q_z|\,v_T}. \qquad (49)$$

It is further essential to verify that the contribution to (33) from the region of values of q and ω where $A = 0$, and from its vicinity, is negligibly small. Since the plasma and sound zeros of $A(\omega, q)$ are different when $q_z R < 1$, the corresponding analysis is much more complicated than when $q_z R \gg 1$. Its principal features are outlined in Appendix 2. But once this is proved, it is easy to show that we can replace the sum in (33), with sufficient degree of accuracy, by

$$1 + \kappa^2/q^2. \qquad (50)$$

We can thus get rid of the series in the denominator of (33). By the same token, the role of the Coulomb interaction reduces in the first approximation to pure screening. The non-static nature of the screening, when $\kappa R \gg 1$ can affect only the numerical factor in the small corrections, is neglected in such estimates.

The next stage consists of estimating the integral of and expression with the denominator of (33) and with a numerator containing the double series. When $\alpha \ll 1$ and $q \ll q_T$, the sum of the series (47) is represented by the following integral (see [9] for derivation), where $w = |q_z|R$:

$$F_q^i(\omega) = \frac{\gamma}{\pi\omega\Omega}\int_{-\infty}^{\infty}\exp\left\{-\lambda^2 + \frac{2i\gamma\omega}{\Omega w}\,\lambda\right.$$
$$\left. - \frac{\gamma^2 u^2}{2}\left[1 - \cos\left(\frac{2\lambda}{\gamma w}\right)\right]\right\}d\lambda. \qquad (51)$$

The denominator of (50) is independent of ω, and the following integral enters into (33):

$$\int_{-\infty}^{\infty} d\omega F_q^e(\omega)\,F_q^i(\omega) = \frac{\gamma^2 R}{2\pi v_T}e^{-u^2/2}\sum_{n=-\infty}^{\infty} I_n\left(\frac{u^2}{2}\right)\int_{-\infty}^{\infty} d\mu$$
$$\times\exp\left[in\gamma^2\mu - \frac{\gamma^4\omega^2\mu^2}{4} - \frac{\gamma^2 u}{2}(1 - \cos\mu)\right]. \qquad (52)$$

When $\gamma^4 w^2 \ll 1$, the difference $1-\cos\mu$ can be expanded in powers of μ and the first term retained; then

$$\int_{-\infty}^{\infty} d\omega F_q^e(\omega)\, F_q^i(\omega) = \frac{1}{\sqrt{\pi}\Omega} e^{-u^2/2} \frac{1}{\sqrt{u^2/\gamma^2+w^2}} \sum_{n=-\infty}^{\infty} I_n\left(\frac{u^2}{2}\right) \times \exp\left(-\frac{n^2}{u^2/\gamma^2+w^2}\right). \quad (53)$$

Thus, we actually obtain instead of intervals (45) and (46) the two following regions of variation of q_z:

$$1 \gtrsim q_z R \gtrsim 1/\gamma^2 \text{ and } 1/\gamma^2 \gtrsim q_z R \gtrsim q_c R. \quad (54)$$

The contribution to $\mathcal{J}$ from the first of these regions is, on the basis of (53)

$$\Delta_1 \mathcal{J} \approx 4\pi^{3/2} \sum_{n=-\infty}^{\infty} \int_0^{\infty} du \int_{1/\gamma^2}^{1} \frac{dw}{\sqrt{w^2+u^2/\gamma^2}} \frac{u^3 I_n(u^2/2)\, e^{-u^2/2}}{(u^2+w^2+\varkappa^2R^2)^2} \times \exp\left(-\frac{n^2}{w^2+u^2/\gamma^2}\right). \quad (55)$$

The second region may not exist at all if $q_c R \gtrsim 1/\gamma^2$ [the lower limit of the integral with respect to w in (55) is then not $1/\gamma^2$ but $q_c R$]. If this region does exist, we have in it

$$\Delta_2 \mathcal{J} \approx 4\pi^{3/2} \sum_{n,N} \int_{q_c R}^{1/\gamma^2} \frac{dw}{w} \int_0^{\infty} du \frac{u^3 I_n(u^2/2)\, e^{-u^2/2}}{(u^2+w^2+\varkappa^2R^2)^2} \times I_N(\gamma^2u^2/2)\, e^{-\gamma^2u^2/2} \exp\left[-(N\gamma^{-2}-n)^2/w^2\right]. \quad (56)$$

Only "resonant" terms, for which $N \approx \gamma^2 n$, can play a role in the series (56) (the others are exponentially small), and consequently the double series is replaced by a single one, in which the zeroth term is the principal one. When $\varkappa R \gtrsim 1$ its order of magnitude is

$$-(1/\gamma\varkappa^2R^2)\ln(q_c R\gamma^2).$$

We note that when $1 \gg \varkappa R \gg 1/\gamma$, the value of this term is

$$-(1/\gamma\varkappa R)\ln(q_c R\gamma^2).$$

In the series (55) the sum of all but the zeroth term is of the same order as the smaller of the two quantities $1/\gamma$ or $1/\varkappa R$. In the calculation of the zeroth term we can replace the lower limit in the integral with respect to w by zero (the error due to such a replacement is small if $\gamma\varkappa R \gg 1$). When $\varkappa R \gg 1$ this term is of order $(\varkappa R)^{-4}\ln\gamma$. We note that when $1/\gamma \ll \varkappa R \ll 1$, its value, accurate to the numbers under the logarithm sign is

$$2\pi^{3/2}\ln[1/(\varkappa R)^2]\ln\gamma. \quad (57)$$

To obtain the final estimates of the corrections $\Delta\mathcal{J}$ to the value $\mathcal{J}$ from the region $q_z R < 1$, we must subtract from the sum of the correct expressions (55) and (56) the contribution from the integral containing for $P_q^{e,i}(\omega)$ expressions (37) and (38) which do not hold in this region. When $\varkappa R \gg 1$ this contribution is

$$\pi^{5/2}/2\varkappa R, \quad (58)$$

and when $\varkappa R \ll 1$

$$\frac{4\pi^{3/2}}{3}\ln\frac{1}{(\varkappa R)^2}. \quad (59)$$

Thus, the correction to $\mathcal{J}$, due to the dependence of the collision operator on the magnetic field, is $\pi^{5/2}/2\varkappa R$ when $\varkappa R \gg \gamma$ and is of order $1/\gamma$ when $\gamma \gg \varkappa R \gg 1$. When $1 \gg \varkappa R \gg 1/\gamma$, if $1/\gamma^2 \gtrsim q_c R$, we have accurate to factors under the logarithm sign

$$\mathcal{J} = \frac{8\pi^{3/2}}{3}\ln(q_T R) + 4\pi^{3/2}\ln\left(\frac{1}{\varkappa R}\right)\ln\gamma. \quad (60)$$

The dependence of this expression on the magnetic field reflects the effect of the magnetic field on collisions with small momentum transfers. Obviously the result (60) could not be obtained from a kinetic equation of the type given in [2], with a collision operator independent of the magnetic field. From the nature of the derivation it might appear that this result has limited applicability, determined by the condition $e^2/\hbar v_z \ll 1$ for all the significant values of the z component of the electron velocity v_z. This result, however differs from the formula obtained by Belyaev [15] by classical analysis only in that the first term in (60) contains q_T rather than kT/e^2. This suggests that the smallness of the Born parameter manifests itself only in collisions with large momentum transfers, and the contribution from collisions with small momentum transfers is independent of whether the Born approximation is valid for their description or not. If this is so, our result (60) is valid under the less stringent condition $e^2/\hbar v_T \ll 1$.

The authors are grateful to V. I. Perel' for a discussion of the work and for many valuable remarks.

APPENDIX 1

Let us calculate the Laplace transform of a plasmon line with one end on the "temperature" axis. Let $z_1 = t_1$, $z_2 = t - i\hbar\lambda$, and let $\hbar a$ be the difference of the electron energies entering and leaving the point z_2. Then the sought quantity is

$$\bar{m}_a(t_1 - t) = -\int_0^{\beta} d\lambda \exp(\hbar a\lambda)\, \bar{l}_q[t_1 - (t - i\hbar\lambda)].$$

Calculating the integral with respect to λ with the aid of (16) and (17b) we get

$$\overline{m}_a(t_1-t)=-\frac{1}{2\pi i\hbar}\int_{\sigma-i\infty}^{\sigma+i\infty}e^{\eta(t_1-t)}\,d\eta\int_{-\infty}^{\infty}\frac{\Phi_{\mathbf{q}}(\omega)}{\eta-i\omega}\,\frac{e^{\hbar a\beta}-e^{\hbar\omega\beta}}{a-\omega}.$$

Expanding the denominator in partial fractions and using (17), we obtain finally

$$\overline{M}_a(\eta)=\frac{1}{i\hbar(\eta-ia)}\{[e^{\hbar a\beta}L(\eta)-\overline{L}(\eta)]-[e^{\hbar a\beta}L(s+ia)-\overline{L}(s+ia)]\}.$$

APPENDIX 2

Let us verify that the contribution to (33) from the region where $A(\omega,\mathbf{q})=0$ and from its vicinity is small. We consider the interval (45), where expressions such as (37) and (38) hold for $P^i_{\mathbf{q}}(\omega)$. If the series (48) contains a large number of significant terms, it can be summed in the case of interest to us ($\alpha\ll 1$, $\hbar\omega\beta\ll 1$, $q_\perp\ll q_T$). As a result of rather cumbersome transformations we obtain for $q_zR\ll 1$

$$\begin{aligned}\operatorname{Re}P^e_{\mathbf{q}}(\omega)=1&-\frac{\omega}{\Omega}\operatorname{ctg}(\pi\delta)\int_0^{\pi}\exp\left[\frac{u^2}{2}(\cos\psi-1)\right]\\&\times\cos\left(\frac{\omega}{\Omega}\psi\right)d\psi-\frac{\omega}{\Omega}\int_0^{\pi}\exp\left[\frac{u^2}{2}(\cos\psi-1)\right]\\&\times\sin\left(\frac{\omega}{\Omega}\psi\right)d\psi+\frac{n_0}{\delta}e^{-u^2/2}I_{n_0}\left(\frac{u^2}{2}\right)\\&+\frac{q_T}{|q_z|}e^{-u^2/2}\left\{I_0\left(\frac{u^2}{2}\right)[W(z_0^+)+W(z_0^-)]\right.\\&\left.+I_{n_0}\left(\frac{u^2}{2}\right)[e^{\alpha n_0}W(z_{n_0}^-)+e^{-\alpha n_0}W(z_{-n_0}^+)]\right\}.\end{aligned}\qquad(A.1)^*$$

Here $\delta=\omega/\Omega-n_0$, where n_0 is the integer closest to ω/Ω. (When $q_zR\sim 1$, Eq. (A.1) yields an estimate of the order of magnitude.)

When $\delta\gg q_zR$ this yields the known expression

$$\operatorname{Re}P^e_{\mathbf{q}}(\omega)=-\frac{q_\perp^2v_T^2}{\omega^2-\Omega^2}-\frac{q_z^2v_T^2}{\omega^2}.\qquad(A.2)$$

It is negative, and therefore $A(\omega,\mathbf{q})$ can vanish. However, in this case $\operatorname{Im}P^e_{\mathbf{q}}(\omega)$ and $\operatorname{Im}P^i_{\mathbf{q}}(\omega)$ are exponentially small. Therefore, by virtue of considerations similar to those advanced in Sec. 8, the contribution from this region and from its vicinity turns out to be small.

An investigation shows that when $u^2\gg 1$, Eq. (A.1) can be negative only near "gyroresonances," when $\delta\ll q_zR$. $A(\omega,\mathbf{q})$ can then vanish only if $n_0/q_zR\gtrsim u\gtrsim n_0$. When $w\ll 1$ and $u\gtrsim n_0$, only the n_0-th term plays any role in the series for $\operatorname{Im}P^e_{\mathbf{q}}(\omega)$ (we shall denote it B_{n_0}) and all others are exponentially small. For B_{n_0} we have ($s\equiv\delta/w$)

$$\begin{aligned}B_{n_0}(s)=&\frac{\sqrt{\pi}}{2}(\varkappa R)^2\left\{\frac{\gamma}{\sqrt{u^2+w^2}}\exp\left[-\frac{\gamma^2n_0^2}{u^2+w^2}\right]\right.\\&\left.+\frac{1}{w}I_{n_0}\left(\frac{u^2}{2}\right)e^{-u^2/2-s^2}\right\}\quad(n_0\neq 0),\end{aligned}\qquad(A.3)$$

$$\begin{aligned}B_0(s)=&\frac{\sqrt{\pi}}{2}(\varkappa R)^2\,s\left\{\frac{\gamma w}{\sqrt{u^2+w^2}}\exp\left[-\frac{s^2\gamma^2w^2}{u^2+w^2}\right]\right.\\&\left.+I_0\left(\frac{u^2}{2}\right)e^{-u^2/2-s^2}\right\}.\end{aligned}$$

The entire region of integration with respect to ω can be subdivided into the intervals

$$(n_0-1/2)\,\Omega\leqslant\omega\leqslant(n_0+1/2)\,\Omega,\qquad(A.4)$$

i.e., $-w/2\leq s\leq w/2$, and with the accuracy employed here the contribution to $\mathcal{J}$ in region (45) can be represented in the form

$$\begin{aligned}\Delta_1\mathcal{J}\approx 8\pi\gamma&\sum_{n=-\infty}^{\infty}{}'\int_{1/\gamma}^{1}d\omega\\&\times\int_0^{\infty}\frac{du u^3I_n(u^2/2)\exp[-u^2/2-\gamma^2n^2/(u^2+w^2)]}{(u^2+w^2)^{5/2}}\int_0^{1/2w}\frac{e^{-s^2}ds}{A_n^2+B_n^2}\\&+8\pi\gamma\int_{1/\gamma}^{1}d\omega\int_0^{\infty}du\,\frac{u^3I_0(u^2/2)\,e^{-u^2/2}}{(u^2+w^2)^{5/2}}\\&\times\int_0^{1/2w}ds\,\frac{\exp[-s^2-s^2\gamma^2w^2/(u^2+w^2)]}{A_0^2+B_0^2}\,ds.\end{aligned}\qquad(A.5)$$

Here

$$\begin{aligned}A_{n_0}\approx 1&+\frac{\varkappa^2R^2}{u^2+w^2}\left\{1+I_{n_0}\left(\frac{u^2}{2}\right)e^{-u^2/2}\frac{q_T}{|q_z|}[e^{\alpha n_0}W(z_{n_0}^-)\right.\\&\left.+e^{-\alpha n_0}W(z_{-n_0}^+)]+\left[1-\frac{n_0\gamma}{\sqrt{u^2+w^2}}W\left(\frac{n_0\gamma}{2\sqrt{u^2+w^2}}\right)\right]\right\},\end{aligned}$$

and A_0 can be readily obtained from (A.1) by expansion in powers of ω/Ω.

When $s\lesssim 1$, the width of the interval Δs, defined by the condition

$$A_n(s_n+\Delta s)=B_n(s_n),\qquad A_n(s_n)=0,\qquad(A.6)$$

is proportional to $B_n(s_n)$ and is consequently exponentially small [we recall that when $w\lesssim 1$, $A(s)$ can have zeros only if $u\lesssim\gamma n$]. Thus, the contribution from the plasma "poles" is proportional in this region to

$$\exp\left[-s_0^2-\frac{\gamma^2n^2}{u^2+w^2}\right]\Big/\left[\exp(-s_0^2)+\exp\left(-\frac{\gamma^2n^2}{u^2+w^2}\right)\right]\qquad(A.7)$$

and is consequently exponentially small.

If $s_0\lesssim 1$, then B is essentially independent of s and A is linear in s, so that it is easy to integrate with respect to s. We can thus readily verify that the contribution from the "poles" is negligibly small in this region. In similar fashion we can verify the smallness of the contribution from the poles in region (46).

*ctg = cot.

[1] L. D. Landau, JETP **7**, 203 (1937).
[2] O. V. Konstantinov and V. I. Perel', JETP **39**, 861 (1960), Soviet Phys. JETP **12**, 597 (1961).
[3] O. V. Konstantinov and V. I. Perel', JETP **39**, 197 (1960), Soviet Phys. JETP **12**, 142 (1961).
[4] I. E. Tamm, Fizika plazmy i problema upravlyaemykh termoyadernykh reaktsii (Plasma Physics and the Problem of Controllable Thermonuclear Reactions) **1**, AN SSSR, 1958, p. 3.
[5] S. I. Braginskii, ibid. p. 178.
[6] R. Kubo, J. Phys. Soc. Japan **12**, 570 (1957).
[7] A. I. Larkin, JETP **37**, 264 (1959), Soviet Phys. JETP **10**, 186 (1960).
[8] V. L. Bonch-Bruevich and A. G. Mironov, FTT **2**, 489 (1960), Soviet Phys.-Solid State **2**, 454 (1960).
[9] Yu. A. Firsov and V. L. Gurevich, JETP **41**, 512 (1961), Soviet Phys. **14**, 364 (1962).
[10] S. Titeica, Ann. Physik **22**, 129 (1935).
[11] E. N. Adams and T. D. Holstein, J. Phys. Chem. Solids **10**, 254 (1959).
[12] V. G. Skobov, JETP **37**, 1467 (1959) and **38**, 1304 (1960), Soviet Phys. JETP **10**, 1039 (1960) and **11**, 941 (1960).
[13] H. Brooks, Phys. Rev. **83**, 879 (1951).
[14] V. P. Silin, JETP **23**, 649 (1952).
[15] S. T. Belyaev, Op. cit.[1], **3**, 1958, p. 66.

Translated by J. G. Adashko
202

COHERENCE PHENOMENA IN THE RADIATION OF IDENTICAL OSCILLATORS CONSTITUTING A CRYSTAL

Č. MUZIKAŘ*

Joint Institute for Nuclear Research

Submitted to JETP editor April 4, 1961

J. Exptl. Theoret. Phys. (U.S.S.R.) 41, 1168-1174 (October, 1961)

A classical theory is given for the electromagnetic interaction of identical oscillators which form a crystal of finite dimensions. General formulas for the radiation field are derived. It is shown that in a crystal of large size there is in most directions a large broadening of the line (as compared with the line of an isolated oscillator) when there is spontaneous emission of radiation by one of the oscillators.

1. INTRODUCTION

THE effect of the interaction of an oscillator with other oscillators of the same kind surrounding it on the properties of the line omitted by the first oscillator has been studied by Dicke [1] and by Faĭn. [2] The case envisaged was that of microwave radiation from bunches of molecules, for which the distance between molecules is much smaller than the wavelength. In this case there is a large broadening of the line, proportional to the number of oscillators in the bunch.

The inverse case, in which the wavelength λ is less than the distance a between radiating systems, has been studied by Podgoretskii and Roĭzen [3]; they considered the cases of two oscillators (a diatomic molecule) and of a long linear chain. The phenomena in such systems are obviously connected with the emission of radiation by atomic nuclei arranged in a crystal, under the conditions in which the Mössbauer effect is observed. The presence of a linear chain of nuclei causes a shift and broadening of the line which depends on the direction of observation and is of the order $(\lambda/a)\gamma_{is}$, where γ_{is} is the line width for the isolated nucleus. Only in certain directions does the shift reach a large value.

When it is extended to the case of three-dimensional crystals, however, the method of Podgoretskii and Roĭzen [3] leads to complications which hinder the further development of the theory. Therefore it is expedient to choose a somewhat different way of solving this problem. In this paper we shall consider a simple cubic lattice whose sites are at the points $\mathbf{r}_s = a\mathbf{s}$, where a is the lattice constant and the components of the vector $\mathbf{s}$ are integers, and shall assume that all of the sites are occupied by identical dipoles, which we shall think of as composed of vibrating particles of charge e and mass μ.

If a dipole were isolated, then after excitation it would emit a line of frequency Ω and width $\gamma + \gamma_e = \gamma_{is}$, where $\gamma_e = (2e^2/3\mu c)\cdot(\Omega/c)^2$ is the partial width caused by the damping owing to radiation, and γ is the partial width associated with loss of energy from the oscillator through other channels. In what follows it is assumed that the time for passage of light through the crystal is much less than the times $1/\gamma_e$ and $1/\gamma$.

2. THE EQUATIONS OF MOTION

We shall denote the dipole moment at the point $\mathbf{r}_s$ and its Fourier transform by $\mathbf{p}_s(t)$ and $\mathbf{p}_s(\omega)$, respectively. At the point $\mathbf{r}$ the dipole $\mathbf{p}_s$ produces an electric field $\mathbf{E}(\mathbf{r}_s; \mathbf{r}, t)$, which we represent by a superposition of plane waves:

$$\mathbf{E}(\mathbf{r}_s; \mathbf{r}, t) = -\frac{1}{(2\pi)^4}\int d\mathbf{k}d\omega G(\mathbf{k}, \omega) \times \left\{(\mathbf{k}\,\mathbf{p}_s(\omega))\,\mathbf{k} - \left(\frac{\omega}{c}\right)^2 \mathbf{p}_s(\omega)\right\} e^{i\mathbf{k}(\mathbf{r}-\mathbf{r}_s)-i\omega t}. \quad (1)$$

Here the retarded Green's function $G = G_0 + G_r$ is defined by the formulas

$$G_0 = 4\pi \mathrm{P}\frac{1}{k^2 - (\omega/c)^2}, \qquad G_r = 4\pi^2 i\,\delta(k^2 - (\omega/c)^2)\,\mathrm{sign}\,\omega. \quad (2)$$

Let the origin of the reference system be inside the crystal. At a sufficiently distant point $\mathbf{R}_0$ the field from the entire crystal is a plane wave prop-

*Charles University, Prague, Czechoslovakia.

agated in the direction $\mathbf{n}_0 = \mathbf{R}_0/R_0$. In the dipole approximation the amplitude of this field is given by the formula

$$\mathbf{E}(\mathbf{R}_0, \omega) = -R_0^{-1}[\mathbf{k}_0 [\mathbf{k}_0 \mathbf{P}(\mathbf{k}_0, \omega)]] e^{i\mathbf{k}_0\mathbf{R}_0}, \quad (3)^*$$

where $\mathbf{k}_0 = \mathbf{n}_0\omega/c$ and

$$\mathbf{P}(\mathbf{k}_0, \omega) = \sum_s \mathbf{p}_s(\omega) e^{-i\mathbf{k}_0\mathbf{r}_s}. \quad (4)$$

The total radiated energy

$$W_{rad} = \int d\mathbf{n}_0 R_0^2 \int dt \mathbf{S}\mathbf{n}_0$$

($\mathbf{S}$ is the Poynting vector) takes the form

$$W_{rad} = \int d\mathbf{n}_0 \int_0^\infty d\omega I(\mathbf{n}_0, \omega). \quad (5)$$

In this formula $d\mathbf{n}_0$ is an element of solid angle and

$$I(\mathbf{n}_0, \omega) = \frac{c}{4\pi^2}\left(\frac{\omega}{c}\right)^4 \mathbf{P}_\perp \mathbf{P}_\perp^* \quad (6)$$

is the density in angle and frequency of the radiation from the crystal; $\mathbf{P}_\perp = \mathbf{P} - (\mathbf{P}\cdot\mathbf{n}_0)\mathbf{n}_0$.

To determine the quantity $\mathbf{P}_\perp$, which is analogous to the function F introduced in the paper of Podgoretskii and Roĭzen,[3] we use the equations of motion of the dipoles. Each dipole is acted on by the following forces: a) elastic and dissipative forces associated with the proper frequency Ω of the vibrations of the isolated dipole and the partial width γ; b) the retarded electric field of all the other dipoles; c) its own electric field, of which we are concerned with only the part associated with G_r in Eq. (1), since the part from G_0 leads to the infinite field mass of the dipole and it is assumed that this mass is already included in the total mass μ; d) the force $\mathbf{f}_s(t)$ by whose action the system is brought into a vibrating state. The nature of this force will be considered in more detail later. We neglect the magnetic interaction of the dipoles, since it brings in only relativistic corrections.

By means of Eq. (1) we get the following equations of motion of the oscillators:

$$\mu(\omega^2 + i\gamma\omega - \Omega^2)\mathbf{p}_s(\omega) = -e\mathbf{f}_s(\omega) + \frac{e^2}{(2\pi)^3}\int d\mathbf{k}\left[e^{i\mathbf{k}\mathbf{r}_s} G(\mathbf{k}, \omega)\left\{(\mathbf{k}\mathbf{P}(\mathbf{k}, \omega))\mathbf{k} - \left(\frac{\omega}{c}\right)^2 \mathbf{P}(\mathbf{k}, \omega)\right\} - G_0(\mathbf{k}, \omega)\left\{(\mathbf{k}\mathbf{p}_s(\omega))\,\mathbf{k} - \left(\frac{\omega}{c}\right)^2 \mathbf{p}_s(\omega)\right\}\right]. \quad (7)$$

Multiplying these equations by $\exp(-i\mathbf{k}_0\cdot\mathbf{r}_s)$ and summing over all s, we arrive at an integral equation for the determination of $\mathbf{P}$:

$$L(\omega)\mathbf{P}(\mathbf{k}_0, \omega) = -\mathbf{F}(\mathbf{k}_0, \omega) + \mathbf{J}_1 + \mathbf{J}_2; \quad (8)$$

$$\mathbf{J}_1 = \frac{e^2}{(2\pi)^3\mu}\int d\mathbf{k} G_r(\mathbf{k}, \omega) S(\mathbf{k} - \mathbf{k}_0)[\mathbf{k}[\mathbf{k}\mathbf{P}(\mathbf{k}, \omega)]], \quad (9)$$

$$\mathbf{J}_2 = \frac{e^2}{(2\pi)^3\mu}\int d\mathbf{k} G_0(\mathbf{k}, \omega)[S(\mathbf{k} - \mathbf{k}_0)\{[\mathbf{k}[\mathbf{k}\mathbf{P}(\mathbf{k}, \omega)]] + (k^2 - (\omega/c)^2)\mathbf{P}(\mathbf{k}, \omega)\} - \{\mathbf{k}[\mathbf{k}\mathbf{P}(\mathbf{k}_0, \omega)]] + (k^2 - (\omega/c)^2)\mathbf{P}(\mathbf{k}_0, \omega)\}], \quad (10)$$

$$L(\omega) = \omega^2 + i\gamma\omega - \Omega^2, \quad (11)$$

$$\mathbf{F}(\mathbf{k}_0, \omega) = \frac{e}{\mu}\sum_s \mathbf{f}_s(\omega) e^{-i\mathbf{k}_0\mathbf{r}_s}, \quad (12)$$

$$S(\mathbf{k} - \mathbf{k}_0) = \sum_s e^{i(\mathbf{k}-\mathbf{k}_0)\mathbf{r}_s}. \quad (13)$$

The structure factor S is a periodic function in the space of the reciprocal lattice, which reduces in our case to a cubic lattice with distance $2\pi/a$ between its nodes. At these nodes the function S has sharp maxima ($S = N_1N_2N_3$, where N_i is the number of oscillators in the direction of the i-th axis of the crystal). Since the integral of S over an elementary cell of the reciprocal lattice is $(2\pi/a)^3$, we can approximate the structure factor (13) in the following way: $S = N_1N_2N_3$ inside a parallelepiped whose edges are $2\pi/N_i a$ and whose center is at the node (hereafter we shall call this parallelepiped the nodal region), and $S = 0$ outside this region. Using the fact that the nodal region is small in comparison with the elementary cell of the reciprocal lattice and that $\mathbf{P}(\mathbf{k}, \omega)$ is a periodic function of the reciprocal lattice, we can replace $\mathbf{P}(\mathbf{k}, \omega)$ by $\mathbf{P}(\mathbf{k}_0, \omega)$ in Eqs. (9) and (10). Thus Eq. (8) is an equation for the vector $\mathbf{P} = \mathbf{P}(\mathbf{k}_0, \omega)$, which does not depend on the variable of integration $\mathbf{k}$. In what follows we shall confine ourselves to crystals of cubical shape ($N_i = N$).

3. DETERMINATION OF THE DIPOLE MOMENT P OF THE SYSTEM

If we substitute for G_r the expression (2), it can be seen from Eq. (9) that the integrand in the formula for $\mathbf{J}_1$ differs from zero only at the points where the sphere $k^2 - (\omega/c)^2 = 0$ (the sphere of propagation Σ) intersects the nodal regions of the reciprocal lattice. To determine them we can use a construction analogous to the well known Ewald construction[4]: For a given frequency ω and a given direction of observation $\mathbf{n}_0$ we lay off from an (arbitrary) node U_0 the vector $-\mathbf{k}_0 = -\omega\mathbf{n}_0/c$, and its end determines the center O of the sphere of propagation Σ (see diagram).

Thus for given ω and $\mathbf{n}_0$ we can determine the nodal regions that contribute to $\mathbf{J}_1$. Denoting these

* $[\mathbf{k}_0[\mathbf{k}_0\mathbf{P}]] = \mathbf{k}_0 \times [\mathbf{k}_0 \times \mathbf{P}]$.

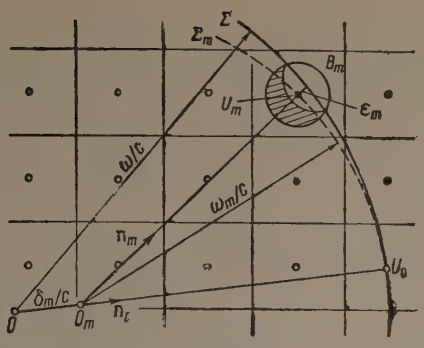

regions by an index m, we get as the expression for $\mathbf{J}_1$

$$\mathbf{J}_1 = i\omega\gamma_e \frac{3}{8\pi} N^3 \sum_{m=0}^{M} \int_{(m)} d\mathbf{n}\,(\mathbf{n}(\mathbf{Pn}) - \mathbf{P}), \qquad (14)$$

where (m) is the solid angle subtended at the center O by the portion of the sphere Σ that intersects the m-th nodal region, and M is the number of regions intersected.

For simplicity let us replace the nodal region by a sphere of radius $\rho = (3/4\pi)^{1/3}(2\pi/Na)$. Because of the smallness of the nodal regions we can neglect the variation of the integrand in Eq. (14) and replace it by a constant value $(\mathbf{P}\cdot\mathbf{n}_m)\mathbf{n}_m - \mathbf{P}$, which is determined in the following way. In the diagram the point O is the center of the sphere of propagation Σ for the frequency ω and direction of observation $\mathbf{n}_0$. The point O_m is the center of the sphere of propagation Σ_m for this same direction of observation but for a frequency ω_m such that the sphere passes exactly through the node U_m. Thus for each direction $\mathbf{n}_0$ and each node U_m one determines a direction $\mathbf{n}_m$ and a frequency ω_m.*

Introducing the notation $\delta_m = \omega - \omega_m$, we get for the distance ϵ_m between the nodal point U_m and the sphere of propagation Σ the value

$$\varepsilon_m = (1 - \mathbf{n}_0\mathbf{n}_m)\,\delta_m/c. \qquad (15)$$

By means of these results the formula (14) can be represented with good accuracy in the form

$$\mathbf{J}_1 = i\omega\gamma_e\left(\frac{4\pi}{3}\right)^{1/3}\frac{3}{8\pi^2}\left(\frac{\lambda}{a}\right)^2 N\sum_m g\left(\frac{\varepsilon_m}{\rho}\right)((\mathbf{Pn}_m)\,\mathbf{n}_m - \mathbf{P}), \qquad (16)$$

where $g(x) = (3\pi/4)(1-x^2)$.

The calculation of $\mathbf{J}_2$ is more complicated. Let us divide the entire $\mathbf{k}$ space into cells B_ν. (Each such cell is essentially a first Brillouin zone.)

*One can obtain all of the points O_m by means of the following construction: we take the nodal point U_0 as the origin and construct the Brillouin zones.[5] The points O_m are the points of intersection of the boundary surfaces of these zones and the straight line that passes through the point O_0 in the direction $\mathbf{n}_0$.

Using Eq. (2) and the properties of the function S, we get

$$\int_{(B_\nu)} d\mathbf{k}\,(S(\mathbf{k}-\mathbf{k}_0) - 1)\,G_0(\mathbf{k},\omega)\left(\mathbf{k}^2 - \left(\frac{\omega}{c}\right)^2\right)$$

$$= 4\pi\int_{(B_\nu)} d\mathbf{k}\,(S(\mathbf{k}-\mathbf{k}_0) - 1) = 0. \qquad (17)$$

Then $\mathbf{J}_2$ takes the form

$$\mathbf{J}_2 = \frac{e^2}{2\pi^2\mu}\sum_\nu \mathrm{P}\int_{(B_\nu)} d\mathbf{k}\left(S(\mathbf{k}-\mathbf{k}_0) - 1\right)\frac{[\mathbf{k}\,[\mathbf{kP}]]}{k^2 - (\omega/c)^2}. \qquad (18)$$

In the calculation of this integral an important part is played by the relative positions of the cell B_ν and the sphere of propagation Σ. Three different cases are possible: 1) the sphere of propagation $k^2 - (\omega/c)^2 = 0$ does not intersect the cell B_ν; 2) it intersects the cell, but not the nodal region (see diagram, $|\epsilon_m| > \rho$); 3) it intersects both the cell and the nodal region ($|\epsilon_m| < \rho$). It can be shown that (owing to the large value of N) the main contribution to the expression (18) comes from the last case. Thus in the formula (18) we are to keep only the integrals

$$\mathrm{P}\int d\mathbf{k}\,[\mathbf{k}\,[\mathbf{kP}]]/(k^2 - (\omega/c)^2) \qquad (19)$$

over nodal regions intersected by the sphere Σ. In these integrals, owing to the antisymmetry of the function $k^2 - (\omega/c)^2$, the unshaded parts of the nodal regions (see diagram) make practically no contribution. Then on replacing the fraction in Eq. (19) by its value at the nodal point, we get as an approximate expression for the integral (19):

$$-\frac{\omega}{c}\left(\frac{2\pi}{Na}\right)^3\frac{[\mathbf{n}_m\,[\mathbf{n}_m\mathbf{P}]]}{2\rho}f\left(\frac{\varepsilon_m}{\rho}\right),\quad f(x) = \frac{3}{2}\left(1 - \frac{x^2}{3}\right)\operatorname{sign} x. \qquad (20)$$

Using all of these results, we arrive at the following approximate expression for $\mathbf{J}_2$:

$$\mathbf{J}_2 = -i\omega\gamma_e\left(\frac{4\pi}{3}\right)^{1/3}\frac{3}{8\pi^2}\left(\frac{\lambda}{a}\right)^2 N\sum_m f\left(\frac{\varepsilon_m}{\rho}\right)((\mathbf{Pn}_m)\,\mathbf{n}_m - \mathbf{P}). \qquad (21)$$

The summation is taken over just the same nodal points as in Eq. (16). We note further that for m = 0 all of the spheres of propagation pass through the nodal point U_0, and therefore $f(\epsilon_0/\rho) = 0$, $g(\epsilon_0/\rho) = 3\pi/4$.

Introducing the notations

$$A = (2\pi)^{-1}(3/4\pi)^{2/3}(\lambda/a)^2 N\gamma_e, \qquad (22)$$

$$\Phi_m = \omega A\,(f(\varepsilon_m/\rho) - ig(\varepsilon_m/\rho)), \qquad (23)$$

we rewrite Eq. (8) for $\mathbf{P}$ in the form

$$\mathcal{L}\mathbf{P} = -\mathbf{F} - \sum_m \Phi_m((\mathbf{Pn}_m)\,\mathbf{n}_m - \mathbf{P}). \qquad (24)$$

Multiplying Eq. (24) by $\mathbf{n}_q$ ($q = 0, 1, 2, \ldots, M$), we get a system of linear equations

$$\left(L - \sum_m \Phi_m\right) \mathbf{P}\mathbf{n}_q + \sum_m \Phi_m (\mathbf{n}_q \mathbf{n}_m)(\mathbf{P}\mathbf{n}_m) = -\mathbf{F}\mathbf{n}_q, \quad (25)$$

from which we can determine the values of $\mathbf{P}\cdot\mathbf{n}_q$ and substitute them in the equation

$$\left(L - \sum_m \Phi_m\right) \mathbf{P}_\perp = -\mathbf{F}_\perp - \sum_m{}' \Phi_m (\mathbf{P}\mathbf{n}_m)\mathbf{n}_{m\perp} \quad (26)$$

for the determination of $\mathbf{P}_\perp$. Equation (26) follows simply from Eqs. (24) and (25). The prime on the summation sign means that the value $m = 0$ is excluded from the sum. The index $\perp$ denotes the component perpendicular to the direction $\mathbf{n}_0$.

Thus the investigation of the effect of the crystal lattice on the line shape of the emitted light reduces to the finding of the nodal regions intersected by the sphere of propagation Σ and the solution of the system of linear equations (25) and (26).

4. SPONTANEOUS EMISSION IN A CRYSTAL OF LARGE SIZE

As an example of the use of these formulas let us consider spontaneous emission. Suppose that for times $t < 0$ all of the oscillators are in the unexcited state, with the exception of the one located at the point $\mathbf{s} = 0$, which is in an excited state with the energy W_0 and begins to radiate at the time $t = 0$. We can obtain a classical model of such a system by assuming that $\mathbf{p}_s(t) = 0$ for $t < 0$ for all oscillators and that at the time $t = 0$ the oscillator at the point $\mathbf{s} = 0$ receives an instaneous impulse. To produce this we set $\mathbf{f}_s(t) = K\delta_{0s}\,\delta(t)$, where $K = (2\mu W_0)^{1/2}$. Then the vector $\mathbf{F}$ in the formulas (24) — (26) takes the form

$$\mathbf{F}_{sp} = (e/\mu)\,K. \quad (27)$$

The use of the retarded Green's function for the electric field of the interaction assures that the condition $\mathbf{p}_s(t) = 0$ is satisfied for $t < 0$. Then since for spontaneous emission the direction of the exciting force is not determinate, we must average $I_{sp}(\mathbf{n}_0, \omega)$ over all directions of the vector $\mathbf{K}$.

We assume that the crystal is sufficiently large. In this case the dimensions of the nodal regions in the reciprocal lattice space are very small and consequently it is most probable that the only intersection is that with the nodal region $m = 0$ (which intersects all the spheres). Thus for most directions of observation $\mathbf{n}_0$ and frequencies ω the sum in Eq. (26) reduces to just the term $m = 0$, and

$$\mathbf{P}_\perp = -\mathbf{F}_\perp (L - \Phi_0)^{-1}. \quad (28)$$

On using the formula (6) for the averaged density of spontaneously emitted radiation, we get

$$\bar{I}_{sp}(\mathbf{n}_0, \omega) = \frac{W_0}{2\pi^2}\left[1 + \left(\frac{\omega - \Omega}{\Gamma/2}\right)^2\right]^{-1} \frac{\gamma_e}{\Gamma^2}, \quad (29)$$

where W_0 is the excitation energy and Γ is the total line width, given by the formula

$$\Gamma = \gamma + \frac{3}{8}\left(\frac{3}{4\pi}\right)^{2/3}\left(\frac{\lambda}{a}\right)^2 N\gamma_e. \quad (30)$$

We obtain the conditions under which we can regard the crystal as large in the sense indicated above in the following way: if $\lambda \ll a$, then there are approximately $(4\pi/3)(\omega/c)^3 (a/2\pi)^3$ nodal points inside the sphere of radius ω/c. The number of nodal regions intersected by the sphere is determined by the number of points inside a spherical shell with the radii $\omega/c \pm \rho$, and is consequently equal to $8\pi\,(3/4\pi)^{1/3}\,(a/\lambda)^2\,(1/N)$. For a large crystal this quantity must be much smaller than unity, and from this we have

$$N \gg 10\,(a/\lambda)^2. \quad (31)$$

If the nonelectromagnetic width γ is not very large in comparison with γ_e, then it can be seen from Eqs. (30) and (31) that $\Gamma \gg \gamma + \gamma_e$. Thus the radiation emitted spontaneously from an oscillator which is a constituent of a large crystal is in most directions a line which retains the Lorentz shape but is much broadened in comparison with the line emitted by an isolated source.

The treatment is complicated for the phenomena that occur for directions of propagation for which the sphere of propagation intersects more than one nodal region. The expression for $\mathbf{P}_\perp$ is now a fraction, with a denominator which consists of two factors; one is $L - \Sigma\Phi_m$, and the other is the determinant of the system (25). The properties of these factors determine the shape of the line. It can be seen at once that the presence of terms $f(\epsilon_m/\rho)$ leads to a shift of the line, and that the presence of the function $g(\epsilon_m/\rho)$ again leads to a broadening of this line. Since the determinant can be a higher-degree polynomial in the frequency ω, the line emitted may have a complicated multiplet structure depending on the direction of observation, and the line loses its Lorentz shape.

For very small crystals the sphere of propagation intersects many nodal regions and it can be shown that in this case the crystal has almost no effect on the line shape.

The scattering of radiation incident on a large crystal is treated in greater detail in[6]. Scattering occurs at the Bragg angle, and the width of the scattered line depends on the ratio of the width of the incident line to the width Γ given by Eq. (30), in accordance with the general theory of scattering.[7]

All of our results are derived for an ideal single crystal, in which identical oscillators are distributed in a strictly periodic crystal lattice. For direct comparison with experiment one must keep in mind the effect of possible violations of these conditions.

In conclusion the writer takes the opportunity to express his gratitude to M. I. Podgoretskii, I. M. Frank, F. L. Shapiro, V. N. Efimov, and Yu. M. Ostanevich for helpful discussions.

[1] R. H. Dicke, Phys. Rev. **93**, 99 (1954).

[2] V. M. Faĭn, Usp. Fiz. Nauk **64**, 273 (1958).

[3] M. I. Podgoretskii and I. I. Roĭzen, JETP **39**, 1473 (1960), Soviet Phys. JETP **12**, 1023 (1961).

[4] R. W. James, The Optical Principles of the Diffraction of X-Rays, London, 1950.

[5] L. Brillouin and M. Parodi, Propagation des Ondes dans les Milieux Periodiques, Paris, 1956.

[6] Č. Muzikař, Joint Inst. Nuc. Res. Preprint P-709, Dubna, 1961.

[7] W. Heitler, The Quantum Theory of Radiation, Oxford, 1954.

Translated by W. H. Furry
203

"METALLIC" REFLECTION OF NEUTRONS

I. I. GUREVICH and P. É. NEMIROVSKII

Submitted to JETP editor April 22, 1961

J. Exptl. Theoret. Phys. (U.S.S.R.) 41, 1175-1177 (October, 1961)

The reflection of neutrons from strongly absorbing media is treated. A formula is found for the reflection coefficient for neutrons in the limit of zero energy. We show that the absorption cross section in the medium tends toward saturation for sufficiently small neutron energies.

THERE are a variety of ways of constructing neutron mirrors.[1,2] We are proposing the use of metallic reflection of neutrons, i.e., their reflection from strongly absorbing media. The theory of the reflection coefficient for neutrons is well known,[3,4] but one usually assumes that the reflecting medium has weak absorption and that the wave vector of the neutron is real.

In a strongly absorbing medium, we cannot neglect the imaginary part of the wave number $k = k_1 + ik_2$, and the wave function for a neutron propagating along the z axis has the form

$$\psi = (2k_2/k_1)^{1/2} e^{i(k_1+ik_2)z}. \quad (1)$$

The normalization has been chosen so that the total number of particles in the medium, which occupies the halfspace $z > 0$, is equal to $1/k_1$. We expand (1) in a Fourier integral:

$$\psi = \int_{-\infty}^{+\infty} c(p)\, e^{ipz} dp. \quad (2)$$

Then

$$c(p) = \left(\frac{k_2}{\pi k_1}\right)^{1/2} \frac{1}{k_2 - i(p - k_1)}. \quad (3)$$

For an undamped plane wave with wave vector p we can write the usual formulas for the absorption and scattering cross sections [cf. [4], formulas (39.6)]:

$$\sigma_c = 4\pi p^{-2}\eta_i (1 - 2\eta_i), \qquad \sigma_s = 4\pi p^{-2}(\eta_r^2 + \eta_i^2), \quad (4)$$

where $\eta = \eta_r + i\eta_i$ is the complex phase of the scattered wave. The total cross sections are given by the following integrals:

$$\bar{\sigma}_c = \int_{-\infty}^{+\infty} \sigma_c(p)\, |c(p)|^2\, pdp, \qquad \bar{\sigma}_s = \int_{-\infty}^{+\infty} \sigma_s(p)\, |c(p)|^2\, pdp \quad (5)$$

(for our normalization, $\int_{-\infty}^{\infty} |c(p)|^2\, p\,dp = 1$). The quantity η is expressed in terms of the quasipotential $u = A\delta(r)$ for the interaction of the nucleon and the nucleus by the formula

$$\eta = -2m\hbar^{-2}pA/4\pi.$$

If $E < 0.025$ ev, A is independent of energy, so that for small p the phase η is proportional to p. If in addition $\eta_i \ll 1$, i.e., $\eta_i^2 \ll \eta_i$, then $p\sigma_c$ is independent of energy, while $p\sigma_s \sim p$. Then

$$\bar{\sigma}_c = -\frac{4\pi}{k_1}\frac{2m}{\hbar^2}\frac{\operatorname{Im} A}{4\pi},$$

$$\bar{\sigma}_s = 4\pi\left(\frac{2m}{\hbar^2}\right)^2\left[\left(\frac{\operatorname{Re} A}{4\pi}\right)^2 + \left(\frac{\operatorname{Im} A}{4\pi}\right)^2\right]. \quad (6)$$

The additivity of the potentials from individual nuclei gives

$$U = V + iW = \rho A,$$

where ρ is the number of nuclei per unit volume in the medium, and U is the potential in the medium. Then

$$W = -\frac{\hbar^2}{2m} k_1 \rho \bar{\sigma}_c, \quad V = \pm\frac{\hbar^2}{2m}\rho\,[4\pi\bar{\sigma}_s - (k_1\bar{\sigma}_c)^2]^{1/2}. \quad (7)$$

If a beam of neutrons with wave number k_0 enters the medium from the space outside, the neutron wave number in the medium is $k^2 = k_0^2 + (\hbar^2/2m)U$, and consequently

$$k^2 = k_0^2 \mp \alpha + ik_1\rho\bar{\sigma}_c, \quad (8)$$

$$\alpha = \rho\,[4\pi\bar{\sigma}_s - (k_1\bar{\sigma}_c)^2]^{1/2}. \quad (9)$$

The upper and lower signs refer to positive and negative scattering amplitudes. Consequently,

$$k_2 = \tfrac{1}{2}\rho\bar{\sigma}_c, \qquad k_1^2 = k_0^2 + \tfrac{1}{4}(\rho\bar{\sigma}_c)^2 \mp \alpha. \quad (10)$$

When the absorption cross section in the medium is small, one obtains the formula for scattering media [cf. [4], formula (43.8)]. But for media with large absorption, at energies of $10^{-6} - 10^{-8}$ ev, the term $k_1\rho\bar{\sigma}_c$ becomes much greater than the other terms in (8) and, in the limit when we neglect the potential scattering, we have

$$k_1 = k_2 = \rho\bar{\sigma}_c/2. \quad (11)$$

The limiting formula for the refractive index is

$$n = (k_1 + ik_2)/k_0 = (\rho\bar{\sigma}_c/k_0)(1 + i). \quad (12)$$

The reflection coefficient for $k_0 \ll \rho\bar{\sigma}_c$ ($|n| \gg 1$) will be given by the formula

$$R = \left|\frac{(n^2 - \sin^2\vartheta)^{1/2} - \cos\vartheta}{(n^2 - \sin^2\vartheta)^{1/2} + \cos\vartheta}\right|^2 = 1 - \frac{4k_0}{\rho\bar{\sigma}_c}\cos\vartheta, \quad (13)$$

where ϑ is the angle to the normal.

In the more general case, when the potential scattering cannot be neglected (in the same approximation with respect to k_0),

$$R = 1 - 4k_1k_0\cos\vartheta/(k_1^2 + k_2^2). \quad (14)$$

For $k_0 \ll \rho\sigma_c$, α the absorption cross section tends toward a limiting value. In fact, according to (6),

$$\sigma_0 = a/k_1. \quad (15)$$

Then, substituting (15) in (9), we get for $k_0 \to 0$,

$$k_1^2 = (\rho a)^2/4k_1^2 \mp \alpha. \quad (16)$$

The expression (16) is an equation for determining the minimum value of k_1 (α does not depend on k_1). Solving this equation, we find

$$k_{1min}^2 = \mp\tfrac{1}{2}\alpha + \tfrac{1}{2}[(\rho a)^2 + \alpha^2]^{1/2}. \quad (17)$$

Consequently for neutrons with zero energy in the vacuum, the real part of the wave number in the medium is different from zero [where the upper sign in (17) refers to the case of a positive scattering amplitude].

Substituting (17) in (15), we get

$$\sigma_{c\,max} = a\left[\tfrac{1}{2}(\rho^2a^2 + \alpha^2)^{1/2} - \tfrac{1}{2}\alpha\right]^{-1/2}.$$

Thus the absorption cross section in the medium remains finite as $k_0 \to 0$, since we always have $\sigma_c \leq \sigma_{c\,max}$. If $\alpha \ll \rho a$,

$$\sigma_{c\,max} = \sqrt{2a/\rho}. \quad (18)$$

In this case the reflection coefficient is equal to

$$R = 1 - 4k_0(2a\rho)^{-1/2}\cos\vartheta. \quad (19)$$

From formula (10) it follows that in a medium with absorption total internal reflection is impossible, although the reflection coefficient can become very large if the absorption is small.

Let us consider a specific example—the isotope Gd^{157}, which has the largest known absorption cross section of all the stable nuclei, $\sigma_c = 2 \times 10^5$ barn for E = 0.025 ev. For gadolinium, $\rho = 2.3 \times 10^{22}$ cm^{-3}. According to (18), $\sigma_{c\,max} = 7.7 \times 10^7$ barns. This cross section is reached for a neutron energy $E \leq 1.6 \times 10^{-7}$ ev ($T < 2 \times 10^{-3}$° K). In this case, $R = 1 - 45\,T^{1/2}\cos\vartheta$ (where T is the neutron energy in degrees).

Thus we see that metallic reflection of neutrons is much less effective than other methods for obtaining neutron mirrors.

We note that the normal vibrations of the atoms of the medium do not change relations (18) and (19), since the Doppler effect does not change cross sections which have a 1/v variation, as follows from the normalization of the wave function to unit flux.

[1] Ya. B. Zel'dovich, JETP **36**, 1952 (1959), Soviet Phys. JETP **9**, 1389 (1959).

[2] V. V. Vladimirskii, JETP **39**, 1062 (1960), Soviet Phys. JETP **12**, 740 (1961).

[3] M. Goldberger and F. Seitz, Phys. Rev. **71**, 294 (1947).

[4] A. I. Akhiezer and I. Ya. Pomeranchuk, Nekotorye Voprosy Teorii Yadra (Some Problems of Nuclear Theory) second edition, Gostekhizdat, 1950, pp. 405-410.

Translated by M. Hamermesh
204

INTERFERENCE BETWEEN DIRECT AND RESONANCE CAPTURE OF SLOW NEUTRONS

I. LOVAS

Central Scientific Research Physics Institute, Budapest

Submitted to JETP editor April 17, 1961

J. Exptl. Theoret. Phys. (U.S.S.R.) **41**, 1178-1184 (October, 1961)

The effective cross section for resonance capture of slow neutrons is known to be symmetric if a compound nucleus is formed. It is shown that when compound nucleus formation and direct capture occur simultaneously, the effective cross section is not symmetric.

1. INTRODUCTION

EXPERIMENTAL and theoretical investigations of direct reactions have been at the center of interest for nuclear physics for many years. Until recently we were able to consider and describe the capture of slow neutrons only by means of statistical theory, based on the Bohr hypothesis of a "compound nucleus". But in studying the anomalies which appear in the γ spectrum from (n,γ) reactions, Lane and Lynn[1] came to the conclusion that a direct mechanism may also play an important role in the process of radiative capture, at least for certain definite groups of nuclei.

According to the statistical theory, the spectral distribution of the primary γ rays appearing in an (n,γ) reaction is proportional to the quantity

$$E_\gamma^3 \rho (E_k - E_\gamma),$$

where E_γ is the energy of the γ ray, E_k is the binding energy of the neutron and $\rho(E)$ is the average level density of the nucleus.

In the case of the capture of slow neutrons, this function has a maximum in the region of 2 — 3 Mev and falls off monotonically toward higher energies. But experiment shows that there are also intensity maxima at higher energies in the γ spectra, at least in the region of nuclei with mass numbers between 70 and 208.[2] As we approach the mass numbers 70 and 208, the peaks which are seen at high energies approach a value corresponding to the binding energy.

Since the 2p and 3p neutron shells close near the mass numbers 70 and 208 respectively, the following explanation of this phenomenon seems very likely. In the field of the nuclear forces, the neutrons are subject to potential scattering; from the free s state they go directly, without compound nucleus formation, into a bound p state, emitting electric dipole radiation. As we approach the mass numbers 70 and 208, the p states correspond to lower and lower excitation, so that the energy of the emitted γ rays increases. Apparently the probability of direct capture is higher the closer the p state is to a pure single particle state.

On the basis of the dispersion theory of nuclear reactions, Lane and Lynn showed that such a direct capture is actually possible and compared the theoretical values for the cross section with the available experimental data;[3] despite the fact that only an order of magnitude comparison was possible, because of the complexity of the phenomena, it seems to be entirely probable that for certain nuclei the process of direct neutron capture actually exists.

From the analysis of Lane and Lynn we see that, in those cases where the final state is an approximate single particle state, the channel region, i.e., the region of configuration space outside the range of nuclear forces, makes a sizable contribution to the matrix element determining the cross section, as had already been pointed out by Thomas.[4] According to them, if the final state is an approximate single particle state, the probability of a transition which leads to this state is increased, and thus it may be possible to explain the anomalies observed in the γ spectra.

From these remarks it follows that it would be extremely useful to carry out a direct experiment to settle unequivocably the question of the existence and role of the direct capture process. The interference that occurs between the direct and resonance capture processes makes it possible, in principle, to set up such a direct experiment. Just as for the case of interference between resonance and potential scattering, here too one may expect that the partial effective cross section for neutron capture accompanied by γ radiation of high energy goes through a minimum value in the region below an isolated resonance, and be-

gins to increase rapidly only after one has passed the resonance.

In the following we shall study the phenomena to be expected in the capture process as a result of the interference between direct and resonance capture.

2. EFFECTIVE CROSS SECTION FOR (n,γ) REACTIONS

We shall consider (n,γ) reactions with slow neutrons, where the orbital angular momentum of the neutron is zero, and assume that the total angular momentum of the system consisting of the neutron and the target nucleus takes on one definite value:

$$\mathbf{J} = \mathbf{s} + \mathbf{s}_n,$$

where $\mathbf{s}$ is the spin of the target nucleus and $\mathbf{s}_n$ is the neutron spin. In this case the effective cross section for the (n,γ) reaction is

$$\sigma_{n\gamma} = \frac{\pi}{k^2}\,\frac{2J+1}{(2s+1)(2s_n+1)}\,|S_{fc}|^2, \qquad (1)$$

where S_{fc} is the corresponding element of the scattering matrix:

$$S_{fc} = \left(\frac{16\pi}{9\hbar}\right)^{1/2} k_\gamma^{*}\,\frac{(\psi_f \mid H^{(1)} \mid \psi_c)}{(2J+1)^{1/2}}. \qquad (2)$$

Here $(\psi_f \mid H^{(1)} \mid \psi_c)$ is the reduced matrix element of the dipole operator between the free state ψ_c and the bound state ψ_f; k_γ is the wave vector of the emitted γ rays.

To determine the reduced matrix element of the dipole operator we must calculate the contributions from the interior of the nucleus and from the channel region. Therefore the functions for the initial and final states must be given both in the interior of the nucleus and also in the channel region. The initial state wave function in the channel is

$$\psi_c = v^{-1/2}\,(I_c(kr) - S_{cc}O_c(kr))\,\varphi_c, \qquad r > R, \qquad (3)$$

where v is the velocity and k the wave vector of the incident neutron ($v = \hbar k/M$, where M is the reduced mass); φ_c is the so-called channel function, which depends on all the internal coordinates of the nucleus and also contains the spin function of the neutron; $I_c(kr)$ and $O_c(kr)$ describe incoming and outgoing waves, and have the asymptotic form:

$$I_c(kr) \to e^{-ikr}, \qquad O_c(kr) \to e^{ikr};$$

S_{cc} is the diagonal element of the scattering matrix.

In the interior of the nucleus, S_{cc} and the function ψ_c can be determined using the R-matrix theory.[5] If we are studying neutron capture in the region of an isolated resonance, we may assume that the matrix

$$R = \sum_{\lambda'} \frac{[\gamma_{\lambda'}\gamma_{\lambda'}]}{E_{\lambda'} - E}$$

splits into two parts:

$$R = \sum_{\lambda' \neq \lambda} \frac{[\gamma_{\lambda'}\gamma_{\lambda'}]}{E_{\lambda'} - E} + \frac{[\gamma_\lambda\gamma_\lambda]}{E_\lambda - E} = R^{\infty} + \frac{[\gamma_\lambda\gamma_\lambda]}{E_\lambda - E}, \qquad (4)$$

where the matrix R^{∞} contains all resonances except for the one near E_λ and is diagonal.

The quantities $\gamma_{\lambda c}$ are the components of the vector for the reduced width of the level, γ_λ, and are defined by the formula

$$\gamma_{\lambda c} = (\hbar^2/2MR)^{1/2}\int X_\lambda \varphi_c^{*}\,dF.$$

In this case the diagonal element of the matrix S can be written in the form

$$S_{cc} = e^{-2i\delta_c'}\left[1 + i\,\frac{\Gamma_{\lambda c}}{E_\lambda + \Delta_\lambda - E - i\Gamma_\lambda/2}\right], \qquad (5)$$

where the relation between the phase shift δ_c' coming from the potential scattering and the phase shift δ_c for an impenetrable sphere is given by

$$e^{-2i\delta_c'} = e^{-2i\delta_c}\left(\frac{1 - R_{cc}^{\infty}L_c^{*}}{1 - R_{cc}^{\infty}L_c}\right).$$

We can then calculate the partial width

$$\Gamma_{\lambda c} = \frac{2P_c\gamma_{\lambda c}^2}{(1 - R_{cc}^{\infty}S_c)^2 + (R_{cc}^{\infty}P_c)^2},$$

the total width

$$\Gamma_\lambda = \sum_c \Gamma_{\lambda c}$$

and the level shift

$$\Delta_\lambda = \sum_c \frac{P_c(R_{cc}^{\infty}P_c) - S_c(1 - R_{cc}^{\infty}S_c)}{(1 - R_{cc}^{\infty}S_c)^2 + (R_{cc}^{\infty}P_c)^2}\,\gamma_{\lambda c}.$$

S_c and P_c denote the real and imaginary parts of the logarithmic derivative L_c calculated at a distance corresponding to the radius of interaction:

$$L_c = \left[kr\,\frac{dO_c(kr)}{d(kr)}\,\frac{1}{O_c(kr)}\right]_{r=R} = S_c + iP_c.$$

In the interior of the nucleus, the function ψ_c has the form

$$\psi_c = -i\hbar^{1/2}e^{-i\delta_c'}\,\frac{\Gamma_{\lambda c}^{1/2}X_\lambda}{E_\lambda + \Delta_\lambda - E - i\Gamma_\lambda/2}, \qquad r < R. \qquad (6)$$

First we determine the contribution to the scattering matrix element from the interior region of the nucleus:

$$S_{fc}^{B} = -i\left(\frac{16\pi}{9}\right)^{1/2} \frac{k_\gamma^{3/2}\Gamma_{\lambda c}^{1/2} e^{-i\delta_c'}}{(2J+1)^{1/2}} \frac{(\psi_f \mid H^{(1)} \mid X_\lambda)}{E_\lambda + \Delta_\lambda - E - i\Gamma_\lambda/2}$$

$$= -ie^{-i\delta_c'} \frac{\Gamma_{\lambda c}^{1/2}\Gamma_{\lambda f}^{1/2}}{E_\lambda + \Delta_\lambda - E - i\Gamma_\lambda/2}. \qquad (7)$$

In this case the integral appearing in the reduced matrix element should be extended over the region $r < R$.

The contribution from the channel region consists of two parts, resonant and nonresonant, as one sees from (5). The determination of the contribution from the resonance channel is done in a way analogous to that for the internal region. In the region of the channels, X_λ corresponds to a continuation of the diverging wave

$$X_\lambda'(r) = (X_\lambda(R)/O_c(kR))\,O_c(kr), \qquad r > R. \qquad (8)$$

Similarly, the final state wave function ψ_f in the channel region has the form

$$\psi_f'(r) = \int \psi_f \varphi_f^* dF \frac{O_f(k_f r)}{O_f(k_f R)} \varphi_f, \qquad r > R, \qquad (9)$$

where φ_f depends on all the coordinates of the total system, which is in a bound final state, except for the radial coordinate of the captured neutron. $O_f(k_f r)$ is the exponentially decreasing radial function for the neutron in the bound final state. Thus the contribution to the scattering matrix element from the resonance is

$$S_{fc}^{K} = -i\left(\frac{16\pi}{9}\right)^{1/2} \frac{k_\gamma^{3/2}\Gamma_{\lambda c}^{1/2} e^{-i\delta_c'}}{(2J+1)^{1/2}} \frac{(\psi_f' \mid H^{(1)} \mid X_\lambda')}{E_\lambda + \Delta_\lambda - E - i\Gamma_\lambda/2}$$

$$= -ie^{-i\delta_c'} \frac{\Gamma_{\lambda c}^{1/2}\delta\Gamma_{\lambda f}^{1/2}}{E_\lambda + \Delta_\lambda - E - i\Gamma_\lambda/2}. \qquad (10)$$

The integration is of course extended over the region $r > R$.

We note that if the penetration factor is small ($P_c \ll 1$), the photon width is real. One can see that the contribution from the resonance channel is significant if the final state function extends out strongly into the channel region. This is the case when the final state is a single particle state or contains a large single particle component. From this it follows that the transition probability is increased for a final state of single particle type. This fact would already explain the anomalies which appear in the γ spectra. But there is still another contribution to the scattering matrix element S_{fc}, coming from the channel region. This contribution comes from the potential scattering, and consequently does not have resonance character:

$$S_{fc}^{p} = \left(\frac{16\pi}{9\hbar v}\right)^{1/2} \frac{k_\gamma^{3/2}}{(2J+1)^{1/2}} (\psi_f' \mid H^{(1)} \mid [I_c - e^{-2i\delta_c'} O_c]\,\varphi_c) = D^p. \qquad (11)$$

The effective cross section corresponding to this contribution may be called the cross section for "direct" capture. Thus the total scattering matrix element will be equal to

$$S_{fc} = S_{fc}^{p} + S_{fc}^{K} + S_{fc}^{B}$$

$$= D^p - ie^{-i\delta_c'} \frac{\Gamma_{\lambda c}^{1/2}\Gamma_{\lambda f}^{1/2}}{E_\lambda + \Delta_\lambda - E - i\Gamma_\lambda/2}$$

$$- ie^{-i\delta_c'} \frac{\Gamma_{\lambda c}^{1/2}\delta\Gamma_{\lambda f}^{1/2}}{E_\lambda + \Delta_\lambda - E - i\Gamma_\lambda/2}, \qquad (12)$$

and the effective cross section will be

$$\sigma_{n\gamma} = \frac{\pi}{k^2} \frac{2J+1}{2(2s+1)} \left\{ |D^p|^2 + \frac{A^2 + 2A\,\mathrm{Re}\,(D^{p*}e^{-i\delta_c'}) - 2xA\,\mathrm{Im}\,(D^{p*}e^{-i\delta_c'})}{x^2+1} \right\};$$

$$A \equiv 2\Gamma_{\lambda c}^{1/2}(\Gamma_{\lambda f}^{1/2} + \delta\Gamma_{\lambda f}^{1/2})/\Gamma_\lambda. \qquad (13)$$

Here we have introduced the quantity $x \equiv [E - (E_\lambda + \Delta_\lambda)/(\Gamma_\lambda/2)]$, which gives the difference between the energy E and the resonance energy $E_\lambda + \Delta_\lambda$, measured in units of the halfwidth.

Since the phase shift for scattering from an impenetrable sphere is $\delta_c = -kR$ (where R is the nuclear radius), and the potential scattering phase shift δ_c' is of order δ_c, for the case of slow neutrons the quantity $e^{-i\delta_c'}$ is approximately equal to unity. By studying the quantities appearing in formula (11), one can easily show that D^p is almost a pure imaginary quantity, so that

$$\mathrm{Re}\,(D^{p*}e^{-i\delta_c'}) \approx 0, \qquad \mathrm{Im}\,(D^{p*}e^{-i\delta_c'}) \approx -|D^p|.$$

Using this, we get

$$\sigma_{n\gamma}(x) = \sigma_n(0)\left\{\frac{\sigma_p}{\sigma_r(0)} + \frac{1 + 2\sqrt{\sigma_p/\sigma_r(0)}\,x}{x^2+1}\right\}, \qquad (14)$$

where

$$\sigma_r(0) = \frac{\pi}{k^2} \frac{2J+1}{2(2s+1)} \frac{\Gamma_{\lambda c}(\Gamma_{\lambda f}^{1/2} + \delta\Gamma_{\lambda f}^{1/2})^2}{\Gamma_\lambda^2/4} \qquad (15)$$

is the effective resonance cross section at the resonance energy, and

$$\sigma_p = \frac{16\pi^2}{9\hbar k^2 v} \frac{k_\gamma^3}{2(2s+1)} |(\psi_f' \mid H^{(1)} \mid [I_c - e^{-2i\delta_c'} O_c]\varphi_c)|^2 \qquad (16)$$

is the effective cross section for "potential" or "direct" capture. Thus, by determining experimentally the energy dependence of the cross section, one can obtain information concerning the ratio of the cross sections. In the figure we show the behavior of $\sigma_{n\gamma}(x)$ for various values of $\kappa = (\sigma_p/\sigma_r(0))^{1/2}$. The difference in the energies

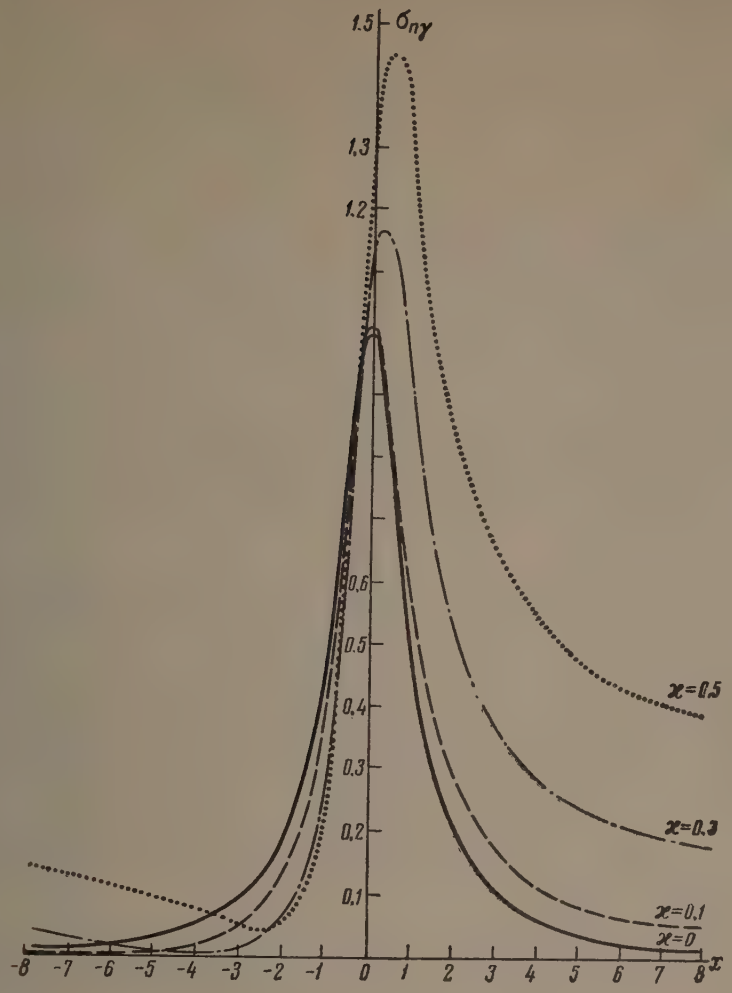

Effective cross section for an (n, γ) reaction in the neighborhood of an isolated resonance.

corresponding to the maximum and minimum effective cross sections is equal to

$$E_{max} - E_{min} = \frac{1}{2}\Gamma_\lambda \sqrt{\sigma_r(0)/\sigma_p + 4}. \qquad (17)$$

3. CONCLUSION

From the arguments given we see that if there is actually a mechanism for direct reaction in (n, γ) reactions then one manifestation of its effects is that, in contrast to our present pictures, the cross section curve will not be symmetric. The experimental determination of the asymmetry and of the ratio $\sigma_p/\sigma_r(0)$ seems to be possible only for those nuclei in which there is an unoccupied state which is close to a single particle p state, and in which isolated resonances occur. It is also obvious that one can exhibit the asymmetry only if one measures the partial cross section $\sigma_{n\gamma}(c \to f)$, i.e., not the effective cross section for the (n, γ) reaction as a whole but only that part which leads to just one final state or several final states with identical character. In practice this means that one selects one or several intense peaks which appear in the high energy region of the γ spectrum, and measures the cross section for those (n, γ) processes in which γ quanta having the selected energy appear.

Formula (14) shows that the detection of the asymmetry is to be expected only for those isolated resonances for which the ratio $\sigma_p/\sigma_r(0)$ is not too small: $\sigma_p/\sigma_r(0) \geq 10^{-2}$.

[1] A. M. Lane and J. E. Lynn, Nuclear Phys. **17**, 563 (1960).

[2] Groshev, Demidov, Lutsenko, and Pelekhov, Paper P/2029, Second International Conference on Peaceful Uses of Atomic Energy, Geneva, 1958, **15**, 138.

[3] A. M. Lane and J. E. Lynn, Nuclear Phys. **17**, 586 (1960).

[4] R. G. Thomas, Phys. Rev. **84**, 1061 (1951).

[5] A. M. Lane and R. G. Thomas, Revs. Modern Phys. **30**, 257 (1958).

Translated by M. Hamermesh
205

LINEAR POLARIZATION OF GAMMA RAYS PRODUCED IN THE (d, pγ) STRIPPING REACTION

NORA MENYHARD and J. ZIMANYI

Central Physics Research Institute, Budapest

Submitted to JETP editor April 17, 1961

J. Exptl. Theoret. Phys. (U.S.S.R.) **41**, 1185-1186 (October, 1961)

The linear polarization of γ rays produced in the $(d, p\gamma)$ reaction is determined by the distorted-wave method. Our results show that as the interaction of deuteron and proton with the target nucleus becomes stronger, the polarization decreases and the polarization plane is displaced.

THE study of various phenomena has been proposed to clarify the mechanism of the stripping reaction. Thus, in the case of the $(d, p\gamma)$ reaction, besides the measurement of the polarization and the angular distribution of protons, measurements of angular p-γ correlation [1] and correlation of circular γ-ray polarization [2,3] have been suggested.

As we know, a simple theory of stripping reactions based on the Born approximation has been inadequate to interpret the results of these measurements. Therefore the interactions of deuteron and proton with the target nucleus as treated by the distorted-wave method have been introduced [1] into the calculation. In this article the linear polarization of γ rays produced in the $(d, p\gamma)$ reaction is computed with account of these interactions.

The correlation function was calculated by the usual method. [4] The linear polarization is given by the formula

$$[W(\varphi + \pi/2) - W(\varphi)] / [W(\varphi + \pi/2) + W(\varphi)],$$

where φ is the angle describing the γ-detector plane of sensitivity to linear polarization, reckoned from an arbitrary x axis in a plane perpendicular to the direction of γ-ray propagation. Choosing the z axis along the direction of γ-ray observation and assuming that the neutron is captured with a definite orbital angular momentum l_n, we obtain the following expression:

$$P_{lin} = \sum_{k>2} h_k |d_{k2}| \cos 2(\varphi - \alpha_{k2}) \Big/ \sum_k g_k d_{k0},$$

where

$$h_k = \Big\{ \sum_{l_n l_n'} \theta_{j_n l_n} \theta_{j_n' l_n} \eta_k(j_n j_n' j_a j_b) \Big\} \times \Big\{ \sum_{LL'} C_L C_{L'} F_k(LL' j_c j_b) (\pm)_{L'} \frac{(LL'11|k2)}{(L'L'1-1|k0)} \Big\},$$

g_k, d_{k2}, d_{k0}, α_k, $\theta_{j_n l_n}$, C_L, F_k, and η_k designate the same quantities as in [5]; j_a is the spin of the target nucleus, j_b the spin of the excited nucleus produced in the process of neutron capture; j_n and l_n are the total and orbital angular momenta of the captured neutron; j_c is the spin of the residual nucleus; 2^L is the multipolarity of the γ radiation. The quantity $(\pm)_{L'}$ is equal to $(-1)^{L'}$ multipled by the parity of radiation with multipolarity $2^{L'}$.

If we detect γ rays in the $\mathbf{k}_d \times \mathbf{k}_p$ direction and choose the z axis to be in this same direction, then when $l_n = 1$ $(k \leq 2)$ we obtain

$$P_{lin} = \frac{\sqrt{6}}{4} \frac{h_2}{g_0 - g_2/2} \lambda \cos 2(\varphi - \alpha_{22}),$$

$$\lambda = -\frac{2}{\sqrt{6}} \frac{|d_{22}|}{d_{20}} \qquad (0 \leqslant \lambda \leqslant 1).$$

In the Born approximation $\lambda = 1$ and $\alpha_{22} = 0$, if φ is measured from the recoil direction. We see that the interaction of the deuteron and the proton with the target nucleus causes the polarization to decrease to the same extent as does the anisotropy of p-γ correlation (cf. [1]); on the other hand, the polarization plane undergoes a rotation by the same angle as does the symmetry axis of p-γ correlation.

It must be observed that since only the quantity α_{k2} participates in the general expression for P_{lin}, the rotation of the polarization plane can be characterized by a single parameter even when $l_n = 2$.

[1] Huby, Refai, and Satchler, Nucl. Phys. **9**, 94 (1958-1959).

[2] G. Satchler, Nucl. Phys. **16**, 674 (1960).

[3] J. Zimanyi, paper delivered at Colloquium on Nuclear Physics, Balatonezed, Hungary (1960).
[4] S. Devons and L. J. B. Goldfarb, Handbuch der Physik 42, 362 (1957).
[5] G. Satchler and W. Tobocman, Phys. Rev. 118, 1566 (1960).

Translated by Mrs. J. D. Ullman
206

REMOVAL OF AMBIGUITIES IN PHASE-SHIFT ANALYSIS

N. P. KLEPIKOV

Nuclear Physics Institute, Moscow State University

Submitted to JETP editor April 25, 1961

J. Exptl. Theoret. Phys. (U.S.S.R.) **41**, 1187-1194 (October, 1961)

We show that the set of n equations obtained from a phase shift analysis of scattered spin-0 and spin-$\frac{1}{2}$ particles with unknown polarization has (in a certain generalized sense) 2^n solutions including some that are nonunitary; furthermore, it is shown that this statement is true also for every subset of n equations of the set of $2n-1$ equations obtained from a phase-shift analysis of scattered spin-zero particles. In both cases the "complete experiment" involving $2n-1$ measurements can be replaced by a "necessary experiment" of just $n+1$ measurements.

1. MULTIPLICITY OF PHASE-SHIFT ANALYSIS

A phase-shift analysis is a method of deriving a matrix from experimental data, such that exact unitarity is obtained by introducing phase shifts. The number of measurements needed at different angles and for a given energy is found to be finite if one restricts the number of states in which one wishes to determine the interaction. In other words, finite accuracy can be obtained for the elements of the scattering matrix as functions of the scattering angle only if one makes use of a finite parametrization.

It is known [1] that the results of a "complete experiment" are sufficient for a phase-shift analysis. Many of the experiments, however, which enter into such a complete set are difficult to perform. It is therefore of some importance to determine the minimum set of measurements necessary for a phase-shift analysis at a given energy, with the subsidiary condition that only the first n phases be considered nonvanishing.

If the measurements are taken over a sufficiently wide energy range, the number of measurements at each energy may be decreased by making use of the causality condition. Additional information is obtained by studying the interference between the interaction being measured and the Coulomb interaction or some other interaction, as calculated theoretically for a number of states. Although in principle interference will give any number of equations for the unique determination of the required phase shifts, experimental accuracy will not often allow the use of all or even nearly all of them.

Thus in a phase-shift analysis one is not dealing with the complete problem of establishing the entire scattering matrix, but the problem of finding for the first n phase shifts values that give the best fit to the experimental data, if one assumes all the other phase shifts negligibly small or given a priori.

In order to obtain a finite number of sets of n phase shifts satisfying the experimental data equally well, one must have at least n independent equations. Such equations are obtained if one expands the experimental angular distributions in a series of Legendre polynomials and then equates coefficients of this expansion with the corresponding expression in terms of the phase shifts.

In studying elastic scattering of spinless particles, a complete experiment requires a measurement of the angular distribution of the scattering. In scattering of spin-$\frac{1}{2}$ particles by spin-0 particles, this experiment requires measurements of the differential cross section and the polarization of the recoil particles as a function of angle. In both cases the Legendre polynomial expansion of the theoretical and experimental angular distributions will lead to a set of equations of the form

$$\sum_{k,l=1}^{n} C_{kl}^{(i)} \sin\delta_k \sin\delta_l \cos(\delta_k - \delta_l) = A_i, \qquad (1)$$

where the $C_{kl}^{(i)}$ are constants, the δ_k are the phase shifts for the different states, the A_i are the expansion coefficients of the experimentally observed differential scattering cross section (divided by λ^2) for an expansion in linearly independent func-

tions of the scattering angle; in the first case $i = 1, \ldots, 2n-1$, while in the second $i = 1, \ldots, n$. For nonzero phase shifts we take here the states in the order S, P, D, ... in the first case, and in the order $S_{1/2}$, $P_{1/2}$, $P_{3/2}$, $D_{3/2}$, ... in the second case.

Before proceeding we must determine the number of solutions of a set of n such equations. It is shown in the Appendix that every set of n equations of the form of (1) has exactly

$$N = 2^n \tag{2}$$

solutions such that $-\pi/2 \leq \mathrm{Re}\,\delta_k \leq \pi/2$. In special cases, when (1) is degenerate and may have an infinite number of solutions, as well as when one of the phase shifts passes through resonance, the number of solutions is defined as the number of solutions at almost all points of a certain region of the n-dimensional complex-valued space of the A_i. Then $N = 2^n$ everywhere.

Thus the experimental data on just the angular distribution of scattering of spin-0 and spin-$\frac{1}{2}$ particles will lead, if the polarization is unknown, to 2^n different solutions. Among these are both unitary (real δ_k) and nonunitary solutions. This result is equally valid for the phase-shift analysis of elastic scattering of spinless particles if one wishes to find the n phase shifts by using only n of all the $2n-1$ expansion coefficients of the angular distribution.

If some of the phase shifts are given and one wishes, as before, to determine only the first n, the number of solutions remains that given in (2). For in this case the left sides of Eq. (1) will contain an additional finite or infinite number of terms of this form in which one of the phase shifts is given. Since the given phase shifts must vanish for zero energy, the result following from (A7) will not change.

We remark that the number of solutions of the set of n equations with n unknowns is independent of the experimental accuracy with which the A_i are determined. On the other hand, the number of solutions admissible (with a given probability) for an overdetermined system depends strongly on this accuracy.

2. EXAMPLES OF AMBIGUITY IN A PHASE SHIFT ANALYSIS

We note first that all the solutions of (1) can be divided into two groups one of which is obtained from the other by the replacement $\delta_k \to -\delta_k$. Further, as has been shown by Minami,[2] if one wants to obtain an even number of phase shifts for a spin 0–spin $\frac{1}{2}$ scattering problem, one finds that the $C_{kl}^{(i)}$ do not change when one interchanges states with the same total angular momentum but with opposite parity. Therefore the associated interchange of these phase shifts will not change the differential cross section, and this fact thus separates all the solutions for this case into two additional classes.

In spin-0–spin-$\frac{1}{2}$ scattering, the equation for a single phase shift

$$\sin^2\alpha = \sin^2\alpha_0 \tag{3}$$

has only the two solutions

$$\alpha_1 = \alpha_0; \qquad \alpha_2 = -\alpha_0.$$

The set of equations for two phase shifts, namely

$$\begin{aligned} &\sin^2\alpha + \sin^2\beta = \sin^2\alpha_0 + \sin^2\beta_0, \\ &\sin\alpha\sin\beta\cos(\alpha-\beta) = \sin\alpha_0\sin\beta_0\cos(\alpha_0-\beta_0) \end{aligned} \tag{4}$$

has the four solutions

$$\begin{aligned} &\alpha_1 = \alpha_0, \quad \beta_1 = \beta_0; \quad \alpha_2 = -\alpha_0, \quad \beta_2 = -\beta_0; \\ &\alpha_3 = \beta_0, \quad \beta_3 = \alpha_0; \quad \alpha_4 = -\beta_0, \quad \beta_4 = -\alpha_0. \end{aligned}$$

For this case the Minami transformation and the change of sign exhaust all possibilities.

The set of equations for three phase shifts, namely

$$\begin{aligned} &\sin^2\alpha + \sin^2\beta + 2\sin^2\gamma = \sin^2\alpha_0 + \sin^2\beta_0 + 2\sin^2\gamma_0, \\ &\sin\alpha\sin\beta\cos(\alpha-\beta) + 2\sin\alpha\sin\gamma\cos(\alpha-\gamma) \\ &\quad = \sin\alpha_0\sin\beta_0\cos(\alpha_0-\beta_0) \\ &\quad + 2\sin\alpha_0\sin\gamma_0\cos(\alpha_0-\gamma_0), \\ &\sin^2\gamma + 2\sin\beta\sin\gamma\cos(\beta-\gamma) \\ &\quad = \sin^2\gamma_0 + 2\sin\beta_0\sin\gamma_0\cos(\beta_0-\gamma_0) \end{aligned} \tag{5}$$

should, according to the above, have eight solutions.

In analyzing the scattering of π mesons by protons, only four solutions have been used heretofore; these are

$$\begin{aligned} &\alpha_1 = \alpha_0, \quad \beta_1 = \beta_0, \quad \gamma_1 = \gamma_0; \\ &\alpha_2 = -\alpha_0, \quad \beta_2 = -\beta_0, \quad \gamma_2 = -\gamma_0; \\ &\alpha_3 = \alpha_0, \quad \beta_3 = \Theta - \beta_0, \quad \gamma_3 = \Theta - \gamma_0, \\ &\Theta = \mathrm{arctg}\,\frac{\sin 2\beta_0 + 2\sin 2\gamma_0}{\cos 2\beta_0 + 2\cos 2\gamma_0} \end{aligned} \tag{6}*$$

(the Fermi-Yang transformation);

$$\alpha_4 = -\alpha_0, \qquad \beta_4 = -\beta_3, \qquad \gamma_4 = -\gamma_3.$$

There exist, however, four other solutions which have real phase shifts for sufficiently small β_0 and γ_0 [if $\alpha_0 \ll 1$, $\beta_0 \ll 1$, $\gamma_0 \ll 1$ and if $\alpha_0^2 \gg 3\gamma_0(\gamma_0 + 2\beta_0)$] and

*arctg = $\tan^{-1}$.

$$\alpha_{5,6} = \operatorname{arctg} \frac{\sin 2\alpha_0 + \sin 2\beta_0 + 2\sin 2\gamma_0}{\cos 2\alpha_0 + \cos 2\beta_0 + 2\cos 2\gamma_0 - 2} - \alpha_0,$$

$$\alpha_{7,8} = -\alpha_{5,6}. \qquad (7)$$

The corresponding values of β and γ are given by expressions which are too complicated to be presented here, although they are easily obtained graphically.

For larger β_0 and γ_0 the last four solutions become nonunitary, i.e., the corresponding phase shifts become complex. At certain energies the complex values for these phase shifts may cross the real axis, and this leads to the additional ambiguities in the phase-shift analysis for real phase shifts, as found by Igushkin.[3]

To find the operator group of order 2^n whose elements will transform a solution of a set of equations such as (1) into another is a problem which has not yet been solved in general. In the examples presented above the groups are Abelian, and are the direct product of n groups of two elements; this would seem to be true for the general case.

3. "NECESSARY EXPERIMENT"

We have seen that among the 2^n solutions of the phase-shift analysis there are both unitary and nonunitary ones. The unitarity condition, written as a reality condition on the phase shifts, is not analytic and can therefore not be included in the integral treated in the Appendix in attempting to reduce the number of solutions. In order to choose a single physically admissible solution from among the 2^n, one must use additional information; nevertheless, it is desirable to find the minimum amount of information necessary. It is then found that the number of measurements necessary to establish the scattering amplitudes is less than the number of measurements in the "complete experiment."

The phase-shift analysis of spin-zero scattering can be carried through in two ways. In the first an electronic computer is used to minimize the sum of the weighted square deviations of the experimental differential cross sections at certain definite angles from the expressions for these cross sections in terms of the phase shifts. In this way one obtains many minima for the sums of the squares, some of which correspond to solutions of the problem, while others arise from different sources entirely. To find the physical solution among them is often quite difficult even if the different minima have different depths.

In the second method one starts by looking for the coefficients of the expansion in Legendre polynomials (or some other linearly independent functions of the cosine of the angle) of the differential cross section. This expansion is unique, and it is rapidly calculated since the problem is linear and its solution does not require successive approximations. One then finds that set of phase shifts which exactly solves the equations obtained by equating the above coefficients to their expressions in terms of the phase shifts.

But the greater the number of A_i coefficients, the lower as a rule the accuracy with which they can be found from given data. Therefore knowledge of the higher $n-1$ among the $2n-1$ quantities A_i determined by the n phase shifts, may be of no help whatsoever, since they are highly inaccurate. In other words, when the experimental errors are large some of Eqs. (1) are "almost missing." Such elimination of some of the conditions may cause ambiguity in the analysis even if there is none in principle (in an "overcomplete experiment").

Instead of this it is best to find just the first (or largest) n coefficients, from which, as has been shown above, one can obtain 2^n solutions for the phase shifts. One can then plot all the curves that remain when one discards the solutions eliminated by the unitarity condition.

If the electronic computer is programmed to choose the best real phase shifts, it is easy to differentiate between the unitary solutions and the nonunitary ones. Indeed, a real solution for the phase shifts has the property that the sum of the square deviations of the A_i from their expressions in terms of the phase shifts vanishes, while nonunitary solutions give more shallow minima. The real parts of solutions with small imaginary parts will in this sense be "almost solutions." The problem of finding all the solutions is simplified by the fact that their total number is known. If the cross section is measured at n points, the first type of analysis will lead to a minimum sum of squares equal to zero for unitary solutions, but to a nonzero value for sets of real phase shifts close to nonunitary solutions. The depth of the minimum may serve as an indication of how close the solution is to unitarity.

It turns out in practice that there are half as many different angular distribution curves as there are sets of phase shifts, since a simultaneous change of sign of all the phase shifts will not change the cross section. Then one can find an angle θ_0 where no pair of the 2^{n-1} curves intersects, and where in fact they are most sepa-

rated. A sufficiently accurate measurement of the cross-section at this angle will eliminate all solutions except two, one of which is causal, while the other is not. In order to identify the correct one, one must make use of interference, for instance with Coulomb scattering. If, further, one has information on the energy dependence of the solutions, one of the solutions, the noncausal one, can be eliminated with the aid of dispersion relations.

In some special cases it may turn out that for a given energy region it is easier to distinguish between the 2^{n-1} curves by measurements not at a single point, but at two or more points.

The question of the number of solutions remaining after the "complete experiment" has been performed will be treated separately.

In order to find all the parameters of an n-parameter curve, one need measure it only at n points. It is assumed, of course, that n has already been chosen from considerations of the nature of the interaction, from analogy, or on the basis of previous experiments. Klepikov and Sokolov [4] (Chapter V) have shown that when a curve with n degrees of freedom is measured at exactly n points, the standard deviations of the coefficients are lower than if the measurements had been performed at more points, but with the same total effort devoted to the measurement. They also show how to find the best measurement points and how most efficiently to distribute the time devoted to measurements at these points for every specific case. It follows from such considerations that the phase-shift analysis of spinless particle scattering is best performed on the basis of cross-section measurements at exactly n points. Subsequently one can eliminate the resulting ambiguity by a single added measurement at the best possible angle θ_0. If the measurements are performed at more than n points, each additional point can be used to reduce the ambiguity, but the effort devoted to the measurements at these points may turn out to be quite inefficiently expended. As for the work involved in finding the best angle θ_0, it is usually considerably less than would be needed for additional measurements.

The phase-shift analysis of scattering of spin-$\frac{1}{2}$ particles by spin-zero particles (or vice versa) can also be performed by the two methods discussed. In this case, however, the differential cross section at any angle is a linear function of the n coefficients A_i. It follows then that there is no additional point at which knowledge of the cross section will decrease the ambiguity of the phase-shift analysis, whose multiplicity, as described above, is 2^n. But the same phase shifts determine the angular dependence of the polarization of the scattered spin-$\frac{1}{2}$ particles. Therefore a polarization measurement at a single successfully chosen angle θ_0 can remove the ambiguity of the analysis. In general (when all the solutions are unitary) one obtains 2^{n-1} different polarization curves, since the polarization is not changed by simultaneously changing the signs of all the phase shifts and interchanging the even-state phase shifts with the odd-state ones of the same total angular momentum (an interchange of the causal and noncausal solutions). If the polarization measurements are impossible, it is impossible to distinguish between four possible sets of phase shifts.

Interference with the Coulomb interaction is an aid in distinguishing the solutions. If the energy dependence of the phase shifts is known, the dispersion relations and the low-energy dependence of the phase shifts can also be used. Indeed, for sufficiently low energies, the momentum dependence of the phase shift is determined entirely by the orbital rather than the total angular momentum; then $\delta_l \sim k^{2l+1}$.

As in the previous case, we can conclude that it is most useful to measure the differential cross section at n points and the polarization at one point. In principle we can choose any n of the $2n-1$ equations for the expansion coefficients of the cross section and the polarization. However, the polarization measurements are usually much more laborious. Furthermore, one must bear in mind the fact that for the polarization these equations are of a different form. Instead of (1), one obtains

$$\sum_{k,\,l=1}^{n} D_{kl}^{(l)} \sin\delta_k \sin\delta_l \sin(\delta_k - \delta_l) = B_l. \qquad (8)$$

Therefore the number of solutions of the mixed system can be either more or less than 2^n (but not more than $2 \times 3^{n-1}$).

We see that in both of the above cases, the "complete experiment" consisting of $2n-1$ measurements can be replaced by a "necessary experiment" of only $n+1$ measurements. As has been stated, the $n+1$ measurements can be chosen so that the information obtained on the phase shifts is greater than in the "complete experiment" involving the same effort.

The author thanks Professor Ya. A. Smorodinskii, S. N. Sokolov, and R. M. Ryndin for very useful discussions.

APPENDIX

NUMBER OF SOLUTIONS OF A PHASE-SHIFT ANALYSIS

N. P. Klepikov and L. A. Aĭzenberg

Equations (1), for which we want to know the number of solutions, can be written in the form

$$f_i(x, a) = \sum_{k,l=1}^{n} C_{kl}^{(i)} \left\{ \frac{x_k x_l (1 + x_k x_l)}{(1 + x_k^2)(1 + x_l^2)} - \frac{a_k a_l (1 + a_k a_l)}{(1 + a_k^2)(1 + a_l^2)} \right\} = 0, \quad \text{(A1)}$$

where $x_k = \tan \delta_k$, $i = 1, \ldots, n$. Equation (A1) contains the experimentally determined values of the A_i in terms of one of the solutions $x_k^{(1)} = a_k$. It is clear that $x_k^{(2)} = -a_k$ is also a solution. However Eqs. (1) or (A1) have also other solutions.

When dealing with elastic scattering, only the real phase-shift (unitary) solutions of these equations are used. Nevertheless we find it convenient to consider the variables x_k and parameters a_k complex. Consider $C^n(x)$, the space of the complex variables $x = (x_1, \ldots, x_n)$, and $C^n(a)$, the space of the complex variables $a = (a_1, \ldots, a_n)$. Reducing the terms of each of the equations of (A1) to their common denominator, we obtain the set of equations

$$F_i(x, a) = 0, \quad \text{(A2)}$$

$(i = 1, \ldots, n)$ involving polynomials of degree 2^n of n variables. Clearly the number of solutions N_2 (counting multiplicities) of (A2) is no less than the number of solutions N_1 of (A1). From elimination theory (see, for instance, van der Waerden,[5] Secs. 77 and 78) it follows that $N_1 \leq N_2 \leq 2^{n^2}$, unless there exists a variable x_i such that

$$D_j(x_1, \ldots, x_{i-1}, x_{i+1}, \ldots, x_n; a_1, \ldots, a_n) = 0$$
$$(j = 1, \ldots, h, h \geqslant 1) \quad \text{(A3)}$$

is an identity in $x_1, \ldots, x_{i-1}, x_{i+1}, \ldots, x_n$. Here the D_j are the resultants of Eq. (A2) with respect to the x_i. Therefore N_2 is always a finite number unless conditions (A3) are fulfilled.

It is possible that these conditions are fulfilled for some a in $C^n(a)$. Let us denote the set of such a by P. In particular, $a = (a_1, \ldots, a_n)$ is in P for spin-0-spin-$\frac{1}{2}$ scattering, with n even, if $a_1 a_2 = -1$, $a_3 a_4 = -1, \ldots, a_{n-1} a_n = -1$. This is easily verified if (1) is written in the form

$$\tfrac{1}{4} \sum_{k,l=1}^{n} C_{kl}^{(i)} [1 + \cos 2(\delta_k - \delta_l) - \cos 2\delta_k - \cos 2\delta_l] = A_i. \quad \text{(A4)}$$

Under this condition $|\delta_1 - \delta_2| = \pi/2, \ldots, |\delta_{n-1} - \delta_n| = \pi/2$, and all terms of the form $\cos 2\delta_1 + \cos 2\delta_2, \ldots, \cos 2\delta_{n-1} + \cos 2\delta_n$ vanish. According to Minami's theorem[2] this exhausts all combinations of terms that do not contain phase differences. Equations (A4) still contain terms with all possible phase differences. We can therefore introduce only a single continuous parameter. According to the mechanism described elsewhere[6] this case can occur if the vertex H is made coincident with the origin O, after which the mechanism can be rotated through any angle about the origin, so that the vanishing of all terms with cosines of double phase shifts indicates that there is no relation of the mechanism to the coordinate system, or that only internal relations exist. Points in $C^n(a)$ at which $a_k = \pm i$ for at least one value of k also present some difficulties on going from (A1) to (A2); in applications, however, these points are never needed.

Let Q denote the set of those a in $C^n(a)$ at which (A2) has at least one solution with at least one infinite coordinate. For real phase shifts this means that at least one of them is equal to $\pi/2$ (resonance). We shall call the points in $C^n(a) - (P + Q)$ ordinary. It is clear that the set of ordinary points is connected; in other words any two ordinary points can be connected by a continuous curve L consisting entirely of ordinary points (see, for instance, Fuks,[7] Sec. 12).

Further, let R(a) be a bounded closed set of ordinary points, and let R(x) be the set of all solutions of (A1) corresponding to points in R(a). Then R(x) is also bounded. Indeed, if this were not the case, there would exist a sequence $x^{(l)}$ in R(x) converging to a point with at least one infinite coordinate. Let x be a solution of (A1) for $a = a^{(l)}$. Since R(a) has no intersection with P, the number of $a^{(l)}$ points is infinite. From the sequence $a^{(l)}$ we can choose a subsequence $a^{(lm)}$ converging to a point $a^{(0)}$ in R(a). Then going to the limit in m in the equations

$$f_i(x^{(lm)}, a^{(lm)}) = 0, \qquad i = 1, \ldots, n \quad \text{(A5)}$$

we would obtain a contradiction with the requirement that $a^{(0)}$ is not in Q.

Levine[8] (see also Cherne[9]) has obtained an integral representation for the number of solutions of the equations

$$\varphi_i(x) = A_i, \quad \text{(A6)}$$

in a bounded region D under the following conditions: (1) the $\varphi_i(x)$ are meromorphic functions, (2) the number of solutions is finite, (3) there are no solutions on the boundary of D.

Let $a^{(1)}$ and $a^{(2)}$ be two ordinary points in $C^n(a)$, and let L be a continuous curve connect-

ing them. As has been shown above, the set of all solutions of (A1) with a in L is bounded in $C^n(x)$. There therefore exists a region D such that all these solutions are in its interior. Using Levine's integral representation, it is easily shown that the number of solutions of (A1) depends continuously on a in L.* It therefore follows that the number of such solutions is the same for all ordinary points.

In order to include also points that are not ordinary, we make the following definition: the system (A1) with $a = a^{(0)}$ in $C^n(a)$ has N solutions in the generalized sense if there exists a neighborhood S of $a^{(0)}$ such that for almost all points in S Eqs. (A2) have exactly N solutions in the usual sense. It is then clear that the number of solutions in the generalized sense is the same for all points in $C^n(a)$.

In order to find this number N, we need only count the number of solutions of (A1) at any ordinary point of $C^n(a)$. We choose the point $a = (0, \ldots, 0)$, and we show that for this point (A1) has only vanishing solutions. It will then follow that $(0, \ldots, 0)$ is an ordinary point of $C^n(a)$. Indeed, for $a_1 = \ldots = a_n = 0$ (zero energy) all the A_i of (1) vanish. This means that the product of the scattering cross section by the square of the wave number also vanishes in the limit. Then the product of the wave number and the scattering amplitude also vanishes. Since it is expanded in orthogonal functions of the angle, $e^{2i\delta_k} - 1$ must also vanish for all k. It follows then that for zero energy the only solutions are $x_1 = \tan \delta_1 = 0, \ldots, x_n = \tan \delta_n = 0$.

All that remains is to count the number of solutions of (A1) for $a = (0, \ldots, 0)$. As is well known, this number can be found in the following way. Let ν_i be the smallest number for which at least one of the partial derivatives of order ν_i of the function $f_i(x, 0)$ does not vanish for $x = (0, \ldots, 0)$. Then

$$N = \prod_{i=1}^{n} \nu_i. \qquad (A.7)$$

It is easily verified that for (A1) $\nu_i = 2$ for all i and therefore

$$N = 2^n. \qquad (A8)$$

We note that this number is considerably below its upper bound $N \leq 2^n$ obtained by elimination theory.

We have thus shown that each of our phase-shift analysis problems has exactly 2^n solutions including, of course, the nonunitary ones.

*It is possible that this continuity can also be proved in a more elementary way.

[1] Puzikov, Ryndin, and Smorodinskii, JETP **32**, 592 (1957), Soviet Phys. JETP **5**, 489 (1957).

[2] S. Minami, Progr. Theoret. Phys. (Kyoto) **11**, 213 (1954).

[3] L. P. Igushkin, A Study of the Uniqueness of a Phase Shift Analysis, Dissertation, Moscow State Univ. (1960).

[4] N. P. Klepikov and S. N. Sokolov, Analysis of Experimental Data by the Method of Maximum Likelihood, Preprint, Joint Inst. Nuc. Res. R-235 (1958).

[5] Van der Waerden, Moderne Algebra, Springer, Berlin, 1930.

[6] N. P. Klepikov, JETP **30**, 1155 (1956), Soviet Phys. JETP **3**, 981 (1956).

[7] B. A. Fuks, Teoriya Analiticheskikh funktsii mnogikh kompleksnykh peremennykh (Theory of Analytic Functions of Many Complex Variables), Gostekhizdat, 1948.

[8] H. Levine, Ann. Math. **71**, 529 (1960).

[9] S. Cherne, Ann. Math. **71**, 536 (1960).

Translated by E. J. Saletan
207

TRANSFORMATION OF SOUND AND ELECTROMAGNETIC WAVES AT THE BOUNDARY OF A CONDUCTOR IN A MAGNETIC FIELD

V. M. KONTOROVICH and A. M. GLUTSYUK

Institute of Radiophysics and Electronics, Academy of Sciences, Ukrainian S.S.R.

Submitted to JETP editor April 25, 1961

J. Exptl. Theoret. Phys. (U.S.S.R.) 41, 1195-1204 (October, 1961)

The electromagnetic field induced when a sound wave strikes the boundary between a conducting and nonconducting medium in a weak magnetic field is calculated. The amplitude of the sound waves outgoing from an interface on which electromagnetic waves are incident is also determined.

1. INTRODUCTION

WHEN a sound wave strikes the boundary of a conductor situated in an external magnetic field, electromagnetic waves are induced by the oscillations of the conducting medium, along with the reflected and refracted sound waves. Accordingly, when an electromagnetic wave is incident on a conductor, sound waves that move away from the interface are produced. They are brought about by the Lorentz force acting in the external magnetic field on the current produced when the electromagnetic wave passes through the conductor.

This mutual convertibility of acoustic and electromagnetic waves [1] can be of interest in the research on magnetoacoustic effects in metals, [2] in sea water, [1] or in plasma, as a possible mechanism of radio emission from the sun and the stars, and can also be used to produce electromagnetic waves with large retardation (on the order of the ratio of the velocity of light to that of sound) and to generate ultrasound directly in a conducting medium (for example, in a metal).

We confine ourselves in this article to a case of a conducting liquid bounding on a non-conducting (liquid or gas) half-space ("air"), where the acoustic and electromagnetic wavelengths in the substance (skin depth) greatly exceed the characteristic mean free path (accordingly, the oscillation frequency ω is much less than the collision frequency $1/\tau$, i.e., $\omega\tau \ll 1$). This means that the hydrodynamic approach is applicable and normal skin effect takes place.

A highly conducting medium ($\sigma/\epsilon \gg \omega$) in a constant magnetic field **B** is characterized by two frequencies:

$$\omega_s = 4\pi\sigma s^2/c^2, \qquad \omega_u = 4\pi\sigma u^2/c^2. \tag{1}$$

Here σ — conductivity, s — velocity of sound, and $u = B/\sqrt{4\pi\rho_0}$ — Alfven velocity. When $\omega = \omega_s$ (or $\omega = \omega_u$) the electromagnetic wavelength in the substance $\lambda\!\!\!^{-}_{em} = c/\sqrt{4\pi\sigma\omega}$ is comparable with the acoustic wavelength $\lambda\!\!\!^{-}_{ac} = s/\omega$ (Alfven wavelength $\lambda\!\!\!^{-}_{a} = u/\omega$). Obviously $\sigma/\epsilon \gg \omega$; in addition, in relatively weak magnetic fields such as we are considering, we have

$$\omega_u/\omega_s = u^2/s^2 \ll 1. \tag{2}$$

In view of the fact that the magnetoacoustic effects, which are quite small by virtue of (2) and which manifest themselves in movements of sufficiently large scale, decrease with increasing ω when $\omega > \omega_s$, we confine ourselves to the frequency region

$$\sigma/\varepsilon \gg \omega \gg \omega_u. \tag{3}$$

We note that the medium can be regarded as infinitely conducting only for frequencies $\omega \ll \sigma/\epsilon$, ω_s, ω_u, i.e., when the skin depth is the smallest of all the characteristic lengths. For liquid metals $\sigma \sim 10^{17}$ sec^{-1}, $\omega_s/2\pi \sim 10^6$ cps, $\omega_u \sim 10^3$ sec^{-1} in a field $B \sim 10^4$ oe; in sea water with $\sigma = 4 \times 10^{10}$ sec^{-1} we have $\omega_s/2\pi \sim 2$ cps and $\omega_u \sim 10^{-12}$ sec^{-1} in the earth's magnetic field ($B \sim 1$ oe).

Subject to limitations (2) and (3), the transformation of acoustic and electromagnetic perturbations can be regarded as particular cases of reflection and refraction of waves in magnetohydrodynamics (more accurately, the conversion of various types of waves into each other). Reflection and refraction in magnetohydrodynamics have been analyzed only for Alfven waves in a perfectly conducting medium. [3] We likewise disregard the general case of arbitrary frequencies and magnetic fields and confine ourselves to the condition

of weak hydromagnetic coupling (2) with finite conductivity of the medium (3).

In the magnetohydrodynamic approximation there exist in the conducting liquid, as is well known, three types of waves (Alfven and fast or slow magnetic sound), in which both "acoustic" (the velocity **v** or the pressure p) and "electromagnetic" quantities (the current **j**, the electric and magnetic field **E** and **H**) oscillate. Under conditions (2) and (3), the Alfven wave and the slow magnetic-sound wave are electromagnetic waves in the medium, while the fast magnetic-sound wave is a sound wave. These waves being modified as follows: the sound wave carries also induced oscillating electromagnetic quantities, while the electromagnetic waves contain acoustic quantities whose reaction on the fields that generate them can be neglected. Since the electromagnetic and acoustic quantities are interrelated in a conducting medium situated in a magnetic field, incidence of any one of the three waves (sound or one of the two electromagnetic waves, which have different polarizations) gives rise to six waves moving away from the boundary (four electromagnetic and two sound). In particular, when a sound wave incident from air is reflected from a liquid surface, electromagnetic wave are produced. The conversion coefficients for these waves are calculated in Secs. 4 and 5, where we also consider the incidence of sound on a conducting medium and determine the coefficients for the conversion of electromagnetic waves into sound waves.

2. WAVES IN A CONDUCTING LIQUID

If we neglect the viscosity and heat conduction of the medium, and also the displacement current, then the dispersion equation connecting the frequency ω with the wave vector **k** of a plane wave in a conducting liquid[4] reduces to

$$[X-(\Omega_u\cos^2\theta-i\Omega)^{-1}]\{X^2(\Omega_u\cos^2\theta-i\Omega) - X(1-i\Omega+\Omega_u)+1\}=0. \quad (4)$$

Here

$$X=(ks/\omega)^2,\ \Omega=\omega/\omega_s,\ \Omega_u=\omega_u/\omega_s,\quad \cos\theta=\varkappa\mathbf{h},\ \varkappa=\mathbf{k}/k,\ \mathbf{h}=\mathbf{B}/B. \quad (5)$$

The electrodynamic and acoustic quantities are expressed in terms of the current by means of the following chain of equations

$$\mathbf{f}=\frac{B}{c}[\mathbf{jh}],\quad \mathbf{v}=\frac{i}{\rho_0\omega}\left\{\frac{X}{1-X}(\varkappa\mathbf{f})\varkappa+\mathbf{f}\right\},$$

$$p=\rho_0 s^2\frac{k}{\omega}(\varkappa\mathbf{v}),\quad \mathbf{E}=\frac{\mathbf{j}}{\sigma}-\frac{B}{c}[\mathbf{vh}],\quad \mathbf{H}=\frac{kc}{\omega}[\varkappa\mathbf{E}]. \quad (6)^*$$

*$[\mathbf{jh}]=\mathbf{j}\times\mathbf{h}$; $(\varkappa\mathbf{v})=\varkappa\cdot\mathbf{v}$.

Under conditions (2) and (3), the dispersion laws become

$$X_a=X_{s1}=i/\Omega,\quad X_a=(sk_a/\omega)^2,\quad X_{s1}=(sk_{s1}/\omega)^2, \quad (7)$$

$$X_{ac}=1-\Omega_u\sin^2\theta/(1+i\Omega),\quad X_{ac}=(sk_{ac}/\omega)^2, \quad (8)$$

where $\mathbf{k_a}$, $\mathbf{k_{sl}}$, and $\mathbf{k_{ac}}$ are the wave vectors of the Alfven, slow magnetic-sound and sound waves. The connection between the fields amplitudes (wave "polarization") in a frame having unit vectors

$$\varkappa=\mathbf{k}/k,\quad \eta=[[\varkappa\mathbf{h}]\varkappa]/\sin\theta,\quad \zeta=[\varkappa\mathbf{h}]/\sin\theta, \quad (9)$$

which are fixed in the wave, is as follows:

in the modified sound wave

$$\mathbf{E}_{ac}=\mathscr{E}_{ac}\zeta_{ac}p_{ac},\quad \mathbf{H}_{ac}=\mathscr{H}_{ac}\eta_{ac}p_{ac},\quad \mathbf{j}_{ac}=J_{ac}\zeta_{ac}p_{ac},$$
$$\mathbf{v}_{ac}=\mathbf{a}p_{ac},\quad \mathbf{a}=\frac{\varkappa_{ac}}{\rho_0 s},\quad \mathscr{E}_{ac}=-\frac{B}{\rho_0 sc}\frac{\sin\theta_{ac}}{1+i\Omega},$$
$$\mathscr{H}_{ac}=-\frac{c}{s}\mathscr{E}_{ac},\quad J_{ac}=i\frac{\omega c}{Bs}\frac{\Omega_u\sin\theta_{ac}}{1+i\Omega}, \quad (10)$$

in the Alfven wave

$$\mathbf{E}_a=\eta_a j_a/\sigma,\quad \mathbf{H}_a=\mathscr{H}_a\zeta_a j_a,\quad \mathbf{j}_a=\eta_a j_a,\quad p_a=0,$$
$$\mathbf{v}_a=\mathbf{V}_a j_a,\quad \mathbf{V}_a=-(iB/\rho_0\omega c)\zeta_a\cos\theta_a,$$
$$\mathscr{H}_a=(c/\sigma s)\sqrt{i/\Omega},\quad \mathrm{Re}\sqrt{i}>0; \quad (11)$$

in the slow magnetic-sound wave

$$\mathbf{E}_{s1}=\zeta_{s1}j_{s1}/\sigma,\quad \mathbf{H}_{s1}=\mathscr{H}_{s1}\eta_{s1}j_{s1},\quad \mathbf{j}_{s1}=\zeta_{s1}j_{s1},$$
$$\mathbf{v}_{s1}=\mathbf{V}_{s1}j_{s1},\quad \mathbf{V}_{s1}=\frac{iB}{\rho_0\omega c}\left(\varkappa_{s1}\frac{\sin\theta_{s1}}{i/\Omega-1}+\eta_{s1}\cos\theta_{s1}\right),$$
$$p_{s1}=P_{s1}j_{s1},\quad P_{s1}=B\sqrt{\frac{i}{4\pi\sigma\omega}}\frac{\sin\theta_{s1}}{1+\Omega i},\quad \mathscr{H}_{s1}=-\mathscr{H}_a. \quad (12)$$

The difference between (8) and the dispersion law for sound

$$X_{ac}=(sk_{ac}/\omega)^2=1 \quad (8')$$

is responsible for the appearance of electric and magnetic fields in the modified wave (10), and also for the additional anisotropic attenuation of the sound, connected with the Joule losses. It will be sufficient in what follows to use the dispersion law (8'), and resort to the more exact expression (8) only in the investigation of the singularities of the conversion coefficient.

We now introduce a coordinate frame fixed to the interface (plane x = 0) and to the external magnetic field **B**. We direct the unit vector $\mathbf{e_x}$ from the liquid into the air. If **q** is the wave-vector component parallel to the interface, φ the angle of incidence, γ the angle between **q** and the plane z = 0 in which the magnetic field **B** is located, and ϵ the angle of inclination of the magnetic field, we obtain

$$\varkappa=\mathbf{e}_x\cos\varphi+\frac{\mathbf{q}}{q}\sin\varphi,\qquad \frac{\mathbf{q}}{q}=\mathbf{e}_y\cos\gamma+\mathbf{e}_z\sin\gamma,$$
$$\mathbf{h}=-\mathbf{e}_x\sin\varepsilon+\mathbf{e}_y\cos\varepsilon,$$
$$\cos\theta=-\cos\varphi\sin\varepsilon+\sin\varphi\cos\gamma\cos\varepsilon. \quad (13)$$

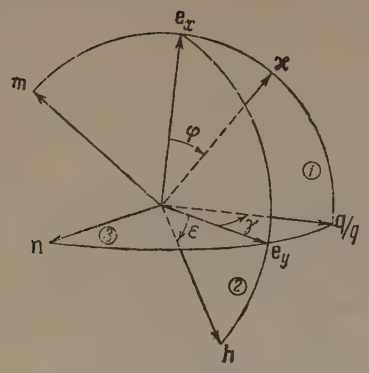

FIG. 1. System of unit vectors fixed in the interface; 1 – plane of incidence; 2 – plane in which the normal to the interface and the constant magnetic field lie; 3 – interface.

To describe the electromagnetic waves in air we introduce the unit vectors (Fig. 1)

$$\mathbf{n} = \left[\frac{\mathbf{q}}{q}\mathbf{e}_x\right], \qquad \mathbf{m} = [\mathbf{n}\varkappa_{e1}];$$

$$\mathbf{n} = \mathbf{e}_y \sin\gamma - \mathbf{e}_z \cos\gamma, \qquad \mathbf{m} = \mathbf{e}_x \sin\varphi_{e1} - \frac{\mathbf{q}}{q}\cos\varphi_{e1}. \quad (14)$$

They are orthogonal to κ_{el}, with $\mathbf{n}$ lying in the interface and $\mathbf{m}$ in the plane of incidence. We choose as the two independent waves with specified value of κ_{el} TE and TM waves with electric or magnetic field respectively parallel to $\mathbf{n}$:

$$\mathbf{E} = E_n\mathbf{n} + H_n\mathbf{m}, \qquad \mathbf{H} = H_n\mathbf{n} - E_n\mathbf{m};$$
$$\omega = ck_{e1}, \qquad \overline{\mathbf{v}_{e1}} = 0, \qquad \overline{p_{e1}} = 0, \qquad \overline{\mathbf{j}_{e1}} = 0. \quad (15)$$

The electric field in the TM wave and the magnetic field in the TE wave are parallel to $\mathbf{m}$.

For sound in air we obviously have

$$\omega = \bar{s}\bar{k}_{ac}, \quad \bar{\mathbf{v}}_{ac} = \bar{\mathbf{a}}\bar{p}_{ac}, \quad \bar{\mathbf{a}} = \bar{\varkappa}_{ac}/\bar{\rho}_0\bar{s},$$
$$\bar{\mathbf{H}}_{ac} = \bar{\mathbf{E}}_{ac} = \bar{\mathbf{j}}_{ac} = 0. \quad (16)$$

The quantities pertaining to air are designated by a bar (except for $\mathbf{E}$ and $\mathbf{H}$ in the electromagnetic wave).

3. BOUNDARY CONDITIONS. CONVERSION OF WAVES

To be specific, we discuss first a sound wave incident from a conducting medium onto the interface. The connection between the angles of reflection, refraction, and conversion (the definition of the latter is obvious) and the angle of incidence φ'_{ac} follows from the equality of the frequencies ω and of the tangential wave-vector components q in the incident plane wave and in all the outgoing waves: $\sqrt{X_i}\sin\varphi_i = \sqrt{X'_{ac}}\sin\varphi_{ac}$. The principal terms of these equations have the form

$$\sin\varphi'_{ac} = \sin\varphi_{ac} = \frac{s}{\bar{s}} \quad \sin\bar{\varphi}_{ac} = \frac{s}{c}\sin\varphi_{e1}$$
$$= \sqrt{\frac{i}{\Omega}}\sin\varphi_a = \sqrt{\frac{i}{\Omega}}\sin\varphi_{e1}. \quad (17)$$

If the angles are complex, the following condition must be satisfied for the outgoing waves

$$\begin{aligned} &\operatorname{Im}\cos\varphi < 0 && x < 0, \\ &\operatorname{Im}\cos\varphi > 0 && x > 0, \end{aligned} \quad (18)$$

so as to make the amplitude decrease with increasing distance from the boundary.

The electromagnetic wave produced in air by the incidence of sound, as follows from "Snell's law" (17), is a surface wave if $\sin\varphi'_{ac} > s/c$, i.e., at all angles of incidence with the exception of the narrow region of angles $\sim 10^{-5}$, corresponding to normal incidence.

When $\varphi'_{ac} \gg s/c$ the "depth of penetration" of the electromagnetic field in air is $1/\operatorname{Im} k_{el}x = \lambda'_{ac}/2\pi\sin\varphi'_{ac}$, where λ'_{ac} is the length of the incident sound wave. The electromagnetic wave propagates along the surface with a velocity equal to the horizontal component of the velocity of light, i.e., at $\varphi'_{ac} \sim 1$, we obtain a slowing-down ratio on the order of $c/s \sim 10^5$. For such a surface wave, both $\sin\varphi_{el}$ and $|\cos\varphi_{el}|$ are on the order of c/s:

$$-i\cos\varphi_{e1} \approx \sin\varphi_{e1} = (c/s)\sin\varphi'_{ac}.$$

According to (14) and (15), it follows therefore that the electric field in a surface TM wave parallel to $\mathbf{m}$ is circularly polarized and is c/s times greater than the magnetic field. Accordingly, in a surface TE wave the magnetic field is c/s times greater than the electric field and is circularly polarized:

$$H_x/H_q = E_x/E_q \approx i, \qquad H_q \equiv (\mathbf{Hq}/q),$$
$$E_q \equiv (\mathbf{Eq}/q). \quad (19)$$

To determine the amplitudes of the outgoing waves from the known amplitudes of the incident waves, we use the boundary conditions on the interface (x = 0), namely the continuity of the pressure, of the tangential components of the magnetic and electric fields, and of the normal velocity component:

$$[\mathbf{H}_t] = [\mathbf{E}_t] = [\mathbf{v}_x] = [p] = 0. \quad (20)$$

Here [A] denotes the jump in the quantity A on the interface. Expanding the quantities in the boundary condition in normal modes (sound and electromagnetic), we can rewrite the boundary conditions (20) with the aid of (10)–(12), (15), and (16) in the form of equations for the amplitudes p_{ac}, j_{sl}, j_a, H_n, E_n, and $\bar{p}$ of the outgoing waves:

$$T_{i1}p_{ac} + T_{i2}j_{sl} + T_{i3}j_a + T_{i4}(-H_n) + T_{i5}(-E_n)$$
$$+ T_{i6}(-\bar{p}) = U_i, \qquad i = 1, 2, \ldots, 6. \quad (21)$$

The matrix T_{ik} has the form

$$\begin{Vmatrix} \mathcal{H}_{ac}\eta_{acy} - \mathcal{H}_a\eta_{ay} & \mathcal{H}_a\zeta_{ay} & n_y & -m_y & 0 \\ \mathcal{H}_{ac}\eta_{acz} - \mathcal{H}_a\eta_{az} & \mathcal{H}_a\zeta_{az} & n_z & -m_z & 0 \\ \mathcal{E}_{ac}\zeta_{acy} & \zeta_{ay}/\sigma & \eta_{ay}/\sigma & m_y & n_y & 0 \\ \mathcal{E}_{ac}\zeta_{acz} & \zeta_{az}/\sigma & \eta_{az}/\sigma & m_z & n_z & 0 \\ a_x & V_{s1x} & V_{ax} & 0 & 0 & \bar{a}_x \\ 1 & P_{s1} & 0 & 0 & 0 & 1 \end{Vmatrix} \quad (22)$$

The right halves U_i of the system (21) are determined by the incident perturbations.

4. CONVERSION COEFFICIENTS

Let us write down the principal terms of the expansion of the coefficients of conversion of sound waves into electromagnetic waves and electromagnetic waves into sound waves in powers of the small Ω_u, Ω_u/Ω, and s/c. The principal term of the determinant of the system (21) is

$$\mathrm{Det}\,|T_{ik}| = -d_1(1-Z)\,\bar{a}_x, \quad (23)$$

where

$$Z = (\bar{\rho}_0\bar{s}/\rho_0 s)\,(\cos\varphi_{ac}/\cos\bar{\varphi}_{ac}), \quad (24)$$

$$d_1 = \frac{1}{\sigma^2}\left(\frac{c}{s}\sqrt{\frac{i}{\Omega}}\cos\varphi_{e1} - \cos\varphi_a\right)\left(\cos\varphi_{e1} - \frac{c}{s}\sqrt{\frac{i}{\Omega}}\cos\varphi_a\right). \quad (25)$$

The term $\cos\varphi_a$ in the first parentheses becomes significant when $\cos\varphi_{el} \to 0$, and it can be shown that (23) in this range of angles is again the principal term of the determinent of the system.

Conversion of Sound Waves into Electromagnetic Waves in Air

When sound is incident from air, the conversion coefficients are

$$H_n/\bar{p}' = 2d_4/d_1(1-Z), \qquad E_n/\bar{p}' = 2d_5/d_1(1-Z). \quad (26)$$

Here $\bar{p}'$ — amplitude of the incident sound wave; H_n and E_n — amplitudes of the fields in the TM and TE waves, respectively;

$$d_4 = \frac{B\zeta_{acx}\sin\theta_{ac}}{\rho_0\sigma^2 s^2(1+i\Omega)\sin\varphi_{ac}}\left(\cos\varphi_a - \sqrt{\frac{i}{\Omega}}\cos\varphi_{ac}\right) \times\left(-\frac{c}{s}\sqrt{\frac{i}{\Omega}}\cos\varphi_a + \cos\varphi_{e1}\right), \quad (27)$$

$$d_5 = \frac{B\eta_{acx}\sin\theta_{ac}}{\rho_0\sigma^2 s^2(1+i\Omega)\sin\varphi_{ac}}\left(\cos\varphi_{ac} - \sqrt{\frac{i}{\Omega}}\cos\varphi_a\right) \times\left(\frac{c}{s}\sqrt{\frac{i}{\Omega}}\cos\varphi_{e1} - \cos\varphi_a\right). \quad (28)$$

When sound is incident from a conducting medium, we obtain the following expressions for the conversion coefficients:

$$\frac{H_n}{p'_{ac}} = \frac{d_1^{pH}}{d_1} - \frac{1+Z}{1-Z}\frac{d_4}{d_1}, \qquad \frac{E_n}{p'_{ac}} = \frac{d_1^{pE}}{d_1} - \frac{1+Z}{1-Z}\frac{d_5}{d_1}. \quad (29)$$

Here p'_{ac} is the amplitude of the sound wave incident from the conductor; d_1^{pH} and d_1^{pE} are obtained respectively from d_4 and $(-1)d_5$ by replacing the parameters of the outgoing sound wave by the parameters of the incident wave ($\varphi_{ac} \to \varphi'_{ac}$ etc).

Conversion of Electromagnetic Waves into Sound Waves in a Conductor

The coefficients of conversion of electromagnetic waves (incident from air) into sound waves (propagating in the conductor) are

$$p_{ac}/H'_n = -P_{s1}\{(1-Z_{s1})\,d_2^{pH} + Z_a d_3^{pH}\}/d_1(1-Z),$$

$$p_{ac}/E'_n = -P_{s1}\{(1-Z_{s1})\,d_2^{pE} + Z_a d_3^{pE}\}/d_1(1-Z). \quad (30)$$

Here E'_n and H'_n are the amplitudes of the incoming TE and TM waves;

$$Z_{s1} = V_{s1x}/P_{s1}\bar{a}_x, \qquad Z_a = V_{ax}/P_{s1}\bar{a}_x;$$

$$d_2^{pH} = \frac{2c}{\sigma s}\zeta_{ax}\frac{\cos\varphi'_{e1}}{\sin\varphi_a}\left(\sqrt{\frac{i}{\Omega}}\cos\varphi_a + \frac{s}{c}\cos\varphi'_{e1}\right), \quad (31)$$

$$d_2^{pE} = \frac{2c}{\sigma s}\eta_{ax}\frac{\cos\varphi'_{e1}}{\sin\varphi_a}\left(\sqrt{\frac{i}{\Omega}}\cos\varphi'_{e1} + \frac{s}{c}\cos\varphi_a\right); \quad (32)$$

d_3^{pH} and d_3^{pE} are obtained from d_2^{pH} and d_2^{pE} by making the substitution

$$\zeta_a \to -\eta_a, \qquad \eta_a \to \zeta_a.$$

Conversion of Sound into Electromagnetic Waves in a Conductor

When sound is incident from air, the conversion coefficients are

$$\frac{j_{s1}}{\bar{p}'} = \frac{-2d_2}{d_1(1-Z)}, \qquad \frac{j_a}{\bar{p}'} = \frac{2d_3}{d_1(1-Z)}; \quad (33)$$

$$d_2 = \frac{cB\cos\varphi_{e1}\sin\theta_{ac}}{\sigma\rho s^3(1+i\Omega)}\left\{\sqrt{\frac{i}{\Omega}}[\eta_{ac}\zeta_a]_x - \frac{s}{c}\frac{\cos\varphi_{e1}}{\sin\varphi_{ac}\sin\varphi_a}\left(\zeta_{acx}\zeta_{ax} + \sqrt{\frac{i}{\Omega}}\eta_{acx}\eta_{ax}\right)\right\}. \quad (34)$$

d_3 is obtained from d_2 by making the substitutions $\zeta_a \to -\eta_a$ and $\eta_a \to \zeta_a$. When the sound is incident from the conductor we have

$$j_{s1}/p'_{ac} = \{(1+Z)\,d_2 - (1-Z)\,d_1^{s1\,\rho}\}/d_1(1-Z),$$
$$j_a/p'_{ac} = -\{(1+Z)\,d_3 - (1-Z)\,d_1^{ap}\}/d_1(1-Z). \quad (35)$$

Here d_1^{slp} and d_1^{ap} are obtained from d_2 and d_3 by replacing the parameters of the outgoing sound wave by the parameters of the incoming wave.

5. INVESTIGATION OF THE CONVERSION COEFFICIENTS

The general formulas become somewhat simpler if we recognize that the acoustic impedance

of air is small compared with the acoustic impedance of the conducting medium. Except for a small range of angles

$$\cos\bar{\varphi}_{ac} \lesssim \bar{\rho}_0\bar{s}/\rho_0 s \ll 1, \qquad (36)$$

corresponding to gliding propagation of sound in air, we can neglect Z, Z_a and Z_{sl} compared with unity. When sound is incident from air, the range of angles (36) is attained but is of no interest, for the sound does not penetrate into the conductor in this case [5] and no electromagnetic waves are produced. On the other hand, when plane homogeneous electromagnetic waves are incident from air or sound waves are incident from a conducting medium, we get

$$Z \sim Z_a \sim Z_{sl} \ll 1 \qquad (37)$$

for all real angles of incidence.

Conversion of Sound Waves into Electromagnetic Waves

With (37) taken into account, the conversion coefficients assume the following form: for incidence from air

$$\frac{E_n}{\bar{p}'} = \frac{2B\,(\sin\varepsilon\sin\varphi_{ac} + \cos\varepsilon\cos\gamma\cos\varphi_{ac})\,(\sqrt{i/\Omega}\cos\varphi_a - \cos\varphi_{ac})}{\rho_0 sc\,(1+i\Omega)\,(1-Z)\left(\sqrt{i/\Omega}\cos\varphi_a - \frac{s}{c}\cos\varphi_{el}\right)}, \qquad (38)$$

$$\frac{H_n}{\bar{p}'} = \frac{2B\sin\gamma\cos\varepsilon\,(\cos\varphi_a - \sqrt{i/\Omega}\cos\varphi_{ac})}{\rho_0 s^2\,(1+i\Omega)\,(1-Z)\,(\cos\varphi_a - (c/s)\sqrt{i/\Omega}\cos\varphi_{el})}; \qquad (39)$$

for incidence from a conductor

$$\frac{E_n}{p'_{ac}} = \frac{2B\,(\sin\varepsilon\sin\varphi'_{ac} - \sqrt{i/\Omega}\cos\varepsilon\cos\gamma\cos\varphi_a)\cos\varphi'_{ac}}{\rho_0 sc\,((s/c)\cos\varphi_{el} - \sqrt{i/\Omega}\cos\varphi_a)\,(1+i\Omega)}, \qquad (40)$$

$$\frac{H_n}{p'_{ac}} = \frac{2B\sin\gamma\cos\varepsilon\cos\varphi'_{ac}}{\rho_0 s^2\,(1+i\Omega)\,((c/s)\cos\varphi_{el} - \sqrt{\Omega/i}\cos\varphi_a)}. \qquad (41)$$

The frequency dependence of the conversion coefficients is determined principally by the frequency dependence of the electromagnetic field in the modified sound wave, i.e., when $\omega \gg \omega_s$ the coefficient decreases as ω_s/ω with increasing frequency. An increase in frequency also brings about a modification in the angular dependence, owing to a certain redistribution of the contributions of the various types of waves, connected with the change in the phase velocities of the electromagnetic waves in the conductor. We confine ourselves in the following estimates to the case $\omega \sim \omega_s$.

In different ranges of sound-incidence angles, the angular dependences and the orders of magnitude of the electric and magnetic fields of TE waves differ appreciably from those of TM waves. At normal incidence ($\varphi'_{ac} < s/c$) the electric and

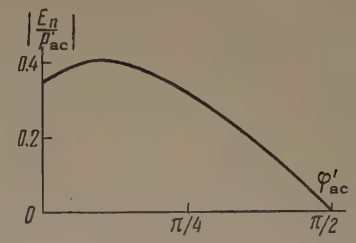

FIG. 2. Dependence of the amplitude of the TE wave on the angle of incidence of a sound wave from a conducting liquid when $\varepsilon = \pi/4$, $\gamma = \pi/3$, and $\Omega = 1$. The scale unit along the ordinate axis is $B\sqrt{2}/\rho_0 sc$.

magnetic fields of electromagnetic waves are equal to each other in air, but in a conducting medium the electric field is c/s times smaller than the magnetic field. Since the electric field of a TE wave lies in the interface, it follows from the continuity of $\mathbf{E}_t$ that the magnetic field of the TE wave is c/s times smaller than the magnetic field of the modified sound. When $\varphi'_{ac} \gg s/c$, the rotating magnetic field is c/s times greater than the electric field, and as a result both fields have the same order of magnitude as in the conductor:

$$E \sim (B/\rho_0 sc)\,p'_{ac}, \qquad H \sim (B/\rho_0 s^2)\,p'_{ac}. \qquad (42)$$

The dependence of E and H on the angle of incidence φ'_{ac} is a smooth one (Fig. 2).

In a TM wave, as in a TE wave, the magnetic field at normal incidence is c/s times smaller than in the modified sound. However, when $\sin\varphi'_{ac} = s/c$ the tangential component $E_q = -H_n\cos\varphi_{el}$ vanishes with $\cos\varphi_{el}$ and the electric field in air, which is orthogonal to the interface, can greatly exceed the field in the conductor. As can be seen from (41), the coefficient of conversion of sound in a TM wave has at this point a very sharp maximum. The magnetic field at the maximum is of the same order of magnitude as the field in the sound wave ($H \sim Bp'_{ac}/\rho_0 s^2$), c/s times greater than the value of H for $\varphi'_{ac} \ll s/c$, and $(c/s)^2$ times greater than the value of H in the surface TM wave (Fig. 3). The half-

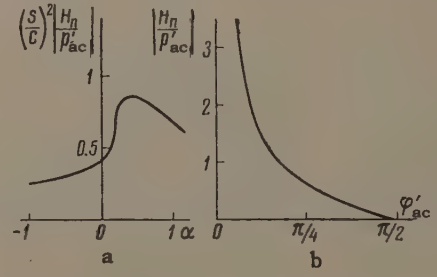

FIG. 3. Dependence of the amplitude of the TM wave on the angle of incidence of a sound wave from a conducting medium when $\varepsilon = \pi/4$, $\gamma = \pi/3$, and $\Omega = 1$. The scale unit along the ordinate axis is $B\sqrt{2}/\rho_0 c^2$. a – region of maximum, $\alpha = (c/s)^3(\varphi'_{ac} - s/c)$; b – surface-wave region ($\sin\varphi'_s > s/c$).

width of this exceedingly narrow maximum, as follows from (41), is of the order of $(s/c)^3$. It follows, however, from the dispersion law (8) that when the angle of incidence is real, $\cos\varphi_{el}$ does not vanish:

$$\cos\varphi_{el} = \sqrt{\Omega_u}\sin\theta_{ac}/\sqrt{1+i\Omega} \quad \text{for} \quad \sin\varphi_{ac} = \frac{s}{c} \qquad (43)$$

(we put $\Omega_u = 0$ in $\sin\theta_{ac}$). Therefore when $\sqrt{\Omega_u} \gg s/c$ we can neglect $\cos\varphi_a$ in the denominator; the height and the width of the maximum are respectively $1/\sqrt{\Omega_u}$ and $(s/c)^2\sqrt{\Omega_u}$.

It is obvious that a similar dependence of the conversion coefficient on the angle of incidence should occur also when the conducting medium is a crystalline solid.

It is seen from (38)—(41) that the conversion coefficients are anisotropic. We can point out the singular cases when there is no conversion of acoustic oscillations into electromagnetic ones. For this purpose it is obviously necessary that the sound propagate in the conducting medium along the magnetic field, for in this case neither fields nor currents are induced. When the sound is incident from the air, the refracted sound wave propagates along the magnetic field without interacting with it if $\gamma = 0$ and $\varphi_{ac} = \epsilon + \pi/2$. As can be seen from (38) and (39), the conversion coefficients for both electromagnetic waves vanish in this case. When incidence is from a conductor, in view of the fact that both the incident and the reflected sound wave must propagate in the liquid in order to have no induction along the magnetic field, there is no connection between the acoustic and electromagnetic oscillations only if the magnetic field is perpendicular to the interface ($\epsilon = \pi/2$) and the wave is normally incident ($\varphi'_{ac} = 0$). We note also that when $\epsilon = \pi/2$ or $\epsilon = 0$ and $\gamma = 0$, only a TE wave is produced in the air, and when $\epsilon = 0$ and $\gamma = \pi/2$ only a TM wave is produced.

Conversion of Electromagnetic Waves into Sound Waves

The coefficients of conversion of electromagnetic waves incident from air into sound waves in a conductor, subject to condition (37), are

$$\frac{p_{ac}}{H'_n} = \frac{B\sin\gamma\cos\varepsilon\cos\varphi'_{el}}{2\pi(1+i\Omega)(\cos\varphi'_{el} + (s/c)\sqrt{\Omega/i}\cos\varphi_a)}, \qquad (44)$$

$$\frac{p_{ac}}{E'_n} = \frac{B\cos\varphi'_{el}(\sin\varepsilon\sin\varphi_a + \cos\varepsilon\cos\gamma\cos\varphi_a)}{2\pi(1+i\Omega)(\cos\varphi_a + (s/c)\sqrt{\Omega/i}\cos\varphi'_{el})}. \qquad (45)$$

Upon incidence of homogeneous plane waves (φ'_{el} real), by virtue of Snell's law (17), the sound and electromagnetic waves propagate in the conductor normally to the interface. This makes it possible to simplify expressions (44) and (45) further, by putting $\sin\varphi_{ac} = \sin\bar{\varphi}_{ac} = \sin\varphi_a = 0$:

$$\frac{p_{ac}}{H'_n} = \frac{B\sin\gamma\cos\varepsilon\cos\varphi'_{el}}{2\pi(1+i\Omega)(\cos\varphi'_{el} - (s/c)\sqrt{\Omega/i})}, \qquad (44')$$

$$\frac{p_{ac}}{E'_n} = \frac{B\cos\varphi'_{el}\cos\varepsilon\cos\gamma}{2\pi(1+i\Omega)(1-(s/c)\sqrt{\Omega/i}\cos\varphi'_{el})}. \qquad (45')$$

We note that in the calculation of the principal terms of the coefficients of conversion of sound into electromagnetic waves we neglect in this approximation the presence of the acoustic field in the modified electromagnetic wave. Accordingly, only the acoustic field of the electromagnetic wave plays a role in the conversion of electromagnetic waves into sound.

The conversion of electromagnetic waves into a sound wave and vice versa is also of interest in investigations of the properties of solids. In this case the angle relationships differ from those obtained for a liquid and will be calculated separately, but the orders of magnitude of the conversion coefficients remain the same:

$$p \sim BH'/4\pi(1+i\Omega), \qquad H \sim Bp'/\rho_0 s^2(1+i\Omega).$$

These estimates are valid down to low temperatures such that the mean free path l of the carriers (electrons) is still considerably less than the mean free path of sound λ and the skin depth δ, i.e., when

$$\sigma \ll \frac{s}{4\pi v_0}\frac{\omega_p^2}{\omega} \sim \frac{10^{26}}{\omega}, \qquad \lambda \gg l, \qquad (46)$$

$$\sigma^{3/2} \ll \frac{1}{(4\pi)^{3/2}}\frac{c}{v_0}\frac{\omega_p^2}{\sqrt{\omega}} \sim \frac{10^{31}}{\sqrt{\omega}}, \qquad \delta \gg l. \qquad (47)$$

Here $v_0 \sim 10^8$ cm/sec is the Fermi velocity and $\omega_p \sim 10^{15}$ sec^{-1} is the plasma frequency of the electrons. Since $v_0/s \gg 1$, this automatically guarantees the inequality $\omega\tau \ll 1$. Let us also rewrite these conditions in different form

$$\Omega \gg v_0 c^2 s^{-3}(\omega/\omega_p)^2 \sim 10^{-17}\omega^2, \qquad (46')$$

$$\Omega^{3/2} \gg v_0 c^2 s^{-3}(\omega/\omega_p)^2. \qquad (47')$$

The authors are grateful to S. Ya. Braude, discussions with whom suggested this work.

APPENDIX

In connection with the vector character of the electrodynamic boundary conditions, the use of the Laplace theorem leads to appreciable simplifications in the calculation of the conversion coefficients.

Let us examine the fourth-order minor obtained by crossing out the last two lines and any columns from the determinant of the system (21) (or from determinants derived from it by Cramer's rule). These determinants are made up of vector components and have the form

$$d = \begin{vmatrix} a_1 & a_2 & a_3 & a_4 \\ b_1 & b_2 & b_3 & b_4 \end{vmatrix}, \qquad (A.1)$$

where $\mathbf{a}_k$ stands for the column $\begin{pmatrix} a_{ky} \\ a_{kz} \end{pmatrix}$, and for d we obtain

$$d = \sum_{i<k,\ l<m} \varepsilon_{iklm} [a_i a_k]_x [b_l b_m]_x. \qquad (A.2)$$

We note that the sum contains only six non-vanishing terms (ϵ_{iklm} is an anti-symmetrical unit tensor). In the calculation of determinants with the aid of (A.2) we use the following corollaries of (13) and (14):

$$[\zeta_i m]_x = -\eta_{ix} \cos\varphi_{e1}/\sin\varphi_i, \quad [\eta_i m]_x = \zeta_{ix} \cos\varphi_{e1}/\sin\varphi_i,$$
$$[\zeta_i n]_x = \zeta_{ix} \cot\varphi_i, \quad [\eta_i n]_x = \eta_{ix} \cot\varphi_i. \qquad (A.3)$$

The text uses the following notation for the minors d: the lower index denotes the number of the column, crossed out together with the sixth column; the upper pair of indices denotes in which column and for what incident wave the change was made in accordance with Cramer's rule.

[1] V. M. Kontorovich, DAN SSSR **137**, 576 (1961).
[2] A. Baños, Phys. Rev. **104**, 300 (1956). S. V. Peletminskii, Ukr. Phys. J. **3**, 611 (1958).
[3] V. C. A. Ferraro, Astrophys. J. **119**, 393 (1954), P. H. Roberts, Astrophys. J. **121**, 720 (1955). R. Simon, Astrophys. J. **128**, 392 (1958). W. E. Williams, Astrophys. J. **131**, 438 (1960).
[4] A. Baños, Proc. Roy. Soc. **A233**, 350 (1955).
[5] L. M. Brekhovskikh, Volny v sloistykh sredakh (Waves in Layered Media) AN SSSR, 1957, p. 19, [transl. Academic Press, New York, (1960)].

Translated by J. G. Adashko
208

A MODEL FOR ANOMALOUS MUON INTERACTION

I. Yu. KOBZAREV and L. B. OKUN'

Institute for Theoretical and Experimental Physics, Academy of Sciences, U.S.S.R.

Submitted to JETP editor April 27, 1961

J. Exptl. Theoret. Phys. (U.S.S.R.) 41, 1205-1214 (October, 1961)

A model is considered in which the muon and electron mass difference is caused by the interaction of the muon with a hypothetical neutral vector meson χ. Possible manifestations of this interaction are discussed. The interaction of the muon neutrino and the baryons with the χ mesons is analyzed.

INTRODUCTION

In all experiments performed so far, the interactions of the electron and the muon are identical, whereas the masses of these particles differ by a factor of more than 200. One can imagine two possibilities: 1) either subsequent experiments will continue to give no evidence for a difference between the electron and muon interactions, or 2) through increased accuracy of the experiments and an analysis of the properties of the muon at small distances, some "anomalous" interaction of the muon will be observed, which is absent in the case of the electron. The second possibility seems to us more natural. As will be shown below, the experiments carried out up to now still leave very much room for a possible anomalous interaction of the muon.

For definiteness, we shall consider a model in which the anomalous interaction is given by the interaction of the muon with a hypothetical neutral vector meson χ. Such a model has a number of attractive features: it is renormalizable, it gives finite results in a number of cases, and it is γ_5 invariant. On the other hand, many of the relations between various physically observable quantities established within the framework of this model should also be qualitatively valid in other models, as, for example, in the case of an anomalous four-fermion interaction.

The anomalous interaction of the muon with a hypothetical intermediate neutral boson has been considered in a number of theoretical papers. Schwinger,[1] Cowland,[2] and Gatland[3] have discussed a model with pseudoscalar and scalar mesons. Jouvet and Goldzahl[4] considered also several aspects of the vector model with which we are concerned (see below). A neutral vector meson χ, if it exists, can interact not only with the muon, but also possibly with certain other particles. The larger the number of particles which interact with the χ meson, the more numerous and varied will also, of course, be the possibilities for an experimental verification of the model.

1. INTERACTION OF THE χ MESON WITH THE MUON

Let us, then, assume that there exists an interaction

$$\sqrt{4\pi} f \psi_\mu \gamma_\alpha \psi_\mu \chi_\alpha,$$

where f is a dimensionless constant and χ_α is the wave function of the χ meson field. In the following we shall call this interaction the f interaction.

The constant f and the mass of the χ meson are parameters of our theory which must be determined from experiment. We shall consider only values of $f < 1$. The only "justification" for this restriction is the absence of a theory of strong interactions. For $f > 1$ we would not be able to employ perturbation theory. The possibility $f^2 = e^2 = \alpha = 1/137$ appears particularly pleasing to us.

1. The mass of the muon. The interaction of the muon with the χ meson might explain the difference between the masses of the muon and the electron. One could think that the bare mass of the muon becomes equal to the mass of the electron if the χ interaction is "switched off" ($m_\mu^0 = m_e$). Since for $f < 1$ the normal polar type mass correction due to the graph of Fig. 1 is small,

$$\delta m_\mu = m_\mu^{0\prime} \frac{3f^2}{4\pi} \ln \frac{\Lambda^2}{m_\chi^2},$$

one can assume that the main part of the muon mass $m_\mu^{0\prime}$ ($m_\mu^{0\prime} \sim m_\mu$) is due to a modification of

FIG. 1

the f interaction at small distances ($r < 1/\Lambda$). This "explanation" of the mass difference between μ and e is no better or worse than the widely known explanation of the mass difference between e and ν by the fact that the electron has an electric charge. For in this case the normal electromagnetic mass correction of the electron is also small,

$$\delta m_e = m_e^{0'} \frac{3e^2}{4\pi} \ln \frac{\Lambda^2}{m_e^{0'2}},$$

and the main part of the electron mass is due to a modification of electrodynamics at distances $r \lesssim 1/\Lambda$.

2. Universality of the weak interaction. The presence of the f interaction should lead to a lowering of the value of the weak coupling constant for μ mesons. For example, the μ-decay constant should become smaller than the vector constant for β decay. The ratio of the probabilities for the decays $\pi \to \mu + \nu$ and $\pi \to e + \nu$, as well as for the decays $K \to \mu + \nu$ and $K \to e + \nu$, should become smaller than predicted by the theory of the universal V-A interaction. This can be easily understood physically: part of the time, when the muon goes over into the state $\mu + \chi$, it cannot participate in the weak interactions. Let us consider, for example, the correction due to the f interaction to the decay of the muon $\mu \to e + \bar{\nu} + \nu$. The effective decay constant G_μ will be equal to

$$G_\mu = GZ_2^{1/2}, \qquad G = 10^{-5} m_N^{-2},$$

where $Z_2^{1/2}$ is the renormalization of the ψ function of the muon owing to the f interaction.

It is natural to expect that the larger renormalization of the mass of the muon δm gives rise to a large renormalization of the ψ function $Z_2^{1/2}$. Unfortunately, the relation between δm and Z_2 established on the basis of Lehmann's spectral representation[5] is rather weak:

$$\delta m_\mu = m_\mu - m_\mu^0 = Z_2 \int_0^\infty [m_\mu \sigma_1(\varkappa^2) + \varkappa \sigma_2(\varkappa^2)]\, d\varkappa^2,$$

$$Z_2 = 1 + \int_0^\infty \sigma_1(\varkappa^2)\, d\varkappa^2,$$

where the spectral functions σ_1 and σ_2 satisfy the conditions

$$\sigma_1(\varkappa^2) \geqslant 0, \qquad \sigma_1(\varkappa^2) \geqslant \sigma_2(\varkappa^2) \geqslant -\sigma_1(\varkappa^2).$$

In first nonvanishing order of perturbation theory (see Fig. 2)

$$Z_2^{-1} = 1 + (f^2/4\pi) \ln(\Lambda^2/m_\chi^2),$$

which gives

$$(G - G_\mu)/G \approx (f^2/8\pi) \ln(\Lambda^2/m_\chi^2).$$

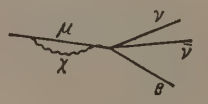

FIG. 2

The analysis of the experimental data indicates that this quantity is not larger than 5%, and may even be equal to zero (taking electromagnetic corrections into account).[6] This imposes definite restrictions on the value of f, m_χ, and Λ. Thus, for $f = 1/2$, $m_\chi = 10$ Bev, $\Lambda = 1000$ Bev, the quantity $(G - G_\mu)/G$ would be larger than 10%. In the following we shall consider two possibilities. In this and the next section, we shall consider a scheme in which only one type of neutrino exists. In such a scheme we expect a violation of the universality of the weak interaction, although we cannot now predict the extent of this violation.

The second possibility, which will be considered in Secs. 3 and 4, is to preserve the universality of the weak interaction even for values of f close to unity by assuming that there exist two types of neutrinos,[7,8] a muonic, ν_μ, and an electronic neutrino, ν_e, and that the muonic neutrino, like the muon, interacts with the χ meson through the f interaction.

3. Anomalous magnetic moment of the muon. The magnetic moment of the muon with account of the electromagnetic corrections is equal to[9]

$$\mu = g_e e/4m_\mu, \qquad g_e/2 = 1 + \alpha/2\pi + 0.75\alpha^2/\pi^2 = 0.001165.$$

The inclusion of the graph of Fig. 3 would lead to an increase in the value of g:

$$g_{e+f}/2 = g_e/2 + \delta; \qquad \delta = \frac{f^2}{\pi} \int_0^1 \frac{x^2(1-x)\,dx}{x^2 + (m_\chi/m_\mu)^2(1-x)}.$$

For $m_\mu/m_\chi \ll 1$ we have*

$$\delta \cong \frac{f^2}{3\pi} \frac{m_\mu^2}{m_\chi^2}.$$

*This formula is contained in a paper by Jouvet and Goldzahl.[4]

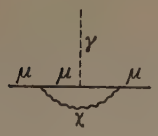

FIG. 3

Recalling that experimentally[10] $(g/2)_{exp} = 1.001145 \pm 0.000022$, we assume

$$(f^2/3\pi)\,(m_\mu^2/m_\chi^2) \lesssim 10^{-5}.$$

From this we obtain the following limit on the mass of the χ meson:

$$m_\chi \gtrsim 100 m_\mu f \approx 10 m_{nucl} f.$$

4. Four-fermion $\mu\mu$ interaction. The exchange of χ mesons should lead to an effective interaction between muons (see the graph of Fig. 4). This interaction has the form

$$\frac{4\pi f^2}{m_\chi^2 - k^2}\,(\bar{u}\gamma_\alpha u)\,(\bar{u}\gamma_\alpha u),$$

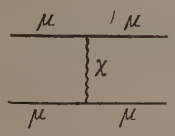

FIG. 4

where k is the four-momentum transferred by the χ meson and the u's are the spinors of the muon field. For $k^2 \ll m_\chi^2$ this interaction has the form of an effective four-fermion interaction

$$F\,(\bar{u}\gamma_\alpha u)\,(\bar{u}\gamma_\alpha u).$$

The data on the anomalous magnetic moment of the muon limit the possible values of the constant F:

$$F = 4\pi f^2/m_\chi^2 \lesssim 12\pi^2 \cdot 10^{-5}/m_\mu^2 = 1/10\, m_{nucl}^2.$$

The presence of such a $\mu\mu$ interaction should, in particular, lead to the creation of muon pairs by muons in the Coulomb field of the nucleus (one of the four graphs for this process is shown in Fig. 5). The contribution of this graph must be compared with the contribution of the pure electrodynamic graphs of the type of Fig. 6. The contributions of these graphs are comparable if

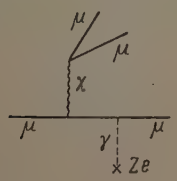

FIG. 5

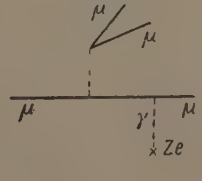

FIG. 6

$$f^2/m_\chi^2 \approx e^2/k^2, \quad \text{or} \quad \sqrt{k^2} \approx 10\, m_\mu \approx 1 \text{ Bev}.$$

Here $e^2 = \alpha = 1/137$, and k is the total four-momentum of the pair. $\sqrt{k^2}$ is the energy of the created pair $\mu^+ + \mu^-$ in its center-of-mass system (c.m.s.).

5. Production and decay of the χ meson. If the energy of the muons is sufficiently large, they can create χ mesons by scattering in the Coulomb field of the nucleus (two graphs of the type of Fig. 7). The cross section for this process $\sigma_{Z\chi}$ can be computed by the Weizsäcker-Williams method if the cross section $\sigma_{\gamma\chi}$ of the corresponding photo process $\gamma + \mu \to \chi + \mu$ is known. The cross section $\sigma_{\gamma\chi}$ is easily computed and is equal to

$$\sigma_{\gamma\chi} \approx (2\pi\alpha f^2/w^2)\ln(w^2/m_\mu^2).$$

Here w is the total energy of the photon and the muon in their c.m.s. (in deriving this formula we have assumed $w \geq m_\chi^2 \geq m_\mu^2$).

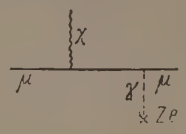

FIG. 7

For the cross section $\sigma_{Z\chi}$ we have

$$\sigma_{Z\chi} = \int \frac{Z^2\alpha}{\pi}\frac{dq^2}{q^2}\frac{dw^2}{w^2}\sigma_{\gamma\chi}.$$

Taking account of the fact that the finite dimensions of the nucleus "cut off" the momenta $\sqrt{q^2} > q_0$ ($q_0 \sim m_\pi A^{-1/3}$, where A is the number of nucleons in the nucleus), and that the conservation laws prescribe that the minimum value of $\sqrt{q^2}$ is equal to $\sqrt{q_{min}^2} = m_\chi^2/2E$ (E is the energy of the muon in the laboratory system), we find that for energies $E \ll E_0 = m_\chi^2/2q_0$ ($q_0^2 \ll q_{min}^2$) the cross section for production of χ mesons is small owing to the "friability" of the nucleus. The main contribution therefore comes from the creation of χ mesons, not on the nucleus as a whole, but on the separate nucleons in the nucleus. For a single proton ($q_0^{(p)} \approx 500$ Mev/c) with $E_\mu \gg m_\chi^2/2q_0^{(p)}$

$$\sigma_\chi \approx 10^{-33} - 10^{-34}\ \text{cm}^2.$$

The lifetime of the χ meson with respect to the decay $\chi \to \mu^+ + \mu^-$, computed in perturbation theory, is equal to

$$\tau = 1/f^2 m_\chi$$

Hence the χ meson should decay within a very short time (10^{-23} to 10^{-25} sec).

In Secs. 2, 3, and 4 we shall consider the possible interactions of the χ meson with other par-

ticles. These interactions would imply the possibility of the decays $\chi \to \nu + \bar{\nu}$, $\chi \to n\pi$, $\chi \to K + \bar{K}$, etc., the corresponding decay rates being comparable with the decay rate for $\chi \to \mu^+ + \mu^-$.

6. Interaction of the χ meson with the photon. Since the χ meson and the photon are vector particles, the transition $\chi \longleftrightarrow \gamma$ is possible (Fig. 8).*

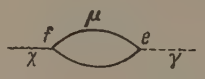

FIG. 8

The perturbation theoretical amplitude for this transition for small k^2 is equal to

$$M_{\chi\gamma} = k^2 (ef/3\pi) \ln (\lambda^2/m_\mu^2),$$

where k is the four-momentum of the photon and λ is the cut-off parameter. The occurrence of this transition implies that all charged particles (electron, proton, etc.) interact with the χ meson, where the coupling constant is equal to

$$f' = (\alpha f / 3\pi) \ln (\lambda^2 / m_\mu^2).$$

For $\lambda \sim 1000$ Bev we have $f' = 0.02\,f$.

Thus there occurs, for example, an effective four-fermion interaction between the muon and the electron

$$F' (\bar{u}_\mu \gamma_\alpha u_\mu)(\bar{u}_e \gamma_\alpha u_e), \text{ where } F' \approx 10^{-2} F.$$

We also obtain an interaction between the electron and the proton $F''(\bar{u}_e \gamma_\alpha u_e)(\bar{u}_p \gamma_\alpha u_p)$ and between two electrons $F''(\bar{u}_e \gamma_\alpha u_e)(\bar{u}_e \gamma_\alpha u_e)$, where $F'' \approx 10^{-4}$ F.

2. INTERACTION OF THE χ MESON WITH THE MUON AND WITH BARYONS

Up to this point we have only considered the interaction of the χ meson with the muon. Let us now discuss what observable effects would arise if the χ meson could also interact with strongly interacting particles. In the spirit of the Sakata model it is natural to consider the interaction of the χ meson with the baryon current J. In choosing a baryon current J which interacts with the χ meson there is some arbitrariness. In the following we shall consider two possible forms of the current:

$$J_\alpha = \bar{\Lambda} \gamma_\alpha \Lambda, \qquad J_\alpha = \bar{p} \gamma_\alpha p + \bar{n} \gamma_\alpha n.$$

This choice corresponds to a highly symmetric scheme of elementary particles.

*For a detailed discussion of this point see[11].

1. Symmetric scheme of elementary particles. If there exists only one type of neutrino, then there is a symmetry between the three leptons (μ^-, e^-, ν) and the three baryons in the Sakata model (Λ, n, p) which shows up in the Lagrangian of the weak interaction, as noticed by Gamba, Marshak, and Okubo.[12] This symmetry can be traced down more deeply* by assuming that all six particles are degenerate if all interactions are "switched off" and that all interactions are of the form of the electromagnetic interaction and are represented by the interaction of a conserved current with a vector field.

The electromagnetic interaction has the form

$$\sqrt{4\pi} e (\bar{e} \gamma_\alpha e + \bar{\mu} \gamma_\alpha \mu - \bar{p} \gamma_\alpha p) A_\alpha.$$

The strong interaction has the form[14,15]

$$\sqrt{4\pi} (\bar{\Lambda} \gamma_\alpha \Lambda + \bar{p} \gamma_\alpha p + \bar{n} \gamma_\alpha n) \rho_\alpha,$$

where ρ_α is the field of the neutral vector mesons (vectons, in the terminology of [15]). The switching-on of a strong charge g separates the baryons from the leptons and gives rise to the baryon masses. The introduction of the electric charges removes the degeneracy between e and ν and between n and p, whereas the degeneracy between n and Λ and between e and μ still persists. This degeneracy can be removed by the f interaction. Here we can assume that the f charge is attached either to the Λ hyperon or to the nucleons.

In the first case the f interaction will be of the form

$$\sqrt{4\pi} f (\bar{\mu} \gamma_\alpha \mu + \bar{\Lambda} \gamma_\alpha \Lambda) \chi_\alpha,$$

and in the second case, of the form

$$\sqrt{4\pi} f (\bar{\mu} \gamma_\alpha \mu + \bar{n} \gamma_\alpha n + \bar{p} \gamma_\alpha p) \chi_\alpha.$$

In this model the f interaction is responsible for the difference in the masses not only of μ and e, but also of Λ and n, and the f charge is a kind of representative of strangeness. Such a scheme, in which all particles are identical if the interactions are turned off and all interactions are universal (the charges of the various particles are identical, unless they are zero), is extremely symmetric and compact and provides a natural explanation of the isotopic invariance and strangeness.

2. Anomalous scattering of muons. The extension of the anomalous interaction to the baryons leads to a difference in the scattering of electrons and muons by nucleons and nuclei. This difference is related to the fact that in the scattering

*Certain other versions of the symmetric scheme have been discussed by the Nagoya group and by Marshak and Okubo.[13]

of muons not only the photon graph (Fig. 9), but also the χ meson graph (Fig. 10) gives a contribution, whereas the scattering of electrons is described by the photon graph alone. The vertex part NNγ has the form

$$\Gamma_\alpha^{(\gamma)} = \gamma_\alpha C_\gamma(q^2) + q_\beta \sigma_{\alpha\beta} M_\gamma(q^2),$$

where $C_\gamma(q^2)$ and $M_\gamma(q^2)$ are the electric and magnetic form factors of the nucleon.

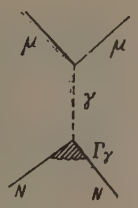

FIG. 9

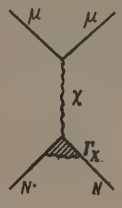

FIG. 10

The vertex part NNχ must have an analogous form:

$$\Gamma_\alpha^{(\chi)} = \gamma_\alpha C_\chi(q^2) + q_\beta \sigma_{\alpha\beta} M_\chi(q^2).$$

The amplitude for eN scattering, corresponding to the graph of Fig. 9, is equal to

$$e^2 q^{-2} (\bar{u}_e \gamma_\alpha u_e)(\bar{u}_N \Gamma_\alpha^\gamma(q^2) u_N).$$

The amplitude for μN scattering corresponding to the sum of the graphs of Figs. 9 and 10 can be written down in an analogous form:

$$e^2 q^{-2} (\bar{u}_\mu \gamma_\alpha u_\mu)(\bar{u}_N \Gamma_\alpha u_N),$$
$$\Gamma_\alpha = \gamma_\alpha C(q^2) + q_\beta \sigma_{\alpha\beta} M(q^2).$$

The deviations of the "effective" μ meson form factors $C(q^2)$ and $M(q^2)$ from the corresponding form factors of the electron are equal to

$$\frac{C(q^2)}{C_\gamma(q^2)} = 1 + \frac{f^2}{e^2}\frac{q^2}{q^2 - m_\chi^2}\frac{C_\chi(q^2)}{C_\gamma(q^2)},$$

$$\frac{M(q^2)}{M_\gamma(q^2)} = 1 + \frac{f^2}{e^2}\frac{q^2}{q^2 - m_\chi^2}\frac{M_\chi(q^2)}{M_\gamma(q^2)}.$$

These deviations can be of order unity for $q \sim 1$ Bev. Unfortunately, the cross section is in this case very small on account of the Coulomb form factor. The data [16] indicate that for momentum transfers $q \sim 300$ Mev/c there is no deviation of the observed angular distribution from the pure electrodynamic distribution within an accuracy of 20%.

In the case of the interaction

$$\sqrt{4\pi} f (\bar{p}\gamma_\alpha p + \bar{n}\gamma_\alpha n)\chi_\alpha,$$

it is easy to see that

$$\Gamma^{(\chi)}(q^2) = \Gamma^{(\gamma)s}(q^2),$$

where $\Gamma^{(\gamma)s}$ is the isoscalar component of the form factor $\Gamma^{(\gamma)}$.

In the case where the Λ particle interacts with the χ meson, the interaction of the χ meson with the nucleons can be due only to graphs of the type of Fig. 11. One should expect in this case that

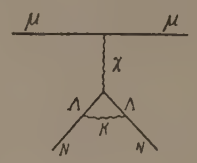

FIG. 11

for nucleons $C_\chi \sim q^2/m_K^2$, $M_\chi \sim 1/m_K$.

3. Pair production by muons. The existence of the interaction

$$\sqrt{4\pi} f (\bar{p}\gamma_\alpha p + \bar{n}\gamma_\alpha n + \bar{\mu}\gamma_\alpha \mu)\chi_\alpha \quad \text{or} \quad \sqrt{4\pi} f (\bar{\Lambda}\gamma_\alpha \Lambda + \bar{\mu}\gamma_\alpha \mu)\chi_\alpha$$

should lead to the production of pairs $\mu^+ + \mu^-$ in nuclear collisions. If the energy in the center of mass system exceeds the threshold for creation of a real χ meson, such pairs will be produced through creation of a real χ meson with subsequent decay $\chi \to \mu^+ + \mu^-$. In practice such a process should look like the emission of a μ^+, μ^- pair from a high energy star. For $f \sim 1$, the probability for this process relative to multiple production processes will be determined by its statistical weight. If the energy is sufficiently large compared to the threshold for χ production, the cross section for production of χ can be of the order of one percent of the total strong interaction cross section. For $f^2 = \alpha$ the probability for χ production will be comparable with the probability for emission of hard photons with energies larger than m_χ. If the energy is insufficient for χ production, the contribution of the graph with a virtual χ meson relative to the contribution of the corresponding electromagnetic graph will be given by the ratio of f^2/m_χ^2 to e^2/k^2.

3. INTERACTION OF THE χ MESON WITH THE MUON AND WITH THE MUONIC NEUTRINO

1. Universality of the weak interaction in the scheme with two neutrinos. If the μ meson is the only lepton with an f interaction and there exists only one neutrino, then the decay $\mu \to e + \gamma$ should occur and the universality of the weak interaction should be strongly violated, as shown above. These difficulties can be avoided by assuming that the neutrinos which appear in the weak current paired with μ and e are different particles. [7] Then the weak lepton current is written in the form

$$J_\alpha = (\bar{\mu}\gamma_\alpha(1+\gamma_5)\,\nu_\mu) + (\bar{e}\gamma_\alpha(1+\gamma_5)\,\nu_e),$$

One further assumes that not only the μ meson, but also the neutrino ν_μ has an f interaction:

$$\sqrt{4\pi} f\,(\bar{\mu}\gamma_\alpha\mu + \bar{\nu}_\mu\gamma_\alpha\nu_\mu)\,\chi_\alpha.$$

We note that the γ_5 invariance of the f interaction insures that the anomalous interaction of the ν_μ neutrino will not give it a nonvanishing mass if the bare mass $m^0_{\nu_\mu}$ is exactly equal to zero.

In the case under consideration the renormalized weak coupling constant is equal to

$$G_\mu = Z_1^{-1}\sqrt{Z_2^\mu Z_2^\nu}\,G,$$

where Z_1, Z_2^μ, and Z_2^ν are the renormalization constants of the $\bar{\mu}\nu_\mu$ vertex parts of the weak interactions and of the Green's functions of the muon and the muonic neutrino. The corresponding first order graphs in perturbation theory are shown in Fig. 12. The renormalization will, in general, be different for the vector and axial vector vertices of the $\bar{\mu}\nu_\mu$ current as a consequence

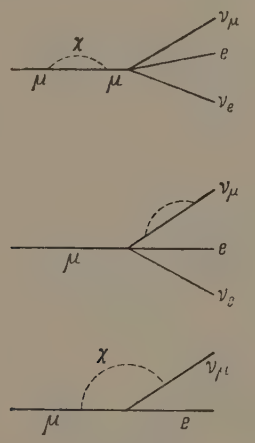

FIG. 12

of the difference between $Z_1(V)$ and $Z_1(A)$. However, it is easily seen that the divergent terms in Z_2 and Z_1 cancel both for G_V and G_A. This is connected with the fact that the divergent terms in Z_2 and Z_1, which are proportional to $\ln(\Lambda^2/m_\chi^2)$, occur in the region of virtual momenta $\Lambda^2 > k^2 > m_\chi^2$. In this region the mass difference of the muon and neutrino can be neglected and the A and V interactions are indistinguishable, so that the divergent terms in Z_2 and Z_1 cancel in the same way as in the case of electrodynamics.

The remaining finite corrections leading to the renormalization of G and to a removal of the equality of $G_V^{(\mu)}$ and $G_A^{(\mu)}$ are of the order

$$f^2\,(m_\mu^2/m_\chi^2)\ln(m_\chi^2/m_\mu^2)$$

and are small for $f^2 \leq 1$ ($m_\mu \ll m_\chi$). We note that the existence of an interaction between the χ meson and the muon and the muonic neutrino gives rise to a form factor in the $\bar{\mu}\nu_\mu$ vertex of the μ decay in the same way as the strong interaction gives rise to a form factor in the $\bar{p}n$ vertex in β decay. This may serve as an explanation for the fact that the equality of the β and μ decay constants is not destroyed by higher corrections in the weak interaction.

2. Interaction of the muonic neutrino. The existence of the interaction $\sqrt{4\pi}\,f\,(\bar{\nu}_\mu\gamma_\alpha\nu_\mu)\,\chi_\alpha$ would lead to interactions of the muonic neutrino which are considerably stronger than in the case where the only interaction of the neutrino is the usual weak interaction. Sufficiently energetic neutrinos will, in particular, lead to the creation of μ meson pairs in the Coulomb field of the nucleus (graph of Fig. 13). The cross section for this process, computed by the Weizsäcker-Williams method, is equal to, for $E_\nu \gg 2m_\mu^2/q_0$,

$$\sigma \sim \frac{e^2F^2Z^2E_\nu q_0}{\pi^3}\ln\frac{q_0E_\nu}{m_\mu^2},$$

where q_0 is the maximal momentum which can be transferred to the nucleus. For $F = \frac{1}{10}m_N^2$,

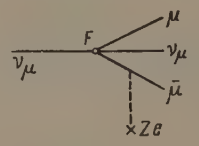

FIG. 13

$Z = 82$, $E_\nu \sim 10$ Bev, this cross section is of the order of 10^{-32} to 10^{-31} cm^2.

Since the χ meson interacts with the electromagnetic currents with a strength given by the constant f' (see Sec. 1, item 6), the muonic neutrinos will also have a similar interaction with a strength given by the constant F'. We note that an interaction of this strength is excluded for the electronic neutrinos by the experiment of Reines and Cowen,[17] which gives the upper limit $\sigma < 10^{-42}$ cm^2 for the cross section of the scattering of a β decay neutrino by an electron.

4. INTERACTION OF χ MESONS WITH MUONS, NEUTRINOS, AND BARYONS

In this section we shall consider the case where the χ meson interacts not only with the current $\bar{\mu}\gamma_\alpha\mu + \bar{\nu}_\mu\gamma_\alpha\nu_\mu$, but also with the baryon currents

$$\bar{n}\gamma_\alpha n + \bar{p}\gamma_\alpha p \quad \text{or} \quad \bar{\Lambda}\gamma_\alpha\Lambda.$$

In this case the scattering of the neutrino by nucleons will be described by the graph of Fig. 14.

FIG. 14

For an interaction of the first type at small energies, where the nucleon form factors are unimportant, the cross section for the scattering of a neutrino by a nucleon will be equal to

$$\sigma = \frac{F^2}{2\pi}\frac{E^2}{1+2E/m_N}\left[1+\frac{4}{3}\frac{(E/m_N)^2}{(1+2E/m_N)^2}\right],$$

where E is the initial energy of the neutrino in the laboratory system and m_N is the nucleon mass.

Beginning with an energy of order 1 Bev, where the cross section reaches values of order 10^{-31} cm^2 (for $F = (1/10)m_N^2$), the cross section will cease to increase because of the nucleon form factor.

In the scattering of a high energy neutrino by nucleons and nuclei the cross section for inelastic processes with creation of π mesons and strange particles will make up a considerable part of the total cross section. We note also that an interaction of this type can lead to the emission of $\bar{\nu}$, ν pairs by metastable nuclei.

CONCLUSION

On the basis of the preceding analysis of the anomalous interaction of the μ meson we can draw the following conclusions:

1. If there exists only one neutrino, one may expect a violation of the universality of the weak interaction.

2. If there exist two neutrinos, one may expect that the muonic neutrino has an anomalous interaction.

The available experimental data do not exclude the possibility of neutrino cross sections of order 10^{-31} cm^2, so that the corresponding experiments are not in contradiction with our arguments. One may think that some of our conclusions are not specific to the model considered by us and will therefore also be valid for more general forms of the structure of the anomalous interaction.

The authors thank A. I. Alikhanov, A. A. Ansel'm, V. N. Gribov, Ya. B. Zel'dovich, B. L. Ioffe, V. A. Lyubimov, V. B. Mandel'tsvaĭg, I. Ya. Pomeranchuk, and B. M. Pontecorvo for numerous discussions of the theoretical questions related to our model and of the possibilities of its experimental verification.

[1] J. Schwinger, Ann. of Phys. **2**, 407 (1957).
[2] W. S. Cowland, Nucl. Phys. **8**, 397 (1958).
[3] I. R. Gatland, Nucl. Phys. **9**, 267 (1958).
[4] B. Jouvet and L. Goldzahl, Nuovo cimento **18**, 702 (1960).
[5] H. Lehmann, Nuovo cimento **11**, 342 (1958).
[6] R. P. Feynman, Proc. of the 1960 Ann. Int. Conf. on High Energy Phys. at Rochester, Univ. of Rochester, 1960, p. 501.
[7] B. Pontecorvo, JETP **37**, 1751 (1959), Soviet Phys. JETP **10**, 1236 (1960).
[8] T. D. Lee and C. N. Yang, Phys. Rev. Lett. **4**, 307 (1960).
[9] C. M. Sommerfield, Phys. Rev. **107**, 328 (1957).
[10] Charpak, Farley, Garwin, Muller, Sens, Telegdi, and Zichichi, Phys. Rev. Lett. **6**, 128 (1961).
[11] Kobzarev, Okun', and Pomeranchuk, JETP (in press).
[12] Gamba, Marshak, and Okubo, Proc. Nat. Acad. Sci. **45**, 881 (1959).
[13] Maki, Nakagawa, Ohnuki, and Sakata, Progr. Theor. Phys. **23**, 1174 (1960). R. Marshak and S. Okubo (preprint).
[14] J. Fujii, Progr. Theor. Phys. **21**, 232 (1959).
[15] I. Kobzarev and L. Okun', JETP (in press).
[16] Heggie, Kim, Masek, and Williams, Proc. of the 1960 Ann. Int. Conf. on High Energy Phys. at Rochester, Univ. of Rochester, 1960, p. 793.
[17] C. L. Cowan Jr. and F. Reines, Phys. Rev. **107**, 528 (1957).

Translated by R. Lipperheide
209

ANALYTIC PROPERTIES OF THE SQUARE DIAGRAM WITH DECAY MASSES

V. N. GRIBOV, G. S. DANILOV, and I. T. DYATLOV

Leningrad Physico-Technical Institute, Academy of Sciences of the U.S.S.R.

Submitted to JETP editor April 28, 1961

J. Exptl. Theoret. Phys. (U.S.S.R.) 41, 1215-1220 (October, 1961)

The analytical properties of the simplest square diagram of perturbation theory are investigated for the case in which the masses of the external particles do not satisfy the condition of stability.

1. In a previous paper by the writers [1]* a study was made of the analytical properties of the simplest square diagram with arbitrary masses (Fig. 1). The specific form of the dispersion representations with respect to energy and momentum transfer (μ_{13} and μ_{24}) for the amplitude A of the diagram was found for any values of the external masses that satisfy the condition of stability:

$$\mu_{ik} = (m_i^2 + m_k^2 - p_{ik}^2)/2m_i m_k > -1.$$

From the study made in I it could be seen that as soon as one of the masses (for example, μ_{12}) has a value that makes decay possible, the corresponding singularity of $\Delta^{(-)}(\mu_{12}, \mu_{23})$ [Eq. I (12)], from which the integration over μ_{13} starts in the dispersion integral for A [Eq. I (29)], goes off into the complex plane; this means that there is a complex singularity of $A(\mu_{ik})$ as a function of μ_{13}, and therefore Im $A \neq 0$ for all real μ_{13} and μ_{24}.

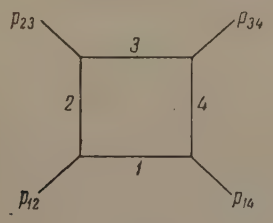

FIG. 1

In the present paper we shall show that in the decay case the imaginary part of A is determined not only by the usual absorption part of the scattering $A_1(\mu_{ik})$ [Eq. I (2)], but also by the decay absorption part $A_d(\mu_{ik})$. The latter is different from 0 for all μ_{13} and μ_{24}. This result, obtained by analytic continuation with respect to the external masses, obviously agrees with the unitarity condition, from which it follows that for a decay value of the mass μ_{12} the imaginary part of the process comes not only from the fact that a real intermediate state with particles 1 and 3 exists, but also from the existence of a real state with particles 1 and 2, through which the process can go (see below, Fig. 3). Thus in the decay case it is possible to write A either in the form of a dispersion integral over a complex path of μ_{13} (or of μ_{24}), or in the form of the integral along the real axis of $\mu_{13}(\mu_{24})$ from $-\infty$ to ∞ of the absorption parts A_1 and A_d (or A_2 and A_d).*

It is obvious that the results obtained not only are valid for the diagram considered, but to some extent characterize the analytic properties of any decay process involving four particles. Moreover, since in the decay case a given diagram can be regarded as the simplest diagram with five external lines [two external lines at the vertex (12)], the existence of complex singularities and absorption parts with respect to different variables (of the type of energy and mass) is for five-branch vertices (and for many-branch vertices) already a general rule, which does not arise as an exception for certain masses of the particles involved, but always exists for definite values of the external parameters (including physical values of these parameters).

2. We consider the case in which only one mass μ_{12} has a decay value, and shall set the others, μ_{23}, μ_{34}, and μ_{14}, equal to each other [the definition of the amplitude A is given by Eq. I (1)], that is,

$$1 > \mu_{23} = \mu_{34} = \mu_{14} = \mu > 0. \qquad (1)$$

According to the analysis carried out in I, the condition (1) means that the singularities of A_1 that correspond to these masses— $\Delta^{\pm}(\mu_{34}, \mu_{14})$ and $\Delta^{\pm}(\mu_{23}, \mu_{34})$ [cf. Eqs. I (12) and I (13)] —are not

*In the present paper we use the notations of [1], which is hereafter cited as I.

*A_2 is the absorption part that corresponds to conditions in which μ_{24} is the energy and μ_{13} is the momentum transfer (Fig. 5, a).

singularities of A (normal case with respect to these masses).

This simple symmetrical case contains within it all the essential features of the decay diagram, and at the same time is free from the superfluous complications characteristic of the case of different masses, which are of no importance in principle. Later we shall indicate the main differences that arise in the general case; they will follow directly from the analysis of I and the considerations given here. It follows from Eqs. I (12) and I (13) that for equal masses the singularities of the absorption part A_1 are of the forms

$$\Delta^{(\pm)} = \Delta^{(\pm)}(\mu_{34}, \mu_{14}) = \Delta^{(\pm)}(\mu_{23}, \mu_{34}) = 1 \text{ or } 2\mu^2 - 1, \quad (2)$$

for the upper and lower signs, respectively, and

$$\Delta^{(\pm)}(\mu_{12}) = \Delta^{(\pm)}(\mu_{12}, \mu_{23}) = \Delta^{(\pm)}(\mu_{12}, \mu_{14})$$

$$= \mu\mu_{12} \pm \sqrt{(1-\mu^2)(1-\mu_{12}^2)}. \quad (3)$$

Analogous simplifications can also be made for the singularities of $\square(\mu_{13})$ and $\square(\mu_{24})$ (cf. I), but their analytic form is not important, and they are shown graphically for the case in which we are interested in Fig. 2 (curves I—V).

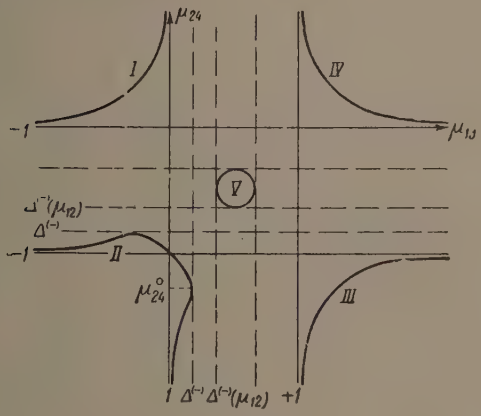

FIG. 2

Let us use the results of I for the case $\theta_{12} + \theta_{23} + \theta_{34} + \theta_{14} < 2\pi$, $\theta_{23} = \theta_{34} = \theta_{14} < \pi/2$, $\theta_{12} < \pi$. Figure 2 shows the positions of the singularities of the absorption part A_1 in this case. For $\mu_{24} > 1$ we have the dispersion relation [Eq. I (29)]:

$$A(\mu_{13}, \mu_{24}) = -\frac{1}{\pi}\int_{-\infty}^{-1} \frac{A_1(\mu_{24}, \mu'_{13})\, d\mu'_{13}}{\mu'_{13} - \mu_{13}} + A_{an}(\mu_{13}, \mu_{24}), \quad (4)$$

$$A_{an}(\mu_{13}, \mu_{24}) = -i\frac{1}{\pi}\int_{-1}^{\Delta^{(-)}(\mu_{12})} \frac{\rho(\mu_{24}, \mu'_{13})\, d\mu'_{13}}{\mu'_{13} - \mu_{13}}, \quad (5)$$

$$\rho = 2\pi\,[\sqrt{K(\mu_{ik})}]^{-1}. \quad (6)$$

$A_1(\mu_{ik})$ and $K(\mu_{ik})$ are defined by the formulas:

$$A_1 = \frac{1}{\sqrt{K(\mu_{ik})}} \ln \frac{V + \sqrt{(\mu_{13}^2 - 1)K(\mu_{ik})}}{V - \sqrt{(\mu_{13}^2 - 1)K(\mu_{ik})}},$$

$$V = (\mu_{13} - 1)[\mu_{24}(\mu_{13} + 1) - \mu(\mu_{12} + \mu)]; \quad (7)$$

$$K(\mu_{ik}) = (\mu_{13}^2 - 1)(\mu_{24}^2 - 1) - 2\mu(\mu_{13} - 1)(\mu_{24} - 1)(\mu + \mu_{12})$$

$$+ (\mu^2 - 1)(\mu - \mu_{12})^2. \quad (8)$$

As compared with the analogous formulas I (3) and I (5) we have changed the sign in Eq. (7) and in the first term of Eq. (4). In the integral (5) $\sqrt{K} = i|\sqrt{K}|$.

For $\mu_{24} < \Delta^{(-)}(\mu_{12})$ [cf. Eq. I (55)] we have

$$A(\mu_{13}, \mu_{24}) = \frac{1}{\pi^2}\iint d\mu'_{13}\, d\mu'_{24} \frac{\rho(\mu'_{13}, \mu'_{24})}{(\mu'_{13} - \mu_{13})(\mu'_{24} - \mu_{24})}$$

$$+ A'_{an}(\mu_{13}, \mu_{24}), \quad (9)$$

$$A'_{an}(\mu_{13}, \mu_{24}) = -\frac{i}{\pi}\int_{\Delta^{(-)}}^{\Delta^{(-)}(\mu_{12})} \frac{\rho(\mu'_{13}, \mu_{24})\, d\mu'_{13}}{\mu'_{13} - \mu_{13}}$$

$$-\frac{2i}{\pi}\int_{\square^{(-)}(\mu_{24})}^{\Delta^{(-)}} \frac{\rho(\mu'_{13}, \mu_{24})\, d\mu'_{13}}{\mu'_{13} - \mu_{13}} \quad (10)$$

for $\mu_{24} > \mu_{24}^0$ [μ_{24}^0 is the point of reversal of the curve of $\square_{II}(\mu_{13})$, cf. Fig. 2], and

$$A'_{an} = -i\frac{1}{\pi}\int_{\Delta^{(-)}}^{\Delta^{(-)}(\mu_{12})} \frac{\rho(\mu'_{13}, \mu_{24})\, d\mu'_{13}}{\mu'_{13} - \mu_{13}} \quad (11)$$

with $\mu_{24} < \mu_{24}^0$.

In the first term of Eq. (9) the integration is taken over the region inside the curve II and $\sqrt{K} > 0$. In Eqs. (10) and (11) $\sqrt{K} = -i|\sqrt{K}|$. As was shown in I, with these definitions curve II is not a singularity of the amplitude A.

3. The formulas (4) — (11) are analytic in μ_{12}, and therefore we can continue them in this variable and obtain a representation of the amplitude A for the decay case. The point $\mu_{12} = -1$ is obviously a singularity of the function A, and therefore the passages around this point by the paths $\mu_{12} \pm i\epsilon$ lead to different results. The Feynman amplitude (with negative imaginary quantities added to the internal masses) corresponds to the path $\mu_{12} - i\epsilon$. With this path all of the formulas (4) — (11) hold as before, but the point $\Delta^{(-)}(\mu_{12})$ of Eq. (3) goes off into the upper half-plane. This means that in the variable μ_{13} (and by symmetry also in μ_{24}) the Feynman amplitude A for the diagram of Fig. 1 with the decay mass has a complex singularity in the upper half-plane. Thus there is no region on the real axis of μ_{13} in which

Im A = 0, and the dispersion relation in μ_{13} contains an integration over a complex path. Since the singularity lies in the upper half-plane and there are no complex singularities in the lower half-plane, we can write instead of the relations (4) — (11) with a complex path relations on the real axis of μ_{13}, but with infinite limits.

Let us examine the case $\mu_{24} > 1$. Then we have from Eqs. (4) and (5)

$$A(\mu_{13}, \mu_{24}) = -\frac{1}{\pi}\int_{-\infty}^{-1}\frac{A_1(\mu'_{13}, \mu_{24})\,d\mu'_{13}}{\mu'_{13}-\mu_{13}} - \frac{1}{\pi}\int_{-\infty}^{+\infty}\frac{A_d(\mu'_{13}, \mu_{24})\,d\mu'_{13}}{\mu'_{13}-\mu_{13}}, \quad (12)$$

$$A_d(\mu_{ik}) = \operatorname{Im} A_{an} \quad (\mu_{13} = \mu_{13} - i\varepsilon). \quad (13)$$

The specific expression for $A_d(\mu_{ik})$ for the diagram of Fig. 1 can be obtained directly from Eq. (13) if we note that it follows from Eqs. (5) and (13) that:

$$A_d(\mu_{13}, \mu_{24}) = -\frac{i}{\pi}\int_{\Delta^{*(-)}(\mu_{12})}^{\Delta^{(-)}(\mu_{12})}\frac{\rho(\mu'_{13}, \mu_{24})\,d\mu'_{13}}{\mu'_{13}-\mu_{13}}, \quad (14)$$

if in Eq. (5) the path from the point -1 runs off at once into the complex region.

The calculation of the integral (14) is not especially difficult, though it is somewhat cumbersome. We are much more interested, however, in the physical meaning of $A_d(\mu_{ik})$ than in the concrete expression, and therefore we shall conduct the calculation of $A_d(\mu_{ik})$ in a different way, which leads to the same result as Eq. (14), but is much more closely connected with the physics.

The region $\mu_{24} > 1$ and $\mu_{13} > -1$ (region I of Fig. 2) is the physical region of the reaction in which particles with momenta p_{12} and p_{23} are converted into particles with momenta p_{34} and p_{14} ($p_{12}, p_{23} \to p_{34}, p_{14}$). In this region, for $\mu_{12} < -1$, the imaginary part of the amplitude A can be found from the relation of unitarity and is equal to the sum of the absorption parts which correspond to the fact that the process goes through real intermediate states with particles (1, 3) and (1, 2) (Fig. 3, a and b). (In Fig. 3 the lines that separate the initial and final states in the unitarity condition are marked with crosses.)

The state (1, 3) leads to the appearance of the absorption part A_1, which is given by Eq. (7) in the region $\mu_{13} < -1$ and is zero for $\mu_{13} > -1$ (Fig. 3, a). Therefore A_d in the physical region $\mu_{13} < -1$ is the decay absorption part with the intermediate state (1, 2) (Fig. 3, b). For $\mu_{13} > -1$,

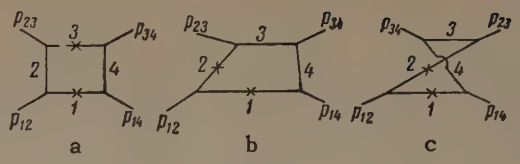

FIG. 3

$\mu_{24} > 1$ there is no physical region of the direct reaction ($p_{12}, p_{23} \to p_{34}, p_{14}$), but here (in region IV, Fig. 2) there is a physical region of the reaction ($p_{14}, p_{23} \to p_{34}, p_{12}$). The diagram of Fig. 1 has no absorption part in the energy of the crossing reaction, $(p_{23} + p_{14})^2$ but in this region it does have a decay absorption part A_d (Fig. 3, c), which is then the imaginary part of A.

In the two physical regions we can find A_d from the unitarity condition, and of course get the same expression in both,

$$A_d = \frac{1}{\sqrt{K(\mu_{ik})}}\ln\frac{V_d + \sqrt{(\mu_{12}^2-1)K(\mu_{ik})}}{V_d - \sqrt{(\mu_{12}^2-1)K(\mu_{ik})}},$$

$$V_d = \mu_{12}\mu_{13}\mu_{24} + \mu(\mu_{13}+\mu_{24}) + \mu[\mu_{12}(\mu-\mu_{12})+1]. \quad (15)$$

Outside the physical regions the imaginary part of A will coincide with the sum of the absorption parts wherever the analytic continuations of A_1 and A_d are real. As is shown in I, A_1 is real right up to the curve II (Fig. 2). As for A_d, if the expression (15) is defined as real in one of the regions I or IV, it must be complex in the other. Since in the physical regions A_d must be a real function, we cannot define the decay absorption part as the expression (15) with the principal value of the logarithm in region I (or IV) and as its analytic continuation in region IV (or I). But if we take A_d as real in both regions I and IV, as follows from the unitarity condition, then in the intermediate region $-1 < \mu_{13} < 1$ we get different values of A_d, depending on which region, $\mu_{13} > 1$ or $\mu_{13} < -1$, we start from for the continuation of the expression (15).

This, however, is only a seeming ambiguity. The formulas (4), (5), (12), and (14) do not contain it. The ambiguity is due to the fact that in the term A_{an} in Eqs. (4) and (5) we can integrate over paths leaving the real axis at different points, i.e., in Eq. (5) we can separate the integrals from the real axis -1 to some point $\tilde{\mu}_{13}$. In Eq. (14) this would correspond to different points of intersection of the path of integration with the real axis. This would also lead to redefinition of A_1 and A_d and to different points $\tilde{\mu}_{13}$, up to which the decay absorption part (15) is defined as the analytic continuation from the right or from the left. If we have

the formulas (4), (5), and (10), then the redefinition of A_d, Eq. (15), occurs at the point $\mu_{13} = -1$.* In the decay case the point $\mu_{13} = -1$ is the only remaining real singularity of A. We can redefine the point $\mu_{13} = \Delta^{(-)}$. Then

$$A(\mu_{13}, \mu_{24}) = -\frac{1}{\pi}\int_{-\infty}^{-1}\frac{A_1(\mu'_{13}, \mu_{24})\,d\mu'_{13}}{\mu'_{13}-\mu_{13}} - \frac{i}{\pi}\int_{-1}^{\Delta^{(-)}}\frac{\rho(\mu'_{13}, \mu_{24})\,d\mu'_{13}}{\mu'_{13}-\mu_{13}}$$

$$-\frac{1}{\pi}\int_{-\infty}^{+\infty}\frac{A'_d(\mu'_{13}, \mu_{24})\,d\mu'_{13}}{\mu'_{13}-\mu_{13}}. \qquad (16)$$

The formula (16) has the convenience that its first two terms are easily continued into the region $\mu_{24} < 1$, and give the first term in Eq. (9). Since all of the formulas remain analytic up to $\mu_{24} \geq \Delta^{(-)}$, Eqs. (12) and (16), with A_1 and A_d defined by Eqs. (7) and (15), remain valid in this entire region.

4. In the region $\mu_{24} < \Delta^{(-)}$ let us first consider values $\mu_{24} < -1$, since they are of the greatest interest. Using the same transformation as in Eq. (12) on the integral (10) over a complex path, to convert it into an integral over μ_{13} from $-\infty$ to $+\infty$, we can identify the various terms in the imaginary part of A with the absorption parts that arise in the physical regions.

The physical region for the reaction of decay of particle p_{12} into p_{14}, p_{23}, p_{34} is in the lower left quadrant of Fig. 2. In this region the imaginary part of A is given by three absorption parts A_d, A_1, and A_2 (Fig. 4, a, b, c). The concrete forms of A_1 and A_d for the diagram in question are given by Eqs. (7) and (15), where the logarithm is defined as the principal value inside curve II of Fig. 2. The quantity A_2 (Fig. 4, c) is the absorption part that arises owing to the fact that for $\mu_{24} < -1$ the decay can go through a real intermediate state with particles 2 and 4. The concrete form of A_2 is obtained from Eq. (7) by the interchange $\mu_{13} \rightleftarrows \mu_{24}$. In the lower right quadrant there is the physical region of the reaction (p_{23}, $p_{34} \rightarrow p_{12}$, p_{14}), in which the nonvanishing absorption parts are A_2 and A_d (Fig. 5, a, b). Thus for $\mu_{24} < -1$ Eq. (9) is equivalent to the following formula:

$$A(\mu_{13}, \mu_{24}) = -\frac{1}{\pi}\int_{-\infty}^{-1}\frac{A_1(\mu'_{13}, \mu_{24})\,d\mu'_{13}}{\mu'_{13}-\mu_{13}}$$

$$-\frac{1}{\pi}\int_{-\infty}^{+\infty}\frac{[A_d(\mu'_{13}, \mu_{24}) + A_2(\mu'_{13}, \mu_{24})]\,d\mu'_{13}}{\mu'_{13}-\mu_{13}}. \qquad (17)$$

*As we go around the point $\mu_{13} = -1$ the integral (5) gets just the added imaginary part that returns the logarithm (15) to its principal value.

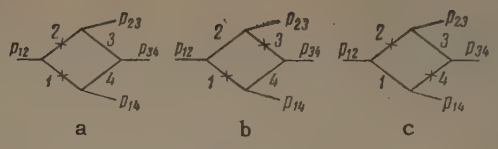

FIG. 4

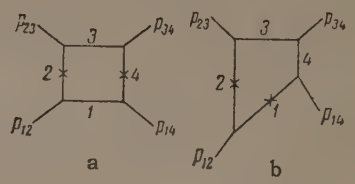

FIG. 5

It can be shown that the formulas (9) — (11) correspond to the definition of A_d and A_2 in which the analytic continuation of Eqs. (7) and (15) from both physical regions is taken up to the point $\mu_{13} = \Delta^{(-)}$.

Finally, in the region $\Delta^{(-)} > \mu_{24} > -1$ the formula (12) is retained, with A_1 and A_d defined by continuation with respect to μ_{24} from the regions II and III; for A_d the redefinition in terms of μ_{13} is accomplished just as in Eq. (17) for $\mu_{13} = \Delta^{(-)}$.

5. If the masses of the particles do not satisfy Eq. (1), but, as before, only one mass has a value permitting decay, then there is nothing new in principle as compared with the case treated in I. The changes correspond entirely to the complications that arise in I, and are explained by the unsymmetrical position of the curves I — IV and the appearance of singularities $\Delta^{(-)}$ of A, which correspond to anomalous masses. This leads to a change of the points of redefinition of the absorption parts (for example, for $\mu_{24} > 1$ the point in question does not coincide with the point $\mu_{13} = -1$, but is equal to one of the $\Delta^{(-)}$). In formulas of the type of Eq. (12) or Eq. (17) there are anomalous added quantities from the other masses (see I).

If we have a diagram with two masses $\mu_{ik} < -1$, another decay absorption part appears, and makes a contribution in Eqs. (12) and (17). If the decay masses are μ_{12} and μ_{23} (two adjacent masses), then the singularity of $\Delta(\mu_{12}, \mu_{23})$ in the variable μ_{13} is on the real axis, and the singularities in μ_{24} go off into the complex plane. As before, the integral (5) will be taken along a real path, but is the integral of a complex function, since in this case the singularity of ρ lies on the path of integration in Eq. (5). The integral (5) can again be transformed into an integral from $-\infty$ to $+\infty$ of the sum of two decay absorption parts. The same result is obtained in the case of masses located along a diagonal.

In a certain sense the decay case is even simpler and more intuitive than the anomalous case (cf. I). This is due to the fact that it is more closely connected with the unitarity relation, and it is from this relation that all of the dispersion parts that occur in the dispersion relations for the decay masses are obtained. This connection is possible owing to the fact that there is no region of real μ_{13} and μ_{24} which would be separated by singularities from all the physical regions. In the anomalous case there is such a region, and the analytic continuation of the unitarity condition into it is difficult.

It is just for this reason that the physical interpretation[2] of the anomalous added terms is not directly connected with the unitarity condition.

[1] Gribov, Danilov, and Dyatlov, JETP 41, 924 (1961), Soviet Phys. JETP 14, 659 (1962).

[2] Y. Nambu, Nuovo cimento 9, 610 (1958). R. Oehme, Phys. Rev. 111, 1430 (1958).

Translated by W. H. Furry
210

THEORY OF REACTIONS INVOLVING THE FORMATION OF THREE PARTICLES NEAR THRESHOLD. THE τ DECAY

V. N. GRIBOV

Leningrad Physico-Technical Institute, Academy of Sciences, U.S.S.R.

Submitted to JETP editor April 28, 1961

J. Exptl. Theoret. Phys. (U.S.S.R.) 41, 1221-1230 (October, 1961)

It is shown that for an arbitrary reaction involving the formation of three particles one can separate (with an accuracy to terms which are linear in energy) the long-range interaction contribution, which is proportional to the pair-interaction amplitudes and cannot be expanded into a series in the above-threshold momenta. A separation of this type allows us to determine the scattering amplitude for unstable particles at zero energy by analyzing the reactions in which they are produced. The reactions $K^+ \to 2\pi^+ + \pi^-$ and $2\pi^0 + \pi^+$ are considered in detail.

1. INTRODUCTION

REACTIONS involving formation of three particles are at present the only practical means of studying interactions between unstable particles. However, it is often impossible to extract information on the amplitudes of interactions of unstable particles from data on the energy and angular distributions in the reactions by which they are produced, owing to the complex character of the production and subsequent three-particle interaction. The only exceptions are cases of sharply pronounced resonances, so that experimental investigations frequently reduce to searches for such resonances.

One of the most important theoretical problems in this field is to ascertain whether it is possible to gain unambiguous information on the amplitude of pair interactions from an analysis of reactions in which three particles are produced. This question is the subject of many papers, most noteworthy of which is that of Chew and Low,[1] who proposed to determine the pair interaction amplitude by analytic continuation of the amplitude of particle production in the momentum transfer variable.

Several methods have been proposed[2-4] for determining the zero-energy amplitude of scattering on stable particles from an analysis of the reactions near threshold. It was shown earlier[2] that the correlation between the momenta of the produced particles depends essentially on the interaction in the final state and can serve as a means of determining the scattering amplitudes.

We shall show in the present paper that it follows even from the results of [2] that the energy distribution of the produced particles also depends appreciably on the scattering amplitudes of the particle pairs.

In view of the presence of interaction in the final state, it becomes impossible to expand the reaction probability in the momenta of the produced particles and to retain only a few terms at low energy. The probability of the reaction depends in essential fashion on the ratios of the particle momenta to their possible maximum value at specified full energy. Accurate to quantities of order $(kr_0)^2$, where k^2 is the mean square of the momentum of the produced particles and r_0 is the interaction radius, this dependence can be determined and the reaction probability expressed in terms of the pair-interaction amplitudes at zero energy and a small number of constant parameters [formulas (5) and (6)]. The additional parameters are due to the interaction at small distances and in the p state of relative motion. The result obtained allows us in principle to determine the pair interaction amplitudes from the momentum distribution of the particles in their production reaction.

In Sec. 3 we rederive the results of [2] by analyzing the analytic properties of the three-particle production amplitude. This derivation is simple and clear.

In Sec. 4 we obtain the distribution over the momenta of the pions produced in the τ and τ' decays ($K^+ \to 2\pi^+ + \pi^-$, $K^+ \to 2\pi^0 + \pi^+$) as a function of the pion-pion scattering amplitudes, a_2 and a_0, and one unknown constant parameter in each reaction [formulas (18), (19), (16) and (13)]. The dependence of the probabilities of both decays on the relative-motion energies of similarly charged

pions is calculated [formula (21) and Fig. 6], as is the dependence on their energies in the K^+ rest system [formula (22) and Fig. 7, the analog of the angular distribution].

The best way of obtaining the scattering amplitude is to study the dependence of the decay probability either on the energy difference in any of the decays or on the relative-motion energy in the $K^+ \to 2\pi^0 + \pi^+$ decay.

2. FORMULATION OF RESULTS

The main result of [2] is that the wave function of three spinless particles [masses m_1, m_2, m_3, momenta p_1, p_2, p_3, and relative pair momenta k_{12}, k_{13}, k_{23} – $\psi_{k_{12},k_{13},k_{23}}(r_1, r_2, r_3)$] has at low energies ($k_{il}r_0 \ll 1$ where r_0 is the interaction radius) in the region $\rho_{12} \sim \rho_{13} \sim \rho_{23} \sim r_0$ ($\rho_{il} = |r_i - r_l|$), accurate to terms of order $k_{il}^2 r_0^2$, the form

$$\psi_{k_{12}, k_{13}, k_{23}}(r_1, r_2, r_3) = C(k_{12}, k_{13}, k_{23})\,\psi_{0,0,0}(r_1, r_2, r_3) + \psi'(1), \tag{1}$$

where $\psi_{0,0,0}(r_1, r_2, r_3)$ is the exact wave function of the three particles at zero energy. $C(k_{12}, k_{13}, k_{23})$ is a standard factor, which depends only on k_{il} and on the zero-energy scattering amplitudes of the particle pairs, a_{il}, which will be written out below. ψ' tends to zero as $k_{li} \to 0$ and contains the dependence on the cosines of the angles between p_3 and k_{12}, p_2 and k_{13}, and p_1 and k_{23}, raised to a power not higher than the first.

Formula (1) follows almost directly from simple considerations, connected with the penetrability of the centrifugal barrier.[2] The factor $C(k_{12}, k_{13}, k_{23})$ takes into account the interaction between particles in configurations such that the distance between two particles is on the order of r_0 and the third is outside the force radius. It is natural for the contribution from the interaction in such configurations to be expressed in terms of the particle-pair scattering amplitudes.

If there are no interactions in such configurations, particles with non-vanishing relative angular momenta can penetrate the region $\rho_{12} \sim \rho_{13} \sim \rho_{23} \sim r_0$ only by overcoming the centrifugal barrier, the penetrability of which is $k_{12}^{\Lambda} p_3^{L}$, $k_{13}^{\Lambda} p_2^{L}$, or $k_2^{\Lambda} p_1^{L}$, where Λ is the angular momentum of the particle pair and L the momentum of the third particle about the center of gravity of the first two. Therefore, for example in the case of a state with zero total momentum, the only states possible (accurate to terms quadratic in the momenta) are those with $L = \Lambda = 1$, and consequently states where the dependence on the angles between the momenta contains the first powers of the cosine.

This is precisely why the function ψ', which contains the contribution of the interactions in configurations other than those indicated above, depends only on the first powers of the cosines. We shall henceforth confine ourselves to states with zero total momentum. In this case, obviously, the most general expression for ψ' has the form

$$\psi' = k_{12}^2 \psi_3' + k_{13}^2 \psi_2' + k_{23}^2 \psi_1', \tag{2}$$

where ψ_i' is independent of the particle momenta.

An expression for $C(k_{12}, k_{13}, k_{23})$ is obtained directly from formulas (26) and (32) of [2]:

$$\begin{aligned} C(k_{12}, k_{13}, k_{23}) &= 1 - ik_{12}a_{12} - ik_{13}a_{13} - ik_{23}a_{23} \\ &+ a_{12}a_{13}[J_1(k_{12}) + J_1(k_{13})] + a_{12}a_{23}[J_2(k_{12}) \\ &+ J_2(k_{23})] + a_{13}a_{23}[J_3(k_{13}) + J_3(k_{23})], \end{aligned} \tag{3}$$

$J_i(k_{il})$ are standard real functions of order k_{il}^2, calculated in [2] [formula (31)] and given below.

Formula (3) differs from the sum of (26) and (32) in [2] in that summation is carried over l and two terms dependent on k_{12} are added. In [2] these terms were left out, for only the dependence on the angle between k_{12} and p_3 was of interest. Addition of these two terms to $C(k_{12}, k_{13}, k_{23})$ ensures independence of ψ' of the higher powers of the cosines of the angles between any of the directions listed above.

The physical meaning of the individual terms in (3) is exceedingly simple. The terms linear in k_{il} correspond to a single account of the interaction. Terms containing $J_i(k_{il})$ are due to two successive particle interactions. These two types of terms can be obtained from the Feynman diagrams shown in Figs. 1 and 2 respectively.[5]

With the aid of (1), (2), and (3) it is easy to calculate the amplitude of a reaction producing three particles with zero total momentum, accurate to terms quadratic in the momenta:

$$\begin{aligned} M(k_{12}, k_{13}, k_{22}) &= M_0\{C^*(k_{12}, k_{13}, k_{23}) + \alpha_1 k_{23}^2 \\ &+ \alpha_2 k_{13}^2 + \alpha_3 k_{12}^2\}, \end{aligned} \tag{4}$$

where M_0 is the amplitude at zero energy. The reaction cross section, averaged over all the orientations of the plane containing the momenta of the resultant particles relative to the momentum of the incident particle, has therefore the form

$$\begin{aligned} d\sigma = M_0^2\{1 &+ 2a_{12}a_{13}[k_{12}k_{13} + J_1(k_{12}) + J_1(k_{13})] \\ &+ 2a_{12}a_{23}[k_{12}k_{23} + J_2(k_{23})] + J_2(k_{12})] + 2a_{13}a_{23}[k_{13}k_{23} \\ &+ J_3(k_{23}) + J_{13}(k_{13})] + \alpha_3 k_{12}^2 + \alpha_1 k_{23}^2 + \alpha_2 k_{13}^2\}\, d\Gamma. \end{aligned} \tag{5}$$

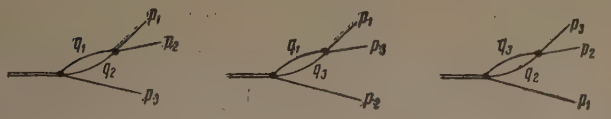

FIG. 1

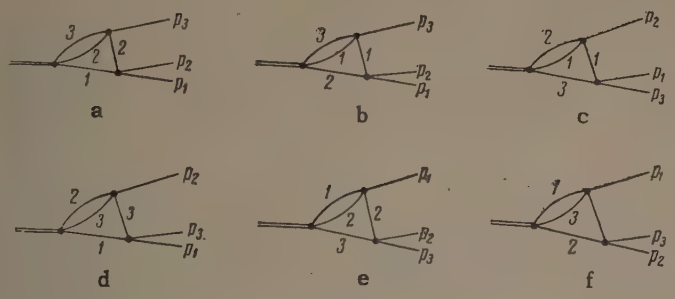

FIG. 2

Terms such as k_{12}^2, k_{13}^2, or k_{23}^2 in $|C(k_{12}, k_{13}, k_{23})|^2$ result in overdetermination of the coefficients α_i, which are not calculated anyway.

It follows from Eq. (5) that a detailed study of the distribution of the momenta of the produced particles will in principle yield the pair interaction amplitudes, since the contribution due to the interaction in the final state depends in a complicated manner on k_{il}, and can therefore be separated from the simple terms such as $\alpha_1 k_{23}^2$ etc.

In conclusion, let us write out an explicit expression for $J_i(k_{il})$, obtained by simple transformation from formula (31) of [2]:*

$$J_i(k_{il}) = I_i(x_{il});$$

$$I_i(x) = -2E\sqrt{\frac{m_1m_2m_3}{m_1+m_2+m_3}}\,\frac{2x\arccos x}{\pi\sqrt{1-x^2}} \times\left[\beta_i + \frac{1}{3}x^2(1-4\beta_i)\right];$$

$$\mu_{il} = \frac{m_i m_l}{m_i+m_l},$$

$$\beta_1 = m_1(m_1+m_2+m_3)/(m_1+m_2)(m_1+m_3),$$

$$x_{il} = k_{il}/\sqrt{2\mu_{il}E}, \qquad (6)$$

where E is the kinetic energy of the produced particles.

Expression (5) for $d\sigma$ has the following interesting property. If we examine it as a function, say, of $E_{12} = k_{12}^2/2\mu_{12}$ it has at first glance a root singularity at $E_{12} = 0$, owing to the terms $k_{12}k_{13}$, and $k_{12}k_{23}$ ($k_{12} = \sqrt{2\mu_{12}E_{12}}$). However, $J_1(k_{12})$ and $J_2(k_{12})$ also have singularities at $E_{12} = 0$:

$$J_1(k_{12}) \approx -k_{12}\sqrt{2\mu_3 E}\,\beta_1, \qquad J_2(k_{12}) \approx -k_{12}\sqrt{2\mu_3 E}\,\beta_2;$$
$$1/\mu_3 = 1/m_3 + 1/(m_1+m_2) \qquad (7)$$

*A misprint in [2] has been corrected in Eq. (6).

and in addition

$$k_{13} = \frac{m_3}{m_1+m_3}k_{12} - \beta_1 p_3, \qquad k_{23} = \frac{m_3}{m_2+m_3}k_{12} - \beta_2 p_3. \qquad (8)$$

When $k_{12} = 0$ we have $p_3 = \sqrt{2\mu_3 E}$, since $k_{12}^2/2\mu_{12} + p_3^2/2\mu_3 = E$, and consequently the singular parts in $K_{12}k_{13} + J_1(k_{12})$ and $k_{12}k_{23} + J_2(k_{12})$ cancel out, and $d\sigma$ does not have a root singularity at $E_{12} = 0$. The situation is obviously the same when $E_{13} = 0$ and $E_{23} = 0$. The situation here is similar to that in electrodynamics in the infrared region, where singularities of the second-approximation diagram [the analog of $J_1(k_{12})$] cancel the singularity of the square of the first approximation (the analog of $k_{12}k_{13}$).

3. ANALYTIC PROPERTIES OF THE REACTION AMPLITUDE NEAR THRESHOLD

In the preceding section we leaned exclusively on the results of [2]. In the present section we re-derive these results by using only the analytic properties of the reaction amplitude. We first follow closely Dyatlov's paper.[5] Consider the amplitude of the process corresponding to the diagram shown in Fig. 3a as a function of the invariants s_{15}, s_{34} and s_{12}, s_{13}, s_{23} near threshold:

$$s_{54} = s_{12} + s_{13} + s_{23} - m_1^2 - m_2^2 - m_3^2$$
$$\approx (m_1+m_2+m_3)^2 + 2(m_1+m_2+m_3)E, \quad E \to 0. \qquad (9)$$

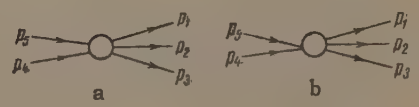

FIG. 3

At sufficiently small E the range of variation of the invariants s_{ik} tends to zero; therefore, if the amplitude has no singularities with respect to any of the invariants near their threshold values, it can be expanded in powers of the deviations from these threshold values. Actually, as a function of the invariants s_{12}, s_{13}, s_{23}, and s_{45}, the amplitude has singularities precisely at the threshold values. These singularities correspond to the diagrams shown in Figs. 1 and 4. Generally speaking, the amplitude has no singularities in s_{15} and s_{34} near threshold and can be expanded in a series. Such an expansion results in terms of the type[5] p_i^2 and $p_5 \cdot p_i$ or $p_4 \cdot p_i$. In the zero-order term of this expansion we should set s_{15} and s_{43} equal to their threshold values, i.e., we should consider the diagram of Fig. 3b instead of 3a.

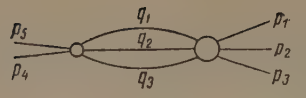

FIG. 4

As was explained in detail in [5], in the first approximation in the above-threshold momenta we can write the amplitude corresponding to the diagram 3b in the form

$$M = M_0(1 + ik_{12}a_{12} + ik_{13}a_{13} + ik_{23}a_{23}),$$
$$k_{il}^2 = [s_{il} - (m_i + m_l)^2]\,\mu_{il}/(m_i + m_l). \qquad (10)$$

As already mentioned, this expression corresponds to an account of the diagrams shown in Fig. 1. We must determine the form of the second-order terms.

We shall show that the amplitude expansion cannot contain terms of the type $k_{12}k_{13}$. Terms of this type have root singularities when $s_{12} = (m_1 + m_2)^2$ and $s_{13} = (m_1 + m_3)^2$ simultaneously, whereas there are no diagrams with such a property. Actually, according to Landau, to find the coefficient of k_{12} it is necessary to integrate over the lines q_1 and q_2 of the diagram of Fig. 1. At the same time (see also [5]) we can neglect the momenta p_1 and p_2 in the remaining parts of the diagram. Under these conditions the diagram as a whole is independent of k_{13} and k_{23}, and therefore cannot contain terms of the indicated type.

Consequently, all that we can add at first glance is an expression of the type

$$\alpha_1 k_{23}^2 + \alpha_2 k_{13}^2 + \alpha_3 k_{12}^2. \qquad (11)$$

This would be correct were the amplitude not to have at $E = 0$ the three-particle singularity shown in Fig. 4. In the presence of this singularity we can have a large number of terms of equal order, such as $\sqrt{E}\,k_{12}$, $k_{12}^2/\sqrt{E}$, ...

Let us examine the three-particle singularity in greater detail. The behavior of the amplitude near this singularity is determined by the integral corresponding to the diagram of Fig. 4, which in the nonrelativistic approximation has the form

$$\int d^3q_1\, d^3q_2\, d^3q_3\, \delta(q_1 + q_3 + q_3)\, \frac{M(q_1q_2q_3)}{E - E(q_1) - E(q_2) - E(q_3)}$$
$$\times A(q_1q_2q_3 \mid p_1p_2p_3). \qquad (12)$$

If M and A are finite near $E = 0$, we find that the contribution of the three-particle singularity is of the order $E^2 \ln E$, and therefore cannot be significant in terms quadratic in the momenta, i.e., linear in the energy.

Thus, the three-particle singularity can contribute to the terms of interest to us only if $M(q_1q_2q_3)$ or $A(q_1q_2q_3 \mid p_1p_2p_3)$ become infinite in the region of integration. The amplitude $M(q_1q_2q_3)$ cannot have poles in the physical region. The amplitude $A(q_1q_2q_3 \mid p_1p_2p_3)$ of the three-particle interaction can have in the physical region poles corresponding to diagrams similar to those shown in Fig. 5.

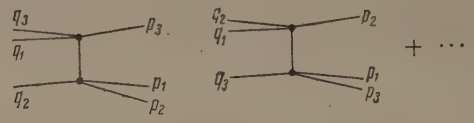

FIG. 5

If we substitute these pole terms in (12) we find that the contribution of the three-particle singularity is of the order $E \ln E$ or $k_{il}^2 \ln E$, i.e., it must be taken into account.

We thus conclude that along with terms written out in (11), it is necessary to take into account the diagrams of Fig. 4, in which A is described by diagrams of Fig. 5. Obviously, these are none other than the diagrams shown in Fig. 2.

4. τ DECAY

In this section we apply the results of the preceding sections to an analysis of the reactions

$$K^+ \to 2\pi^+ + \pi^-, \qquad K^+ \to 2\pi^0 + \pi^+.$$

We shall denote by M^- and M^+ the amplitudes of the first and second reactions, respectively. Particles with like charges will be denoted by the indices 1 and 2.

Unlike [2] we do not confine ourselves to the dependence on the angle between p_3 and k_{12}. Furthermore, the Clebsch-Gordan coefficients in [2] have been incorrectly calculated and are corrected here.

We note first that only one of the three unknown parameters in (4) and (5), namely α_1, α_2, and α_3, remains. By virtue of the symmetry of the amplitude relative to the momenta of particles with like charges, $\alpha_1 = \alpha_2$. By virtue of

$$k_{12}^2 + k_{13}^2 + k_{23}^2 = \tfrac{3}{2}\varkappa^2, \qquad \varkappa^2 = \mu\,[M_K - 3\mu], \qquad (13)$$

the quantity $k_{13}^2 + k_{23}^2$ is expressed in terms of k_{12}^2 and κ^2. The constant term $3\alpha_1\kappa^2/2$ is not essential, since it influences only the normalization of the energy distribution.

The essential difference between the reactions considered here and those described in the earlier sections is that, along with simple scattering, charge exchanges $\pi^+ + \pi^- \rightleftarrows \pi^0 + \pi^0$ are possible in the final state. It is therefore convenient to introduce in place of a_{il} the quantities a_0 and a_2 —the scattering lengths in states with isotopic

spins T = 0 and T = 2. In terms of a_0 and a_2, we have for the scattering amplitudes a_s^{++}, a_s^{+-}, a_s^{00}, a_s^{0+}, and a_s^{0-} the following expressions

$$a_s^{++} = a_s^{0+} = a_s^{-0} = a_2, \quad a_s^{+-} = \tfrac{1}{3}(2a_0 + a_2),$$

$$a_s^{00} = \tfrac{1}{3}(2a_2 + a_0).$$

The upper signs obviously denote the charges of the scattered particles: the charge-exchange amplitude is $a_e = (a_2 - a_0)/3$.

It is easy to write out in terms of these amplitudes the contribution to the matrix elements M^- and M^+ from the diagrams shown in Figs. 1 and 2. The contribution from the diagram of Fig. 1 to the matrix element M^- has the form

$$[ik_{12}a_2 + i(k_{13} + k_{23})\tfrac{1}{3}(2a_0 + a_2)]\, M_0^-$$
$$+ i(k_{13} + k_{23})\tfrac{1}{3}(a_2 - a_0) M_0^+, \qquad (14a)$$

and the contribution to the matrix element M^+ is

$$[ik_{12}\tfrac{1}{3}(2a_2 + a_0) + i(k_{13} + k_{23})a_2]\, M_0^+$$
$$+ ik_{12}\tfrac{2}{3}(a_2 - a_0) M_0^-. \qquad (14b)$$

The contribution to M^- from diagrams 2a and 2b is

$$2J(k_{12})[\tfrac{1}{3}a_2(2a_0 + a_2) M_0^- + \tfrac{1}{3}a_2(a_2 - a_0) M_0^+];$$

that from diagrams 2c and 2d is

$$[J(k_{13}) + J(k_{23})][\tfrac{1}{3}(2a_0 + a_2) a_2 M_0^- + \tfrac{1}{3}(a_2 - a_0) a_2 M_0^+] \qquad (15a)$$

and that from diagrams 2e and 2f is

$$J(k_{13}) + J(k_{23})][\tfrac{1}{3}(2a_0 + a_2)\tfrac{1}{3}(2a_0 + a_2) M_0^-$$
$$+ \tfrac{1}{3}(2a_0 + a_2)\tfrac{1}{3}(a_2 - a_0) M^+ + \tfrac{1}{3}(a_2 - a_0) a_2 M_0^+].$$

The contributions from the corresponding diagrams to M^+ are

$$2J(k_{12})\{\tfrac{1}{3}(2a_2 + a_0) a_2 M_0^+ + \tfrac{1}{3}(a_2 - a_0) a_2 M_0^-$$
$$+ \tfrac{1}{3}(a_2 - a_0)\tfrac{1}{3}(2a_0 + a_2) M_0^- + \tfrac{1}{9}(a_2 - a_0)^2 M_0^+\},$$
$$(J(k_{13}) + J(k_{23}))\{a_2\tfrac{1}{3}(2a_2 + a_0) M_0^+ + a_2\tfrac{2}{3}(a_2 - a_0) M_0^-\},$$
$$(J(k_{13}) + J(k_{23}))\, a_2^2 M_0^+, \qquad (15b)$$

where $M_0^\pm$ are the matrix elements at zero energy.

The functions $J(k_{il})$ have been defined in (6). In our case (for equal masses) they are all equal to

$$J(k_{il}) = I(x_{il}) = -\frac{\sqrt{3}}{\pi}\varkappa^2 \frac{x_{il}\arccos x_{il}}{(1 - x_{il}^2)^{1/2}}\left(1 - \frac{8}{9}x_{il}^2\right),$$

$$x_{il} = \frac{k_{il}}{\varkappa}. \qquad (16)$$

Collecting terms from (14) and (15) and recognizing that the matrix elements can contain terms in the form αk_{12}^2, we obtain

$$M^- = M_0^-\{1 + ik_{12}a_2 + i(k_{13} + k_{23})\tfrac{1}{3}[2a_0 + a_2$$
$$+ \rho(a_2 - a_0)] + 2J(k_{12})\, a_2\tfrac{1}{3}[2a_0 + a_2 + \rho(a_2 - a_0)]$$
$$+ (J(k_{13}) + J(k_{23}))[\tfrac{1}{3}(2a_0 + a_2) + a_2]$$
$$\times \tfrac{1}{3}[2a_0 + a_2 + \rho(a_2 - a_0)]$$
$$+ \tfrac{1}{3}(a_2 - a_0)\, a_2\rho] + \alpha_- k_{12}^2\}; \qquad (17a)$$

$$M^+ = M_0^+\{1 + ik_{12}\tfrac{1}{3}[2a_2 + a_0 + 2\rho^{-1}(a_2 - a_0)]$$
$$+ i(k_{13} + k_{23})\, a_2 + [J(k_{13}) + J(k_{23})]$$
$$\times [\tfrac{1}{3}a_2(2a_2 + a_0 + 2\rho^{-1}(a_2 - a_0)) + a_2^2] + 2J(k_{12})$$
$$\times a_2[\tfrac{1}{3}(2a_2 + a_0) + \tfrac{2}{3}\rho^{-1}(a_2 - a_0)]$$
$$+ 2J(k_{12})\tfrac{1}{9}(a_2 - a_0)^2(1 - 2\rho^{-1}) + \alpha_+ k_{12}^2\},$$
$$\rho = M_0^+/M_0^-. \qquad (17b)$$

Squaring (17a) and (17b) and taking account of the fact that conservation of combined parity calls for real matrix elements M_0^- and M_0^+, we find that the probabilities of the decays $K^+ \to 2\pi^+ + \pi^-$ and $K^+ \to 2\pi^0 + \pi^+$ are respectively equal to

$$dW^{(-)} = |M_0^-|^2\{1 + \beta_1[k_{12}(k_{13} + k_{23}) + 2J(k_{12}) + J(k_{13})$$
$$+ J(k_{23})] + \beta_2[k_{13}k_{23} + J(k_{13}) + J(k_{23})]$$
$$+ \beta_3[J(k_{13}) + J(k_{23})] + \alpha_- k_{12}^2\}d\Gamma, \qquad (18a)$$

$$dW^{(+)} = |M_0^+|^2\{1 + \gamma_1[k_{12}(k_{13} + k_{23}) + 2J(k_{12})$$
$$+ J(k_{13}) + J(k_{23})] + \gamma_2[k_{13}k_{23} + J(k_{13})$$
$$+ J(k_{23})] + \gamma_3 2J(k_{12}) + \alpha_+ k_{12}^2\}\, d\Gamma; \qquad (18b)$$

$$\beta_1 = \tfrac{2}{3}a_2(2a_0 + a_2 + \rho(a_2 - a_0)],$$
$$\gamma_1 = \tfrac{2}{3}a_2[2a_2 + a_0 + 2\rho^{-1}(a_2 - a_0)]$$
$$\beta_2 = \tfrac{2}{9}[2a_0 + a_2 + \rho(a_2 - a_0)]^2, \qquad \gamma_2 = 2a_2^2,$$
$$\beta_3 = \tfrac{2}{9}\rho(a_2 - a_0)^2(2 - \rho), \quad \gamma_3 = -\tfrac{2}{9}\tfrac{1}{\rho}(a_2 - a_0)^2(2 - \rho). \qquad (19)$$

We note that (18a) and (18b) differ in structure from (5). In particular, the terms proportional to β_3 and γ_3 have root singularities for $E_{13} = 0$, $E_{23} = 0$, and $E_{12} = 0$ respectively, and these singularities do not cancel. This is a consequence of the possibility of going from one channel to the other via charge exchange, and is a phenomenon of the same type as discussed in [3,4].

Formulas (18) and (19) determine the dependence of the probabilities of both decays on all the variables and make it possible, in principle, to de-

termine the amplitudes a_2 and a_0 from their experimental analysis, in spite of the fact that the parameters α_- and α_+ are not expressed in terms of the scattering amplitudes.

It is most natural to regard $dW^{(-)}$ and $dW^{(+)}$ as a function of the orthogonal coordinates on a Dalitz diagram. It is convenient to choose as one of the variables $x^2 = k_{12}^2/k_m^2$ — the ratio of the square of the relative momentum of like charged pions to its maximum value. k_{12}^2 is simply related to the customarily used variable ϵ, the energy of the third pion:

$$\varepsilon = (M_K^2 + 3\mu^2 - 4k_{12}^2)/2M_K,$$

$$k_m^2 = \tfrac{1}{4}(M_K^2 - 2\mu M_K - 3\mu^2) \approx \varkappa^2. \qquad (20)$$

For the second variable we choose z, the difference between the energies of like charged pions divided by the maximum value of this difference.

For convenience in the experimental analysis, it is useful to have decay-probability formulas integrated over one of the variables. Integrating with respect to z, we obtain the so-called energy distribution

$$dW^{(-)}(x) = |M_0^-|^2\{1 + \varkappa^2[\beta_1 F_1(x) + \beta_2 F_2(x) + \beta_2 F_3(x) + \alpha_- x^2]\}\, d\Gamma_{x^2}, \qquad (21a)$$

$$dW^{(+)}(x) = |M_0^+|^2\{1 + \varkappa^2[\gamma_1 F_1(x) + \gamma_2 F_2(x) + \gamma_3 2J(x) + \alpha_+ x^2]\}\, d\Gamma_{x^2}. \qquad (21b)$$

The functions $F_1(x)$, $F_2(x)$, $F_3(x)$, and $J(x)$ are plotted in Fig. 6 and are written out in the Appendix. In the calculation of $F_i(x)$ we have left out terms of the form $a + bx^2$, since they enter either into the normalization or in $\alpha_\pm$. As can be seen from Fig. 6, the curves for F_1, F_2, and F_3 differ little from straight lines and it is therefore little likely that it will be possible to determine a_0 and a_2 from an analysis of the energy distribution in the reaction $K^+ \to 2\pi^+ + \pi^-$ only.

It follows, however, from the same diagram that owing to the presence of the term $2\kappa^2\gamma_3 J(x)$ the energy distribution in the reaction $K^+ \to 2\pi^0 + \pi^+$ differs appreciably from $\alpha_+ x^2$, and can therefore be used to determine the charge-exchange amplitude. The effect of this term on the energy distribution is also anomalously exaggerated by the fact that $\rho = 1/4$, and consequently

$$\gamma_3 = -\tfrac{16}{9}(a_2 - a_0)^2.$$

It is clear from all the foregoing that the corrections to the energy distribution, calculated in [6,7], cannot be successful since they are reduced to a calculation of first-order diagrams (Fig. 1), which in many cases are almost completely cancelled by the diagrams shown in Fig. 2.

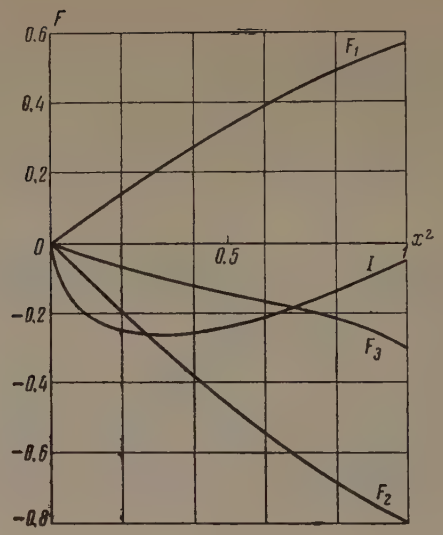

FIG. 6

Integrating (18a) and (18b) with respect to x^2, we obtain an analog of the angular distribution

$$dW^{(-)}(z) = |M_0^-|^2\{1 + \varkappa^2[\beta_1\varphi_1(z) + \beta_2\varphi_2(z) + \beta_3\varphi_3(z)]\}\, d\Gamma_z, \qquad (22a)$$

$$dW^{(+)}(z) = |M_0^+|^2\{1 + \varkappa^2[\gamma_1\varphi_1(z) + \gamma_2\varphi_2(z) + \gamma_3\varphi_4(z)]\}\, d\Gamma_z. \qquad (22b)$$

The functions $\varphi_1(z)$, $\varphi_2(z)$, $\varphi_3(z)$, and $\varphi_4(z)$ are shown in Fig. 7 and are given in the Appendix. A study of the dependence of $dW^{(-)}$ and $dW^{(+)}$ on z can serve as a means of determining a_2 and a_0, but statistics on the order of 10^4 events are needed for this case.

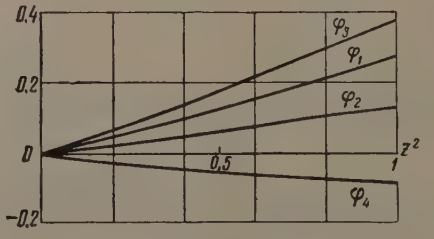

FIG. 7

In conclusion, I am deeply grateful to L. D. Landau and I. T. Dyatlov for useful discussions.

APPENDIX

$$F_1(x) = \int_{z_1}^{z_2} k_{12}(k_{13}+k_{23})\frac{dz}{4x^2x\sqrt{1-x^2}} + 2I(x) + F_3(x) = 2I(x) + F_3(x) + \begin{cases} \frac{\sqrt{3}x}{\sqrt{1-x^2}}\left(1-\frac{8}{9}x^2\right) & x^2 < \frac{3}{4} \\ 1 & x^2 > \frac{3}{4}, \end{cases} \tag{A1}$$

$$F_2(x) = F_3(x) + \int_{z_1}^{z_2} k_{13}k_{23}\frac{dz}{4x^2x\sqrt{1-x^2}} = F_3(x) + \frac{(3-2x^2)^2}{16\sqrt{3}x\sqrt{1-x^2}} \arcsin\frac{2x\sqrt{3(1-x^2)}}{3-2x^2} + \frac{1}{8}|3-2x^2|, \tag{A2}$$

$$F_3(x) = \int_{z_1}^{z_2} [I(x_{13}) + I(x_{23})]\frac{dz}{4x^2x\sqrt{1-x^2}} = \begin{cases} -\frac{2}{9}\frac{\arcsin x}{x\sqrt{1-x^2}}\left[1+\frac{\sqrt{3}x^2}{\pi}(3-4x^2)\right] + \frac{1}{6}(3-4x^2) & x^2 < \frac{3}{4} \\ -\frac{2}{9}\frac{2\arccos x}{x\sqrt{1-x^2}}\left[1+\frac{\sqrt{3}x^2}{2\pi}(4x^2-3)\right] + \frac{1}{3}(4x^2-3) & x^2 > \frac{3}{4}. \end{cases} \tag{A3}$$

$I(x)$ is given by Eq. (16) in the text, and $z_{1,2} = \mp 2x\sqrt{1-x^2}$.

$$\varphi_1(z) = \int k_{12}(k_{13}+k_{23})\frac{dx^2}{x^2\sqrt{1-z^2}} + \varphi_3(z) + \varphi_4(z) = \varphi_3(z) + \varphi_4(z) + \frac{3}{16}\frac{(\sqrt{3}+z)^2}{\sqrt{2(1-z^2)}}\arccos\frac{1+\sqrt{3}z}{(\sqrt{3}+z)} + \frac{1}{16}(1+\sqrt{3}z)$$

$$+ \begin{cases} \frac{3}{16}\frac{(\sqrt{3}-z)^2}{\sqrt{2(1-z^2)}}\arccos\sqrt{\frac{1}{3}} + \frac{1}{16\sqrt{1-z^2}}(1+2\sqrt{3}z-5z^2), & z < \frac{\sqrt{3}}{2}, \\ \frac{3}{16}\frac{(\sqrt{3}-z)^2}{\sqrt{2(1-z^2)}}\arccos\frac{\sqrt{3}z-1}{(\sqrt{3}-z)} + \frac{\sqrt{3}z-1}{16}, & z > \frac{\sqrt{3}}{2}, \end{cases} \tag{A4}$$

$$\varphi_2(z) = \varphi_3(z) + \int k_{13}k_{23}\frac{dx^2}{x^2\sqrt{1-z^2}} = \varphi_3(z) + \frac{3}{8}\begin{cases} \frac{1}{\sqrt{1-z^2}}\left[\frac{2}{3}(2-z^2) - \frac{z^2}{2}\operatorname{arcsh}\frac{4}{3}\right], & z < \frac{\sqrt{3}}{2} \\ \frac{5}{3} - \frac{z^2}{2\sqrt{1-z^2}}\operatorname{arcsh}\frac{2\sqrt{1-z^2}}{z^2}, & z > \frac{\sqrt{3}}{2}, \end{cases} \tag{A5}*$$

$$\varphi_3(z) = \int (I(x_{13}) + I(x_{23}))\frac{dx^2}{x^2\sqrt{1-z^2}} = -\frac{1}{3\sqrt{3}}\frac{\arccos z}{\sqrt{1-z^2}}\left[1+\frac{(\sqrt{3}-2z)(1+\sqrt{3}z)}{\pi}\right]$$

$$-\frac{1}{3\sqrt{3}}\begin{cases} \frac{\pi-\arccos z}{\sqrt{1-z^2}}\left[1+\frac{(\sqrt{3}+2z)(1-\sqrt{3}z)}{\pi}\right], & z < \frac{\sqrt{3}}{2}, \\ \frac{5\arccos z}{\sqrt{1-z^2}}\left[1-\frac{(\sqrt{3}+2z)(1-\sqrt{3}z)}{5\pi}\right] - \sqrt{3}-2z, & z > \frac{\sqrt{3}}{2}, \end{cases} \tag{A6}$$

$$\varphi_4(z) = \int I(x)\frac{dx^2}{x^2\sqrt{1-z^2}} = -\frac{1}{2\sqrt{3}}\frac{\arccos z}{\sqrt{1-z^2}}\left(1+\frac{2z}{3\pi}\right) - \frac{z}{3\sqrt{3}};$$

$$\frac{1}{2}(1-\sqrt{1-z^2}) < x^2 < \frac{1}{2}(1+\sqrt{1-z^2}), \quad z > 0. \tag{A7}$$

[1] G. F. Chew and F. E. Low, Phys. Rev. **113**, 1380 (1959).

[2] V. N. Gribov, Nucl. Phys. **5**, 633 (1958).

[3] A. A. Ansel'm and V. N. Gribov, JETP **36**, 1890 (1959) and **37**, 501 (1959), Soviet Phys. JETP **9**, 1345 (1959) and **10**, 354 (1960).

[4] V. N. Gribov, JETP **38**, 553 (1960), Soviet Phys. JETP **11**, 400 (1960).

[5] I. T. Dyatlov, JETP **37**, 1330 (1959), Soviet Phys. JETP **10**, 947 (1960).

[6] N. N. Khuri and S. B. Treiman, Phys. Rev. **119**, 1115 (1960).

[7] R. E. Sawyer and K. G. Wale, Phys. Rev. **119**, 1426 (1960).

*Arcsh = $\sinh^{-1}$.

Translated by J. G. Adashko
211

EFFECT OF EXTERNAL FIELDS ON THE MOTION AND GROWTH OF BUBBLES IN BOILING LIQUIDS

G. A. ASKAR'YAN

P. N. Lebedev Physics Institute, Academy of Sciences, U.S.S.R.

Submitted to JETP editor April 29, 1961

J. Exptl. Theoret. Phys. (U.S.S.R.) 41, 1231-1232 (October, 1961)

It is noted that the growth of bubbles and boiling conditions of heated or saturated liquids can be controlled by employing external fields, which influence the bubble motion on which the thermodynamic growth conditions depend. The growth of bubbles in an accelerated bubble chamber can either be hindered or enhanced. Local inhomogeneous electric or magnetic fields which keep the bubbles near the vessel walls or repel them can be used to change the boundary conditions for boiling and heat exchange with the wall. The effects considered can be used, for example, to improve storage conditions of liquefied gases, heat exchange control, control of boiling, etc.

1. ACCELERATED BUBBLE CHAMBER

THE growth of a bubble in an effervescing liquid leads to local cooling of the liquid near the bubble. Consequently the translational motion of the bubble through new regions of the liquid can change appreciably the thermodynamic condition of the bubble growth. In particular, if there are no forces causing the bubble to float up, its growth can be appreciably hindered.

The bubbles can be kept from floating up in a "dropping" bubble chamber, which is allowed to fall freely during the time of bubble growth. It is much easier to make a "falling" bubble chamber than a "falling" cloud chamber [1] since the short bubble-growth time t makes it sufficient for the chamber to fall a short distance (let $s = gt^2/2$; usually $t \approx 10^{-3}$—10^{-2} sec, i.e., the path of the chamber need not exceed several millimeters). The start of chamber motion can be synchronized with the pressure drop. It is also possible to impart to the chamber an acceleration much greater than that of gravity, thus increasing sharply the Archimedean force that pushes the bubbles out of the liquid. All this allows us to study the influence of the motion of the bubble on its growth and to investigate, for example, the growth of the bubble under exceedingly simple thermodynamic conditions, which are amenable to simulation and to calculation (see, for example, [2,3]).

The compensation for the gravitational force in the falling bubble chamber can also eliminate convection in the working liquid and reduce distortion of the tracks.

2. EFFECT OF EXTERNAL INHOMOGENEOUS FIELDS ON THE MOTION OF BUBBLES IN LIQUIDS

In addition to the inertia forces and the gravity force $\mathbf{f}_g = \rho\mathbf{g}$, the liquid may be acted upon by inhomogeneous electric or magnetic fields (see, for example, [4,5]). The volume force acting on the liquid produces an additional Archimedean force acting on the bubble.

The total force acting on the bubble as a whole is

$$\mathbf{F} = \int_S \left\{ \varepsilon \left[\mathbf{E}(\mathbf{En}) - \tfrac{1}{2} E^2 \mathbf{n} \right] + \mu \left[\mathbf{H}(\mathbf{Hn}) - \tfrac{1}{2} H^2 \mathbf{n} \right] \right\} ds = \tfrac{4}{3} \pi a^3 \mathbf{f}_{dip} .$$

The condition for the equilibrium of the bubble in the liquid in the presence of gravitational force and electric or magnetic field is $-\mathbf{f}_g = \mathbf{f}_{dip}$, where $\mathbf{f}_{dip}$ is the force per unit bubble volume acting on the dipole moment of the bubble

$$\mathbf{f}_{dip} = -\frac{3}{4\pi} \left\{ \frac{\varepsilon - 1}{\varepsilon + 2} \nabla E^2_{ext} + \frac{\mu - 1}{\mu + 2} \nabla H^2_{ext} \right\} .$$

We consider here, for simplicity, bubbles with dimensions small compared with the characteristic dimensions of the field variation and for which the surface pressure is considerably greater than the pressure of the electromagnetic field on the surface of the bubble. In this case the principal role of the inhomogeneous electromagnetic field is to displace the bubble as a whole, and its deformation can be neglected. It is obvious that the equilibrium conditions and the force per unit vol-

ume tending to move the bubble are independent of its dimensions.

Let us estimate the necessary field gradients. The Archimedean force (due to gravity) becomes commensurate with the forces in the electric and magnetic field if $\chi_e \nabla E^2 \sim g$ and $\chi_m \nabla H^2 \sim g$, where χ_e and χ_m are the electric and magnetic polarizabilities per units mass of liquid. For typical values, $\chi_e \sim 0.3\ g^{-1}\ cm^3$ and $\chi_m \sim 10^{-6}\ g^{-1}\ cm^3$, we find that in a field with characteristic inhomogeneity dimension $l \sim 0.3$ cm the necessary field amplitudes are $E_0 \sim 10$ kv/cm and $H_0 \sim 10^4$ oe. Such fields can be readily realized in a thin layer near the chamber walls.

We note, for example, that the paramagnetic susceptibility of oxygen is hundreds of times greater, so that the fields can be decreased or their effective zone of action increased.

It is possible to control by means of inhomogeneous fields not only bubble growth but also the boiling conditions on the boundaries and the heat exchange at the walls; if the bubbles are kept at the walls by local fields, heat exchange between the liquids and the walls becomes difficult, and after the bubbles are removed heat exchange is facilitated. Inhomogeneous fields can be induced from the outside even in the case of a conducting wall (magnetic poles near the walls of a vessel containing a diamagnetic or paramagnetic liquid).

The foregoing possibilities of influencing the boiling and evaporation of liquids by using local inhomogeneous fields to retain or remove the bubbles near the walls can also be used to improve the conditions of storage of liquefied gases, to control evaporation, etc.

[1] N. N. Das Gupta and S. K. Ghosh, Revs. Modern Phys. **18**, 225 (1946).

[2] M. S. Plesset and S. A. Zwick, J. Appl. Phys. **23**, 95 (1952); **25**, 493 (1954).

[3] S. A. Zwick, Phys. Fluids **3**, 685 (1960).

[4] L. D. Landau and E. M. Lifshitz, Élektrodinamika sploshnykh sred (Electrodynamics of Continuous Media) Gostekhizdat, 1957.

[5] J. A. Stratton, Electromagnetic Theory, McGraw Hill, 1941.

Translated by J. G. Adashko
212

PROPOSED RELATION BETWEEN THE POSITION OF A POLE OF THE SCATTERING AMPLITUDE AND THE VALUE OF THE RESIDUE AT THE POLE

L. A. KHALFIN

Mathematics Institute, Academy of Sciences, U.S.S.R.

Submitted to JETP editor May 4, 1961

J. Exptl. Theoret. Phys. (U.S.S.R.) 41, 1233-1240 (October, 1961)

The question is investigated as to whether dispersion relations can in principle give a definite relation between the position of a pole and the residue at the pole, i.e., between the mass and the interaction constant. It is shown that restrictions on the possible values of the interaction constant[1-3,7] are a consequence of the use of models in the examples treated in the papers in question. It is proved that in the general case, if we start from only the dispersion relations and the unitarity relation for the forward scattering amplitude, there are no restrictions on the possible values of the interaction constant.

SEVERAL recent papers[1,2] have studied the question as to whether dispersion relations in principle give a definite connection between the position of a pole and its residue, i.e., between the mass and charge of particles. A nonrelativistic quantum-mechanical example[1] and a more general field example[2] show that it appears at first glance that there is in principle such a connection, or more exactly, that for a given position of the pole (a given mass) there is an upper bound on the residue (the charge). In a recent paper by Zachariasen[3] an interesting model of a quantum field theory is proposed, which is also free from internal contradictions only when there are definite restrictions on the possible values of the interaction constants (g^2 and λ) of the theory.

We shall show that these restrictions arise only because of the model nature of the examples considered, so that the results of[1-3] are of a model nature in a double sense, and do not follow at all from the dispersion relations in the general case. More exactly we shall show that if we start only from the dispersion relations for the forward scattering amplitude, the unitarity relation ("optical" theorem), and the supplementary condition associated with short-range action,[2] [1)] then there are no restrictions on the possible values of the interaction constant g^2.

1. As is well known,[4] the causality condition together with the principle of spectral representation leads to the analytic character of the forward scattering amplitude $f(E)$ in the complex E plane with cuts along the semiaxes $-\infty$, $-\mu$ and μ, ∞, where μ is the mass of the particles being scattered. For the usual case of scattering of mesons by nucleons[4] which we consider here, in the unphysical region $-\mu < E < \mu$, $\operatorname{Im} f(E)$ is proportional to a δ function:

$$\operatorname{Im} f(E) = g^2 \delta(E - E_0), \tag{1}$$

where E_0 is the pole of the scattering amplitude $f(E)$ which is fixed by the masses of the π meson and nucleon, and the negative quantity $-g^2$, i.e., the residue of $f(E)$ at the pole $E = E_0$, is related in a definite way to the meson-nucleon interaction constant. We note that the presence of a single isolated pole and the absence of a continuous spectrum in the unphysical region is a consequence of the present known "spectrum" of elementary particles.

On the usual assumptions about the degree of the asymptotic behavior of $|f(E)|$ for $|E| \to \infty$ one gets dispersion relations connecting the real part $\operatorname{Re} f(E)$ and the imaginary part $\operatorname{Im} f(E)$ of the forward scattering amplitude[4]; in particular, the dispersion relation without subtractions[2)] is of the form

$$\operatorname{Re} f(E) = -\frac{g^2}{E - E_0} + \frac{1}{\pi} P \int_{\mu}^{\infty} \frac{\operatorname{Im} f(E')}{E' - E}\, dE' + \frac{1}{\pi} P \int_{-\infty}^{-\mu} \frac{\operatorname{Im} f(E')}{E' - E}\, dE'. \tag{2}$$

[1)] This is equivalent to the assumption that there are no scattering phase shifts for large values of l.

[2)] Hereafter when speaking of dispersion relations we shall have in mind just the dispersion relation (2), since the treatment of dispersion relations with subtractions is a natural extension.

The unitarity relation for the forward scattering amplitude f(E) reduces to the optical theorem [4]:

$$\operatorname{Im} f(E) = \frac{k}{4\pi}\sigma(E) = \frac{k}{2}\int_0^{\pi} \sin\theta\, |f(E,\theta)|^2 d\theta + \frac{k}{4\pi}\sigma_{\text{inel}}(E),$$
$$E \geqslant \mu, \quad k^2 \equiv E^2 - \mu^2, \quad f(E,0) \equiv f(E), \qquad (3)$$

where $f(E,\theta)$ is the scattering amplitude at the angle θ and $\sigma_{\text{inel}}(E)$ is the total cross section for inelastic processes (in particular, many-particle processes). For $E < -\mu$ we can use the condition of crossing symmetry [4]

$$f^*(-E) = f_{\text{an}}(E), \qquad (4)$$

where $f_{\text{an}}(E)$ is the forward scattering amplitude of the antiparticles.

We note a fact of importance for what follows. As Lehmann [5] has shown, $f(E,\theta)$ is an analytic function of θ for all finite $|E| < \infty$, so that the region of analyticity (the Lehmann ellipse) surely includes the physical region $0 \leq \theta \leq \pi$.

The meaning of the dispersion relations is in particular that one cannot prescribe independently the behaviors of Re f(E) and Im f(E) in a certain energy interval, but that the real part Re f(E) for a certain value of E is determined by the behavior of Im f(E) as a function of E over the entire range of variation of the energy. At the same time, and it is very important to emphasize this, the dispersion relations in themselves do not put any important restrictions on the choice of Im f(E), and thus provide a constructive method for fixing the forward scattering amplitude f(E) in terms of a given E_0 (position of the pole), given g^2 (the residue at the pole, which is equivalent to giving the interaction constant), and the value of Im f(E) in the physical region $-\infty < E < -\mu$ and $\mu < E < \infty$, and indeed for arbitrary Im f(E) [naturally Im f(E) must be such that the integrals in Eq. (2) converge].

The analytic property of the forward scattering amplitude, and consequently also the dispersion relations, are, like the unitarity relation, derived on the most general assumptions [4] regarding the form of the interaction, and consequently are valid for arbitrary values of the interaction constant. Thus the unitarity relation (3), and also the dispersion relation (2), are identities with respect to the value of the interaction constant, and consequently with respect to the value of the residue $-g^2$.

2. It is quite obvious that from the two identities with respect to the value of g^2 —the dispersion relation (2) and the unitarity relation (3)—one cannot derive any restrictions on the possible values of g^2, provided these identities are not mutually (internally) contradictory for certain values of g^2. Here mutual contradiction is understood in the sense that for certain values of g^2 one cannot construct any forward scattering amplitude f(E) (other than one that is identically zero) with residue at the pole $E = E_0$ equal to $-g^2$ and with an imaginary part Im f(E) in the physical region which satisfies the unitarity relation.

A possible contradiction between the dispersion relation (2) and the unitarity relation (3) in the general case could be caused by the following circumstance. The unitarity relation (3) connects the imaginary part Im f(E) of the forward elastic scattering amplitude with the absolute values $|f(E,\theta)|$ of the elastic scattering amplitude at arbitrary angles and with the cross sections of inelastic (in particular, of many-particle) processes. Since we are investigating possible contradictions only for the dispersion relation and the unitarity relation for the forward scattering amplitude f(E), the elastic scattering amplitudes $f(E,\theta)$ at nonzero angles ($\theta \neq 0$) and the amplitudes for inelastic processes must be regarded as "external" functions, which in general do not depend on the elastic forward scattering amplitude f(E). But since according to Eq. (3) Im f(E) can, in general, depend on $|f(E,0)|^2 = |f(E)|^2$, and consequently also on Re f(E), the unitarity relation (3) could have as a consequence a definite, local connection between Re f(E) and Im f(E), independent in its explicit form of the value of g^2 and of the dispersion relations.

At the same time the dispersion relations (2) also establish a definite connection between Re f(E) and Im f(E), which does depend explicitly on the value of g^2 and which is in general nonlocal. This could have the result that the dispersion relations (2) and the unitarity relation (3), in serving independently of each other to give connections between Re f(E) and Im f(E), would be inconsistent for certain values of g^2.

It is not hard to show, however, that in the general case the unitarity condition (3) does not lead at all to a local connection between Re f(E) and Im f(E). In fact, as can be seen from Eq. (3), Im f(E) can depend on $|f(E,0)| = |f(E)|$ only through the fact that $|f(E,0)|$ occurs in the integrand. But by a theorem of Lehmann [5] the integrand $\sin\theta\,|f(E,\theta)|^2$ has no singularity in the range of integration, so that the value of the integrand $\sin\theta\,|f(E,\theta)|^2$ at the one point $\theta = 0$ is immaterial to the value of the integral (the more so because of the factor $\sin\theta$), and consequently, generally speaking, Im f(E) does not depend on

$|f(E)|$. Thus in the general case no (local) connection between Re $f(E)$ and Im $f(E)$ arises from the unitary condition. Consequently, in the general case the dispersion relations and the unitarity relation are consistent, and thus cannot impose any restrictions on the possible value of the interaction constant g^2.

3. Of course, in special cases of models Im $f(E)$ can turn out to depend on the value of the integrand $|f(E,\theta)|^2$ at $\theta = 0$, which in turn leads by Eq. (3) to a local connection between Re $f(E)$ and Im $f(E)$, and consequently to a possible incompatibility of the unitarity relation and the dispersion relations for certain values of g^2. Then from the two incompatible conditions involving g^2 (the unitarity condition and the dispersion relation) one can also get limitations on the possible values of the coupling constant g^2. It is quite clear, however, from what has been said that the restrictions on g^2 so obtained relate solely to the model and really only show for what values of g^2 one can treat the special case of the model without contradiction.

According to Eq. (3) Im $f(E)$ can depend on the value of the integrand $|f(E,\theta)|^2$ at $\theta = 0$ only if the values of $|f(E,\theta)|^2$ in some finite range of θ (in particular in the neighborhood $\theta \sim 0$) are determined by the values of $|f(E,\theta)| = |f(E)|$,[3] i.e., if important restrictions on the dependence of $f(E,\theta)$ on θ are postulated a priori. In particular, it would be sufficient for this to assume that in some arbitrarily small (but finite) region in E and θ

$$|f(E,\theta)| = |f(E,0)| = |f(E)|. \qquad (5)$$

But in virtue of Lehmann's theorem [5] and the fact that the partial amplitudes for elastic scattering are analytic in the energy (for finite energies), the relation (5) would hold for all E and θ, and thus the elastic scattering would reduce to pure s scattering.

It is precisely this special case that has been considered up to now.[1,3,7] In the paper by Castillejo and others [7] this model was used for the scattering of scalar mesons by stationary nuclei, and in the paper by Gribov and others [1] it was used for nonrelativistic scattering by a singular (delta-function) potential. In [7] a restriction on the value of the residue at the pole was obtained for the first time by means of the apparatus of R functions. It is now clear that this restriction is entirely due to the fact that for the model considered all of the elastic scattering reduced to pure s scattering.

Thus if the elastic scattering reduces to pure s scattering, then for the analytic forward scattering amplitude we indeed do get from the dispersion relations and the unitarity relation a restriction on the maximum value of the residue at the pole.[4] Actually, however, this restriction on the possible value of the residue at the pole only means that it is only for $g^2 < g^2_{max}$ that elastic scattering for which the amplitude at $\theta = 0$ has analytic properties (satisfies the dispersion relations) can be treated without contradiction as pure s scattering.

In this connection we note that in the treatment of the problem of scattering by a potential the partial amplitude for s scattering has the necessary analytic properties (satisfies the dispersion relations) only if the finite interaction radius r_0 is equal to zero,[8] i.e., only for the model of the singular potential,[1] [5] for which the entire elastic scattering reduces to pure s scattering.

4. As has already been pointed out, a local connection between Re $f(E)$ and Im $f(E)$, and consequently also possible restrictions on the value of g^2, can arise if we make drastic (model) assumptions about the dependence of $f(E,\theta)$ on θ, and in particular if we assume that the elastic scattering is completely described by a finite number of scattering phase shifts. This assumption actually means that in the neighborhood of $\theta = 0$ the amplitude $f(E,\theta)$ is a sufficiently smooth function (since it does not contain high phase shifts), and this in turn has the consequence that in the neighborhood of $\theta = 0$ the quantity $|f(E,\theta)|$ is to a large extent determined by its value at $\theta = 0$. But then, according to the unitarity relation (3), we arrive at a local connection between Re $f(E)$ and Im $f(E)$, and consequently, at possible restrictions on the maximum value of g^2, which are generalizations of those known for the case in which the finite set of phase shifts reduces to the s phase shift alone.[1,7]

It is very important to emphasize that in virtue of the often-used theorem of Lehmann [5] and of the analytic properties of the partial scattering

[3] We note that if in some range of θ, $|f(E,\theta)|^2$ should depend explicitly on $|f(E)|$, then by the method of [6] one could also obtain restrictions on the asymptotic behavior of $|f(E)|$ for $|E| \to \infty$.

[4] This restriction can also be obtained on the basis of the fact that when the elastic scattering reduces to pure s scattering there is an upper limit on $|f(E)|$ which does not depend on the value of g^2.[6]

[5] From this same fact it follows at once that for scattering by a potential with a finite radius the main conclusions of the paper by Gribov and others [1] are incorrect. In [1] this conclusion is reached by indirect arguments.

amplitudes, the elastic scattering amplitude cannot be described exactly by a finite number of phase shifts in some restricted range of energies and by a different (finite or infinite) number of phase shifts in another range of energies; it must be described by the same number of phase shifts for all finite values of the energy. This assertion does not contradict the well known procedure (based, for example, on the uncertainty relation) of separating the phase shifts into the large (important) a_l with $l < kr_0$ and the small (unimportant) a_l with $l > kr_0$, in the case of a short-range interaction with a finite radius r_0.[6] We further emphasize that the separation into large and small phase shifts does not depend on the "strength" g^2 of the interaction (the coupling constant), because it depends only on the energy E and the interaction radius r_0, which by its very definition does not depend on the interaction constant.[7] It is not hard to convince oneself of this for the case of scattering by a potential, and also for scattering in quantum field theory. In fact, in the pole approximation, we have for the phase shifts a_l [10]

$$a_l = i\mu f^{(1)}(k^2)\, k^{-1} Q_l\,(1 + \mu^2/2k^2), \qquad (6)$$

where Q_l are Legendre functions of the second kind, $\mu \sim 1/r_0$ is the mass of the mesons transmitting the interaction, and $f^{(1)}(k^2)$ is a dimensionless function proportional to g^2. From Eq. (6) and the asymptotic properties of the Q_l there follows, independently of the value of g^2, a separation of the phase shifts into the large (important) ones with $l \ll k/\mu = kr_0 \ll 1$,

$$a_l = \frac{i\mu f^{(1)}(k^2)}{k} \frac{l!\cdot 2^{l+1}}{(2l+1)!!} \left(\frac{k}{\mu}\right)^{2l+2} \qquad (7)$$

and the "small" (unimportant) ones with $l \gg k/\mu = kr_0 \gg 1$,

$$a_l = i\mu f^{(1)}(k^2)\, k^{-1} \sqrt{\pi/2\mu l}\, e^{-\mu l/k}. \qquad (8)$$

Thus the additional condition associated with the short-range nature of the force—the separation of the phase shifts into large (important) and small (unimportant) phase shifts—is an identity with respect to g^2, just as are the dispersion relations and the unitarity relation.

[6] It also follows from the uncertainty relation that the number of important phase shifts (in any case of nonvanishing phase shifts) for an interaction with a finite radius ($0 < r_0 < \infty$) increases with increasing energy. On the basis of Lehmann's theorem [5] it follows from this that an interaction with a finite radius must be described by an infinite number of phase shifts.

[7] The radius r_0 of the interaction is determined by the mass of the particles that transmit the interaction, and its "strength" (g^2) by their number.

In a paper by Ansel'm and others [2] an attempt is made to obtain restrictions on the maximum value of the interaction constant by starting from the dispersion relations for the forward scattering amplitude (in particular for scattering of π mesons by nucleons), the unitarity relation ("optical" theorem), and the short-range nature of the interaction. From what has been said above it is clear that if we start from these three identities in g^2, which do not internally contradict each other, we cannot obtain any restrictions on the possible values of g^2; consequently, the authors of [2] have essentially made assumptions that are particularly dependent on a model.

To derive restrictions on the maximum value of the interaction constant by the method of [2] it suffices to get a nontrivial ($C \neq 0$) lower bound on the quantity $\operatorname{Im} f(E)/|f(E)|^2$ in some arbitrary (finite) energy range,

$$\operatorname{Im} f(E) / |f(E)|^2 \geqslant C > 0, \qquad (9)$$

which does not depend on g^2. In [2] an estimate of the type (9) is obtained in the following way. It is assumed that in a given energy range $E \in [E_1, E_2]$ the forward scattering amplitude $f(E)$ is completely described by a finite number l_{max} of phase shifts a_l; this number is given by

$$l_{max} = k_2 r_0, \qquad (10)$$

where k_2 corresponds to the energy E_2 and r_0 is the radius of the interaction. Then

$$\operatorname{Im} f(E)/|f(E)|^2 \equiv F(a_l;\, l_{max},\, k)$$

$$= \operatorname{Im}\Big(\frac{1}{2ik}\sum_{l=0}^{l_{max}} a_l\,(2l+1)\Big)\Big/\Big|\frac{1}{2ik}\sum_{l=0}^{l_{max}} a_l\,(2l+1)\Big|^2 \qquad (11)$$

and by regarding $F(a_l)$ as a function of the variables a_l ($l = 0, 1, 2, \ldots, l_{max}$) we easily get a bound for F [2]:

$$\operatorname{Im} f(E)/|f(E)|^2 = F \geqslant C(k_2;\, l_{max},\, k), \qquad (12)$$

where C is the absolute minimum of $F(a_l)$ with respect to all possible a_l. Here it is essential that, since by hypothesis [2] l_{max} is determined by k_2 and r_0 only, and does not depend on g^2 [cf. Eq. (10)], the bound (12) contains a constant C that does not depend on g^2. Without writing out the explicit form of C, we merely note that when $l_{max} \to \infty$, $C \to 0$, and the bound (12) becomes a trivial one. Thus we again verify that to obtain a relation (12) with $C \neq 0$ it is necessary to assume that the forward scattering amplitude is completely (exactly) described by a finite number l_{max} of phase shifts a_l, which does not depend on g^2.

It is not hard to verify that the method of the paper of Ansel'm and others,[2] which we have just explained, cannot be applied in the general case. In fact, from the separation of the phase shifts into "large" and "small" (important and unimportant) phase shifts we can conclude nothing except that for $l < l_{max}$, where l_{max} is given by Eq. (10), the phase shifts are "large," and for $l > l_{max}$ they are "small." It by no means follows, however, (cf. footnote [6]) that, as is required for the method of [2] to apply, l_{max} gives a maximum (finite) number of phase shifts a_l which completely (exactly) describe the forward scattering amplitude, independent of the value of g^2. The only case in which this is true is the highly special case of a model in which the forward scattering amplitude $f(E)$ is completely described by (the same) finite number of phase shifts a_l for all energies E ($\mu < E < \infty$). Only for this model case [with l_{max} fixed a priori, and not at all by Eq. (10)] is the bound (12) valid, and consequently only in this model case does one get on the basis of Eq. (12) a restriction on the possible values of g^2.

The meaning of this restriction is of course that only for $g^2 < g^2_{max}$ can we treat without contradiction the model case in which the forward scattering amplitude, while possessing analytic properties (i.e., satisfying dispersion relations) is completely described for all energies by a fixed finite number of phase shifts. In actual problems we must suppose that this model picture cannot apply. In fact, as can be seen, for example, from the formulas for phase shifts with sufficiently large l ($l \gg kr_0 \gg 1$)—in the pole approximation[10] of Eq. (7) or from a quasi-classical treatment of scattering by a potential[9]—the "unimportant" phase shifts a_l increase with increase of the interaction constant g^2. Therefore we cannot proceed independently of g^2 to neglect phase shifts a_l for large $l > kr_0$ (see also footnote [6]).

The only bound on $\operatorname{Im} f(E)/|f(E)|^2$ that is valid in this case is the trivial one ($C = 0$). In fact, from obvious physical considerations (positiveness of cross sections)

$$\frac{\operatorname{Im} f(E)}{|f(E)|^2} \geqslant \frac{\operatorname{Im}\left(\frac{1}{2ik}\sum_{l=0}^{L} a_l(2l+1)\right)}{\{[\operatorname{Re} f(E)]^2 + [\operatorname{Im} f(E)]^2\}}. \tag{13}$$

But it by no means follows from this that in $\operatorname{Re} f(E)$ we need keep only the finite number of phase shifts a_l ($l = 0, 1, 2, \ldots, L$) that is taken for the calculation of $\operatorname{Im} f(E)$ in the numerator.[8] For the estimate of $\operatorname{Im} f(E)/|f(E)|^2$ not to be in contradiction with the dispersion relations, even when it is assumed that only a finite number L of phase shifts are "important," one must express $\operatorname{Re} f(E)$ in the denominator of Eq. (13) in terms of $\operatorname{Im} f(E)$ by means of the dispersion relation (2). But then

$$\frac{\operatorname{Im} f(E)}{|f(E)|^2} \geqslant \operatorname{Im}\left(\frac{1}{2ik}\sum_{l=0}^{L} a_l(2l+1)\right) \Big/ \left\{\left[\operatorname{Im}\left(\frac{1}{2ik}\sum_{l=0}^{L} a_l(2l+1)\right)\right]^2 + \left[-\frac{g^2}{E-E_0} + \frac{1}{\pi} P\int \operatorname{Im}\left(\frac{1}{2ik'}\sum_{l=0}^{L} a_l(k')(2l+1)\right) \times \frac{dE'}{E'-E}\right]^2\right\} \equiv \Phi(a_l, L, k, g^2, E_0), \tag{14}$$

where Φ already depends explicitly on g^2.

To obtain a lower bound on Φ we can proceed in analogy with [2], and find the absolute minimum of Φ with respect to the a_l for fixed L, k, g^2, E. Consequently, the bound on Φ also depends on g^2. It is not hard to see from Eq. (14) that the only bound on $\operatorname{Im} f(E)/|f(E)|^2$ that is independent of g^2 is the trivial one ($C = 0$).

5. Thus it has been shown that the dispersion relations for the forward scattering amplitude, the unitarity relation ("optical" theorem), and the condition of short-range forces [separation of the phase shifts into "large" (important) and "small" (unimportant) phase shifts] do not depend on the value of the interaction constant and are internally noncontradictory, and that consequently one cannot, using only these conditions, get any restrictions on the possible values of the interaction constant g^2.[9] A similar conclusion is also found when one considers also the dispersion relations (spectral representations) and unitarity relations for the (elastic) scattering amplitude at nonzero angles. One here makes essential use of the property of crossing symmetry of the theory (the presence of a cut on the left) (cf. investigation of the Lee model in a paper by Ter-Martirosyan[12]). It is true that it may be that if we examine the spectral representations and unitarity conditions for all amplitudes (including many-particle amplitudes), they will turn out to be compatible only for quite definite values of the interaction constant and the masses

[8] This assertion is not in contradiction with the fact that, for example in a paper by Pomeranchuk,[11] in determining restrictions on the asymptotic behavior of $|f(E)|$ the same finite number of phase shifts has been taken for both $\operatorname{Re} f(E)$ and $\operatorname{Im} f(E)$, because in[11] g^2 is regarded as fixed.

[9] Owing to this there is no meaning in the hypothesis[2,13] that the strong interaction is the strongest of all possible interactions.

of the particles, but at present it would be unrealistic to discuss this possibility in the framework of the existing theory.

Thus the answer to the question stated at the beginning of this paper must be negative in the general case. Possible restrictions on the maximum value of g^2 can be obtained only for cases of very special models, and actually indicate for which values of g^2 these model cases can be treated without contradiction. The interaction constants, like the masses of the particles, are parameters in the present theory.

In conclusion I express my gratitude to Academician Ya. B. Zel'dovich, V. N. Gribov, I. T. Dyatlov, and A. A. Ansel'm for the opportunity to become acquainted with their papers [1,2] prior to publication.

I am grateful to Professor Ya. A. Smorodinskii and the members of the seminar of the Laboratory of Theoretical Physics of the Joint Institute for Nuclear Research for a discussion. I am grateful to Professor G. I. Petrashen' for his constant interest and a discussion of the work.

Note added in proof (September 4, 1961). The results obtained in the present paper are also fully applicable to papers [14,15] in which the interaction constant is entirely determined in terms of the masses of the interacting particles.

[1] Gribov, Zel'dovich, and Perelomov, JETP **40**, 1190 (1961), Soviet Phys. JETP **13**, 836 (1961).

[2] Ansel'm, Gribov, Danilov, Dyatlov, and Shekhter, JETP **41**, 619 (1961), Soviet Phys. JETP **14**, 444 (1962).

[3] F. Zachariasen, Phys. Rev. **121**, 1851 (1961).

[4] Bogolyubov, Medvedev, and Polivanov, Voprosy teorii dispersionnykh sootnoshenii (Topics in the Theory of Dispersion Relations), Fizmatizdat, 1958.

[5] H. Lehmann, Nuovo cimento **10**, 579 (1958).

[6] L. A. Khalfin, JETP **40**, 493 (1961), Soviet Phys. JETP **13**, 345 (1961).

[7] Castillejo, Dalitz, and Dyson, Phys. Rev. **101**, 453 (1956).

[8] N. G. van Kampen, Phys. Rev. **91**, 1267 (1953).

[9] L. D. Landau and E. M. Lifshitz, Quantum Mechanics, Pergamon, 1958.

[10] L. B. Okun' and I. Ya. Pomeranchuk, JETP **36**, 300 (1959), Soviet Phys. JETP **9**, 207 (1959).

[11] I. Ya. Pomeranchuk, JETP **34**, 725 (1958), Soviet Phys. JETP **7**, 499 (1958).

[12] K. A. Ter-Martirosyan, JETP **37**, 1005 (1959), Soviet Phys. JETP **10**, 714 (1960).

[13] G. F. Chew and S. C. Frautschi, Phys. Rev. Letters **5**, 580 (1960).

[14] L. D. Landau, JETP **39**, 1856 (1960), Soviet Phys. JETP **12**, 1294 (1961).

[15] Y. Nambu and J. Sakurai, Phys. Rev. Letters **6**, 377 (1961).

Translated by W. H. Furry
213

TRANSPORT EQUATION FOR A DEGENERATE SYSTEM OF FERMI PARTICLES

G. M. ÉLIASHBERG

Leningrad Physico-Technical Institute, Academy of Sciences, U.S.S.R.

Submitted to JETP editor May 8, 1961

J. Exptl. Theoret. Phys. (U.S.S.R.) **41**, 1241-1251 (October, 1961)

Applying the temperature-dependent diagram technique and the method of analytic continuation, we give a derivation of the transport equation for the distribution function of excitations in a degenerate Fermi system. The analytic properties of the four-vertex part are studied and the equation for it is extended. We consider briefly whether the results obtained can be applied to the microscopic theory of a Fermi liquid.

1. It is well known that a degenerate Fermi system has an excitation branch of the Fermi type, and the excitations are weakly damped when their momenta are sufficiently close to the limiting Fermi momentum. This property is the basis of the semi-phenomenological theory of a Fermi liquid given by Landau. An application of the quantum field-theoretical methods made it possible to obtain a microscopic interpretation of the most important quantities in the Fermi-liquid theory.[1-3]

The present paper is devoted to a derivation of a transport equation for a degenerate Fermi system. To be specific, we consider the electric conductivity of a normal metal. An application of the temperature-dependent diagram technique and the method of analytic continuation[4] yielded an equation for the distribution function of the excitations in which the collision integral was expressed in terms of the four-vertex part Γ. The connection between the collision integral and Γ is, of course, independent of the character of the transport problem. The results obtained can thus be helpful for studying different problems about the kinetics of a Fermi liquid.

2. When we use the temperature-dependent diagram technique to calculate the conductivity, it is convenient to start from the expression (see [5])

$$\sigma_{\mu\nu}(\mathbf{k}, \omega) = \left(\frac{e}{m}\right)^2 \iint \frac{d^3p d^3p'}{(2\pi)^6} p_\mu \frac{K^R_{pp'}(\mathbf{k}, \omega) - K^R_{pp'}(\mathbf{k}, 0)}{i\omega} p', \quad (1)$$

where e and m are the electronic charge and mass,* k and ω the wave vector and the frequency of the external field, and $K^R_{pp'}(\mathbf{k}, \omega)$ the Fourier component of the retarded commutator

$$\tilde{K}^R_{pp'}(\mathbf{k}, t) = i\langle [e^{i(H-\mu N)t} a^+_{p'-k/2} a_{p'+k/2} e^{-i(H-\mu N)t}, a^+_{p+k/2} a_{p-k/2}]\rangle \theta(t). \quad (2)$$

*We use a system of units in which $\hbar = 1$.

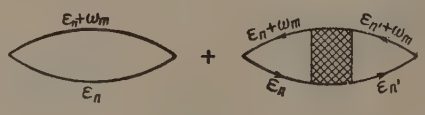

FIG. 1

The average is over a grand canonical ensemble.

We now introduce the function

$$\tilde{K}_{pp'}(\mathbf{k}, \tau) = \langle T_\tau (e^{(H-\mu N)\tau} a^+_{p'-k/2} a_{p'+k/2} e^{-(H-\mu N)\tau}) a^+_{p+k/2} a_{p-k/2}\rangle.$$

The Fourier component of this function

$$K_{pp'}(k, \omega_m) = \frac{1}{2}\int_{-1/T}^{1/T} e^{\omega_m \tau} \tilde{K}_{pp'}(\mathbf{k}, \tau)\, d\tau; \quad \omega_m = 2m\pi i T \quad (3)$$

and the quantity $K^R_{pp'}(\mathbf{k}, \omega)$ are values of the same function, which is analytic in the upper half-plane, respectively in the points ω_m $(m > 0)$ on the imaginary axis and on the real axis. Moreover,

$$K^R_{pp'}(\mathbf{k}, 0) = K_{pp'}(\mathbf{k}, 0). \quad (4)$$

One can check this by performing a Lehmann expansion of the functions K^R and K.

The function $K_{pp'}(\mathbf{k}, \omega_m)$ can be represented by a sum of the diagrams depicted in Fig. 1. These diagrams correspond to the expression

$$K_{pp'}(\mathbf{k}, \omega_m) = -T\sum_n G_{p+k/2}(\varepsilon_n + \omega_m) G_{p-k/2}(\varepsilon_n) \delta_{p-p'} - T^2 \sum_{nn'} G_{p+k/2}(\varepsilon_n + \omega_m) G_{p-k/2}(\varepsilon_n) \Gamma_{pp'k}(\varepsilon_n, \varepsilon_{n'}; \omega_m) \times G_{p'+k/2}(\varepsilon_{n'} + \omega_m) G_{p'-k/2}(\varepsilon_{n'}). \quad (5)$$

Here $G_p(\epsilon_n)$ is the temperature-dependent Green's function defined at the set of points $\epsilon_n = (2n+1)\pi i T$, and $\Gamma_{pp'k}(\epsilon_n, \epsilon_{n'}; \omega_m)$ is the four-vertex part.

3. In order to carry out an analytic continuation in (5) it is necessary to elucidate the analytic properties of Γ. To do this we consider the Lehmann

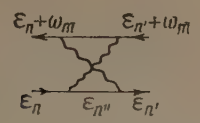

FIG. 2

expansion (given in the Appendix) of the two-particle Green's function $K(\epsilon_n, \epsilon_{n'}; \omega_m)$ with which $\Gamma(\epsilon_n, \epsilon_{n'}; \omega_m)$ is connected in the well-known way. (We dropped the momentum subscripts as they will not interest us in this section.)

It is clear from that expansion that $K(\epsilon, \epsilon'; \omega)$ as function of the complex variables ϵ, ϵ', and ω has singularities when

$$\begin{aligned}
&\text{a) } \operatorname{Im}\varepsilon = 0, \quad \operatorname{Im}(\varepsilon+\omega) = 0, \quad \operatorname{Im}\varepsilon' = 0, \\
&\quad \operatorname{Im}(\varepsilon'+\omega) = 0; \\
&\text{b) } \operatorname{Im}(\varepsilon+\varepsilon'+\omega) = 0; \\
&\text{c) } \operatorname{Im}\omega = 0, \quad \operatorname{Im}(\varepsilon-\varepsilon') = 0.
\end{aligned} \tag{6}$$

These singularities correspond to cuts parallel to the real axis in the complex planes of each argument. The whole space of the variables ϵ, ϵ', and ω is thus divided into several regions in each of which Γ is an analytic function of any of its arguments, while the values of the other arguments are fixed.

Green's functions which are external end points of Γ and which are included in K also possess singularities of the type a). Therefore the presence of these singularities in the function K still does not mean that they also occur in the function Γ. However, a study of the separate diagrams of the vertex part shows that Γ has singularities of the type a). As an example we consider the diagram given in Fig. 2. This diagram corresponds to the expression

$$\begin{aligned}
\Gamma_1(\varepsilon_n, \varepsilon_{n'}; \omega_m) = &T\sum_{n''} G(\varepsilon_{n''}) G(\varepsilon_n+\varepsilon_{n'}+\omega_m-\varepsilon_{n''}) \\
&\times D(\varepsilon_n-\varepsilon_{n''}) D(\varepsilon_{n''}-\varepsilon_{n'}).
\end{aligned}$$

Here D is some boson Green's function corresponding to the interaction. It is most convenient to study the analytic properties of this diagram by substituting for the summation over n'' an integration:

$$\begin{aligned}
\Gamma_1(\varepsilon_n, \varepsilon_{n'}; \omega_m) = &\frac{1}{4\pi i}\int_C dz \operatorname{th}\frac{z}{2T} G(z)\, G(\varepsilon_n+\varepsilon_{n'} \\
&+\omega_m - z) D(\varepsilon_n - z) D(z-\varepsilon_{n'}) + T[G(\varepsilon_n) G(\varepsilon_{n'} \\
&+\omega_m) D(0) D(\varepsilon_n-\varepsilon_{n'}) + G(\varepsilon_{n'}) G(\varepsilon_n+\omega_m) \\
&\times D(\varepsilon_n-\varepsilon_{n'}) D(0)].
\end{aligned} \tag{7}*$$

The contour C is depicted in Fig. 3; it goes around all poles of $\tanh(z/2T)$ except $z = \epsilon_n$ and $z = \epsilon_{n'}$ and does not contain other singularities of the integrand. The integrals over the arcs of the large circle are equal to zero. The integrals over the small circles are compensated by terms outside the integral. Taking into account that

$$\operatorname{th}\frac{\varepsilon+\varepsilon_n}{2T} = \operatorname{cth}\frac{\varepsilon}{2T} \quad \text{and} \quad \operatorname{th}\frac{\varepsilon+\omega_m}{2T} = \operatorname{th}\frac{\varepsilon}{2T},$$

we get thus for Γ_1 the expression

$$\begin{aligned}
\Gamma_1(\varepsilon_n, \varepsilon_{n'}; \omega_m) = &\frac{1}{4\pi i}\int_{-\infty}^{\infty} d\varepsilon'' \Big\{ \operatorname{th}\frac{\varepsilon''}{2T}[G^R(\varepsilon'') \\
&- G^A(\varepsilon'')] G(\varepsilon_n+\varepsilon_{n'}+\omega_m-\varepsilon'') \\
&\times D(\varepsilon_n-\varepsilon'') D(\varepsilon''-\varepsilon_{n'}) + \operatorname{th}\frac{\varepsilon''}{2T}[G^A(-\varepsilon'') \\
&- G^R(-\varepsilon'')] G(\varepsilon''+\varepsilon_n+\varepsilon_{n'}+\omega_m) D(-\varepsilon''-\varepsilon_{n'}-\omega_m) \\
&\times D(\varepsilon''+\varepsilon_n+\omega_m) + \operatorname{cth}\frac{\varepsilon''}{2T}[D^A(-\varepsilon'') \\
&- D^R(-\varepsilon'')] G(\varepsilon''+\varepsilon_n) G(\varepsilon_{n'}+\omega_m-\varepsilon'') D(\varepsilon''+\varepsilon_n \\
&-\varepsilon_{n'}) + \operatorname{cth}\frac{\varepsilon''}{2T}[D^R(\varepsilon'') - D^A(\varepsilon'')] G(\varepsilon''+\varepsilon_{n'}) \\
&\times G(\varepsilon_n+\omega_m-\varepsilon'') D(\varepsilon_n-\varepsilon_{n'}-\varepsilon'')\Big\}.
\end{aligned} \tag{8}$$

The integration in the vicinity of $\epsilon'' = 0$ must refer to the principal value. Since the functions G and D have singularities when the imaginary parts of their arguments tend to zero, the diagram considered here will give all singularities (6), as can be seen from (8).

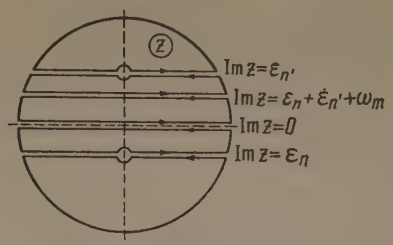

FIG. 3

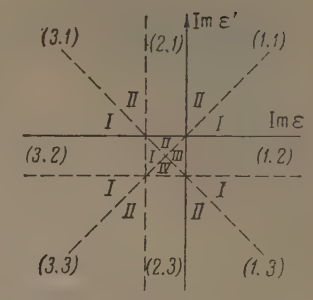

FIG. 4

We shall in the following be interested in the properties of $\Gamma(\epsilon, \epsilon'; \omega)$ as functions of ϵ and ϵ' for fixed values of ω, with $\operatorname{Im}\omega > 0$. It is convenient in that case to represent the analytic properties of Γ as in Fig. 4, where the singularities (6) are plotted in the Im ϵ, Im ϵ' plane. The lines drawn in the figure divide the plane into 16 regions, each of which corresponds to a function Γ which is analytic in that region in any of its arguments. The rectangular regions in the figure are numbered by two indices (i, k), each of which takes on three values. Some of these regions are divided into parts by the diagonal cuts. These parts are denoted by Roman numbers. Such a system of notation is also used for the Γ functions (for instance, $\Gamma^{I}_{1,1}$).

4. We can now carry out the analytic continuation in Eq. (5). To do this we first replace the

*th = tanh, cth = coth, ch = cosh.

sums over n and n′ by integrals, in the same way as was done in the case of the diagram of Fig. 2. We can write

$$T\sum_{n'}\Gamma(\varepsilon_n, \varepsilon_{n'}; \omega_m)\, G(\varepsilon_{n'}+\omega_m)\, G(\varepsilon_{n'}) = \frac{1}{4\pi i}\int_{L'} dz'\, \mathrm{th}\frac{z'}{2T}\,\Gamma(\varepsilon_n, z'; \omega_m)\, G(z'+\omega_m)\, G(z'),$$

where the integration is performed in the positive direction along the edges of the cuts: Im z′ = 0, Im z′ = $-\omega_m$, Im z′ = ϵ_n, and Im z′ = $-\epsilon_n-\omega_m$, while near the points z′ = ϵ_n and z′ = $-\epsilon_n-\omega_m$ the principal value of the integral must be taken. One verifies easily, by writing out explicitly the integrals over the different parts of the contour L′, that the expression obtained has singularities at Im z = 0 and Im z = $-\omega_m$, as function of the complex variable z corresponding to ϵ_n. Using this fact we can replace the sum over n in Eq. (5) by an integral. As a result we obtain an expression which is an analytic function of ω in the upper half-plane. Performing the analytic continuation with respect to ω on the real axis we get finally

$$K^R(\omega) = -\frac{1}{4\pi i}\int_{-\infty}^{\infty} d\varepsilon\Big[\mathrm{th}\frac{\varepsilon}{2T}K_1(\varepsilon,\omega) + \Big(\mathrm{th}\frac{\varepsilon+\omega}{2T} - \mathrm{th}\frac{\varepsilon}{2T}\Big)K_2(\varepsilon,\omega) - \mathrm{th}\frac{\varepsilon+\omega}{2T}K_3(\varepsilon,\omega)\Big], \tag{9}$$

where

$$K_i(\varepsilon,\omega) = g_i(\varepsilon,\omega)\Big\{1 + \frac{1}{4\pi i}\int d\varepsilon'\,\mathcal{T}_{ik}(\varepsilon,\varepsilon';\omega)\,g_k(\varepsilon',\omega)\Big\}, \tag{10}$$

$$g_1(\varepsilon,\omega) = G^R(\varepsilon+\omega)\,G^R(\varepsilon),$$
$$g_2(\varepsilon,\omega) = G^R(\varepsilon+\omega)\,G^A(\varepsilon),$$
$$g_3(\varepsilon,\omega) = G^A(\varepsilon+\omega)\,G^A(\varepsilon). \tag{11}$$

The quantities $\mathcal{T}_{ik}$ are connected with the functions Γ_{ik} which arise because of the analytic continuation of the vertex part, as follows:

$$\mathcal{T}_{11}(\varepsilon,\varepsilon';\omega) = \mathrm{th}\frac{\varepsilon'}{2T}\Gamma^{\mathrm{I}}_{11}(\varepsilon,\varepsilon;\omega) + \mathrm{cth}\frac{\varepsilon'-\varepsilon}{2T}[\Gamma^{\mathrm{II}}_{11}(\varepsilon,\varepsilon';\omega) - \Gamma^{\mathrm{I}}_{11}(\varepsilon,\varepsilon';\omega)],$$

$$\mathcal{T}_{12}(\varepsilon,\varepsilon';\omega) = \Big(\mathrm{th}\frac{\varepsilon'+\omega}{2T} - \mathrm{th}\frac{\varepsilon'}{2T}\Big)\Gamma_{12}(\varepsilon,\varepsilon';\omega),$$

$$\mathcal{T}_{13}(\varepsilon,\varepsilon';\omega) = -\mathrm{th}\frac{\varepsilon'+\omega}{2T}\Gamma^{\mathrm{I}}_{13}(\varepsilon,\varepsilon';\omega) - \mathrm{cth}\frac{\varepsilon'+\varepsilon+\omega}{2T}[\Gamma^{\mathrm{II}}_{13}(\varepsilon,\varepsilon';\omega) - \Gamma^{\mathrm{I}}_{13}(\varepsilon,\varepsilon';\omega)],$$

$$\mathcal{T}_{21}(\varepsilon,\varepsilon';\omega) = \mathrm{th}\frac{\varepsilon'}{2T}\Gamma_{21}(\varepsilon,\varepsilon';\omega),$$

$$\mathcal{T}_{22}(\varepsilon,\varepsilon';\omega) = \Big(\mathrm{cth}\frac{\varepsilon'-\varepsilon}{2T} - \mathrm{th}\frac{\varepsilon'}{2T}\Big)\Gamma^{\mathrm{II}}_{22}(\varepsilon,\varepsilon';\omega) + \Big(\mathrm{cth}\frac{\varepsilon'+\varepsilon+\omega}{2T} - \mathrm{cth}\frac{\varepsilon'-\varepsilon}{2T}\Big)\Gamma^{\mathrm{III}}_{22}(\varepsilon,\varepsilon';\omega) + \Big(\mathrm{th}\frac{\varepsilon'+\omega}{2T} - \mathrm{cth}\frac{\varepsilon'+\varepsilon+\omega}{2T}\Big)\Gamma^{\mathrm{IV}}_{22}(\varepsilon,\varepsilon';\omega),$$

$$\mathcal{T}_{23}(\varepsilon,\varepsilon';\omega) = -\mathrm{th}\frac{\varepsilon'+\omega}{2T}\Gamma_{23}(\varepsilon,\varepsilon';\omega),$$

$$\mathcal{T}_{31}(\varepsilon,\varepsilon';\omega) = \mathrm{th}\frac{\varepsilon'}{2T}\Gamma^{\mathrm{I}}_{31}(\varepsilon,\varepsilon';\omega) + \mathrm{cth}\frac{\varepsilon'+\varepsilon+\omega}{2T}[\Gamma^{\mathrm{II}}_{31}(\varepsilon,\varepsilon';\omega) - \Gamma^{\mathrm{I}}_{31}(\varepsilon,\varepsilon';\omega)],$$

$$\mathcal{T}_{32}(\varepsilon,\varepsilon';\omega) = \Big(\mathrm{th}\frac{\varepsilon'+\omega}{2T} - \mathrm{th}\frac{\varepsilon'}{2T}\Big)\Gamma_{32}(\varepsilon,\varepsilon';\omega);$$

$$\mathcal{T}_{33}(\varepsilon,\varepsilon';\omega) = -\mathrm{th}\frac{\varepsilon'+\omega}{2T}\Gamma^{\mathrm{I}}_{33}(\varepsilon,\varepsilon';\omega) - \mathrm{cth}\frac{\varepsilon'-\varepsilon}{2T}[\Gamma^{\mathrm{II}}_{33}(\varepsilon,\varepsilon';\omega) - \Gamma^{\mathrm{II}}_{33}(\varepsilon,\varepsilon';\omega)]. \tag{12}$$

The problem of the analytic continuation of (5) is solved by Eqs. (9) to (12).

5. For the following it is necessary to elucidate some properties of the Green's functions

$$G^R(x,x') = -i\langle\{\psi(x),\psi^+(x')\}\rangle\theta(t-t'),$$
$$G^A(x,x') = i\langle\{\psi(x),\psi^+(x')\}\rangle\theta(t'-t).$$

In the momentum representation we can write

$$G^R_{\mathbf{p}}(\varepsilon) = [\varepsilon - \varepsilon^0_{\mathbf{p}} - \Sigma^R_{\mathbf{p}}(\varepsilon)]^{-1}, \tag{13}$$

where $\epsilon^0_{\mathbf{p}} = (p^2/2m)-\mu$. The fact that there are weakly damped fermion excitations present in the system corresponds to a well-defined small imaginary part of $\Sigma^R_{\mathbf{p}}(\epsilon)$, namely such that, if the temperature is sufficiently low and $\epsilon \sim T$, $\epsilon^0_{\mathbf{p}} \sim T$; $\mathrm{Im}\,\Sigma^R_{\mathbf{p}}(\epsilon) \ll T$. It follows from this that if $\epsilon \sim T$ and $v|p-p_0| \sim T$ (v is the velocity on the Fermi surface),

$$\mathrm{Im}\,G^R_{\rho}(\varepsilon) = -\pi a\delta(\varepsilon - \varepsilon_{\mathbf{p}}), \tag{14}$$

where $\epsilon_{\mathbf{p}}$ is the root of the equation $\epsilon - \epsilon^0_{\mathbf{p}} - \mathrm{Re}\,\Sigma^R_{\mathbf{p}}(\epsilon) = 0$, and

$$a = \Big[1 - \frac{\partial}{\partial\varepsilon}\mathrm{Re}\,\Sigma^R_{\mathbf{p}}(\varepsilon)|_{\varepsilon=\varepsilon_{\mathbf{p}}}\Big]^{-1} \tag{15}$$

We consider now the quantities g_i defined by Eqs. (11). When $\omega \ll T$ and $vk \ll T$,

$$g_1(P,K) \approx |G^R(P)|^2; \qquad P = (\varepsilon, \mathbf{p}), \qquad K = (\omega, \mathbf{k}),$$

i.e., we can assume that g_1 is in that case independent of ω and $\mathbf{k}$. If this quantity occurs in an integral where values $\epsilon \sim T$ and $v|p-p_0| \sim T$ are important, we can use for it the simple expression

$$g_1(P,K) \approx a^2(\varepsilon - \varepsilon_{\mathbf{p}} + i\delta)^{-2}, \qquad \delta = +0. \tag{16}$$

The quantity $g_3 = g_1^*$ has the same properties. Only the function $g_2(P,K) = G^R_{\mathbf{p}+\mathbf{k}/2}(\epsilon+\omega)\cdot G^R_{\mathbf{p}-\mathbf{k}/2}(\epsilon)$ depends appreciably on ω and $\mathbf{k}$ for small values of ω and k.

We shall see that in all integrals which contain g_2 the domain of integration is limited by the values $\epsilon \sim T$ and $v|p-p_0| \sim T$. We can thus write for $\omega \ll T$ and $vk \ll T$

$$g_2(P,K) \approx 2\pi i a^2\delta(\varepsilon - \varepsilon_{\mathbf{p}})/(\omega - \mathbf{vk} + 2i\gamma_{\mathbf{p}}) \tag{17}$$

where

$$\mathbf{v} \equiv \mathbf{p}/m^* = a\,[\mathbf{p}/m + \nabla_{\mathbf{p}} \operatorname{Re} \Sigma_{\mathbf{p}}(\varepsilon)|_{\varepsilon=\varepsilon_{\mathbf{p}}}], \quad (18)$$

$$\gamma_{\mathbf{p}} = -a \operatorname{Im} \Sigma^R_{\mathbf{p}}(\varepsilon_{\mathbf{p}}) > 0. \quad (19)$$

In accordance with what was said before, $\gamma_{\mathbf{p}} \ll T$ when $v|p - p_0| \sim T$.

6. We consider now in somewhat greater detail the properties of the quantities $\mathcal{T}_{ik}$. We note first that some graphic representation of these quantities is possible. We introduce the irreducible parts $\mathcal{T}^{(1)}_{ik}$ which are obtained, as the result of the analytic continuation and of applying Eq. (12), from all diagrams $\Gamma^{(1)}(\epsilon_n, \epsilon_{n'}; \omega_m)$ which do not contain a pair of lines of the type $G(\epsilon_n + \omega_m)\,G(\epsilon_n)$. One can then easily verify that $\mathcal{T}_{ik}$ satisfies the equation

$$\mathcal{T}_{ik}(P, P'; K) = \mathcal{T}^{(1)}_{ik}(P, P'; K) + \frac{1}{2i(2\pi)^4}\int d^4P''\,\mathcal{T}^{(1)}_{il}(P, P''; K)\,g_l(P'', K)\,\mathcal{T}_{lk}(P'', P'; K). \quad (20)$$

This means that $\mathcal{T}_{ik}$ can be written as the sum of diagrams containing different numbers of irreducible parts $\mathcal{T}^{(1)}$, which we depict by shaded rectangles and which are joined by pairs of lines g_l which we shall call sections l.

We saw that from among the three functions g_i only g_2 depends appreciably on ω and k when ω and k are small. It is thus expedient to introduce for each of the functions $\mathcal{T}_{ik}$ the totality of diagrams $\mathcal{T}^{(0)}_{ik}$ which does not contain the section 2. We shall then have instead of the set of Eqs. (20) one equation for $\mathcal{T}_{22}$:

$$\mathcal{T}_{22}(P, P'; K) = \mathcal{T}^{(0)}_{22}(P, P'; K) + \frac{1}{2i(2\pi)^4}\int d^4P''\,\mathcal{T}^{(0)}_{22}(P, P''; K)\,g_2(P'', K) \times \mathcal{T}_{22}(P'', P'; K), \quad (21)$$

whereas all other quantities $\mathcal{T}_{ik}$ can be expressed in terms of $\mathcal{T}_{22}$ and $\mathcal{T}^{(0)}_{ik}$ as is shown in Fig. 5. If $vk \ll T$ we can assume that all $\mathcal{T}^{(0)}_{ik}$ are independent of k. The dependence of these quantities on ω occurs in practice only because of the hyperbolic functions in (12). In particular, the functions $\mathcal{T}_{12}$ and $\mathcal{T}_{32}$ are proportional to $\tanh[(\epsilon+\omega)/2T] - \tanh(\epsilon/2T)$ and tend to zero for $\omega = 0$. Therefore, when $\omega = 0$ the functions $\mathcal{T}_{ik}$, with the exception of $\mathcal{T}_{22}$, do not contain diagrams which have at least one section 2.

We need relations connecting the derivatives of the Green's functions with the quantities $\mathcal{T}_{ik}$ at K = 0. These relations can be obtained in a way similar to the one used for T = 0 [2] or through an analytic continuation of the relations for the temperature-dependent diagram technique. [6] We shall therefore give them without derivation

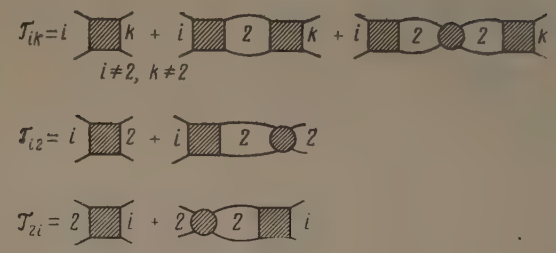

FIG. 5

$$\frac{\partial}{\partial\varepsilon}[G^R_{\mathbf{p}}(\varepsilon)]^{-1} = 1 + \frac{1}{2i(2\pi)^4}\int d^4P'\,\{\mathcal{T}_{11}(P, P')\,[G^R(P')]^2 + \mathcal{T}_{13}(P, P')\,[G^A(P')]^2\}, \quad (22)$$

$$\frac{\partial}{\partial p}[G^R_{\mathbf{p}}(\varepsilon)]^{-1} = -\frac{\mathbf{p}}{m} - \frac{1}{2i(2\pi)^4}\int d^4P'\,\mathbf{p}'\,\{\mathcal{T}_{11}(P, P')\,[G^R(P')]^2 + \mathcal{T}_{13}(P, P')\,[G^A(P')]^2\}. \quad (23)$$

7. We show now that the conductivity $\sigma_{\mu\nu}$ can be expressed in terms of the single function $\mathcal{T}_{22}$ only, while the other $\mathcal{T}_{ik}$ determine the values of renormalization constants.

Bearing in mind the case $\omega \ll T$, $kv \ll T$ we retain a dependence on ω and k only in g_2 and $\mathcal{T}_{i2}$. It then follows from (1) and (9) that we need only be interested in those diagrams $K_1(\epsilon, \omega)$ and $K_3(\epsilon, \omega)$ which contain at least one section 2. All those diagrams and also the diagrams forming $K_2(\epsilon, \omega)$ are illustrated in Fig. 6, in which the rectangles correspond to the quantities $\mathcal{T}^{(0)}$ which do not contain sections 2, and a circle represents $\mathcal{T}_{22}$. Substituting the expressions for the K_i corresponding to these diagrams into (9) and (1), and applying Eq. (17), we get

$$\sigma_{\mu\nu}(\mathbf{k}, \omega) = \frac{i}{2}\left(\frac{e}{m}\right)^2 a^2 \left\{\int \frac{d^3p}{(2\pi)^3}\,Q^{(1)}_{\mu}(\mathbf{p})\,\frac{(1/2T)\,\mathrm{ch}^{-2}(\varepsilon_{\mathbf{p}}/2T)}{\omega - \mathbf{vk} + 2i\gamma_{\mathbf{p}}} \times Q^{(2)}_{\nu}(\mathbf{p}) + \frac{a^2}{2}\int \frac{d^3p\,d^3p'}{(2\pi)^6}\,Q^{(1)}_{\mu}(\mathbf{p}) \times \frac{(1/2T)\,\mathrm{ch}^{-2}(\varepsilon_{\mathbf{p}}/2T)\,\mathcal{T}_{22}(p, p'; k, \omega)}{[\omega - \mathbf{vk} + 2i\gamma_{\mathbf{p}}](\omega - \mathbf{v'k} + 2i\gamma_{p'})}\,Q^{(2)}_{\nu}(\mathbf{p}'), \quad (24)$$

where $Q^{(1)}_{\mu}(\mathbf{p})$ and $Q^{(2)}_{\mu}(\mathbf{p})$ are the values at $\epsilon = \epsilon_{\mathbf{p}}$ of the following quantities

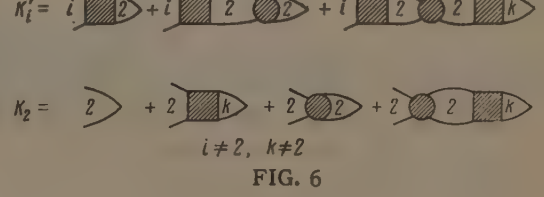

FIG. 6

$$Q_\mu^{(1)} = p_\mu + \frac{2T}{\omega}\operatorname{ch}^2\frac{\varepsilon}{2T}\frac{1}{2i(2\pi)^4}\int d^4P''\, p_\mu''\operatorname{th}\frac{\varepsilon''}{2T}\,[g_1(P'')$$
$$\times \mathcal{T}_{12}^{(0)}(P'', P; \omega) - g_3(P'')\,\mathcal{T}_{32}^{(0)}(P'', P'; \omega)], \qquad (25)$$

$$Q_\mu^{(2)} = p_\mu + \frac{1}{2i(2\pi)^4}\int d^4P''\,[\mathcal{T}_{21}^{(0)}(P, P'')\,g_1(P'')$$
$$+\mathcal{T}_{23}^{(0)}(P, P'')\,g_3(P'')]\,p_\mu''. \qquad (26)$$

We took here into account that $\mathcal{T}_{2i}^{(0)}(P, P''; K) \approx \mathcal{T}_{2i}^{(0)}(P, P''; 0)$. The quantities $\mathcal{T}_{i2}(P'', P; \omega)$ contain a factor $(\omega/2T)\cosh^{-2}(\epsilon_p/2T)$, and are otherwise independent of ω.

Using Eqs. (12) we can write

$$Q_\mu^{(1)} = p_\mu + \frac{1}{2i(2\pi)^4}\int d^4P''\,p_\mu''\operatorname{th}\frac{\varepsilon''}{2T}\,[g_1(P'')\,\Gamma_{12}^{(0)}(P'', P)$$
$$-g_3(P'')\,\Gamma_{32}^{(0)}(P'', P)],$$
$$Q_\mu^{(2)} = p_\mu + \frac{1}{2i(2\pi)^4}\int d^4P''\,p_\mu''\operatorname{th}\frac{\varepsilon''}{2T}\,[\Gamma_{21}^{(0)}(P, P'')\,g_1(P'')$$
$$-\Gamma_{23}^{(0)}(P, P'')\,g_3(P'')].$$

By considering the separate diagrams of the vertex part or the Lehmann expansion for the two-particle Green's function (see Appendix) one can easily check that

$$\Gamma_{i2}(P'', P) = \Gamma_{2i}(P, P''), \qquad \Gamma_{12}(P, P'') = [\Gamma_{32}(P, P'')]^*.$$

Thus, $\mathbf{Q}^{(1)} = \mathbf{Q}^{(2)} = \mathbf{Q}$, where $\mathbf{Q}$ is a real quantity. It is clear that

$$\mathbf{Q}(\mathbf{p}) = \alpha\mathbf{p}. \qquad (27)$$

From our earlier considerations it follows that

$$\alpha^2 = (m/am^*)^2. \qquad (28)$$

We write the quantities $\mathcal{T}_{21}^{(0)}$ and $\mathcal{T}_{23}^{(0)}$ which occur in (26) in the following form:

$$\mathcal{T}_{2i}^{(0)}(P, P'') = \tfrac{1}{2}\left[\mathcal{T}_{1i}(P, P'') + \mathcal{T}_{3i}(P, P'')\right] + \left\{\mathcal{T}_{2i}^{(0)}(P, P'')\right.$$
$$\left. -\tfrac{1}{2}\left[\mathcal{T}_{1i}(P, P'') + \mathcal{T}_{3i}(P, P'')\right]\right\}.$$

A simple, though rather tedious study of the separate diagrams shows that when $\epsilon \sim T$ the second term differs from zero only in an interval $\epsilon'' \sim T$, while outside that interval it decreases exponentially. Assuming that all diagrams have this property we get the result that one can in (26) replace $\mathcal{T}_{2i}^{(0)}$ by $\frac{1}{2}[\mathcal{T}_{1i} + \mathcal{T}_{3i}]$. Indeed, if we substitute the difference $\mathcal{T}_{2i}^{(0)} - \frac{1}{2}[\mathcal{T}_{1i} + \mathcal{T}_{3i}]$ into (26), we find that in the integral the values $\epsilon'' \sim T$, $v|p''-p_0| \sim T$ are the important ones. Since we are, moreover, interested in the value of $\mathbf{Q}(\mathbf{p})$ when $v|p-p_0| \sim T$ one may assume that the above-mentioned difference depends only on $p-p''$. We get thus when we use Eq. (16) and integrate over $\epsilon_{p''} = v(p''-p_0)$ the result that the integral vanishes. Equation (28) follows then from (23) and (18). Equations (24), (27), and (28) completely determine the connection between $\sigma_{\mu\nu}$ and $\mathcal{T}_{22}$.

8. We now introduce the quantity $f_p(k, \omega)$, which is the change in the excitation distribution function which is linear in the external field $\mathbf{E}$, starting from the equation

$$j_\mu(k, \omega) = \frac{e}{m^*}\int\frac{d^3p}{(2\pi)^3}\,p_\mu\, f_p(k, \omega).$$

It then follows from (24), (27), and (28) that

$$f_p(k, \omega) = \frac{i}{2}\frac{e}{m^*}\frac{(1/2T)\operatorname{ch}^{-2}(\epsilon_p/2T)}{\omega - vk + 2i\gamma_p}$$
$$\times E_\nu\left\{p_\nu + \frac{1}{2}\int\frac{d^3p'}{(2\pi)^3},\ \frac{a^2\mathcal{T}(p, p'; k, \omega)}{\omega - v'k + 2i\gamma_{p'}}\,p_\nu'\right\}. \qquad (29)$$

(Here and henceforth we drop the subscripts in $\mathcal{T}_{22}$.) The equation for $f_p(k, \omega)$ follows directly from Eq. (21) for $\mathcal{T}$. Introducing, as usual, instead of f_p a function φ_p such that $f_p(k, \omega) = \varphi_p(k, \omega)\,dn_p/d\epsilon_p$, where $n_p = (e^{\epsilon_p/T}+1)^{-1}$, we get

$$i(\omega - vk)\,\varphi_p(k, \omega) = e\,vE + i\frac{a^2}{2}\int\frac{d^3p'}{(2\pi)^3}\,\mathcal{T}^{(0)}(p, p'; k, \omega)\,\varphi_{p'}(k, \omega)$$
$$+2\gamma_p\varphi_p(k, \omega). \qquad (30)$$

The quantity $\mathcal{T}^{(0)}$ representing all diagrams that do not contain sections 2 consists of an irreducible part $\mathcal{T}^{(1)}$ which neither contains sections 1 nor 3 and of diagrams which have different numbers of sections 1 and 3. Such diagrams are illustrated in Fig. 7. It is clear that they all contain the quantity $\mathcal{T}_{i2}(P, P')$ and it then follows from (12) that they are all proportional to $(\omega/2T)\cosh^{-2}(\epsilon_p/2T)$.

If we also split off from $\mathcal{T}^{(1)}$ the part proportional to ω we write $\mathcal{T}^{(0)}$ in the form

$$\mathcal{T}^{(0)}(p, p'; \omega) = \mathcal{T}^{(1)}(p, p') + \frac{\omega}{2T}\operatorname{ch}^{-2}\frac{\epsilon_p}{2T}\,\mathcal{T}^{(2)}(p, p'). \qquad (31)$$

By studying separate diagrams or from the Lehmann expansion for the two-particle Green's function we can check that $\mathcal{T}(P, P'; K)$ is a purely imaginary quantity for $K = 0$. Since $g_2(P, K)$ is real at $K = 0$, $\mathcal{T}^{(1)}(P, P')$ is also a purely imaginary quantity. The expression

$$I = \frac{ia^2}{2}\int\frac{d^3p'}{(2\pi)^3}\,\mathcal{T}^{(1)}(p, p')\,\varphi_{p'}(k, \omega) + 2\gamma_p\,\varphi_p(k, \omega) \qquad (32)$$

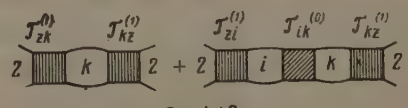

$i \neq 2,\ k \neq 2$

FIG. 7

is thus the collision integral in the transport equation (30). We explain the significance of the second term in (31) in the following.

9. There is, of course, a direct connection between the transport equation and Eq. (21) for the vertex part $\mathcal{J}$ not only for the problem of electrical conductivity considered here. In order to establish the connection between the quantity $\mathcal{J}$ introduced by us and the vertex part occurring in the zero-temperature diagram technique, we show how one can obtain from (21) the equation for zero sound in a Fermi liquid.[1]

We consider Eq. (21) in the limiting case $\omega\tau \gg 1$, where τ is the relaxation time which is of the order of magnitude of $\gamma_{\mathbf{p}}^{-1}$. Since the collision integral (32) can be written in the form φ/τ for estimating purposes, it follows that $\mathcal{J}^{(1)}$ is of the order of magnitude of $\mu/p_0^3\tau T$. On the other hand, if we estimate the simplest diagrams we get easily the result that $\mathcal{J}^{(2)}$ in (31) is of the order of magnitude μ/p_0^3. Therefore, when $\omega\tau \ll 1$, the quantity $\mathcal{J}^{(0)} \approx \mathcal{J}^{(1)}$, whereas for $\omega\tau \gg 1$

$$\mathcal{J}^{(0)}(\mathbf{p}, \mathbf{p}'; \omega) \approx \frac{\omega}{2T} \operatorname{ch}^{-2}\frac{\varepsilon_{\mathbf{p}}}{2T}\, \mathcal{J}^{(2)}(\mathbf{p}, \mathbf{p}').$$

We shall be interested just in that case. Neglecting in (21) terms of the order of magnitude $(\omega\tau)^{-1}$, we get

$$\mathcal{J}(\mathbf{p}, \mathbf{p}'; \mathbf{k}, \omega) = \frac{\omega}{2T} \operatorname{ch}^{-2}\frac{\varepsilon_{\mathbf{p}'}}{2T}\, \mathcal{J}^{(2)}(\mathbf{p}, \mathbf{p}') + \frac{a^2}{2}\int \frac{d^3p''}{(2\pi)^3}\frac{1}{2T}\operatorname{ch}^{-2}\frac{\varepsilon_{\mathbf{p}''}}{2T}\,\frac{\omega \mathcal{J}^{(2)}(\mathbf{p}, \mathbf{p}'')}{\omega - \mathbf{v}''\mathbf{k} + i\delta}\,\mathcal{J}(\mathbf{p}'', \mathbf{p}'; k, \omega). \quad (33)$$

Introducing the notation

$$\mathcal{J}(\mathbf{p}, \mathbf{p}'; 0, \omega) = \frac{\omega}{2T}\operatorname{ch}^{-2}\frac{\varepsilon_{\mathbf{p}'}}{2T}\,\Gamma^{\omega}(\mathbf{p}, \mathbf{p}') \quad (\omega\tau \gg 1), \quad (34)$$

we get for $\mathbf{k} = 0$ for Γ^{ω} the equation

$$\Gamma^{\omega}(\mathbf{p}, \mathbf{p}') = \mathcal{J}^{(2)}(\mathbf{p}, \mathbf{p}') + \frac{a^2}{2}\int \frac{dp''}{(2\pi)^3}\frac{1}{2T} \times \operatorname{ch}^{-2}\frac{\varepsilon_{\mathbf{p}''}}{2T}\,\mathcal{J}^{(2)}(\mathbf{p}, \mathbf{p}'')\,\Gamma^{\omega}(\mathbf{p}'', \mathbf{p}'). \quad (35)$$

In the integral term in this equation and also in Eq. (33) practically only the quantity $\cosh^{-2}(\epsilon_{\mathbf{p}''}/2T)$ depends on the magnitude of the vector $\mathbf{p}''$. Integrating over $\mathbf{p}''$ and eliminating $\mathcal{J}^{(2)}$ from (35) and (33) we get thus

$$\mathcal{J}(\mathbf{p}, \mathbf{p}'; \mathbf{k}, \omega) = \frac{\omega}{2T}\operatorname{ch}^{-2}\frac{\varepsilon_{\mathbf{p}'}}{2T}\,\Gamma^{\omega}(\mathbf{p}, \mathbf{p}') + \frac{a^2 p_0}{(2\pi)^3}\int d\sigma_{\mathbf{p}''} \times \frac{\mathbf{p}''\mathbf{k}\,\Gamma^{\omega}(\mathbf{p}, \mathbf{p}'')}{\omega - \mathbf{v}''\mathbf{k} + i\delta}\,\mathcal{J}(\mathbf{p}'', \mathbf{p}'; \mathbf{k}, \omega). \quad (36)$$

To find the natural vibrations corresponding to zero sound we must drop the free term. The equation we obtain then is the same as Landau's equation.[1] We can thus conclude that the quantity Γ^{ω} is the same as the corresponding quantity occurring in the zero-temperature diagram technique.

(The case $\omega\tau \gg 1$ corresponds for $T = 0$ to the limiting transition $k = 0$, $\omega \to 0$.) When deriving Eq. (36) we completely neglected terms of the order $(\omega\tau)^{-1}$. When such terms are taken into account it is possible to obtain the damping of zero sound and also to consider other phenomena connected with damping. To do this, it is, however, necessary to study in detail the structure of the quantities $\mathcal{J}^{(1)}$ and $\gamma_{\mathbf{p}}$, which is outside the framework of the present paper.

The author is very grateful to L. É. Gurevich and V. I. Perel' for discussing a number of problems connected with the present paper.

APPENDIX

We perform the spectral expansion of the two-particle temperature-dependent Green's function

$$K(x_1x_2; x_3x_4) = \langle T\psi(x_1)\psi(x_2)\psi^+(x_3)\psi^+(x_4)\rangle,$$

where

$$\psi(x) = e^{(H-\mu N)\tau}\,\psi(r)\,e^{-(H-\mu N)\tau}.$$

This function consists of 24 parts corresponding to different permutations of the ψ operators. All permutations fall into six cycles with four permutations in each.

The contribution from the cycle created by the order 1-2-3-4 is equal to

$$\begin{aligned} K_1(x_1x_2; x_3x_4) = \sum_{\alpha_1\alpha_2\alpha_3\alpha_4} & \langle\alpha_1|\psi(r_1)|\alpha_2\rangle\langle\alpha_2|\psi(r_2)|\alpha_3\rangle \\ & \times \langle\alpha_3|\psi^+(r_3)|\alpha_4\rangle\langle\alpha_4|\psi^+(r_4)|\alpha_1\rangle \exp\{E_1(\tau_1-\tau_4) \\ & + E_2(\tau_2-\tau_1) + E_3(\tau_3-\tau_2) + E_4(\tau_4-\tau_3)\} \\ & \times [e^{-E_1/T}\theta(\tau_1-\tau_2)\theta(\tau_2-\tau_3)\theta(\tau_3-\tau_4) \\ & - e^{-E_2/T}\,\theta(\tau_2-\tau_3)\,\theta(\tau_3-\tau_4)\theta(\tau_4-\tau_1) \\ & + e^{-E_3/T}\,\theta(\tau_3-\tau_4)\theta(\tau_4-\tau_1)\theta(\tau_1-\tau_2) \\ & - e^{-E_4/T}\theta(\tau_4-\tau_1)\theta(\tau_1-\tau_2)\,\theta(\tau_2-\tau_3)]. \end{aligned} \quad (A.1)$$

Here all energies E_i are calculated from μN_i. We choose from the four differences $\tau_i - \tau_k$ any three independent ones, for instance $t_1 = \tau_1 - \tau_2$, $t_2 = \tau_2 - \tau_3$, and $t_3 = \tau_3 - \tau_4$ and carry out in them a periodic continuation from the interval $(-1/T, 1/T)$ onto the whole axis of imaginary times. To do this one needs expand (A.1) in a triple Fourier series in terms of t_1, t_2, and t_3, taking into account that we must have $|t_1 + t_2 + t_3| \equiv |\tau_1 - \tau_4| \leq 1/T$. Carrying out next a Fourier-series expansion in all four τ_i, we get for the Fourier components the expression

$$K_1(\varepsilon_1\varepsilon_2; \varepsilon_3\varepsilon_4) = T^{-1}\delta(\varepsilon_1 + \varepsilon_2 - \varepsilon_3 - \varepsilon_4)\,K_1'(\varepsilon_1\varepsilon_2; \varepsilon_3\varepsilon_4).$$

The function K_1' depends in actual fact on three variables for which we choose $\epsilon = \epsilon_4$, $\epsilon' = \epsilon_2$, and $\omega = \epsilon_1 - \epsilon_4 = \epsilon_3 - \epsilon_2$. In terms of these variables

$$K_1'(\varepsilon, \varepsilon'; \omega) = \sum_{\alpha_1\alpha_2\alpha_3\alpha_4} A(1,2,3,4) \times \left\{ \frac{e^{-E_1/T}}{(E_2-E_1-\varepsilon-\omega)(E_3-E_1-\varepsilon-\varepsilon'-\omega)(E_4-E_1-\varepsilon)} - \frac{e^{-E_2/T}}{(E_1-E_2+\varepsilon+\omega)(E_3-E_2-\varepsilon')(E_4-E_2+\omega)} + \frac{e^{-E_3/T}}{(E_1-E_3+\varepsilon+\varepsilon'+\omega)(E_2-E_3+\varepsilon')(E_4-E_3+\varepsilon'+\omega)} - \frac{e^{-E_4/T}}{(E_1-E_4+\varepsilon)(E_2-E_4-\omega)(E_3-E_4-\varepsilon')} \right\}, \quad (A.2)$$

where $\epsilon = (2n+1)\pi iT$; $\omega = 2m\pi iT$; the quantity $A(1,2,3,4)$ is the product of matrix elements of the ψ operators occurring in (A.1). The corresponding formulae for the other cycles are obtained from (A.2) by simple permutations of the indices.

[1] L. D. Landau, JETP **35**, 97 (1958), Soviet Phys. JETP **8**, 70 (1959).

[2] L. P. Pitaevskii, JETP **37**, 1794 (1959), Soviet Phys. JETP **10**, 1267 (1960).

[3] V. I. Karpman, JETP **39**, 185 (1960), Soviet Phys. JETP **12**, 133 (1961).

[4] A. A. Abrikosov, L. P. Gor'kov, and I. E. Dzyaloshinskii, JETP **36**, 900 (1959), Soviet Phys. JETP **9**, 636 (1959); E. S. Fradkin, JETP **36**, 1286 (1959), Soviet Phys. JETP **9**, 912 (1959).

[5] V. I. Perel' and G. M. Éliashberg, JETP **41**, 886 (1961), Soviet Phys. JETP **14**, 633 (1962).

[6] E. S. Fradkin, JETP **38**, 157 (1960), Soviet Phys. JETP **11**, 114 (1960).

Translated by D. ter Haar
214

CONCERNING THE ELECTROMAGNETIC STRUCTURE OF THE K MESON

A. A. STARTSEV

Moscow State University

Submitted to JETP editor May 9, 1961

J. Exptl. Theoret. Phys. (U.S.S.R.) 41, 1252-1253 (October, 1961)

An expression for the isovector part of the electromagnetic form factor of the K meson has been deduced by applying the dispersion relation technique to the problem of the electromagnetic structure of the K meson. The electromagnetic radius of the K meson is calculated under the assumption of a narrow $\pi\pi$ resonance.

SEVERAL authors have in recent times successfully applied the double dispersion relation technique to the discussion of reactions involving π mesons and nucleons as well as to the problem of the electromagnetic structure of the nucleon and the pion. We are thus encouraged to go on to the consideration of reactions involving strange particles. In the same way as the pion-pion interaction plays a fundamental role in the problem of the scattering of nucleons and pions, the πK interaction is the determining factor in reactions involving strange particles. This last interaction has been given considerable attention in recent times. Since direct experiments on πK scattering are at present impossible, one may obtain information on the πK interaction from the analysis of various reactions in which K mesons participate. Thus the analysis of experiments on K^-N scattering[1] and K^+N scattering[2] with the help of the double dispersion representation leads to certain conclusions concerning the amplitude of the process $\pi + \pi \to K + \bar{K}$.

In view of the success of the dispersion representation approach in the investigation of the electromagnetic form factor of the nucleon[3] and of the K^-N scattering[1] and the K^+N scattering[2] it is possible to obtain some information on the electromagnetic structure of the K meson.

Let us consider the current density operator of the K meson taken between a kaon-antikaon state and the vacuum. Owing to Lorentz and gauge invariance it can be written in the form

$$\langle p_1 p_2 \mid j_\mu(0) \mid 0\rangle = (p_1 - p_2)_\mu F_K(t)/\sqrt{p_{10}p_{20}}, \quad (1)$$

where p_1 and p_2 are the four-momenta of the kaon and antikaon, and

$$t = -(p_1 - p_2)^2 = (p_{10} - p_{20})^2 - (\mathbf{p}_1 - \mathbf{p}_2)^2.$$

The form factor of the K meson $F_K(t)$ can be divided up into an isoscalar and an isovector part:

$$F_K(t) = F_K^S(t) + \tau_3 F_K^V(t), \quad F_K^S(0) = F_K^V(0) = e/2.$$

We shall restrict our discussion to the isovector part $F_K^V(t)$, which satisfies the dispersion relation

$$F_K^V(t) = \frac{e}{2} + \frac{t}{\pi}\int_{4\mu^2}^{\infty} \frac{\operatorname{Im} F_K^V(t')\,dt'}{t'(t'-t)} \quad (2)$$

We have performed a subtraction in order to improve the convergence of the integral.

In calculating $\operatorname{Im} F_K^V(t)$ with the help of the unitarity condition we shall take only two-pion intermediate states into account. We have then

$$\operatorname{Im} F_K^V(t) = \frac{e}{2\pi}\frac{q^3}{4E} b_1^+(t)\, F_\pi(t), \quad (3)$$

where $q^2 = t/4 - \mu^2$, $E = \sqrt{q^2 + m_K^2}$, $F_\pi(t)$ is the form factor of the pion, and $b_1(t)$ is the partial amplitude for the process $\pi + \pi \to K + \bar{K}$ in the state $T = J = 1$.

Assuming a narrow resonance of the $\pi\pi$ interaction in the state $T = J = 1$, we can express $b_1(t)$ approximately as[4]

$$b_1(t) = (\xi/4\pi)\, F_\pi(t),$$

where ξ is some phenomenological constant. Hence

$$F_K^V(t) = \frac{e}{2}\left[1 + \frac{t}{\pi^2}\left(\frac{\xi}{4\pi}\right)\int_{4\mu^2}^{\infty} \frac{q'^3}{4E'}\frac{|F_\pi(t')|^2}{t'(t'-t)}\,dt'\right]. \quad (4)$$

We shall use the following expression for F_π:[5]

$$F_\pi(t) = \frac{11.3}{11.5 - t - i\,2.32}.$$

This expression agrees roughly with the pion form factor of Frazer and Fulco,[3] but is more convenient for calculations. To simplify matters, we make the replacement

$$|F_\pi(t)|^2 = \frac{(11.3)^2}{2.32}\frac{\gamma}{(t-t_r)^2+\gamma^2} \to \frac{(11.3)^2}{2.32}\pi\delta(t_r - t), \quad (5)$$

where $t_r = 11.5\,\mu^2$ and $\gamma = 2.32\,\mu^2$. Then

$$F_K^V(t) = \frac{e}{2}\left(1 + A\frac{\xi}{4\pi}\frac{t}{t_r - t}\right), \quad (6)$$

where $A \approx 0.576$.

With the help of (6) we can calculate the isovector radius of the K meson:

$$\langle (r_K^V)^2 \rangle \approx 6A\xi/t_r 4\pi \approx 0.3\xi/4\pi.$$

The analysis of the energy dependence of the K^-N and K^+N scattering phases[1,2] shows that $0.5 \leq \xi/4\pi \leq 1$ for $t_r = 11.5\mu^2$. We then obtain

$$5.4 \cdot 10^{-14}\text{cm} \leqslant r_K^V \leqslant 7.8 \cdot 10^{-14}\text{ cm},$$

which is in approximate agreement with the electromagnetic dimensions of the nucleon.

The author expresses his gratitude to A. M. Brodskii for a useful discussion and also to D. Ivanenko for his interest in this work.

[1] Ferrari, Frye, and Pusterla, Phys. Rev. Lett. 4, 615 (1960).

[2] B. W. Lee, Phys. Rev. 121, 1550 (1961).

[3] W. R. Frazer and J. R. Fulco, Phys. Rev. Lett. 2, 365 (1959); Phys. Rev. 117, 1609 (1960).

[4] B. W. Lee and K. S. Cho, Modified Static Equations for the πK Interaction. Effect of Pion-pion Resonance (preprint).

[5] S. C. Frautschi and J. D. Walecka, Phys. Rev. 120, 1486 (1960).

Translated by R. Lipperheide
215

ON THE THEORY OF THE SPIN ECHO

A. R. KESSEL'

Physico-Technical Institute, Kazan' Branch, Academy of Sciences, U.S.S.R.

Submitted to JETP editor May 11, 1961

J. Exptl. Theoret. Phys. (U.S.S.R.) 41, 1254-1257 (October, 1961)

A theoretical discussion is given of the effect of two resonance pulses—an acoustic and an electromagnetic one, and also of two acoustic pulses—on the nuclear spin system in a cubic crystal. Expressions describing the effect of the acoustic pulse on the free precession signal due to the electromagnetic pulse and expressions for the spin echo signals are obtained.

1. At the present time a large amount of varied information on the internal structure of many materials and on processes which occur in them is obtained from experiments involving spin echo and free nuclear precession produced by resonant electromagnetic pulses. An examination of similar phenomena involving acoustic pulses appears to be of interest.

It has been shown previously [1,2] that in cubic crystals an acoustic pulse of Larmor frequency $\omega_0 = \gamma H_0$ applied at $t = 0$, and an acoustic pulse of frequency $\omega = 2\omega_0$ applied at $t = \tau$, give rise to a spin echo signal at $t = 2\tau$. A single acoustic pulse does not give rise to a free precession signal [2] and alters the z component of magnetization from M_0 to $M_0 \cos\beta$ or $M_0 \cos 2\gamma$ [3] (β and γ will be defined later in terms of parameters describing the substance and the pulse).

In order to carry out an experiment with two acoustic pulses it is necessary to introduce into the crystal sound at the Larmor frequency and at double the Larmor frequency, or to reduce to one-half the magnitude of the magnetic field within a time $\tau < T_1$ (T_1 is the longitudinal relaxation time). These difficulties can be avoided if one electromagnetic and one acoustic pulse is applied to the substance.

Since the z component of the magnetization does not precess, its response to an acoustic pulse could be determined, for example, from the magnitude of the free precession signal from the second electromagnetic pulse. It is, therefore, of interest to study the results of applying an acoustic and an electromagnetic pulse to a nuclear spin-system. In the present article we examine the theory of this phenomenon for the case $I = 1$.

2. We consider a cubic crystal containing nuclei of spin $I = 1$ and of quadrupole moment Q placed in a magnetic field H_0. We follow the method of calculation presented in [2].

If acoustic oscillations are introduced into the crystal along the C_4 symmetry axis longitudinal acoustic standing waves are set up in the crystal.[2] The operator for the interaction of the ultrasound with the nucleus giving rise to resonance transitions in the Zeeman spectrum is given by [2]

$$\hat{h}(t) = -\hbar\,[2\omega_1(\hat{I}_x\hat{I}_z + \hat{I}_z\hat{I}_x) + \omega_2(\hat{I}_+ + \hat{I}_-)]\cos\omega t,$$

$$\omega_1 = \frac{3e^2Qq_1Ak}{8I(2I-1)\hbar}\sin\mathbf{kR}\sin 2\theta,$$

$$\omega_2 = \frac{3e^2Qq_1Ak}{8I(2I-1)\hbar}\sin\mathbf{kR}\sin^2\theta, \qquad (1)$$

where 2A and $\mathbf{k}$ are the oscillation amplitude and the propagation vector lying in the xy plane and making an angle θ with respect to the z axis chosen parallel to H_0, and eq_1 is the electric field gradient with respect to a displacement between the particles resulting from the oscillations about the equilibrium distance between them; $\mathbf{R}$ is the position vector of the nucleus in the coordinate system fixed in the crystal. We neglect the time required to set up the standing waves in the crystal.

For a pulse with the oscillating magnetic field $2H_1 \cos\omega t$ directed parallel to the x axis, the operator for the interaction with the nucleus is, as is well known,

$$\hat{h}(t) = -\hbar\omega^1(\hat{I}_+ + \hat{I}_-)\cos\omega t, \qquad \omega^1 = \gamma H_1. \qquad (2)$$

After the pulse has been applied the wave function for the nuclear spin can be represented in the form

$$\Psi(t) = \sum_m C_m(t_\omega)\, e^{-iE_m t/\hbar}\chi_m, \qquad (3)$$

where $C_m(t)$ is determined by the Schrödinger equation with the Hamiltonian $\hat{\mathcal{H}}_0 + \hat{h}(t)$, with the operator $\hat{h}(t)$ given in the form (1) or (2), while $\hat{\mathcal{H}}_0$, E_m and χ_m are respectively the Hamiltonian, its eigenvalue, and its eigenfunction in the absence of a pulse.

In the case of an acoustic pulse of frequency $\omega = \omega_0 = \gamma H_0$ and of duration $t_\omega \gg \omega^{-1}$ we obtain* for $C_m(t)$

$$C_{\pm 1}(t) = C^0_{\pm 1}\cos^2\frac{|\omega_1|t}{2} + C^0_{\mp 1}\sin^2\frac{|\omega_1|t}{2} \pm \frac{i}{\sqrt{2}}\,\mathrm{sign}\omega_1\, C^0_0 \sin|\omega_1|t,$$

$$C_0(t) = C^0_0\cos|\omega_1|t + \frac{i}{\sqrt{2}}\,\mathrm{sign}\,\omega_1\,(C^0_1 - C^0_{-1})\sin|\omega_1|t, \quad (4)$$

where $C^0_m = C_m(t=0)$.

For an acoustic pulse with $\omega = 2\omega_0$ and $t_\omega \gg \omega^{-1}$ we have

$$C_{\pm 1}(t) = C^0_{\pm}\cos|\omega_2|t + i\,\mathrm{sign}\,\omega_2\, C^0_{\mp 1}\sin|\omega_2|t, \quad C_0(t) = C^0_0. \quad (5)$$

For an electromagnetic pulse we have

$$C_{\pm 1}(t) = C^0_{\pm 1}\cos^2\frac{\omega^1 t}{2} - C^0_{\mp 1}\sin^2\frac{\omega^1 t}{2} + \frac{i}{\sqrt{2}}C^0_0\sin\omega^1 t,$$

$$C_0(t) = C^0_0\cos\omega^1 t + \frac{i}{\sqrt{2}}(C^0_1 + C^0_{-1})\sin\omega^1 t. \quad (6)$$

With the aid of (3) — (6) we can evaluate the expectation values for the components of the nuclear spin. When two pulses are applied this procedure is carried out twice, with the nuclear state just before the second pulse being given by formula (3) with $t = \tau$.

In order to obtain the resultant magnetization it is necessary to add the expectation values of the components of the spin of all the nuclei in the sample. In order to do this, we shall average over the nuclear position vector, treating $\mathbf{k}\cdot\mathbf{R}$ as arbitrary, and over the frequency distribution, which we assume to be Gaussian.[5] Since at $t = 0$ the nuclei were in thermal equilibrium we shall make use of Boltzman statistics for the initial distribution of the N nuclei of the sample.

The results of such a program of calculations for different combinations of pulses are given in the table where

$$\alpha = \omega^1 t_\omega, \quad \beta = |\omega_1| t_\omega, \quad \gamma = |\omega_2| t_\omega,$$

$$f(p) = \exp[-i\omega_0 p - p^2/2T_2^{*2}],$$

a bar over an expression denotes averaging over the nuclear coordinates, and T_2^{*-2} is the mean square deviation of the frequency from γH_0.

The average value of the x and y components of the spin of an individual nucleus after an acoustic pulse of frequency ω_0 is proportional to

First pulse	Second pulse	$M^+ = M_x + iM_y$ in units of $2N\gamma\hbar^2\omega_0/3kT$
ac., $\Delta m = 1$	e.m.	$i\sin\alpha\,\overline{\cos\beta}\,f(t-\tau)$
ac., $\Delta m = 1$	ac., $\Delta m = 1$	0
ac., $\Delta m = 1$	ac., $\Delta m = 2$	$\mathrm{sign}(\omega_1\omega_2)\,\overline{\sin\beta\sin\gamma}\,f(t-2\tau)$
ac., $\Delta m = 2$	e.m.	$i\sin\alpha\,\overline{\cos 2\gamma}\,f(t-\tau)$
ac., $\Delta m = 2$	ac., $\Delta m = 1$	$\mathrm{sign}(\omega_1\omega_2)\,\overline{\sin\beta\sin 2\gamma}\,\{\overline{\cos^2(\beta/2)}\,f(t+\tau) + \overline{\sin^2(\beta/2)}\,f(t-3\tau)\}$
ac., $\Delta m = 2$	ac., $\Delta m = 2$	0
e.m.	ac., $\Delta m = 1$	$i\frac{1}{2}\sin\alpha\,\{\overline{(\cos 2\beta + \cos\beta)}\,f(t) + \overline{(\cos 2\beta - \cos\beta)}\,f(t-2\tau)\}$
e.m.	ac., $\Delta m = 2$	$i\sin\alpha\,\overline{\cos\gamma}\,f(t)$

sign $\omega_1 \cdot \sin|\omega_1|t_\omega$. In averaging over the coordinates, this expression vanishes if the dimension of the sample parallel to the direction of propagation of sound is an even multiple n of half a wavelength. If n is odd, then the total magnetization is determined by the nuclei situated in a layer half a wavelength thick in the direction perpendicular to the direction of propagation of sound.

For a sample of linear dimensions ~ 1 cm and for a frequency $\nu \sim 10^7$ cps this layer will contain $\sim 1\%$ of all the nuclei. Moreover, as a result of averaging over the initial conditions it turns out that the total magnetization in the x and y directions is proportional to $(\hbar\omega_0/kT)^2$, i.e., it is smaller by a factor $(\hbar\omega_0/kT)$ than the magnetization due to the electromagnetic pulse $(\hbar\omega_0/kT) \sim 10^{-6}$ at $T \sim 300°$ K and $H_0 \sim 10$ kilogauss. Therefore, it is impossible to observe the free precession signal due to an acoustic pulse.

3. It should be noted that the results shown in the table have been obtained by neglecting terms proportional to $(\hbar\omega_0/kT)^2$. Also we have not taken into account here processes associated with longitudinal relaxation, for, as is well known, in a solid the nuclear longitudinal relaxation times satisfy $T_1 \gg T_2^*$.

From the table it can be seen that in those cases when the electromagnetic pulse follows the acoustic pulse only a free precession signal appears following the second pulse. The ratio of this signal to the free precession signal due to a single electromagnetic pulse is equal to $P = \overline{\cos|\omega_{1,2}|t_\omega}$. This can be easily understood if we take into account the fact that a single acoustic pulse does not give rise to a free precession signal and alters the value of the z-component of the magnetization from M_0 to $M_0\cos|\omega_{1,2}|t_\omega$ and that, moreover, the free precession signal following the electromagnetic pulse is proportional to the magnetization existing before it was applied.

*I take this opportunity to note that the expression sign $\omega_{1,2}$ has been omitted for the corresponding formulas of [2]. Apart from the sign, however, this does not affect the results of [2].

In those cases when the acoustic pulse follows the electromagnetic one a free precession signal from the first electromagnetic pulse is present and, therefore, a spin echo signal can be produced. In this case, as expected, no free precession signal is produced by the second pulse.

The ratio of the spin echo signal due to the electromagnetic and the acoustic pulses giving rise to the $\Delta m = 1$ transitions, to the echo signal due to two electromagnetic pulses [5] is given by

$$P' = \overline{(\cos 2\beta - \cos 3\beta)} / 2 \sin^3 \frac{\alpha}{2}.$$

A measurement of the values of P and P′ provides a method for studying the changes in the crystalline electric fields at nuclear sites as a result of the application of ultrasound.

The author is grateful to Professor S. A. Al'tshuler for his interest in this work.

[1] A. R. Kessel', FTT **2**, 1944 (1960), Soviet Phys.-Solid State **2**, 1751 (1960).

[2] A. R. Kessel', JETP **39**, 872 (1960), Soviet Phys. JETP **12**, 604 (1961).

[3] N. G. Koloskova and U. Kh. Kopvillem, FMM (Phys. of Metals and Metallography) **10**, 818 (1960).

[4] D. J. Bolef and M. Menes, Phys. Rev. **114**, 1441 (1959).

[5] Das, Saha, and Roy, Proc. Roy. Soc. (London) **A227**, 407 (1955).

Translated by G. Volkoff
216

A NEW METHOD OF CALCULATING THE ENERGY SPECTRUM OF CARRIERS IN SEMICONDUCTORS. I. NEGLECTING SPIN-ORBIT INTERACTION

G. E. PIKUS

Institute of Semiconductors, Academy of Sciences, U.S.S.R.

Submitted to JETP editor May 11, 1961

J. Exptl. Theoret. Phys. (U.S.S.R.) 41, 1258-1273 (October, 1961)

A new method is developed for constructing the Hamiltonian for carriers in semiconductors in the "effective mass" approximation in the presence of external fields and deformations, which allows the symmetry requirements to be taken into account without directly using perturbation theory.

1. INTRODUCTION

THE effective-mass method used to consider the motion of carriers in a periodic lattice perturbed by external electric and magnetic fields has been derived by a number of authors (see, for example, [1,2]). This method is used for calculating the energy spectrum of carriers in semiconductors and its change during deformation, [3,4] and in the theory of scattering it leads directly to the "deformation potential" method. [5,6]

In the method the wave function Ψ, which is a solution of the Schrödinger equation

$$\hat{\mathcal{H}}\Psi = (\hat{\mathcal{H}}_0 + \hat{\mathcal{H}}_1)\,\Psi = i\hbar\partial\Psi/dt, \qquad (1)$$

is written approximately as the sum of the products of smooth functions $F_i(\mathbf{r},t)$ and Bloch functions

$$\varphi_{i\mathbf{k}_0} = u_{i\mathbf{k}_0} \exp\,[i\,(\mathbf{k}_0\mathbf{r} - Et/\hbar)],$$

which are the eigenfunctions of the operator $\hat{\mathcal{H}}_0 = -(\hbar^2/2m)\nabla^2 + V_0(\mathbf{r})$ at an extremum point $\mathbf{k}_0$:

$$\Psi = \sum_{i=1}^{n} F_i\varphi_i. \qquad (2)$$

Here in general the band is assumed degenerate at the point $\mathbf{k}_0$ i.e., to the eigenvalue $E_{\mathbf{k}_0}$ correspond n eigenfunctions $\varphi_{i\mathbf{k}_0}$.

The method is, of course, only valid when a number of conditions are satisfied—to be explicit: for free electrons described in this approximation by plane waves, the wave vector $\mathbf{k}$, reckoned from the point $\mathbf{k}_0$, must be sufficiently small as compared with a vector of the reciprocal lattice; the external fields appearing in $\hat{\mathcal{H}}_1$ must be sufficiently smooth; if these fields depend on time, the characteristic frequencies must be small compared with the quantity $\Delta E/\hbar$, where ΔE is the distance between nearest bands.

When these conditions are satisfied, the system of differential equations determining the functions F_i has the form

$$\mathcal{D}_{ij}(\mathcal{K})\,F_j = i\hbar\,\partial F_i/\partial t. \qquad (3)$$

The matrix $\mathcal{D}$, which is the Hamiltonian in the effective-mass method, depends on the operators $\mathbf{k}$, on the external electric and magnetic fields, on the deformation tensor ϵ, etc. For simplicity in what follows, we shall use a single symbol $\mathcal{K}$ for all these scalar, vector, and tensor quantities.

Various variants of perturbation theory are generally used both to prove the applicability of the effective mass method and to construct the Hamiltonian $\mathcal{D}$. To construct $\mathcal{D}(\mathcal{K})$ the calculation has to be carried to second and higher orders of perturbation. Although the constants entering into $\mathcal{D}$ can in principle also be calculated by these methods, they are in practice determined from experiment. Thus, once the validity of the effective-mass method is proved, it is not necessary to use explicitly the rather cumbersome methods of perturbation theory to calculate $\mathcal{D}(\mathcal{K})$ for each specific case, since the form of this matrix is uniquely determined by the symmetry properties.

A number of workers [7,8] have successfully used various ways of constructing $\mathcal{D}$ directly. In the present work we develop a general method of constructing the operator $\mathcal{D}(\mathcal{K})$, starting directly from the symmetry conditions and the invariance of the Schrödinger equation under time inversion.

In the first part we shall not take spin-orbit interaction into account, so as to be able to display the principles of the method more simply. In the second part [9] it will be shown how spin-orbit interaction can be accurately taken into account within the framework of this method. For clarity we shall consider several examples in the

first and, especially, in the second part. Using the method we shall consider the change of the energy spectrum of carriers in semiconductors with the wurtzite and germanium structures during deformation.

Other examples are contained in the article by the author and Bir devoted to calculating the effect of deformation on the electrical properties of p and n type InSb [10] and the article by the author [11] where the energy spectrum in tellurium is calculated.

2. SYMMETRY CONDITIONS

The operator $\hat{\mathcal{H}}_0$ in (1) is invariant under all the operations of the space group characterizing the symmetry of the crystal, i.e., in particular to the operations of the wave vector group $G_{\mathbf{k}_0}$, i.e., those operations of the complete space group which move $\mathbf{k}_0$ to equivalent points differing from $\mathbf{k}_0$ by one of the reciprocal lattice vectors.

Under these operations the functions $\varphi_{i\mathbf{k}_0}$ transform linearly into one another

$$\hat{G}\varphi_i(\mathbf{r}) = \varphi_i(\hat{G}^{-1}\mathbf{r}) = G^0_{i'i}\varphi_{i'}(\mathbf{r}). \tag{4}$$

Here $G^0_{i'i}$ are the matrix elements of the representation T_0 according to which the $\varphi_i(\mathbf{r})$ transform.

For brevity we shall omit the label $\mathbf{k}_0$ on φ_i and G, here and below. The operator $\hat{\mathcal{H}}_1$ in (1) is not in general invariant under these operations.

If we apply to (1) the transformation $\hat{G}$, going from $\mathbf{r}$ to $\mathbf{r}' = \hat{G}\mathbf{r}$, then, in place of the system of equations (3), we obtain a new system

$$\mathcal{D}(\hat{G}\mathcal{H})\,F = i\hbar\partial F/\partial t. \tag{5}$$

The form of the matrix $\mathcal{D}$ depends on the choice of a definite representation, i.e., on the basis: in (3) $\mathcal{D}(\mathcal{H})$ is written in the basis $\varphi_i(\mathbf{r})$, and in (5) $\mathcal{D}(\hat{G}\mathcal{H})$ is written in the basis $\varphi_i(\hat{G}\mathbf{r}) = \hat{G}^{-1}\varphi_i(\mathbf{r})$. If $\hat{G}$ appears in the wave vector group, then, using (4), we can rewrite $\mathcal{D}(\mathcal{H})$ in the same basis as $\mathcal{D}(\hat{G}\mathcal{H})$, and then both these matrices must be identical.

Consequently,

$$G^0\mathcal{D}(\mathcal{H})\,G^{0-1} = \mathcal{D}(\hat{G}\mathcal{H}). \tag{6}$$

This equation also determines the requirements imposed on $\mathcal{D}(\mathcal{H})$ by the symmetry conditions.

The matrix $\mathcal{D}$ is of dimension $n \cdot n$. It is therefore possible to take, as the basis for constructing $\mathcal{D}$, n^2 linearly independent matrices A_l with constant coefficients, i.e., not depending on $\mathcal{H}$. Since these matrices form a complete set, any of the matrices $G^0A_lG^{0-1}$ can be expanded in terms of them, and, consequently,

$$G^0A_l\,G^{0-1} = G_{l'l}A_{l'}.$$

It is easily verified that the matrices $G_{l'l}$ of dimensions $n^2 \cdot n^2$ form a representation of the group $G_{\mathbf{k}_0}$. This representation is reducible in the general case.

The matrices A_l can be chosen so that this representation is made irreducible. Then the matrices A_{sl}, being the basis of an irreducible representation T_s of the group $G_{\mathbf{k}_0}$, transform only into one another, i.e.,

$$G^0A_{sl}\,G^{0-1} = \hat{G}A_{sl} = G^s_{l'l}\,A_{sl'}. \tag{7}$$

We label the matrices A_{sl} with two symbols here: the first gives the number of the representation, s, according to which they transform, and the second, l, the number of the matrix in the representation; l takes values from 1 to m_s, where m_s is the dimension of the representation. Clearly, $\Sigma_s m_s = n^2$.

As is well known, [12] the wave vector group has two types of representation: for one of them under translation by a reciprocal lattice vector $\mathbf{t}$ we have $(0\,|\,\mathbf{t})_{l'l} = e^{i\mathbf{k}_0\cdot\mathbf{t}}\delta_{l'l}$. The wave functions $\varphi_{i\mathbf{k}_0}$ transform according to these representations. For the other type of representation $(0\,|\,\mathbf{t})_{l'l} = \delta_{l'l}$. These representations of the group $G_{\mathbf{k}_0} = (g\,|\,\tau)$ coincide with the representations of the corresponding point group $\bar{G}$ with elements $(g\,|\,0)$. The matrices A_{sl} also transform according to these representations. Knowing the representation T_0 according to which the functions $\varphi_{i\mathbf{k}_0}$ transform, the irreducible representations according to which the matrices A_{sl} transform can be established. We write (7) in expanded form:

$$A_{st,ij} = G^{0-1}_{i'i'}\,G^0_{j'j}\,G^s_{l'l}\,A_{sl',i'j'} = G^s_{l,ij;\,l',i'j'}A_{sl',\,i'j'}. \tag{7a}$$

From a well-known theorem of group theory [12,13] the number of linearly independent groups of m_s matrices transforming according to the representation T_s is n_s:

$$n_s = \frac{1}{h}\sum_{G\in\bar{G}_{\mathbf{k}_0}} G^s_{l,\,ij;\,l,\,ij} = \frac{1}{h}\sum_{G\in\bar{G}_{\mathbf{k}_0}} \chi_s(G)\,|\,\chi_0(G)\,|^2, \tag{8}$$

where χ_0 and χ_s are the characters of the representations T_0 and T_s.

The summation here is carried over all the elements of the factor group $\bar{G}_{\mathbf{k}_0}$ of the wave vector group $G_{\mathbf{k}_0}$ which contains h elements. In other words, n_s is the number of identity representations contained in the direct product $T_0 \times T_0^* \times T_s$, or, correspondingly, the number of representations T_s contained in $T_0 \times T_0^*$. If $n_s > 1$ i.e., if T_s comes in more than once in $T_0 \times T_0^*$, then several groups of linearly independent matrices A_{sl} transform according to this representation. In

order to distinguish these groups, we introduce a third label, t, and shall label these matrices A^t_{sl}. Of course, the form of these matrices depends on the choice of a concrete representation T_0.

We consider below in detail the methods of constructing these matrices; meanwhile we shall assume them to be known, and shall show how then to construct $\mathcal{D}(\mathcal{K})$, satisfying condition (6) and the conditions associated with the invariance of the Schrödinger equation to time inversion.

We express $\mathcal{D}(\mathcal{K})$ in terms of the basis matrices A^t_{sl} and write it in the form

$$\mathcal{D}(\mathcal{K}) = \sum_{t,r,s} C_s^{tr} \sum_l A^t_{sl} f^r_{sl}(\mathcal{K}). \qquad (9)$$

Here $f(\mathcal{K})$ are functions of the variables k_i, H_i, ϵ_{ij}, etc., and their products, which we wish to include in $\mathcal{D}$. For example, to calculate the spectrum it is only necessary to include in $\mathcal{D}$ functions of k_i. Depending on the problem considered, we can either limit ourselves to linear or quadratic terms, or include terms of higher orders. Various functions of $\mathcal{K}$, for example k_x^2, H_x^2, ϵ_{xx}, etc., can be associated with one matrix A^t_{sl}. We distinguish these functions by an index r. The coefficients C_s^{tr} are constants of the substance. If the matrices $\sum_l A^t_{sl} f^r_{sl}(\mathcal{K})$ are Hermitian these constants are real.

Let us see how to choose $f(\mathcal{K})$ so that condition (6) is satisfied.

We substitute (9) in (6). Then, taking (7) into account and comparing terms in the independent constants C_s^{tr} in (9), we obtain

$$\sum_l \hat{G} A^t_{sl} \cdot \hat{G} f^r_{sl}(\mathcal{K}) = \sum_l A^t_{sl} f^r_{sl}(\mathcal{K}). \qquad (10)$$

Analogously to (4), $\hat{G}f(\mathcal{K}) = f(\hat{G}^{-1}\mathcal{K})$ here. Equation (10) means that each of the sums over l in (9) should transform according to an identity representation. Consequently, the matrices A_{sl}, which transform according to the representation T_s, must have as multipliers the functions $f_{sl}(\mathcal{K})$, which transform according to a conjugate (equivalent) representation T_s^*, i.e., so that

$$\hat{G} f_{sl}(\mathcal{K}) = f_{sl}(G^{-1}\mathcal{K}) = G^{s*}_{l'l} f_{sl'}(\mathcal{K}) = G^{s-1}_{ll'} f_{sl'}(\mathcal{K}). \qquad (11)$$

In fact, Eq. (10) follows at once from (7) and (11).

Thus, to construct $\mathcal{D}$ it is necessary to construct functions of $\mathcal{K}$, which transform according to the irreducible representations contained in the direct product $T_0 \times T_0^*$. Functions $f(\mathcal{K})$, transforming according to other representations, cannot appear in $\mathcal{D}$. In practice, the construction of such functions presents no difficulty. All the quantities $\mathcal{K}$ are scalars, the components of polar or axial vectors or tensors and their symmetrized products, and they can be expressed in terms of irreducible representations by the usual methods of group theory.[13]

We shall not linger especially on this question, and point out only one particular case: according to [6], to take account of scattering by nonpolar optical vibrations, it is necessary to include in $\mathcal{D}$ functions of the components of the vector **u**, which describes the displacement of one of the sublattices relative to the other. This vector transforms as a usual polar vector under all operations which do not interchange the sublattices, but changes sign under those operations which do interchange the sublattices. It is necessary to take this fact into account when expressing $f(u_i)$ in irreducible representations.

3. INVARIANCE UNDER TIME INVERSION

If in the original equation (1) we change t into $-t$, and then go to the conjugate equation and replace in it H_i by $-H_i$ and $\hat{k}_i$ by $-\hat{k}_i$, we obtain the equation

$$\hat{\mathcal{H}}'^* \Psi'^* = i\hbar \partial \Psi'^* / \partial t.$$

If the system of differential equations (3) follows from (1), then we obtain similarly from this equation the system

$$\mathcal{D}'^* F'^* = i\hbar \partial F'^* / \partial t. \qquad (12)$$

The prime signifies here the replacement of k_i by $-k_i$ and H_i by $-H_i$.

The Hamiltonians $\hat{\mathcal{H}}$ and $\hat{\mathcal{H}}^*$ are in general different. For them to coincide it is necessary to change H_i into $-H_i$ and k_i into $-k_i$ in $\hat{\mathcal{H}}$.[2,14] Consequently, the wave functions Ψ'^*, as well as the functions Ψ, are eigenfunctions of $\hat{\mathcal{H}}$, corresponding to the same value of the energy and the same value of the wave vector **k**, if, of course, **k** also remains an integral of motion in the "perturbed" equation (1).

Since $\hat{\mathcal{H}}_0^* \equiv \hat{\mathcal{H}}$, the functions $\hat{S}\varphi_i = \varphi_i^*$ are the basis of Eq. (12). If these functions are linearly related to the φ_i, which are the basis of $\mathcal{D}$ in (3), then $\mathcal{D}$ and $\mathcal{D}'^*$ can be written in a single basis. Since in this case the functions Ψ and Ψ'^* coincide, the matrices $\mathcal{D}$ and $\mathcal{D}'^*$, being written in a single basis, must also exactly coincide. This requirement imposes additional conditions on $\mathcal{D}(\mathcal{K})$. As Wigner [14] has shown, there is a linear relationship between φ_i and φ_i^* when the representation T_0 is real (case a). If the representations

T_0 and T_0^* are essentially complex and non-equivalent (case b) and $\mathbf{k}_0$ and $-\mathbf{k}_0$ appear in a single star, or if these representations are complex and equivalent (case c), they must be combined into one, i.e., in this case there is additional degeneracy.

If $\mathbf{k}_0$ and $-\mathbf{k}_0$ do not appear in a common star, there is no additional degeneracy at the point $\mathbf{k}_0$, and $E(\mathbf{k})$ must satisfy only the usual condition following from the equality of $\hat{\mathcal{H}}$ and $\hat{\mathcal{H}}'^*$: $E(\mathbf{k}) = E(-\mathbf{k})$. Knowing the characters of the representation, it is possible, using Herring's formula,[12,15] to decide to which case this representation belongs:

$$\frac{M}{h'}\sum_{\substack{(g|\tau)^2\in G_{\mathbf{k}_0}\\ \hat{g}\mathbf{k}_0=-\mathbf{k}_0}}\chi(g|\tau)^2=\begin{cases}1 - \text{ case } a,\\ 0 - \text{ case } b,\\ -1 - \text{ case } c.\end{cases} \tag{13}$$

Summation here is performed over the operations of the factor group of the complete space group $G' = (g|\tau)$, for which $\hat{g}\mathbf{k}_0 = -\mathbf{k}_0$; h' is the number of elements of this group, and M is the number of vectors in the star of $\mathbf{k}_0$. It is clear that the operations $(g|\tau)^2$ always appear in the wave vector group $G_{\mathbf{k}_0}$. From (13) it follows that, if $\mathbf{k}_0$ and $-\mathbf{k}_0$ appear in different stars, then we are concerned with case b. In this case, which we shall label as b_3, no additional conditions apart from (6) are imposed on $\mathcal{D}$.

We shall consider in greater detail the case when invariance to time inversion leads to additional requirements on $\mathcal{D}$.

Case a: representation T_0 real.

1) a_1; $\mathbf{k}_0$ equivalent to $-\mathbf{k}_0$.

In this case

$$\hat{S}\varphi_i = \varphi_i^* = S_{i'i}\varphi_{i'}. \tag{14}$$

Since $\hat{S}\hat{S} = 1$, and S is a unitary matrix, then

$$S = S^{*-1} = \tilde{S}, \tag{15}$$

where $\tilde{S}$ signifies the matrix obtained by transposing S. The matrix $\mathcal{D}'^*$ in the representation φ_i, must coincide with $\mathcal{D}$, and, consequently, taking into account (15) and the fact that $\mathcal{D}$ is Hermitian,

$$\mathcal{D} = S\mathcal{D}'^*S^{-1} = S\tilde{\mathcal{D}}'S^{-1} = (S^{-1}\mathcal{D}'S)^{\sim}, \tag{16}$$

it follows from (16) and (6) that

$$(G^0S)^{-1}\mathcal{D}'(\hat{G}\mathcal{H})(G^0S) = \tilde{\mathcal{D}}(\mathcal{H}). \tag{17}$$

We substitute $\mathcal{D}$ in the form (9) into (17), remembering that $f(\mathcal{H})$ is a homogeneous function of $\mathcal{H}$, and, therefore,

$$f(\mathcal{H}') = \gamma f(\mathcal{H}), \tag{18}$$

where $\gamma = \pm 1$, depending on the "parity" of $f(\mathcal{H})$.

We then obtain equations similar to (7a)

$$A^t_{sl,ij} = (G^0S)^{ts}_{l,ij;r,i'j'}A^t_{sl',i'j'}$$

$$= \gamma(G^0S)^*_{i'j}(G^0S)_{j'i}G^{*s}_{i'l}A^t_{sl'i'j'}. \tag{19}$$

We introduce the expanded group consisting of the elements of G and GS, the matrix elements of which are defined by (7a) and (19), and find n_S:

$$n_s = \frac{1}{2h}\sum_{G\in\bar{G}_{\mathbf{k}_0}} G^{0ts}_{l,ij;l,ij} + (G^0S)^{ts}_{l,ij;l,ij}$$

$$= \frac{1}{2h}\sum_{G\in\bar{G}_{\mathbf{k}_0}}\chi_s(G)\,[\chi_0^2(G) + \gamma\chi_0(G^2)]. \tag{20}$$

Thus, we learn that, because $\hat{G}$ and $\hat{S}$ commute, and because of (16), it follows that $SG^{*0}S^* = SG^{0*}S^{-1} = G^0$, and also that $\chi_0^*(G) = \chi_0(G)$.

Thus, in case a_1, for even functions $f(\mathcal{H})$, the number n_S is equal to the number of representations T_S contained in the symmetric product $[T_0^2]$, and for odd, in the antisymmetric one $\{T_0^2\}$.

2) a_2; $\mathbf{k}_0$ not equivalent to $-\mathbf{k}_0$.

In this case the functions $\hat{S}\varphi_{i\mathbf{k}_0} = \varphi^*_{i\mathbf{k}_0}$ are linearly related, not to $\varphi_{i\mathbf{k}_0}$, but to $\varphi_{i,-\mathbf{k}_0}$. However, according to (13), there are in this case in the space group operations R that turn $\mathbf{k}_0$ into $-\mathbf{k}_0$. Therefore the functions $\hat{R}\hat{S}\varphi_{i\mathbf{k}_0}(\mathbf{r}) = \varphi^*_{i\mathbf{k}_0}(R^{-1}\mathbf{r})$ can be linearly expressed in terms of $\varphi_{i\mathbf{k}_0}(\mathbf{r})$:

$$\hat{R}\hat{S}\varphi_i = R_{i'i}\varphi_{i'}. \tag{21a}$$

Since $\hat{R}$ and $\hat{S}$ commute, and $\hat{S}^2 = 1$, it follows that

$$\hat{R}\varphi_i = R^*_{i'i}\varphi_{i'}. \tag{21b}$$

In order to write the matrix $\mathcal{D}'^*$ in (13) in the same basis as $\mathcal{D}$ in (3), we apply to the original equation the transformation $\hat{R}$, translating from $\mathbf{r}$ to $\mathbf{r}' = \hat{R}\mathbf{r}$. Instead of $\mathcal{D}'^*(\mathcal{H})$ in (12), we then obtain $\mathcal{D}'^*(\hat{R}\mathcal{H})$, where the basis of this matrix will already be the functions $\varphi_i^*(\hat{R}\mathbf{r}) = \hat{R}^{-1}\hat{S}\varphi_i = (\hat{R}^{-1})_{i'i}\varphi_{i'}$. In the basis $\varphi_i(\mathbf{r})$ this matrix must coincide with $\mathcal{D}$. Consequently,

$$R^{-1}\mathcal{D}'(\hat{R}\mathcal{H})R = \mathcal{D}(\mathcal{H}). \tag{22}$$

Here the matrix of the inverse operator $\hat{R}^{-1}$ is

$$(\hat{R}^{-1})_{ij} = R^{*-1}_{ij} = R_{ji}, \tag{23}$$

which follows directly from the relationship $(\hat{R}^{-1}\hat{R})_{ij} = \hat{R}^{-1*}_{il}R_{lj} = \delta_{ij}$, and the fact that R is unitary.

An expanded group can be introduced, consisting of the elements of $G_{\mathbf{k}_0}$ and R. All the elements of R can be obtained by multiplying one of the elements of R_0 by all the elements of $G_{\mathbf{k}_0}$. In fact, the product of any of the elements of R by R_0 does not change $\mathbf{k}_0$, and therefore this element of the space group RR_0 is one of the elements of G.

The functions φ_i and $\varphi_I = \hat{S}\varphi_i$ are the basis of this expanded group. For $\hat{G}$ the only matrix elements different from zero are G_{ij} and $G_{IJ} = G_i^{*j}$, but for $\hat{R}$, only R_{iJ} [$= R_{ij}$ in the notation of Eq. (21)] and $R_{Ij} = R_{ij}^*$ are non-zero. For the matrix products, for example in (22), the usual laws of multiplication are then valid, but summation must be made over all intermediate indices and i and I. Thus $\mathcal{D}_{IJ} = \mathcal{D}_{ij}^*$. Similarly in (23), as for usual operators, $(\hat{R}^{-1})_{iJ} = R_{iJ} = R_{Ji}^* = R_{ji}$.

If $\mathcal{D}$ is expressed in terms of the matrices A_{sl}^t according to (9), and A_{sl}^t and f_{sl}^r are chosen so that they transform according to the irreducible representations of the point group, corresponding to the expanded group G, $R - T_S'$, and (9) is substituted in (22), we obtain in analogy to (7a)

$$A_{slij}' = R_{l,ij;t,i'j'}^{ts} A_{st'i'j'}^t = \gamma R_{j'j} R_{i'i}^{*s} A_{st'i'j'}^t. \qquad (24)$$

Thus we learn from (18) and from the fact that $\mathcal{D}$ is Hermitian that

$$\sum_t A_{tij}^* f_t'^* (\hat{R}\mathcal{K}) = \gamma \sum_t A_{tji} f_t (\hat{R}\mathcal{K}).$$

When calculating n_S it is necessary to sum the characters over all the elements of the expanded group (G and $R = R_0G$):

$$n_s = \frac{1}{2h}\left[\sum_{G\in\bar{G}_{\mathbf{k}_0}} G_{l,ij;t,ij}^{ts} + \sum_{R\in R_0\bar{G}_{\mathbf{k}_0}} R_{l,ij;t,ij}^{ts}\right]$$

$$= \frac{1}{2h}\sum_{G\in\bar{G}_{\mathbf{k}_0}} \chi_s(G)|\chi_0(G)|^2 + \gamma\chi_s(R_0G)\,\chi_0[(R_0G)^2]. \qquad (25)$$

Here $(\hat{R}^2)_{ii} = R_{iJ}R_{Ji} = R_{ij}R_{ji}^*$.

Cases b and c: representations T_0 and T_0^* complex.

1) b_1 and c_1; $\mathbf{k}_0$ equivalent to $-\mathbf{k}_0$.

In these cases there is additional degeneracy at the point $\mathbf{k}_0$, and the functions φ_i and $\varphi_I = \hat{S}\varphi_i = \varphi_i^*$ are linearly independent and are united into a single representation. Under all the operations of $G_{\mathbf{k}_0}$ the "diagonal" parts of the matrix $\mathcal{D}$ — $\mathcal{D}_{ij}$ and $\mathcal{D}_{IJ}$ —, and the "non-diagonal" parts— $\mathcal{D}_{iJ}$ and $\mathcal{D}_{Ij}$ —each transform into themselves. Of course, the matrix elements between the same functions must be equivalent, both in the matrix $\mathcal{D}$, constructed in the basis φ_i, φ_I, and in $\mathcal{D}'^*$, constructed in the basis $\bar{\varphi}_i = \hat{S}\varphi_i = \varphi_I$ and $\bar{\varphi}_I = \hat{S}\varphi_I = S^2\varphi_i = \varphi_i$. Therefore

$$\mathcal{D}_{ij}'^* = \mathcal{D}_{Ji}' = \mathcal{D}_{IJ}, \qquad (26a)$$

$$\mathcal{D}_{Ij}'^* = \mathcal{D}_{Ij}' = \mathcal{D}_{iJ}. \qquad (26b)$$

These conditions do not impose additional limitations on any of the "diagonal" parts of $\mathcal{D}$, and the number of groups of matrices A_{sl}^t with a non-zero diagonal part n_S is defined by the general equation (8). As regards the "non-diagonal" parts, it follows from (26b), (18), and (9) that

$$A_{slIj}' = \gamma A_{slJi}. \qquad (27)$$

It is, therefore, also possible here to introduce an expanded group G, GS. Then the effect of the operator $\hat{G}$ on the matrix elements A_{Slij} is determined by (7a), and the elements of (GS) are, according to (7a) and (27),

$$A_{slIj}' = (GS)_{l,Ij;t',i'j'}^{ts} A_{st'i'j'}^t = \gamma G_{j'j}^{0*} G_{i'i}^{0} G_{i'i}^{*s} A_{st'i'j'}^t. \qquad (28)$$

Since $G_{JI}^{0*} = G_{ji}^0$, it follows from (28) and (7a) that for the "non-diagonal" parts n_S is determined in this case also by (20).

2) b_2 and c_2; $\mathbf{k}_0$ not equivalent to $-\mathbf{k}_0$.

In this case also there is additional degeneracy. In the space group there is an operation R converting $\mathbf{k}_0$ into $-\mathbf{k}_0$, and the functions referring to the same point $\mathbf{k}_0$, i.e., φ_i and $\varphi_I = \hat{R}_0\hat{S}\varphi_i = \varphi_i^*(\hat{R}_0^{-1}\mathbf{r})$, where R_0 is one of the operations of R, are united in a single representation. If $\mathcal{D}$ is written in the basis φ_i, φ_I, then $\mathcal{D}'^*$ is in the basis $S\varphi_i$ and $S\varphi_I = \hat{R}_0\varphi_i$.

In order to write $\mathcal{D}'^*$ in the same basis as $\mathcal{D}$, we apply, as in case a_2, a transformation R. Then, instead of $\mathcal{D}'^*(\mathcal{K})$, we obtain $\mathcal{D}'^*(R\mathcal{K})$ in the basis

$$\bar{\varphi}_i = \hat{R}^{-1}\hat{S}\varphi_i = (R_0R)^{-1}\varphi_I,$$

$$\bar{\varphi}_I = R^{-1}S\varphi_I = S^2R_0R^{-1}\varphi_i = R_0R^{-1}\varphi_i.$$

The functions $\varphi_i(\mathbf{r})$ and $\hat{R}\varphi_i^*(\mathbf{r})$ here are linearly independent and are not expressible in terms of one another, but the operation R_0R appears in the group $G_{\mathbf{k}_0}$, and, therefore,

$$\varphi_I = (R_0R)_{i'i}\bar{\varphi}_{i'}, \quad \varphi_i = (RR_0^{-1})_{i'i}\bar{\varphi}_{I'}. \qquad (29)$$

Of course, the matrix (R_0R) cannot here be considered as the product of two matrices R_0 and R, which in general do not exist separately.

It follows from (29) that

$$\mathcal{D}_{ij} = (R_0R)_{i'i}\mathcal{D}_{I'J'}'^*(\hat{R}\mathcal{K})(RR_0^{-1})_{j'j}. \qquad (30a)$$

$$\mathcal{D}_{Ij} = (R_0R)_{i'i}\mathcal{D}_{i'J'}'^*(\hat{R}\mathcal{K})(RR_0^{-1})_{j'j}^* = (RR_0^{-1})_{j'j}\mathcal{D}_{J'i'}'(\hat{R}\mathcal{K})(R_0R)_{i'i}^* \qquad (30b)$$

These conditions do not impose additional limitations on any of the "diagonal" parts of $\mathcal{D}$, and the corresponding value of n_S, as above, is determined by (11). For the "non-diagonal" parts we have, according to (30b), (18), and (7):

$$A_{slIj}' = R_{lIj;t'i'j'}^{ts} A_{st',i'j'}^t = \gamma(RR_0^{-1})_{i'j}(R_0R)_{j'i} R_{t'i}^{*s} A_{st'i'j'}^t. \qquad (31)$$

If the expanded group G and $R = R_0G$ is introduced, then it follows from (10) and (31) that in this case n_S for the "non-diagonal" parts is determined by (25).

From (11), (20), and (25) are obtained the formulae, previously derived by Rashba,[8] for determining the points of zero slope, i.e., those points where no terms linear in k appear in $\mathcal{D}$, i.e., where, for the corresponding representations T_S, $n_S = 0$ for $\gamma = -1$.

4. CONSTRUCTION OF THE MATRIX $\mathcal{D}$

The definite form of the matrix A^t_{sl} is determined by the choice of a definite representation T_0 according to which the basis functions transform. The more detailed methods of constructing them depends on the properties of this representation. We shall consider these methods.

1. The wave vector group G_{k_0} equivalent to the point group. As is well known,[12] in a number of cases the matrix elements of the representation $T_0 - (g \mid \tau_g)_{ij}$ — can be expressed as the products of matrix elements of the corresponding representation of the point group $\bar{\bar{G}} - (g \mid 0)_{ij}$ and $e^{-ik_0\tau_g}$:

$$G_{ij} = \bar{\bar{G}}_{ij} e^{-ik_0\tau_g}. \tag{32}$$

For this to be so, it is necessary that (32) satisfy the multiplication law of elements of the wave vector group, i.e., that

$$[(\alpha \mid \tau_\alpha)(\beta \mid \tau_\beta)]_{ij} = (\alpha\beta)_{ij} e^{-ik_0(\tau_\alpha + \tau_\beta)} = (\alpha\beta \mid \hat{\alpha}\tau_\beta + \tau_\alpha)$$
$$= (\alpha\beta)_{ij} e^{-ik_0(\hat{\alpha}\tau_\beta + \tau_\alpha)}.$$

This condition is satisfied when

$$\psi_{\alpha\beta} = \exp\{-ik_0(\hat{\alpha}\tau_\beta = \tau_\beta)\} \equiv 1$$

for all the operations of G_{k_0}, which occurs for all points k_0 lying inside the Brillouin zone and often also for points on the surface. In these conditions the factor group $\bar{G}_{k_0}$ is isomorphous with the point group $\bar{\bar{G}}$. Thus, to satisfy (6) it is necessary and sufficient according to (32) that

$$\bar{\bar{G}}_0 \mathcal{D}(\mathcal{K}) \bar{\bar{G}}_0^{-1} = \mathcal{D}(\hat{G}\mathcal{K}) \tag{33}$$

and, therefore, as the basis of $\mathcal{D}$, the eigenfunctions u_i of the point group $\bar{\bar{G}}$ can be chosen, which transform according to the representation $\bar{T}_0$. Since any point group is a sub-group of the complete space group, the functions u_i can consist of the eigenfunctions $Y^{j\pm}_m$ of any of the representations of the complete space group D which contain $\bar{T}_0$:

$$u_i = a^i_{j,m\pm} Y^{j\pm}_m. \tag{34}$$

If the representation $\bar{T}_0$ is irreducible, then only spherical functions $Y^{j\pm}_m$ with one value of j appear in the u_i in (34). For the matrices A^t_{sl} we can thus use the well-known matrices of the components of the axial vector J_i and their products — $\varphi^t_{s,l}(J_i)$, constructed from the corresponding basis functions u_i. The matrices $\varphi^t_{sl}(J)$ transform under the operations of $\bar{\bar{G}}$ just as the operator $\varphi^t_{sl}(\hat{J})$. In fact, the matrix elements $\varphi^t_{sl}(\hat{J})$ are non-zero only in the case when they are invariant under the operations $\bar{\bar{G}}$. Consequently,

$$\bar{\bar{G}}^0 \varphi^t_{sl}(J) \bar{\bar{G}}^{0-1} = \varphi^t_{sl}(\hat{G}^{-1}J) = G^s_{l'l}\varphi^t_{sl'}(J), \tag{35}$$

which agrees with (7). Therefore, in the present case it is necessary to construct the operator

$$\hat{\mathcal{D}} = \sum_{t,r,s} C^{t,r}_s \sum_l \varphi^t_{sl}(\hat{J}) f^r_{sl}(\mathcal{K}), \tag{36}$$

invariant under the operations G, i.e., satisfying the condition

$$\sum_l \varphi^t_{s,l}(\hat{G}\hat{J}) f^r_{sl}(\hat{G}\mathcal{K}) = \sum_l \varphi^t_{sl}(\hat{J}) f^r_{sl}(\mathcal{K}), \tag{37}$$

and its matrix constructed in the basis u_i will then satisfy condition (10).

Now, according to (11), $\varphi_{sl}(\hat{J})$ and $f(\mathcal{K})$ must transform according to conjugate (equivalent) representations. The construction of these functions and of the operator $\mathcal{D}$ itself is very simple. The construction of the matrices $\varphi_{sl}(J)$ is more complicated.

The general number of linearly independent matrices $\varphi^t_{sl}(J)$ in the space of the functions $Y^{j\pm}_m$ is $(2j+1)^2$, while the number of linearly independent matrices in the space u_i is equal to the square of the dimensions of the representation T_0 — n_s^2, and n_s matrices from them transform according to each of the representations T_S, where n_S is given by equation (8). Applying the usual methods of group theory,[12] it can at once be established in which of the representations $D^{\pm}_j$ a given representation $\bar{T}_0$ is contained. Of course, j must be taken as small as possible; then the actual breaking up of this representation into irreducible representations, i.e., the determination of $a^i_{j,m}$ in (34) and the construction of the corresponding matrices $\varphi(J)$, becomes simplest. If $n < 2j+1$, then some of the $(2j+1)^2$ matrices $\varphi(J)$ either become zero or linearly dependent. Therefore, if a greater number of the group of matrices transform according to the representation T_S than given by (8), the "superfluous" matrices must not be included in $\mathcal{D}$. If $n = 2j+1$, i.e., the representation $\bar{T}_0$ coincides with $D^{\pm}_j$, then the matrices $\varphi(J)$ can be taken in any representation with the given j. In this case the method described here coincides with Luttinger's method.[7]

If there are two representations T_{01} and T_{02} for which the moduli of the characters coincide,

then the same $f(\mathcal{K})$ appear in $\mathcal{D}(\mathcal{K})$ according to (8). It is not, however, obvious whether the determinants $\|\mathcal{D}(\mathcal{K})\|$ are always the same for both representations. For two-dimensional representations the equality of the determinants follows from the method of constructing $\mathcal{D}$ described below. It is apparent from (6) that the determinants are also equal if the representations T_{01} and T_{02} differ only in parity, and also in the more general case when the group $G'' = Ge^{-i\pi\delta}G$, where $e^{-i\pi\delta}G = \chi_{01}(G)/\chi_{02}(G)$, is isomorphous with the group G. In these cases it is sufficient to construct $\mathcal{D}$ only for that representation T_{0i} which is contained in $D_j^{\pm}$ with the minimum j.

The additional requirements associated with invariance to time inversion imply that the part of the terms for which, according to (20) or (25) $n_S = 0$, is excluded from $\mathcal{D}$ in the corresponding cases. In case a_1 it is also possible to use directly relation (16), since

$$S\varphi^*(J)\,S^{-1} = SS\varphi(J^*)\,S^{-1}S^{-1} = \varphi(J^*) = \gamma'\varphi(J), \quad (38)$$

where $\varphi(J^*)$ is the matrix of the operator $\varphi(\hat{J}^*)$, the complex conjugate of $Q(\hat{J})$. Here $\gamma' = \pm 1$, depending on the parity of $\varphi(\hat{J})$. It therefore follows from (16) that in case a_1 there can appear in $\mathcal{D}$ in (36) only even products with $\gamma\gamma' = 1$, i.e., those not changing sign on replacing k_i, H_i and J_i by $-k_i$, $-H_i$ and $-J_i$. In the other cases this simple rule is not, of course, valid.

2. Unifying several representations. In some cases, for example, when it is necessary to take account of the effect of the nearest zones, and also in cases $b_{1,2}$ and $c_{1,2}$, when complex representations are combined, it is necessary to construct $\mathcal{D}$ for the reducible representation T_0 which contains several irreducible representations T_{0i}. If the group G_{k_0} is equivalent, in the sense given above, to the point group $\bar{\bar{G}}$, then $\mathcal{D}$ can be constructed analogously. If all the irreducible representations are contained in the same representation $D_j^{\pm}$, then their basis functions can be constructed from $Y_m^{j\pm}$ with the same j, and, as above, for the matrices A_{sl}^t can be taken the matrices $\varphi_{sl}^t(J)$, constructed from the corresponding basis functions.

If the irreducible representations T_{0i} are contained in different representations $D_j^{\pm}$ with j differing by not more than unity, then, depending on the parity of these representations, it is simplest to choose as these matrices the matrices of either the axial vector J or the polar vector A.[13] If T_0 contains, for example, two representations T_{01} and T_{02} of dimensions n_1 and n_2, then in all there are $(n_1+n_2)^2$ non-zero linearly independent matrices. Of these $2n_1n_2$ matrices transform according to the irreducible representations contained in $T_{01}\times T_{02}^* + T_{01}^*\times T_{02}$, and have only non-zero "interband" matrix elements. For the remaining $n_1^2 + n_2^2$ matrices, which transform according to the representations contained in $|T_{01}|^2 + |T_{02}|^2$, the intraband matrix elements are non-zero. As regards the conditions imposed by invariance under time inversion, in obtaining the equations of Sec. 2 we have nowhere supposed that the representation T_0 is irreducible, and all these equations therefore remain in force.

When combining two complex representations in cases $b_{1,2}$ and $c_{1,2}$, it is also necessary to take into account the additional conditions (26a) and (30a) imposed on the "diagonal" parts of the matrix $\mathcal{D}$.

3. The group G_{k_0} not equivalent to the point group. In this case, when the quantity $\psi_{\alpha\beta}$ is not equal to unity for all G_{k_0}, the quantities G_{ij} cannot be represented in the form (32), and the factor group $\bar{G}_{k_0}$ of the space group $\underline{G}_{k_0}$ contains more elements than the point group $\bar{\bar{G}}$. This case, which is more complicated, can occur at separate points on the zone surface; then there is usually degeneracy at such a point. In the case of twofold degeneracy, $\mathcal{D}$ can be immediately constructed by the method described in the following section. For higher degeneracy $\mathcal{D}$ can be constructed as follows.

We reduce the symmetry of the group G_{k_0} by excluding elements with non-primitive translations, so that the new group $\tilde{G}_{k_0}$ becomes equivalent to the point group. In this group the representation T_0 can be reducible, and breaks down into irreducible representations $\tilde{T}_{0i}$. By combining these representations it is possible by the method given above to construct a matrix $\tilde{\mathcal{D}}$, satisfying Eq. (6) for the operations $\tilde{G}$. On increasing the symmetry, i.e., going from $\tilde{G}_{k_0}$ to G_{k_0}, the form of $\mathcal{D}$ can change only due to some of the constants C_s^{tr} becoming zero and some of them becoming equal. If, using relation (8), n_S is found for both groups, and $\mathcal{D}$ and $\tilde{\mathcal{D}}$ are written in the general form (9) without explicitly writing out the matrices A_{sl}^t, then, by comparing these expressions, it is usually possible to establish at once which of the constants become zero or equal on going from $\tilde{\mathcal{D}}$ to $\mathcal{D}$, and, simultaneously, to find $\mathcal{D}$. To simplify the calculations it is, of course, necessary to choose the group $\tilde{G}_{k_0}$ so that the symmetry remains the maximum possible.

4. Twofold degeneracy. In the case of twofold degeneracy at the point k_0, both the determinant $\|\mathcal{D} - E\|$ and the matrix $\mathcal{D}$ can be constructed

without using concrete basis functions. From (6) follows the obvious identity

$$\| \mathcal{D}(\mathcal{K}) - E \| = \| \mathcal{D}(\hat{G}\mathcal{K}) - E \|, \tag{39}$$

i.e., the determinant $\| \mathcal{D}(\mathcal{K}) - E \|$ must be invariant to the operations $\hat{G}$. We write the matrix $\mathcal{D} - E$ in the form

$$\mathcal{D} - E = \begin{vmatrix} a_0 + a_1 - E & a_{12} \\ a_{12}^* & a_0 - a_1 - E \end{vmatrix}. \tag{40}$$

Then

$$\| \mathcal{D} - E \| = (E - a_0)^2 - a_1^2 - |a_{12}|^2. \tag{41}$$

Here we have formally replaced all operators in a_i by numbers. We remember that only symmetrized products of operators appear in $\mathcal{D}$. It is clear from (39) that only functions $f(\mathcal{K})$ appear in a_0 which are invariant to $\hat{G}$, i.e., transform according to an identity representation, but in $a_2 = a_1^2 + |a_{12}|^2$ there appear only quadratic invariants of $f(\mathcal{K})$, which transform according to non-identity representations. These invariants can be constructed uniquely. Since in the direct product $T_S \times T_{S'}$ an identity representation is contained only once if $s = s'$, and not at all if $s \neq s'$, only products of $f(\mathcal{K})$ can appear in a_2 which transform according to the same representation —one product for each irreducible representation T_S for which n_S is non-zero according to (8), (20), or (25). These formulae therefore uniquely determine $\| \mathcal{D} - E \|$.

For two-dimensional representations T_0 the product $T_0 \times T_0^*$ breaks down either into four one-dimensional irreducible representations or into two one-dimensional, including the identity T_1, and one two-dimensional.

In the first case, when all the representations T_S are one-dimensional,

$$a_0 = \sum_r C_1^r f_1^r(\mathcal{K}), \qquad a_2 = \sum_{r,s=2,3,4} |C_s^r f_s^r(\mathcal{K})|^2. \tag{42}$$

It is apparent that $\mathcal{D}$ can be chosen in any form satisfying (42) and the condition that it be Hermitian.

If all the $f_S^r(\mathcal{K})$ are chosen real, then $\mathcal{D}$ can, for example, be written in the form

$$\mathcal{D} = \sum_{r,s} C_s^r A_s f_s^r(\mathcal{K}), \tag{43}$$

where $A_1 = I$, and A_2, A_3, and A_4 are the Pauli matrices σ_x, σ_y, and σ_z. We note that, irrespective of the choice of basis, we have $\mathrm{Sp}\, A_S = 0$ for any matrix A_S transforming according to the one-dimensional non-identity representation. In fact, $\mathrm{Sp}(G^0 A_S G^{0-1}) = \mathrm{Sp}\, A_S$. On the other hand, for the one-dimensional representations $GA_S = e^{i\varphi_G} A_{S'}$, and, consequently, $\mathrm{Sp}\, \hat{G}A_S = e^{i\varphi_G}\, \mathrm{Sp}\, A_S$. Since for non-identity representations all the $e^{i\varphi_G}$ cannot be equal to unity, for them $\mathrm{Sp}\, A_S = 0$. Therefore A_S can always be represented as the sum of Pauli matrices, and by unitary transformations they can be brought to the form described above. This does not, of course, mean that the corresponding matrices transform as spin operators.

In the second case, when one of the representations, T_3, is two-dimensional, the $f_{3l}^r(\mathcal{K})$ transforming according to this representation can always be chosen so that $f_{32}^r(\mathcal{K}) = f_{31}^{r*}(\mathcal{K})$ and $|f_{31}^r(\mathcal{K})|^2$ is invariant under G. Then

$$a_2 = \sum_r |C_2^r f_2^r(\mathcal{K})|^2 + |C_3^r f_{31}^r(\mathcal{K})|^2. \tag{44}$$

If here $f_2^r(\mathcal{K})$ is real, then $\mathcal{D}$ can be expressed in the form

$$\mathcal{D} = \sum_{r,s,l} C_s^r A_{sl} f_{sl}^r(\mathcal{K}), \tag{45}$$

where

$$A_1 = I = \begin{vmatrix} 1 & 0 \\ 0 & 1 \end{vmatrix}, \quad A_2 = \sigma_z = \begin{vmatrix} 1 & 0 \\ 0 & -1 \end{vmatrix}, \quad A_{31} = \sigma_+ = \begin{vmatrix} 0 & 1 \\ 0 & 0 \end{vmatrix},$$
$$A_{32} = \sigma_- = \begin{vmatrix} 0 & 0 \\ 1 & 0 \end{vmatrix}. \tag{46}$$

Of course, all the $f_{3l}^r(\mathcal{K})$ with equal indices l must transform according to the same representation, i.e., according to the representation T_S, for which all the matrix elements coincide and not only the characters.

With the choice of $f_{Sl}^r(\mathcal{K})$ and the matrices A_{Sl} given above, the operator $\mathcal{D}$ satisfies both condition (39) and the requirement that it be Hermitian. The method proposed here for constructing $\mathcal{D}$ for twofold degenerate representations is the most simple. This method is close to that used by Rashba.[8]

In conclusion we consider a concrete example.

5. THE EFFECT OF DEFORMATION ON THE ENERGY SPECTRUM OF CARRIERS IN WURTZITE TYPE CRYSTALS

The space group of wurtzite C_{6v}^4 has been investigated in detail by Rashba.[8] He has constructed the wave vector group for the various points and calculated the spectrum at these points. For degenerate representations the possible points of zero slope in wurtzite are: a) for the representations Δ_5 and Δ_6, all the points on the Δ axis apart from A; b) for the representations P_3, the point H (in the notation of [8]). We consider the change of the spectrum for the corresponding representations under deformation.

Table I*. Characters of the representations for the point Δ

Number of elements	Elements of the class	Δ_1	Δ_2	Δ_3	Δ_4	Δ_5	Δ_6
1	$(\varepsilon \mid 0)$	1	1	1	1	2	2
2	$(\delta_6 \mid 1/2\, t_0)$, $(\delta_6^{-1} \mid 1/2\, t_0)$	η_k	η_k	$-\eta_k$	$-\eta_k$	$-\eta_k$	η_k
2	$(\delta_3 \mid 0)$, $(\delta_3^{-1} \mid 0)$	1	1	1	1	−1	−1
1	$(\delta_2 \mid 1/2\, t_0)$	η_k	η_k	$-\eta_k$	$-\eta_k$	$2\eta_k$	$-2\eta_k$
3	$(\sigma_1 \mid 0)$, $(\sigma_2 \mid 0)$, $(\sigma_3 \mid 0)$	1	−1	1	−1	0	0
3	$(\sigma_1' \mid 1/2\, t_0)$, $(\sigma_2' \mid 1/2\, t_0)$, $(\sigma_3' \mid 1/2\, t_0)$	η_k	$-\eta_k$	$-\eta_k$	η_k	0	0

*$\eta_k = \exp(ik_z t_0/2)$. For the point Γ the quantity $\eta_k = 1$.

1) The point Δ. The characters of the representations at the points Δ calculated by Rashba are given in Table I.

The twofold representations Δ_5 and Δ_6 belong to the case b_3 and, consequently, according to (8), there can appear in $\mathcal{D}$ matrices A_{Sl} and $f(\mathcal{K})$, which transform according to the representations $\Delta_5 \times \Delta_5^* = \Delta_6 \times \Delta_6^* = \Gamma_1 + \Gamma_2 + \Gamma_5$.

The functions $f(\mathcal{K})$, transforming according to these representations, are given in Table III. We limit ourselves here to terms quadratic in **k** and linear in ϵ. The matrices mentioned transform according to these representations. We choose the functions $f(\mathcal{K})$ in accordance with the requirements of Sec. 3, item 4, taking in particular (44) into account. Therefore, according to (45),

$$\mathcal{D} = A_1 (B_0 k_z + B_1 k_z^2 + B_2 k_\perp^2 + C_1 \varepsilon_{zz} + C_2 \varepsilon_\perp) + B_3 (A_{31} k_+^2 + A_{32} k_-^2) + C_3 (A_{31} \varepsilon_+ + A_{32} \varepsilon_-). \quad (47)$$

Here

$$k_\pm = k_x \pm i k_y, \qquad k_\perp^2 = k_x^2 + k_y^2,$$
$$\varepsilon_\pm = \varepsilon_{xx} \pm 2i\varepsilon_{xy} - \varepsilon_{yy}, \qquad \varepsilon_\perp = \varepsilon_{xx} + \varepsilon_{yy},$$

B_i and C_i are constants of the substance and the matrices A_{Sl} are given by (46).

For the representations Γ_5 and Γ_6, which belong to case a_1, there can, according to (20), only appear in $\mathcal{D}$ even functions of $\mathcal{K}$, which transform according to $[\Gamma_{5,6}^2] = \Gamma_1 + \Gamma_5$ (and odd functions transforming according to $\{\Gamma_{5,6}^2\} = \Gamma_2$). Therefore, at this point $B_0 = 0$. In addition, the point of zero slope can be any of the points Δ. At these points, according to (47), the solution of the secular equation $\| \mathcal{D} - E \| = 0$ has the form

$$E(k, \varepsilon) = \lambda \pm \{B_3^2 k_\perp^4 + 2B_3 C_3 [(\varepsilon_{xx} - \varepsilon_{yy})(k_x^2 - k_y^2) + 4\varepsilon_{xy} k_x k_y] + C_3^2 [(\varepsilon_{xx} - \varepsilon_{yy})^2 + 4\varepsilon_{xy}^2]\}^{1/2}, \quad (48)$$

where

$$\lambda = B_1 k_z^2 + B_2 k_\perp^2 + C_1 \varepsilon_{zz} + C_2 \varepsilon_\perp.$$

The splitting of the terms at $\mathbf{k} = 0$ is

$$\delta E_0 = 2 \mid C_3 \mid [(\varepsilon_{xx} - \varepsilon_{yy})^2 + 4\varepsilon_{xy}^2]^{1/2}. \quad (49)$$

Close to the extremum, i.e., for $E(k) \ll \delta E_0$, the surfaces of constant energy have the form of ellipsoids:

$$E_{1,2} = \pm \frac{\delta E_0}{2} + \lambda \pm \frac{2C_3 B_3}{\delta E_0} [(k_x^2 - k_y^2)(\varepsilon_{xx} - \varepsilon_{yy}) + 4k_x k_y \varepsilon_{xy}]. \quad (50)$$

For large k, when $E(k) \gg \delta E_0$,

$$E = \lambda \pm \mid B_3 \mid k_\perp^2 \pm \frac{B_3 C_3}{\mid B_3 \mid k_\perp^2} [(\varepsilon_{xx} - \varepsilon_{yy})(k_x^2 - k_y^2) + 4\varepsilon_{xy} k_x k_y]. \quad (51)$$

Therefore, according to [16], large values of the piezoresistance coefficients, $\Pi_{xxxx} = \Pi_{yyyy}$, $\Pi_{xxyy} = \Pi_{yyxx}$, and Π_{xyxy}, can be expected here —these constants being proportional to C_3/kT. Of course, all these formulae are valid only in the case when the splitting of the bands δE_0 caused by the deformation exceeds the spin-orbit splitting.

2) The point H. The characters of the representations at the points P are given in Table II. The twofold degenerate representation H_3 belongs to the case a_2. To construct $\mathcal{D}$ according to (25), it is necessary to construct $f(\mathcal{K})$ which transform according to the irreducible representations of the expanded group G, R, containing the elements G_H and $G_H R_0$. This group coincides with the group Γ, and we have already constructed the corresponding functions (Table III). Substituting in (25) the values of the corresponding characters from Tables I and II, we find that there can appear in $\mathcal{D}$ odd

Table II*. Characters of the representations for the point P

Number of elements	Elements of the class	P_1	P_2	P_3
1	$(\varepsilon \mid 0)$	1	1	2
2	$(\delta_3 \mid 0)$, $(\delta_3^{-1} \mid 0)$	1	1	−1
3	$(\sigma_1' \mid 1/2\, t_0)$, $(\sigma_2' \mid 1/2\, t_0)$, $(\sigma_3' \mid 1/2\, t_0)$	η_k	$-\eta_k$	0

*For the point H the quantity $\eta_k = i$, and for the point K the quantity $\eta_k = 1$.

Table III*. The distribution of $f(\mathscr{K})$ and A_{sl} over the irreducible representations Γ and K

Representation Γ	Representation K	$f(\mathscr{K})$ odd	$f(\mathscr{K})$ even	A_{sl}
Γ_1	K_1	k_z	k_z^2; $k_\perp^2$; ε_{zz}; $\varepsilon_\perp$	A_1
Γ_4		—	—	
Γ_2	K_2	—	—	A_2
Γ_3		—	—	
Γ_5	K_3	—	k_+^2, k_-^2; $\varepsilon_+, \varepsilon_-$	A_{31}, A_{32}
Γ_6		k_+, k_-	$k_+ k_z$, $k_- k_z$; ε_{+z}, ε_{-z}	

* $k_\pm = k_x \pm ik_y$, $k_\perp^2 = k_x^2 + k_y^2$, $\varepsilon_\pm = \varepsilon_{xx} \pm 2i\varepsilon_{xy} - \varepsilon_{yy}$, $\varepsilon_\perp = \varepsilon_{xx} + \varepsilon_{yy}$, $\varepsilon_{\pm z} = \varepsilon_{xz} \pm i\varepsilon_{yz}$.

functions transforming according to the representations Γ_2 and Γ_5, and even functions transforming according to Γ_1 and Γ_6. We emphasize that the matrix $\mathscr{D}$ must be invariant to the operations of the point group K corresponding to the group H, and there must appear in $\mathscr{D}$ products of $f_{sl}(\mathscr{K})$ and A_{sl}, which transform according to the equivalent representations of the group K appearing in $H_3H_3^*$, i.e., K_1, K_2, and K_3. These functions can transform according to different representations of the group Γ, since two representations Γ_i correspond to each representation K_i, as is seen from Table III.

We construct $\mathscr{D}$ using the functions from Table III:

$$\mathscr{D} = A_1 (B_1 k_z^2 + B_2 k_\perp^2 + C_1 \varepsilon_{zz} + C_2 \varepsilon_\perp) + B_3 (A_{31} k_+ + A_{32} k_-) k_z + C_3 (A_{31} \varepsilon_{+z} + A_{32} \varepsilon_{-z}), \quad (52)$$

where $\epsilon_{\pm z} = \epsilon_{xz} \pm i\epsilon_{yz}$, and the matrices A_{sl} are given by (46). Solving the secular equation $\| \mathscr{D} - E \| = 0$ we have

$$E(k, \varepsilon) = \lambda \pm \{B_3^2 k_\perp^2 k_z^2 + 2B_3 C_3 (k_x \varepsilon_{xz} + k_y \varepsilon_{yz}) k_z + C_3^2 (\varepsilon_{xz}^2 + \varepsilon_{yz}^2)\}^{1/2}, \quad (53)$$

where λ is given by (48).

Consequently, the splitting of the bands at $k = 0$ is

$$\delta E_0 = 2 | C_3 | (\varepsilon_{xz}^2 + \varepsilon_{yz}^2)^{1/2}. \quad (54)$$

The spectrum close to the extremum for small values of k is:

$$E_{1,2} = \pm \frac{\delta E_0}{2} + \lambda \pm \frac{2B_3 C_3}{\delta E_0} (k_x k_z \varepsilon_{xz} + k_y k_z \varepsilon_{yz}). \quad (55)$$

The spectrum for large k is:

$$E = \lambda \pm | B_3 k_\perp k_z | \pm \frac{B_3 C_3}{| B_3 k_\perp k_z |} (\varepsilon_{xz} k_x k_z + \varepsilon_{yz} k_y k_z). \quad (56)$$

Therefore, according to [16], there will be large piezoresistance coefficients $\Pi_{xzxz} = \Pi_{yzyz}$.

It is curious here that for any deformation all the extrema at different points of the star H are displaced equally, as is seen from (49). This means that no effects arise associated with the displacement of the extrema relative to one another, as are observed, for example, in n-Ge and n-Si.[17]

[1] S. I. Pekar, Issledovaniya po Élektronnoĭ Teorii Kristallov (Studies in the Electronic Theory of Crystals), Gostekhizdat 1951, p. 26.

[2] J. M. Luttinger and W. Kohn, Phys. Rev. **97**, 869 (1955).

[3] E. N. Adams, Phys. Rev. **96**, 803 (1954).

[4] G. E. Pikus and G. L. Bir, FTT **1**, 154 and 1642 (1959), Soviet Phys.-Solid State **1**, 136 (1959) and 1502 (1960).

[5] J. Bardeen and W. Shockley, Phys. Rev. **80**, 72 (1950).

[6] G. E. Pikus, ZhTF **28**, 2390 (1958), Soviet Phys.-Tech. Phys. **3**, 2194 (1959). G. L. Bir and G. E. Pikus, FTT **2**, 2287 (1960), Soviet Phys.-Solid State **2**, 2039 (1961).

[7] J. M. Luttinger, Phys. Rev. **102**, 1030 (1956).

[8] É. I. Rashba, FTT **1**, 407 (1959); Soviet Phys.-Solid State **1**, 368 (1959).

[9] G. E. Pikus, JETP **41**, 1507 (1961), Soviet Phys. JETP, in press.

[10] G. L. Bir and G. E. Pikus, FTT **3**, 3058 (1961), Soviet Phys.-Solid State **3**, in press.

[11] G. E. Pikus, FTT **3**, 2819 (1961), Soviet Phys.-Solid State **3**, in press.

[12] G. L. Lyubarskii, Teoriya Grupp i ee Primenenie v Fizike (Group Theory and its Application in Physics), Gostekhizdat 1957.

[13] L. D. Landau and E. M. Lifshitz, Quantum Mechanics, Pergamon, 1958, Chap. XII.

[14] E. Wigner, Gött. Nachr. **5**, 546 (1932).

[15] C. Herring, Phys. Rev. **52**, 361 (1937).

[16] G. E. Pikus and G. L. Bir, FTT **1**, 1828 (1959), Soviet Phys.-Solid State **1**, 1675 (1960).

[17] C. S. Smith, Phys. Rev. **94**, 42 (1954).

Translated by K. F. Hulme
217

CORRELATION OF MOTION OF FOUR NUCLEONS IN THE Po^{212} NUCLEUS

I. M. BAND, L. A. SLIV, and Yu. I. KHARITONOV

Leningrad Physico-Technical Institute, Academy of Sciences, U.S.S.R.

Submitted to JETP editor May 12, 1961

J. Exptl. Theoret. Phys. (U.S.S.R.) **41**, 1274-1284 (October, 1961)

The spectrum of the excited states and the transitions between these states are calculated for a nucleus with two nucleon pairs in excess of the filled shells. Residual pair interaction is taken into account along with the self-consistent potential. The importance of taking np forces in such nuclei into account is demonstrated.

1. INTRODUCTION

THE self-consistent potential acting on an individual nucleon, as well as the residual pair forces in the nucleus, have already been determined in earlier investigations.[1-4] The self-consistent potential consists of two principal parts, central V_C and surface V_S. The central potential is

$$V_C(i) = V(r_i) - \lambda\left(\frac{\hbar}{2Mc}\right)^2 \frac{\mathbf{l}_i\mathbf{s}_i}{r_i}\frac{\partial V(r_i)}{\partial r_i},$$

$$V(r_i) = -V_0/[1+e^{\alpha(r_i-r_0)}]. \quad (1)$$

The parameters α, λ, and V_0 were calculated from the energies of the ground and excited levels of nuclei with filled shells ± one nucleon (for more details, see [1]). The surface potential V_S is due to the quadrupole interaction between the outer particle and the core particles, and is usually represented in the form

$$V_S(i) = -\varkappa(r_i)\sqrt{\frac{\hbar\omega}{2C}}\sum_\mu (b_\mu + (-1)^\mu b^+_{-\mu})\, Y_{2\mu}(\vartheta_i, \varphi_i). \quad (2)$$

Here b^+ and b are the phonon creation and annihilation operators. The parameters $\hbar\omega$ and C, which characterize the phonon energy and the deformability of the surface respectively, were determined from the E2-transition probabilities and the quadrupole moments.[4] In the region of heavy nuclei, $\hbar\omega = 2-3$ Mev and $C = (1-2)\times 10^3$ Mev. For the radial matrix elements we have the following estimate

$$\langle n|\varkappa(r_i)|n'\rangle \approx (-1)^{n+n'}(35-40)\ \text{Mev}$$

where n is the principal quantum number.

In nuclei with two nucleons (holes) in excess of twice-filled shells, in addition to the self-consistent field, pair forces begin to play an important role which must be correctly accounted for. The pair interaction operator was taken in the form[2,3]

$$V_p(ij) = -(v_s\pi_s + v_t\pi_t)\exp\{-|\mathbf{r}_i-\mathbf{r}_j|^2/\rho^2\}. \quad (3)$$

Here v_S and v_t are the parameters of the singlet and triplet interaction, π_S and π_t are the operators of singlet and triplet projection, and ρ is the effective radius of interaction. The parameters v_S, v_t, and ρ were determined separately for the nn, pp, and np pairs in the corresponding nuclei. The results obtained show that v_S is somewhat greater for the pp pair than for the nn pair, but we cannot say that this difference has physical meaning and is not the result of inaccurate knowledge of the energy of the single-particle levels in the Pb^{210} and Po^{210} nuclei. For the np pair in Bi^{209} the main contribution to the interaction energy is made by triplet forces, and the parameter v_t determined for this case is more reliable.

2. SINGULARITIES IN THE FOUR-PARTICLE PROBLEM

The problem of determining the states of four interacting nucleons in the nucleon has its own singularities, which greatly complicate the solution. We consider, for example, as in the case of two nucleons, five neutron and five proton single-particle levels (see Fig. 1). We then obtain for the neutron pair and for the proton pair 225 configurations, each multiply degenerate. Even if we confine ourselves to the zeroth-approximation levels, with energies ≤3.5 Mev, we obtain more than 70 levels with spin $I = 0^+$, more than 270 levels with spin $I = 2^+$, etc. These are only levels without phonons ($N = 0$); if states with $N \neq 0$ are taken into account, the number of levels increases still more. Naturally, not all these levels must be taken into account if we are interested in excitations not higher than 3 Mev, for after excluding the pair interaction the levels will be approximately 6 Mev apart. But in order to calcu-

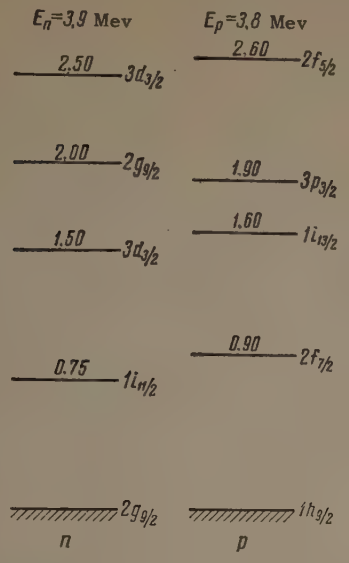

FIG. 1. Single-particle levels of Po^{212} nucleons.

late correctly the configuration mixture, it is necessary to take into account a sufficient number of levels, and this leads to great computational difficulties, which so far could not be overcome even in the simple problem without account of the interaction with the surface. Only programming for a computer resulted in a complete solution of the entire four-particle problem.

On the basis of the data accumulated in the earlier investigations, we can formulate the following assumptions of importance to the four-nucleon problem.

1. The nucleons move in the self-consistent potential (1) and (2).

2. The residual forces are short-range pair forces.

3. The parameters of the pair forces are the same for all particle pairs (isotopic independence of the pair forces). Naturally, small deviations of the parameters of the pair forces or of the self-consistent field are actually possible. But if these deviations are significant, they can be observed and subsequently accounted for.

We chose for the pair-force parameters the values $\rho = 2f$, $v_S = 30-36$ Mev, and $v_t = 15-20$ Mev. These are precisely the forces obtained for Pb^{210}, Bi^{210}, and Po^{210}.

3. METHOD OF CALCULATION

In the present problem we consider a system of four nucleons (2n + 2p) moving in a central field, and a nuclear surface executing quadrupole oscillations. The nuclear surface is needed only to account for the V_S interaction. The single-particle and phonon functions were determined from the equations

$$H_0(i)\,|\,n_i l_i j_i m_i\rangle = E_i^{(0)}\,|\,n_i l_i j_i m_i\rangle, \qquad i = 1, 2, 3, 4; \tag{4}$$

$$H_S\,|\,NRM_R\rangle = (N + {}^5/_2)\hbar\omega\,|\,NRM_R\rangle;$$

$$H_0(i) = p_i^2/2M + V_C(i), \tag{4'}$$

where $n_i l_i j_i m_i$ are the quantum numbers of the i-th nucleon, N is the number of phonons with energy $\hbar\omega$, while R and M_R are the angular momentum of the phonon and its projection on the z axis.

In the zeroth approximation the eigenfunction of the entire system, corresponding to a definite momentum I, projection M, and parity ν, is written in the form

$$|\,[(n_1 l_1 j_1, n_2 l_2 j_2)\,J_{12}]_a\,,\ [(n_3 l_3 j_3,\ n_4 l_4 j_4)\,J_{34}]_a,\ J;\ NR;\ IM\nu\rangle. \tag{5}$$

The indices 1 and 2 pertain to neutrons while 3 and 4 pertain to protons. The index a denotes antisymmetrization of the functions. We have in mind here the following connections between the angular momenta:

$$\mathbf{j}_1 + \mathbf{j}_2 = \mathbf{J}_{12}, \quad \mathbf{j}_3 + \mathbf{j}_4 = \mathbf{J}_{34},$$

$$\mathbf{J}_{12} + \mathbf{J}_{34} = \mathbf{J}, \quad \mathbf{J} + \mathbf{R} = \mathbf{I}.$$

The total Hamiltonian of the system is

$$H = \sum_{i=1}^{4} H_0(i) + H_S + \sum_{i=1}^{4} V_S(i) + \sum_{i<j}^{4} V_p(ij). \tag{6}$$

We seek the solution of the Schrödinger equation with Hamiltonian (6) in the form of an expansion in the eigenfunctions (5):

$$\Big|\,IM\nu\rangle = \sum_{\alpha} c^I(\alpha)\,\Big|\,[(j_1 j_2)\,J_{12}]\ ,\ [(j_3 j_4)\,J_{34}]_a,\ J;\ NR;\ IM\nu\rangle,$$

$$\alpha \equiv (j_1 j_2 J_{12} j_3 j_4 J_{34} J N R). \tag{7}$$

To abbreviate the notation, the index j_i denotes the set of three quantum numbers $m_i l_i j_i$.

The eigenvalues and the coefficients $C^I(\alpha)$ of expansion in eigenfunctions of the Hamiltonian (6) are obtained by diagonalizing the energy matrix. To set up the energy matrix it is necessary to calculate the matrix elements of the operators $\Sigma V_p(ij)$ and $\Sigma V_S(i)$. The matrix element of the pair interaction has six terms and its value is

$$\langle [(j_1 j_2)\,J_{12}]_a,\ [(j_3 j_4)\,J_{34}]_a,\ J;\ NR;\ IM\nu\Big|\sum_{i<j}^{4} V_p(ij)\Big|$$

$$\to [(j_1' j_2')J_{12}']_a, [(j_3' j_4')\,J_{34}']_a,\ J';\ N'R';\ IM\nu\rangle$$

$$= \delta_{NN'}\delta_{RR'}\delta_{JJ'}\{\delta_{J_{12}J_{12}'}\delta_{J_{34}J_{34}'}[\delta_{j_3 j_3'}\delta_{j_4 j_4'}$$

$$\times \langle [(j_1 j_2)\,J_{12}M_{12}]_a\,|\,V_p(12)\,|\,[(j_1' j_2')\,J_{12}M_{12}]_a\rangle$$

$$+ \delta_{j_1 j_1'}\delta_{j_2 j_2'}\langle [(j_3 j_4)\,J_{34}M_{34}]_a\,|\,V_p(34)\,|\,[(j_3' j_4')\,J_{34}M_{34}]_a\rangle]$$

$$+ 4\langle [(j_1 j_2)\,J_{12}]_a,\ [(j_3 j_4)\,J_{34}]_a,$$

$$JM\,|\,V_p(13)\,|\,[(j_1' j_2')\,J_{12}']_a,\ [(j_3' j_4')\,J_{34}']_a; JM\rangle\}. \tag{8}$$

This general expression must be reduced to a form which is simplest and most convenient for machine computation. Let us rewrite (8) in the form of a sum of the matrix elements of the non-antisymmetrized functions

$$\delta_{NN'}\delta_{RR'}\delta_{JJ'}\Big\{\delta_{J_{12}J'_{12}}\delta_{J_{34}J'_{34}}\Big[\delta_{j_3j'_3}\delta_{j_4j'_4}N_{j_1j_2}N_{j'_1j'_2}$$
$$\times\sum_P(-1)^pP\langle(j_1j_2)\ J_{12}M_{12}\,|\,V_p(12)\,|\,(j'_1j'_2)J_{12}M_{12}\rangle$$
$$+\delta_{j_1j'_1}\delta_{j_2j'_2}N_{j_3j_4}N_{j'_3j'_4}$$
$$\times\sum_P(-1)^pP\langle(j_3j_4)\ J_{34}M_{34}\,|V_p(34)\,|\,(j'_3j'_4)\ J_{34}M_{34}\rangle\Big]$$
$$+4N_{j_1j_2}N_{j'_1j'_2}N_{j_3j_4}N_{j'_3j'_4}\sum_P(-1)^pP\ \langle(j_1j_2)\ J_{12},\ (j_3j_4)\ J_{34};$$
$$\to JM\,|V_p(13)\,|\,(j'_1j'_2)\ J'_{12},\ (j'_3j'_4)\ J'_{34};\ JM\rangle\Big\}. \qquad (9)$$

Here P is the operator which permutes the indices inside each of the pairs j_1j_2, j_3j_4, $j'_1j'_2$, and $j'_3j'_4$. The summation extends over all the different permutations which actually change the arrangement of the indices. Each pair of indices makes its own contribution to the power p of the factor (-1). If the permutation j_ij_k is even the corresponding term vanishes, and if it is odd its value is $(j_i+j_k-J_{ik}+1)$. The normalizing factors of the functions of the particle pair j_ij_k have the form

$$N_{j_ij_k}=1/\sqrt{2}+(1-1/\sqrt{2})\,\delta_{j_ij_k}. \qquad (10)$$

In order to calculate the matrix element of the np interaction, it is necessary to go over in the last term of (9) to a different coupling scheme, in which the first particle is connected with the third and the second with the fourth. Then

$$\langle(j_1j_2)\ J_{12},\ (j_3j_4)\ J_{34};\ JM\,|V_p(13)\,|\,(j'_1j'_2)\ J'_{12},\ (j'_3j'_4)\ J'_{34};\ JM\rangle$$
$$=\delta_{j_2j'_2}\delta_{j_4j'_4}\sum_{J_{13}J_{24}}A\begin{Bmatrix}j_1 & j_2 & J_{12}\\ j_3 & j_4 & J_{34}\\ J_{13} & J_{24} & J\end{Bmatrix}A\begin{Bmatrix}j'_1 & j_2 & J'_{12}\\ j'_3 & j_4 & J'_{34}\\ J_{13} & J_{24} & J\end{Bmatrix}$$
$$\times\langle(j_1j_3)\ J_{13}M_{13}\,|V_p(13)\,|\,(j'_1j'_3)\ J_{13}M_{13}\rangle. \qquad (11)$$

Here $A\{\ \}$ are normalized generalized Racah coefficients.

This formula is difficult to compute, for it calls for double summation of a rather complicated expression. We make therefore the following transformations. We represent the pair interaction operator in the form of two terms

$$V_p(13)=V(|\mathbf{r}_1-\mathbf{r}_3|)\,[a+b(\sigma_1\sigma_3)]$$
$$=V_p^{(a)}(13)+V_p^{(b)}(13); \qquad (12)$$
$$V_p^{(a)}(13)=a\sum_k f_k(\mathbf{T}^k(1)\,\mathbf{T}^k(3)), \qquad (12')$$
$$V_p^{(b)}(13)=b\sum_k f_k(\mathbf{T}^k(1)\,\mathbf{T}^k(3))(\sigma_1\sigma_3)$$
$$=b\sum_{kk'}(-1)^{k+k'+1}f_k(\mathbf{U}^{k'}(1)\,\mathbf{U}^{k'}(3)). \qquad (12'')$$

Here $\mathbf{U}^{k'}$ is the tensor product of the tensor operators $\mathbf{T}^k$ and σ:

$$U^{k'}_{q'}=[\mathbf{T}^k\times\sigma]^{k'}_{q'}=\sum_{q\mu}C^{k'q'}_{kq1\mu}T^k_q\sigma_\mu, \qquad (13)$$
$$=k-1,\ k,\ k+1;\ q'=-k',\ -k'+1,\ \ldots,\ k';$$
$$f_k=\int\exp\left\{-\left(\frac{\mathbf{r}_1-\mathbf{r}_3}{\rho}\right)^2\right\}P_k\cos\omega_{13})\,d\Omega, \qquad (14)$$
$$a=(v_s+3v_t)/4,\qquad b=-(v_s-v_t)/4. \qquad (15)$$

Then

$$\langle(j_1j_3)\ J_{13}M_{13}\,|V_p(13)\,|\,(j'_1j'_3)\ J_{13}M_{13}\rangle=(-1)^{j_1+j'_3-J_{13}}$$
$$\times2\sum_{kk'}F^k\langle l_1\|\mathbf{T}^k\|l'_1\rangle\langle l_3\|\mathbf{T}^k\|l'_3\rangle\ W\,[j_1j'_1j_3j'_3;\ k'J_{13}]$$
$$\times\left[a\delta_{kk'}A\begin{Bmatrix}l_1 & 1/2 & j_1\\ l'_1 & 1/2 & j'_1\\ k & 0 & k\end{Bmatrix}A\begin{Bmatrix}l_3 & 1/2 & j_3\\ l'_3 & 1/2 & j'_3\\ k & 0 & k\end{Bmatrix}\right.$$
$$\left.-b(-1)^{k+k'}\left(\frac{2k'+1}{2k+1}\right)A\begin{Bmatrix}l_1 & 1/2 & j_1\\ l'_1 & 1/2 & j'_1\\ k & 1 & k'\end{Bmatrix}A\begin{Bmatrix}l_3 & 1/2 & j_3\\ l'_3 & 1/2 & j'_3\\ k & 1 & k'\end{Bmatrix}\right], \qquad (16)$$

where F^k are radial integrals of the Slater type.

In each term of (16) the dependence of J_{13} enters only in the form $(-1)^{-J_{13}}W\,[j_1j'_1j_3j'_3;\ k'J_{13}]$. This enables us to sum over J_{13} and J_{24} in (11), using the relations

$$\sum_{J_{13}J_{24}}(-1)^{-J_{13}}W\,[j_1j'_1j_3j'_3;\ k'J_{13}]\,A\begin{Bmatrix}j_1 & j_2 & J'_{12}\\ j_3 & j_4 & J'_{34}\\ J_{13} & J_{24} & J\end{Bmatrix}A\begin{Bmatrix}j'_1 & j_2 & J'_{12}\\ j'_3 & j_4 & J'_{34}\\ J_{13} & J_{24} & J\end{Bmatrix}$$
$$=(-1)^{j'_1+j_2+j'_3+j_4+j_1+j'_3+J_{34}+J'_{34}+J}[(2J_{12}+1)\,(2J'_{12}+1)$$
$$(2J_{34}+1)\,(2J'_{34}+1)]^{1/2}\,W\,[j_1j'_1J_{12}J'_{12};\ k'j_2]$$
$$W\,[j_3j'_3J_{34}J'_{34};\ k'j_4]\,W\,[J_{12}J'_{12}J_{34}J'_{34};\ k'J]. \qquad (17)$$

Finally, the matrix element of the operator $V_p(13)$ becomes

$$\langle(j_1j_2)\ J_{12},\ (j_3j_4)\ J_{34},\ JM\,|V_p(13)\,|\,(j'_1j'_2)\ J'_{12},\ (j'_3j'_4)$$
$$\times\ J'_{34};\ JM\rangle\Big|=(-1)^{j'_1+j_3+j'_3+j_4+J_{34}+J'_{34}+J}\ \delta_{j_2j'_2}\delta_{j_4j'_4}$$
$$\times[(2J_{12}+1)\ (2J'_{12}+1)\ (2J_{34}+1)\,(2J'_{34}+1)]^{1/2}2\sum_{kk'}F^k$$
$$\times\langle l_1\|\mathbf{T}^k\|l'_1\rangle\langle l_3\|\mathbf{T}^k\|l'_3\rangle W\,[j_1j'_1J_{12}J'_{12};k'j_2]\,W\,[j_3j'_3J_{34}J'_{34};\ k'j_4]$$
$$\times W\,[J_{12}J'_{12}J_{34}J'_{34};\ k'J]\left[a\delta_{kk'}A\begin{Bmatrix}l_1 & 1/2 & j_1\\ l'_1 & 1/2 & j'_1\\ k & 0 & k\end{Bmatrix}A\begin{Bmatrix}l_3 & 1/2 & j\\ l'_3 & 1/2 & j\\ k & 0 & k\end{Bmatrix}\right.$$
$$\left.-b(-1)^{k+k'}\left(\frac{2k'+1}{2k+1}\right)A\begin{Bmatrix}l_1 & 1/2 & j_1\\ l'_1 & 1/2 & j'_1\\ k & 1 & k'\end{Bmatrix}A\begin{Bmatrix}l_3 & 1/2 & j_3\\ l'_3 & 1/2 & j'_3\\ k & 1 & k'\end{Bmatrix}\right]. \qquad (18)$$

Formulas (16) and (18), apart from a factor, differ only in the fact that one Racah coefficient in the former is replaced by a product of three Racah coefficients in the latter. Inasmuch as (16) and (18) are of the same type, it is convenient to use formula (16) for the calculation of the matrix elements of the nn and pp interaction.

The matrix elements of the V_S interaction were calculated with the formula

$$\langle [(j_1 j_2) J_{12}]_a [(j_3 j_4) J_{34}]_a, J, NR; IM\nu | V_S | [(j_1' j_2') J_{12}']_a [(j_3' j_4') J_{34}']_a, J'; N'R'; IM\nu \rangle$$

$$= 2\delta_{N,N\pm 1} (-1)^{1+\sum_{i=1}^{4}(n_i+n_i')} |\langle n | \varkappa(r_i) | n' \rangle| \sqrt{\frac{5}{4\pi}\frac{\hbar\omega}{2C}}$$

$$\times \langle NR \| b \| N'R' \rangle \sqrt{(2J+1)(2J'+1)}\, W[IRJ'2; JR']$$

$$\times \Big\{ \delta_{j_3 j_3'} \delta_{j_4 j_4'} \delta_{J_{34} J_{34}'} (-1)^{J_{34}-J_{12}'-J-J_{12}} \sqrt{(2J_{12}+1)(2J_{12}'+1)}$$

$$\times W[J_{12} J J_{12}' J'; J_{34} 2]\, N_{j_1 j_2} N_{j_1' j_2'} \sum_P P \delta_{j_2 j_2'} (-1)^{p+j_2-j_1'}$$

$$\times \langle l_1 j_1 \| T^2 \| l_1' j_1' \rangle W[j_1 J_{12} j_1' J_{12}'; j_2 2]$$

$$+ \delta_{j_1 j_1'} \delta_{j_2 j_2'} \delta_{J_{12} J_{12}'} (-1)^{J_{12}-J'} \sqrt{(2J_{34}+1)(2J_{34}'+1)}$$

$$\times W[J_{34} J J_{34}' J'; J_{12} 2]\, N_{j_3 j_4} N_{j_3' j_4'} \sum_P P \delta_{j_4 j_4'} (-1)^{p+j_4-j_3'}$$

$$\times \langle l_3 j_3 \| T^2 \| l_3' j_3' \rangle W[j_3 J_{34} j_3' J_{34}'; j_4 2] \Big\}. \qquad (19)$$

As noted earlier, even if we confine ourselves to single-particle levels lying within 3 Mev, the energy matrices are still found to be of rather large order. For comparison with experiment, it is sufficient to calculate accurately the positions of the first three levels with given I, which are the most sensitive to the parameters of the pair interaction. We stipulate that the error in the determination of the energies of these levels be less than 0.1 Mev. Then, to obtain this accuracy, there is no need to operate with high-order matrices. It was established that if we cross out from the matrix with given spin I the columns in which the ratio of the non-diagonal matrix elements a_{ik} to the difference between diagonal elements, namely $a_{ik}/(a_{ii}-a_{kk})$, does not exceed 0.05 ($i = 1, 2, 3$; $k > 3$), then each of the levels $i = 1, 2, 3$ will shift by not more than 0.1 Mev. This was carefully investigated by testing many matrices.

In the present four-particle problem for I = 0 we first calculated and investigated in detail a 46-th order matrix (with N = 0). For I = 2 we calculated the first three rows of a 200-th order matrix and checked which of the high levels can be neglected. It was thus established that the 31-th order matrices,* with which we subsequently operated, guarantee the required accuracy in the determination of the energy and the level functions.

4. SPECTRUM OF Po^{212}

Let us trace the formation and shifts of the levels, by successively turning on the interaction in parts. The single-particle levels of the four particles (Fig. 1) will be multiply degenerate. When the pair interaction diagonal matrix elements are added, the degeneracy is lifted. The matrix elements of the nn and pp interaction are strongly dependent on the intermediate momenta J_{12} and J_{34} (see [2]) and give rise to momentum level splits. The matrix elements of the np interaction depend weakly on either the intermediate momenta or on the total momentum I, and therefore produce a parallel downward shift of all the levels without an appreciable distortion of the preceding splitting. The result is the level scheme shown in Fig. 2.

We then take account of the non-diagonal matrix elements, in other words the interaction between the levels. We first turn on only the matrix ele-

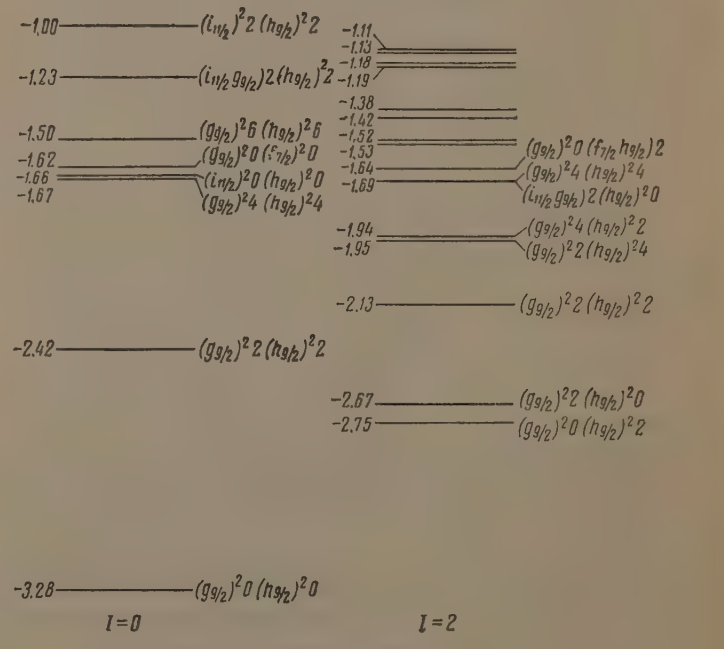

FIG. 2. Lower levels of four Po^{212} nucleons with account of the single-particle energy and the diagonal matrix elements of the pair interaction. The configuration is indicated on the right and the energy on the left. The energy is referred to the single-particle ground level.

*Including levels with N = 0, 1, and 2.

ments of the nn and pp forces. The first level* $I = 0_1^+$ will interact both via the nn forces and the pp forces [with levels 4, 7, etc. in downward order on Fig. 2; see formula (8)], and will drop more than twice as far as in the case of a single pair.

On the other hand, the first level $I = 2_1$ will interact only via the nn forces (with levels 3, 5, 9 ... on Fig. 2), while the second level $I = 2_2$ will interact only via the pp forces (with levels 3, 4, etc), and consequently both will drop lower than the level $I = 0_1$. We then find that the two levels with $I = 2$ will lie ~ 1 Mev above the $I = 0_1$ level and will be close to each other. Such a level scheme disagrees with experiment. We now take into account the level interaction due to the np forces. It must be noted that the nondiagonal np matrix elements between the levels of the main configuration are approximately four times greater than for a single particle pair, and are comparable in magnitude with the matrix elements of the nn and pp forces in the case $I = 0$, when the latter are large. The np interaction of all the lower levels will therefore be strong and the first levels with given I will move down owing to repulsion. But the 2_1 level will drop farther than the 0_1 level because the $I = 2$ levels are denser than the $I = 0$ levels. Thus, a certain sequence of equidistant levels 0_1–2_1–2_2 is formed, with properties similar to those of the vibrational levels, but actually entirely different in nature. An account of the np forces is essential not only for the levels $I = 2$, but also for all levels of the four-particle system.

Finally, let us take into account the interaction between the external particles and the surface and let us calculate the entire spectrum. Figure 3 shows the calculated level scheme of Po^{212}, obtained with parameters $\rho = 2f$, $v_i = 15$ Mev, $v_s = 35$ Mev, $\hbar\omega = 3$ Mev, and $C = 1000$ Mev. For comparison, the experimental level scheme is shown on the right. The Po^{212} nucleus was experimentally investigated by many authors [5-9] and the results obtained in different laboratories are quite close to each other. It is also important to verify the correctness of the calculated binding energy for the ground state. The measured energy required to remove two neutrons and two protons from Po^{212} is 19.4 Mev. The single-particle energy of the four particles in potential (1) is $-(7.8 + 7.6) = -15.4$ Mev (see [1]), the energy of interaction with the surface is -0.7 Mev (for $C = 1000$ Mev), and the energy of Coulomb repulsion between two protons is $+0.4$ Mev. Consequently

*The parity sign will henceforth be omitted where self-evident.

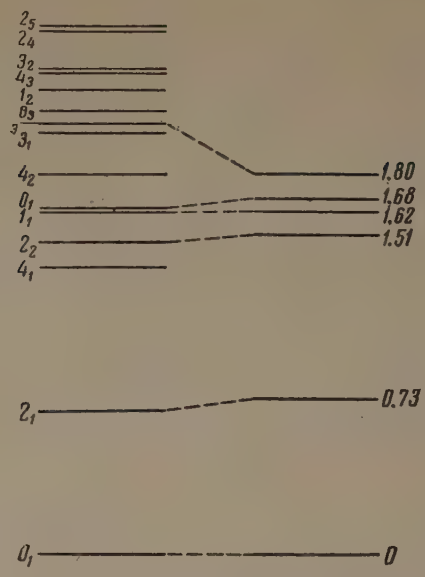

FIG. 3. Level scheme of Po^{212} after diagonalization of the matrices. The experimental level scheme is shown on the right.

the pair energy of the four particles is -3.7 Mev. The calculated total pair energy for the chosen parameters is -3.8 Mev.

To illustrate the sensitivity of the level scheme and of the binding energy to the choice of parameters, Table I lists the energies of the first three levels with spins $I = 0$ and 2 for different parameter combinations. By plotting different curves we can determine the dependence of the energy, of the distance between levels, etc. on the choice of each parameter separately.

Table I. Energies of the first three levels with spins $I = 0$ and 2 as a function of the potential parameters

Parameters*				$I = 0$	$I = 2$
v_t	v_s	$\hbar\omega$	C		
15	35	0		−3.75 −2.42 −1.94	−3.22 −2.69 −2.21
15	35	3	1000	−4.50 −2.87 −2.40	−3.82 −3.02 −2.48
15	35	3	1500	−4.26 −2.73 −2.24	−3.67 −2.93 −2.30
15	30	3	1000	−4.10 −2.64 −2.12	−3.56 −2.73 −2.20
20	35	3	1000	−4.88 −3.20 −2.77	−4.28 −3.34 −2.66
20	40	3	1000	−5.24 −3.45 −3.06	−4.54 −3.54 −2.88
15	35	3	2000	−4.14 −2.68 −2.20	−3.58 −2.85 −2.36

*All values are in Mev. $\rho = 2f$.

Table II. Fundamental coefficients $c^I(\alpha)$ of the eigenfunction expansion of the Po^{212} levels

$I=0$			$I=2$			
$(j_1j_2)J_{12}, (j_3j_4)J_{34}; J; NR$	0_1	0_2	$(j_1j_2)J_{12}, (j_3j_4)J_{34}; J; NR$	2_1	2_2	2_3
$(g_{9/2})^2\,0\,(h_{9/2})^2\,0;\ 0;\ 00$	0.80	−0.39	$(g_{9/2})^2\,0\,(h_{9/2})^2\,2;\ 2;\ 00$	0.63	−0.60	0.18
$(g_{9/2})^2\,2\,(h_{9/2})^2\,2;\ 0;\ 00$	0.36	0.77	$(g_{9/2})^2\,2\,(h_{9/2})^2\,0;\ 2;\ 00$	0.55	0.66	0.20
$(g_{9/2})^2\,4\,(h_{9/2})^2\,4;\ 0;\ 00$	0.12	0.26	$(g_{9/2})^2\,2\,(h_{9/2})^2\,2;\ 2;\ 00$	−0.26	−0.04	0.88
$(g_{9/2})^2\,6\,(h_{9/2})^2\,6;\ 0;\ 00$	0.04	0.05	$(g_{9/2})^2\,2\,(h_{9/2})^2\,4;\ 2;\ 00$	0.18	−0.18	−0.01
$(i_{13/2})^2\,0\,(h_{9/2})^2\,0;\ 0;\ 00$	0.10	−0.17	$(g_{9/2})^2\,4\,(h_{9/2})^2\,2;\ 2;\ 00$	0.17	0.21	0.02
$(g_{9/2})^2\,0\,(f_{7/2})^2\,0;\ 0;\ 00$	0.09	−0.12	$(g_{9/2})^2\,4\,(h_{9/2})^2\,4;\ 2;\ 00$	−0.04	−0.01	0.29
$(g_{7/2})^2\,0\,(h_{9/2})^2\,0;\ 0;\ 00$	0.12	−0.09	$(g_{7/2})^2\,0\,(h_{9/2})^2\,2;\ 2;\ 00$	0.10	−0.11	0.04
$(g_{9/2})^2\,0\,(i_{13/2})^2\,0;\ 0;\ 00$	−0.01	0.09	$(g_{9/2})^2\,2\,(i_{13/2})^2\,0;\ 2;\ 00$	−0.08	−0.12	−0.05
$(g_{9/2})^2\,0\,(h_{9/2})^2\,2;\ 2;\ 12$	−0.24	−0.03	$(i_{13/2})^2\,0\,(h_{9/2})^2\,2;\ 2;\ 00$	0.07	−0.09	0.05
$(g_{9/2})^2\,2\,(h_{9/2})^2\,0;\ 2;\ 12$	−0.28	−0.03	$(g_{9/2})^2\,0\,(h_{9/2})^2\,0;\ 0;\ 12$	−0.17	−0.01	−0.07
$(g_{9/2})^2\,2\,(h_{9/2})^2\,2;\ 2;\ 12$	0.08	0.21	$(g_{9/2})^2\,0\,(h_{9/2})^2\,2;\ 2;\ 12$	0.11	−0.07	−0.13
$(g_{9/2})^2\,2\,(h_{9/2})^2\,4;\ 2;\ 12$	−0.07	−0.17	$(g_{9/2})^2\,0\,(h_{9/2})^2\,4;\ 4;\ 12$	−0.12	0.13	−0.09
$(g_{9/2})^2\,4\,(h_{9/2})^2\,2;\ 2;\ 12$	−0.08	−0.17	$(g_{9/2})^2\,4\,(h_{9/2})^2\,0;\ 4;\ 12$	−0.10	−0.14	−0.05
$(d_{5/2}g_{9/2})\,2\,(h_{9/2})^2\,0;\ 2;\ 12$	−0.11	0.06	$(g_{9/2})^2\,2\,(h_{9/2})^2\,0;\ 2;\ 12$	0.10	0.09	−0.12
$(g_{9/2})^2\,0\,(h_{9/2})^2\,0;\ 0;\ 20$	0.06	—	$(g_{9/2})^2\,2\,(h_{9/2})^2\,2;\ 4;\ 12$	−0.18	−0.01	0.02
$(g_{9/2})^2\,4\,(h_{9/2})^2\,0;\ 4;\ 24$	0.04	0.02	$(g_{9/2})^2\,0\,(h_{9/2})^2\,2;\ 2;\ 24$	0.03	0.01	—

Table II lists the coefficients $C^I(\alpha)$ needed to construct the lower-state functions [see formula (7)]. All the functions are characterized by a large configuration mixture and this greatly influences the properties of the levels.

5. γ-TRANSITION PROBABILITIES

The γ-transition probability is sensitive to the structure of the initial and final state functions. This can be traced by calculating the reduced transition probability $B(\lambda)$, which is connected with the total transition probability $T(\lambda)$ by the relation

$$T(\lambda;\ I\to I') = B(\lambda; I\to I')\,(\Delta E)^{2\lambda+1}, \tag{20}$$

$$B(\lambda;\ I\to I') = \frac{8\pi\,(\lambda+1)}{\lambda\,[(2\lambda+1)!!]^2\,\hbar\,(\hbar c)^{2\lambda+1}\,(2I+1)} \times \Big|\sum_{p\alpha\alpha'} c^I(\alpha)\,c^I(\alpha')\,\langle\alpha I\nu\|\mathfrak{M}_p(\lambda)\|\alpha' I'\nu'\rangle + \sum_{\alpha\alpha'} c^I(\alpha)\,c^I(\alpha')\,\langle\alpha I\nu\|\mathfrak{M}_s(\lambda)\|\alpha' I'\nu'\rangle^2\Big|. \tag{21}$$

$\mathfrak{M}_p(\lambda)$ and $\mathfrak{M}_s(\lambda)$ are the operators of the nucleon and collective transitions with multipolarity λ.

The sum in (21) breaks up into two parts; one corresponds to partial phononless transitions, and the other is connected with the change in the number of phonons. The contribution from the second part of the sum is essential for E1 transitions.

Table III lists the calculated values of $B(\lambda)$ for transitions between levels up to an excitation energy ~ 2 Mev. The value of $B(\lambda)$ varies within wide limits and is an individual characteristic of each transition separately. A distinguishing feature of the transition $2_1 \to 0_1$ is that all the members of the sum (21) have the same sign. Both parts of the sum give approximately the same contribution when C = 1000 Mev. On the whole the probability of the $2_1 \to 0_1$ transition with C = 1000 Mev is found to be five times larger than the so-called single-particle probability. The $2_2 \to 0_1$ transition differs strongly from the preceding one. The difference in the signs of $c^I(\alpha)$ causes the principal terms of the sum (21) to drop out and

Table III. Reduced probabilities* of γ transitions from Po^{212} levels

Transition	C = 1000 Mev		C = 2000 Mev	
	$B(E2)\cdot10^{-11}$, $sec^{-1}\cdot Mev^{-5}$	$B(M1)\cdot10^{-11}$, $sec^{-1}\cdot Mev^{-3}$	$B(E2)\cdot10^{-11}$, $sec^{-1}\cdot Mev^{-5}$	$B(M1)\cdot10^{-11}$, $sec^{-1}\cdot Mev^{-3}$
$2_1 \to 0_1$	4.30		2.20	
$2_2 \to 0_1$	0.05		0.01	
$2_2 \to 2_1$	0.04	61.00	0.02	68.00
$1_1 \to 0_1$		11.54		11.50
$1_1 \to 2_1$	1.60	5.03	1.04	4.90
$0_2 \to 2_1$	2.70		4.00	
$2_3 \to 0_1$	0.20		0.21	
$2_3 \to 2_1$	2.20	0.01	0.77	0.01
$2_3 \to 4_1$	0.38		0.10	
$2_3 \to 2_2$	0.44	4.90	0.33	5.80
$2_4 \to 2_1$	0.14	1.20	0.03	7.60
$4_1 \to 2_1$	7.20		3.30	

*The eigenfunctions were calculated with parameters $\rho = 2f$, $v_t = 15$ Mev, $v_s = 35$ Mev, $\hbar\omega = 3$ Mev, and C = 1000 and 2000 Mev.

$B(E_2)$ becomes two or three orders smaller than the first transition. This transition is particularly sensitive to the parameters of the forces.

The $2_2 \rightarrow 2_1$ transition has high intensity. In this case the electric component of the transition is small because of the strong quenching in the sum (21), while the magnetic component is, to the contrary, large. The $2_3 \rightarrow 2_1$ transition differs from the preceding one in that the magnetic component is small and the electric one increases sharply. The direct transition $2_3 \rightarrow 0_1$ has a noticeable intensity and can be observed. From the 1_1 level there is an intense M_1 transition to the ground level 0_1 and a mixed $(E_2 + M_1)$ transition to the excited level 2_1.

Most transitions in Table III have been experimentally observed, but only their multipolarities and relative intensities have been determined (see, for example, [7]). All the known experimental data on γ transitions are in good agreement with the theoretical calculations. This shows that an account of the mixture of configurations makes it possible to calculate the γ-transition picture sufficiently completely. As to the absolute values of the transition probabilities, these have been determined earlier from a comparison of the intensity of the γ line and the long-range α particles from a given level. In this case the α-decay probability was found from a semi-empirical formula verified against the transitions from the ground levels. The data on $B(\lambda)$ in Table III show that this method yields too high a probability. For example, the probability of the $2_1 \rightarrow 0_1$ transition is estimated in [7] to be 2.5×10^{-12} sec, while from Table III we get for probability not more than 1.2×10^{-11} sec.

The theoretical spectrum contains levels with spins $I = 3$ and 4, the 4_1 level being rather low. Since however, the β decay of Bi^{212} to these levels is strongly forbidden and the γ transitions to the 4_1 level have a low probability, it is quite difficult to observe these levels.

In the discussion of the spectra of Bi^{210} and Po^{210}, a suggestion has been made that the single-particle levels $i_{11/2}$ and $i_{13/2}$ move approximately 0.5 Mev below their positions in Pb^{209} and Bi^{209}, because the boundary of the potential V_C is less diffuse. This raises the question of the positions of these levels in Po^{212}. All the previous calculations were made without lowering the $i_{11/2}$ and $i_{13/2}$ levels. To verify the effect of the change in the positions of these single-particle levels, we calculated the spectrum with $i_{11/2}$ and $i_{13/2}$ dropped 0.5 Mev. It turned out that all the levels previously-present up to 1.8 Mev barely shifted, but new levels appeared, which we denote by 0_i, 1_i, and 2_i^-. The 0_i level lies near 2_1, 1_i lies near 1_1, and 2_i^- is higher than 2.2 Mev. It is very difficult to detect these levels by the γ rays,* nor are any other means clear. Since the investigation has shown that a shift of the $i_{11/2}$ and $i_{13/2}$ levels in Po^{212} within the indicated limits does not greatly affect all the results obtained, the question loses its urgency.

6. CONCLUSIONS

1. The previously obtained self-consistent and pair potentials were applied to a nucleus with two particle pairs in excess of the filled shells. The results show that an account of these potentials is sufficient to determine and describe in detail the pattern of excited states of such a nucleus.

2. We calculated the spectrum of Po^{212}, the binding energy, and the γ-transition probabilities. All the known levels have been found and their properties explained. The additional levels that should exist are indicated.

3. The theoretical results cannot be reconciled with the experimental data without account of the np interactions.

4. The method developed can be readily generalized to include the case of 8 nucleons $(4n + 4p)$ in excess of the filled shells.

[1] L. A. Sliv and B. A. Volchok, JETP **36**, 539 (1959), Soviet Phys. JETP **9**, 374 (1959).

[2] Guman, Sliv, and Sogomonova, JETP **40**, 341 (1961), Soviet Phys. JETP **13**, 232 (1961).

[3] Sliv, Sogomonova, and Kharitonov, JETP **40** 946 (1961), Soviet Phys. JETP **13**, 661 (1961).

[4] V. N. Guman, JETP **41**, 800 (1961), Soviet Phys. JETP **14**, 574 (1962).

[5] Sergeev, Krisyuk, Latyshev, Trofimov, and Remennyi, JETP **33**, 1140 (1957), Soviet Phys. JETP **6**, 878 (1958).

[6] G. T. Emery and W. R. Kane, Phys. Rev. **118**, 755 (1960).

[7] Gangarskii, Gusinskii, and Lemberg, Izv. AN SSSR, ser. fiz. **24**, 1449 (1960), Columbia Techn. Transl. p. 1443.

[8] Giannini, Prosperi, and Scinti, Nucl. Phys. **19**, 380 (1960).

[9] Schupp, Daniel, Eakins, and Jensen, Phys. Rev. **120**, 189 (1960).

*Thus, $B(E2; 2_2 \rightarrow 0_i) = 4 \times 10^7$; $B(E2; 2_3 \rightarrow 0_i) = 6 \times 10^7$; $B(E2; 1_i \rightarrow 2_1) = 7 \times 10^6$; $B(M1; 1_i = 0_i) = 10^{10}$. All are two or three orders smaller than for those observed.

Translated by J. G. Adashko
218

PHOTOPRODUCTION OF NEUTRINOS ON ELECTRONS AND NEUTRINO RADIATION FROM STARS

V. I. RITUS

P. N. Lebedev Physics Institute, Academy of Sciences, U.S.S.R.

Submitted to JETP editor May 15, 1961

J. Exptl. Theoret. Phys. (U.S.S.R.) 41, 1285-1293 (October, 1961)

Photoproduction of a neutrino-antineutrino pair on an electron is considered. The cross section for this process is calculated, and the photoneutrino emission by a degenerate or nondegenerate electron gas at high temperature and density is determined in the nonrelativistic approximation. The photoneutrino emission from an electron gas of density 10^5 g/cm^3 at temperatures $\kappa T \geq 40$ kev (κ is Boltzmann's constant) exceeds the neutrino bremstrahlung radiation under the same conditions [4] by two orders of magnitude. In stars with high temperature and density (such as novae between bursts, etc.) the energy radiated in the form of photoneutrinos exceeds the usual photon luminosity.

1. INTRODUCTION

ACCORDING to the theory of Feynman and Gell-Mann [1] there is a direct neutrino-electron scattering process $\nu + e \rightarrow \nu' + e'$ with a matrix element

$$G2^{-1/2}(\bar{e}'\gamma_\mu(1+\gamma_5)\nu)(\bar{\nu}\gamma_\mu(1+\gamma_5)e) \qquad (1)$$

which is of first order in the weak interaction coupling constant. Direct experimental study of this process is extremely difficult at the present time; however, its existence can lead to macroscopic effects which are important in astrophysics. In 1941 Gamow and Schoenberg [2] showed that at the high temperatures and densities which exist in the interiors of stars in the last stages of evolution the process of nuclear electron capture and subsequent beta decay

$$N_Z^A + e^- \rightarrow N_{Z-1}^A + \nu, \qquad N_{Z-1}^A \rightarrow N_Z^A + e^- + \bar{\nu}, \qquad (2)$$

with the emission of two neutrinos, becomes possible. Although the cross section for this process is very small, the energy carried out of the star by neutrinos from this process can exceed the energy emitted in the form of photons. This is because neutrinos travel out freely from the star's interior, while photons have a very short free path and are therefore radiated only by the external envelope of the star. It should be noted, however, that process (2) has an energy threshold, and therefore stellar neutrino emission from this process depends on the presence of nuclei with a low threshold.

Pontecorvo [3] pointed out that if the direct electron-neutrino interaction (1) occurs then neutrino pair bremstrahlung can occur in the scattering of an electron by a nucleus:

$$e + A \rightarrow \nu + \bar{\nu} + e' + A'. \qquad (3)$$

This process is unlike process (2) in that it does not have a threshold; in stars with high temperatures and densities and also high Z it can be an important energy radiation mechanism. [3] Gandel'man and Pinaev [4] showed that in stars with Z about 10, temperature $\kappa T \geq 30$ kev, and density $\rho > 10^5$ g/cm^3, the energy carried off by neutrinos formed in process (3) exceeds the energy radiated in the form of photons.

We wish to point out that the existence of a direct electron-neutrino interaction also leads to the photoproduction of neutrino pairs on electrons:

$$\gamma + e \rightarrow e' + \nu + \bar{\nu}. \qquad (4)$$

This process is first order in the weak interaction and electromagnetic coupling constants. Since the photon number density increases very rapidly with temperature and can be comparable with and even exceed the density of electrons and nuclei at high temperatures, process (4), like process (3), can be an important energy radiation mechanism in stars with high temperature and density.

In this work we calculate the neutrino pair photoproduction cross section on electrons and the photoneutrino radiation by a degenerate or nondegenerate electron gas as a function of temperature

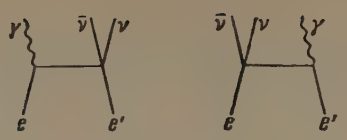

FIG. 1

and density. We show that the photoneutrino radiation by an electron gas is two orders of magnitude greater than the neutrino bremstrahlung radiation under the same conditions. This is mainly due to the fact that the neutrino pair photoproduction cross section increases rapidly with photon energy and the neutrino bremstrahlung cross section increases with increasing energy, while the photon spectrum is shifted to higher energies as compared to the electron spectrum at the same temperature.

2. CROSS SECTION FOR NEUTRINO PAIR PHOTOPRODUCTION OF ELECTRONS

We let $p = (\mathbf{p}, E)$ and $p' = (\mathbf{p}', E')$ be the initial and final electron four-momenta and $k = (\mathbf{k}, \omega)$, $q_1 = (\mathbf{q}_1, \epsilon_1)$, and $q_2 = (\mathbf{q}_2, \epsilon_2)$ be the four-momenta of the photon, neutrino, and antineutrino. The formation of a neutrino-antineutrino pair in the collision of a photon and an electron is described by the two Feynman diagrams shown in Fig. 1. The matrix element for this process is

$$M = \frac{eG}{2\sqrt{\omega}}\{(\bar{\nu}_n\gamma_\mu(1+\gamma_5)(i\hat{p}_1+m)^{-1}\hat{e}e)(\bar{e}'\gamma_\mu(1+\gamma_5)\nu_a) + (\bar{e}'\hat{e}(i\hat{p}_2+m)^{-1}\gamma_\mu(1+\gamma_5)\nu_a)(\bar{\nu}_n\gamma_\mu(1+\gamma_5)e)\}, \quad (5)$$

where e_μ is the photon polarization four vector and

$$p_1 = p + k, \quad p_2 = p' - k, \quad p_f = p' + q_1 + q_2, \quad p_i = p + k.$$

For calculation, it is convenient to use a Fierz transformation to obtain M in the form $(\bar{e}'Oe)(\bar{\nu}O\nu)$. Then

$$M = \frac{eG}{2\sqrt{\omega}}(\bar{e}'[\gamma_\mu(1+\gamma_5)(i\hat{p}_1+m)^{-1}\hat{e} + \hat{e}(i\hat{p}_2+m)^{-1}\gamma_\mu(1+\gamma_5)]e) \times(\bar{\nu}_n\gamma_\mu(1+\gamma_5)\nu_a). \quad (6)$$

We then obtain for the differential cross section averaged over initial electron spin direction and photon polarization and summed over final electron spin directions

$$d\sigma = -\frac{1}{(2\pi)^5(pk)}\int\frac{1}{4}\sum|F|^2\delta^4(p_f-p_i)\frac{d^3p'\,d^3q_1\,d^3q_2}{E'\varepsilon_1\varepsilon_2}, \quad (7)$$

where F is the invariant amplitude, $M = (\omega EE'\epsilon_1\epsilon_2)^{-1/2}F$ and

$$-(4e^2G^2)^{-1}\sum|F|^2 = [m^2(p'q_1)(p_1q_2) + (pk)(p'q_1)(kq_2)](pk)^{-2} + [(pp')[(p_2q_1)(pq_2) + (p'q_1)(p_1q_2)] - (kp)(p'q_1)(p+p', q_2) + (kp')\times(p+p', q_1)(pq_2)]/(pk)(p'k) + [m^2(p_2q_1)(pq_2) + (p'k)(kq_1)(pq_2)](p'k)^{-2}. \quad (8)$$

Integrating over the neutrino and antineutrino momenta with the aid of the formula

$$\int(aq_1)(bq_2)\delta^4(q-q_1-q_2)\frac{d^3q_1\,d^3q_2}{\varepsilon_1\varepsilon_2} = \frac{\pi}{6}[2(aq)(bq) + (ab)q^2],$$

we obtain

$$d\sigma = \frac{e^2G^2}{12(2\pi)^4(pk)}\left\{-q^2(q^2+m^2)\left[\frac{m^2}{(kp)^2}+\frac{m^2}{(kp')^2}+\frac{2(pp')}{(kp)(kp')}\right] + 4q^2 + \frac{2(q^2-m^2)(kq)^2}{(kp)(kp')}\right\}\frac{d^3p'}{E'}, \quad (9)$$

where $q = q_1 + q_2 = p + k - p'$.

In the following we make the nonrelativistic approximation that ω/m, $|\mathbf{p}|/m$, and $|\mathbf{p}'|/m$ are all much less than one. Then the differential cross section (9) in the center-of-mass system is

$$d\sigma = \frac{e^2G^2}{(2\pi)^4m^2\omega}\left\{\frac{3\omega^2-\mathbf{p}'^2}{6} - \frac{\omega^2+\mathbf{p}'^2}{12\omega^4}[\mathbf{kp}']^2 + \frac{1}{3}\mathbf{kp}'\right\}d^3p'. \quad (10)^*$$

In order to write the differential cross section (10) in the laboratory system, it is sufficient to make the replacements $\mathbf{p}' \to \mathbf{p}' - \mathbf{p} - \mathbf{k}$, $\mathbf{k} \to \mathbf{k}$, $d^3p' \to d^3p'$.

We note that in general the number of final states of an electron with momentum $\mathbf{p}'$ is given by $(1-n_{\mathbf{p}'})\,d^3p'/(2\pi)^3$, where $n_{\mathbf{p}'}$ is the occupation number of the state with momentum $\mathbf{p}'$. Thus the differential cross section (10) has an additional factor $(1-n_{\mathbf{p}'})$ in the general case. In a medium with temperature T

$$n_{\mathbf{p}'} = \left[\exp\left(\frac{E'-\mu}{\varkappa T}\right)+1\right]^{-1},$$

where μ is the chemical potential; in the center of mass system $n_{\mathbf{p}'}$ must be replaced by $n_{\mathbf{p}'+\mathbf{p}+\mathbf{k}}$ in the nonrelativistic case. The integration over $\mathbf{p}'$ of the differential cross section (10) with the weight function $1-n_{\mathbf{p}'+\mathbf{p}+\mathbf{k}}$ cannot be done analytically. Therefore we consider two extreme cases.

1. Nondegenerate electrons. In this case $n_{\mathbf{p}'} \ll 1$, and the total cross section for photoproduction of neutrino pairs on nondegenerate electrons obtained by integrating (9) over $\mathbf{p}'$ is

$$\sigma = \frac{\alpha g^2}{12\pi^2}\left(\frac{\hbar}{mc}\right)^2\frac{1}{x(x+\sqrt{x^2+1})}\left\{\left[\frac{8}{3}x^4+\frac{10}{3}x^2+\frac{2}{3}-\frac{5}{4x^2} + \left(\frac{8}{3}x^3+2x-\frac{25}{6x}\right)\sqrt{x^2+1}\right]\ln\left(x+\sqrt{x^2+1}\right) - \left[\frac{35}{9}x^4+\frac{11}{18}x^2-\frac{25}{6}+\left(\frac{20}{9}x^3+\frac{3}{2}x-\frac{5}{4x}\right)\sqrt{x^2+1}\right]\right\}. \quad (11)$$

*$[\mathbf{kp}'] = \mathbf{k}\times\mathbf{p}'$.

Here $\alpha = e^2/4\pi = 1/137$ and $g = m^2G = 3.0 \times 10^{-12}$ are dimensionless constants and $x = \omega/m$, where ω is the photon energy in the center-of-mass system. In the nonrelativistic approximation

$$\sigma(\mathbf{k}, \mathbf{p}) = \frac{4\alpha g^2}{35\pi^2}\left(\frac{\hbar}{mc}\right)^2\left(\frac{\omega}{mc^2}\right)^4 = 1{,}13\cdot 10^{-48}\left(\frac{\omega}{mc^2}\right)^4 \text{cm}^2. \quad (11')$$

2. Completely degenerate electrons. In this case $n_{\mathbf{p}'+\mathbf{p}+\mathbf{k}} = 1$ if $|\mathbf{p}'+\mathbf{p}+\mathbf{k}| < p_0$ and $n_{\mathbf{p}'+\mathbf{p}+\mathbf{k}} = 0$ if $|\mathbf{p}'+\mathbf{p}+\mathbf{k}| > p_0$, where p_0 is the Fermi momentum. By using the properties of the dependence of the differential cross section on $\mathbf{p}'$ and the fact that $|\mathbf{p}| \leq p_0$, the nonrelativistic total cross section for photoproduction of neutrino pairs on degenerate electrons can be written in the form

$$\sigma(\mathbf{k}, \mathbf{p}) = \frac{e^2G^2}{(2\pi)^4 m^2\omega}\int_{p_0-P}^{\omega} \mathbf{p}'^2\, dp' \int_{\frac{p_0^2-\mathbf{p}'^2-P^2}{2p'P}}^{1} d\cos\theta' \int_0^{2\pi} d\varphi' \quad (12)$$

$$\times\left\{\frac{3\omega^2-\mathbf{p}'^2}{6} - \frac{\omega^2+\mathbf{p}'^2}{12\omega^4}\right.$$

$$\left.\times\,[\mathbf{k}\mathbf{p}']^2 + \frac{1}{3}\mathbf{k}\mathbf{p}'\right\}\theta(P+\omega-p_0),$$

where $\mathbf{P} = \mathbf{p} + \mathbf{k}$, θ' is the angle between $\mathbf{p}'$ and $\mathbf{P}$, φ' is the angle between the planes $(\mathbf{p}', \mathbf{P})$ and $(\mathbf{k}, \mathbf{P})$, and $\theta(x)$ is one for $x > 0$ and zero for $x < 0$. The explicit expression for $\sigma(\mathbf{p}, \mathbf{k})$ is cumbersome and therefore we do not give it here; in the following only the value of this integral at the point $|\mathbf{p}| = p_0$, $P = p_0$ will be needed.

3. PHOTONEUTRINO RADIATION POWER OF AN ELECTRON GAS

The energy carried off by the neutrino pair in a single photoproduction event is $\epsilon_1 + \epsilon_2 = E + \omega - E'$. Therefore the energy carried off by neutrinos from a unit volume of electron gas per unit time (the photoneutrino radiation power per unit volume of medium) is

$$Q_\nu = \iint \frac{2d^3k}{(2\pi)^3}\frac{2d^3p}{(2\pi)^3} n_\gamma(\mathbf{k})\, n_e(\mathbf{p})\, v_{\text{rel}} \int (E+\omega-E')$$

$$\times\, d\sigma(\mathbf{k}, \mathbf{p}, \mathbf{p}'), \quad (13)$$

where $n_\gamma(\mathbf{k})$ and $n_e(\mathbf{p})$ are the momentum distributions of photons and electrons:

$$n_\gamma(\mathbf{k}) = \frac{1}{e^{\omega/\kappa T}-1}, \quad n_e(\mathbf{p}) = \frac{1}{e^{(E-\mu)/\kappa T}+1}, \quad (14)$$

and $v_{\text{rel}} = 1 - \mathbf{p}\cdot\mathbf{k}/E\omega$ is the relative velocity of the photon and electron.

From energy and momentum conservation it follows that $E - E' \ll \omega$ in the nonrelativistic case. Therefore the energy carried off by the neutrino pair in a single photoproduction is equal to the photon energy $\epsilon_1 + \epsilon_2 = \omega$ and the last integral in (13), which is usually called the effective deceleration, is simply

$$\int (E + \omega - E')\, d\sigma(\mathbf{k}, \mathbf{p}, \mathbf{p}') = \omega\sigma(\mathbf{k}, \mathbf{p}). \quad (15)$$

We consider two cases in which Q_ν can be evaluated analytically.

1. Nondegenerate electrons. In this case $n_e(\mathbf{p}) = C\exp(-E/\kappa T) \ll 1$ and $\sigma(\mathbf{k}, \mathbf{p})$ is given by (11'). After integrating, we obtain

$$Q_\nu = \frac{4\cdot 7!\zeta(8)}{35\pi^4}\alpha g^2 mc^2 \frac{mc^2}{\hbar}\left(\frac{\kappa T}{mc^2}\right)^8 n_e, \quad (16)$$

Substituting numerical values into (16) and assuming that the medium is almost completely ionized, so that the electron density is related to the matter density ρ by $n_e = 6 \times 10^{23}\,\rho/\mu_e$, where $\mu_e^{-1} = \Sigma_i C_i Z_i/A_i$ with C_i the weight concentration of element with atomic number A_i and charge Z_i, we obtain (with T in kev)

$$Q_\nu = 3{,}32\cdot 10^{-8} T^8\,(\rho/\mu_e)\ \text{erg/sec-cm}^3 \quad (17)$$

2. Strongly degenerate electrons. In this case $p_0^2/2m \gg \kappa T$ and $n_e(\mathbf{p}) = 1$ if $|\mathbf{p}| < p_0$, $n_e(\mathbf{p}) = 0$ if $|\mathbf{p}| > p_0$; p_0 is the Fermi momentum, which is related to the electron density by

$$p_0/mc = (3\pi^2 n_e)^{1/3}(\hbar/mc) = 1.01\cdot 10^{-2}\,(\rho/\mu_e)^{1/3}; \quad (18)$$

$\sigma(\mathbf{p}, \mathbf{k})$ is given by Eq. (12). We note that $\sigma(\mathbf{k}, \mathbf{p})$ depends on k and p only through ω, $|\mathbf{p}|$, and P $= |\mathbf{p}+\mathbf{k}|$; namely, $\sigma(\mathbf{k}, \mathbf{p}) = \sigma(\omega, p, P)\times\theta(P+\omega-p_0)$. Therefore the integration over the direction of $\mathbf{p}$ in (13) can be replaced by an integration over P between the limits $|p-\omega|$ and $p+\omega$. We then obtain

$$\int \sigma(\mathbf{k}, \mathbf{p})\, d\Omega_{\mathbf{p}} = \frac{2\pi}{\omega p}\left\{\theta(p - p_0 + 2\omega)\int_{p_0-\omega}^{p+\omega}\sigma(\omega, p, P)\, PdP\right.$$

$$\left. - \theta(|p-\omega| - p_0 + \omega)\int_{p_0-\omega}^{|p-\omega|}\sigma(\omega, p, P)\, PdP\right\}.$$

Then integrating over $|\mathbf{p}|$ between zero and p_0, we obtain

$$\int \sigma(\mathbf{k}, \mathbf{p})\, d^3p = \frac{2\pi}{\omega}\left\{\int_{p_0-2\omega}^{p_0} p\, dp \int_{p_0-\omega}^{p_0+\omega}\sigma(\omega, p, P)\, PdP + \ldots\right\}, \quad (19)$$

where the dots stand for terms proportional to $\theta(2\omega - p_0)$ and $\theta(\omega - p_0)$. In the strongly degenerate case $p_0 \gg \kappa T$; in the integration over ω these terms will therefore be exponentially small [of order $\exp(-p_0/2\kappa T)$ and $\exp(-p_0/\kappa T)$] in comparison with the integral over ω of the term written out in (19); hence, they will be neglected. Furthermore, since the main contribution of the first term in (19) to the integral over ω comes from frequencies ω near $\kappa T \ll p_0$, we can write

	T, kev	Q_ν erg/sec · cm³	q_ν erg/sec · cm³
Degenerate gas	1	$2.08 \cdot 10^{-4}$	$1.41 \cdot 10^{-1}$
	5	$4.06 \cdot 10^{3}$	$1.17 \cdot 10^{3}$
	10	$2.08 \cdot 10^{5}$	$4.66 \cdot 10^{4}$
	20	$1.06 \cdot 10^{8}$	$1.20 \cdot 10^{6}$
Nondegenerate gas	30	$1.09 \cdot 10^{9}$	$3.05 \cdot 10^{7}$
	40	$1.08 \cdot 10^{10}$	$1.10 \cdot 10^{8}$
	50	$6.50 \cdot 10^{10}$	$3.05 \cdot 10^{8}$
	70	$9.55 \cdot 10^{11}$	$1.38 \cdot 10^{9}$
	100	$1.66 \cdot 10^{13}$	$6.87 \cdot 10^{9}$

$$\int_{p_0-2\omega}^{p_0} p\,dp \int_{p_0-\omega}^{p+\omega} \sigma(\omega, p, P) P dP \approx 2\omega p_0 \int_{p_0-\omega}^{p_0+\omega} \sigma(\omega, p_0, P) P dP$$

$$\approx (2\omega p_0)^2 \sigma(\omega, p_0, p_0). \qquad (20)$$

From Eq. (12) we obtain to lowest order in ω/p_0

$$\sigma(\omega, p_0, p_0) = (2\pi)^{-3} \tfrac{4}{35} (e^2 G^2/m^2)\, \omega^4.$$

Then, to lowest order in $\kappa T/p_0$, we obtain

$$Q_\nu = \frac{12 \cdot 8!\, \zeta(9)}{35\pi^4} \alpha g^2 mc^2 \frac{mc^2}{\hbar} \left(\frac{\kappa T}{mc^2}\right)^9 n_e \frac{mc}{p_0}. \qquad (21)$$

Using (18) and substituting numerical values, we obtain

$$Q_\nu = 1.5 \cdot 10^{-7} T^9 (\rho/\mu_e)^{2/3} \text{ erg/sec-cm}^3. \qquad (22)$$

The table lists the photoneutrino radiation power Q_ν per unit volume of electron gas (degenerate and nondegenerate) in erg/sec-cm³ as a function of temperature for a density $\rho = 10^5$ g/cm³. The corresponding values of the neutrino bremstrahlung radiation power q_ν found from the formula of Gandel'man and Pinaev[4] are also shown.

4. NEUTRINO RADIATION BY STARS

If the distributions of temperature and density in a star are known, then Eqs. (17) and (22) enable us to find the energy emitted by the star in the form of neutrinos. It is advantageous to compare this energy L_ν, which we will call the neutrino "luminosity" of the star, with the usual photon luminosity L_γ.

1. Nondegenerate star configurations. If the energy emission in the star occurs uniformly over the whole volume (uniform source model) or if all the star's energy is emitted at the center (point source model), then it follows from general properties of the equation for equilibrium of the star that the liminosity L_γ is related to the temperature T_c and density ρ_c at the star's center by[5]

$$L_\gamma = C\mu^{-0.5} \rho_c^{-2.5} b T_c^8, \qquad (23)$$

where b is the constant in Kramer's formula for the photon mean free path:

$$l = b\rho^{-2} T^{3.5},$$
$$\mu^{-1} = \sum_i C_i (Z_i + 1)/A_i. \qquad (24)$$

The value of the constant C and the temperature and density distributions are different in the two models and must be found by numerical integration of the equilibrium equations.

In the following we consider the point source model, since it corresponds more nearly to reality. The temperature and density distributions in this model were found by Cowling[6] by numerical integration of the equilibrium equations. Since the temperature falls rapidly, and the density even more rapidly, with distance from the star's center, the central values of the temperature and density do not characterize the temperature and density of the main stellar mass. We therefore introduce the mean temperature $\bar{T}$ and mean density $\bar{\rho}$ defined by

$$\bar{T} = \frac{1}{M} \int \rho T dv, \qquad \bar{\rho} = \frac{1}{v} \int \rho dv. \qquad (25)$$

By using the distributions $\rho(r)$ and $T(r)$, it can be shown[5,6] that the central temperature and density are related to the mean temperature and density and also to the mass and radius of the star by

$$T_c = 1.85\,\bar{T} = 6.28 \cdot 10^{-23} \mu M R^{-1},$$
$$\rho_c = 37.0\,\bar{\rho} = 8.84 M R^{-3}. \qquad (26)$$

Here and in the following temperatures are in kev and densities in g/cm³. With the values found by Cowling for the constants, we obtain*

$$L_\gamma = 7.22 \cdot 10^{35} \mu^{-0.5} \rho_c^{-2.5} b T_c^8 = 1.19 \cdot 10^{34} \mu^{-0.5} \bar{\rho}^{-2.5} b \bar{T}^8. \qquad (27)$$

We integrate Q_ν over the volume of the star, using the distributions[6] $\rho(r)$ and $T(r)$ and Eq. (26), which relates R, T_c, and ρ_c. We obtain the result†

$$L_\nu = 1.45 \cdot 10^{25} \mu_e^{-1} \mu^{-1.5} \rho_c^{-0.5} T_c^{9.5}$$
$$= 0.822 \cdot 10^{27} \mu_e^{-1} \mu^{-1.5} \bar{\rho}^{-0.5} \bar{T}^{9.5}. \qquad (28)$$

*We note that in the corresponding equation [Eq. (16)] in the paper of Gandel'man and Pinaev,[4] the value of the constant is too large by a factor of 5.1. This also affects their Eq. (19).

†We note that in Eq. (18) in the paper of Gandel'man and Pinaev[4] the value of the constant in the expression for the neutrino bremstrahlung luminosity is two or three times too large due to the use of a rough approximation for the temperature and density instead of the numerical values given by Cowling.

The ratio of the photoneutrino and photon luminosities is

$$L_\nu/L_\gamma = 2.01\cdot10^{-11}\,T_c^{1.5}\rho_c^2/b\mu_e\mu = 0.69\cdot10^{-7}\bar{T}^{1.5}\bar{\rho}^2/b\mu_e\mu. \quad (29)$$

This ratio is of the order of unity for $\bar{\rho} = 3\times10^2$ and $\bar{T} = 10$ kev, for example, which apparently prevail in the stars like subdwarfs which flare up from time to time as novae.[7-9] In stars which are evolving into white dwarfs, $T_c \approx 40$ kev, $\rho_c \approx 5\times10^4$ g/cm^3 (see Öpick[10]); then $L_\nu/L_\gamma \approx 10$.

2. Degenerate star configurations. Since the thermal conductivity of a degenerate electron gas is very high (soft photons cannot be absorbed by the electrons), the temperature is constant in the interior of a star that consists of a degenerate gas. On the other hand, the equation of state of the degenerate gas depends weakly on the temperature. If we neglect this dependence, the density distribution in the star depends on just one parameter, for example, the Fermi momentum at the center of the star $x_c = (p_0/mc)_c$. In a nonrelativistic electron gas x_c^2 is small, and in this case the density distribution is determined by the Lane-Emden polytrope with index $\frac{3}{2}$, namely, $\rho(r) = \rho\, f_{3/2}^{3/2}(3.654\, r/R)$, where $f_{3/2}(\xi)$ is the Lane-Emden function with index $\frac{3}{2}$ (see [11], Sec. 105, or [5], Ch. 11).

We integrate the photoneutrino radiation power of a degenerate electron gas over the stellar volume, using

$$\int \rho^{2/3}\,dv = M\bar{\rho}^{-1/3}\,3\left(\frac{\rho_c}{\bar{\rho}}\right)^{2/3}\int_0^1\left(\frac{\rho}{\rho_c}\right)^{2/3}x^2\,dx,$$

where the quantity

$$3\left(\frac{\rho_c}{\bar{\rho}}\right)^{2/3}\int_0^1\left(\frac{\rho}{\rho_c}\right)^{2/3}x^2dx$$

depends weakly on the parameter x_c^2, and is equal to 8.400 for small x_c^2. Then

$$L_\nu = 1{,}29\cdot10^{-7}M\Gamma^9/\mu_e^{2/3}\bar{\rho}^{1/3}. \quad (30)$$

On the other hand, Schatzman[12] showed that the photon luminosity of a degenerate star is related to its temperature and mass by $T = 6.17\times10^7(L_\gamma/M)^{2/7}$ (with T in degrees) or

$$L_\gamma = 2{,}88\cdot10^{-3}\,MT^{7/2}, \quad (31)$$

if T is expressed in kev. Thus, the ratio of photoneutrino and photon luminosities is

$$L_\nu/L_\gamma = 4.48\cdot10^{-5}\,T^{5.5}/\mu_e^{2/3}\bar{\rho}^{1/3}. \quad (32)$$

This ratio is of the order of unity for $\bar{\rho} = 10^5$ g/cm^3 and $T = 20$ kev. In white dwarfs with $\bar{\rho} \approx 10^5$ and $T \approx 5$ kev, this gives $L_\nu/L_\gamma \approx 10^{-3}$.

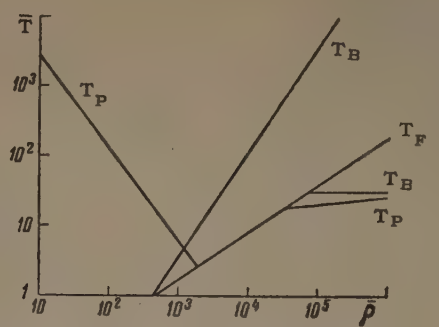

FIG. 2. Mean stellar temperatures and densities for which the photoneutrino and neutrino bremstrahlung luminosities are equal to the photon luminosity.

The dependence of L_ν/L_γ on temperature and density is most conveniently discussed with the aid of a diagram. In Fig. 2 the line labelled T_F separates the degenerate gas region (below T_F) from the nondegenerate gas region (above T_F). The lines T_P in both the degenerate and nondegenerate regions correspond to the mean temperatures and densities for which the photoneutrino luminosity is equal to the usual photon luminosity; above these lines $L_\nu/L_\gamma > 1$ and below them $L_\nu/L_\gamma < 1$. Similarly, the lines T_B correspond to the temperatures and densities for which the neutrino bremstrahlung luminosity is equal to the photon luminosity; The points below T_B in the degenerate region correspond to temperatures and densities for which $L_\nu/L_\gamma > 1$ (and vice versa). As is evident from Fig. 2, the region of stellar temperatures and densities for which the photoneutrino luminosity is greater than or equal to the photon luminosity is much larger than the region in which the neutrino bremstrahlung luminosity exceeds the photon luminosity, and includes the latter as a particular case.

The most interesting region to us is that around $\rho = 5\times10^2$ g/cm^3 and $T = 10$ kev. These appear to be the densities and temperatures of novae before and after bursts[7-9] (it is known that the same star can flare up as a nova several times and that its mass and luminosity are the same before and after a burst). Stars evolving into white dwarfs have even greater temperatures and densities.[10] Equation (29) and Fig. 2 show that the photoneutrino luminosity is near the photon luminosity or exceeds it in the region of densities greater than 5×10^2 and temperatures greater than 5 kev; therefore neutrino photoproduction must play a significant role in the energy balance in such stars.

What are the greatest stellar neutrino luminosities? It is doubtful that the neutrino current increases strongly during a nova burst, since the energy released during a nova burst is about 10^{45}

erg,[7] which is 10^{-4} of the star's thermal energy. Therefore the mean stellar temperature and consequently the neutrino luminosity are not significantly increased during a nova burst.

A different situation can be observed in a supernova burst. Then the energy release is comparable with the star's thermal energy[7] and amounts to about 10^{50} erg. In such a case, a star with mass near that of the sun (2×10^{33} g) is heated up to a temperature of 50 to 100 kev. Since the photoneutrino radiation power per gram of material is $10^6 - 10^8$ erg/g-sec at these temperatures, the neutrino luminosity of a supernova is $10^{39} - 10^{41}$ erg/sec. This is comparable with the usual supernova luminosity ($10^7 - 10^8$ times the sun's). During a burst which lasts 50 to 100 days, the neutrinos carry off $10^{46} - 10^{48}$ erg, which is $10^{-4} - 10^{-2}$ of the total energy released. Thus, although the neutrino luminosity during a stellar supernova burst is colossal, neutrino processes do not play as large a role in the energy balance of supernovae as they can play in novae before and after bursts and in stars evolving into white dwarfs.

Note added in proof (September 19, 1961). After this article was submitted for publication, a paper on the same subject was published by Chiu and Stabler [Phys. Rev. 122, 137 (1961)]. However, they do not consider the photoneutrino radiation by a nonrelativistic degenerate electron gas. Moreover, it should be noted that owing to the use of an unusual relation between probability and cross section [for the customary relation, see C. Møller, Kgl. Danske Videnskab. Selsk., Mat.-fys. Medd. 23, 1 (1945)] their expression for the photoproduction cross section differs from ours by a factor $(pk)/E\omega$ and is not relativistically invariant. We also note that they used Heaviside units, but mistakenly set $e^2/\hbar c = 1/137$, instead of $e^2/4\pi\hbar c = 1/137$, and their results are therefore too small by a factor 4π.

[1] R. Feynman and M. Gell-Mann, Phys. Rev. 109, 193 (1958).

[2] G. Gamow and M. Schoenberg, Phys. Rev. 59, 539 (1941).

[3] B. M. Pontecorvo, JETP 36, 1615 (1959), Soviet Phys. JETP 9, 1148 (1959).

[4] G. M. Gandel'man and V. S. Pinaev, JETP 37, 1072 (1959), Soviet Phys. JETP 10, 764 (1960).

[5] S. Chandrasekhar, An Introduction to the Study of Stellar Structure, University of Chicago Press, Chicago 1939.

[6] T. G. Cowling, Monthly Notices, Royal Astr. Soc. 96, 42 (1936).

[7] L. H. Aller, Astrophysics, N. Y. 1959.

[8] M. L. Humason, Astrophys. Journ. 88, 228 (1938).

[9] Z. Kopal, Vistas in Astronomy, v. 2, Pergamon Press, London 1956.

[10] E. I. Öpick, Nuclear Processes in Stars (Russ. Transl.), IIL, Moscow 1957.

[11] L. D. Landau and E. M. Lifshitz, Statistical Physics, Pergamon, 1958.

[12] E. Schatzman, Ann. d'ast. 8, 143 (1945); 10, 19 (1947).

Translated by M. Bolsterli
219

POSSIBILITY OF POLARIZING AN ELECTRON BEAM BY RELATIVISTIC RADIATION IN A MAGNETIC FIELD

I. M. TERNOV, Yu. M. LOSKUTOV, and L. I. KOROVINA

Moscow Power Institute

Submitted to JETP editor May 17, 1961

J. Exptl. Theoret. Phys. (U.S.S.R.) 41, 1294-1295 (October, 1961)

Spin flip due to radiation produced by the motion of electrons in a uniform magnetic field is considered. It is shown that an initially unpolarized beam becomes partially polarized, with the magnetic moment primarily in the direction of the field.

THE solutions corresponding to the two polarization states for a Dirac electron moving in a uniform magnetic field (cf. [1] Sec. 28; this reference contains a detailed bibliography on this problem) can be used to compute the probability of radiative quantum transitions in which the electron spin reverses direction. Assuming for simplicity that in the initial state the electron has no momentum along the field we obtain the following expression for the difference in radiation intensity, $\Delta W_{-1,1}$ (W_{-1} is the radiation intensity for the case where the magnetic moment is initially antiparallel to the field and the final position is parallel, while W_1 applies to the inverse case):

$$\Delta W_{-1,1} = W_{-1} - W_1 \approx \frac{35\sqrt{3}}{16} \frac{ce_0^2}{R^2} \left(\frac{\hbar}{m_0 cR}\right)^2 \left(\frac{E}{m_0 c^2}\right)^8. \quad (1)$$

Here R is the radius of curvature of the electron orbit, E/m_0c^2 is the kinetic energy of the moving electron divided by its rest energy, and e_0 is the electron charge.

This formula indicates that the predominant quantum transitions will be those which leave the spin magnetic moment oriented in the direction of the magnetic field. Thus it appears that partial polarization can be realized in an electron beam that is initially unpolarized (an effect peculiar to emission).

The process in question should occur, for example, when electrons move in accelerators or storage rings. The effect should be stronger in the latter case because the particle storage time in storage rings is rather large. A macroscopic consequence of this effect is the appearance of a magnetic field in addition to that produced by the current; the additional magnetic field is proportional to the number of polarized electrons in the beam and reaches some fixed value in the course of time.

In addition, the beam polarization causes an additional spin-orbit interaction, which should cause splitting of the electron energy levels.

In conclusion we note that the result given in (1) also holds if the motion of the electron along the field is bounded by infinite potential walls.

The authors are indebted to Professor A. A. Sokolov for discussions.

[1] A. A. Sokolov, Vvedenie v kvantovuyu elektrodinamiku (Introduction to Quantum Electrodynamics) Fizmatgiz, 1958.

Translated by H. Lashinsky
220

THE MÖSSBAUER EFFECT IN MONO- AND DIATOMIC CUBIC LATTICES

Yu. KAGAN and V. A. MASLOV

Submitted to JETP editor May 17, 1961

J. Exptl. Theoret. Phys. (U.S.S.R.) 41, 1296-1303 (October, 1961)

We treat monatomic and diatomic cubic crystals, including both noncentral and central nearest neighbor interactions. An expression is derived for the Mössbauer effect at T = 0 and at arbitrary temperatures. We analyze the case of a diatomic lattice in which one of the atoms is the radiator. We show, in particular, that for a light radiator in a diatomic lattice the effect may be larger than for a monatomic lattice with the same Debye temperature. We find that in general for a diatomic lattice the Debye temperature does not even approximately characterize the probability of the Mössbauer effect.

INTRODUCTION

THE probability of recoilless resonant emission or absorption of γ quanta in a solid (the Mössbauer effect) depends on a quantity which is an integral characteristic of the phonon spectrum (cf. [1,2]). So far, in calculating the effect, the isotropic model and a Debye spectrum for the vibration frequencies have been used. The probability then depends on the ratio $R/k\Theta$, where R is the recoil energy and Θ the Debye temperature.

We know that the spectrum of vibrations of a real crystal is markedly different from the Debye spectrum. This immediately raises the question of the sensitivity of the Mössbauer effect to the shape of the spectrum, and whether one can use the single parameter Θ for analyzing the intensity. Of special interest in this connection are crystals with different atoms in the unit cell, where the nucleus of one of the atoms is the active nucleus.

The central point here is the analysis of the role of the optical branches, especially when there is a sizeable difference in the masses of the atoms. In particular, such an analysis should help solve the problem of whether one can obtain a sizeable effect for nuclei with a large recoil energy (i.e., relatively light nuclei) if they are incorporated into a multiatomic unit cell. We note that this problem is extremely complicated even for the case of diatomic lattices. The reason for this is principally that one must find the amplitudes of the normal modes for each atom separately, and also must include the different types of vibration branches.

In the present paper we carry out the analysis for monatomic and diatomic lattices with cubic symmetry. We use a model of the simple cubic crystal with nearest neighbor interactions (of both noncentral and central type). This model has been used in recent years for the analysis of the vibration spectra of crystals (cf. the review article [3]). An important point is that the frequency spectra obtained for the case of a monatomic lattice have all the singularities which are predicted by the general theory.[4] In the case of a diatomic lattice, the frequency distribution has an incorrect root singularity at the top of the acoustic branch and at the bottom edge of the optical branch, which is a consequence of omitting the interaction with next nearest neighbors. But a weak singularity of this type gives practically no contribution to integrals over the spectrum for the characteristic quantities, which are the only quantities of interest in the present work. Aside from this, the spectrum for the diatomic lattice has all the singularities of the general type.

1. MONATOMIC LATTICE. T = 0.

The probability for the absorption (or emission) of γ quanta in a monatomic crystal, not accompanied by any change in the phonon spectrum, is given by the expression

$$W = e^{-Z}, \tag{1.1}$$

$$Z = R\frac{v_0}{(2\pi)^3}\sum_\alpha\int d^3\mathbf{f}\,\frac{|\mathbf{q}\mathbf{V}_\alpha(\mathbf{f})|^2}{\hbar\omega_\alpha}(2n_\alpha(\mathbf{f})+1), \tag{1.2}$$

where $\mathbf{f}$, $\omega_\alpha(\mathbf{f})$ are the wave vector and frequency of a phonon corresponding to the α-th branch; $\mathbf{V}_\alpha$ is the polarization vector; n_α is the equilibrium

density of phonons; $\mathbf{q}$ is a unit vector along the direction of incidence of the γ quantum, v_0 is the volume of the unit cell. For a cubic lattice at $T = 0$ we have

$$Z = R\frac{v_0}{(2\pi)^3}\frac{1}{3}\sum_\alpha\int d^3f\,\frac{1}{\hbar\omega_\alpha} = R\int\frac{1}{\hbar\omega}\psi(\omega)\,d\omega, \qquad (1.3)$$

where $\psi(\omega)$ is the frequency distribution in the phonon spectrum, normalized to unity.

Let us consider a cubic crystal and include only the interaction with nearest neighbors. In this case the equations of motion for displacements along the three cubic axes are independent. We have the same secular equation for all of them:

$$m\omega^2 = 2\sum_{i=1}^{3}\gamma_i(1-\cos\varphi_i), \qquad (1.4)$$

where γ_1 is the central force constant, $\gamma_2 = \gamma_3$ is the noncentral force constant; $\varphi_i = f_i a$ $(-\pi \le \varphi_i \le \pi)$.

Let us determine the frequency distribution function for such a lattice. The form of Eqs. (1.4) and the fact that all values of f_i in the space of the reciprocal lattice, and consequently all the φ_i, have the same statistical weight permits us to use the solution of the familiar random walk problem. A direct application of the general scheme gives the following expression for the distribution function (cf. the corresponding expression in [3]):

$$g(\omega^2) = \frac{1}{2\pi}\int_{-\infty}^{\infty}\exp\left\{-i\omega^2\rho + i\frac{2}{m}(\gamma_1+2\gamma_2)\rho\right\}$$

$$\times J_0\left(\frac{2\gamma_1}{m}\rho\right)J_0^2\left(\frac{2\gamma_2}{m}\rho\right)d\rho, \qquad (1.5)$$

where J_0 is the Bessel function of zero order.

The function $g(\omega^2)$ is normalized by the condition

$$\int_0^\infty g(\omega^2)\,d(\omega^2) = 1. \qquad (1.6)$$

From this,

$$\psi(\omega) = 2\omega g(\omega^2). \qquad (1.7)$$

We substitute (1.7) and (1.5) in (1.3) and, using the fact that J_0 is an even function, go over to an integral over positive values of ρ. We interchange the order of integration and carry out the ω integration explicitly. The result is

$$Z = \frac{R}{\hbar\sqrt{\pi}}\int_0^\infty\frac{1}{\sqrt{\rho}}\sin\left(\frac{2(\gamma_1+2\gamma_2)}{m}\rho+\frac{\pi}{4}\right)J_0\left(\frac{2\gamma_1}{m}\rho\right)J_0^2\left(\frac{2\gamma_2}{m}\rho\right)d\rho \qquad (1.8)$$

The expression for Z contains two independent parameters γ_1 and γ_2. In place of these we introduce two new parameters,

$$\xi = \gamma_1/\gamma_2 \qquad (1.9)$$

and the Debye temperature Θ. We determine the latter by a comparison with the classical Debye formula for the low temperature specific heat of the lattice, using the dispersion law in the form (1.4). We have

$$\Theta = (\hbar/k)\,(36\pi^4\gamma_2^2\gamma_1/m^3)^{1/6}. \qquad (1.10)$$

With (1.9) and (1.10), we transform (1.8) to the form

$$Z = \frac{R}{k\Theta}\left(\frac{9\pi}{2}\xi\right)^{1/6}\int_0^\infty\frac{1}{\sqrt{y}}\sin\left[(2+\xi)y+\frac{\pi}{4}\right]J_0(\xi y)\,J_0^2(y)\,dy. \qquad (1.11)$$

Assuming R/Θ fixed, we consider Z as a function of ξ. It is easy to show that $Z \to 0$ both for $\xi \to 0$ and for $\xi \to \infty$. But at both limits Z tends to zero slowly ($\sim \xi^{1/6}$ for $\xi \to 0$ and $\sim \xi^{-1/3}$ for $\xi \to \infty$), and over a wide range of variation of ξ it changes slightly. This is shown clearly in Fig. 1,

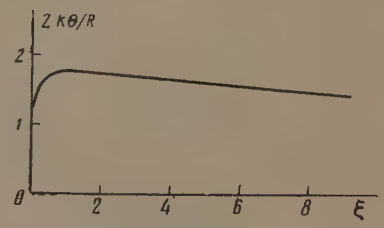

FIG. 1

where we plot the curve

$$Zk\Theta/R = f(\xi).$$

If we relate γ_1 and γ_2 to the elastic constants, it can be shown that $\xi = c_{11}/c_{44}$. From the tabulated data for c_{11} and c_{44} it follows that as a rule ξ lies in the interval $0.2 - 5$. Consequently in most cases the value of Z at $T = 0$ will be determined mainly by the constant Θ alone.

But the actual value of $Zk\Theta/R$ is different from $3/2$, its value for a Debye spectrum.

2. DIATOMIC LATTICE. T = 0.

In the case of a lattice with several atoms in the unit cell, where one of them is the radiator (we give it the subscript 1), the probability for the Mössbauer effect has the form (1.1) with Z defined by the expression [2]

$$Z = R_1\frac{v_0}{(2\pi)^3}\sum_\alpha\int d^3f\,\frac{|\mathbf{q}\mathbf{V}_{1\alpha}^*(\mathbf{f})|^2}{\hbar\omega_\alpha(\mathbf{f})}(2n_\alpha(\mathbf{f})+1). \qquad (2.1)$$

Here $V^i_{j\alpha}(f)$ is the complex amplitude which appears in the expansion of the displacement of the j-th atom in normal coordinates (cf. [2]). These amplitudes are normalized by the condition

$$\sum_{j,i} V^i_{j\alpha}(f)\, V^{i*}_{j\alpha}(f) = 1. \qquad (2.2)$$

To find the explicit form of $V^i_{j\alpha}$, we must bring in the equations of motion.

Let us consider a simple diatomic cubic lattice and include nearest neighbor interactions. The equations of motion for displacements along the three cubic axes are again independent, and the secular system of sixth order reduces to three identical pairs of equations (cf. [2]):

$$u_1^x [m_1\omega^2 - 2(\gamma_1 + 2\gamma_2)] + u_2^x 2\sum_i \gamma_i \cos\varphi_i = 0,$$

$$u_1^x \cdot 2\sum_i \gamma_i \cos\varphi_i + u_2^x [m_2\omega^2 - 2(\gamma_1 + 2\gamma_2)] = 0. \qquad (2.3)$$

The u^x_i are the amplitudes in the expansion in plane waves of the displacement of the i-th atom along the x axis. The rest of the notation is the same as in Sec. 1. From (2.3) we easily find the dispersion law:

$$\omega^2_\pm = (m_1^{-1} + m_2^{-1})(\gamma_1 + 2\gamma_2)$$

$$\pm\sqrt{(m_1^{-1} - m_2^{-1})^2(\gamma_1 + 2\gamma_2)^2 + 4X^2/m_1m_2}, \qquad (2.4)$$

$$X = \sum_i \gamma_i \cos\varphi_i. \qquad (2.5)$$

The plus sign refers to the optical branch, the minus sign to the acoustic branch.

If we go over to normal vibrations, we can establish a relation between the amplitudes u^x_i and V^x_i:

$$u_i^x = V_i^x \sqrt{\hbar(2n+1)/m_i\omega N}.$$

Then using one of Eqs. (2.3) and the relation (2.2), we find

$$|V^x_{i\alpha}|^2 = \frac{m_2\omega_\alpha^2 - 2(\gamma_1 + 2\gamma_2)}{2m_2\omega_\alpha^2 - 2(\gamma_1 + 2\gamma_2)(m_2/m_1 + 1)}. \qquad (2.6)$$

The subscript α takes on two values, corresponding to the acoustical and optical branches. (In this model for the crystal, the polarization vector for each branch is directed exactly along one of the cubic axes).

Since (2.6) contains dependence only on ω^2, we can go over in (2.1) to an integration over frequency. We introduce the frequency distribution function $g(\omega^2)$ with the normalization (1.6). We then have for T = 0,

$$Z = \frac{4R_1}{\hbar}\int_0^\infty \frac{m_2\omega^2 - 2(\gamma_1 + 2\gamma_2)}{2m_2\omega^2 - 2(\gamma_1 + 2\gamma_2)(m_2/m_1 + 1)} g(\omega^2)\, d\omega. \qquad (2.7)$$

The function $g(\omega^2)$ is easily related to the distribution function G(X) for the quantity X of (2.5), if we use the monotonic character of the function $\omega^2_\pm(X)$ (cf. Eq. (2.4)). The same arguments as in the monatomic case lead to the expression

$$G(X) = \frac{1}{2\pi}\int_{-\infty}^{\infty} e^{-i\rho X} J_0(\rho\gamma_1) J_0^2(\rho\gamma_2)\, d\rho. \qquad (2.8)$$

Changing to an integration over X in (2.7), we find

$$Z = \frac{2R_1}{\hbar}\left\{\int_0^{\gamma_1+2\gamma_2} \frac{m_2\omega_-^2 - 2(\gamma_1 + 2\gamma_2)}{\omega_-[2m_2\omega_-^2 - 2(\gamma_1 + 2\gamma_2)(m_2/m_1 + 1)]} G(X)\, dX \right.$$

$$\left. + \int_0^{\gamma_1+2\gamma_2} \frac{m_2\omega_+^2 - 2(\gamma_1 + 2\gamma_2)}{\omega_+[2m_2\omega_+^2 - 2(\gamma_1 + 2\gamma_2)(m_2/m_1 + 1)]} G(X)\, dX\right\}. \qquad (2.9)$$

Here the $\omega^2_\pm$ are defined in accordance with (2.4).

Let us consider the limiting cases. Suppose first that $\epsilon = m_2/m_1 \ll 1$. We expand (2.4) in powers of ϵ. Then, keeping the first two terms of the series,

$$\omega_- = \omega_1\sqrt{1 - t^2}\,(1 - \epsilon t^2/2), \qquad \omega_+ = \omega_1\epsilon^{-1/2}(1 + \epsilon t^2/2), \qquad (2.10)$$

where we have used the notation

$$\omega_1 = \frac{2}{m_1}\sum_i \gamma_i, \qquad t = \sum_i \gamma_i \cos\varphi_i \Big/ \sum_i \gamma_i. \qquad (2.11)$$

The form of the expressions for $\omega_\pm$ enables us to carry out the X integration in (2.9). Omitting the computations, we give the final result for the contributions to Z from the acoustical and optical branches:

$$Z_- = \frac{2R_1}{k\Theta}\left(\frac{9\pi^4}{16}\xi(2+\xi)^3\right)^{1/6}\left\{\int_0^\infty J_0(y(2+\xi)) J_0(\xi y) J_0^2(y)\, dy \right.$$

$$- \epsilon\int_0^\infty \left[J_0(y(2+\xi)) - \frac{1}{2y(2+\xi)} J_1(y(2+\xi))\right]$$

$$\left. \times J_0(\xi y) J_0^2(y)\, dy\right\}, \qquad (2.12)$$

$$Z_+ = \frac{2R_1}{k\Theta}\left(\frac{36}{\pi^2}\xi(2+\xi)^3\right)^{1/6}\epsilon^{2/3}\int_0^\infty \left[\frac{2\cos(y(2+\xi))}{y^2(2+\xi)^2}\right.$$

$$\left. + \left(1 - \frac{2}{y^2(2+\xi)^2}\right)\frac{\sin(y(2+\xi))}{y(2+\xi)}\right] J_0(\xi y) J_0^2(y)\, dy;$$

$$Z = Z_- + Z_+. \qquad (2.13)$$

In these expressions, ξ is defined by (1.9), and the Debye temperature for the lattice is

$$\Theta = \frac{\hbar}{k}\left(\frac{288\,\pi^4\gamma_2^2\gamma_1}{(m_1+m_2)^3}\right)^{1/6}. \qquad (2.14)$$

From the form of the expressions (2.12) and (2.13) it follows that the main contribution to Z comes from the acoustical branch. The contribution from the optical branches is $\sim \epsilon^{3/2}$, which is related to the fact that $\omega_+ \sim \epsilon^{-1/2}$, while the square of the amplitude $|V_1|^2$ for these branches is $\sim \epsilon$, i.e., within the framework of this model for the crystal, for $\epsilon \ll 1$ a heavy atom is hardly displaced in the optical branches.

In Fig. 2 we give the results obtained by numerical integration for the coefficients of the zeroth and first powers of ϵ in (2.12) as a function of ξ ($Zk\Theta/R_1 = A - B\epsilon$). In the interval of variation of ξ which is of practical interest, the coefficients A and B change very little.

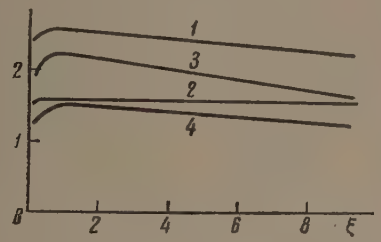

FIG. 2. Curve 1 – A(ξ), 2 – B(ξ), 3 – C(ξ), 4 – D(ξ).

Now we consider the opposite limiting case ($\epsilon \gg 1$), where the radiator is a light atom. From (2.4) we have approximately

$$\omega_- = \omega_1\varepsilon^{-1/2}(1 - t^2/2\varepsilon), \qquad \omega_+ = \omega_1(1 + t^2/2\varepsilon). \qquad (2.15)$$

Substituting these values in (2.9) and carrying out the X integration, we get the expressions

$$Z_- = \frac{2R_1}{k\Theta}\left(\frac{9\pi^4}{16}\xi(2+\xi)^3\right)^{1/6}\varepsilon^{-1}\int_0^\infty \left[J_0(y(2+\xi)) - \frac{J_1(y(2+\xi))}{y(2+\xi)}\right] J_0(\xi y)\, J_0^2(y)\, dy, \qquad (2.16)$$

$$Z_+ = \frac{2R_1}{k\Theta}\left(\frac{36}{\pi^2}\xi(2+\xi)^3\right)^{1/6}\left\{\varepsilon^{-1/2}\int_0^\infty \frac{\sin(y(2+\xi))}{y(2+\xi)} J_0(\xi y)\, J_0^2(y)\, dy - \varepsilon^{-3/2}\int_0^\infty \left[\frac{2\cos(y(2+\xi))}{y^2(2+\xi)^2} + \left(\frac{4}{3} - \frac{2}{y^2(2+\xi)^2}\right)\frac{\sin(y(2+\xi))}{y(2+\xi)}\right] J_0(\xi y)\, J_0^2(y)\, dy\right\}. \qquad (2.17)$$

From (2.16) and (2.17) we get the important result that for $\epsilon \gg 1$ the expansion of Z in powers of $1/\epsilon$ begins with $\epsilon^{-1/2}$. As a consequence there is marked reduction in the increase of Z (decrease of the Mössbauer effect) with decreasing mass of the radiating nucleus; instead of the $1/m_1$ dependence we get a $1/\sqrt{m_1}$ dependence. Thus the Mössbauer effect for a light atom may be much more likely in a diatomic lattice than in a monatomic lattice with the same Debye temperature. Physically this gain is related to the fact that for $\epsilon \gg 1$ the light atom vibrates mainly in the optical branches. But the band of optical frequencies corresponds to a region whose characteristic frequencies are $\sqrt{\epsilon}$ times greater than the frequencies of the acoustic band.

The coefficients of the different powers of ϵ have the same order of magnitude and the same type of variation with ξ as in the preceding section. This is apparent from Fig. 2, where we give the coefficients of $\epsilon^{-1/2}$ and ϵ^{-1} in the expansions (2.17) and (2.16):

$$Zk\Theta/R_1 = C\varepsilon^{-1/2} + D\varepsilon^{-1}.$$

Figure 3 shows the dependence of $Zk\Theta/R_1$ on ϵ for a particular value of the parameter ξ ($\xi = 1$), obtained by numerical double integration of (2.9).

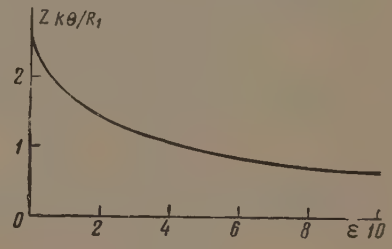

FIG. 3

This curve enables us to follow the manner in which the probability for the Mössbauer effect changes for a fixed Debye temperature, over the whole range of values for the ratio of the masses of atoms in the unit cell.

The results of this section indicate that, in the case of a diatomic lattice with an arbitrary ratio of masses, the Debye temperature does not even approximately characterize the magnitude of the Mössbauer effect. For example it is easy to find a case where a larger Debye temperature corresponds to a smaller effect.

3. MONATOMIC LATTICE. T ≠ 0.

Now let us consider the temperature dependence of the Mössbauer effect for a monatomic lattice of the same type as in Sec. 1. Transforming the general expression (1.2), we have

$$Z = R\frac{v_0}{(2\pi)^3}\int d^3f\,\frac{1}{\hbar\omega}\,\mathrm{cth}\,\frac{\hbar\omega}{2kT}. \qquad (3.1)^*$$

We use the transformation

*cth = coth.

$$\frac{1}{x}\operatorname{cth} x = \int_0^\infty e^{-x^2 t}\,\theta(t)\,dt, \qquad (3.2)$$

$$\theta(t) = \sum_{n=-\infty}^{\infty} e^{-\pi^2 n^2 t}. \qquad (3.3)$$

(When we replace t by $-it'/\pi$, the function $\theta(t)$ goes over into the function $\theta_2(t')$, which coincides with the Jacobi theta function of the third kind.) Then

$$Z = \frac{R}{2kT}\frac{v_0}{(2\pi)^3}\int d^3 f \int_0^\infty e^{-\beta^2\omega^2 t}\,\theta(t)\,dt, \qquad (3.4)$$

where $\beta = \hbar/2kT$.

We substitute the expression (1.4) for ω^2 into (3.4) and integrate over the phase volume

$$Z = \frac{R}{2kT}\int_0^\infty \exp\left[-\frac{2\beta^2}{m}(\gamma_1 + 2\gamma_2)\,t\right]\theta(t)$$

$$\times\, I_0\left(\beta^2\frac{2\gamma_1}{m}t\right) I_0^2\left(\beta^2\frac{2\gamma_2}{m}t\right) dt. \qquad (3.5)$$

Here I_0 is the Bessel function of pure imaginary argument.

Now we make the change of variables $\beta^2 2\gamma t/m = x$ in (3.5). Using the definitions (1.9) and (1.10) we finally get

$$Z = 2\pi\left(\frac{9\pi}{2}\xi\right)^{1/3}\frac{R}{k\Theta}\frac{T}{\Theta}$$

$$\times \int_0^\infty e^{-(2+\xi)x}\,\theta\left(4\pi\left(\frac{9\pi}{2}\xi\right)^{1/3}\frac{T^2}{\Theta^2}x\right) I_0(\xi x)\, I_0^2(x)\,dx. \qquad (3.6)$$

From (3.6) it follows that $Zk\Theta/R$ is a function only of T/Θ and the parameter ξ. In Fig. 4 we show this dependence for two values of ξ. The curve for $\xi = 10$ practically coincides with the one for $\xi = 0.1$. For comparison we show the dotted curve, corresponding to a Debye spectrum. We see that the percentage variation of Z with T/Θ does not change much in the interval of values of ξ which is of most interest, and is comparatively close to the Debye case.

4. DIATOMIC LATTICE. T ≠ 0.

Using the results of Sec. 2, we find the following general expression for Z at an arbitrary temperature:

$$Z = \frac{R_1}{k\Theta}\,4\left(\frac{9\pi^4}{2}\xi(2+\xi)^3\frac{\varepsilon^3}{(1+\varepsilon)^3}\right)^{1/4}\sum_\alpha \int_0^1 dt \frac{F(t)\,|V_{1\alpha}(t)|^2}{\psi_\alpha(t)}$$

$$\times \operatorname{cth}\left[\frac{1}{4}\left(\frac{2}{9\pi^4}\frac{(2+\xi)^3}{\xi}\frac{(1+\varepsilon)^3}{\varepsilon^3}\right)^{1/4}\psi_\alpha(t)\frac{\Theta}{T}\right]; \qquad (4.1)$$

$$F(t) = \frac{1}{\pi}\int_0^\infty \cos\rho t\,(2+\xi)\,J_0(\xi\rho)\,J_0^2(\rho)\,d\rho,$$

$$\psi_\alpha(t) = [1 + \varepsilon \pm ((1-\varepsilon)^2 + 4\varepsilon t^2)^{1/2}]^{1/2}. \qquad (4.2)$$

$|V_{1\alpha}(t)|^2$ is determined by (2.6) with the value of t given by (2.11).

From the form of (4.1) it follows that $Zk\Theta/R_1$ depends on T/Θ and the parameters ξ and ϵ. The general analysis of this expression shows that the dependence on ϵ leads in the general case to a qualitative change in the way Z increases with temperature, as compared to the case of a

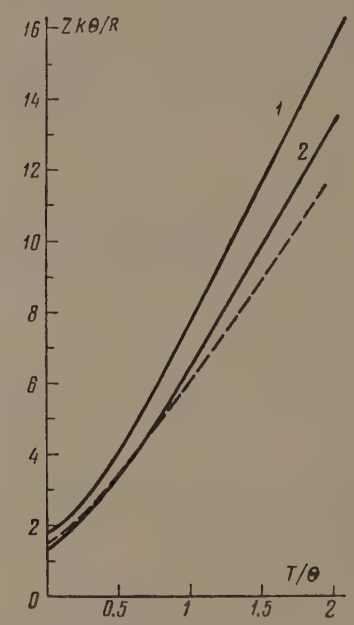

FIG. 4. Curve 1 – $\xi = 1$; curve 2 – $\xi = 0.1$.

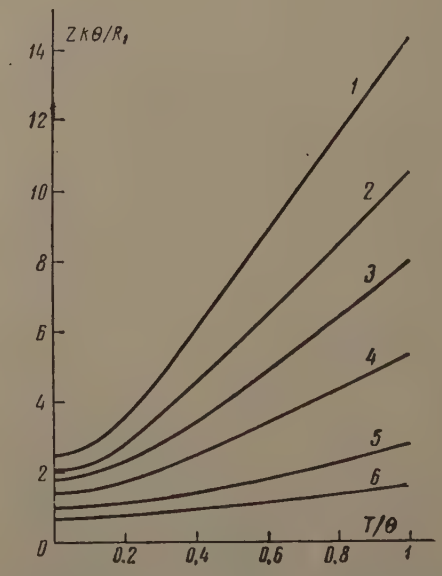

FIG. 5. Curve 1 – ε = 0.1; curve 2 – ε = 0.5; curve 3 – ε = 1; curve 4 – ε = 2; curve 5 – ε = 5; curve 6 – ε = 10.

monatomic lattice. Thus, when the radiator is the light atom and $\epsilon \gg 1$, one observes a slow variation of Z with T/Θ. As ϵ decreases the rate of increase becomes more marked, and for $\epsilon \lesssim 1$ it has a character close to that for the monatomic lattice. Such a change in the temperature dependence of the effect is related to the change in the relative importance of the optical and acoustical branches in the vibrations of the radiating atom, when there is a markedly different type of thermal excitation for the two types of phonons. (The excitation of optical phonons starts at much higher temperatures.)

Figure 5 shows curves of $Zk\Theta/R_1$ for several values of ϵ, and $\xi = 1$. We note that from our results it is clear that for an arbitrary diatomic lattice one can draw no conclusions concerning the value of the Debye temperature from the relative rate of decrease of the Mössbauer effect with temperature.

[1] W. Visscher, Annals of Physics **9**, 194 (1960).

[2] Yu. Kagan, JETP **40**, 312 (1960), Soviet Phys. JETP **13**, 211 (1961).

[3] A. Maradudin et al., Revs. Modern Phys. **30**, 175 (1958).

[4] L. Van Hove, Phys. Rev. **89**, 1189 (1953).

Translated by M. Hamermesh
221

CORRELATION BETWEEN THE MEAN NUMBER AND MEAN ENERGY OF PROMPT FISSION NEUTRONS AND THE PROPERTIES OF THE FISSIONING NUCLEUS

V. P. KOVALEV and V. S. STAVINSKII

Submitted to JETP editor May 17, 1961

J. Exptl. Theoret. Phys. (U.S.S.R.) **41**, 1304-1306 (October, 1961)

Experimental data on the mean number $\bar{\nu}$ and mean energy $\bar{E}$ of prompt fission neutrons are considered. A correlation is established between $\bar{\nu}$ and the spontaneous fission periods of even-even isotopes. It is noted that $\bar{E}$ has a tendency to split up, depending on the parity of the nucleons of the fissioning nucleus. An analysis reveals that the properties of the fissioning nucleus that are related to the parity of the nucleons influence the fission process at all its stages up to disintegration.

A study of the systematics of spontaneous fission periods T_f and fission thresholds E_f [1] reveals that the properties of the original nucleus which are associated with the parity of the nucleons influence the fission process up to the saddle-point stage. Experimental data on the mean number and the mean energy of the prompt fission neutrons permits one to confirm the influence of these properties on the fission process and on later stages right up to disintegration.

The following graph presents the experimental dependence of $\bar{\nu}$ on Z^2/A (black dots). The data were taken from the work of Bondarenko et al. [2]

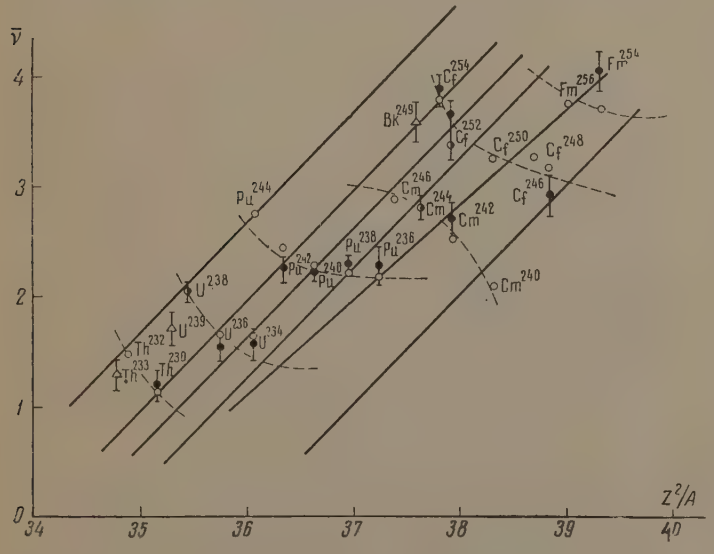

The solid lines connect nuclei that differ by $\Delta Z = 2$ and $\Delta A = 6$. The broken lines connect isotopes of a given element. The plotted values of $\bar{\nu}$ fall near the intersections of these lines. The graph of $\log T_f$ vs. Z^2/A [3] forms a similar grid. Thus, for even-even nuclei there is a distinct correlation between $\bar{\nu}$ and $\log T_f$.

Since there is a comparatively simple semi-empirical formula [1] for $\log T_f$, it is natural for one to attempt to establish a similar formula for $\bar{\nu}$. An analysis of the experimental data on even-even nuclei led to the following semi-empirical formula for $\bar{\nu}$:

$$\bar{\nu} = 0.7Z^2/A - 23.3 + 0.55\,(0.9 + 0.38Z - Z^2/A)\,\delta M. \quad (1)$$

Here δM is the difference between the ground-state mass M of the fissioning nucleus and the mass as computed by the semi-empirical Green formula.

In formula (1) the first two terms correspond to a straight line passing through maximum stability with respect to spontaneous fission, while the third term accounts for the correlation with the mass of the fissioning nucleus. The values computed by formula (1) are shown in the graph (the light circles). The experimental values of M used in the computation were taken from Glass et al. [4]

The systematics of $\bar{\nu}$ has been studied earlier. [2,5] Crane et al. [5] have noted that $\bar{\nu}$ has a general tendency to increase with the mass number of the fissioning nucleus. Bondarenko et al. [2] have attempted a more detailed systematization. An energy balance equation was used to compute $\bar{\nu}$. The computed values of $\bar{\nu}$ for U^{238} and Pu^{238} are in poor agreement with the experimental data. This may be due to the fact that in their investigation the authors disregarded the effect of the correlation between the kinetic energy of the fragments and δM, which must occur, especially if it is assumed, as they have, that $E_\gamma = \text{const}$.

The satisfactory agreement between formula (1) and the experimental data permits $\bar{\nu}$ to be

estimated for those even-even isotopes for which the experimental data are either lacking or unreliable. Specifically, for Th^{232} formula (1) gives $\bar{\nu} = 1.54$, which, together with the observed $\bar{\nu}$ for U^{238}, correlates very well with the spontaneous fission periods of these nuclei.

The aggregate of experimental values for $\bar{E}$ [6-10] makes it possible to advance the theory that the mean energy of the fission neutrons depends on the parity of the nucleons in the fissioning nucleus. If the Z^2/A dependence of the hardness parameter, $B = 2\bar{E}/3$, of the fission neutron spectra is plotted, then it can be seen that this parameter is an increasing function of Z^2/A, as has been noted earlier.[11] The one difference which is observed is that the values of B for isotopes with odd A run somewhat higher ($\Delta B \approx 0.1$) than for even isotopes, i.e., a splitting appears in $\bar{E}$ between isotopes with even and odd A. This split in the value of $\bar{E}$ which depends on the parity of A explains the difference between the computed and experimental data for U^{239}.[9,11]

A direct relation between $\bar{E}$ and $\bar{\nu}$ was discovered by Terrel (see Leachman[7]) in an analysis of even-even isotopes and is of the form

$$\bar{E} = 0.78 + 0.62\sqrt{\bar{\nu} + 1}. \qquad (2)$$

It is not difficult to see that formula (2) is not in agreement with the experimental data for the odd isotopes Th^{233} and U^{239}.[8,9] Formula (2) was based on the assumption that temperature T of the fragments is related to their excitation energy E_{ex} by the relationship $T \sim \sqrt{E_{ex}}$. If the function $\bar{E}(Z^2/A)$ is known, then formula (2) can be used to relate $\bar{\nu}$ to Z^2/A for even-even isotopes. The expression thus obtained for $\bar{\nu}$ fails to agree even qualitatively with the form of formula (1). If it is assumed that T depends only slightly on E_{ex}, then for the even-even isotopes we find

$$\bar{E} = 0.78 + 2(0.41 + 0.067\bar{\nu}). \qquad (3)$$

The formula for $\bar{\nu}$ obtained by using Eq. (3) is analogous in form to formula (1). If the kinetic energy of an incident neutron is changed from thermal to ~14 Mev, then $\bar{\nu}$ is approximately doubled. According to the equation $T \sim \sqrt{E_{ex}}$, this corresponds to a temperature change of 40 — 50%. Equation (3) means a change in T of ~20% which is in better agreement with the conclusion derived from an analysis of the spectra of inelastically scattered neutrons,[12] that the nuclear temperature depends only slightly on the excitation energy.

The authors wish to express their gratitude to Professor I. I. Bondarenko for a discussion of this paper.

[1] W. J. Swiatecki, Phys. Rev. **100**, 937 (1955); Phys. Rev. **101**, 97 (1956).

[2] Bondarenko, Kuz'minov, Kutsaeva, Prokhorova, and Smirenkin, Second International Conference on the Peaceful Uses of Atomic Energy, Paper No. 2187 (Geneva, 1958).

[3] A. Ghiorso, First International Conference on the Peaceful Uses of Atomic Energy, Vol. 8, Paper No. 718 (Geneva, 1955).

[4] Glass, Thompson, and Seaborg, J. Inorg. Nucl. Chem. **1**, 3 (1955).

[5] Crane, Higgins, and Bowman, Phys. Rev. **101**, 1804 (1955).

[6] Smith, Fields, Friedman, Cox, and Sjoblum, Second International Conference on the Peaceful Uses of Atomic Energy, Paper No. 690 (Geneva, 1958).

[7] R. Leachman, ibid, Paper No. 2467.

[8] Zamyatnin, Safina, Gutnikova, and Ivanova, Atom. Energiya (Atomic Energy) **4**, 337 (1958); transl. in Soviet Journal of Atomic Energy **4**, 443 (1958).

[9] Vasil'ev, Zamyatnin, Il'in, Sirotinin, Toropov, and Fomushkin, JETP **38**, 671 (1960), Soviet Phys. JETP **11**, 483 (1960).

[10] V. I. Kalashnikova, Dissertation, Inst. Atom. Energy, Acad. Sci. (1959).

[11] V. P. Kovalev and V. S. Stavinskii, Atomn. Energiya **5**, 649 (1958); Transl. in Soviet Journal of Atomic Energy **5**, 1588 (1958).

[12] V. S. Stavinskii, Dissertation, Moscow Eng. Phys. Inst. (1959).

Translated by A. Skumanich
222

A NEW TREATMENT OF THE GRAVITATIONAL FIELD

A. M. BRODSKII, D. IVANENKO, and G. A. SOKOLIK

Moscow State University

Submitted to JETP editor May 18, 1961

J. Exptl. Theoret. Phys. (U.S.S.R.) 41, 1307-1309 (October, 1961)

As is well known, the requirement of gauge invariance of the equations for arbitrary spin induces a vector field, where the vector character of the field is prescribed by the locality of the transformation. Similarly, we can derive in as natural a manner a gravitational interaction in terms of a tensor field, by assuming that the parameters of the Lorentz group depend on the coordinates. It can be shown that the known affinity coefficients can be obtained in the case of a spinor field. Gravitational coupling to a scalar field for the Klein-Gordon equation is given by the ordinary affinity coefficients.

SAKURAI[1] has recently proposed an interesting method of introducing vector boson fields. To each conservation law there corresponds a phase transformation which induces a vector field, in the same way as charge conservation, connected with invariance under the transformation $\psi' = \psi e^{i\Lambda(x)}$, leads to the introduction of the electromagnetic field described by the gauge invariant vector potential $A'_\mu = A_\mu + \partial\Lambda/\partial x^\mu$. The isotopic conservation laws (baryon charge, isospin, strangeness) correspond to invariance with respect to definite phase transformations. In contrast to the usual treatment, the phase transformation parameter is in this case not considered constant, but depends on the coordinates in such a way that it has differing values only in points separated by space-like distances. In other words, we impose the natural requirement that the phase transformations in such points be independent of one another.

Since phase transformations with coordinate-dependent parameters do not any more commute with derivative operators, they will give rise to additional terms in the field equations which cannot have any physical meaning. One therefore introduces new vector fields which transform in such a way under the gauge transformation as to cancel these additional terms. This is completely analogous to the procedure one uses in the case of the electromagnetic field. We should like to call attention to the fact that, by analogous considerations, one can introduce not only vector fields, but also tensor fields with zero rest mass (in the case of an exact conservation law), and, in particular, a field with spin 2.

This is a natural way of introducing a field which is in many respects equivalent to the gravitational field and yet follows from considerations which are different from the usual ones of Einstein. We must start with a generalized Lorentz transformation the parameters of which, while always satisfying the condition

$$a_{\mu\nu}a^{\nu\pi} = \delta_\mu^\pi, \tag{1}$$

are not constant, but depend on the coordinates in such a way that for all time-like vectors a^α ($a^\alpha a_\alpha < 0$)

$$a^\alpha \partial a_{\mu\nu}/\partial x^\alpha = 0. \tag{2}$$

For space-like a^α the left-hand side of (2) is arbitrary. As a result, the components of the Minkowski metric tensor $g_{\mu\nu}$, viewed locally, will depend in a definite way on the coordinates, conserving everywhere the Galilean values $g^{(0)}_{\alpha\beta}(x)$ (orthogonal system rotating around spatial directions). Since the metric tensor depends on the coordinates, the differentiations in the field equations must be replaced by covariant differentiations which give rise to the appearance of an additional term involving a Christoffel symbol with a $g_{\mu\nu}$ of the particular form mentioned above. At the same time the Lorentz transformation can be given the form of a phase transformation, which emphasizes the analogy to the introduction of other boson fields even more (see below).

For clarity, let us first consider the simplest case of the equation for a scalar field φ, which can be written in covariant form:

$$g^{\alpha\beta}\frac{\partial^2\varphi}{x\partial^\alpha \partial x^\beta} + \frac{1}{\sqrt{-g}}\frac{\partial\sqrt{-g}g^{\alpha\beta}}{\partial x^\alpha}\frac{\partial\varphi}{\partial x^\beta} - m^2\varphi = 0. \tag{3}$$

In our case the metric tensor $g_{\alpha\beta}$ in (3) must have the Galilean values everywhere, and its derivative in space-like directions must be different from zero:

$$g^{\alpha\beta}(x) = g^{(0)\,\alpha\beta}(x);$$

$$\sqrt{-g} = 1, \qquad a^\nu \partial g^{\alpha\beta}(x)/\partial x^\nu = 0, \qquad a^\nu a_\nu < 0. \tag{4}$$

Using (4) and writing $g^{\alpha\beta}(x) = g^{\alpha\beta}(0) + h^{\alpha\beta}(x)$, we find from (3) that a Lorentz transformation of the above-mentioned type takes the free scalar field equation into the form

$$g^{(0)\,\alpha\beta}\frac{\partial^2\varphi}{\partial x^\alpha \partial x^\beta} + \frac{\partial h^{\alpha\beta}(x)}{\partial x^\alpha}\frac{\partial\varphi}{\partial x^\beta} - m^2\varphi = 0. \tag{5}$$

In order to remove the additional term involving $\partial h^{\alpha\beta}/\partial x^\alpha$, which does not have any physical meaning by itself, we must, according to the basic novel idea, introduce a field with the corresponding gauge group transformations. This field will evidently be related to the field φ in the same way as the linearized gravitational field and must, by gauge invariance, have a vanishing mass.

In the general case of a field with arbitrary spin we can start with the equation

$$\Gamma_i \partial_i \Psi + im\Psi = 0. \tag{6}$$

We give the Lorentz transformation the form of a phase transformation by associating with it the matrix

$$l_{ij} = \exp\left[\frac{i}{2}\,\varepsilon_{sp} h_i^s h_m^p\,(g_{im}\delta_{lj} - g_{il}\delta_{mj})\right], \tag{7}$$

where h_l^s are the unit vectors of the orthogonal coordinates and ϵ_{sp} are the group parameters. Let us now assume that the h_m^l are not constant, but are functions of the coordinates in the sense explained above. Then the transformations (7) will not take Eq. (6) into itself but into

$$\Gamma_i(\partial_i + S\partial_i S^{-1})\Psi + im\Psi = 0, \tag{8}$$

where

$$l_{ik} S\Gamma_k S^{-1} = \Gamma_l, \qquad S = \exp\left[i\varepsilon_{ik} h_s^i h_p^k I_{ps}\right], \tag{9}$$

where the I_{ps} are the infinitesimal generators of the representation of the Lorentz group. In the general case we must therefore also introduce a compensating field Φ_σ which transforms under gauge transformations as

$$\Phi'_\sigma = l_\sigma^\alpha(\Phi_\alpha + S\partial_\alpha S^{-1}). \tag{10}$$

Using the following formula for the derivative of an operator exponential [2]

$$\frac{d}{dt}e^{A(t)} = e^{A(t)}\int_0^1 e^{-sA(t)}A'(t)\,e^{sA(t)}\,ds \tag{11}$$

and the relations of the Lie algebra, we can write the expression for $S\partial_\alpha S^{-1}$ in the form

$$S\partial_\alpha S^{-1} = I_{ml}\frac{\partial\varepsilon_{sl}}{\partial x_\alpha}\int_0^1 \exp\{it(\varepsilon_{ms}\delta_{pl} + \varepsilon_{lp}\delta_{sm} + \varepsilon_{sl}\delta_{pm} + \varepsilon_{pm}\delta_{sl})\}\,dt. \tag{12}$$

Here we have made use of the formula [3]

$$e^{\varepsilon_i \chi_i}\chi_k e^{-\varepsilon_i\chi_i} = \langle k|e^{\varepsilon_i b^i}|\alpha\rangle\chi_\alpha, \tag{13}$$

where $\langle k|b^i|\alpha\rangle = |c_{ik}^\alpha|$, and the c_{ik}^α are the structure coefficients of the associated Lie algebra χ_i. If (13) is substituted in the relation $[\chi_i\chi_j] = c_{ij}^\alpha\chi_\alpha$ for the Lie algebra, it leads to the well known Jacobi identity.

In the particular case of the Dirac equation,

$$\Gamma_\alpha = \gamma_\alpha. \tag{14}$$

From this we find the known affinity coefficients obtained earlier [4,5] by covariant differentiation of the spinors. In the case of the Klein-Gordon equation we obtain the expression quoted earlier.

We note that one can take account of the nonlinear character of the gravitational field with the help of interaction terms in the equations for the new field itself, which must be introduced owing to the presence of derivative terms in the equations.

Finally, we call attention to the fact that the conservation law for isotopic spin and, possibly, baryon number are not exact, [6,7] which induces a nonvanishing rest mass in the corresponding boson fields of Sakurai. In analogy, the presence of gauge noninvariant terms (of the type of the cosmological term) in the gravitational field equations can be related to the violation of Lorentz invariance at small distances of the order $\lambda^{-1/2}$.

[1] J. Sakurai, Ann. Phys. **11**, 1 (1960). (See also R. Utyama, Phys. Rev. **101**, 1596 (1956).)

[2] Yu. L. Daletskii and S. G. Kreĭn, DAN SSSR **76**, 1 (1951).

[3] G. A. Sokolik, Collection, Teoriya élementarnykh chastits (Theory of Elementary Particles), Uzhgorod (1960).

[4] V. Fock and D. Ivanenko, Compt. rend. **188**, 1470 (1929).

[5] A. Sokolov and D. Ivanenko, Kvantovaya teoriya polya (Quantum Theory of Fields), Gostekhizdat (1952).

[6] A. M. Brodskii and D. D. Ivanenko, Nucl. Phys. **13**, 447 (1959).

[7] J. A. Wheeler, Rendiconti Varenna, Corso **11** (1960).

Translated by R. Lipperheide
223

ON THE $\bar{K} + N \rightarrow \Lambda(\Sigma) + \gamma$ PROCESS

L. I. LAPIDUS and CHOU KUANG-CHAO

Joint Institute for Nuclear Research

Submitted to JETP editor May 18, 1961

J. Exptl. Theoret. Phys. (U.S.S.R.) **41**, 1310-1314 (October, 1961)

Some information on $\Lambda(\Sigma) + \pi \rightarrow \Lambda(\Sigma) + \gamma$ processes can be obtained by investigating the $\bar{K} + N \rightarrow \Lambda(\Sigma) + \gamma$ reaction. A detailed phenomenological analysis of these processes in the s state is performed. The Kroll-Ruderman theorem for photoproduction of pions on hyperons near threshold is considered.

1. One of the most important problems in elementary-particle physics is the study of interactions between unstable particles, where for lack of an unstable-particle target it becomes necessary to use indirect methods for this purpose.

We have shown earlier [1] that by using the unitarity condition for the S matrix we can establish certain relations between the matrix elements for the processes $\bar{K} + N \rightarrow \bar{K} + N$, $\bar{K} + N \rightarrow \Lambda(\Sigma) + \pi$ and $\Lambda(\Sigma) + \pi \rightarrow \Lambda(\Sigma) + \pi$ for states with arbitrary values of the angular momentum. It is therefore necessary to obtain certain information on the processes $\Lambda(\Sigma) + \pi \rightarrow \Lambda(\Sigma) + \pi$ by analyzing the cross sections and polarizations of the baryons in elastic scattering and in reactions involving K mesons and nucleons. Similar conclusions were reached later by other authors. [2,3] In [2] and [3] there is a detailed analysis of elastic scattering and interaction of K mesons with nucleons in the s state. Existing experimental data allow us to establish the phase difference of the s waves in $\pi\Sigma$ scattering with isospin I = 1 and I = 0.

In order to obtain certain information on the electromagnetic and strong interactions of hyperons, we consider in the present article the processes

$$\bar{K} + N \rightarrow \Lambda(\Sigma) + \gamma. \tag{1}$$

The S-matrix unitarity conditions cause the matrices for the processes $\pi + \Lambda(\Sigma) \rightarrow \Lambda(\Sigma) + \gamma$ to be related with the matrix elements of processes (1).

2. For simplicity we consider the reactions (1) in the s state only. We use the K-matrix method developed in [3]. For our problem it is convenient to use a symmetrical and Hermitian K matrix, expressed in terms of a T matrix with the aid of the relation

$$K = T - i\pi K\rho T = T - i\pi T\rho K, \tag{2}$$

where ρ is the density matrix of the phase volume for the intermediate states with fixed total energy. For two-particle (binary) reactions with a definite angular momentum, the matrix ρ is diagonal. In the relativistic normalization of the wave functions, the diagonal elements of the ρ matrix are

$$\rho_{nn} = M_n k/\pi E, \tag{3}$$

where k is the relative momentum of the particle in the c.m.s., M_n is the mass of the baryons in the intermediate states, and E is the total energy of the system:

$$E = (k^2 + M_n^2)^{1/2} + (k^2 + m^2)^{1/2}. \tag{4}$$

If we introduce the notation

$$K' = \pi\rho^{1/2}K\rho^{1/2}, \qquad T' = \pi\rho^{1/2}T\rho^{1/2}, \tag{5}$$

then Eq. (2) can be rewritten as

$$K' = T' - iK'T' = T' - iT'K'. \tag{6}$$

From (6) we obtain

$$T' = (1 - iK')^{-1}K' = K'(1 - iK')^{-1}. \tag{7}$$

The cross section of reaction (1) expressed in terms of the T′ matrix, in a state with definite angular momentum J and with definite parity, is

$$\sigma(i \rightarrow j) = 4\pi k_i^{-2}(J + 1/2)\,|\langle j|T'|i\rangle|^2. \tag{8}$$

Let us consider the submatrices of the introduced K and T matrices, which we denote by

$$\begin{aligned}
\alpha &= \langle \bar{K}N|K|\bar{K}N\rangle, & T_{KK} &= \langle \bar{K}N|T|\bar{K}N\rangle,\\
\beta &= \langle \bar{K}N|K|Y\pi\rangle, & T_{KY} &= \langle \bar{K}N|T|Y\pi\rangle,\\
\beta^+ &= \langle Y\pi|K|\bar{K}N\rangle, & T_{YK} &= \langle Y\pi|T|\bar{K}N\rangle,\\
\gamma &= \langle Y\pi|K|Y\pi\rangle, & T_{YY} &= \langle Y\pi|T|Y\pi\rangle,\\
\xi &= \langle \bar{K}N|K|Y\gamma\rangle, & T_{K\gamma} &= \langle \bar{K}N|T|Y\gamma\rangle,\\
\xi^+ &= \langle Y\gamma|K|\bar{K}N\rangle, & T_{\gamma K} &= \langle Y\gamma|T|\bar{K}N\rangle,\\
\eta &= \langle Y\pi|K|Y\gamma\rangle, & T_{Y\gamma} &= \langle Y\pi|T|Y\gamma\rangle,\\
\eta^+ &= \langle Y\gamma|K|Y\pi\rangle, & T_{\gamma Y} &= \langle Y\gamma|T|Y\pi\rangle,\\
\zeta &= \langle Y\gamma|K|Y\gamma\rangle, & T_{\gamma\gamma} &= \langle Y\gamma|T|Y\gamma\rangle.
\end{aligned} \tag{9}$$

We denote the submatrices of the K′ and T′ matrices by the corresponding primed letters. We neglect the matrix ζ, which is at least one order of magnitude smaller than the other matrices.

If we introduce

$$K_0 = \begin{pmatrix} \alpha & \beta \\ \beta^+ & \gamma \end{pmatrix}, \quad \delta = \begin{pmatrix} \xi \\ \eta \end{pmatrix}, \tag{10}$$

then we can write

$$K = \begin{pmatrix} K_0 & \delta \\ \delta^+ & 0 \end{pmatrix}. \tag{11}$$

From (5), (7), (10), and (11) we readily find that

$$\begin{aligned}
T'_{KK} &= (1 - iX')^{-1} X', \\
T'_{K\gamma} &= (1 - iX')^{-1} \beta' (1 - i\gamma')^{-1} \\
&= (1 - i\alpha')^{-1} \beta' (1 - iZ')^{-1}, \\
T'_{\gamma K} &= (1 - iZ')^{-1} \beta'^T (1 - i\alpha')^{-1} \\
&= (1 - i\gamma')^{-1} \beta'^T (1 - iX')^{-1}, \\
T'_{\gamma\gamma} &= (1 - iZ')^{-1} Z', \; T'_{K\gamma} \\
&= (1 - iX')^{-1} \xi' + i (1 - iX')^{-1} \beta' (1 - i\gamma')^{-1} \eta', \\
T'_{\gamma\gamma} &= i (1 - iZ')^{-1} \beta'^T (1 - i\alpha')^{-1} \xi' + (1 - iZ')^{-1} \eta', \\
T'_{\gamma K} &= \xi'^T (1 - iX')^{-1} + i\eta'^T (1 - i\gamma')^{-1} \beta'^T (1 - iX')^{-1}, \\
T'_{\gamma\gamma} &= i\xi'^T (1 - i\alpha')^{-1} \beta' (1 - iZ')^{-1} + \eta'^T (1 - iZ')^{-1},
\end{aligned} \tag{12}$$

where

$$\begin{aligned}
X' &= \alpha' + i\beta' (1 - i\gamma')^{-1} \beta'^T, \\
Z' &= \gamma' + i\beta'^T (1 - i\alpha')^{-1} \beta'.
\end{aligned} \tag{13}$$

3. In our discussion it is sufficient to take into account the electromagnetic interaction in first-order perturbation theory, considering separately the contributions from the iso-scalar and iso-vector parts of the electromagnetic interaction.

We start from the iso-scalar current. In this case the total isospin is I = 0 for the $\Lambda + \gamma$ system and I = 1 for the $\Sigma + \gamma$ system. We denote by ξ^0_Λ, ξ^1_Σ, η^0_Λ, and η^1_Σ the matrix elements with iso-scalar current for the processes $\bar{K} + N \to \Lambda(\Sigma) + \gamma$ and $\Lambda(\Sigma) + \pi \to \Lambda(\Sigma) + \gamma$, respectively. In the case of the iso-vector current, the total isospin is I = 1 for the $\Lambda + \gamma$ system and I = 0 or 1 for the $\Sigma + \gamma$ system. The corresponding matrix elements will be denoted by ξ^1_Λ, ξ^1_Σ, ξ'^1_Σ, η^1_Λ, η^0_Σ, and η'^1_Σ.

Let us consider the channels with isospin I = 0. In this case the submatrices α, β, and γ are simply numbers. Expressions (13) are then reduced to

$$X = \alpha + i\pi\beta^2\rho_\Sigma/(1 - i\pi\rho_\Sigma\gamma) = a + ib, \tag{14}$$

where

$$\begin{aligned}
a &= \alpha - \pi^2\beta^2\gamma\rho^2_\Sigma/[1 + \pi^2\rho^2_\Sigma\gamma^2], \\
b &= \pi\beta^2\rho_\Sigma/[1 + \pi^2\rho^2_\Sigma\gamma^2] > 0.
\end{aligned} \tag{15}$$

Substituting (14) in (12) we get

$$\begin{aligned}
T'_{KK} &= (1 - iX')^{-1} X' = \pi\rho_K (a^0 + ib^0) \Delta_0^{-1}, \\
T'_{\Sigma K} &= \pi^{1/2}\rho_K^{1/2} (b^0)^{1/2} e^{i\lambda_\Sigma} \Delta_0^{-1},
\end{aligned} \tag{16}$$

where

$$\tan\lambda_\Sigma = \pi\rho_\Sigma\gamma, \qquad \Delta_0 = 1 - i\pi\rho_K (a^0 + ib^0).$$

Formulas (16) for the processes $\bar{K} + N \to \bar{K} + N$ and $\bar{K} + N \to \Sigma + \pi$ were obtained by many authors.[3]

Let us write

$$\begin{aligned}
T'_{\gamma K} &= \xi^T (1 - iX')^{-1} + i\eta^T (1 - i\gamma')^{-1} \beta'^T (1 - iX')^{-1} \\
&= \begin{pmatrix} T'_{\Lambda\gamma K} \\ T'_{\Sigma\gamma K} \end{pmatrix}, \quad \eta^T = \begin{pmatrix} \eta^0_{\Lambda\Sigma} \\ \eta^0_{\Sigma\Sigma} \end{pmatrix}, \quad \xi^T = \begin{pmatrix} \xi^0_{\Lambda K} \\ \xi^0_{\Sigma K} \end{pmatrix}.
\end{aligned} \tag{17}$$

From (14)—(17) we readily find that

$$\begin{aligned}
T'_{\Lambda\gamma K} &= \pi\rho_{\gamma\Lambda}^{1/2}\rho_K^{1/2} [\xi^0_{\Lambda K} + i\eta^0_{\Lambda\Sigma}\pi^{1/2}\rho_\Sigma^{1/2} (b^0)^{1/2} e^{i\lambda_\Sigma}] \Delta_0^{-1}, \\
T'_{\Sigma\gamma K} &= \pi\rho_{\gamma\Sigma}^{1/2}\rho_K^{1/2} [\xi^0_{\Sigma K} + i\eta^0_{\Sigma\Sigma}\pi^{1/2}\rho_\Sigma^{1/2} (b^0)^{1/2} e^{i\lambda_\Sigma}] \Delta_0^{-1}.
\end{aligned} \tag{18}$$

We note that $T'_{\Lambda\gamma K}$, $T'_{\Sigma\gamma K}$, and $T'_{\Sigma K}$ have almost the same energy dependence in the low-energy region, where (assuming the relative parity of the hyperons to be positive) the energy dependence of ρ_Σ, ρ_Λ, $\rho_{\gamma\Lambda}$, and $\rho_{\gamma\Sigma}$ can be neglected.

Let us proceed to examine the channels with isospin I = 1. In this case γ and β are matrices,

$$\gamma = \begin{pmatrix} \gamma_{\Lambda\Lambda} & \gamma_{\Sigma\Lambda} \\ \gamma_{\Lambda\Sigma} & \gamma_{\Sigma\Sigma} \end{pmatrix}, \quad \beta = (\beta_{\Lambda K}, \beta_{\Sigma K}). \tag{19}$$

It is easy to verify that in this case X is simply a complex number

$$X = a^1 + ib^1, \tag{20}$$

where

$$a^1 = \alpha - \pi\beta\rho_Y^{1/2} \frac{1}{1 + \gamma'^2} \gamma'\rho_Y^{1/2}\beta^T, \qquad b^1 = \pi\beta\rho_Y^{1/2} \frac{1}{1 + \gamma'^2} \rho_Y^{1/2}\beta^T \tag{21}$$

From (12), (13), and (19)—(21) it follows that

$$\begin{aligned}
T'_{KK} &= \pi\rho_K (a^1 + ib^1) \Delta_1^{-1}, \quad T'_{\Lambda K} = \pi^{1/2}\rho_K^{1/2} (b^1_{\Lambda K})^{1/2} e^{i\lambda_{\Lambda K}} \Delta_1^{-1}, \\
T'_{\Sigma K} &= \pi^{1/2}\rho_K^{1/2} (b^1_{\Sigma K})^{1/2} e^{i\lambda_{\Sigma K}} \Delta_1^{-1},
\end{aligned} \tag{22}$$

where

$$\begin{aligned}
\pi^{1/2}\rho_K^{1/2} b^{1/2}_{\Lambda K} e^{i\lambda_{\Lambda K}} &\equiv \langle \Lambda | (1 - i\gamma')^{-1} \beta'^T | K \rangle, \\
\pi^{1/2}\rho_K^{1/2} b^{1/2}_{\Sigma K} e^{i\lambda_{\Sigma K}} &\equiv \langle \Sigma | (1 - i\gamma')^{-1} \beta'^T | K \rangle, \\
\Delta_1 &= 1 - i\pi\rho_K (a^1 + ib^1),
\end{aligned} \tag{23}$$

and the quantities $b_{\Lambda K}$ and $b_{\Sigma K}$ are related with b by the equation $b_{\Lambda K} + b_{\Sigma K} = b$. If we represent the matrices ξ and η in the form

$$\xi = (\xi_{\Lambda K}, \xi_{\Sigma K}), \quad \eta = \begin{pmatrix} \eta_{\Lambda\Lambda} & \eta_{\Sigma\Lambda} \\ \eta_{\Lambda\Sigma} & \eta_{\Sigma\Sigma} \end{pmatrix}, \tag{24}$$

then the matrix elements $T'_{\gamma\Lambda K}$ and $T'_{\gamma\Sigma K}$ become

$$T'_{\gamma\Lambda K} = \pi\rho_{\gamma\Lambda}^{1/2}\rho_K^{1/2}\Delta_1^{-1}[\xi_{\Lambda K} + i\eta_{\Lambda\Lambda}\pi^{1/2}\rho_\Lambda^{1/2}b_{\Lambda K}^{1/2}e^{i\lambda_{\Lambda K}} + i\eta_{\Lambda\Sigma}\pi^{1/2}\rho_\Sigma^{1/2}b_{\Sigma K}^{1/2}e^{i\lambda_{\Sigma K}}], \quad (25)$$

$$T'_{\gamma\Sigma K} = \pi\rho_{\gamma\Sigma}^{1/2}\rho_K^{1/2}\Delta_1^{-1}[\xi_{\Sigma K} + i\eta_{\Sigma\Lambda}\pi^{1/2}\rho_\Lambda^{1/2}b_{\Lambda K}^{1/2}e^{i\lambda_{\Lambda K}} + i\eta_{\Sigma\Sigma}\pi^{1/2}\rho_\Sigma^{1/2}b_{\Sigma K}^{1/2}e^{i\lambda_{\Sigma K}}]. \quad (26)$$

To simplify matters we introduce new symbols

$$\begin{aligned}
\alpha_\Lambda^0 &= \pi^{1/2}\rho_{\gamma\Lambda}^{1/2}[\xi_{\Lambda K}^0 + i\eta_{\Lambda\Sigma}^0\pi^{1/2}\rho_\Sigma^{1/2}(b^0)^{1/2}e^{i\lambda_\Sigma}],\\
\alpha_\Sigma^0 &= \pi^{1/2}\rho_{\gamma\Sigma}^{1/2}[\xi_{\Sigma K}^0 + i\eta_{\Sigma\Sigma}^0\pi^{1/2}\rho_\Sigma^{1/2}(b^0)^{1/2}e^{i\lambda_\Sigma}],\\
\alpha_\Lambda^1 &= \pi^{1/2}\rho_{\gamma\Lambda}^{1/2}[\xi_{\Lambda K}^1 + i\eta_{\Lambda\Lambda}^1\pi^{1/2}\rho_\Lambda^{1/2}(b_{\Lambda K}^1)^{1/2}e^{i\lambda_{\Lambda K}} + i\eta_{\Lambda\Sigma}^1\pi^{1/2}\rho_\Sigma^{1/2}(b_{\Sigma K}^1)^{1/2}e^{i\lambda_{\Sigma K}}],\\
\alpha_\Sigma^1 &= \pi^{1/2}\rho_{\gamma\Sigma}^{1/2}[\xi_{\Sigma K}^1 + i\eta_{\Sigma\Lambda}^1\pi^{1/2}\rho_\Lambda^{1/2}(b_{\Lambda K}^1)^{1/2}e^{i\lambda_{\Lambda K}} + i\eta_{\Sigma\Sigma}^1\pi^{1/2}\rho_\Sigma^{1/2}(b_{\Sigma K}^1)^{1/2}e^{i\lambda_{\Sigma K}}],\\
\alpha_\Sigma'^1 &= \pi^{1/2}\rho_{\gamma\Sigma}^{1/2}[\xi_{\Sigma K}'^1 + i\eta_{\Sigma\Lambda}'^1\pi^{1/2}\rho_\Lambda^{1/2}(b_{\Lambda K}^1)^{1/2}e^{i\lambda_{\Lambda K}} + i\eta_{\Sigma\Sigma}'^1\pi^{1/2}\rho_\Sigma^{1/2}(b_{\Sigma K}^1)^{1/2}e^{i\lambda_{\Sigma K}}],
\end{aligned} \quad (27)$$

with which the cross sections of the processes (1) can be written in the following form:

Process:	Cross section:
$K^- + p \to \Lambda^0 + \gamma$ $\bar{K}^0 + n \to \Lambda^0 + \gamma$	$\frac{2\pi m_K}{E_K k}\left\lvert\frac{\alpha_\Lambda^0}{\Delta_0} \pm \frac{\alpha_\Lambda^1}{\Delta_1}\right\rvert^2$,
$K^- + p \to \Sigma^0 + \gamma$ $\bar{K}^0 + n \to \Sigma^0 + \gamma$	$\frac{2\pi m_K}{E_K k}\left\lvert-\frac{\alpha_\Sigma^0/\sqrt{3}}{\Delta_0} \pm \frac{\alpha_\Sigma^1}{\Delta_1}\right\rvert^2$,
$K^- + n \to \Sigma^- + \gamma$ $\bar{K}^0 + p \to \Sigma^+ + \gamma$	$\frac{2\pi m_K}{E_K k}\left\lvert\frac{\alpha_\Sigma^1 \pm \alpha_\Sigma'^1/\sqrt{2}}{\Delta_1}\right\rvert^2$.

Thus, the experimental investigation of the processes $\bar{K} + N \to \Lambda(\Sigma) + \gamma$ in $\bar{K}p$ and $\bar{K}d$ collisions can yield certain information on the matrix elements α_Λ and α_Σ. Naturally, this information is not sufficient to reconstitute the matrix elements ξ and η, which describe the photoproduction of mesons on hyperons. Nonetheless they may prove useful for a study of the interaction between hyperons and mesons or photons.

4. A powerful method for the analysis of strong interactions is the method of dispersion relations (d.r.), the use of which yields in many cases interesting results in the low-energy region. It can be assumed that the d.r. method is applicable to the photoproduction of mesons and hyperons. In the present paper we confine ourselves to a generalization of the Kroll-Ruderman theorem for photoproduction of pions near threshold.[4]

Let us assume that the Λ and Σ hyperons have a positive relative parity and that the K meson is pseudoscalar. If the created particles have low energies account of the electric dipole radiation is sufficient. The generalized Kroll-Ruderman theorem states that, accurate to $m_\pi/M \approx 15\%$, the matrix for the electric dipole transition is determined completely by the pion-hyperon coupling constant.

Let us write the Hamiltonian of the pion-hyperon interaction in the form

$$\mathcal{H} = ig_{\Sigma\Lambda}\bar{\Psi}_\Sigma\gamma_5\Psi_\Lambda\Psi_\pi + ig_{\Sigma\Sigma}([\bar{\Psi}_\Sigma\gamma_5\Psi_\Sigma]\Psi_\pi) + \text{Herm. conj.} \quad (28)$$

Following Low's method[5] we can obtain

$$\eta_{\Lambda\Sigma}^0 \sim m_\pi/M, \quad \eta_{\Sigma\Lambda}^1 \sim m_\pi/M, \quad \eta_{\Sigma\Sigma}^1 \sim m_\pi/M,$$
$$\eta_{\Sigma\Lambda}'^1 = \eta_{\Lambda\Sigma}'^1 = \sqrt{2}\alpha^{1/2}f_{\Sigma\Lambda}[1 + O(m_\pi/M)],$$
$$\eta_{\Sigma\Sigma}'^1 = \alpha^{1/2}f_{\Sigma\Sigma}[1 + O(m_\pi/M)], \quad \eta_{\Sigma\Sigma}^0 \approx m_\pi/M.$$

Here m_π is the pion mass, M is the hyperon mass, $\alpha = \epsilon^2/4\pi = 1/137$, and $f^2 = g^2/8\pi M$.

[1] L. I. Lapidus and Chou Kuang-chao, JETP **37**, 283 (1959), Soviet Phys. JETP **10**, 199 (1960).

[2] Jackson, Ravenhall, and Wyld, Nuovo cimento **9**, 834 (1958). R. H. Dalitz and S. F. Tuan, Ann. of Physics **8**, 100 (1959). M. Ross and G. Snow, Phys. Rev. **115**, 1773 (1959).

[3] R. H. Dalitz and S. F. Tuan, Ann. of Physics **10**, 307 (1960). P. T. Mathews and A. Salam, Nuovo cimento **13**, 382 (1959). J. D. Jackson and H. Wyld, Nuovo cimento **13**, 84 (1959).

[4] K. M. Kroll and M. A. Ruderman, Phys. Rev. **93**, 233 (1954).

[5] F. E. Low, Phys. Rev. **97**, 1392 (1955).

Translated by J. G. Adashko
224

NUCLEAR RECOIL IN THE EQUIVALENT PHOTON METHOD

A. M. BADALYAN

Submitted to JETP editor May 26, 1961

J. Exptl. Theoret. Phys. (U.S.S.R.) 41, 1315-1323 (October, 1961)

The region of nuclear recoil q^2, in which the Weizsäcker-Williams relation is valid, is investigated by considering the bremsstrahlung of an electron in the nuclear field as an example. It is shown that the region of permissible values of q^2 depends on whether the cross section is averaged over the directions of nuclear recoil or not. It is also demonstrated that the Weizsäcker-Williams relation is violated in a narrow region of q^2 corresponding to strictly forward radiation by the electron. The treatment is of a completely covariant nature.

1. INTRODUCTION

THE method of equivalent photons was proposed initially [1,2] for the calculation of several electromagnetic processes. The justification of the method was semi-qualitative and its field of application was limited to the calculation of total cross sections. In several recent papers [3-5] this method is used to solve a new group of problems, including those involving processes with strong interactions [4] and the calculation of radiative corrections. [5] In these papers, however, the method is applied to cross sections averaged over the polarizations and integrated over the nuclear recoil directions. The recent results [6] on the covariant form of the equivalent photon spectrum, for an arbitrary process in the field of a heavy particle, make it possible for the first time to take covariant account of the dependence of the cross section on the direction of the nuclear recoil. The approximations used in the equivalent-photon method have likewise not been examined before.

We show in the present paper that the derivation of the fundamental relation of the method (the Weiszäcker-Williams relation), connecting the cross section $d\sigma_b$ of the considered process* and the cross section $d\sigma_C$ of the photo process,

$$d\sigma_b = N d\sigma_C, \qquad (1.1)$$

entails two approximations.

1) Separation of the equivalent-photon spectrum N in $d\sigma_b$. It is shown in [6] that the separation of the spectrum N is connected only with a new gauge for the field of the heavy particle. This means that by using the gauge-invariance condition we can rewrite (1.1) in the form

$$d\sigma_b = N d\sigma_q, \qquad (1.2)$$

where the cross section $d\sigma_q$ describes a process that differs from the photoprocess in that $q^2 \neq 0$ for the incoming photon (q^2 is the invariant square of the nuclear recoil momentum). The polarization $\tilde{e}$ of the incoming photon is determined here by the direction of the nuclear recoil (Sec. 4).

2) Replacement of the cross section $d\sigma_q$ by its value at the "pole" when $q^2 = 0$, i.e., by $d\sigma_C$. The conditions under which such extrapolation is possible were not made clear and this problem can apparently not be analyzed in general form. Furthermore, the limit of applicability of this method for the given process will depend, for example, on whether the cross section under consideration is averaged over the polarization or not.

We investigate here the nuclear recoil region where relation (1.1) holds, using as an example the bremsstrahlung of an electron in the field of the nucleus. We consider two cases: a) $d\sigma_b$ depends on the direction of the nuclear recoil (Secs. 2—6), in which case the incident photon is polarized in the corresponding Compton effect; b) $d\sigma_b$ is averaged over the nuclear recoil directions (Appendix), and then the corresponding cross section $d\sigma_C$ is averaged over the polarization of the incident photon. We shall show that 1) if the term in $d\sigma_b$ dependent on the direction of the nuclear recoil is small, the limits of applicability of the method are the same in cases a and b; 2) if this term in $d\sigma_b$ is appreciable, the limits of applicability of (1.1) change, the region of permissible values of q^2 becoming narrower; 3) for a relativistic electron when the frequency of the radiated photon is of the same order as the energy of the incoming electron, relation (1.1) is violated in a narrow region corresponding to strictly forward radiation.

*We consider a certain process which includes exchange of one virtual photon upon collision of two particles, of which one is heavy (nucleus).

The entire analysis in the present paper is completely covariant.

2. BREMSSTRAHLUNG CROSS SECTION

The bremsstrahlung of an electron in the field of the nucleus corresponds to two diagrams (see the figure). If the nuclear spin is assumed to be zero, then the differential cross section of the

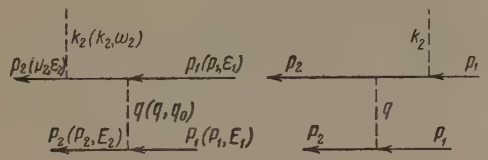

process (after averaging over the electron spin before and after the scattering and polarization of the photon) has the following form (see the figure for notation)

$$d\sigma_b = \frac{Z^2\alpha^3}{\pi^2}\frac{F_{\alpha\beta}P_\alpha P_\beta}{q^4}\frac{1}{(J\varepsilon_1 E_1)}\frac{dp_2}{2\varepsilon_2}\frac{dk_2}{2\omega_2}\frac{dP_2}{2E_2}\delta^4(q+p_1-k_2-p_2), \tag{2.1}$$

$$q = P_1 - P_2. \tag{2.2}$$

$J\epsilon_1 E_1$ assumes the role of invariant current density of the colliding particles (with masses m and M):

$$J\varepsilon_1 E_1 = [(p_1P_1)^2 - m^2M^2]^{1/2} \tag{2.3}$$

(the density of the electrons and nuclei in their rest system is assumed equal to unity). In the coordinate system in which one of the particle is at rest (prior to collision) J is the velocity of the second particle.

The 4-vector P, namely

$$P = P_1 + P_2, \tag{2.4}$$

defines the polarization of the pseudophoton (virtual quantum). The Lorentz condition is satisfied here:

$$qP = 0. \tag{2.5}$$

We note, however, that $P^2 < 0$ and therefore the normalization condition $P^2 = 1$, which usually applies to polarization vectors, cannot be imposed on this vector.

We introduce the usual invariant variables

$$m^2\varkappa_1 = q^2 + 2qp_1 = 2k_2p_2, \quad m^2\varkappa_2 = q^2 - 2qp_2 = -2k_2p_1,$$
$$m^2\varkappa_1 = -(\omega^2 - m^2) < 0, \tag{2.6}$$

where w is the total energy of the final photon and electron ($ab = \mathbf{a}\cdot\mathbf{b} - a_0b_0$). In these variables the matrix $F_{\alpha\beta}$ is written in the form

$$F_{\alpha\beta} = -\frac{\varkappa_1}{\varkappa_2}\left(1-\frac{q^2}{m^2\varkappa_1}\right)^2 F^{(1)}_{\alpha\beta} - \frac{\varkappa_2}{\varkappa_1}\left(1-\frac{q^2}{m^2\varkappa_2}\right)^2 F^{(2)}_{\alpha\beta}$$
$$-\frac{8}{\varkappa_1^2\varkappa_2^2}\xi_\alpha\xi_\beta + \frac{q^2}{m^2}\left(\delta_{\alpha\beta} - \frac{q_\alpha q_\beta}{q^2}\right)F^{(0)}_{\alpha\beta}; \tag{2.7}$$

$$F^{(1,2)}_{\alpha\beta} = \delta_{\alpha\beta} - (qp_i)^{-1}(q_\alpha p_{i\beta} + q_\beta p_{i\alpha})$$
$$+ q^2(qp_i)^{-2}p_{i\alpha}p_{i\beta}, \quad i = 1, 2,$$

$$\xi_\alpha = m^{-1}\left(\varkappa_2 p_{1\alpha} + \varkappa_1 p_{2\alpha} - \tfrac{1}{2}q_\alpha(\varkappa_1 - \varkappa_2)\right),$$

$$F^{(0)} = -2(1/\varkappa_1 + 1/\varkappa_2)^2. \tag{2.8}$$

The symmetrical matrix $F_{\alpha\beta}$ has the gauge-invariance property

$$F_{\alpha\beta}q_\beta = 0. \tag{2.9}$$

The same property is possessed by all the quantities in (2.7). If we use the Lorentz condition (2.5), then some of the terms in the cross section vanish after multiplication by $P_\alpha P_\beta$.

3. COMPTON-EFFECT CROSS SECTION

The formula for the differential cross section of the Compton scattering can be written in a form similar to (2.1) (with averaging over the spins of the electron and polarization of the final photon)

$$d\sigma_C = \frac{4\alpha^2}{m^2|\varkappa_1|}\Phi_{\alpha\beta}e_\alpha e_\beta\frac{dp_2}{2\varepsilon_2}\frac{dk_2}{2\omega_2}\delta^4(k_1 + p_1 - k_2 - p_2). \tag{3.1}$$

The notation here is analogous to that of (2.6)—(2.9). The expression for $\Phi_{\alpha\beta}$ is obtained from (2.8) with $q^2 = 0$:

$$\Phi_{\alpha\beta} = -\frac{\varkappa_1}{\varkappa_2}\Phi^{(1)}_{\alpha\beta} - \frac{\varkappa_2}{\varkappa_1}\Phi^{(2)}_{\alpha\beta} - \frac{8}{\varkappa_1^2\varkappa_2^2}\xi_\alpha\xi_\beta;$$

$$\Phi^{(1,2)}_{\alpha\beta} = \delta_{\alpha\beta} - (k_1p_i)^{-1}(k_{1\alpha}p_{i\beta} + k_{1\beta}p_{i\beta}), \quad i = 1, 2,$$
$$\xi_\alpha = m^{-1}(\varkappa_2 p_{1\alpha} + \varkappa_1 p_{2\alpha}), \tag{3.2}$$

where k_1 is the wave vector of the incoming quantum, $-m^2\kappa_1/2 = J\epsilon_1\omega_1$ is in this case an invariant current obtained from (2.3) with $M = 0$, and e is the polarization of the incoming quantum ($e^2 = 1$).

The usual expression for the Compton effect is obtained by leaving out of (3.1) the terms that do not contribute to the cross section by virtue of the Lorentz gauge. We then have, in particular,

$$\Phi_{\alpha\beta}e_\alpha e_\beta = -\frac{\varkappa_1}{\varkappa_2} - \frac{\varkappa_2}{\varkappa_1} - 8\frac{[\varkappa_2(p_1e) + \varkappa_1(p_2e)]^2}{m^2\varkappa_1^2\varkappa_2^2}. \tag{3.3}$$

4. EQUIVALENT-PHOTON SPECTRUM

The gauge-invariance condition (2.1) enables us to introduce in place of the time-like polarization vector P a new space-like vector $\tilde{e}$. Following [6], we define this vector in such a way that its

scalar component vanishes in the frame where the electron is at rest, i.e., $\tilde{e}$ is subject to the condition

$$\tilde{e}p_1 = 0, \tag{4.1}$$

$$\tilde{e} = f^{-1}(P - q(p_1P/p_1q)) \quad (\tilde{e}^2 = 1), \tag{4.2}$$

$$f = [P^2 + q^2(p_1P/p_1q)^2]^{1/2}. \tag{4.3}$$

The pseudophoton polarization vector $\tilde{e}$ no longer satisfies the Lorentz condition (2.5)

$$\tilde{e}q \neq 0. \tag{4.4}$$

We therefore separate from q a vector q_1 orthogonal to $\tilde{e}$:

$$q = q_1 + q_2, \qquad q_1 = q - \tilde{e}(\tilde{e}q), \tag{4.5}$$

$$q_1\tilde{e} = 0. \tag{4.6}$$

The vector q_1 is time-like

$$q_1^2 = q^2P^2/f^2 < 0. \tag{4.7}$$

If along with making the gauge transformation $P \to f\tilde{e}$, we replace P_2 in the bremsstrahlung cross section (2.1) by q and make the substitution ($P = 2P_1 - q$)

$$d\mathbf{P}_2/2E_2 \to d^4P_2\delta(P_2^2 + M^2) \to d^4q\delta(qP),$$

it becomes convenient to rewrite (2.1) in the form of (1.2), with

$$d\sigma_q = \frac{2\alpha^2}{|qp_1|}F_{\alpha\beta}\tilde{e}_\alpha\tilde{e}_\beta\frac{dp_2}{2\varepsilon_2}\frac{dk_2}{2\omega_2}\delta^4(q + p_1 - p_2 - k_2), \tag{4.8}$$

$$N = \frac{Z^2\alpha}{2\pi^2}\frac{|qp_1|}{(J\varepsilon_1E_1)}\frac{f^2}{q^4}d^4q\delta(qP). \tag{4.9}$$

$d\sigma_q$ describes a process that differs from the Compton effect only in that $q^2 \neq 0$ for the incoming photon, whose polarization does not satisfy the Lorentz condition. N is the differential spectrum of the pseudophotons, written in fully covariant form. Formula (4.9) coincides in fact with the expression given in [6] for the spectrum [(formula (6)]. They differ only in the normalization of the cross section and of the square of the matrix element.

We note that (4.9) coincides with the conventional expression for the spectrum [see, for example,[4] Eq. (2.16)] if the following conditions are satisfied

$$m^2M^2 \ll (p_1P_1)^2, \qquad |qp_1| \ll |p_1P_1|. \tag{4.10}$$

The first condition in (4.10) denotes* that the velocity of the electron relative to the nucleus is $v \sim 1$, while the second condition is that of the external field. We shall not repeat here the known expressions for the spectrum.

*Conditions (4.10) can apply not only to the case of a heavy nucleus ($M \to \infty$), but also to the analogous process occurring upon collision of particles of equal mass, say two electrons (if $v \to 1$).

5. LIMITS OF APPLICABILITY OF THE WEIZSÄCKER-WILLIAMS RELATION

Relation (1.2) is exact, while (1.1) is approximate. It holds only in that region of nuclear recoil (q^2) where $d\sigma_q$ coincides with $d\sigma_C$. We shall determine below the region of such values of q^2 and show that in this region $d\sigma_q$ determines the cross section for Compton scattering of a photon with wave vector q_1 and polarization $\tilde{e}$.

The Compton-effect cross section [see (3.3)] has two terms, one independent of the photon polarization

$$-\varkappa_1/\varkappa_2 - \varkappa_2/\varkappa_1 \equiv F_{12}, \tag{5.1}$$

and another determined by e:

$$-8[\varkappa_2(ep_1) + \varkappa_1(ep_2)]^2/m^2\varkappa_2^2\varkappa_1^2 \equiv -F_3. \tag{5.2}$$

We consider the Compton scattering photons with $e = \tilde{e}$. Therefore, by virtue of (4.1),

$$F_3 = 8(\tilde{e}p_2)^2/m^2\varkappa_2^2. \tag{5.3}$$

The conditions under which $d\sigma_q$ coincides with $d\sigma_C$ will be considered separately for the case when a) $F_3 \ll F_{12}$ and b) $F_3 \sim F_{12}$. Only in case b) can the dependence of the cross section on the direction of the nuclear recoil $\tilde{e}$ be accounted for in the method of equivalent photons.

The cross section $d\sigma_q$ [cf. (2.7) and (3.2)] contains, in addition to the corresponding Compton terms, the term

$$F^{(0)}m^{-2}(q^2 - (\tilde{e}q)^2) \equiv F^{(0)}q_1^2/m^2, \tag{5.4}$$

which is missing from $d\sigma_C$. It is obvious that $d\sigma_q$ and $d\sigma_C$ can be regarded as equal only in that region of q^2 where this term is small compared with the other terms that determine $d\sigma_q$. This condition is explained in Sec. 6.

Before we proceed to cases a) and b) we note that by considering the limits of variation of the parameters κ_1 and κ_2,

$$\varkappa_{2\,max} = -\varkappa_1, \qquad \varkappa_{2\,min} = \varkappa_1/(\varkappa_1 - 1), \tag{5.5}$$

we can readily show that

$$F_{12} \geqslant 2, \qquad F_3 \leqslant 2.$$

It also follows from (5.5) that

$$\begin{aligned} &\varkappa_2 \sim |\varkappa_1| \quad |\varkappa_1| \lesssim 1, \\ &1 \lesssim \varkappa_2 \leqslant |\varkappa_1| \quad |\varkappa_1| \gg 1. \end{aligned} \tag{5.6}$$

We shall assume further that $\kappa_2 \sim |\kappa_1|$ and consequently $F_{12} \sim 1$, after which we shall consider the case

$$\kappa_2 \ll |\kappa_1|, \tag{5.7}$$

which is possible when $|\kappa_1| \gg 1$.

It follows from (5.5) and (5.6) that

$$\text{a) } F_3 \ll 1, \quad |\tilde{e}p_2| \ll m\kappa_2, \tag{5.8}$$

$$\text{b) } F_3 \sim F_{12} \sim 1, \quad |\tilde{e}p_2| \sim m\kappa_2. \tag{5.9}$$

Case a). Comparing the coefficients preceding $F^{(1,2)}_{\alpha\beta}$ and $\Phi^{(1,2)}_{\alpha\beta}$ in (2.7) and (3.2), we obtain the first condition for q^2:

$$q^2 \ll m^2 |\kappa_1|. \tag{I'}$$

(We shall therefore no longer distinguish between $m^2\kappa_1$ and $2qp_1$ or $m^2\kappa_2$ and $-2qp_2$.)

It is obvious that by virtue of condition (4.1) and the Lorentz condition $(\tilde{e}k_1 = 0)$ we have

$$\Phi^{(1,2)}_{\alpha\beta}\tilde{e}_\alpha\tilde{e}_\beta = F^{(1)}_{\alpha\beta}\tilde{e}_\alpha\tilde{e}_\beta = 1. \tag{5.10}$$

But

$$F^{(2)}_{\alpha\beta}\tilde{e}_\alpha\tilde{e}_\beta = 1 + (\tilde{e}q)(\tilde{e}p_2)/qp_2 + q^2(\tilde{e}p_2)^2/(qp_2)^2. \tag{5.11}$$

Equations (5.10) and (5.11) can be regarded as equivalent by stipulating that the second and third terms (5.11) be much smaller than unity.

Let us estimate the absolute value of $\tilde{e}q$ in (5.11):

$$\tilde{e}q = -q^2 f^{-1}(p_1 P)/p_1 q. \tag{5.12}$$

If we assume [see (4.3)]*

$$f^2 \approx q^2 (p_1P)^2/(p_1q)^2, \tag{5.13}$$

then

$$|\tilde{e}q| \approx \sqrt{q^2} \tag{5.14}$$

and the third term in (5.11) can be regarded as the square of the second term. It is therefore sufficient to require that

$$\sqrt{q^2}\,|\tilde{e}p_2/qp_2| \ll 1. \tag{II'}$$

By virtue of (5.8), condition (II') is satisfied if (I') is satisfied, and we can assume that the first two terms in (2.8) coincide with F_{12}.

Let us consider the third term in (2.7):

$$8\frac{(\tilde{e}\xi)^2}{m^2\kappa_1^2\kappa_2^2} = 8\frac{\left[\kappa_1(\tilde{e}p_2) - \frac{1}{2}(\tilde{e}q)(\kappa_1-\kappa_2)\right]^2}{m^2\kappa_1^2\kappa_2^2}. \tag{5.15}$$

According to condition (5.8), the term with $(\tilde{e}p_2)^2$ is small compared with F_{12}. The other two terms with $\tilde{e}q$ in (5.15) can be neglected if

$$q^2 \ll m^2\kappa_1^2, \tag{I''}$$

$$\sqrt{q^2}\,|\tilde{e}p_2| \ll m^2\kappa_1^2. \tag{II''}$$

Condition (II'') is weaker than (I''). Condition (I'') supplements (I') if $|\kappa_1| \ll 1$. Combining (I') and (I'') we conclude that in case a) the equivalent-photon method is applicable in the nuclear-recoil region defined by the condition

$$q^2 \ll \begin{cases} m^2\kappa_1^2, & |\kappa_1| \lesssim 1 \\ m^2|\kappa_1|, & |\kappa_1| \gtrsim 1 \end{cases}. \tag{Ia}$$

The Appendix contains similar conditions for the case of cross sections integrated over the nuclear-recoil directions. It follows from (Ia) and (A.1) that these conditions coincide in case a).

Case b). In this case, conditions (I')—(II') and (I'')—(II'') obviously remain in force. However, unlike case a), fulfillment of (I') and (I'') does not guarantee fulfillment of (II')—(II''), since $|\tilde{e}p_2| \sim m\kappa_2$. We must stipulate in addition that the term with $\tilde{e}q$ in (5.15) be small compared with F_3, i.e.,

$$\sqrt{q^2} \ll |\tilde{e}p_2| \sim m\kappa_2, \quad \kappa_2 \sim -\kappa_1,$$

or

$$\sqrt{q^2} \ll m|\kappa_1|. \tag{5.16}$$

Combining conditions (I) and (II) with (5.8) and (5.16), we find that in case b) relation (1.1) is valid if

$$\sqrt{q^2} \ll \begin{cases} m|\kappa_1|, & |\kappa_1| \lesssim 1 \\ m, & |\kappa_1| \gtrsim 1 \end{cases}. \tag{Ib}$$

Thus, in case b) there exists a nuclear-recoil region (Ib) where on the one hand we can neglect the nuclear recoil, i.e., q^2, and on the other hand we can take into account the nuclear-recoil direction, which is characterized by the polarization vector $\tilde{e}$. However, region (Ib) of q^2 is found to be narrower than in case a), where the nuclear recoil is not considered at all.

We have not considered as yet the range $\kappa_2 \ll |\kappa_1|$. It is obvious from the form of $F_{\alpha\beta}\tilde{e}_\alpha\tilde{e}_\beta$ that in this case the main contribution to the cross section is due to the term with $F^{(1)}_{\alpha\beta}\tilde{e}_\alpha\tilde{e}_\beta$, the value of which is

$$-\kappa_1/\kappa_2 \gg 1.$$

Then in the entire permissible range of q^2 we have

$$q^2 \ll m^2|\kappa_1| \tag{5.17}$$

or, since $|\kappa_1| \gg 1$,

$$q^2 \lesssim m^2.$$

*It will be shown below that assumption (5.13) excludes only a narrow region of values of q^2, corresponding to strictly forward radiation of a relativistic electron.

we can neglect the contributions of the other terms in $d\sigma_q$ (and $d\sigma_C$). Condition (5.17) is weaker than (Ia).

6. VIOLATION OF THE WEIZSÄCKER-WILLIAMS RELATIONS IN FORWARD RADIATION OF A RELATIVISTIC ELECTRON

The requirement that the term

$$F^{(0)}q_1^2/m^2, \qquad F^{(0)} = -2(1/\varkappa_1 + 1/\varkappa_2)^2,$$

in $d\sigma_q$, a term missing from the Compton-effect cross section, be small compared with the other terms of $d\sigma_2$, leads to another limitation, in addition to (Ia) [or (b)], on the limits of applicability of the Weizsäcker-Williams relation (1.1).

The following relation will be useful in the subsequent estimates:

$$f^2 (qp_1)^2 \geqslant -q^2P^2m^2. \tag{6.1}$$

(This inequality can be readily proved by changing to a frame in which the electron is at rest; (6.1) then goes into the condition $q_\perp^2 \geq 0$, where $q_\perp$ is the q component perpendicular to the vector p_1). The equality sign in (6.1) corresponds to the minimum and maximum values of q^2 for a specified qp_1. The quantities q^2_{max} that follow from (6.1) do not satisfy condition (Ia) and are of no interest to us.

Using (4.3) and introducing $1 - v^2 \equiv -m^2P^2/(p_1P)^2$, we rewrite (6.1) in the form

$$m^2q^2v^2/(1-v^2) \geqslant (qp_1)^2. \tag{6.2}$$

Condition (6.2) imposes an upper limit on the permissible range of $|qp_1|$. We note that conditions (Ia) and (6.2) are compatible if

$$1 - v^2 \ll 1 \text{ for } |\varkappa_1| \lesssim 1 \quad \text{or} \quad |\varkappa_1|(1-v^2) \ll 1 \text{ for } |\varkappa_1| \gg 1. \tag{6.3}$$

The equality in (6.1) determines the minimum value of q^2 corresponding to forward radiation. We obtain from (6.1)

$$|q_1|^2 = -q^2P^2/f^2 \leqslant (qp_1)^2/m^2 \tag{6.4}$$

$$F^{(0)}q_1^2/m^2 \lesssim (\varkappa_1+\varkappa_2)^2/2\varkappa_1^2, \qquad m^2\varkappa_1 \approx 2qp_1. \tag{6.5}$$

When this term is small, there are two possibilities.

$$1)\ |\varkappa_1 + \varkappa_2| \ll |\varkappa_1|, \qquad \varkappa_2 \sim -\varkappa_1.$$

It follows from (6.5) and (5.5) that in this case $F^{(0)}q_1^2/m^2 \ll F_{12}$, and can be neglected, regardless of the value of q_1^2. Condition (6.6) holds for radiation of a nonrelativistic electron* and when the relativistic electron radiates photons with frequency $\omega \ll \epsilon_1$.

$$2)\ |\varkappa_1 + \varkappa_2| \sim |\varkappa_1|. \tag{6.7}$$

This condition corresponds to an emitted photon with energy ω (in the laboratory system) of the same order as the energy ϵ_1 of the initial electron ($\epsilon_1 \gg m$). Then

$$F^{(0)}q_1^2/m^2 \sim 2|q_1^2|/\varkappa_2^2m^2. \tag{6.8}$$

For forward radiation, i.e., when $q^2 = q^2_{min}$, it follows from (4.7) that

$$F^{(0)}q_1^2/m^2 \sim \varkappa_1^2/\varkappa_2^2. \tag{6.9}$$

Since $|\kappa_1| > \kappa_2$, this term is either greater than or of the same order as F_{12}, and cannot be neglected. The region where the term $F^{(0)}q_1^2/m^2$ is significant is very narrow

$$\Delta q^2 \approx q^2(1-v^2).$$

Outside this region we can assume $f^2 \approx q^2(p_1P)^2/(p_1q)^2$ and obtain from (4.7)

$$q_1^2 \approx -(qp_1)^2(1-v^2)/m^2. \tag{6.10}$$

Substituting (6.10) in (6.8) we obtain

$$F^{(0)}q_1^2/m^2 \approx \varkappa_1^2(1-v^2)/\varkappa_2^2. \tag{6.11}$$

This term is small compared with F_{12} if [see (6.6) and (6.7)]

$$1 - v^2 \ll \begin{cases} 1, & |\varkappa_1| \lesssim 1 \\ 1/|\varkappa_1|, & |\varkappa_1| \gg 1 \end{cases}. \tag{III}$$

[Conditions (III) coincide with (6.3)].

Thus, when conditions (III) are satisfied, we can replace for a relativistic electron $d\sigma_q$ by the Compton scattering cross section $d\sigma_C$, in the entire range of q^2 allowed by conditions (Ia) [or (Ib)], except for the narrow region corresponding to forward radiation.

In conclusion, the author is deeply grateful to Ya. A. Smorodinskii for constant interest in the work and for valuable comments.

APPENDIX

We give here an invariant expression for the bremsstrahlung cross section $d\bar{\sigma}_b$, integrated

*It must be noted that the limitations considered earlier (Sec. 5) are not connected with any conditions whatever on the electron velocity. Therefore, if we take for the spectrum N in (1.1) its exact expression (4.9), we can speak of the equivalent-photon method in the nonrelativistic region for the case of q^2 defined by conditions (1b) [or (1a)].

over the nuclear recoil directions [we have assumed that $1-v^2 \equiv -m^2P^2/(p_1P)^2 \approx m^2M^2/(p_1P_1)^2$]:

$$d\bar{\sigma}_b = N d\bar{\sigma}_q, \tag{A.1}$$

$$N = \frac{Z^2\alpha}{\pi}\frac{dq^2}{q^4}\frac{d(qp_1)}{qp_1}\{q^2 - (qp_1)^2(1-v^2)\}, \tag{A.2}$$

$$d\bar{\sigma}_q = 2\pi r_0^2 \frac{m^2}{2|qp_1|}\frac{d\varkappa_2}{W^{5/2}}\bar{F}_{\alpha\beta}\tilde{e}_\alpha\tilde{e}_\beta, \tag{A.3}$$

where

$$W = [4m^{-2}q^2 + (\varkappa_1 - m^{-2}q^2)^2],$$

$$\bar{F}_{\alpha\beta} = -m^{-2}q^2(\delta_{\alpha\beta} - q_\alpha q_\beta/q^2)\varphi_1(q^2, \varkappa_1, \varkappa_2) + (\varkappa_1 - m^{-2}q^2)^2 \times\left(\delta_{\alpha\beta} - \frac{p_{1\alpha}q_\beta + p_{1\beta}q_\alpha}{qp_1} + q^2\frac{p_{1\alpha}p_{1\beta}}{(qp_1)^2}\right)\varphi_2(q^2, \varkappa_1, \varkappa_2),$$

$$\begin{aligned}\varphi_1 = {} & 4\varkappa_1^{-1}\varkappa_2^{-2}\{4\varkappa_1^4 - 2\varkappa_1^4\varkappa_2 - \varkappa_1^4\varkappa_2^2 - 12\varkappa_1^3 + 20\varkappa_1^3\varkappa_2 - 2\varkappa_1^3\varkappa_2^2 \\ & - \varkappa_1^3\varkappa_2^3 - 24\varkappa_1^2\varkappa_2 + 16\varkappa_1^2\varkappa_2^2 + 2\varkappa_1^2\varkappa_2^3 - 12\varkappa_1\varkappa_2^2 \\ & + q^2m^{-2}(-8\varkappa_1^3 + 8\varkappa_1^3\varkappa_2 - 2\varkappa_2^3\varkappa_1 + 3\varkappa_1^3\varkappa_2^2 + 16\varkappa_1^2 \\ & - 42\varkappa_1^2\varkappa_2 + 6\varkappa_1^2\varkappa_2^2 + 2\varkappa_1^2\varkappa_2^3 + 32\varkappa_1\varkappa_2 - 28\varkappa_1\varkappa_2^2 \\ & + 16\varkappa_2^2 + 2\varkappa_2^3) + q^4m^{-4}(4\varkappa_1^2 - 10\varkappa_1^2\varkappa_2 - 3\varkappa_1^2\varkappa_2^2 + 24\varkappa_1\varkappa_2 \\ & - 4\varkappa_1\varkappa_2^2 - \varkappa_1\varkappa_2^3 + 4\varkappa_2^2 + 2\varkappa_2^3) + q^6m^{-6}(4\varkappa_1\varkappa_2 + \varkappa_1\varkappa_2^2)\},\end{aligned}$$

$$\begin{aligned}\varphi_2 = {} & \varkappa_1^{-2}\varkappa_2^{-2}\{\varkappa_1^2(-\varkappa_1^3\varkappa_2 + 4\varkappa_1^2 - 4\varkappa_1^2\varkappa_2 + 8\varkappa_1\varkappa_2 - 4\varkappa_1\varkappa_2^2 \\ & - \varkappa_1\varkappa_2^3 + 4\varkappa_2^2) + 2q^2m^{-2}(-\varkappa_1^4 + 2\varkappa_1^4\varkappa_2 + 8\varkappa_1^3 \\ & - 7\varkappa_1^3\varkappa_2 - 2\varkappa_1^3\varkappa_2^2 - 16\varkappa_1^2 + 32\varkappa_1^2\varkappa_2 - 3\varkappa_1^2\varkappa_2^2 \\ & - 2\varkappa_1^2\varkappa_2^3 - 32\varkappa_1\varkappa_2 + 24\varkappa_1\varkappa_2^2 + \varkappa_1\varkappa_2^3 - 16\varkappa_2^2) \\ & + q^4m^{-4}(4\varkappa_1^3 - 7\varkappa_1^3\varkappa_2 - 16\varkappa_1^2 + 40\varkappa_1^2\varkappa_2 + 2\varkappa_1^2\varkappa_2^2 \\ & - 64\varkappa_1\varkappa_2 + 20\varkappa_1\varkappa_2^2 - \varkappa_1\varkappa_2^3 - 16\varkappa_2^2) \\ & + 2q^6m^{-6}(-\varkappa_1^2 + 3\varkappa_1^2\varkappa_2 \\ & - 10\varkappa_1\varkappa_2 + \varkappa_1\varkappa_2^2 - \varkappa_2^2) - 2\varkappa_1\varkappa_2q^8m^{-8}\}.\end{aligned}$$

We cite without derivation the conditions under which $d\bar{\sigma}_q$ (A.3) coincides with the Compton-scattering cross section $d\bar{\sigma}_C$, averaged over the polarizations of the initial photon,

$$d\bar{\sigma}_C = 2\pi r_0^2\frac{d\varkappa_2}{\varkappa_1^2}\left\{-\frac{\varkappa_1}{\varkappa_2} - \frac{\varkappa_2}{\varkappa_1} + 4\left(\frac{1}{\varkappa_1} + \frac{1}{\varkappa_2}\right)^2 - 4\left(\frac{1}{\varkappa_1} + \frac{1}{\varkappa_2}\right)\right\}. \tag{A.4}$$

These conditions are

$$q^2 \ll \begin{cases} m^2\varkappa_1^2, & |\varkappa_1| \lesssim 1 \\ m^2|\varkappa_1|, & |\varkappa_1| \gg 1 \end{cases}, \tag{A.I}$$

$$1 - v^2 \ll \begin{cases} 1, & |\varkappa_1| \lesssim 1. \\ 1/|\varkappa_1|, & |\varkappa_1| \gg 1 \end{cases} \tag{A.II}$$

As in the case considered earlier (Sec. 6), the Weizsäcker-Williams relation (1.1) is violated in a narrow region of q^2 near q^2_{min}.

It is easy to see that (A.I) and (A.II) coincide with conditions (Ia) and (III).

[1] G. Weizsäcker, Z. Physik **88**, 612 (1934).
[2] E. Williams, Phys. Rev. **45**, 729 (1934).
[3] F. E. Low, Phys. Rev. **120**, 582 (1960).
[4] I. Ya. Pomeranchuk and I. M. Shmushkevich, Nucl. Phys. **23**, 452 (1961).
[5] K. Mork and H. Olsen, Nuovo cimento **8**, 395 (1960).
[6] A. M. Badalyan and Ya. A. Smorodinskii, JETP **40**, 123 (1961), Soviet Phys. JETP **13**, 865 (1961).

Translated by J. G. Adashko
225

ADIABATIC PERTURBATION OF DISCRETE SPECTRUM STATES

A. M. DYKHNE

Institute for Radioelectronics, Siberian Division, Academy of Sciences, U.S.S.R.

Submitted to JETP editor May 27, 1961

J. Exptl. Theoret. Phys. (U.S.S.R.) **41**, 1324-1327 (October, 1961)

The probabilities for quantum transitions between the states of a discrete spectrum are calculated for a system in adiabatic conditions, no assumptions being made regarding the form of the Hamiltonian. The calculations are performed with an accuracy to a pre-exponential factor of the order of unity.

THE author has calculated previously [1] for a one-dimensional linear oscillator the probabilities of quantum transitions under the influence of an adiabatic change in the frequency. In the present communication we calculate the transition probabilities in an arbitrary quantum system which is under adiabatic external conditions. Such a system is described by a Hamiltonian that varies "slowly" with the time. We assume that the time dependence of the Hamiltonian is analytic. We are interested in transitions between discrete spectrum states. Accordingly, we seek a solution of the Schrödinger equation in the form

$$\psi(x, t) = \sum_n a_n(t)\,\psi_n(x, t)\exp\left\{-i\int^t E_n(t')\,dt'\right\}. \quad (1)$$

Here $\psi_n(x,t)$ satisfies an equation with a Hamiltonian that has a parametric time dependence

$$H(t)\,\psi_n(x, t) = E_n(t)\,\psi_n(x, t), \quad (2)$$

and x denotes the set of all the coordinates.

Since we intend to continue the solutions of (2) into the region of complex t, we subject the functions $\psi_n(x,t)$ to analytic orthonormalization conditions (without complex conjugation)

$$\int \psi_n(x, t)\,\psi_m(x, t)\,dx = \delta_{mn}. \quad (3)$$

Substituting (1) into the temporal Schrödinger equation and using (2), we obtain

$$\dot a_n + \sum_{m\neq n} c_{mn}a_m \exp\left\{i\int^t \omega_{nm}(t')\,dt'\right\} = 0,$$

$$c_{mn} = \int \psi_m(x, t)\,\psi_n(x, t)\,dx,$$

$$\omega_{mn}(t) = E_n(t) - E_m(t), \qquad \hbar = 1. \quad (4)$$

These equations must be solved subject to initial conditions*

$$a_n(t) \to \delta_{nk} \text{ as } t \to -\infty. \quad (5)$$

The adiabaticity condition $\omega T \gg 1$ (ω is the characteristic frequency $E_n - E_m$ of the Hamiltonian $H(t)$ and T is the characteristic time of its variation) implies smallness of c_{nm}/ω. This enables us to solve (4) by successive approximation.

In the first approximation we have

$$a_n(+\infty) = \int_{-\infty}^{\infty} c_{nk}\exp\left\{i\int^t \omega_{nk}(t')\,dt'\right\}dt. \quad (6)$$

The integral in (6) is calculated by the steepest descent method, and we obtain the well known result that the transition probabilities are exponentially small if the different terms n and k do not cross. If any two terms cross, then, as can be readily shown, the corresponding matrix element c_{nk} vanishes and there are no transitions between such states in the first approximation. As can be seen from (6), the probabilities are maximal for transitions to "neighboring" levels, such as are of interest to us.

It is easy to show (see, for example, [1]) that (6) yields the correct order of magnitude of the result (correct order of the exponential function), but an incorrect factor preceding the exponential function.

To obtain the correct pre-exponential factor it would be necessary to take into account the next orders of perturbation theory, all of which give results of the same order of magnitude. In practice, naturally, this is not feasible. However, if we consider the system (4) with t complex, we can readily show that a contribution to the transition probability is made only by the neighborhoods of the singular points of the Hamiltonian.

In fact, this property is possessed by all the terms of the perturbation-theory series. We can therefore solve the system (4) in the neighborhoods of the singular points of the Hamiltonian

*It is assumed that H(t) tends to constant values $H_\pm$ as $t \to \pm\infty$.

and then "join" the resultant solutions with the constant amplitudes a_n for $t \to \pm\infty$. It is obvious that the singularities of the Hamiltonian can be due only to crossing of the terms (for a complex value of the time t), or to splitting of the discrete term from the continuous spectrum. We consider the case when the singularities of the former type are significant.

If the Hamiltonian H has no special form then, generally speaking, only two terms can cross at a given point t_0.* To calculate the greatest transition probability within neighboring levels it is necessary to take into account only the point of intersection of these terms, i.e., to retain in the system (4) only the matrix elements c_{mn} corresponding to two levels. The system (4) is then transformed into two equations:

$$\dot{a}_1 + c_{12}\exp\left\{i\int^t \omega(t')\,dt'\right\}a_2 = 0,$$
$$\dot{a}_2 + c_{21}\exp\left\{-i\int^t \omega(t')\,dt'\right\}a_1 = 0. \qquad (7)$$

As can be seen from (5) and (3), $c_{21} = -c_{12}$. Thus, Eq. (7) contains two functions $\omega(t)$ and $c(t) \equiv c_{12}(t)$. To solve the system we must investigate the behavior of these functions near the point t_0 where the terms cross.

Solving the stationary solution for the two terms in the vicinity of the intersection point, we can obtain a relation between the transition frequency at the instant t and the frequency at the instant t_1 (see [2]):

$$\omega_{12}(t) = \{[\omega_{12}(t_1) + v_{11}(t_1, t) - v_{22}(t_1, t)]^2 + 4v_{12}^2(t_1, t)\}^{1/2}; \qquad (8)$$

here

$$v_{ik} = \int \psi_i(x, t_1)\,[H(t) - H(t_1)]\,\psi_k(x, t_1)\,dx.$$

It is natural to assume that the radicand in (8) has a simple zero when $t = t_0$; thus, $\omega(t)$ behaves like $(t - t_0)^{1/2}$ near the point of intersection of the terms.

The wave functions of the stationary states in the vicinity of the point of intersection of the terms are connected with the functions at the instant t_1 by the equations

$$\psi_1(t) = [(1+k)^{1/2}\psi_1(t_1) - (1-k)^{1/2}\psi_2(t_1)]/\sqrt{2},$$
$$\psi_2(t) = [(1-k)^{1/2}\psi_1(t_1) + (1+k)^{1/2}\psi_2(t_1)]/\sqrt{2}. \qquad (9)$$

Here

$$k(t_1, t) = [\omega(t_1) + v_{11}(t_1, t) - v_{22}(t_1, t)]/\omega(t). \qquad (10)$$

Taking into account the fact that the wave functions at the instant t_1 are orthonormalized, we can readily obtain from (9)

$$c(t) = \int \dot{\psi}_2(x, t)\,\psi_1(x, t)\,dt = -\dot{k}/2(1-k^2)^{1/2}. \qquad (11)$$

Using (10) and noting that as $t \to t_0$ the numerator in (10) tends to a constant value, we can easily obtain

$$c(t) = \dot{\omega}/2i\omega. \qquad (12)$$

In the vicinity of the term crossing point the system (7) has the form

$$\dot{a}_1 + \frac{\dot{\omega}}{2i\omega}a_2\exp\left\{i\int^t \omega(t')\,dt'\right\} = 0,$$
$$\dot{a}_2 - \frac{\dot{\omega}}{2i\omega}a_1\exp\left\{-i\int^t \omega(t')\,dt'\right\} = 0. \qquad (13)$$

These equations are conveniently solved with initial conditions

$$a_2 \to 0, \qquad a_1 \to 1 \text{ as } t \to -\infty. \qquad (14)$$

We introduce a new unknown function y(t) with the aid of the equality

$$y(t) = \frac{a_1}{\sqrt{\omega}}\exp\left\{-\frac{i}{2}\int^t \omega(t')\,dt'\right\} + \frac{ia_2}{\sqrt{\omega}}\exp\left\{\frac{i}{2}\int^t \omega(t')\,dt'\right\}. \qquad (15)$$

It is easy to verify that y(t) satisfies the equation

$$\ddot{y} + (\omega(t)/2)^2 y = 0. \qquad (16)$$

From (14) and (15) follows an initial condition for

$$y \sim \exp\left\{-\frac{i}{2}\int^t \omega(t')\,dt'\right\} \text{ as } t \to -\infty. \qquad (17)$$

As $t \to +\infty$ we obtain

$$y \to A\exp\left\{-\frac{i}{2}\int^t \omega(t')\,dt'\right\} + R\exp\left\{\frac{i}{2}\int^t \omega(t')\,dt'\right\}. \qquad (18)$$

The value of R was calculated by Pokrovskii and Khalatnikov, who investigated the above-barrier reflection of a quasi-classical particle. Its value is

$$R = i\exp\left\{i\int^{t_0} \omega(t)\,dt\right\}. \qquad (19)$$

Comparing (18) and (15), we obtain the transition amplitude

$$a_2(+\infty) = \exp\left\{i\int^{t_0} \omega(t)\,dt\right\}. \qquad (20)$$

We see that the absolute value of the factor in front of the exponential function in the expression for the transition amplitude is unity. Expression (20) actually contains an arbitrary phase (since the lower limit of integration has not been defined). The phase of the transition amplitude can be determined accurate to π. Assume that when $t \to -\infty$ the wave function is

*The linear oscillator is in a class by itself, for all terms cross when $\omega = 0$.

$$\psi(t) \to \psi_1(x, -\infty) \exp[-iE_1(-\infty)\, t]. \quad (21)$$

By virtue of conditions (3), the wave function $\psi_1(x, t)$ is defined apart from the sign. As $t \to +\infty$

$$\psi(t) \to a_1(+\infty)\, \psi_1(x, +\infty) \exp[-iE_1(+\infty)\, t] + a_2(+\infty)\, \psi_2(x, +\infty) \exp[-iE_2(+\infty)\, t]. \quad (22)$$

Comparing (1) with (21) and (22) we can readily determine the phase of the transition amplitude, i.e., establish the lower limit of the integral in (19). Elementary calculations yield for $a_2(+\infty)$ the final expression

$$a_2(+\infty) = \exp\left\{ i \int_{-\infty}^{t_0} [E_1(t) - E_1(-\infty)]\, dt - i \int_{+\infty}^{t_0} [E_2(t) - E_2(+\infty)]\, dt + i\, [E_1(-\infty) - E_2(+\infty)]\, t_0 \right\}. \quad (23)$$

The transition probability is

$$w_{12} = \exp\left\{ i \int_{t_0^*}^{t_0} \omega(t)\, dt \right\}. \quad (24)$$

The formulas obtained determine completely the probability of transition of the quantum system to a "neighboring" level, with a maximum order of magnitude. As for transitions to farther levels, transitions through a virtual level can compete here with the above-considered process of "direct" transition. This question needs, however, additional investigation.

The author is sincerely grateful to Academician L. D. Landau for numerous valuable hints.

[1] A. M. Dykhne, JETP **38**, 570 (1960), Soviet Phys. JETP **11**, 411 (1960).

[2] L. D. Landau and A. M. Lifshitz, Quantum Mechanics, Pergamon, 1958.

[3] V. L. Pokrovskii and I. M. Khalatnikov, JETP **40**, 1713 (1961), Soviet Phys. JETP **13**, 1207 (1961).

Translated by J. G. Adashko
226

A MORE PRECISE DETERMINATION OF THE KINETIC COEFFICIENTS OF A PLASMA

O. V. KONSTANTINOV and V. I. PEREL'

Leningrad Physico-Technical Institute, Academy of Sciences, U.S.S.R.

Submitted to JETP editor May 29, 1961

J. Exptl. Theoret. Phys. (U.S.S.R.) 41, 1328-1329 (October, 1961)

Kinetic coefficients containing the exact values of the Coulomb logarithm are derived for a plasma. The case $\omega\tau \ll 1$, $e^2/\hbar v \ll 1$ is considered.

THE kinetic coefficients of a fully ionized gas are known with logarithmic accuracy.[1] This is connected with the logarithmic divergence of the Coulomb bremsstrahlung cross section for large impact parameters. One usually deals with this difficulty by artificially cutting off the interaction at distances of the order of the Debye radius. With the help of the methods of quantum field theory one can consistently take account of the collective interactions and obtain an expression for the renormalized scattering probability which does not contain divergences. Such an expression for the case where the de Broglie wavelength of the electron $\hbar/mv$ is much larger than the range of the essential interaction e^2/kT (e and m are the charge and mass of the electron, v is the thermal velocity of the electron, and T is the temperature) has been obtained in a number of papers.[2-4]

Since the renormalized scattering probability automatically cuts off the interaction for large impact parameters, it is possible to obtain the exact values of the terms in the argument of the logarithm appearing in the expressions for the kinetic coefficients. This has been done for the specific energy losses of a fast particle going through a plasma,[2] for the diffusion coefficient of the plasma perpendicular to the magnetic field[5] (for the case $\omega_c\tau \gg 1$, $\omega_c \ll \omega_0$, where ω_c is the cyclotron frequency, τ is the relaxation time, and ω_0 is the plasma frequency), and for the high frequency conductivity of the plasma[6] for $\omega\tau \gg 1$, where ω is the frequency of the electromagnetic wave. In the present paper we have carried out a similar more precise determination of the coefficients which determine the particle currents and the heat in the plasma in the presence of an electric field and of temperature and concentration gradients for $\omega\tau \ll 1$ (ω is the frequency of the process).

Our starting point is the kinetic equation with the collision integral obtained earlier in [3]. In solving it we have used the usual method of expanding the distribution function in a series of Laguerre polynomials (see, for example, the paper of Landshoff[7]). The result of the calculation can be written in the form

$$\mathbf{j} = \sigma\left(\mathbf{E} - \frac{1}{ne}\nabla p\right) + \tau\nabla T, \quad \mathbf{q} = -K\nabla T - \mu\left(\mathbf{E} - \frac{1}{ne}\nabla p\right), \tag{1}$$

where $\mathbf{E}$ is the electric field intensity, p is the pressure, n is the concentration, $\mathbf{j}$ is the current density, and $\mathbf{q}$ is the density of the heat flow. The kinetic coefficients σ, τ, μ, and K have the form

$$\sigma = 1.95\frac{ne^2}{m\nu_0}\frac{1}{\lambda_\sigma}, \qquad \tau = 1.39\frac{nek}{m\nu_0}\frac{1}{\lambda_\tau},$$
$$\mu = 6.25\frac{nekT}{m\nu_0}\frac{1}{\lambda_\mu}, \qquad K = 7.62\frac{nk^2T}{m\nu_0}\frac{1}{\lambda_K}. \tag{2}$$

Here

$$\nu_0 = \tfrac{2}{3}\pi(e^2/kT)^2(8kT/\pi m)^{1/2}n.$$

The difference between these formulas and the results of Landshoff[7] consists in that in our case the logarithm λ is definite (up to a term of order λ^{-1}) and has a different value for the different kinetic coefficients:

$$\lambda_\sigma = \ln\frac{1.2}{\eta}, \qquad \lambda_\mu = \ln\frac{1.3}{\eta}, \qquad \lambda_\tau = \ln\frac{1.6}{\eta},$$
$$\lambda_K = \ln\frac{1.7}{\eta}. \tag{3}$$

Here $\eta = (e\hbar/kT)(2\pi n_0/m)^{1/2}$ is the ratio of the de Broglie wavelength of the electron to the Debye radius.

These results were obtained by considering the first three Laguerre polynomials in the expansion of the distribution function. The calculations are similar to those carried out by Landshoff, but the intermediary expressions are considerably more involved and have therefore not been quoted.

[1] L. Spitzer, The Physics of Fully Ionized Gases, Interscience Publishers, N. Y. (1956).

[2] A. I. Larkin, JETP **37**, 264 (1959), Soviet Phys. JETP **10**, 186 (1960).

[3] O. V. Konstantinov and V. I. Perel', JETP **39**, 861 (1960), Soviet Phys. JETP **12**, 597 (1960).

[4] V. P. Silin, JETP **40**, 1768 (1961), Soviet Phys. JETP **13**, 1244 (1961).

[5] V. L. Gurevich and Yu. A. Firsov, JETP (in press).

[6] V. I. Perel' and G. M. Éliashberg, JETP (in press).

[7] R. Landshoff, Phys. Rev. **76**, 904 (1949).

Translated by R. Lipperheide
227

Letters to the Editor

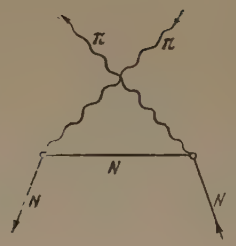

SCATTERING OF 7–8 Bev NEGATIVE PIONS ON NUCLEONS WITH LARGE MOMENTUM TRANSFER

R. A. ARIPOV,* V. G. GRISHIN, L. V. SIL'-VESTROV, and V. N. STREL'TSOV

Joint Institute for Nuclear Research

Submitted to JETP editor August 7, 1961

J. Exptl. Theoret. Phys. (U.S.S.R.) **41**, 1330-1331 (October, 1961)

In the study of the scattering of high-energy elementary particles, cases associated with a large momentum transfer between the colliding particles as a result of their interaction are of great interest.

Examples of such processes are reactions in which the particles are scattered at c.m.s. angles close to 180°. The study of such reactions, in particular, can serve as a check of the conclusions of Gell-Mann and Zachariasen[1] that large momentum transfers should still occur at high energies. Moreover, Pomeranchuk has shown (see, for example, [12]) that the pole of the diagram in the figure should give an appreciable contribution to the cross section for the scattering of high-energy π^+ mesons by protons at 180° c.m.s. The angular distribution of the scattered π^+ mesons described by this diagram should have a maximum at 180° with a width of about 30° at 7–8 Bev/c; this corresponds to the backward scattering of π^+ mesons in the l.s. An estimate of the cross section for such a process gives the value $d\sigma/d\Omega\ (180°) \approx 0.5$ mb/sr. The total cross section for the scattering of 7–8 Bev/c π^+ mesons backward in the l.s. should then also be ≈ 0.5 mb.

We have studied the following reactions in which π^- mesons are scattered backward in the l.s. on nucleons:

$$\pi^- + n \to \pi^- + n, \quad (1)$$

$$\pi^- + p \to \pi^- + p, \quad (2)$$

$$\pi^- + p \to \pi^0 + n. \quad (3)$$

Reaction (1) is the charge-conjugate analog of the above-mentioned reactions involving the scattering of π^+ mesons by protons. Consequently, the characteristics discussed above should be present in this case, too.[2] It is also obvious that the diagram should give a contribution to the cross section of reaction (3). This is not the case, however, for the scattering of π^- mesons on protons of type (2) because of the law of charge conservation.

The experiment was performed with a 24-liter propane bubble chamber placed in a magnetic field of 13 700 oe. The chamber was exposed to a 7–8 Bev/c π^- meson beam.

To find events corresponding to reaction (3), two observers scanned independently about 30 000 photographs. They recorded cases in which the primary mesons vanished. The efficiency for finding such events was $\sim 95\%$. A total of 579 cases in which the vanishing of the pions was associated with 230 γ quanta was found. The γ quanta had an angle of emission $\theta \geq 90°$ l.s. in only three cases. From this we can estimate the upper limit of the cross section σ_3 for reaction (3), since if the π^0 meson is scattered backward in the l.s., at least one γ quantum from the decay of this π^0 should also be emitted backward. This estimate is

$$\sigma_3 (\geqslant 90°) \leqslant 0.1 \text{ mb}$$

To find events corresponding to reactions (1) and (2), we scanned twice about 6000 photographs. We recorded cases with negative relativistic particles emitted at an angle $\geq 90°$ l.s. (process 1) and similar cases accompanied by the forward emission of a charged particle (process 2). The efficiency of finding such events was close to 100%.

As a result, we found four events which did not contradict the kinematics of reaction (1). Under the assumption that the carbon nuclei behave as a single effective quasi-free neutron,[3] we obtained an estimate of the upper limit of the cross section for this reaction:

$$\sigma_1 (\geqslant 90°) \leqslant 0.06 \text{ mb}$$

The result is in agreement with a similar estimate made by Bayukov et al.[2] for 2.8-Bev/c π^- mesons.

We also found three cases which did not contradict the kinematics of the elastic scattering of π^- mesons backward in the l.s. on protons. This corresponds to the cross section

$$\sigma_2 (\geqslant 90°) \leqslant 0.02 \text{ mb}$$

The estimate of the cross sections for processes (3) and particularly (1) obtained in this way is considerably less than that calculated from the diagram, which apparently indicates that other possible processes compete with this diagram. Moreover, the estimates of the cross sections for all three scattering processes are of the same order of magnitude, i.e., there is no difference between processes to which this diagram gives a contribution and those for which a contribution is impossible.

The authors thank M. I. Podgoretskii for discussion of the results and for valuable advice, the bubble chamber crew of the Joint Institute for Nuclear Research for providing the pictures and M. A. Balashova, T. A. Zhuravleva, O. V. Kol'ga, M. I. Filippova, V. D. Shopkova, and N. V. Sharikova, for helping scan the photographs.

*Physico-technical Institute, Academy of Science, Uzbek S.S.R.

[1] M. Gell-Mann and F. Zachariasen, Preprint, 1961.

[2] Bayukov, Leksin, Suchkov, Shalamov, and Shebanov, JETP **41**, 52 (1961), Soviet Phys. JETP **14**, 40 (1962).

[3] Bannik, Gal'per, Grishin, Kotenko, Kuzin, Kuznetsov, Merzon, Podgoretskii, and Sil'vestrov, JETP **41**, 1394 (1961), translation in press.

[4] Bayukov, Leksin, and Shalamov, Preprint, Inst. of Theoret. and Exptl. Phys., 1961.

Translated by E. Marquit
228

ANISOTROPY OF THE ODD PHOTOMAGNETIC EFFECT

I. K. KIKOIN and S. D. LAZAREV

Submitted to JETP editor July 17, 1961

J. Exptl. Theoret. Phys. (U.S.S.R.) **41**, 1332-1333 (October, 1961)

IT has been shown previously[1,2] that the even photomagnetic effect in germanium is markedly anisotropic. The odd photomagnetic effect is usually considered to be isotropic. When there is a strictly linear variation of the odd photomagnetic e.m.f. on the magnetic field strength, it is expected to be anisotropic for a cubic crystal. However, it is known that for sufficiently strong magnetic fields

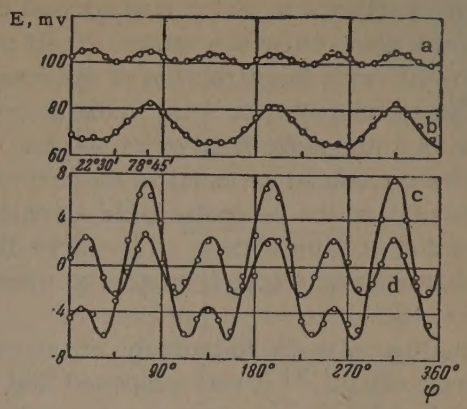

FIG. 1

the odd photomagnetic e.m.f. in germanium ceases to vary linearly with the field, and even passes through a maximum at some value of the field. In these conditions the possibility of anisotropy arising even in the odd photomagnetic effect is not excluded.

To clarify the question of the existence of anisotropy in the odd photomagnetic effect, we have studied single-crystal specimens of n- and p-germanium in magnetic fields up to 25 000 oe. The specimens studied, like those described previously,[1] were in the form of circular discs with 32 electrodes around the periphery. The specimens could be rotated about an axis coinciding with the normal to the plane of the disc. The angle φ between the crystallographic axes and the direction of the magnetic field was thereby changed. Also the specimens could be turned so that the angle θ between the normal to the specimen surface and the direction of the magnetic field was changed.

Figure 1a shows the anisotropy curve of the odd effect, i.e., the variation of the odd photomagnetic e.m.f. on the angle φ for a specimen of p-germa-

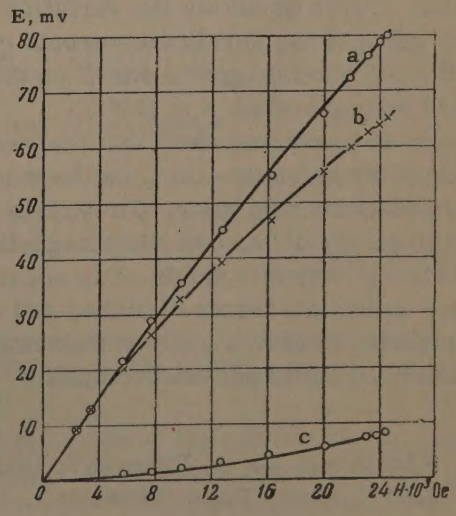

FIG. 2

nium, the [111] axis of which was normal to the plane of the disc, while the normal itself made an angle $\theta = 90°$ with the direction of the magnetic field. The measurements were made at room temperature in a magnetic field of 24,500 oe. The e.m.f. was measured as usual in the direction perpendicular to the magnetic field direction and the direction of illumination. The curve 1b refers to the photomagnetic e.m.f. measured when the angle $\theta \approx 130°$.

By analogy with the anisotropy of the even photomagnetic effect,[2] it was supposed that the measured odd photomagnetic e.m.f. can be regarded as the sum of isotropic and anisotropic components. It is clear that the purely anisotropic component can be obtained by measuring the odd photomagnetic e.m.f. in the direction of the magnetic field or its projection on the plane of the surface. Experiments performed in fact confirmed the presence of an odd photomagnetic e.m.f. when measuring it in the direction of the magnetic field, i.e., in the direction in which there is no isotropic odd photomagnetic effect. The variation of this photomagnetic e.m.f. on the angle φ is given in Fig. 1d (the continuous curve is the function $E = a \sin 6\varphi$). Figure 1c shows the anisotropy curve for the same specimen when $\theta = 75°$ (the continuous curve is the function $E = a \sin 3\varphi + b \sin 6\varphi$).

Curves are given in Fig. 2 showing the variation of the extreme values of the odd photomagnetic e.m.f. with the magnetic field strength. Curves 2a and 2b refer to the photomagnetic e.m.f. measured in the "usual" direction (perpendicular to the magnetic field) for two values of φ: 75°45′ and 22°30′ (see Fig. 1b). The specimen was oriented relative to the magnetic field so that $\theta \approx 130°$. For this value of θ the anisotropic component of the photomagnetic e.m.f. attains a maximum value. Curve 2c shows the variation of the extremal value of the purely anisotropic component of the odd photomagnetic e.m.f. on the magnetic field strength when $\theta \approx 130°$.

The curves presented show that the variation of the odd photomagnetic e.m.f. on the magnetic field is essentially nonlinear. To explain the observed anisotropy of the odd photomagnetic effects in strong magnetic fields, it is apparently necessary to include terms of higher odd degree in the magnetic field in a general phenomenological equation of the Kagan-Smorodinskii[3] type.

[1] I. K. Kikoin and Yu. A. Bȳkovskii, DAN SSSR **116**, 377 (1957), Soviet Phys.-Doklady **2**, 442 (1958).

[2] I. K. Kikoin and S. D. Lazarev, DAN SSSR **135**, 1371 (1960), Soviet Phys.-Doklady **5**, 1313 (1961).

[3] Yu. Kagan and Ya. A. Smorodinskii, JETP **34**, 1346 (1958), Soviet Phys. JETP **7**, 929 (1958).

Translated by K. F. Hulme
229

RESISTANCE OF THIN SINGLE-CRYSTAL WIRES

B. N. ALEKSANDROV and M. I. KAGANOV

Physico-Technical Institute, Academy of Sciences, Ukrainian S.S.R.

Submitted to JETP editor July 25, 1961

J. Exptl. Theoret. Phys. (U.S.S.R.) 41, 1333-1336 (October, 1961)

MEASUREMENT of the electrical conductivity of thin metal wires is usually used to determine electron mean free paths.[1] In the standard method for this, the results obtained for the dependence of resistivity on wire diameter are compared with the theoretical curve obtained by Dingle.[2] It must be remembered that Dingle's results were obtained on the assumption of an isotropic, quadratic dispersion law for the electrons. As a result, the ratio ρ/ρ_∞ (ρ_∞ is the resistivity of an infinitely thick wire and ρ that of a wire of diameter d) is expressed as a function of d/λ only (λ is the electron mean free path).

One of us (B. A.) has measured the dependence of the resistivity of tin single crystal wires on diameter. The tin used in the experiments was first subjected to zone refinement.[3] The purity is

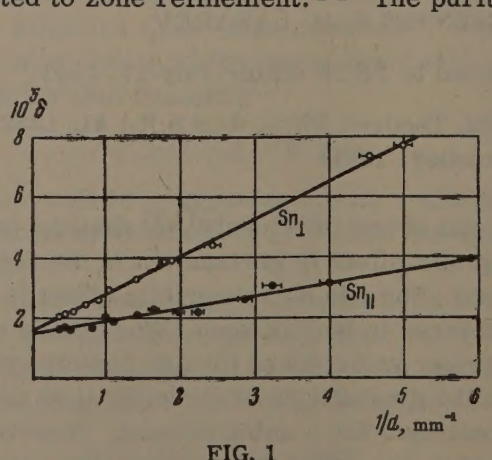

FIG. 1

calculated as 99.99986% ($\delta_{4.2\infty} = 1.5 \times 10^{-5}$). The results obtained are shown in Fig. 1 in the form of the dependence of $\delta = R_{4.2}/R_{293}$ ($R_{4.2}$ is the electrical resistance of a wire at 4.2° K, and R_{293} the resistance of the same wire at 20° C) on the reciprocal of the diameter. The lower curve refers to wires with axis parallel to the principal crystal axis ($Sn_{\parallel}$), and the upper curve to wires with axis perpendicular to the principal axis ($Sn_{\perp}$). In the latter case the wire axis coincides with the [110] direction. These orientations of the single crystals were determined with an accuracy of 2—4°. Since δ was measured with an accuracy not worse than 2—3%, while the error in determining 1/d increased with decreasing diameter, we can say that the slope of the straight lines in Fig. 1 were determined with an accuracy of 1—3%. The slope of the line for $Sn_{\perp}$ is approximately three times greater than for $Sn_{\parallel}$, i.e., the difference in slopes lies definitely outside the experimental errors.*

It is only possible to take a theoretical discussion of the electrical conductivity of single crystal wires to the end (starting from the assumption of an arbitrary dispersion law for the electrons) for the case when the mean free path λ is appreciably greater than the wire diameter. If the axis of the cylindrical wire is perpendicular to the symmetry plane of the crystal, the mean electrical conductivity $\sigma(d)$ is of the form

$$\sigma(d) \approx \frac{8de^2}{3\pi(2\pi\hbar)^3} I, \qquad I = \oint \frac{(\mathfrak{N}\mathbf{b})^2}{\sqrt{1-(\mathfrak{N}\mathbf{b})^2}}\, dS, \tag{1}$$

where **b** is a unit vector in the direction of the axis of the wire, $\mathfrak{N}$ is a unit vector normal to the Fermi surface, dS is an element of area on the Fermi surface, and the integration is over the whole surface. We should note that in the derivation of this expression there are no additional restrictions other than those usually assumed to be fulfilled (for example, it was assumed that the temperature is considerably below the Fermi energy). In particular, (1) is also valid for the model of a Fermi liquid. If we introduce the Gaussian curvature of the Fermi surface $K(\theta, \varphi)$ and choose the direction of the vector **b** as the polar axis, then (1) can be written in the following form:

$$\sigma(d) \approx \frac{8\,de^2}{3\pi(2\pi\hbar)^3} \oint \frac{\cos^2\theta\, d\theta\, d\varphi}{K(\theta, \varphi)}. \tag{2}$$

The integrals in (1) and (2) cannot, naturally, be evaluated without an assumption about the dispersion law for the electrons. For a quadratic, anisotropic dispersion law

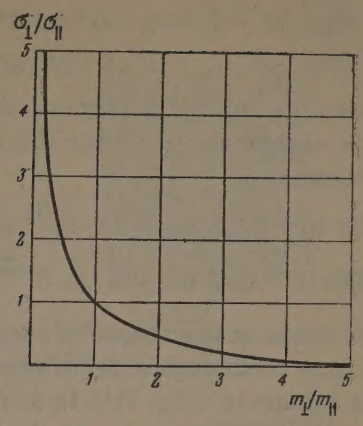

FIG. 2

$$\varepsilon(p) = \frac{p_1^2}{2m_1} + \frac{p_2^2}{2m_2} + \frac{p_3^2}{2m_3}, \tag{3}$$

and taking the vector **b** to be parallel to the first axis, we obtain

$$\sigma(d) = \frac{4\,de^2}{3\pi\hbar}\left(\frac{3n}{8\pi}\right)^{2/3}(k_2k_3)^{-1/3}[F(k_2, k_3) + F(k_3, k_2)], \tag{4}$$

where n is the number of electrons per unit volume,

$$k_2 = \frac{m_1}{m_2}, \qquad k_3 = \frac{m_1}{m_3},$$

$$F(k_2, k_3) = \int_0^{\pi/2} \frac{d\varphi}{(k_2\cos^2\varphi + k_3\sin^2\varphi)^{1/2}}. \tag{5}$$

For the isotropic case ($k_2 = k_3 = 1$) we obtain the well known Dingle formula:[2]

$$\sigma(d) \approx (4de^2/3\hbar)\,(3n/8\pi)^{2/3} = \sigma_{\infty}\, d/\lambda.$$

If $m_2 = m_3 = m_{\perp}$, while $m_1 = m_{\parallel}$, then

$$\sigma(d) \equiv \sigma(d)_{\parallel} = \frac{4\,de^2}{3\hbar}\left(\frac{3n}{8\pi}\right)^{2/3}\left(\frac{m_{\perp}}{m_{\parallel}}\right)^{1/3}. \tag{6}$$

If $m_1 = m_2 = m_{\perp}$, while $m_3 = m_{\parallel}$ ($k_2 = 1$, $k_3 = k = m_{\perp}/m_{\parallel}$), then

$$\sigma(d) \equiv \sigma(d)_{\perp} = \frac{4\,de^2}{3\pi\hbar}\left(\frac{3n}{8\pi}\right)^{2/3}\left(\frac{m_{\parallel}}{m_{\perp}}\right)^{1/3}[F(1, k) + F(k, 1)]. \tag{7}$$

From (6) and (7) we obtain

$$\frac{\sigma_{\perp}(d)}{\sigma_{\parallel}(d)} = \frac{1}{\pi k}[F(1, k) + F(k, 1)] \approx \begin{cases} \dfrac{1}{\pi k}\ln\dfrac{1}{k}, & k \ll 1 \\ 1, & k = 1 \\ \dfrac{\ln k}{\pi k^{3/2}}, & k \gg 1 \end{cases} \tag{8}$$

The dependence of $\sigma_{\perp}(d)/\sigma_{\parallel}(d)$ on the ratio of effective masses [Eq. (8)] is shown graphically in Fig. 2.

From the slope of the curves of Fig. 1 and the values $\rho_{\parallel 293} = 14.3 \times 10^{-6}$ ohm cm and $\rho_{\perp 293} = 9.85 \times 10^{-6}$ ohm cm,[4] we determined the products

$[d\Delta\rho(d)]_{\parallel} = d[\rho_{\parallel}(d) - \rho_{\parallel}(\infty)] = 0.61 \cdot 10^{-11}\,\Omega \cdot \mathrm{cm}^2$,

$[d\Delta\rho(d)]_{\perp} = 1.22 \cdot 10^{-11}\,\Omega \cdot \mathrm{cm}^2$.

Using this data we can determine the values of the integrals entering into (1) for the two crystallographic directions:

$$I_{\parallel} = 1{,}335 \cdot 10^{-48}/[d\Delta\rho(d)]_{\parallel} = 2.2 \cdot 10^{-37} \text{ cgs esu}$$

$$I_{\perp} = 1.335 \cdot 10^{-48}/[d\Delta\rho(d)]_{\perp} = 1.1 \cdot 10^{-37} \text{ cgs esu} \quad (9)$$

The difference in the slopes of the curves of Fig. 1 are thus connected with different values of the surface integrals [Eq. (1)] in different crystallographic directions, i.e., with the shape of the Fermi surface for tin. From this point of view, an experimental study of the difference in the slopes of the straight lines (in δ, 1/d coordinates) for Pb, Cu, Au, Ag and possibly Al in the [100] and [111] directions is of interest; these are the directions in which maximum differences of conductivity of thin wires of cubic crystals are expected (the existence of complicated open Fermi surfaces are assumed for these metals, except Al[5]).

If the crystal anisotropy is described in terms of effective masses, then for tin, for which $\Delta\rho_{\parallel}(d)/\Delta\rho_{\perp}(d) = 0.5$ (at 4.2° K) we must take $m_{\perp}/m_{\parallel} = 1.85$ from Fig. 2 and $n = 4.4 \times 10^{22}$ [calculated according to (6)].

Since the number of atoms per unit volume $n_A = 3.7 \times 10^{22}\ \mathrm{cm}^{-3}$ for tin, there must be $n/n_A = 1.2$ conduction electrons per atom. Naturally, this number cannot be considered the true number of conduction electrons per atom as it was obtained from very simplifying assumptions about a quadratic dispersion law, while from galvanomagnetic and magnetic experiments it is known that the Fermi surface for tin is very complicated.[6]

*A detailed discussion of the experimental method and results will be given separately.

[1] A. Eucken and F. Förster, Götting. Nachrichten 1, 43, 129 (1934). L. Riedel, Ann. Physik Lpz. 28, 603 (1937). E. R. Andrew, Proc. Phys. Soc. A62, 77 (1949). J. E. Kunzler and C. A. Renton, Phys. Rev. 108, 1397 (1957). H. Meissner, Phys. Rev. 109, 668 (1958). H. Meissner and R. Zdanis, Phys. Rev. 109, 681 (1958). B. N. Aleksandrov and B. I. Verkin, JETP 34, 1655 (1958), Soviet Phys. JETP 7, 1137 (1958). J. L. Olsen, Helv. Phys. Acta 31, 713 (1958). R. Nossek, Zs. Naturforsch. 14a, 840 (1959). T. Frederking and R. Reimann, Helv. Phys. Acta 33, 998 (1960).

[2] R. B. Dingle, Proc. Roy. Soc. A201, 545 (1950).

[3] B. N. Aleksandrov, FMM 9, 53 (1960), Phys. Met. and Metall. 9, 46 (1960).

[4] Sb. Fiz. Konstant, (Table of Physical Constants), ONTI, 1937.

[5] N. E. Alekseevskii and Yu. P. Gaĭdukov, JETP 37, 672 (1959), Soviet Phys. JETP 10, 481 (1960).

[6] Alekseevskii, Gaĭdukov, Lifshitz, and Peschanskii, JETP 39, 1201 (1960), Soviet Phys. JETP 12, 837 (1961); A. V. Gold and M. G. Priestley, Phil. Mag. 5, 1089 (1960).

Translated by R. Berman
230